

**PREDICTION OF SHEAR STRENGTH OF REINFORCED
AND PRESTRESSED CONCRETE BEAMS
BY FINITE ELEMENT METHOD**

By

MOHAMED MOHAMED AHMED ABDEL-KADER

**A thesis submitted for the degree of
Doctor of Philosophy**

In the Name of ALLAH

**Department of Civil Engineering
University of Glasgow**

© M. M. A. Abdel-Kader

November 1993

ProQuest Number: 13832072

All rights reserved

INFORMATION TO ALL USERS

The quality of this reproduction is dependent upon the quality of the copy submitted.

In the unlikely event that the author did not send a complete manuscript and there are missing pages, these will be noted. Also, if material had to be removed, a note will indicate the deletion.



ProQuest 13832072

Published by ProQuest LLC (2019). Copyright of the Dissertation is held by the Author.

All rights reserved.

This work is protected against unauthorized copying under Title 17, United States Code
Microform Edition © ProQuest LLC.

ProQuest LLC.
789 East Eisenhower Parkway
P.O. Box 1346
Ann Arbor, MI 48106 – 1346

TABLE OF CONTENTS

ACKNOWLEDGEMENTS.....	i
SUMMARY.....	ii
NOTATIONS.....	iii

CHAPTER 1 INTRODUCTION

1.1 Introduction.....	1
1.2 Purpose of study.....	3
1.3 Organisation of the thesis.....	4

CHAPTER 2 : ON SHEAR IN REINFORCED CONCRETE

2.1 Introduction.....	5
2.2 Definitions related to shear.....	5
2.3 Mechanisms of shear transfer.....	7
2.3.1 Shear transfer by aggregate interlock.....	10
2.3.2 Aggregate interlock.....	10
2.3.3 Dowel action.....	10
2.3.4 Interaction between aggregate interlock and dowel action.....	12
2.3.5 Arch action.....	13
2.3.6 Web reinforcement.....	13
2.4 Mechanisms of shear failure.....	15
2.4.1 Beams without web reinforcement.....	16
2.4.2 Beams with web reinforcement.....	16
2.5 Factors affecting the shear capacity.....	18
2.5.1 Reinforcement details.....	18
2.5.2 Concrete properties.....	19
2.5.3 Beam dimensions.....	21
2.5.4 Other factors.....	21
2.6 Types of failures.....	24
2.6.1 Flexural failure.....	24
2.6.2 Shear failure.....	24
2.7 Methods of analysis of shear capacity.....	26
2.7.1 Beams without web reinforcement.....	27
2.7.1.1 Analytical shear compression theories.....	27
2.7.1.2 Concept of concrete arches.....	27
2.7.1.3 Concept of the compression truss model.....	29
2.7.2 Arch analogies.....	30
2.7.3 Frame Analogies.....	32
2.7.4 Truss analogies.....	33
2.7.4.1 Morsch model (or the 45° truss model).....	34



In the Name of ALLAH

"Most Gracious, Most Merciful"

"He Who taught (the use of) the Pen,"

"Taught man that which he Knew not."

2.7.4.2 Collins and Mitchell truss model	36
2.7.4.3 Mander's model	38
TABLE OF CONTENTS	
2.7.5 Modified Compression Field Theory	43
2.7.5.1 Stress-strain relationships	44

ACKNOWLEDGEMENTS	i
SUMMARY	ii
NOTATIONS	iii

CHAPTER 1 : INTRODUCTION

1.1 Introduction	1
1.2 Purpose of study	3
1.3 Organisation of the thesis	4

CHAPTER 2 : ON SHEAR IN REINFORCED CONCRETE

2.1 Introduction	5
2.2 Definitions related to shear	5
2.3 Mechanisms of shear transfer	7
2.3.1 Shear transfer by shear stress in concrete	10
2.3.2 Aggregate interlock	10
2.3.3 Dowel action	10
2.3.4 Interaction between aggregate interlock and dowel action	12
2.3.5 Arch action	13
2.3.6 Web reinforcement	13
2.4 Mechanisms of shear failure	15
2.4.1 Beams without web reinforcement	16
2.4.2 Beams with web reinforcement	16
2.5 Factors affecting the shear strength	18
2.5.1 Reinforcement details	18
2.5.2 Concrete properties	19
2.5.3 Beam dimensions	21
2.5.4 Other factors	23
2.6 Types of failures	24
2.6.1 Flexural failure	24
2.6.2 Shear failure	24
2.7 Methods of analysis of shear failure	26
2.7.1 Beams without web reinforcement	27
2.7.1.1 Analytical shear compression theories	27
2.7.1.2 Concept of concrete cantilever	29
2.7.1.3 Concept of the compressive force path	29
2.7.2 Arch analogies	30
2.7.3 Frame Analogies	32
2.7.4 Truss analogies	32
2.7.4.1 Morsch model: (or the 45° truss model)	34

2.7.4.2	Collins and Mitchell truss model	36
2.7.4.3	Modified truss model	38
2.7.5	Modified Compression Field Theory	43
2.7.5.1	Stress-strain relationships.....	44

CHAPTER 3 : MATERIAL BEHAVIOUR AND NUMERICAL MODELLING

3.1	Introduction.....	47
3.2	Modelling of concrete.....	49
3.2.1	Concrete in compression.....	50
3.2.1.1	Uniaxial stress	50
3.2.1.2	Biaxial stress	53
3.2.1.3	Triaxial stress	60
3.2.1.4	Compression softening.....	62
3.2.2	Concrete in tension	63
3.2.2.1	Tensile strength of concrete	63
3.2.2.2	Cracking of concrete	65
3.2.2.3	Tension stiffening	74
3.2.2.4	Tension softening.....	76
3.2.3	Concrete in shear.....	77
3.2.3.1	Shear retention factor	81
3.2.4	Yield criterion	84
3.2.4.1	2-D yield criterion.....	84
3.2.4.2	3-D yield criterion.....	88
3.3	Modelling of steel.....	92
3.3.1	Smearred model:.....	92
3.3.2	Discrete model:	94
3.3.3	Embedded model:	94
3.4	Interaction between concrete and steel	95
3.4.1	Bond-slip.....	95
3.4.2	Dowel action	96

CHAPTER 4 : THE FINITE ELEMENT AND NUMERICAL METHODS OF ANALYSIS

4.1	Introduction.....	100
4.2	Finite element concept and formulation	100
4.3	Discretisation by finite element	101
4.4	Isoparametric elements:	104
4.4.1	Shape functions:.....	104
4.4.2	Stress-strain relationships	107
4.4.3	Element stiffness matrix.....	111
4.4.4	Stiffness matrix of embedded bar	111
4.4.5	Numerical integration	113
4.5	The equation solution technique.....	114

4.6 Numerical methods of analysis.....	116
4.6.1 Incremental procedure.....	117
4.6.2 Iterative procedure	118
4.6.3 Incremental-Iterative procedure.....	118
4.7 Convergence criteria.....	119
4.8 Basic steps in nonlinear program.....	120

CHAPTER 5 : COMPARISON BETWEEN THE PREDICTIONS OF 3-D AND 2-D FINITE ELEMENT MODELS

5.1 Introduction.....	123
5.2 Features of the 3-D and 2-D versions used in the analysis.....	123
5.3 Prediction of the behaviour of a plain concrete prism.....	128
5.4 Prediction of the behaviour of a rectangular beam without web reinforcement.....	140
5.5 Prediction of the behaviour of a rectangular beam with web reinforcement.....	152
5.6 Prediction of the behaviour of a Tee beam.....	161
5.7 Conclusions.....	166

CHAPTER 6 : PRELIMINARY PARAMETRIC STUDY

6.1 Introduction.....	172
6.2 Analysis of Bresler and Scordelis's beams	173
6.2.1 Effect of shear retention factor.....	181
6.2.1.1 Beams without shear reinforcement.....	181
6.2.1.2 Beams with shear reinforcement.....	193
6.2.2 Effect of tensile strength of concrete	219
6.2.2.1 Beams without shear reinforcement.....	220
6.2.2.2 Beams with shear reinforcement.....	226
6.2.3 Effect of the value of the compressive strain at peak stress.....	234
6.2.4 Effect of tension softening of concrete	245
6.2.4.1 Beams without shear reinforcement.....	246
6.2.4.2 Beams with shear reinforcement.....	247
6.2.5 Effect of compressive strength of concrete.....	264
6.2.6 Effect of compression softening of concrete.....	269
6.3 Conclusions.....	302

CHAPTER 7 : PARAMETRIC STUDY CONTINUED

7.1 Introduction.....	304
7.2 Data of beams	304
7.2.1 Krefeld and Thurston's beams.....	304
7.2.2 Clark's beams	314
7.2.3 Mphonde and Frantz's beams.....	314

7.3	Analysis of beams.....	324
7.3.1	Beams without shear reinforcement.....	328
7.3.1.1	Results of Krefeld and Thurston's beams.....	329
7.3.1.2	Clark's beams	329
7.3.1.3	Mphonde and Frantz's beams.....	329
7.3.2	Beams with shear reinforcement.....	334
7.3.2.1	Krefeld and Thurston's beams.....	334
7.3.2.2	Clark's beams	334
7.4	Prediction of failure mode	338
7.5	Conclusions.....	353

CHAPTER 8 : PRESTRESSED CONCRETE BEAMS

8.1	Introduction.....	356
8.2	Arthur's beams	356
8.3	Elzanaty, et al's beams	386
8.4	Conclusions.....	400

CHAPTER 9 : REINFORCED CONCRETE TEE-BEAMS

9.1	Introduction.....	401
9.2	Kotsovos, et al's beams.....	401
9.3	Taylor's beams	415
9.4	Conclusions.....	432

CHAPTER 10 : CONCLUSIONS AND RECOMMENDATIONS

10.1	General conclusions.....	434
10.2	Recommendations for future work	439
REFERENCES		446

ACKNOWLEDGEMENTS

The work described in this thesis was carried out in the Department of Civil Engineering at the University of Glasgow, under the general guidance of Professor A. Coull whose interest and encouragement are gratefully acknowledged.

The author is indebted to Dr. P. Bhatt for his valuable supervision, patience, encouragement and advice throughout the course of this study.

I wish also to express my thanks to Professor D. R. Green, Professor D. Muirwood, and Dr. J. G. Herbertson, past, and present heads of Department of Civil Engineering for making the facilities available.

Grateful thanks are due to:

Dr. D. V. Phillips, Dr. T. J. A. Agar, and Dr. P. D. Arthur for their interest and useful discussions.

The research staff and students of Civil Engineering Department, especially Dr. B. Zhang, Dr. B. Famiyesin, Dr. A. Khan, Dr. H. Musavi, Dr. A. Bensalem, Mr. A. Hamidon, Mr. S. D. Djellab, Mr. B. Khaled, Mr. Khalifa for their useful discussions.

My wife and lovely daughter and sons Heba, Ali, and Tarek for their patience and moral support and for my parents, sisters, and brothers for their valuable encouragement throughout the years.

This study was made possible by the award of a scholarship by the Egyptian Government. I am grateful to it.

SUMMARY

This thesis presents a 2-D finite element model that can be used to predict the shear strength of reinforced and prestressed concrete beams. A comparison between the predictions of 3-D and 2-D finite element models was made first, from which it was concluded that the 2-D finite element model is sufficient to predict the behaviour of reinforced concrete beams.

To improve the results of the 2-D finite element, five parameters which have a significant effect on the prediction of the failure load and the corresponding mode of failure were studied. These parameters are: (i) shear retention factor, (ii) tensile strength of concrete, (iii) magnitude of the strain corresponding to the peak stress in the stress-strain curve of concrete in compression, (iv) tension softening of concrete, and (v) compression softening of concrete. The developed model is used in a nonlinear finite element program. Only smeared cracking approach was used.

After developing, the model was tested against more than two hundred reinforced and prestressed concrete beams from seven previous experimental investigations. These beams were with and without shear reinforcement having rectangular, I, and Tee cross-sections. The beams covered important variables affecting the shear strength of reinforced concrete beams such as: shear span to depth ratio a/d , amount of shear reinforcement, effective depth and width of beam, and compressive strength of concrete. Most of the beams failed in shear. Because of the fact that in many previous studies on a small number of beams, the emphasis had been placed purely on the prediction of the failure load, very often the corresponding mode of failure differed significantly from the actual mode of failure. In this study particular emphasis is placed on the predicted mode agreeing with the actual mode of failure. The model was capable of predicting to good accuracy the failure load, the mode of failure, the load-deflection curve, and the stresses in reinforcement.

NOTATIONS

Major symbols used in the text are listed below. Others are defined when they first appear. Some symbols have different meanings in different contexts; these are clearly defined at the appropriate place.

a	Shear span.
a/d	Shear span over effective depth ratio.
A_c	Area of concrete section.
A_s	Area of tensile reinforcement.
A_{sv}	Cross sectional area of a vertical stirrup.
b	Width of a section.
$[B]$	Strain matrix.
$[D]$	Elasticity matrix for any material.
d	Effective depth of beam.
E	Young's modulus.
f_c'	Cylinder compressive strength of concrete.
f_{cc}	Intermediate yield surface strength of concrete.
f_{cu}	Cube compressive strength of concrete.
f_t'	Tensile strength of concrete.
f_y	Yield strength of steel.
G_o	Shear modulus of uncracked concrete.
G_{cr}	Shear modulus of cracked concrete.
$[K]$	Stiffness matrix.
L. F.	Load factor = computed load / Experimental failure load.
m	Ratio of tensile to compressive strengths of concrete.
M	Bending moment at any stage of loading.
$N(\xi, \eta)$	Shape function matrix.

P	Applied load.
q	Intensity of the uniformly distributed load.
s, s_v	Spacing of stirrups.
$[T]$	Transformation matrix for cracks.
Tol	Specified convergence tolerance.
V	Shear force.
v_c	Shear stress carried by concrete.
u, v, w	Displacements at a point in X, Y, Z directions respectively.
X, Y, Z	Rectangular cartesian coordinates.
x, y, z	Coordinates at a point in X, Y, Z system.
α	Ratio of the principal stresses = σ_1 / σ_2 .
β	Shear retention factor = $\frac{G_{cr}}{G_o}$.
β_{min}	Minimum shear retention factor.
$\{\delta\}$	Displacement vector.
$\{\epsilon\}$	Strain vector.
ϵ	Normal strain.
ϵ_1, ϵ_2	Principal strains.
ϵ_{cc}	Compressive strain at peak of stress.
ϵ_{cr}	Cracking strain of concrete.
ϵ_{max}	Maximum compressive strain of concrete.
ϵ_n, ϵ_t	Strain normal and tangential to the surface of crack.
ϵ_{tmax}	The tensile strain after which concrete does not carry tensile stress.
ϵ_x, ϵ_y	Strain components in the cartesian coordinates.
ϵ_{ys}	Yield strain of steel.
ξ, η	Intrinsic coordinates of any point within the element.
ϕ	Reinforcement bar diameter.
ρ	Percentage of tensile steel = $\frac{A_s}{bd}$.
ν	Poisson's ratio.

Π	Total potential.
π_e	Total potential of element.
$\{\sigma\}$	Stress vector.
$\{\sigma_0\}$	Initial stress vector.
σ_{oct}	Octahedral normal stress.
σ_n	Normal stress.
$\sigma_x, \sigma_y, \sigma_{xy}$	Stress components in a cartesian coordinates.
σ_1, σ_2	Principal stresses.
τ_{xy}	Shear stresses in xy plane.
τ_{oct}	Octahedral shear stress.

CHAPTER 1

INTRODUCTION

1.1 Introduction

This thesis is concerned with the development of a two dimension (2-D) finite element model that gives 'good' predictions of the shear strength of reinforced and prestressed concrete beams. Although many attempts have been made, the prediction of the response of reinforced concrete structures failing in shear is not an easy task. A brief review of the available important investigations include the following.

Starting with Ngo and Scordelis (1967) who developed the first linear elastic finite element model which was used in the analysis of the behaviour of reinforced concrete members, a lot of work using the finite element method has been done. Cedolin and DeiPoli (1977) developed a finite element model, which incorporated the available experimental results on concrete nonlinear behaviour under biaxial stresses, and predicted the load-deflection curve for two beams failing in shear. In 1978, Cedolin and Nilson studied the convergence of iterative methods applied to finite element analysis of reinforced concrete on one beam without shear reinforcement failing in shear. Arnesen, et al. (1980) developed a finite element model and compared the results of the model with four tests. Bedard and Kotsovos (1985) tried to ensure the generality of their finite element model to the analysis of concrete structures. They analysed three structural configurations: deep beam with openings and web reinforcements, four shear panels, and a plain concrete sphere in addition to results of nine examples (mainly on beams and plain concrete prisms) reported in their paper. In 1987, Cervera, Hinton and

Hassen used 3-D finite element model and compared the results with: two panels, four slabs, two deep beams and beam without shear reinforcement. Chang, et al. (1987) compared the numerical results obtained from their finite element analysis with four reinforced concrete panels. In 1988, Balakrishnan and Murray published three papers which described a constitutive model for smeared cracking nonlinear finite element analysis of reinforced concrete structures and they compared the results of their model with eleven beams and nine panels. After modification of layered shell element to more accurately model shear behaviour, Harmon and Zhangyuan (1989) compared the results of their model with two beams: one failing in flexure and the other beam without stirrups failing in shear, in addition to four plates and concrete shell. Recently, Vidosa, et al. (1991) introduced 3-D non-linear finite element model and studied its generality in three papers. They analysed eight structures: a beam and a shear wall both failing in flexure, two beams with and without shear reinforcement failing in shear, T-beam, two slabs exhibiting punching failure, and two prism under strip or patch loading. After development of the compression-field theory, Vecchio and Collins (1986) introduced the modified compression-field theory which was incorporated in nonlinear finite element program by Vecchio (1989). Vecchio predicted the ultimate loads for three different types of test specimens: panel, deep beam, and beam with shear reinforcement. Stevens, et al. (1991) incorporated the modified compression field theory in nonlinear finite element program (FIERCM) which was described by Vecchio (1989) as a more complex program and by simple program Vecchio obtained better results. Stevens, et al. demonstrated the power of their program by analysing a beam with shear reinforcement and a deep beam.

The above literature review shows that in most of the previous finite element modelling:

- only a few beams or a definite class of beams have been analysed,
- parametric studies have been done on only a few beams,

- the relationship between the ultimate load and the mode of failure has not been studied in most of the above investigations.

1.2 Purpose of study

Among the finite element models that have been developed to predict the behaviour of reinforced concrete structures are the simple model which neglects many factors including even the shear resistance of concrete after cracking and the sophisticated one which takes everything into account such as the bond slip between the concrete and reinforcement, softening of concrete in tension, and softening of concrete in compression. Also, material models for concrete and reinforcement are based on different theories e.g. nonlinear elasticity theory, plasticity theory, endochronic theory, or modified compression-field theory. They deal with concrete after cracking as a smeared model, discrete model, crack band model, or fracture mechanics model. The common aspect between these models, as mentioned above, is that all of them have used for the analysis only a small numbers of experimental tests which do not cover all the factors influencing the behaviour of reinforced concrete. In other words the generality of any one of these models has not been established and it is difficult to judge which model gives best predictions for any kind of structures.

The purpose of this study is to attempt to find out the features of a finite element model which is able to predict, with reasonable accuracy, the ultimate load and the mode of failure for a large number of beams which cover all factors influencing the behaviour of reinforced concrete beams. To determine this finite element model many parameters that affect the prediction should be studied. In this study some parameters which many think have a significant effect on the prediction will be studied.

These parameters are:

- (i) shear retention factor,

- (ii) tensile strength of concrete,
- (iii) magnitude of the strain corresponding to the peak stress in the stress-strain curve of concrete in compression,
- (iv) tension softening of concrete,
- (v) compression softening of concrete.

1.3 Organisation of the thesis.

Chapter 2 focuses on the shear in reinforced concrete, while Chapter 3 reviews the behaviour of material (steel and concrete) and numerical modelling.

In Chapter 4, the finite element method and numerical methods have been discussed. A comparison between the predictions of a 3-D finite element model and 2-D one has been made in Chapter 5. In Chapter 6 a parametric study of some factors affecting the prediction of shear strength has been done on rectangular beams with and without shear reinforcement.

In Chapter 7 about hundred and fifty rectangular beams with and without shear reinforcement have been analysed and some factors which affect on the prediction of reinforced concrete failing in shear have been studied. Prestressed concrete beams have been analysed in Chapter 8. The analysis of reinforced concrete Tee beams is presented in Chapter 9. The final conclusions and recommendations for future work are given in Chapter 10.

2.2 Definitions related to shear

In this section the definitions related to the shear in reinforced concrete beams used in this thesis are introduced.

CHAPTER 2

ON SHEAR IN REINFORCED CONCRETE

2.1 Introduction

The ACI-ASCE Committee 426 (1974) stated that despite the tremendous number of references on the prediction of the strengths of reinforced concrete members subjected to shear forces, the question of shear strength is far from settled. This is because of the complexities involved in formulating rational analytical solutions. Shear failure due to web crushing, which is likely to occur in a thin-webbed I-beam, does not seem to be open to any precise mathematical treatment (Kar 1969). Chana (1987) reported that a theoretical analysis of splitting failures is difficult owing to the complex nature of stress conditions present in the dowel splitting region. As a result of this, he concluded that shear design methods for members without web reinforcement are likely to remain empirical in basis. At present, although there is no final solution of the problem, considerable progress has been achieved towards the solution of the problem.

In this chapter, a brief review of basic facts about mechanisms of shear resistance, modes of failure, and theories of analysis of shear in reinforced concrete beams are given.

2.2 Definitions related to shear

In this section the definitions related to the shear in reinforced concrete beams used in this thesis are introduced.

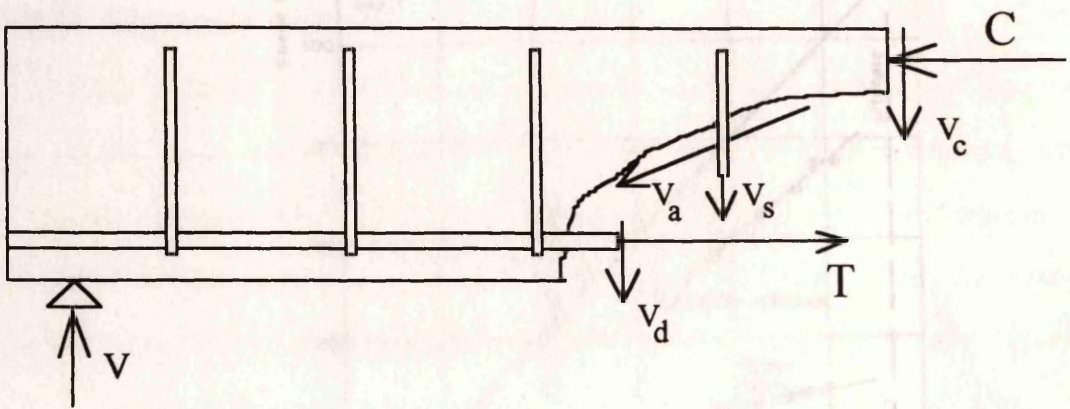
- **Shear stress:** is the average shear force per unit area resisting this shear force.
- **Shear strength:** is the maximum shear force that the beam can carry.
- **Shear transfer:** is the transmission of the force by shear from one plane to another.
- **Shear span:** is the length of the beams subjected to uniform shear force. It is denoted by a
- **a/d ratio:** The ratio a/d takes into account the ratio between the bending moment M and shear force V occurring simultaneously at the same cross section ($a/d = M/(Vd)$). This is in a beam loaded by two concentrated loads at equal distances from the supports.
- **Flexural crack:** is a nearly vertical crack formed at the middle of the beam starting from the tension face due to bending of the beam.
- **Shear crack:** There are two types of shear cracks which may develop in reinforced concrete beams. These types are the flexure-shear and web-shear cracks.
- **Flexure-shear crack:** is an inclined crack originating from the top of a previously existing flexural crack.
- **Web-shear crack:** is an inclined crack forming in a beam without flexural crack in its vicinity. This kind of shear cracking is more likely to occur in tee and thin-webbed beams.
- **Aggregate interlock action:** is due to the interlocking of the irregular concrete surfaces on each side of the crack. It provides a resisting force similar to a frictional force.
- **Dowel action:** is the resistance to shear across a crack provided by the longitudinal reinforcing bars.
- **Shear retention factor (β):** is the ratio of the residual shear modulus of concrete after cracking G_{cr} to the shear modulus before cracking G_o ($\beta = \frac{G_{cr}}{G_o}$).

2.3 Mechanisms of shear transfer

As defined before, shear transfer means transmission of the force by shear from one plane to another. This transmission may occur in various ways in reinforced concrete members. Shear stress in concrete, aggregate interlock, dowel action, arch action, and web reinforcement are the main types of shear transfer (Fig.2.1). The relative contribution of these components vary considerably as the applied load is increased. In beams without web reinforcement, after cracking the shear resistance is distributed approximately in the following proportions (Houde and Mirza 1974; Taylor 1974):

	Houde and Mirza (1974)	Taylor (1974)
Aggregate interlock	50%	33 - 50%
Compression zone	30%	20 - 40%
Dowel action	20%	15 - 25%

Fig. 2.2 illustrates the distribution of shear forces in a typical beam tested by Taylor (1974). Shear stresses were measured on the two lines marked 1 and 2 (Fig. 2.2a). These lines were located at the head of major cracks on the beam across which displacements had been measured in the test. The line on the Fig. 2.2b at 45° is the line that should be achieved if the three components (dowel, aggregate interlock, and compression zone shear forces) added up to the full imposed shear force. This did not happen probably due to slight under-estimation of dowel and aggregate interlock forces in the experiment because the movement of the crack before the instrumentation was applied could not be measured. The figure shows that up to the point of cracking, the beam behaves elastically and the shear force is distributed through the concrete. After cracking, as the applied shear force increases, the rate of increase of the shear force carried by aggregate interlock becomes more than that of the shear forces carried by both dowel action and compression zone.



V_c = shear carried by concrete in compression zone

V_s = shear carried by stirrups

V_a = shear carried by aggregate interlock

V_d = shear carried by dowel action

V = total shear force

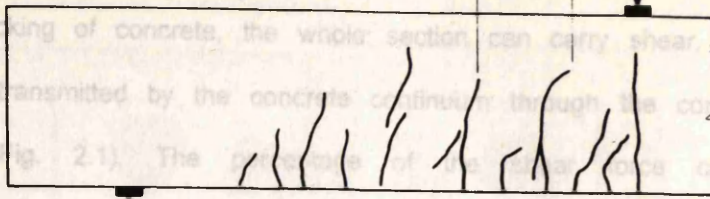
T = tensile force in bar

C = compressive force in concrete

Fig. 2.1 Forces acting at inclined crack for beams with web reinforcement.

2.3.1 Shear transfer by shear stress in concrete

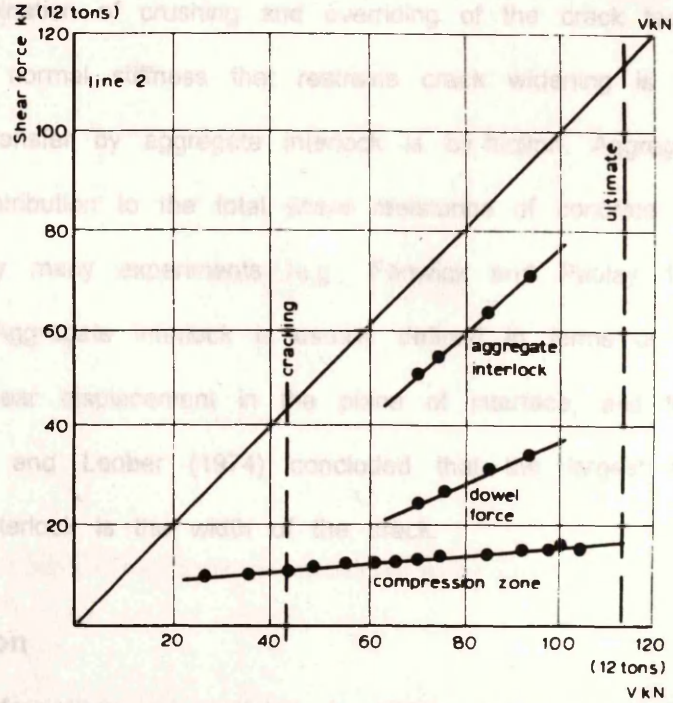
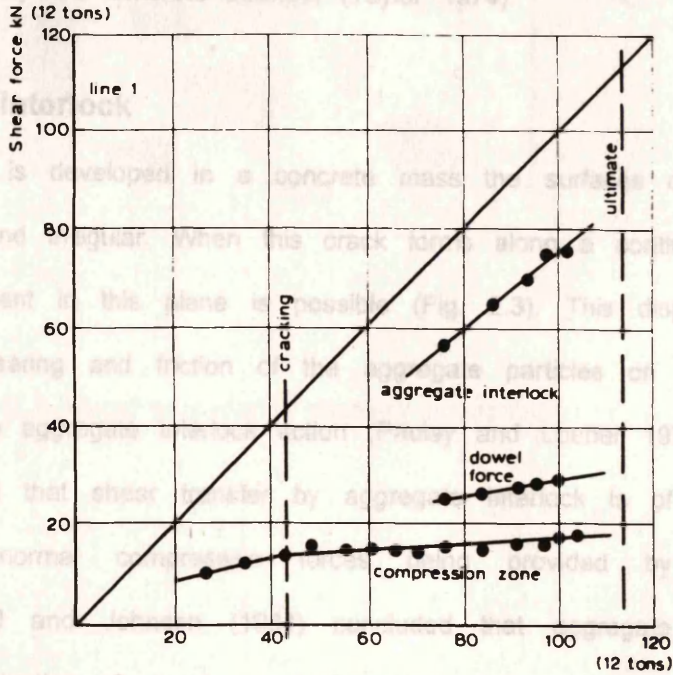
Before cracking of concrete, the whole section can carry shear. After cracking, shear can be transmitted by the concrete continuously through the compression zone only (V_c in Fig. 2.1). The compression zone is influenced by the size of the zone and its ultimate shear capacity is affected by the concrete strength (Taylor 1974).



(a)

2.3.2 Aggregate interlock

When a crack is developed in a concrete mass, the surface of the crack are usually rough and irregular. When this crack forms a continuous plane, a parallel displacement in this plane is possible (Fig. 2.3). This displacement is restricted by the bearing and friction of the aggregate particles of the cracked surface which is the aggregate interlock (Taylor 1974). Dwyer et al. (1987) stated that shear transfer by aggregate interlock is a function of the nature with the normal stress. The shear transfer is provided by embedded reinforcement. Millard and Taylor (1974) studied the aggregate interlock mechanism results from a compression zone overlying of the crack and can be predicted if the residual crack width is known. This means that shear transfer by aggregate interlock is a function of the crack width. It has a significant contributor to the total shear resistance if the concrete has been proved by many experiments (e.g. Taylor and Loaber 1974, 1978, 1984, and Loaber 1974). Aggregate interlock is a function of the average shear stress, the shear displacement in the plane of the crack, and the angle of the crack. Taylor and Loaber (1974) concluded that the shear transfer factor affecting aggregate interlock is a function of the average shear stress.



(b)

2.3.3. Dowel action

Siding shear deformations are resisted, in addition to aggregate interlock, by dowel action. Dowel action is the resistance to shear transfer provided by the reinforcement bars crossing the crack. Dowel action is a function of the shear stress, the shear displacement in the plane of the crack, and the angle of the crack. Taylor and Loaber (1974) concluded that the shear transfer factor affecting aggregate interlock is a function of the average shear stress.

Fig. 2.2 Distribution of shear force in beam without web reinforcement.

2.3.1 Shear transfer by shear stress in concrete

Before cracking of concrete, the whole section can carry shear. After cracking, shear can be transmitted by the concrete continuum through the compression zone only (V_c in Fig. 2.1). The percentage of the shear force carried by the compression zone is influenced by the size of the zone and its ultimate shear capacity is affected by the concrete strength (Taylor 1974).

2.3.2 Aggregate interlock

When a crack is developed in a concrete mass the surfaces of the crack are usually rough and irregular. When this crack forms along a continuous plane, a parallel displacement in this plane is possible (Fig. 2.3). This displacement is restricted by the bearing and friction of the aggregate particles on the cracked surface which is the aggregate interlock action (Paulay and Loeber 1974). Divakar, et al. (1987) stated that shear transfer by aggregate interlock is of a frictional nature with the normal compressive forces being provided by embedded reinforcement. Millard and Johnson (1984) concluded that aggregate mechanism results from a combination of crushing and overriding of the crack faces and can be predicted if the normal stiffness that restrains crack widening is known. This means that shear transfer by aggregate interlock is by friction. Aggregate interlock has a significant contribution to the total shear resistance of concrete beams. This has been proved by many experiments (e.g., Fenwick and Paulay 1968; Paulay and Loeber 1974). Aggregate interlock is usually defined in terms of the average shear stress, the shear displacement in the plane of interface, and the width of the crack. Paulay and Loeber (1974) concluded that the largest single factor affecting aggregate interlock is the width of the crack.

Fig. 2.4 Interactive effect between concrete and reinforcement: Dowel effect.

2.3.3. Dowel action

Sliding shear deformations are resisted, in addition to aggregate interlock, by dowel action of the reinforcing bars (Fig. 2.4). When aggregate interlock



Fig. 2.3 Shear transfer by aggregate interlock.

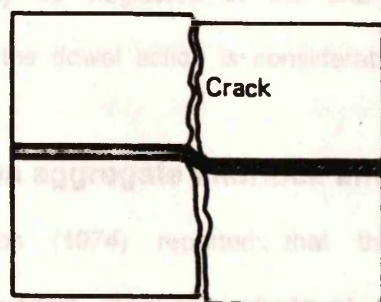


Fig. 2.4 Interactive effect between concrete and reinforcement: Dowel effect.

diminishes with a large crack opening, dowel bars play a major role in preventing sliding shear failure. Soroushian, et al. (1986) concluded that the main factor influencing the dowel behaviour is the diameter of the bar. Axial load in the dowel bar can also have an important effect if it approaches the axial yield strength (Soroushian, et al. 1986). Other factors that influence dowel behaviour include the steel and concrete strengths as well as the inclination of the dowel bar and the concrete cover.

Hofbeck, et al. (1969) concluded that dowel action of reinforcing bars crossing the shear plane is insignificant in initially uncracked concrete, but is substantial in concrete with a pre-existing crack along the shear plane.

The amount of vertical shear resisted by the longitudinal reinforcement is limited by the tensile strength of the concrete beam at the level of the steel; an amount in excess of this limiting value causes splitting of the beam along the reinforcement. As the tensile strength of concrete is low and the vertical tensile stresses are concentrated near the plane of the diagonal tension crack, usually the contribution of the longitudinal reinforcement to transfer of shear cannot be large. Due to this Ruble, et al. (1955) stated that ordinary shear resistance of the longitudinal reinforcement may be neglected in the analysis. However if the bars are well supported by links, then the dowel action is considerably enhanced.

2.3.4 Interaction between aggregate interlock and dowel action

Swamy and Andriopoulos (1974) reported that there is an interaction or interdependence between aggregate interlock and dowel action and it is difficult to separate the effects of one from the other. The relative shear contributions of aggregate interlock and dowel action and their combined contribution will depend primarily on the development of the diagonal crack both in the web and at the level of the tension steel, and hence on the amount of tension steel, the moment-shear ratio, the amount and position of web reinforcement, and concrete strength. Swamy and Andriopoulos said "*the hazards and limitations of trying to*

separate the effects of aggregate interlock and dowel action are far too obvious".

More experimental study is required of both the aggregate interlock and dowel action mechanisms before their combined action in reinforced concrete can be predicted with confidence (Millard and Johnson 1984).

2.3.5 Arch action

Beams may be visualised as composed of two parts: an arch portion, above, and a beam portion, below the diagonal crack. When there is no web reinforcement the arch acts as if there is a hinge under the applied load (Fig. 2.5), because of the relatively small zone of concrete remaining intact. The negative bending moment along the arch produced by this action reduces the compressive stress at the top fibre. When the web reinforcement is added, the stirrups forces represent a distributed load along the arch, which tends to cause a larger compressive stress at the top fibre (Scordelis, et al. 1974). For arch action to develop, a horizontal reaction component is required at the base of the arch. In beams, this is usually provided by the tie of the longitudinal bars. Frequently deep beams fail due to a failure of the anchorage of the bars. In beams, arch action occurs not only outside the outermost cracks but also between diagonal tension cracks. Web reinforcement produces an additional arch support (Fig. 2.6). The location of the stirrups is very important. It was found (Kani 1969) that stirrups close to the base of diagonal cracks can provide support to the arches.

2.3.6 Web reinforcement

The stirrups remain practically unstressed until diagonal tension cracking occurs; afterward the stirrup strains increase rapidly. Stirrups reduce the maximum principal concrete stresses in the vicinity of the diagonal crack and thus inhibit the growth of these cracks (Scordelis, et al. 1974).

Fig. 2.6 Arch supports provided by three main types of web reinforcement.

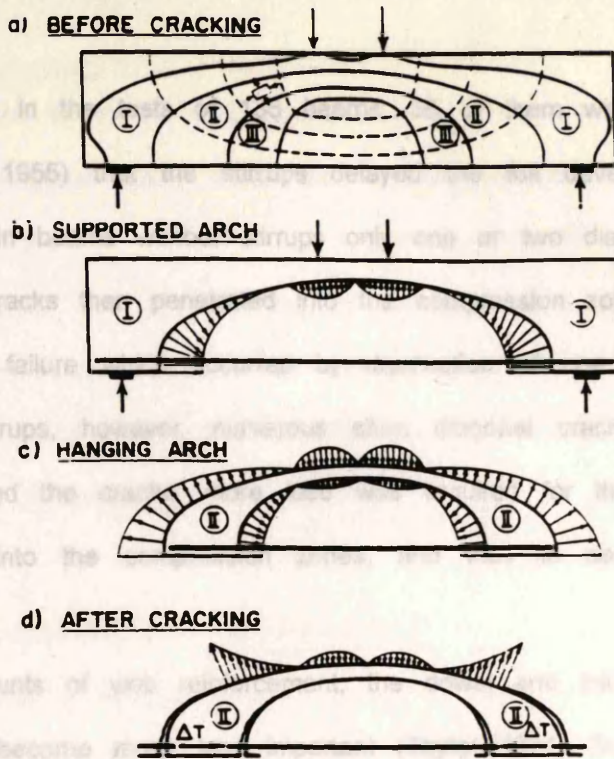


Fig. 2.5 Arch analogy for reinforced concrete beam without web reinforcement.

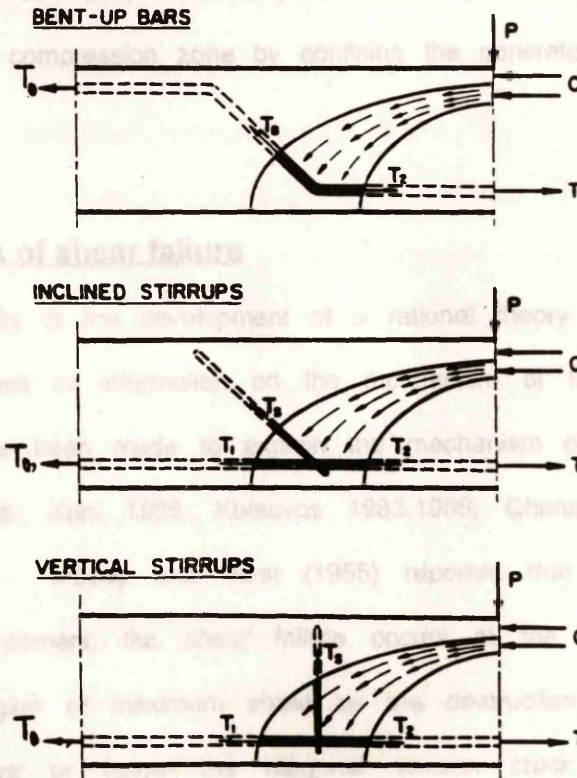


Fig. 2.6 Arch supports provided by three conventional types of web reinforcement.

It was observed in the tests of 136 beams, 35 of them with web reinforcement (Moody, et al. 1955) that the stirrups delayed the full development of diagonal tension cracks. In beams without stirrups only one or two diagonal tension cracks formed; these cracks then penetrated into the compression zones of concrete and precipitated the failure which occurred by destruction of one of these zones. In beams with stirrups, however, numerous short diagonal cracks formed since the stirrups distributed the cracks; more load was required for the cracks to develop and penetrate into the compression zones, and thus to cause crushing of the concrete.

With large amounts of web reinforcement, the dowel and interlock contributions to shear capacity become much less important (Taylor 1974; Scordelis, et al. 1974). This means that not only stirrups carry shear themselves but also they limit the maximum dowel shear and thus reduce the tendency for horizontal splitting. Moreover, stirrups may transfer a small force across the crack by dowel action (see e.g., Ruble, et al. 1955) due to possible kinking and they tend to enhance the strength of the compression zone by confining the concrete.

2.4 Mechanisms of shear failure

A major difficulty in the development of a rational theory for shear design is identified as the lack of information on the mechanism of failure (Chana 1988). Many attempts have been made to explain the mechanism of shear failure (e.g., Moody, et al. 1955; Kani 1966; Kotsovos 1983,1986; Chana 1987; and Bazant and Kazemi 1991). Moody and Viest (1955) reported that for beams with or without web reinforcement, the shear failure occurs at the section of maximum moment in the region of maximum shear by the destruction of the compression zone directly above or below the diagonal tension crack. Kotsovos (1983) concluded that there is no single cause of diagonal failure and it is not

considered realistic to expect that theories based on the assumption of a unique mechanism of diagonal failure could lead to safe design procedures. For beams with a/d smaller than 2.5 subjected to two point load, Kotsovos (1984) reported that their failure is due to branching of diagonal crack within the shear span toward the compressive zone of the middle span (Fig. 2.7) and not due to crushing of the compressive region of the loading point as for beams with a/d greater than 2.5 (Kotsovos 1986).

2.4.1 Beams without web reinforcement

Shear failures of beams without web reinforcement are brittle in nature and, hence, there is little information on beam displacements approaching failure, and during the immediate post-peak or failing branch phase (Chana 1987). Chana (1988) concluded that shear failures of beams without web reinforcement are initiated by dowel splitting. The dowel action of the main reinforcement causes splitting of the concrete along the steel. As the dowel force is lost, shear force is transferred and the diagonal crack extends into the compression zone, which fails on account of excessive principal tensile stress. Taylor (1974) also concluded that the sequence of failure is initiated by dowel cracking. The aggregate interlock is the next to fail, causing an abrupt and sometimes explosive failure of the compression zone. It can be understood from these conclusions that the failure is initiated by dowel action but is completed by failing or crushing of the compression zone. In other words, the magnitude of the failure load depends on the resistance of the compression zones at the end of the diagonal tension crack.

2.4.2 Beams with web reinforcement

The presence of web reinforcement has no important effect on the behaviour of beams prior to the formation of initial diagonal tension cracks. The strains in the stirrups are practically zero and the load deflection curve for a beam without

web reinforcement is the same for a typical beam with web reinforcement (Moody, et al. 1964). After the formation of a diagonal crack, the interaction between the web reinforcement and the crack provides additional shear strength beyond that of a beam without web reinforcement.

2.5. Factors affecting the shear strength

The factors influencing the shear strength of reinforced concrete beams failing in shear are numerous and complex (Bresler and Mau, 1987). They include: the proportions and shape of the beam, the structural restraints and the interaction of the beam with other components in the system, the amount and arrangement of tensile, compressive, and transverse reinforcement, the degree of prestress, the load distribution and loading history, the properties of the concrete and steel, the concrete placement and curing, and the environmental history.

(a) Generally accepted

These factors may be classified to four groups: reinforcement details, concrete properties, beam dimensions, and other factors, e.g. type of loading and degree of prestress.

2.5.1 Reinforcement details

Longitudinal reinforcement

Percentage of tensile steel $\rho = \frac{A_s}{bd}$, A_s - cross-sectional area of tensile steel

b = beam width, and d = effective depth. It is a significant parameter affecting the shear strength of reinforced concrete beams (Kari, 1980; Taylor, 1976; Ghossein, et al. Andriopoulos 1974; Elzanaty, et al. 1966a). As ρ increases the diagonal cracks become narrower and shorter. Therefore the shear strength increases with an increase of ρ .

Fig. 2.7 Cause of failure for beams with a/d smaller than 2.5.

In the Canadian code, the longitudinal reinforcement is assumed to resist, in addition to the bending moment at the midspan section, an equivalent axial tension caused by shear (Collins and Mitchell 1988, see Sec. 2.7.4.2).

web reinforcement is the same for a typical beam with web reinforcement (Moody, et al. 1954). After the formation of a diagonal crack, the interaction between the web reinforcement and the crack provides additional shear strength beyond that of a beam without web reinforcement.

2.5. Factors affecting the shear strength

The factors influencing behaviour and strength of reinforced concrete beams failing in shear are numerous and complex (Bresler and MacGregor 1967). They include: the proportions and shape of the beam, the structural restraints and the interaction of the beam with other components in the system, the amount and arrangement of tensile, compressive, and transverse reinforcement, the degree of prestress, the load distribution and loading history, the properties of the concrete and steel, the concrete placement and curing, and the environmental history.

These factors may be classified to four groups; reinforcement details, concrete properties, beam dimensions, and other factors, e.g. type of loading and degree of prestress.

2.5.1 Reinforcement details

Longitudinal reinforcement:

Percentage of tensile steel ρ ($=\frac{A_s}{bd}$; A_s =cross-sectional area of tensile steel,

b = beam width, and d = effective depth) is a significant parameter affecting the shear strength of reinforced concrete beams (Kani 1966; Taylor 1974; Swamy and Andriopoulos 1974; Elzanaty, et al. 1986a). As ρ increases the flexural cracks become narrower and shorter. Therefore, the shear strength increases due to an increase of both dowel action and aggregate interlock contributions.

In the Canadian code, the longitudinal reinforcement is designed to resist, in addition to the bending moment at the midspan section, an equivalent axial tension caused by shear (Collins and Mitchell 1986, see Sec. 2.7.4.2). Kani 1966

Web reinforcement:

Beams with web reinforcement fail at higher loads and are capable of developing substantially higher deflections, thus exhibiting greater ductility (Bresler and Scordelis 1963). The stirrups not only carry shear themselves but also enhance the strength of other shear transfer mechanisms. The functions of the web reinforcement may be summarised as follows:

- Carrying a part of the additional shear after diagonal tension cracking (some Codes assume that the additional shear is resisted by stirrups only).
- Increase the strength of the dowel action. The stirrups provide support for the longitudinal steel and prevent the bars from splitting from the surrounding concrete.
- Increase both the shear carried by aggregate interlock and shear strength of the uncracked compression zone. The stirrups help to contain the crack, limiting its propagation and keeping its width small.
- Stirrups also increase the strength of concrete in compression by providing confinement.
- They may transfer a small force across the crack by dowel action.

Compression reinforcement:

Moody and Viest (1955) reported that if the shear failure is caused by the destruction of the compression zone of concrete at the end of diagonal crack, compression reinforcement located in this compression zone will increase shear strength by preventing failure of concrete.

2.5.2 Concrete properties**Concrete strength:**

Some investigators concluded that concrete compressive strength (from about 17.0 to 34.0 MPa) has little or no effect on the shear strength (e.g., Kani 1966;

2.5.3 Beam dimensions

Taylor 1974). But some investigators concluded that it has effect on shear strength. Iyengar and Rangan (1966), based on tests by Moody et al. (1954), concluded that concrete strength (from about 14.0 to 41.0 MPa) has a definite influence on the shear strength of beam in medium and higher ranges of a/d (i.e. $a/d > 2.0$). Clark (1951) reported that the shear capacity of a beam increases with the strength of concrete (from about 14.0 to 41.0 MPa) when the other factors are the same (a/d was small, from 1.17 to 2.43).

After using the high-strength concrete (up to about 83.0 MPa), Elzanaty, et al. (1986a) found that the shear strength of beams with or without web reinforcement increased with the increase of concrete strength. Mphonde and Frantz (1984) concluded that the effect of concrete strength (from 21.0 to 103.0 MPa) on shear capacity becomes more significant as the a/d ratio decreases. Also, failures become more sudden and explosive as the compressive strength increases, especially at lower a/d values.

Aggregate type:

In lightweight concrete, the actual performance in shear depends on the aggregate type (Taylor 1974). With some aggregates, the crack goes right through the aggregate and low shear strengths are obtained. In other cases, a rough cracked surface is obtained and shear test results much closer to those from dense concrete are obtained. Akhtaruzzaman and Abul Hasnat (1986) found that the shear strength of brick-aggregate concrete beams without web reinforcement is higher than that of normal weight concrete beams. The percentage of increase depends on concrete strength and a/d ratio. They reported that this increase in the shear strength of brick-aggregate concrete beams is due to its higher tensile strength.

2.5.3 Beam dimensions

***a/d* ratio:**

The ratio a/d takes into account the ratio between the bending moment M and shear force V occurring simultaneously at the same cross section ($a/d = M/(Vd)$). It is now well established that a/d ratio is one of the most important, if not the only important factor influencing the shear strength of reinforced concrete beams.

Many investigators (e.g., Mphonde and Frantz 1984) found that there is much more scatter in the ultimate shear strengths as a/d ratio decreases due to the possible variation of failure modes. Mphonde and Frantz (1984) found that at a/d ratio of 1.5 (with other properties remaining constant) failure was either by crushing of the arch rib and the beam attained high capacity or by extension of the inclined crack through to the top surface and the beam failed at lower capacity.

An increase in a/d ratio causes a decrease in shear strength. This is because flexural cracks in beams with high a/d ratios will be well developed, decreasing interlock capacity (Taylor 1974).

The mode of diagonal failure has been found by many investigators to be primarily dependent upon a/d ratio (Kani 1964, 1966). Kotsovos (1983) classified the mode of failure according a/d ratio to four types as shown in Fig. 2.8.

Depth of the beam:

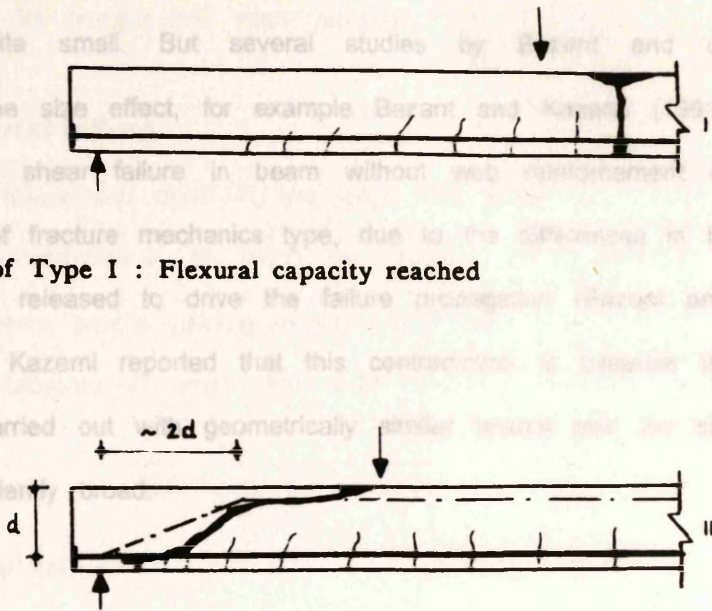
Ahmed, et al. (1986) observed that the shear capacity of beam decreases with increased depth for a constant a/d ratio.

Size effect:

The size effect is defined by comparing geometrically similar specimens or structures of different sizes. When these specimens or structures fail at the same nominal stress, this means there is no size effect.

Tests on four beams, each beam is a scale model of the other three, by Ivey and Buth (1967) indicated that if the effect of beam size is present, it is probably quite small. But several studies by Bazant and co-workers have addressed the size effect, for example Bazant and Kazemi (1991) concluded that the diagonal shear failure in beam without web reinforcement exhibits a strong size effect of fracture mechanics type, due to the differences in the stored energy that can be released to drive the failure propagation (Bazant and Kazemi 1991). Bazant and Kazemi reported that this contradiction of behaviour in the previous tests were not carried out with geometrically similar beams over the size range tested

Failure of Type I : Flexural capacity reached

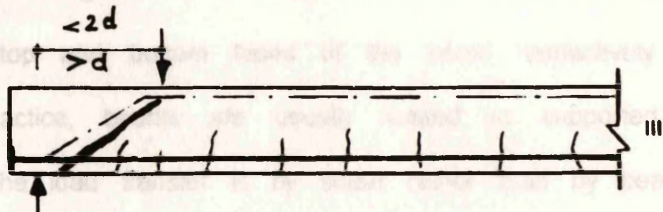


2.2 Failure of Type II: Flexural capacity not reached

Type of loading:

(1) *Indirect loading*: In most tests, all loads are applied to the top surface of the beam (usually directly under beams). In practice, all loads should be applied to the top and bottom surfaces (indirect loading). Indirectly loaded beams are weaker than directly loaded beams. Tests and Neville (1970), Clark (1951) reported that the important factor that affects the shear capacity of a beam

Failure of Type III: Flexural capacity not reached



Failure of Type IV: Flexural capacity reached

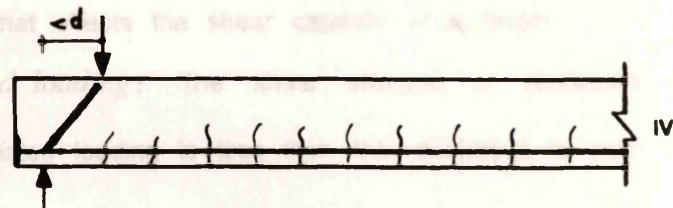


Fig. 2.8 Types of behaviour exhibited by beams without web reinforcement subjected to two-point loading.

2.6 Types of failures

Tests on four beams, each beam is a scale model of the other three, by Ivey and Buth (1967) indicated that if the effect of beam size is present, it is probably quite small. But several studies by Bazant and co-workers have addressed the size effect, for example Bazant and Kazemi (1991) concluded that the diagonal shear failure in beam without web reinforcement exhibits a strong size effect of fracture mechanics type, due to the differences in the stored energy that can be released to drive the failure propagation (Bazant and Kazemi 1991). Bazant and Kazemi reported that this contradiction is because the previous tests were not carried out with geometrically similar beams and the size ranges tested were insufficiently broad.

2.6.2 Shear failure

2.5.4 Other factors

Type of loading:

(1) *Indirect loading*: In most tests on beams, the loads and reactions are applied on the top and bottom faces of the beam respectively (directly loaded beams). In practice, beams are usually loaded or supported by intersecting beams so that the load transfer is by shear rather than by bearing on the top and bottom surfaces (indirectly loaded beams). For a/d ratio less than 2.5, indirectly loaded beams are weaker than directly loaded beams (Ferguson 1956; Taub and Neville 1970). Clark (1951) reported that the loading condition is an important factor that affects the shear capacity of a beam.

(2) *Repeated loading*: The shear strength of reinforced concrete beams subjected to repeated loading is less than that subjected to static loading.

Degree of prestress:

The shear strength is strongly affected by the prestress force (Cederwall, et al. 1974). An increase in prestress in the prestressed concrete beams increase the strength in shear (Zwoyer and Siess 1954).

2.6 Types of failures

In considering the mode of failure of reinforced concrete beam, one has to consider both its flexural and shear capacity.

2.6.1 Flexural failure

Flexural failure can occur in two ways (Fig. 2.9):

- (1) flexure compression, in which the crushing of concrete in the compression zone occurs before yielding of the main steel.
- (2) flexure tension, in which the main reason for failure is yielding of main steel.

2.6.2 Shear failure

Many types of shear failure have been reported in the literature. Some of these types have clear definition while the others are difficult to identify clearly. Some of these types of failure are described below (Fig. 2.9):

- (1) **Shear-compression failure:** A beam is said to fail in shear-compression when the concrete crushes under compressive stress above an inclined crack which has formed in the shear span and which itself extends to or from the level of the horizontal tensile reinforcement (Evans and Schumacher 1963). In this mode of shear failure, the concrete compression zone is either crushed or ruptured along the diagonal crack (Kar 1969). Shear compression failure is the most frequently observed mode of shear failure especially in prestressed concrete beams.

A closely related mode of failure is:

DT-C failure: A crushing disintegration failure above or at the end of a horizontal crack in the compression zone (Krefeld and Thurston 1966b).

- (2) **Shear-proper failure:** Failure defined as shear proper generally takes place by shearing off of the compression zone of the concrete along the line of

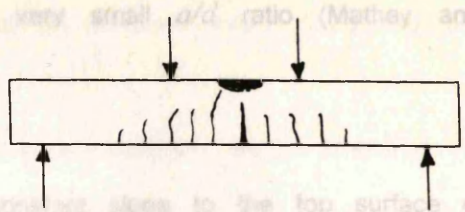
Fig. 2.9 Different types of failures.

the diagonal tension crack in beams having very small a/d ratio (Mathay and

- **Flexure** —
 ↗ Compression
 ↘ Tension

A closely related mode of failure is

DT failure: A diagonal crack at nearly 45° slope to the top surface of the beam (Krefeld and Thurston 1966b).



(3) Diagonal-tension failure: The failure occurs as a result of the longitudinal splitting in the compression zone near the load and by horizontal splitting along the tensile reinforcement.

- **Shear-Compression, DT-C**

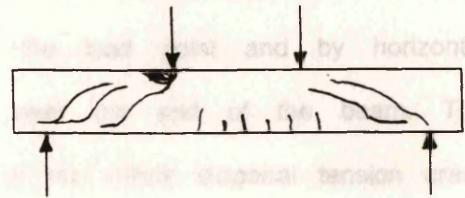
The failure occurs shortly after the formation of a diagonal tension crack (Bresler and Scordelis 1963).

A closely related mode of failure is

DT-R failure: A failure associated with diagonal cracks in adjacent segments at the end of the horizontal chord. A diagonal tension crack in the compression zone, which has developed in the previous segment, may

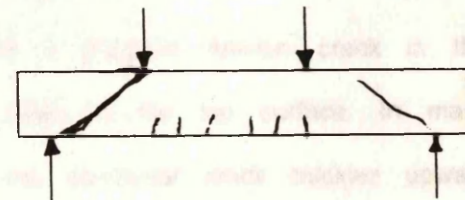
- **Shear-Propagated, DT**

cases a thin layer of concrete above the diagonal crack thickens upward (Krefeld and Thurston 1966b).



(4) DT-S failure: A sliding type of failure along a diagonal chord, or at the end of a horizontal chord at the compression zone (Krefeld and Thurston 1966b).

- **Diagonal-Tension, DT-R**



2.7 Methods of analysis

For all beams falling in either of the above categories, the behaviour of the beam is governed by the shear stress distribution (Moody 1893).

- **DT-S**

None of the shear stress theories is sufficiently general to describe the behaviour of beams. It is difficult to generalise about the nature of shear stress distribution (1937).

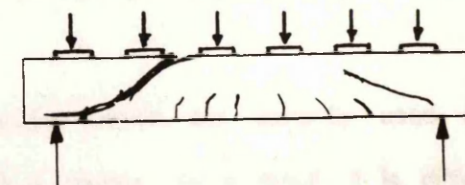
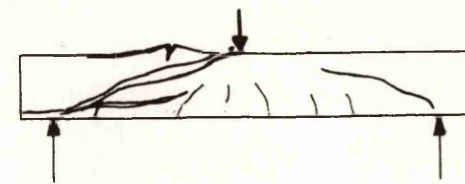


Fig. 2.9 Different types of failures.

the diagonal tension crack in beams having very small a/d ratio (Mathey and Watstein 1963).

A closely related mode of failure is:

DT failure: A diagonal crack at nearly constant slope to the top surface of the beam (Krefeld and Thurston 1966b).

- (3) Diagonal-tension failure: The failure occurs as a result of the longitudinal splitting in the compression zone near the load point and by horizontal splitting along the tensile reinforcement near the end of the beam. The failure occurs shortly after the formation of the critical diagonal tension crack (Bresler and Scordelis 1963).

A closely related mode of failure is:

DT-R failure: A failure associated with relative rotation of adjacent segments at the end of the horizontal portion of a diagonal tension crack in the compression zone which has extended close to the top surface. In many cases a thin layer of concrete above the horizontal crack buckles upward (Krefeld and Thurston 1966b).

- (4) DT-S failure: A sliding type of failure along a diagonal plane above or at the end of a horizontal crack in the compression zone (Krefeld and Thurston 1966b).

2.7 Methods of analysis of shear failure

For all beams failing in shear, up to the formation of diagonal tension cracks the behaviour of all beams is the same as that of beams failing in flexure (Moody, et al. 1955).

None of the shear failure theories or analogies which are currently used are sufficiently general to consider all possible failure modes. As a result, it is difficult to generalise about the nature of shear failures (Bresler and MacGregor 1967).

Beams can fail in combined bending and shear in different ways, depending on the geometry and properties of the beams.

In the past there were two basic approaches to analyse shear problems in reinforced concrete: (1) arch, frame, and truss analogies, and (2) limit analysis mechanisms. The mechanism method cannot satisfy the compatibility condition, unless the concrete and steel are assumed to have infinite plasticity (Mau and Hsu 1990). Arch, frame, and truss models represent behaviour of reinforced concrete beams subjected to flexure and shear. It is generally agreed by researchers in recent years that the truss model theory provides a more promising way to handle shear failure mechanisms.

In this section a brief review of the arch, frame, and truss models is introduced with emphasis on truss models.

2.7.1 Beams without web reinforcement

Various theoretical approaches have been suggested for the behaviour of beams without web reinforcement under action of shear forces. Some of these approaches are briefly reviewed in this section.

2.7.1.1 Analytical shear compression theories:

These theories consider the load carrying capacity of concrete in its compression zone due to shear (e.g., Bresler and Pister 1958; Ojha 1967). The forces acting on the free body above the shear crack are shown in Fig. 2.10. In this approach any forces transfer across the inclined crack by dowel action or aggregate interlock action is ignored. The external load is supported by an inclined thrust in the concrete above the crack and the horizontal component of the thrust at the support is resisted by tension steel acting as a tie (Fig. 2.10).

These theories are now only of historical interest. They represent the first serious attempts to analyse the shear capacity of beams without stirrups. However, it should be noted that these theories are unrealistic, in that they ignore any shear

force transfer across the diagonal crack. Acharya and Kemp (1965) showed by means of a series of careful experiments that this assumption leads to unacceptably high stress in the concrete at the tip of the diagonal crack.

2.7.1.2

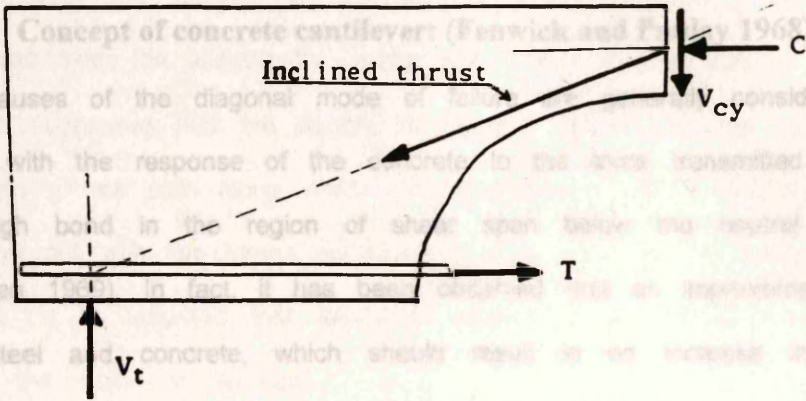
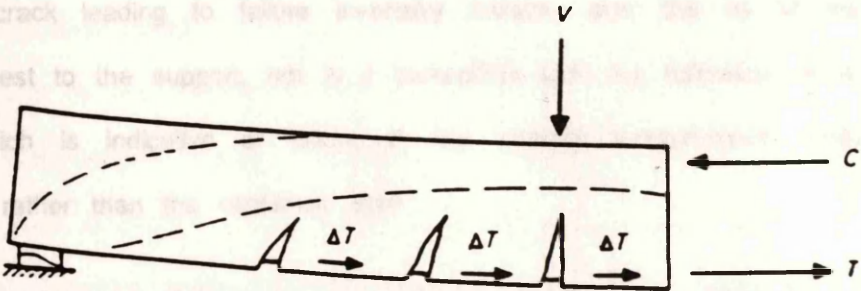


Fig. 2.10 Forces acting on free body above shear (ignored are: dowel and aggregate interlock).

Fig. 2.11.

Kotsovos stated that in spite of a number of relative disadvantages of the shear conditions of a concrete cantilever, the shear stress distribution along the diagonal crack leading to failure is probably similar to that of the concrete crack closest to the supports, with a maximum shear stress at a diagonal crack, which is inclined at an angle to the horizontal. The shear stress distribution in a concrete cantilever is shown in Fig. 2.11.



2.7.1.3

Concept of the concrete cantilever (Lefas 1990).

Fig. 2.11 Concrete cantilevers.

The concept of the concrete cantilever is based on the assumption that load-carrying capacity is a result of resistance of a length of concrete in the region of the shear stress distribution. The middle of the cross section is transmitted to the wall, and a compressive force may be visualized as a flow of longitudinal stresses, with varying sections perpendicular to the path direction and with the compressive force representing the

force transfer across the diagonal crack. Acharya and Kemp (1965) showed by means of a series of careful experiments that this assumption leads to unacceptably high stress in the concrete at the tip of the diagonal crack.

2.7.1.2 Concept of concrete cantilever: (Fenwick and Paulay 1968)

The causes of the diagonal mode of failure are generally considered to be associated with the response of the concrete to the force transmitted to it from steel through bond in the region of shear span below the neutral axis (Kani 1964; Regan 1969). In fact, it has been observed that an improvement of bond between steel and concrete, which should result in an increase in the force transmitted to the concrete, leads to a significant reduction of the load sufficient to cause diagonal failure (Fenwick and Paulay 1968). It has been suggested that, under the action of the bond forces, concrete between consecutive flexural cracks reacts as a cantilever fixed to the compression zone of the beam (Kani 1964), Fig. 2.11.

Kotsovos stated that in spite of a number of detailed investigations of the stress conditions of a concrete cantilever, the above assumption neither explains why the diagonal crack leading to failure invariably initiates near the tip of the flexural crack closest to the support, nor is it compatible with the formation of a diagonal crack, which is indicative of failure of the support (compressive zone) of the cantilever rather than the cantilever itself.

2.7.1.3 Concept of the compressive force path: (Kotsovos 1983; Kotsovos and Lefas 1990)

The concept of the compressive force path is related to arch action and assumes that load-carrying capacity of a beam is associated with the strength of concrete in the region of the path along which compressive force of the middle cross section is transmitted to the supports. The path of a compressive force may be visualized as a flow of compressive stresses, with varying sections perpendicular to the path direction and with the compressive force representing the

stress resultant at each section (Fig. 2.12). It is assumed that the shape of the path is a bilinear. The junction between the two parts of this bilinear path occurs at a distance which depends on the a/d ratio. It is approximately equal to the shear span from the support for beams with $a/d < 2$ and twice the beam effective depth from the support for beams with $a/d > 2$ (Fig. 2.8).

It has been suggested that the causes of diagonal failure are very closely related to the shape of the path along which the compressive force is transmitted to the supports and not with the stress conditions in the region of the beam below the neutral axis. It is assumed that failure is related to the development of tensile stresses in the region of the path.

On the basis of the concept of the compressive force path, it has also been found that collapse of beams never occurs after the compressive strength of concrete is exceeded, and that even in the compressive zone where concrete fails under combined compressive and tensile stresses, failure occurs by splitting of the compressive zone connecting the point where the load is applied to the supports rather than by crushing of the loading point region (Fig. 2.13).

2.7.2 Arch analogies

The aims of arch analogies were to reduce the complexity and indeterminacy of the actual cracked beams. Observation of crack patterns in different beams suggested such analogies. For example, in a beam cracked as shown in Fig. 2.5 an element between adjacent cracks can be isolated and considered as a tied arch freebody. The dowel action in the longitudinal reinforcement is neglected. The transverse shear is carried by stress components along the arbitrary arch boundaries in the uncracked parts of the beam. The arch ribs are capable of supporting transverse loads only as long as they act essentially in compression, not in bending. Without transverse reinforcement only short deep beams can develop tied-arch action. As the length of the span increases, bending develops in the rib and failure occurs. With transverse reinforcement (Fig. 2.6), it is possible

to develop arch action in longer spans, and substantial shear loads can be transmitted essentially by compression forces in the arch ribs.

Partly because the geometry of the arch rib elements is not precisely defined, and partly because the model is a simplification of the actual behaviour, the model to describe beam behaviour is more than as a precise analytical model (Baker and MacGregor 1967).

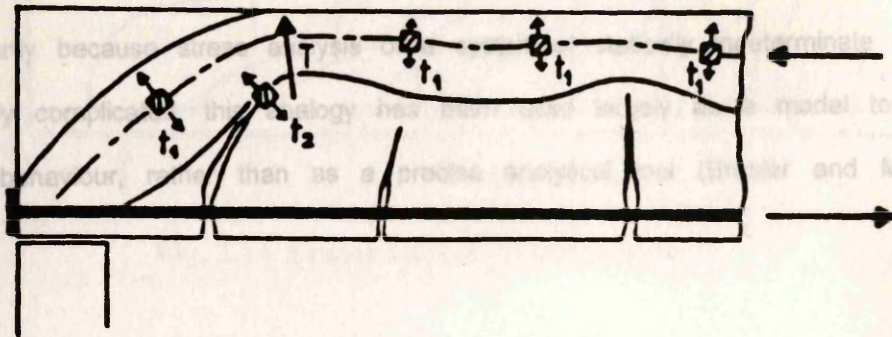
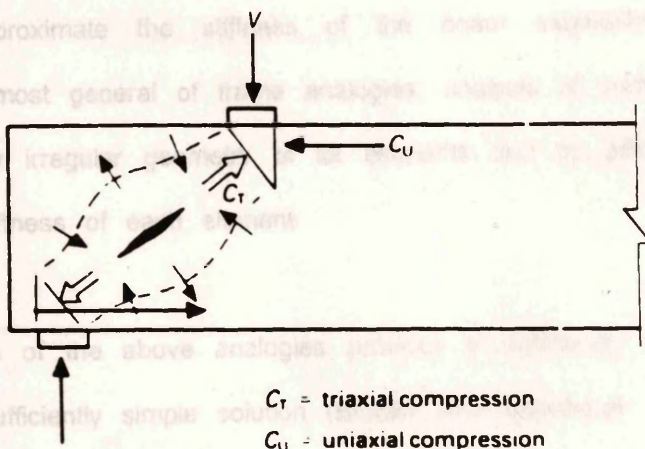


Fig. 2.12 Path of compressive force indicating locations of tensile stress.

2.7.3 Frame Analogies

This model was proposed as an analogy consisting of uniaxial concrete elements, which more nearly approximate the geometry of the arch ribs in a cracked beam, and linear steel elements, which represent longitudinal and transverse reinforcement (Fig. 2.14). The steel reinforcement, wherever it crosses a crack, is capable of resisting both axial and shear forces. The nodes are considered rigid joints, and stiffness of the frame elements is adjusted to the length to approximate the stiffness of the beam. Although this is perhaps, the most general of frame analogies, it is complicated by the need to account for the appropriate stiffness of the joints.



2.7. Fig. 2.13 Stress conditions within shear span for Type IV behaviour (see Fig. 2.8).

For beams with transverse reinforcement a more useful model for the design is based on the concept of a trapezoidal arch (Baker and MacGregor 1967). The first step in the development of this model is presented at the beginning of this chapter (see the trapezoidal model or 45° truss model). Recently, there are many variations on the truss model in the literature.

to develop arch action in longer spans, and substantial shear loads can be transmitted essentially by compression forces in the arch ribs.

Partly because the geometry of the arch rib elements is not precisely defined, and partly because stress analysis of a system of statically indeterminate arches is relatively complicated, this analogy has been used largely as a model to describe beam behaviour, rather than as a precise analytical tool (Bresler and MacGregor 1967).

Fig. 2.14 Frame analogy (after Rowatt)

2.7.3 Frame Analogies

This model was proposed as an analogy consisting of curvilinear concrete elements, which more nearly approximate the geometry of the concrete segments in a cracked beam, and linear steel elements, which represent longitudinal and transverse reinforcement (Fig. 2.14). The steel reinforcement, wherever it crosses a crack, is capable of resisting both axial and dowel forces. The nodal points are considered rigid joints, and stiffness of the frame elements is varied along their length to approximate the stiffness of the beam segments. Although this is, perhaps, the most general of frame analogies, analysis of such a frame is greatly complicated by irregular geometry of its elements and by difficulty of defining the appropriate stiffness of each element.

However none of the above analogies provides a sufficiently accurate and, at the same time, sufficiently simple solution (Bresler and MacGregor 1967).

2.7.4 Truss analogies

For beams with transverse reinforcement, a more familiar and generally more useful model for the designer is based on an analogous truss (Bresler and MacGregor 1967). The first truss model in reinforced concrete beams was presented at the beginning of this century (known as Morsch model or 45° truss model). Recently, there are many variations on the truss models in the literature.

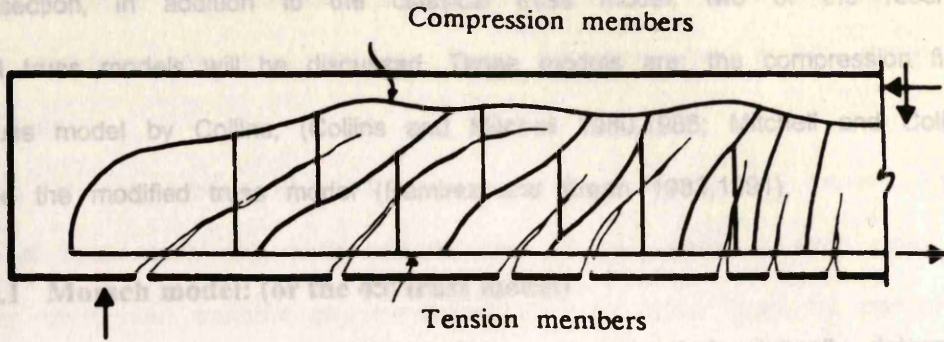
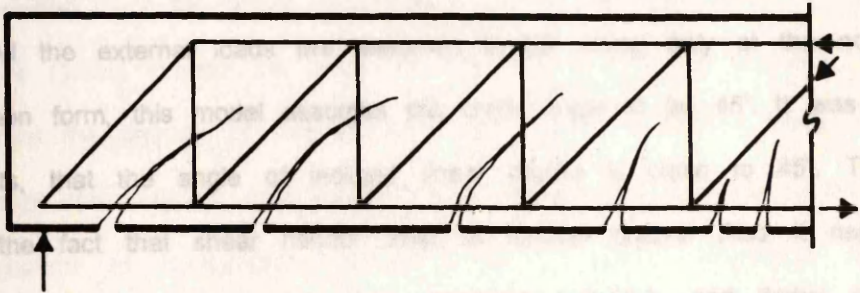
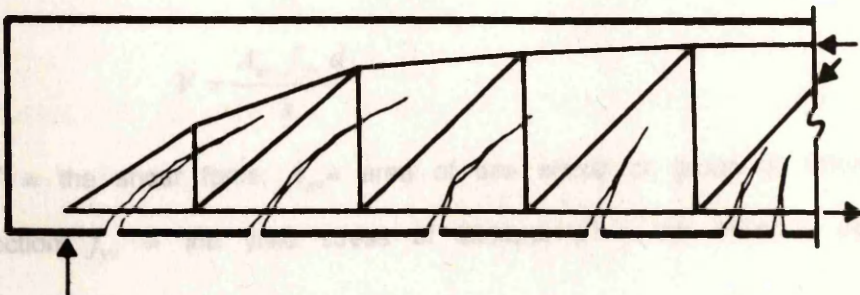


Fig. 2.14 Frame analogy (after Rusch).



a) Classical truss analogy



b) Modified truss analogy

Fig. 2.15 Truss analogy.

In this section, in addition to the classical truss model, two of the recently developed truss models will be discussed. These models are; the compression field theory truss model by Collins, (Collins and Mitchell 1980,1986; Mitchell and Collins 1974) and the modified truss model (Ramirez and Breen 1983,1991).

2.7.4.1 Morsch model: (or the 45° truss model)

In this model the beam is replaced by a pin-connected, statically determinate truss in which the concrete compression zone is represented by the compression chord, the tensile steel reinforcement is represented by the tension chord, the transverse reinforcement corresponds to the tension web members, and the concrete between inclined cracks corresponds to compression web members (Fig. 2.15a). All the external loads are assumed to be acting only at the nodes. In its common form, this model assumes the crack angle to be 45°. It was observed from tests, that the angle of inclined shear cracks is close to 45°. The model ignores the fact that shear cannot exist at flexural cracks. Also it neglects the shear resistance by compression zone, aggregate interlock, and dowel action; i.e., it assumes that failure is caused by yielding of the web reinforcement. The traditional Morsch theory was widely used in codes of practice (e.g., CP-114 1957) and when it is used, the web reinforcement (vertical stirrups) can be calculated from the following equation,

$$V = \frac{A_{sv} f_{yv} d}{s_v}$$

where V = the shear force; A_{sv} = area of one stirrup or group of stirrups at one cross section; f_{yv} = the yield stress of stirrups; d = the effective depth; s_v = spacing of stirrups.

Although the model is simple to use, it does not give results which are in general agreement with test results.

2.7.4.2. Collins and Mitchell truss model: (Collins and Mitchell 1986)
 In order to improve the predictions of the truss model, many attempts have been made to introduce new truss models. These attempts were mainly along the following lines :

1. Sloping of compression chord to take account of direct arch action. In a classical truss model the cords are assumed to be parallel to each other. As neither chord can transmit any transverse load, all shear must be carried by the inclined web members. To account for the experimentally observed shear capacity of the concrete in a beam with or without web reinforcement, the compression chord of the truss may be assumed curved (Fig. 2.15b). This modified truss begins to approach the arch analogy described previously.
2. Generalization of the angle of inclination of the concrete struts θ . Collins and Mitchell (1986) related the angle of inclination θ with the economical need to minimize the amount of web reinforcement. They choose the lower value of θ at which the diagonal compressive stress reaches the diagonal crushing stress.
3. Introduction of compatibility conditions. Collins (1973) developed compatibility equation to determine the angle of inclination of the concrete struts. This angle is assumed to coincide with the angle of inclination of the principal compression stress and strain, this theory is also known as the compression field theory. In this theory, the average strain condition should satisfy Mohr's strain circle and the stress in the concrete struts should satisfy Mohr's stress circle.
4. Introduction of the softening of concrete struts. After the discovery of the softening of concrete struts, Vecchio and Collins (1981) developed the quantification of this phenomena. They proposed a softened stress-strain curve, in which the softening effect depends on the ratio of the two principal strains. Based on combining the equilibrium, compatibility, and softened stress-strain relationships, the softened truss model theory has been proposed by Hsu (see Hsu 1988,1991; Belarbi and Hsu 1990; Mau and Hsu 1987,1990).

2.7.4.2 Collins and Mitchell truss model:(Collins and Mitchell 1986)

This truss model concentrates on the conditions at the mid-depth of the beam. The model assumes that the shear stresses are uniformly distributed over the cross section of the beam. The truss consists of compression struts and a tension tie. The shear force on the section is resisted by diagonal compressive stresses in the concrete. By assuming that the principal tensile stresses in the concrete is equal zero, the principal compressive stress in the concrete can be related to the shear stress on the concrete by the following equilibrium equation, which is derived from Mohr's circle (Fig. 2.16)

$$f_2 = \left(\tan \theta + \frac{1}{\tan \theta} \right) \left(\frac{V_f}{b_v d_v} \right)$$

The cross-sectional dimensions of the member calculated from the following condition

$$f_2 < f_{2\max}$$

where $f_{2\max}$ is diagonal crushing strength of concrete which is related to the principal tensile strain ε_1 by the following equation

$$f_{2\max} = \frac{\lambda \phi_c f'_c}{(0.8 + 170\varepsilon_1)} \leq \lambda \phi_c f'_c$$

where λ is a factor accounting for lightweight concrete and ϕ_c is the material resistance factor for concrete in the Canadian Code ($\phi_c = 0.60$). The principal tensile strain ε_1 , the principal compressive strain ε_2 , the longitudinal strain at mid depth ε_x , the transverse strain ε_y , and the principal compressive strain direction θ are interrelated by the requirements of compatibility (see Fig. 2.17) as follows:

$$\varepsilon_1 = \varepsilon_x + (\varepsilon_x + \varepsilon_2) / \tan^2 \theta$$

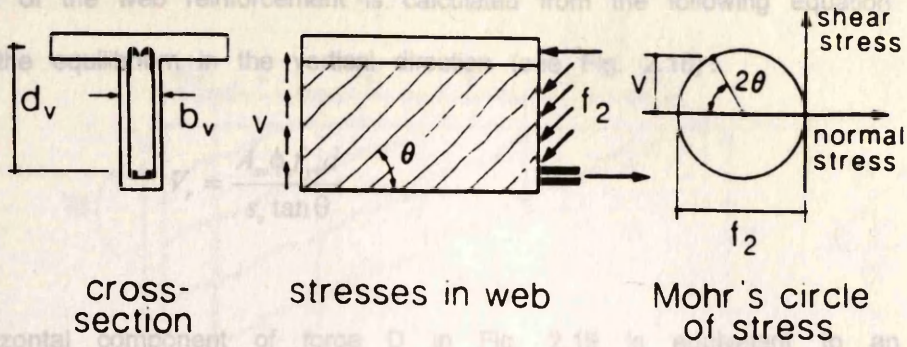


Fig. 2.16 Concrete stresses in web of beam.

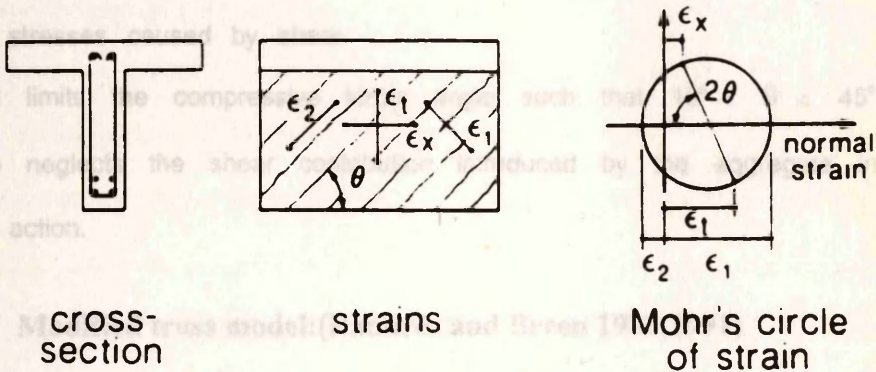


Fig. 2.17 Concrete strains at middepth of beam.

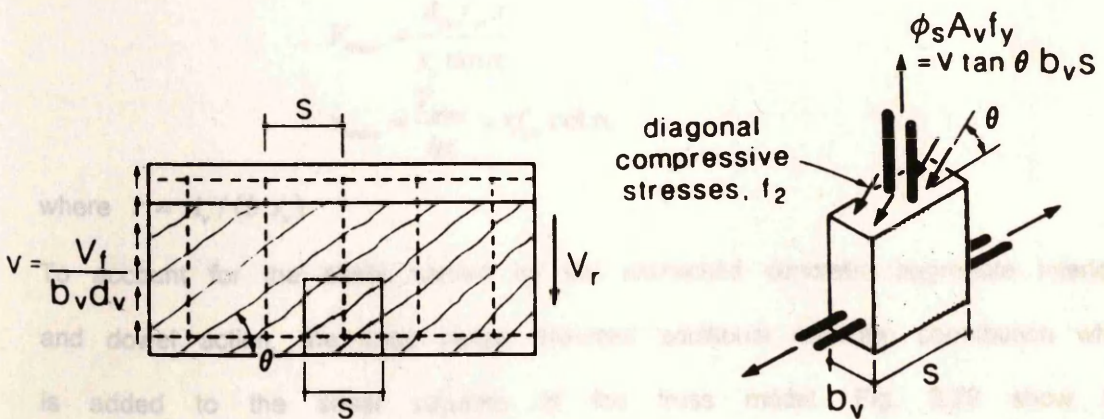


Fig. 2.18 Design of transverse reinforcement for shear.

The area of the web reinforcement is calculated from the following equation which satisfies the equilibrium in the vertical direction (see Fig. 2.18):

$$V_r = \frac{A_{sv} \phi f_{yv} d}{s_v \tan \theta}$$

The horizontal component of force D in Fig. 2.19 is equivalent to an axial compression on the concrete. This compression needs to be equilibrated by tensile forces ($V_f / \tan \theta$) in the longitudinal reinforcement (Fig. 2.18). The model suggests that the longitudinal reinforcement is designed to a larger moment of $M_f + 0.5(V_f / \tan \theta)d_v$ to give the additional longitudinal reinforcement to balance the tensile stresses caused by shear.

The model limits the compressive struts angle such that $15^\circ < \theta < 45^\circ$. The model also neglects the shear contribution introduced by the aggregate interlock and dowel action.

2.7.4.3 Modified truss model:(Ramirez and Breen 1983,1991)

The modified truss model consists of a parallel chord truss with the diagonal forming a uniform compression field as shown in Fig. 2.19. The shear capacity of the model is given by:

$$V_{truss} = \frac{A_{sv} f_{yv} z}{s_v \tan \alpha}$$

$$v_{truss} = \frac{V_{truss}}{bz} = r f_{yv} \cot \alpha$$

where $r = A_{sv} / (b \cdot s_v)$

To account for the shear carried by the uncracked concrete, aggregate interlock, and dowel action, the truss model assumed additional concrete contribution which is added to the shear capacity of the truss model. Fig. 2.20 show this contribution which is a function of the applied load. For example, when the applied load causes shear stress $V/(b \cdot z)$ less than $2\sqrt{f'_c}$, the contribution v_c is

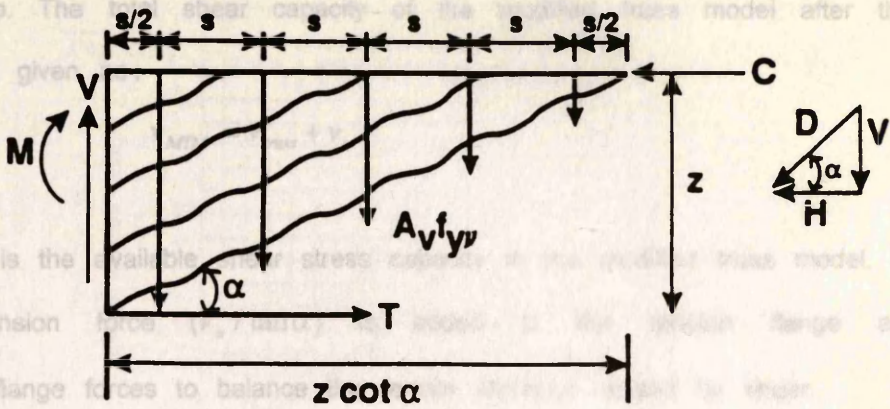


Fig. 2.19 Truss model for beams and beam-type regions.

1. The modified truss model is more conservative for shear design than the total shear is resisted by truss action with shear flow by diagonal concrete struts plus web reinforcement.

2. Limitation on θ : The range of θ is the range of θ in the ACI model ($25^\circ < \theta < 45^\circ$) with the suggestion for using the lower bound ($\theta = 25^\circ$) (2.21a), while in the modified truss model the range is $25^\circ < \theta < 45^\circ$ (2.21b).

3. Comparison with the ACI model: The ACI model is compared to the modified truss model with respect to the shear capacity of reinforced concrete beams. The ACI model is compared to the modified truss model with respect to the shear capacity of reinforced concrete beams. The ACI model is compared to the modified truss model with respect to the shear capacity of reinforced concrete beams. The ACI model is compared to the modified truss model with respect to the shear capacity of reinforced concrete beams.

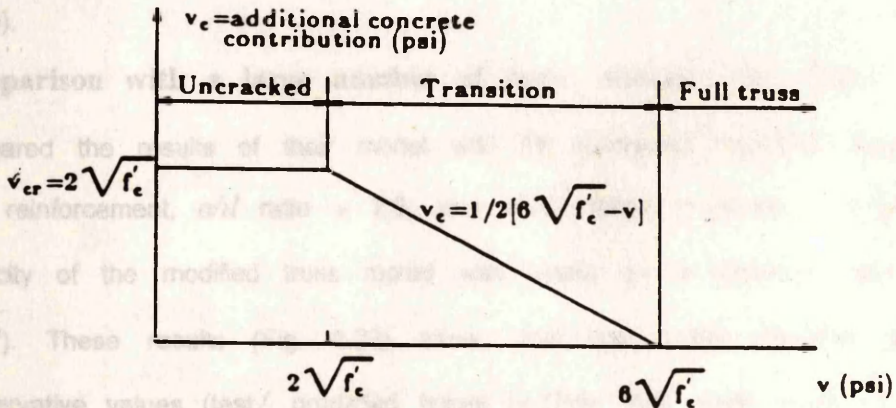


Fig. 2.20 Diminishing concrete contribution for reinforced concrete beams.

constant ($=2\sqrt{f'_c}$), while when it causes shear stress equal $6\sqrt{f'_c}$ the contribution becomes zero. The total shear capacity of the modified truss model after this contribution is given as:

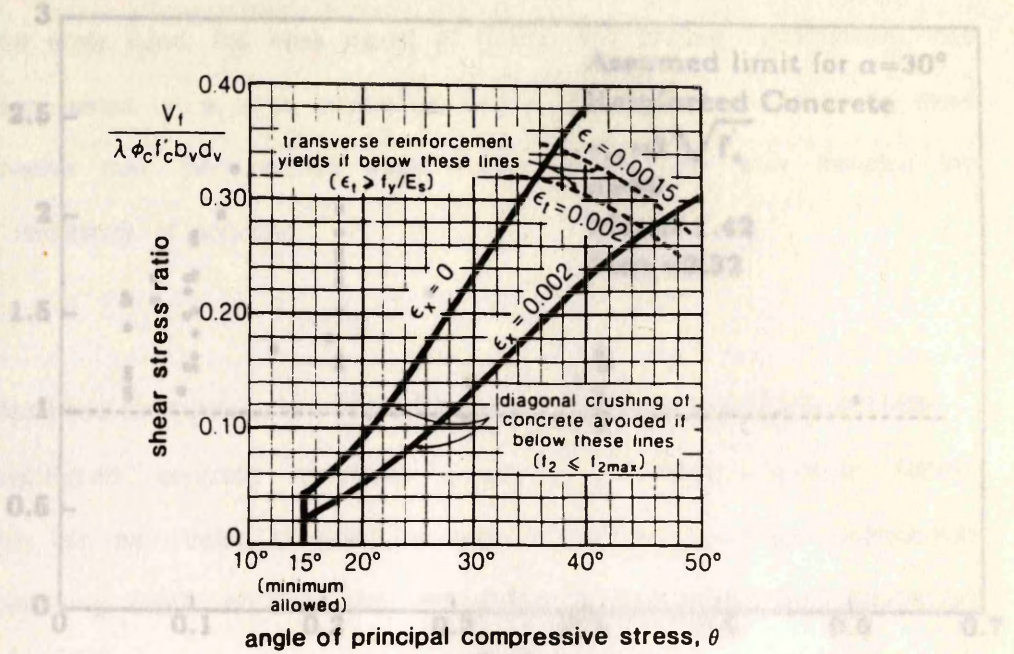
$$v_{MTM} = v_{truss} + v_c$$

where v_{MTM} is the available shear stress capacity in the modified truss model.

Additional tension force ($V_u / \tan\alpha$) is added to the tension flange and compression flange forces to balance the tensile stresses caused by shear.

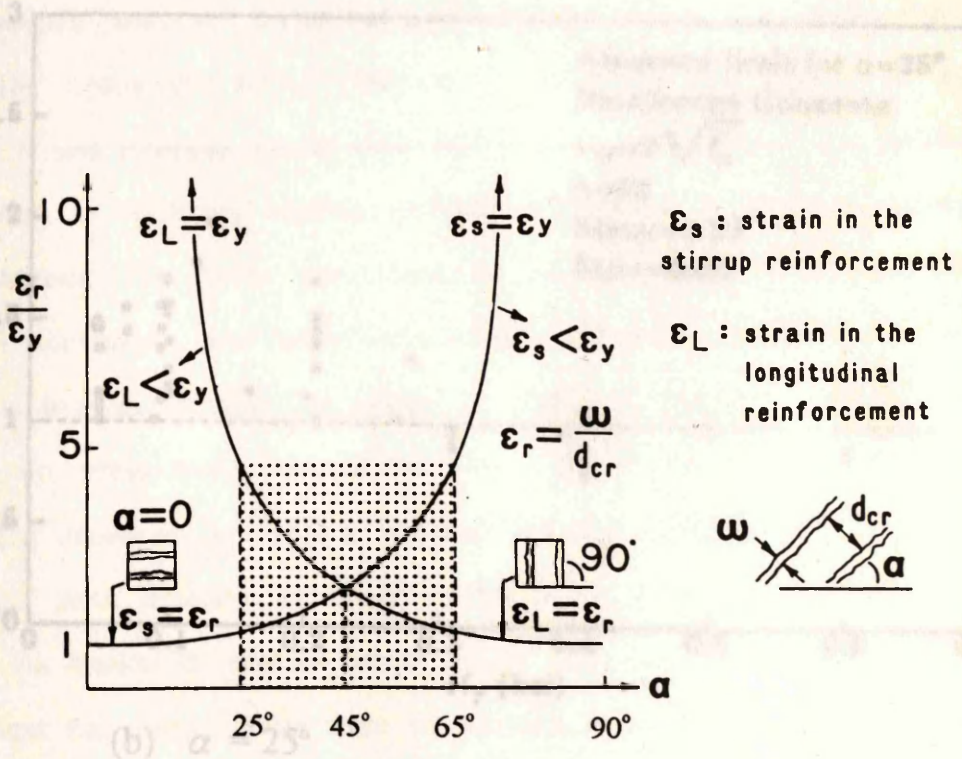
The modified truss model differs from the truss model of Collins and Mitchell in the following aspects:

1. **The modified truss model is more economical:** The model assumes that the total shear is resisted by truss action and beam action, the truss action consists of diagonal concrete struts plus web reinforcement.
2. **Limitation on θ :** The range of θ in the Model of Collins and Mitchell is $15^\circ < \theta < 45^\circ$ with the suggestion for using the lowest possible value of θ (Fig. 2.21a), while in the modified truss model the range is $30^\circ < \theta < 65^\circ$ (Fig. 2.21b).
3. **Comparison with a large number of tests.** Ramirez and Breen (1991) compared the results of their model with 59 reinforced concrete beams with web reinforcement, a/d ratio > 2.0 , and which failed in shear. The predicted capacity of the modified truss model was based on a minimum value of θ ($=30^\circ$). These results (Fig. 2.22) show that the model provided generally conservative values (test/ predicted failure > 0.94) with mean value $=1.42$ and standard deviation $= 0.32$. The prediction becomes quite conservative for beams with $r_{fyv} < 1.38 \text{ MPa}$ (200 psi) and unconservative values for beams with $r_{fyv} > 2.07 \text{ MPa}$ (300 psi). If the value of θ decreases the conservatism decreases but the results will be unacceptable unconservative for beams with $r_{fyv} > 2.07 \text{ MPa}$ (300 psi).



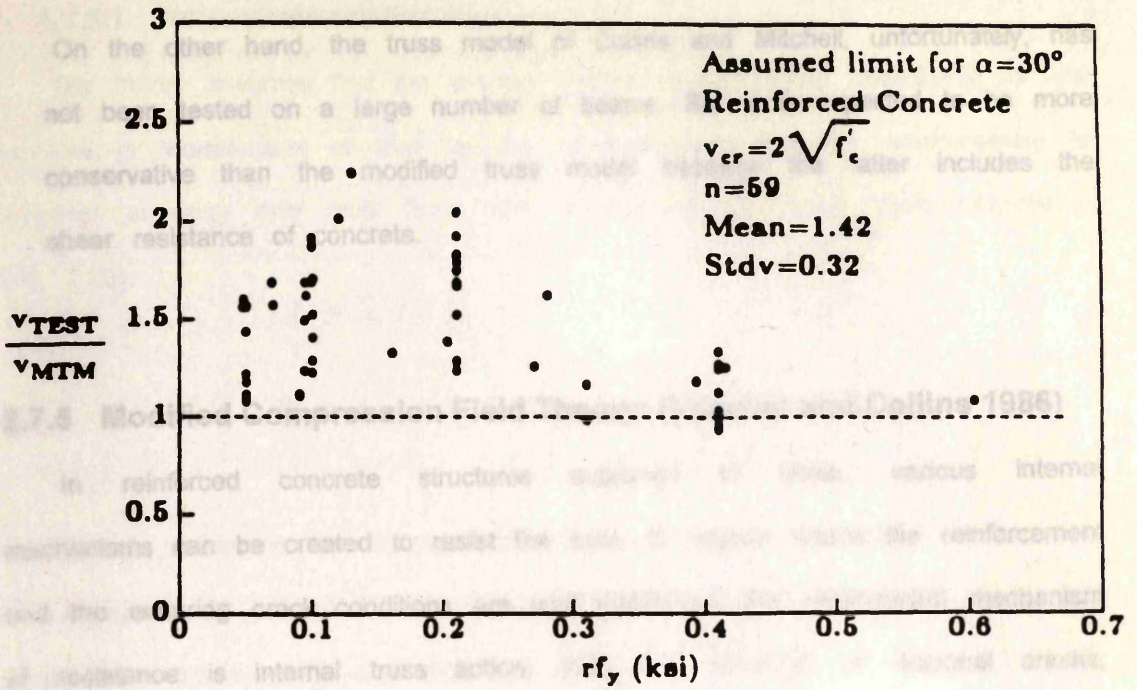
(a) $\alpha = 30^\circ$

Fig. 2.21a Choice of θ in Collins and Mitchell's truss model

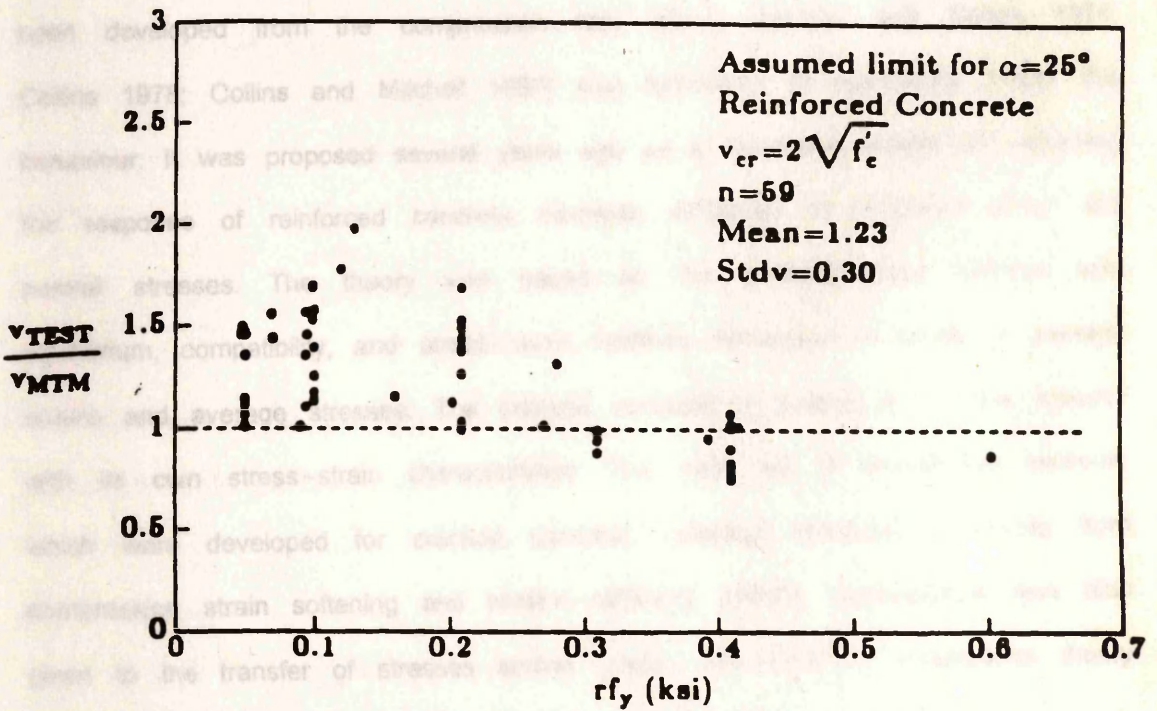


(b) α

Fig. 2.21b Choice of the compressive struts angle (α) in Modified truss model (Ramirez and Breen 1991)



(a) $\alpha = 30^\circ$



(b) $\alpha = 25^\circ$

Fig. 2.22 Evaluation of reinforced concrete beams with concrete contribution of Fig. 2.20 (Ramirez and Breen 1991)

2.7.5.1 Stress-strain relationships:

On the other hand, the truss model of Collins and Mitchell, unfortunately, has not been tested on a large number of beams. But it is expected to be more conservative than the modified truss model because the latter includes the shear resistance of concrete.

(Fig. 2.23)

$$f_s = E_s \epsilon \leq f_{sy}$$

2.7.5 Modified Compression Field Theory: (Vecchio and Collins 1986)

In reinforced concrete structures subjected to shear, various internal mechanisms can be created to resist the load. In regions where the reinforcement and the ensuring crack conditions are well distributed, the predominant mechanism of resistance is internal truss action. With the formation of diagonal cracks, compression struts develop in concrete while the longitudinal and transverse reinforcement act as tension ties. The modified compression field theory, which has been developed from the compression field theory (Mitchell and Collins 1974; Collins 1978; Collins and Mitchell 1980) was formulated to specifically model this behaviour. It was proposed several years ago as a theoretical model for predicting the response of reinforced concrete elements subjected to in-plane shear and normal stresses. The theory was based on the smeared-crack concept with equilibrium, compatibility, and stress-strain relations formulated in terms of average strains and average stresses. The cracked concrete is treated as a new material with its own stress-strain characteristics. This new set of constitutive relations, which were developed for cracked concrete, reflected significant influences from compression strain softening and tension-stiffening effects. Consideration was also given to the transfer of stresses across cracks. The modified compression theory also includes the change in the angle of inclination of the cracks.

The theory was based on the smeared-crack concept with stress-strain relationship for concrete formulated in terms of average strains and average stresses.

2.7.5.1 Stress-strain relationships:

The theory assumes that the average stress-average strain relationship for the concrete is independent of that for the reinforcement. Also the reinforcement is assumed to carry only axial force with bilinear uniaxial stress-strain relationship (Fig. 2.23),

$$f_{sx} = E_s \cdot \epsilon \leq f_{yx}$$

$$f_{sy} = E_s \cdot \epsilon \leq f_{yy}$$

In order to determine the average stress-average strain relationship, Vecchio and Collins tested 30 reinforced concrete panels under uniform stresses. Based on these test results, they quantified the observed softening of concrete in the principal compressive direction as a function the coexisting principal tensile in addition to the principal compressive strain as follows (Fig. 2.23):

$$f_{c2} = f_{c2max} \cdot \left[2 \left(\frac{\epsilon_2'}{\epsilon_c'} \right) - \left(\frac{\epsilon_2'}{\epsilon_c'} \right)^2 \right]$$

where

$$\frac{f_{c2max}}{f_c'} = \frac{1}{0.8 - 0.34 \epsilon_1' / \epsilon_c'} \leq 1.0$$

Also, they derived an expression for the average tensile stresses that exist in the cracked concrete as follows (Fig. 2.23):

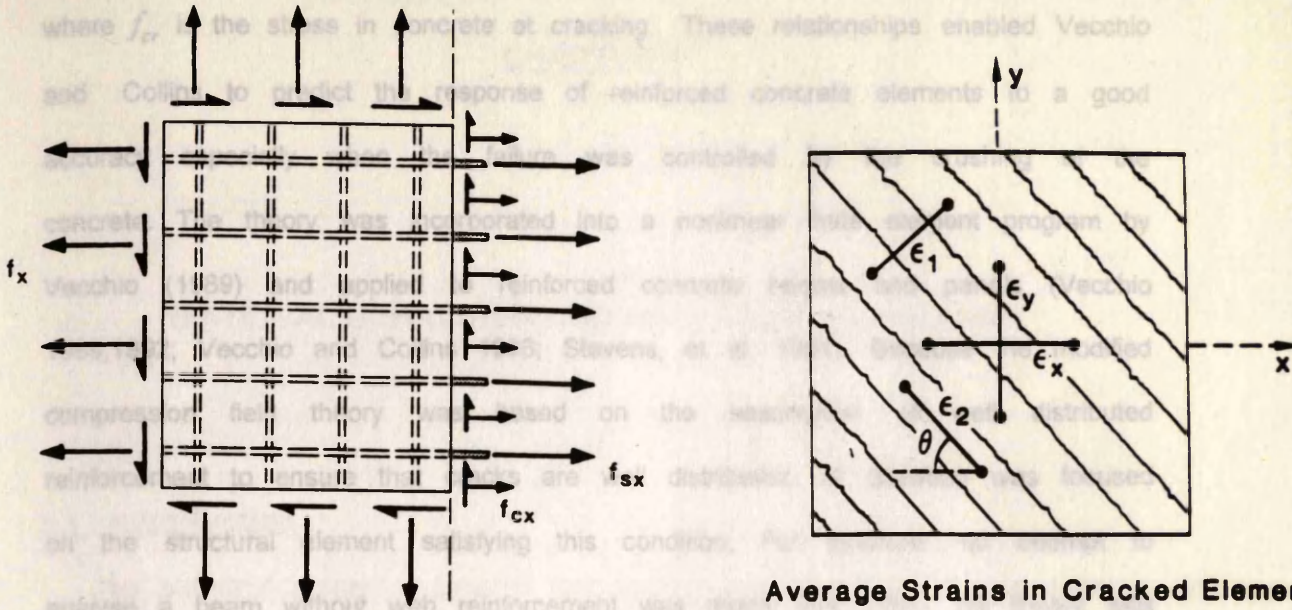
Before cracking,

$$f_{c1} = E_c \cdot \epsilon_1$$

After cracking,

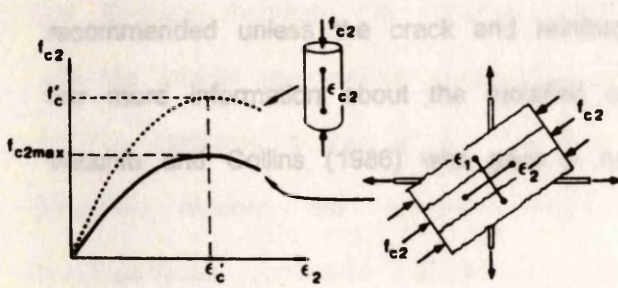
$$f_{c1} = \frac{f_{cr}}{1 + \sqrt{200 \epsilon_1}}$$

Fig. 2.23 Assumed stresses-strain relationships for concrete and steel in Modified compression-tension theory.

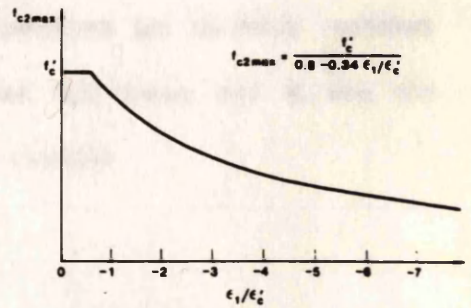


Free-body diagram of part of element.

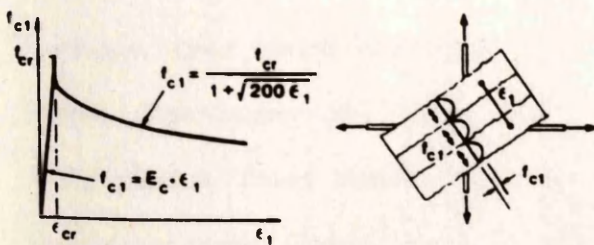
Average Strains in Cracked Element



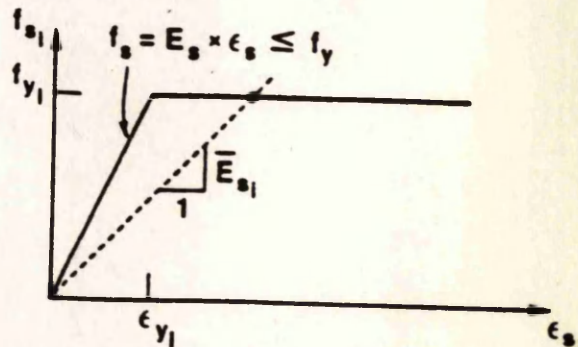
Stress-Strain Relationship for Cracked Concrete in Compression



Proposed Relationship for Maximum Compressive Stress



Average Stress-Strain Relationship for Cracked Concrete in Tension



Reinforcing Steel

Fig. 2.23 Assumed stresses -strain relationships for concrete and steel in Modified compression field theory.

where f_{cr} is the stress in concrete at cracking. These relationships enabled Vecchio and Collins to predict the response of reinforced concrete elements to a good accuracy especially when the failure was controlled by the crushing of the concrete. The theory was incorporated into a nonlinear finite element program by Vecchio (1989) and applied to reinforced concrete beams and panels (Vecchio 1989,1992; Vecchio and Collins 1986; Stevens, et al. 1991). Because the modified compression field theory was based on the assumption of well distributed reinforcement to ensure that cracks are well distributed, all attention was focused on the structural element satisfying this condition. For example, no attempt to analyse a beam without web reinforcement was made. And when the theory was used to analyse pushoff specimens tested by Hofbeck, et al. (1969), Vecchio and Nieto (1991) concluded that the application of the analysis procedure is not recommended unless the crack and reinforcement conditions are discretely modelled. For more information about the modified compression field theory and its use see Vecchio and Collins (1986) who gave a numerical example.

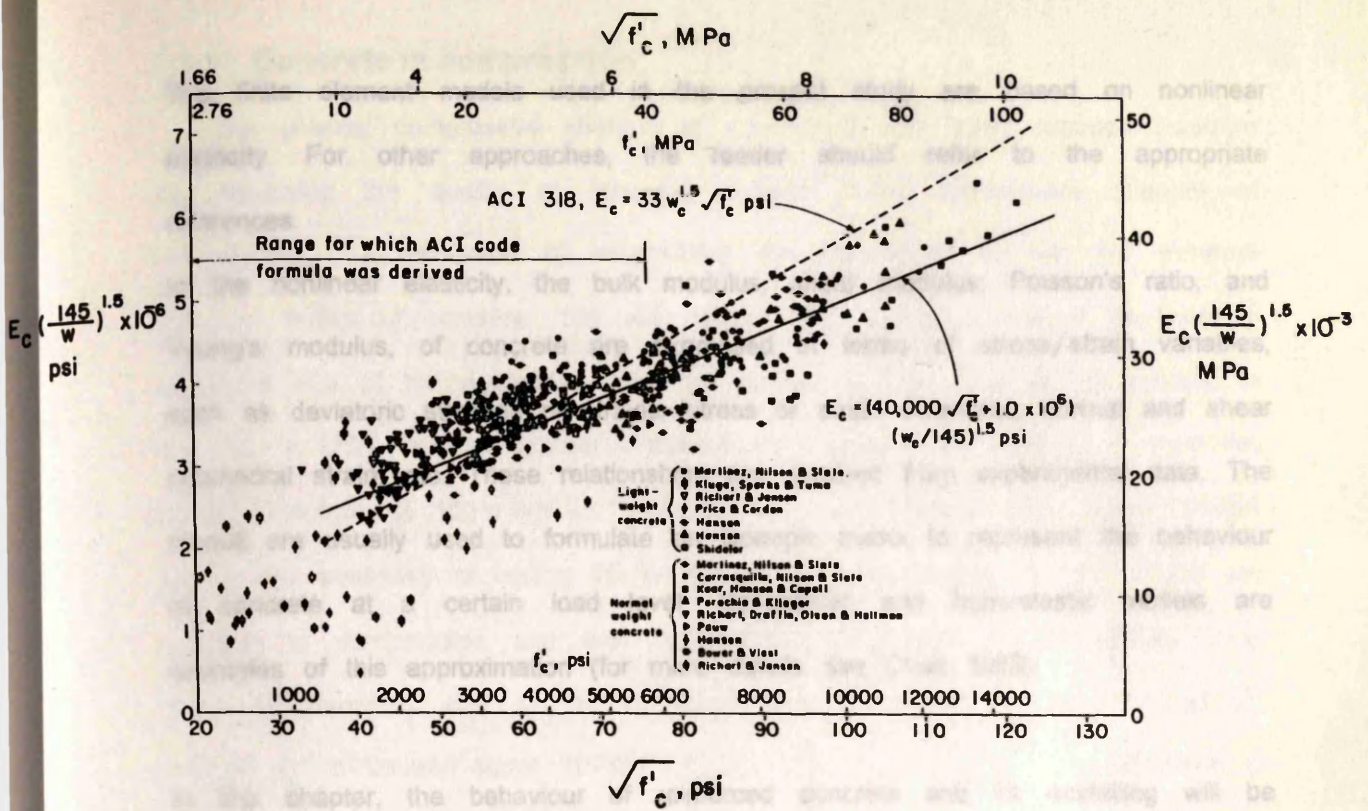
CHAPTER 3

MATERIAL BEHAVIOUR AND NUMERICAL MODELLING

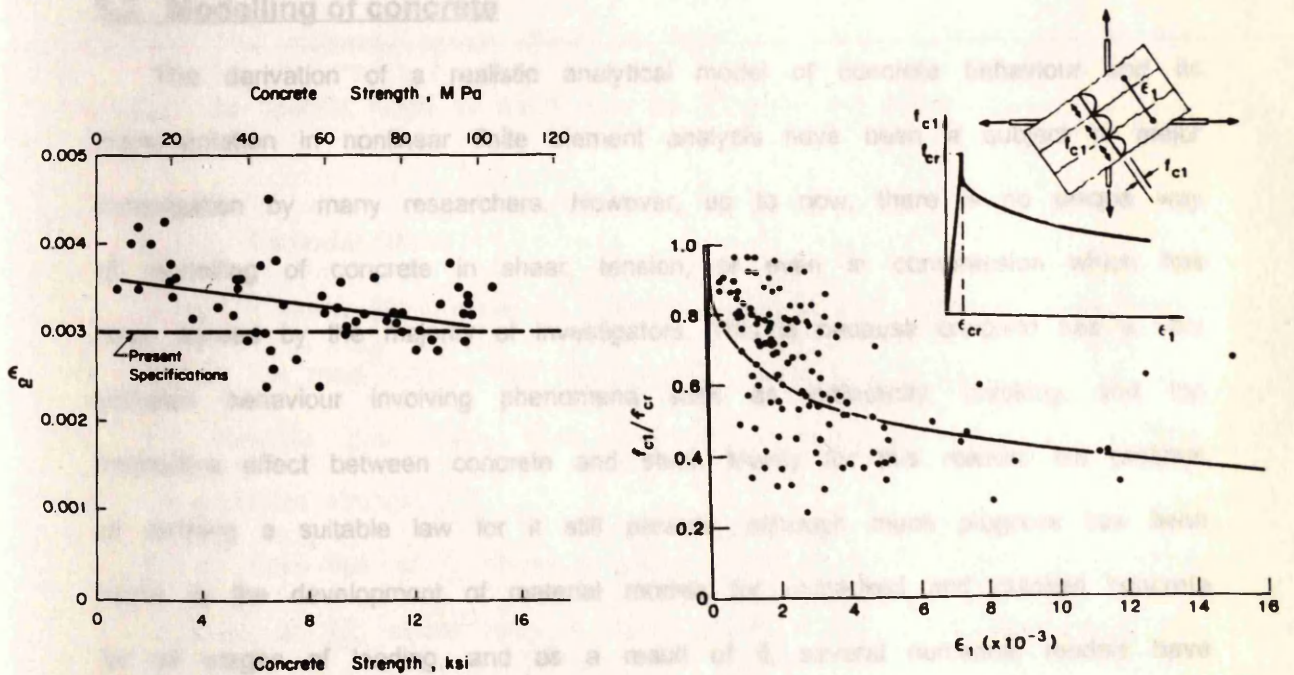
3.1 Introduction

The statistical scatter of concrete test results tends to support the view that a perfect match between an analytical and experimental data is neither possible nor really necessary (Meyer 1982). Figure 3.1 shows three examples of this scatter for the Young's modulus, the concrete strain at failure (ACI-Committee-363 1984), and the tensile stress-strain curve of concrete (Vecchio and Collins 1986). In view of this statistical scatter of concrete test data, it appears questionable whether complex models are justified. Reinforced concrete is considered as a heterogeneous, composite material. At macroscopic level, it consists of two major components: steel reinforcements and concrete. In the modelling of its nonlinear stress-strain behaviour, a general approach is to treat the response of each component separately, then obtain their combined effects by imposing the condition of material continuity. To model the nonlinear response of concrete as a continuum, three distinct approaches have been employed; nonlinear elasticity based models (Palaniswamy and Shah 1974; Cedolin, et al. 1977; Elwi and Murray 1979), plasticity based models (Chen and Chen 1975a, b; Bazant and Kim 1979), endochronic theory (Bazant and Bhat 1976; Bazant 1978; Bazant and Shieh 1978, 1980; and Al-Manaseer 1983). A comprehensive evaluation of these approaches was given by Chen and Teng (1980).

Fig. 3.1 Scatter of concrete test results



(a) Modulus of elasticity versus concrete compressive strength (ACI-Committee-363 1984).



(b) Ultimate concrete flexural strain versus concrete compressive strength (ACI-Committee-363 1984).

(c) Test data for cracked concrete in tension (Vecchio and Collins 1986).

Fig. 3.1 Scatter of concrete test results.

3.2.1 Concrete in compression

The finite element models used in the present study are based on nonlinear elasticity. For other approaches, the reader should refer to the appropriate references.

In the nonlinear elasticity, the bulk modulus, shear modulus, Poisson's ratio, and Young's modulus, of concrete are expressed in terms of stress/strain variables, such as deviatoric stresses or strains, stress or strain invariants, normal and shear octahedral strain, etc. These relationships are obtained from experimental data. The moduli are usually used to formulate an isotropic matrix to represent the behaviour of concrete at a certain load level. Hypoelastic and hyperelastic models are examples of this approximation (for more details see Chen 1982).

In this chapter, the behaviour of reinforced concrete and its modelling will be reviewed with the focus on the modelling chosen in the present study.

3.2 Modelling of concrete

The derivation of a realistic analytical model of concrete behaviour and its implementation in nonlinear finite element analysis have been a subject of major investigation by many researchers. However, up to now, there is no unique way of modelling of concrete in shear, tension, or even in compression which has been agreed by the majority of investigators. This is because concrete has a very complex behaviour involving phenomena such as inelasticity, cracking, and the interactive effect between concrete and steel. Mainly for this reason, the problem of defining a suitable law for it still persists, although much progress has been made in the development of material models for uncracked and cracked concrete for all stages of loading, and as a result of it, several numerical models have been developed (Chen 1982).

A brief summary of the behaviour of concrete and its modelling in compression, tension, and shear will be given in this section.

3.2.1 Concrete in compression

The uniaxial compressive strength of concrete is the most common measure for assessing the quality of concrete. Uniaxial cube compressive strength of concrete f_{cu} is evaluated by determining the strength of 28 day old standard 150 mm cubes of concrete. 100 mm cubes are sometimes used if the nominal maximum size of the aggregate does not exceed 25 mm. This is the practice in the UK. In USA, uniaxial cylinder compressive strength of concrete f'_c is evaluated by the strength of 152 x 305 mm cylinder specimens. Nasser and Kenyon (1984) studied the possibility of testing 76 x 152 mm cylinders instead of 152 x 305 mm cylinders in compression and they concluded that it can be successfully used where the maximum size of the aggregate does not exceed 25 mm. The cylinder strength f'_c is usually about 70–90% of the cube strength f_{cu} . The difference is due to the frictional forces which develop between the platen plates of the testing machine and the contact face of the test specimen. These end forces produce a multiaxial stress state which increases the apparent cube compressive strength of concrete. The multiaxial stress effects are significant throughout the cube. In the cylinder, the specific height to width ratio will minimise this effect.

3.2.1.1 Uniaxial stress

A typical stress–strain curve for concrete under uniaxial compression is shown in Fig. 3.2. The main experimental observations can be summarised as follows:

- The concrete has nearly linear behaviour up to 30% of its maximum compressive strength f'_c .
- Stress above 30% of f'_c shows a gradual increase in deformation up to about 75–90% of f'_c ; where upon it bends more sharply when approaching the peak strength f'_c .
- Beyond the peak strength f'_c , the stress–strain curve has a descending branch until crushing failure occurs at some ultimate strain (ϵ_{max}).

Fig. 3.2 Uniaxial compressive stress–strain curves for concrete with different strengths

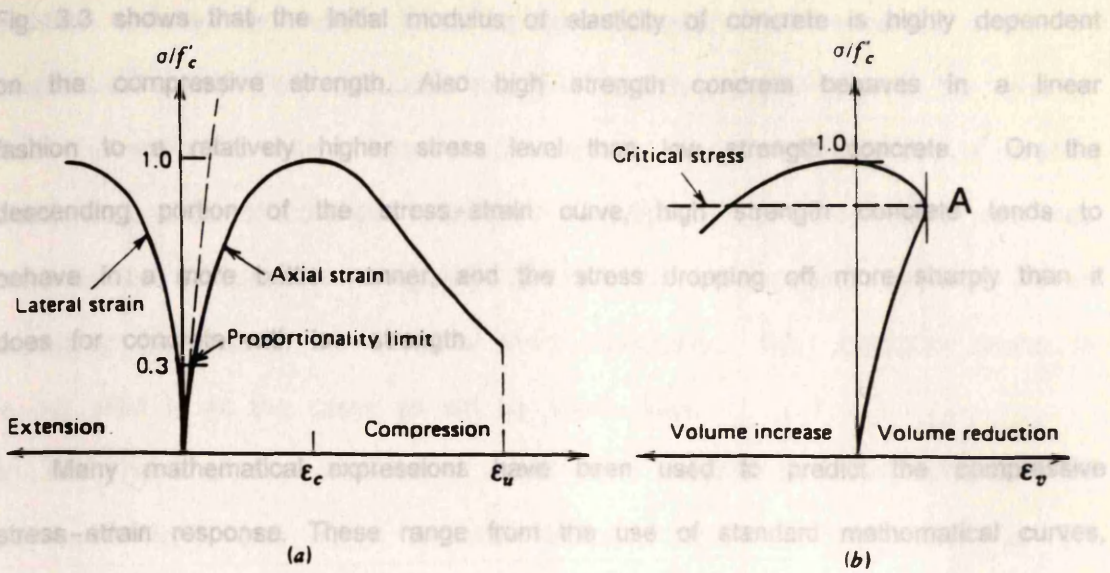


Fig. 3.2 Typical stress-strain curves for concrete in uniaxial compression test.
(a) Axial and lateral strains. (b) volumetric strain ($\epsilon_v = \epsilon_1 + \epsilon_2 + \epsilon_3$)

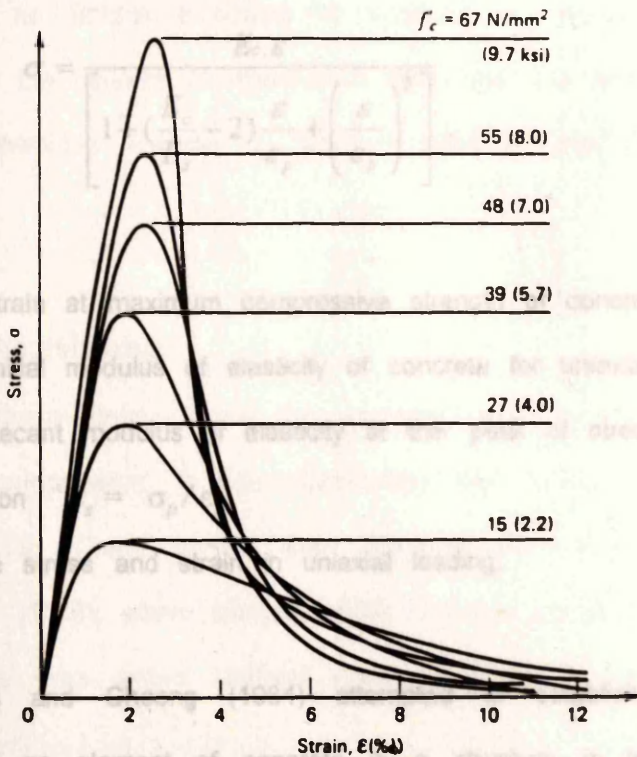


Fig. 3.3 Uniaxial compressive stress-strain curves for concrete with different strengths ,

Fig. 3.3 shows that the initial modulus of elasticity of concrete is highly dependent on the compressive strength. Also high strength concrete behaves in a linear fashion to a relatively higher stress level than low strength concrete. On the descending portion of the stress-strain curve, high strength concrete tends to behave in a more brittle manner, and the stress dropping off more sharply than it does for concrete with low strength.

Many mathematical expressions have been used to predict the compressive stress-strain response. These range from the use of standard mathematical curves, to more complex formulae based on curve fitting techniques.

Equation 3.1 originally proposed by Liu, et al. (1972), representing uniaxial stress-strain curve for concrete is commonly used for numerical analysis. And it will be used in the present study for the ascending portion of the uniaxial compressive stress-strain curve.

$$\sigma = \frac{E_c \varepsilon}{\left[1 + \left(\frac{E_c}{E_s} - 2 \right) \frac{\varepsilon}{\varepsilon_p} + \left(\frac{\varepsilon}{\varepsilon_p} \right)^2 \right]} \quad (3.1)$$

where;

ε_p is the strain at maximum compressive strength of concrete σ_p .

E_c is the initial modulus of elasticity of concrete for uniaxial loading.

E_s is the secant modulus of elasticity at the peak of stress and given by the expression $E_s = \sigma_p / \varepsilon_p$.

σ and ε are stress and strain in uniaxial loading.

Kotsovos and Cheong (1984) attempted to establish to what extent the behaviour of an element of concrete in a structure is realistically described by stress-strain relationships obtained from tests on concrete specimens, such as

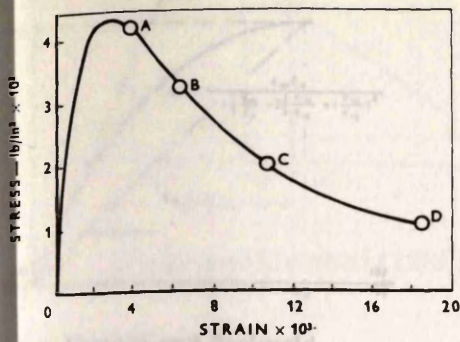
cylinders, prisms, or cubes, subjected to concentric and eccentric states of compressive stress. They concluded that the ascending portion (up to the level at which the specimen volume becomes a minimum, point A in Fig. 3.2b) of stress-strain relationships of concrete established from the uniaxial compression tests was found to be sufficient to completely describe the deformational response of an element of concrete of the structural forms investigated. This conclusion seems to be not valid in all the cases as will be shown later.

On the shape of the compressive stress-strain curves, much experimental work has been done, and many numerical formulae have been proposed. Fig. 3.4 shows some different shapes which have been experimentally reported, while Figs. 3.5 and 3.6 show some curves that have been derived numerically. From these figures the following observations can be made:

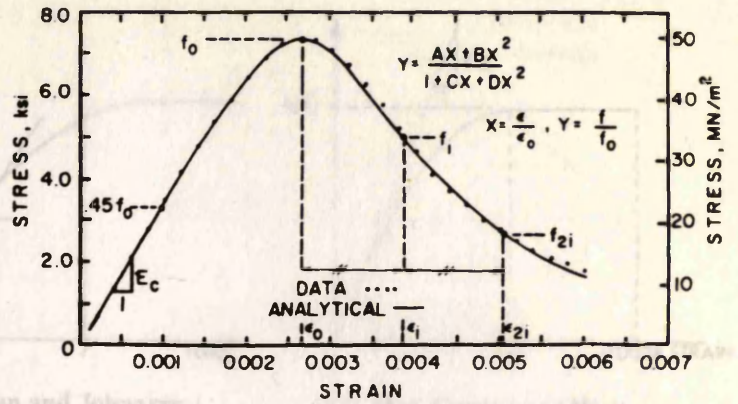
- The compression softening of concrete has been proved by all the experimental works, however, the maximum compressive strain is different from test to test (Fig. 3.4).
- There is no unique modelling of concrete in compression that has been agreed by the majority of researchers (see Figs. 3.5 and 3.6).
- Many researchers assume a minimum value of post-crushing strength (Fig. 3.6).

3.2.1.2 Biaxial stress

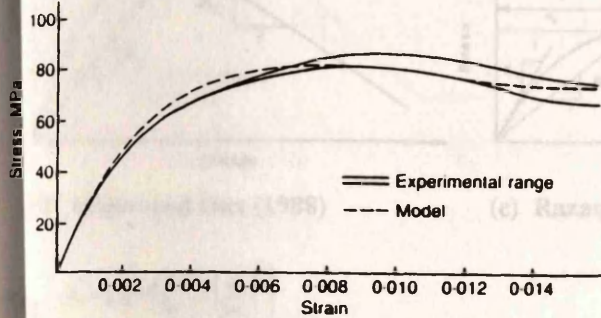
Typical stress-strain curves for concrete under biaxial states of stress in compression-compression, tension-compression and tension-tension are shown in Figures 3.7-3.9. These curves were obtained from the experimental tests of Kupfer, et al. (1969), where normal weight concrete specimens of dimension 200 x 200 x 50 mm were tested. Uniaxial stress-strain curves are also shown in these figures.



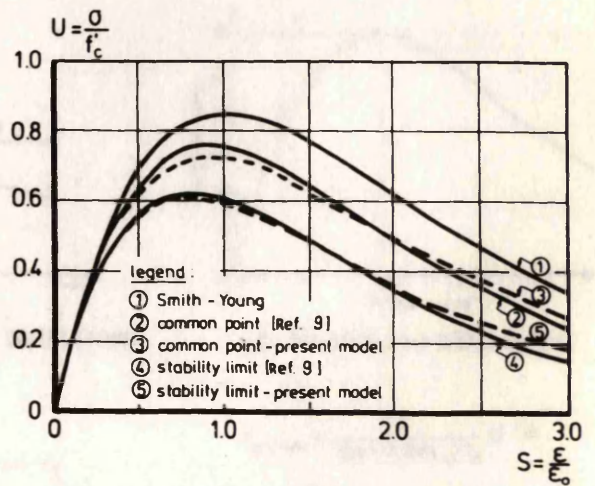
(a) Barnard (1964)



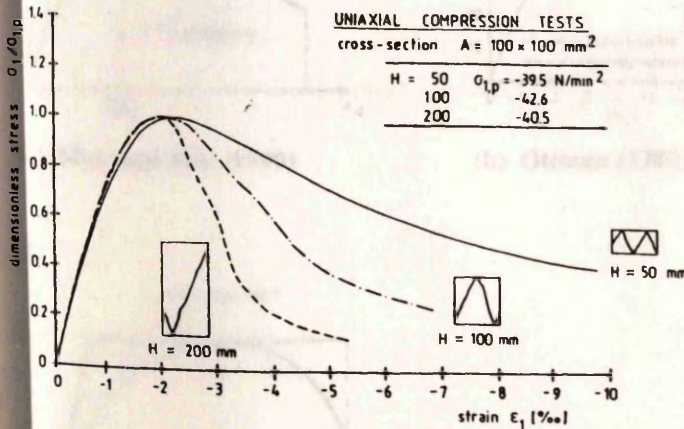
(b) Wang, et al. (1978)



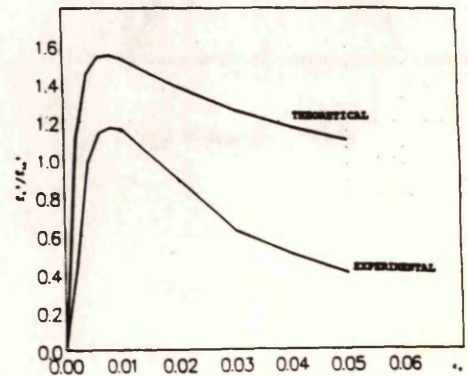
(c) Ahmad and Abdel-Fattah (1991)



(d) Yankelevsky and Reinhardt (1987)



(e) Van Mier (1986)



(f) Krauthammer, et al. (1988)

Fig. 3.4 Different shapes of compressive stress-strain curve of concrete.

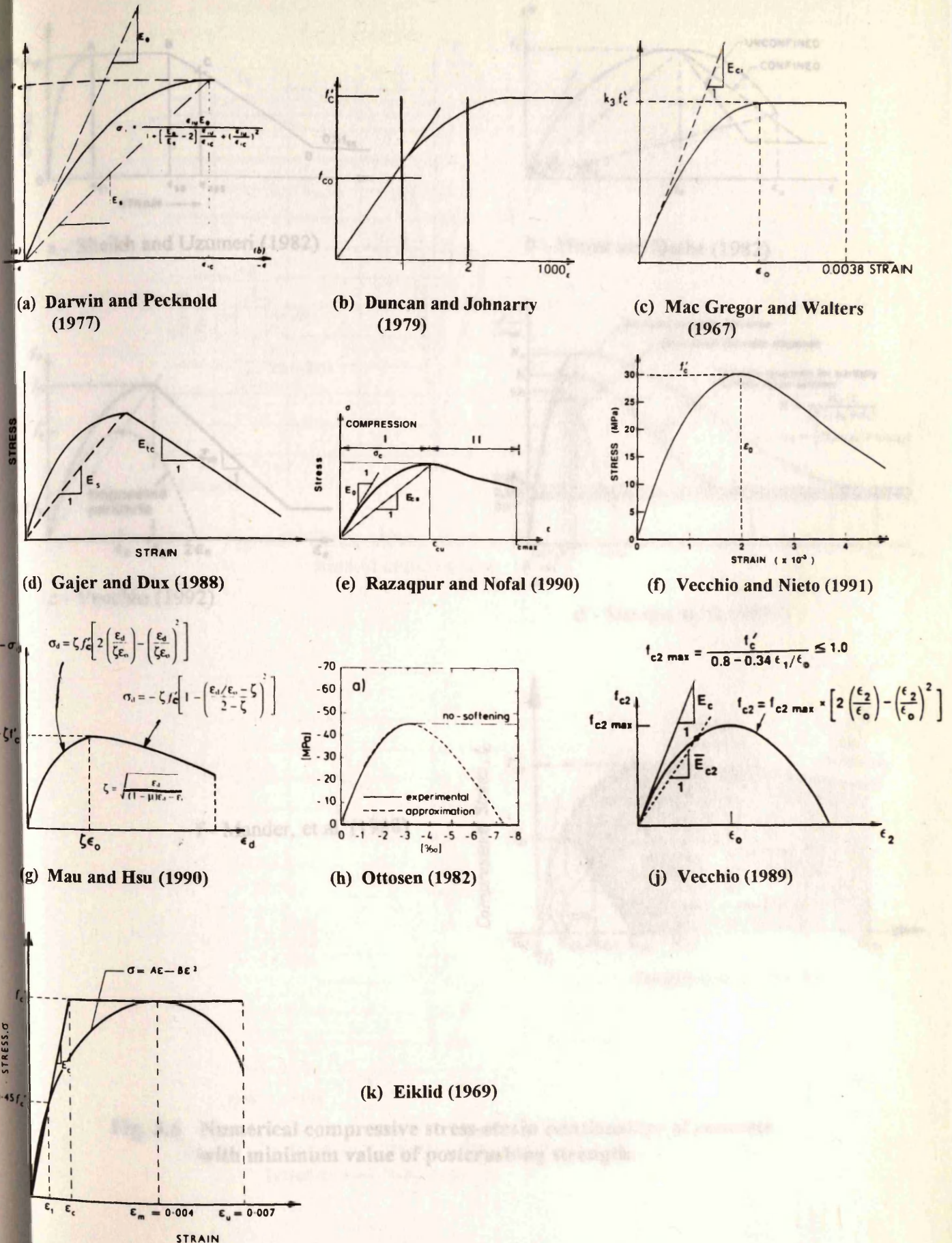


Fig. 3.5 Different numerical compressive stress-strain relationships of concrete.

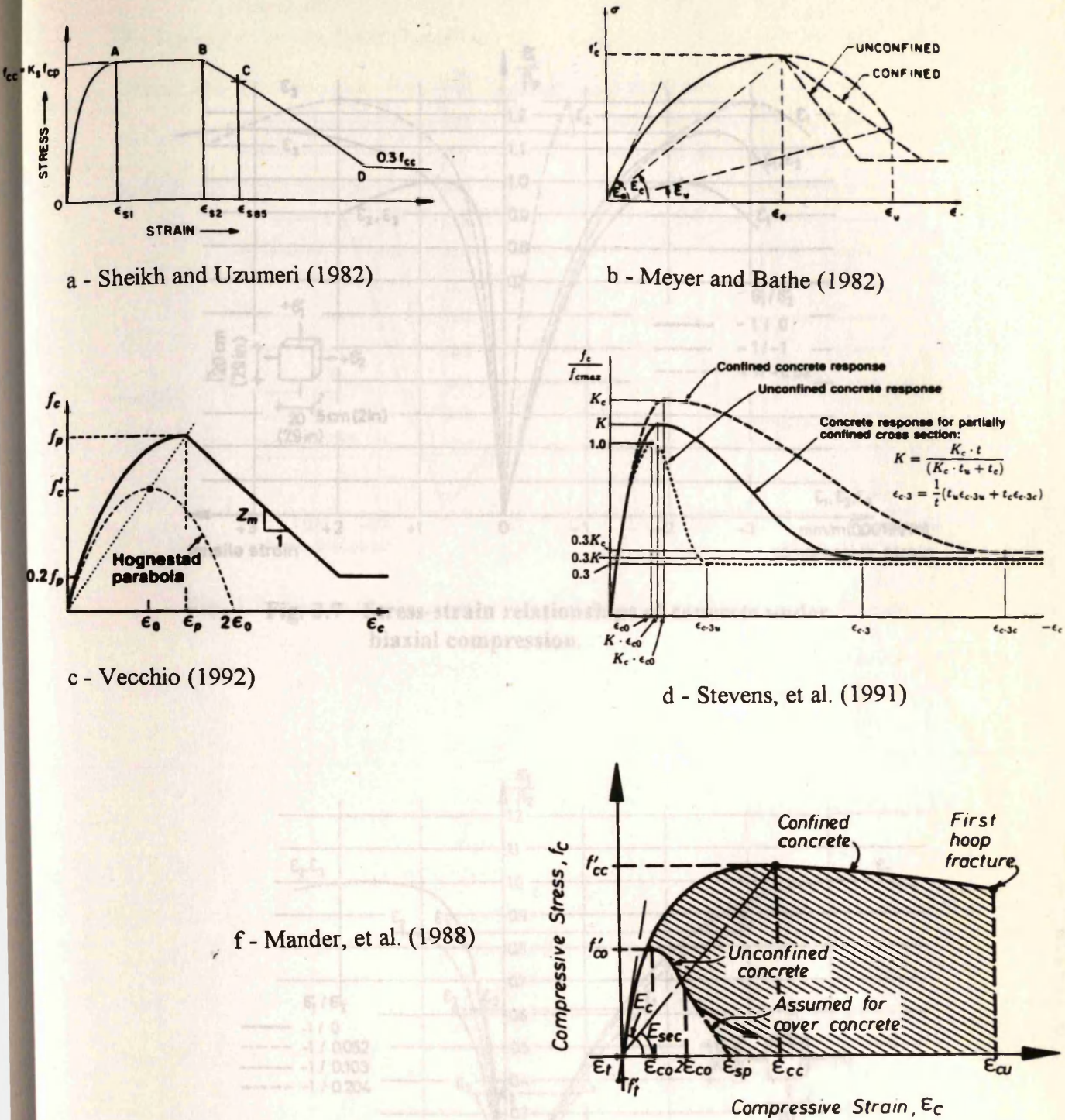


Fig. 3.6 Numerical compressive stress-strain relationships of concrete with minimum value of postcrushing strength.

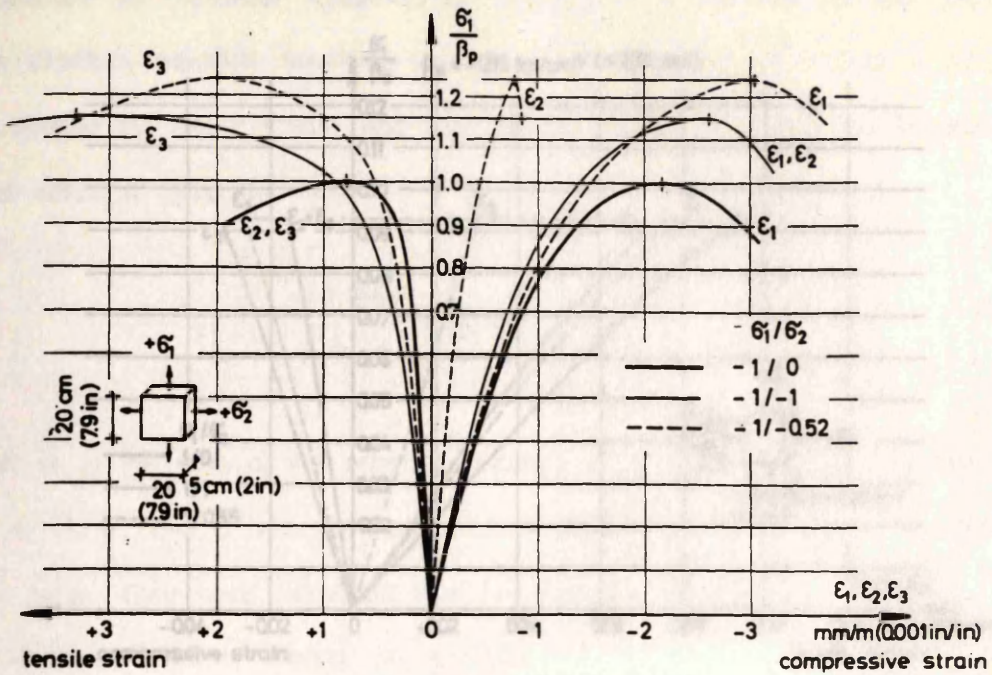


Fig. 3.7 Stress-strain relationships of concrete under biaxial compression.

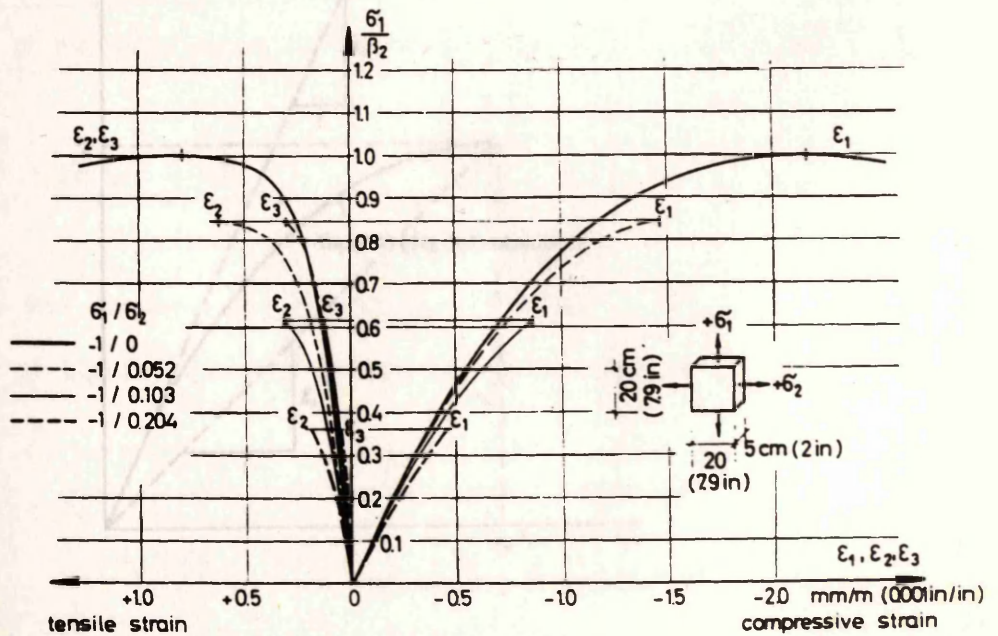


Fig. 3.8 Stress-strain relationships of concrete under combined tension and compression.

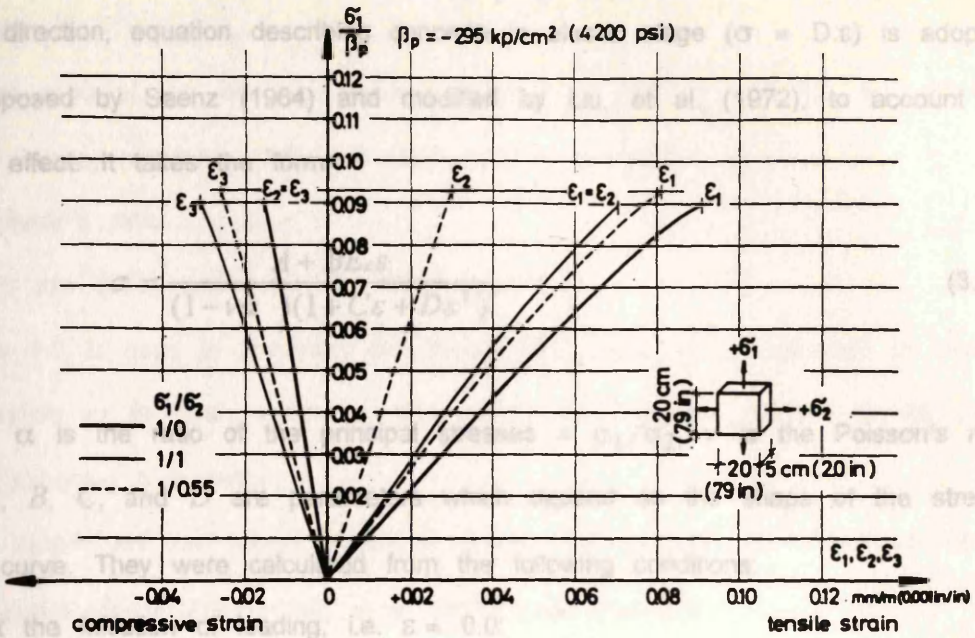


Fig. 3.9 Stress-strain relationships of concrete under biaxial tension.

$$d\sigma/d\epsilon = E_c / (1 - \nu\alpha) \quad \alpha = 0$$

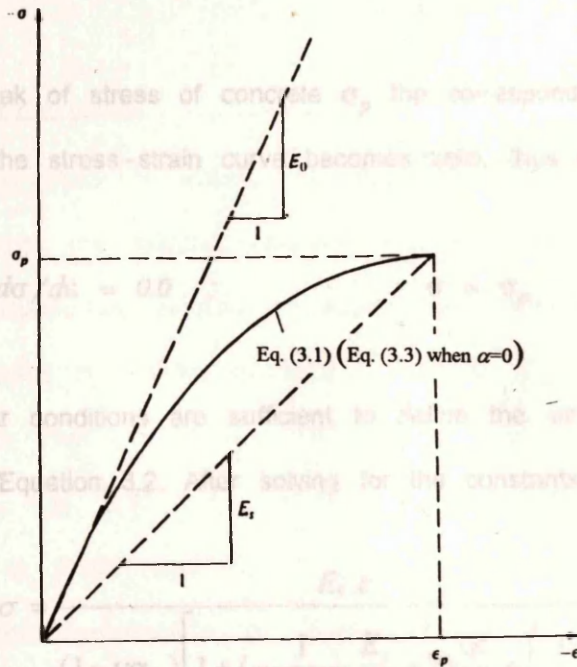


Fig. 3.10 Equivalent uniaxial stress-strain curve

where

σ_p is the ultimate strength of concrete in compression

ϵ_p is the strain at maximum compressive strength of concrete

E_c is the initial modulus of elasticity of concrete for uniaxial loading

To account for nonlinear stress-strain relationship of concrete in the principal stress direction, equation describing concrete in elastic stage ($\sigma = D.\varepsilon$) is adopted as proposed by Saenz (1964) and modified by Liu, et al. (1972), to account for biaxial effect. It takes the form:

$$\sigma = \frac{A + BE_c\varepsilon}{(1 - \nu\alpha)(1 + C\varepsilon + D\varepsilon^2)} \quad (3.2)$$

where; α is the ratio of the principal stresses = σ_1/σ_2 , ν is the Poisson's ratio and A , B , C , and D are parameters which depend on the shape of the stress-strain curve. They were calculated from the following conditions:

- 1) At the initiation of loading, i.e. $\varepsilon = 0.0$:

$$d\sigma/d\varepsilon = E_c/(1 - \nu\alpha); \quad \sigma = 0.0$$

- 2) At the peak of stress of concrete σ_p the corresponding strain is ε_p and the slope of the stress-strain curve becomes zero, thus at $\varepsilon = \varepsilon_p$ we have:

$$d\sigma/d\varepsilon = 0.0 ; \quad \sigma = \sigma_p$$

The above four conditions are sufficient to define the unknown parameters A , B , C , and D of Equation 3.2. After solving for the constants we have (Fig. 3.10):

$$\sigma = \frac{E_c.\varepsilon}{(1 - \nu\alpha) \left[1 + \left(\frac{1}{1 - \nu\alpha} \frac{E_c}{E_s} - 2 \right) \frac{\varepsilon}{\varepsilon_p} + \left(\frac{\varepsilon}{\varepsilon_p} \right)^2 \right]} \quad (3.3)$$

where:

σ_p is the ultimate strength of concrete in compression, equal f'_c .

ε_p is the strain at maximum compressive strength of concrete.

E_c is the initial modulus of elasticity of concrete for uniaxial loading.

E_s is the secant modulus of elasticity at the peak of stress and given by the expression $E_s = \sigma_p / \varepsilon_p$.

α is the ratio of the principal stresses = σ_1 / σ_2 (If $\alpha = 0$, i.e. for uniaxial state of stress, equations (3.1) and (3.3) become identical).

ν is Poisson's ratio.

σ and ε are stress and strain in biaxial loading.

Equation 3.3 is used to generate the stress-strain behaviour of concrete in biaxial compression up to peak strain ε_p , after which this equation ceases to be valid due to softening deformation.

Further details on the biaxial states of stress can be found in references, e.g.;

Darwin and Pecknold (1977); Liu, et al. (1972); and Van Mier (1986).

Roosstad, et al. (1974), Darwin and Pecknold (1977), Tasuj, et al. (1978), and Van Mier (1986).

3.2.1.3 Triaxial stress

In a triaxial state of stress, the strength of concrete can be increased considerably above the uniaxial strength, in particular, under hydrostatic stress conditions. A considerable amount of research has been performed to study the strength of concrete in a three-dimensional state of stress (Kotsovos, et al. 1977, 1978, 1979, 1980; Elwi and Murray 1979; Murray 1979; Ahmad and Shah 1982; Van Mier 1986). Figs. 3.11 and 3.12 show a stress-strain curves from the tests by Richart, et al. (1928) and Balmer (1949). These tests were conducted under different volumetric compression (or confining) stresses. As these curves show, depending on the confining stress, concrete act as a quasi-brittle, plastic-softening, or plastic-hardening material. This is because under higher confining stresses the possibility of bond cracking is greatly reduced and the failure mode shifts from cleavage to crushing of cement paste (Chen 1982). Figs. 3.11 and 3.12 show that the axial strength increases with increasing

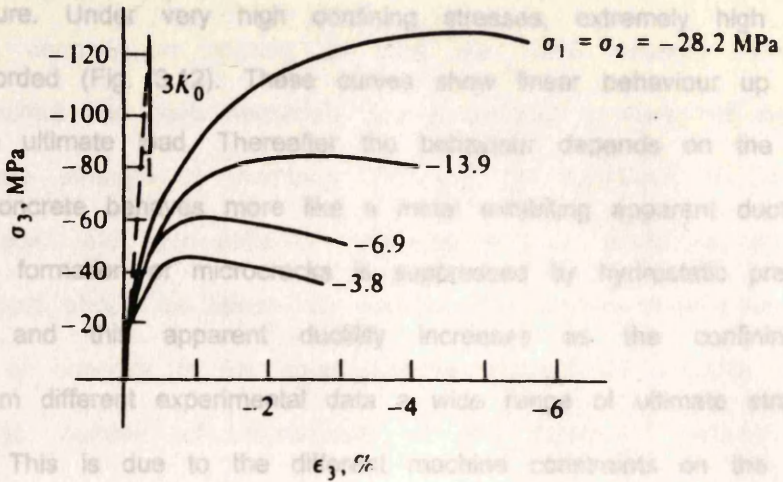


Fig. 3.11 Triaxial stress-strain relationship for concrete (Richart, et al. 1928).

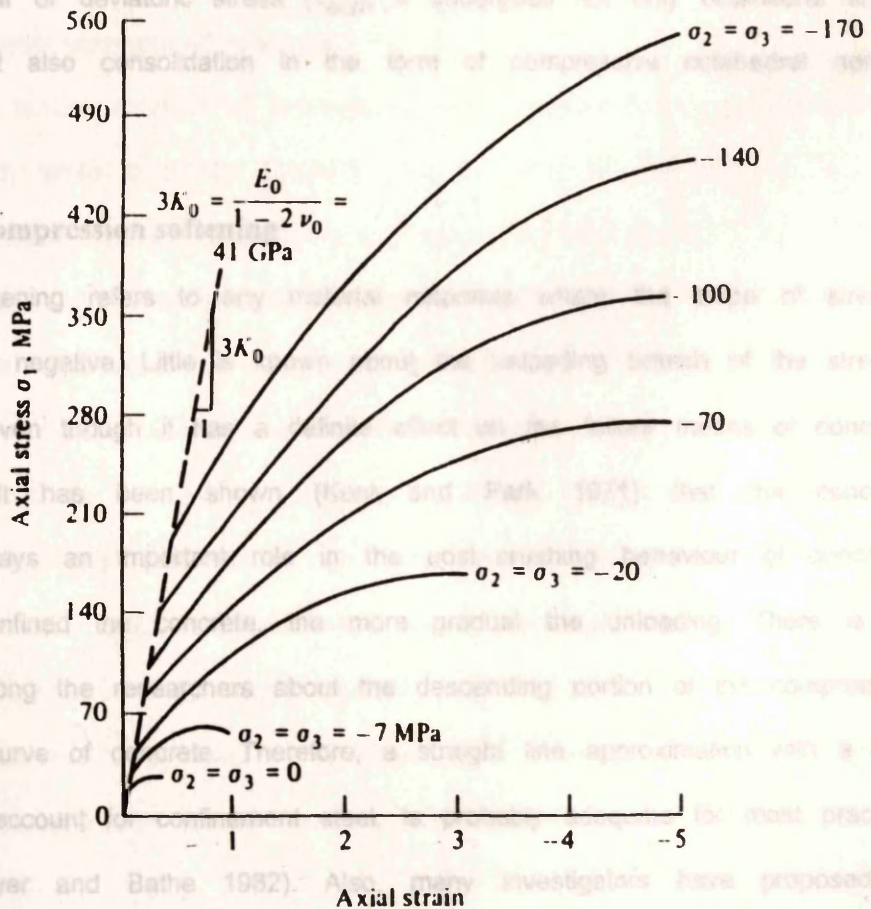


Fig. 3.12 Triaxial stress-strain relationship for concrete. (Balmer 1949).

3.2.2 Concrete in tension

confining pressure. Under very high confining stresses, extremely high strengths have been recorded (Fig. 3.12). These curves show linear behaviour up to about 30-40% of the ultimate load. Thereafter the behaviour depends on the confining pressure and concrete behaves more like a metal exhibiting apparent ductility. This is because the formation of microcracks is suppressed by hydrostatic pressure on the specimen and this apparent ductility increases as the confining stress increases. From different experimental data a wide range of ultimate strains have been reported. This is due to the different machine constraints on the specimen boundaries. The boundary constraints will inhibit transverse deformation affecting the value of the moduli.

Analysis of test data by Kotsovos and Newman (1978) indicates that when concrete is subjected to a constant hydrostatic stress (constant σ_{oct}) and an increasing shear or deviatoric stress (τ_{oct}), it undergoes not only octahedral shear strain γ_{oct} but also consolidation in the form of compressive octahedral normal strain ϵ_{oct} .

3.2.1.4 Compression softening

Strain softening refers to any material response where the slope of stress-strain curve is negative. Little is known about the unloading branch of the stress-strain curve, even though it has a definite effect on the failure modes of concrete structures. It has been shown (Kent and Park 1971) that the concrete confinement plays an important role in the post-crushing behaviour of concrete. The better confined the concrete, the more gradual the unloading. There is no agreement among the researchers about the descending portion of the compressive stress-strain curve of concrete. Therefore, a straight line approximation with a free parameter to account for confinement steel, is probably adequate for most practical purposes (Meyer and Bathe 1982). Also, many investigators have proposed to credit concrete with a residual post-crushing strength of between 10 and 40% of f_c' (see Fig. 3.6).

3.2.2 Concrete in tension

Strength of concrete in tension is very low. Until recently, the tensile behaviour in concrete has been neglected, this is because it does not significantly affect the ultimate strength of members (this will be discussed in Sec. 5-3). However, to predict the load-deflection characteristics of structures, the tensile strength of concrete should be taken into account. The primary reason for the low tensile strength of concrete is the heterogeneous structure of concrete. Concrete contains a large number of microcracks at the interfaces between coarse aggregate and mortar, this even before any load has been applied. Much experimental work on the complete tensile stress-strain relationship has been done. Fig.3.13 shows tensile stress-strain curves including unloading portion (ACI Committee-224 1986).

Fig. 3.13 Tensile stress-strain curves for concrete including unloading portion (ACI Committee-224 1986)

3.2.2.1 Tensile strength of concrete

The uniaxial tensile strength of concrete is rarely measured or reported in the experiments and, when it is, its accuracy may be open to question due to the scatter in the tensile strength test. There are three methods of tests used to find the tensile strength of plain concrete; the direct tension test, the beam test, and the splitting test. Very often the tensile strength of concrete is not measured but has to be inferred from compressive strength. The best property used to calculate the tensile strength is the uniaxial compressive strength of concrete f'_c because it is usually tested and reported in the experimental works. There are many empirical equations which estimate the tensile strength from the cylinder compressive strength f'_c . From these equations, two equations (3.4 and 3.5) have been chosen for this study (Fig. 3.14). These two equations are plotted against some previous experimental results obtained from Raphael (1984).

$$f_t' = 0.10 f'_c \quad \text{MPa} \quad (3.4)$$

$$f_t' = 0.54 \sqrt{f'_c} \quad \text{MPa} \quad (3.5)$$

Fig. 3.14 Estimating tensile strength f_t' from compressive strength f'_c

3.2.2.2 Cracking of concrete

Progressive cracking is one of the most important nonlinear characteristics

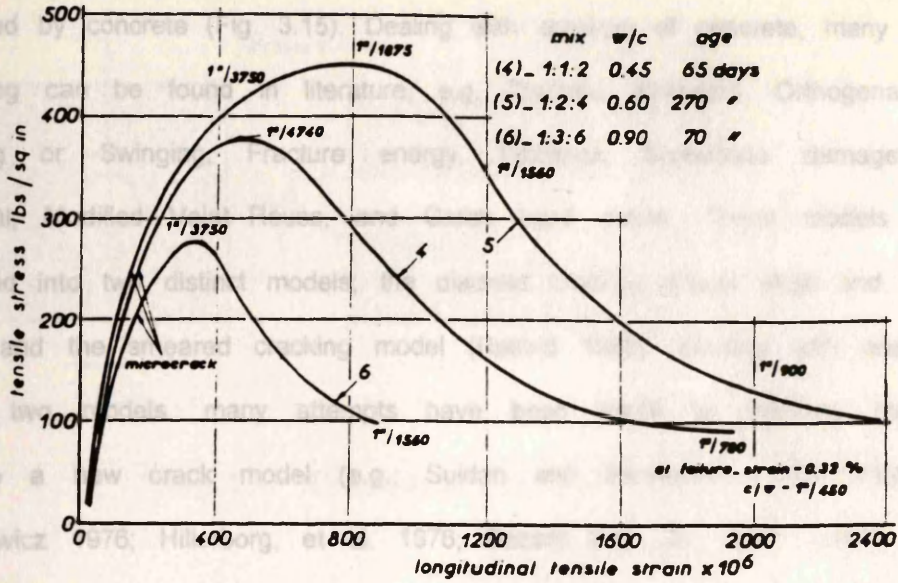


Fig. 3.13 Tensile stress-strain curves for concrete including unloading portion (ACI-Committee-224 1986).

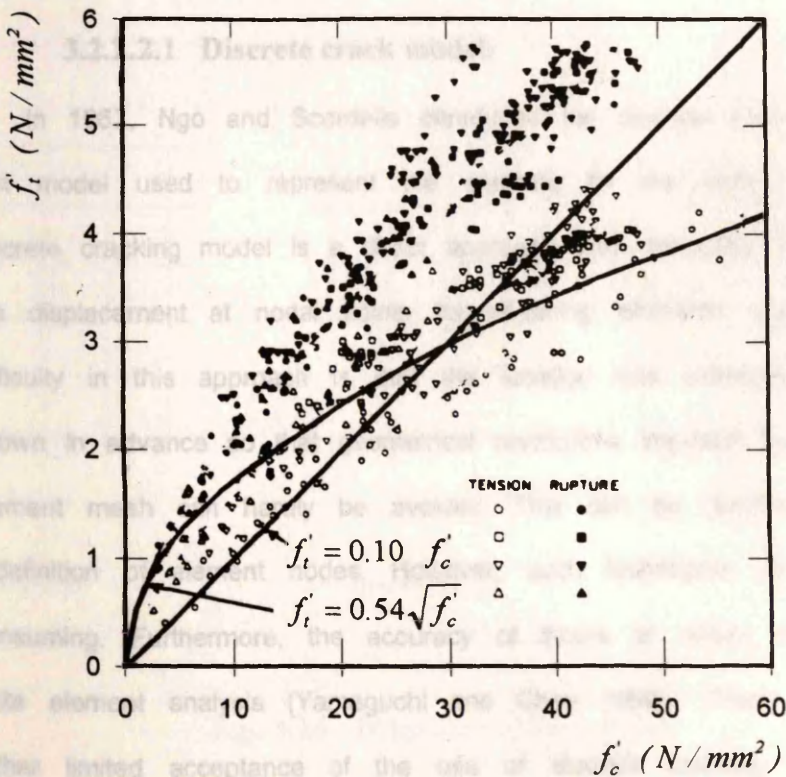


Fig. 3.14 Estimating tensile strength f_t' from compressive strength f_c' .

3.2.2.2 Cracking of concrete

Progressive cracking is one of the most important nonlinear characteristics displayed by concrete (Fig. 3.15). Dealing with cracking of concrete, many ways of modelling can be found in literature, e.g. Discrete, Smeared, Orthogonal, Fixed, Rotating or Swinging, Fracture energy, Fictitious, Composite damage, Local, Nonlocal, Modified Voigt-Reuss, and Crack band model. These models can be classified into two distinct models; the discrete cracking model (Ngo and Scordelis 1967) and the smeared cracking model (Rashid 1968). Starting with one of the above two models, many attempts have been made to improve, modify, or develop a new crack model (e.g., Suidan and Schnobrich 1973; Phillips and Zienkiewicz 1976; Hillerborg, et al. 1976; Bazant and Oh 1983; Bazant and Lin 1988; Gajer and Dux 1988 and 1990; Yamaguchi and Chen 1990, and Dahlblom and Ottosen 1990).

A brief review of some of these models are presented in the following.

3.2.2.2.1 Discrete crack model:

In 1967, Ngo and Scordelis introduced the discrete crack model which is the first model used to represent the cracking for the finite element method. The discrete cracking model is a direct approach and simulates cracks by disconnecting the displacement at nodal points for adjoining elements (Fig. 3.16). The obvious difficulty in this approach is that the location and orientation of cracks are not known in advance so that geometrical restrictions imposed by the preselected finite element mesh can hardly be avoided. This can be rectified to some extent by redefinition of element nodes. However, such techniques are complex and time-consuming. Furthermore, the accuracy of stress at nodes is relatively poor in a finite element analysis (Yamaguchi and Chen 1990). These difficulties result in a rather limited acceptance of the use of discrete cracking representations in the finite element analysis of concrete structures. One of the recent discrete crack model is the fictitious crack model.

Fictitious crack model:

Crack Widths
Not to Scale

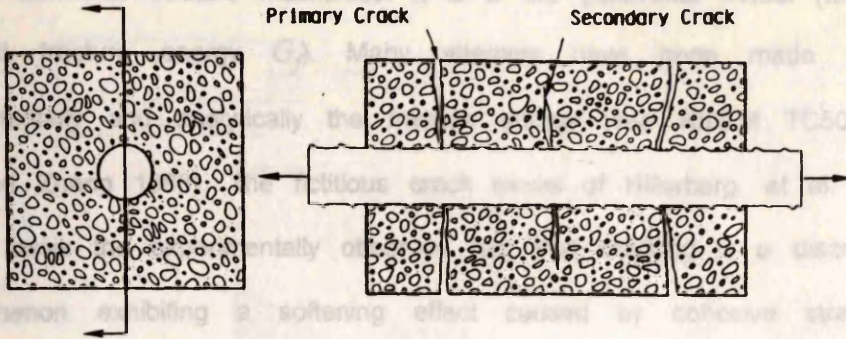
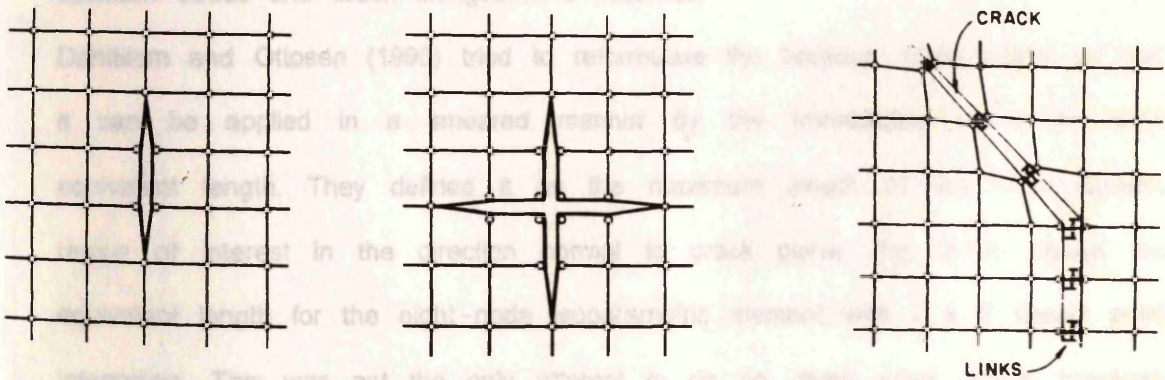


Fig. 3.15 Cracking of concrete.



Single crack

Double crack

Crack and aggregate interlock

Fig. 3.16 Discret cracking model.

Fictitious crack model:

The fictitious crack model, in its original form, is a discrete approach based on the nonlinear fracture mechanics. It is a two parameter model (tensile strength f_t' and fracture energy G_f). Many attempts have been made to determine experimentally and analytically the fracture energy (see RILEM TC50-FMC 1985; Wu and Zhang 1988). The fictitious crack model of Hillerborg, et al. (1976) takes as its basis the experimentally observed fact that cracking is a discrete, localized phenomenon exhibiting a softening effect caused by cohesive stresses in the microcracked region. For a concrete bar loaded in tension into its post-peak region, the fictitious crack model assumes that elastic unloading occurs over the entire length of the bar, and an additional elongation occurs in an infinitely thin cracked zone (Fig. 3.17). Instead of describing the cracking process by a relationship between stresses and strains, the fictitious crack model describes the behaviour of the infinitely thin cracking zone by a constitutive relation expressed in terms of normal stress σ and crack elongation normal to the crack plane w_c . Fig. 3.17 shows this description of the fictitious crack model where a linear relation between stress and crack elongation is assumed.

Dahlblom and Ottosen (1990) tried to reformulate the fictitious crack model so that it can be applied in a smeared manner by the introduction of a so-called equivalent length. They defined it as the maximum length of the finite element region of interest in the direction normal to crack plane. Fig. 3.17b shows the equivalent length for the eight-node isoparametric element with 2 x 2 Gauss point integration. This was not the only attempt to do so, there were others, however, they did not obtain entirely satisfactory results (Dahlblom and Ottosen 1990). For more information about fictitious crack model see Hillerborg, et al. (1976); and Dahlblom and Ottosen (1990).

Fig. 3.18 Tensile stress-strain curves for concrete

3.2.2.2.2 Smearred-crack model:

The first smeared crack model, which over the years became the most practical model for numerical analysis of fractured concrete, was introduced by Hillerborg (1988). The original idea of Hillerborg was to represent the effect of a

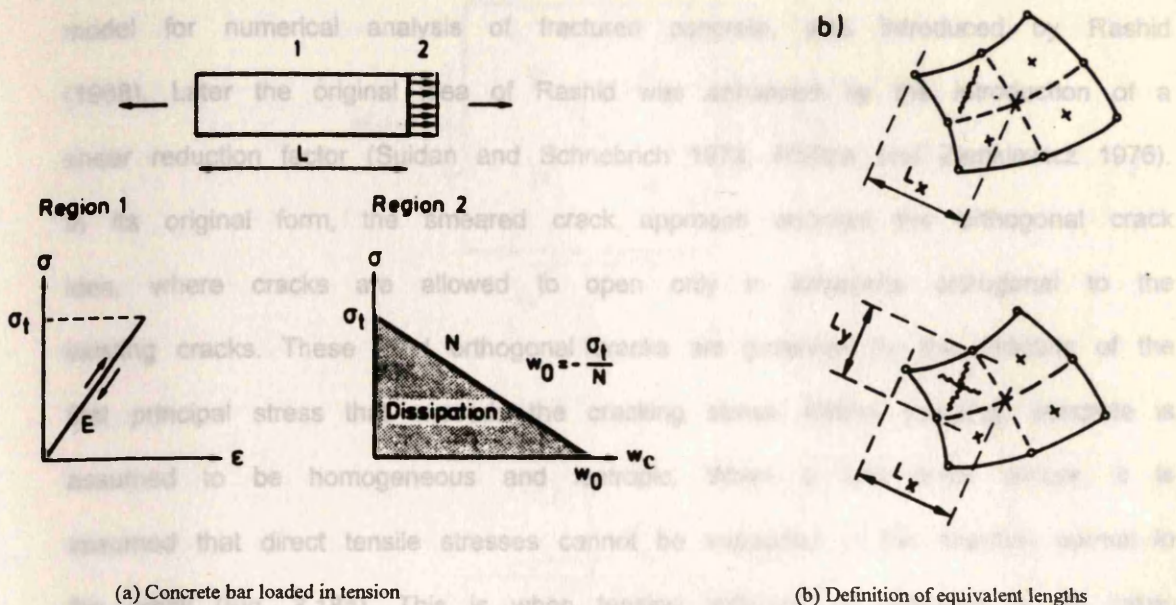


Fig. 3.17 Fictitious crack model (Hillerborg, et al. 1976).

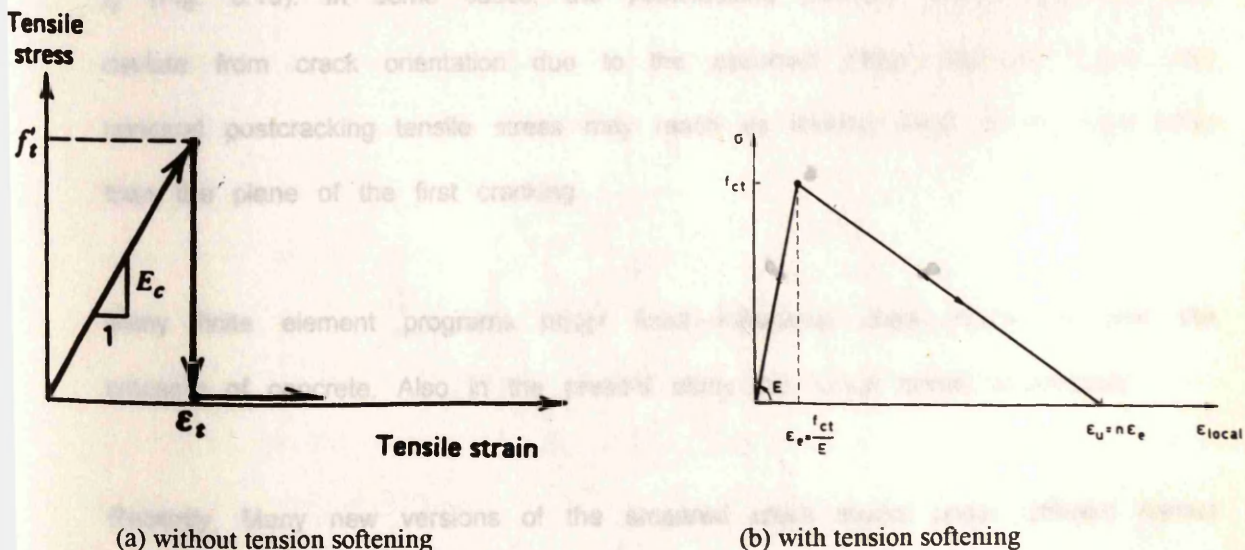


Fig. 3.18 Tensile stress-strain curves for concrete.

3.2.2.2 Smearred-crack model:

The first smeared crack model, which over the years became the most practical model for numerical analysis of fractured concrete, was introduced by Rashid (1968). Later the original idea of Rashid was enhanced by the introduction of a shear reduction factor (Suidan and Schnobrich 1973; Phillips and Zienkiewicz 1976). In its original form, the smeared crack approach adopted the orthogonal crack idea, where cracks are allowed to open only in directions orthogonal to the existing cracks. These fixed orthogonal cracks are governed by the direction of the first principal stress that exceeds the cracking stress. Before cracking, concrete is assumed to be homogeneous and isotropic. When a first crack occurs, it is assumed that direct tensile stresses cannot be supported in the direction normal to the crack (Fig. 3.18a). This is when tension stiffening or softening is not taken into account. But when it is taken into account, a value of tensile stress as a certain function of strain normal to the crack can be allowed to across the crack (Fig. 3.18b). On further loading, it is possible that new cracks will occur. Second crack occurs when the stress parallel to the first crack σ_t^* becomes greater than f_t' (Fig. 3.19). In some cases, the postcracking principal stress directions may deviate from crack orientation due to the assumed shear retention factor. The principal postcracking tensile stress may reach its limiting value on a plane other than the plane of the first cracking.

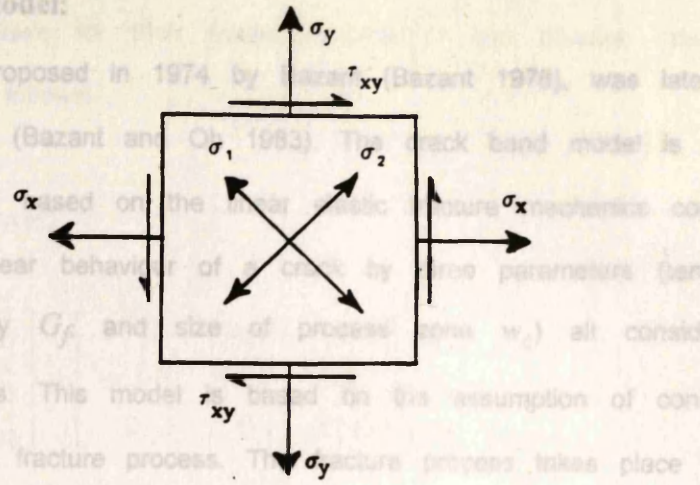
Many finite element programs adopt fixed-orthogonal crack model to treat the cracking of concrete. Also in the present study this crack model is adopted.

Recently, Many new versions of the smeared crack model under different names have been introduced. A brief review on two from these models is presented here.

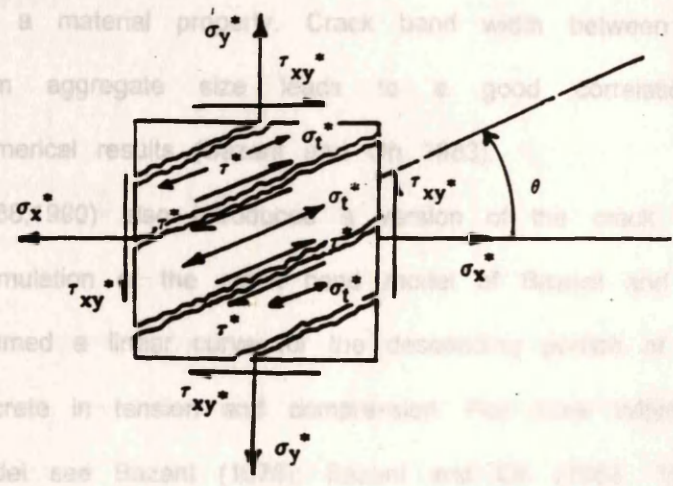
Fig. 3.19 Smearred-crack model

Crack band model:

This model proposed in 1974 by Bazant (Bazant 1978), was later called the crack band model (Bazant and Oh 1983). The crack band model is essentially a smeared approach based on the composite material mechanics concept, which describes the bilinear behavior of concrete by three parameters (tensile strength f_t , fracture energy G_f and size of process zone w_f) all considered to be material parameters. This model is based on the assumption of constant energy release during the fracture process. The fracture process takes place in bands of certain width called crack bands (Bazant and Oh 1983). The width of the crack



band is treated as a material property. Crack band width between 3 and 10 times the maximum aggregate size is a good correlation between experimental and numerical results. Gajer and Dux (1988) proposed a modification of the crack band model which yields the formulation of the crack band model. Gajer and Dux assumed a linear stress-strain curve of concrete in tension. For more information about the crack band model see Bazant (1988), Bazant and Oh (1983, 1984, 1985), Bazant and Pijaudier-Cabot (1988), Pijaudier-Cabot and Bazant (1987), Bazant and Oh (1988), Gajer and Dux (1988, 1990).



It is worth commenting that an application of the crack band model to problems is still not forth coming. Yamaguchi and Chen (1990) proposed a cracking model for the finite element analysis of crack propagation in concrete materials. Yamaguchi and Chen reported that the crack band model and the composite damage model (which is another crack model proposed by William

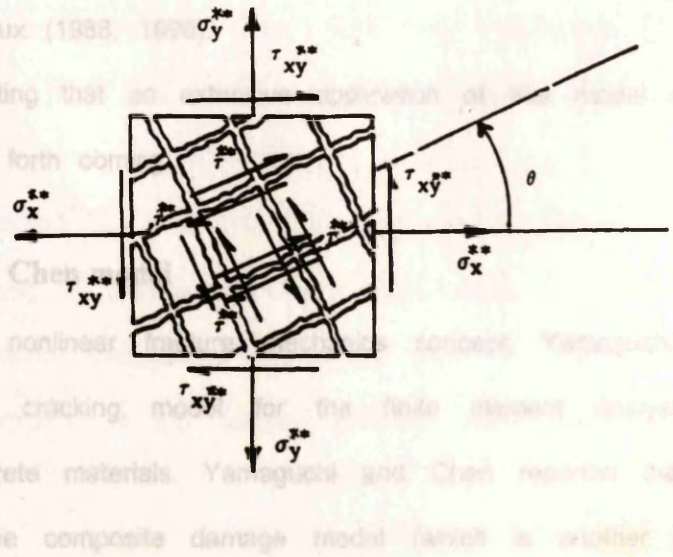


Fig. 3.19 Smeared-crack model

Crack band model:

This model proposed in 1974 by Bazant (Bazant 1976), was later called the crack band model (Bazant and Oh 1983). The crack band model is essentially a smeared approach, based on the linear elastic fracture mechanics concept, which describes the bilinear behaviour of a crack by three parameters (tensile strength f_t' , fracture energy G_f , and size of process zone w_c) all considered to be material parameters. This model is based on the assumption of constant energy release during the fracture process. The fracture process takes place in bands of certain width called crack bands (Bazant and Oh 1983). The width of the crack band is treated as a material property. Crack band width between 3 and 10 times the maximum aggregate size leads to a good correlation between experimental and numerical results (Bazant and Oh 1983).

Gajer and Dux (1988,1990) also introduced a version of the crack band model which yields the formulation of the crack band model of Bazant and Oh (1983). Gajer and Dux assumed a linear curve for the descending portion of the stress-strain curve of concrete in tension and compression. For more information about the crack band model see Bazant (1976); Bazant and Oh (1983, 1984); Bazant and Pijaudier-Cabot (1988); Pijaudier-Cabot and Bazant (1987); Bazant and Lin (1988); Gajer and Dux (1988, 1990).

It is worth commenting that an extensive application of this model on full-scale problems is still not forth coming.

Yamaguchi and Chen model

Based on the nonlinear fracture mechanics concept, Yamaguchi and Chen (1990) proposed a cracking model for the finite element analysis of crack propagation in concrete materials. Yamaguchi and Chen reported that the crack band model and the composite damage model (which is another crack model proposed by Willam, et al. in 1984) are special cases of the proposed model.

The constitutive laws for their model consists of two phases; intact layer and cracked layer as follows:

Phase *a* (intact layer)

$$\begin{Bmatrix} \varepsilon_{11}^a \\ \varepsilon_{22}^a \\ \gamma_{12}^a \end{Bmatrix} = \begin{bmatrix} 1/E & -\nu/E & 0 \\ -\nu/E & 1/E & 0 \\ 0 & 0 & 1/G \end{bmatrix} \begin{Bmatrix} \sigma_{11}^a \\ \sigma_{22}^a \\ \sigma_{12}^a \end{Bmatrix} \quad (3.6)$$

Phase *b* (cracked layer)

$$\begin{Bmatrix} \varepsilon_{11}^b \\ \varepsilon_{22}^b \\ \gamma_{12}^b \end{Bmatrix} = \begin{bmatrix} 1/E & -\nu/E & 0 \\ -\nu/E & 0 & 0 \\ 0 & 0 & 1/\beta G \end{bmatrix} \begin{Bmatrix} \sigma_{11}^b \\ \sigma_{22}^b \\ \sigma_{12}^b \end{Bmatrix} + \begin{Bmatrix} 0 \\ e(\sigma_{22}^b) \\ 0 \end{Bmatrix} \quad (3.7)$$

where β = the shear retention factor; and $e(\sigma_{22}^b)$ is the softening function, whose value increases as σ_{22}^b decreases. β is assumed to be constant. Directions 1 and 2 are the directions parallel and normal to the crack, respectively. The advantage of this model is that it does not place any restrictions on the form of the softening function (Yamaguchi and Chen only presumed linear softening behaviour). Equations (3.6) and (3.7) show that during the process of crack-opening, phase (*b*) experiences strain-softening behaviour due to cracking, whereas phase (*a*) is subjected to unloading behaviour. These behaviours have been observed experimentally by Gopalaratnam and Shah (1985).

The relationship between incremental stress and strain for this model which can be used in construction of the tangent stiffness matrix in a nonlinear finite element analysis is:

$$\begin{Bmatrix} d\sigma_{11} \\ d\sigma_{22} \\ d\sigma_{12} \end{Bmatrix} = \frac{1}{\Delta} \begin{bmatrix} 1/\bar{E} & \nu/E & 0 \\ \nu/E & 1/E & 0 \\ 0 & 0 & \bar{G}\Delta \end{bmatrix} \begin{Bmatrix} d\varepsilon_{11} \\ d\varepsilon_{22} \\ d\gamma_{12} \end{Bmatrix} \quad (3.8)$$

where

$$\begin{Bmatrix} d\sigma_{11} \\ d\sigma_{22} \\ d\sigma_{12} \end{Bmatrix} = \begin{bmatrix} E & 0 & 0 \\ 0 & 0 & 0 \\ 0 & 0 & 0 \end{bmatrix} \begin{Bmatrix} de \\ d\sigma_{22} \\ de \end{Bmatrix} \quad (3.9)$$

$$\bar{E} = \left(\frac{v^a}{E} + v^b \frac{de}{d\sigma_{22}} \right)^{-1}$$

$$\bar{G} = \frac{\beta G}{v^a \beta + v^b}$$

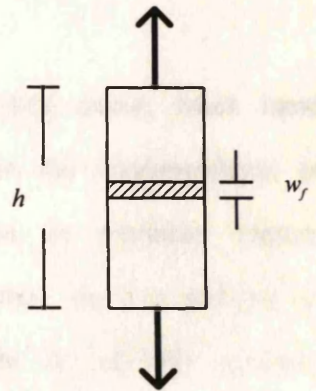
$$\Delta = \frac{1}{E\bar{E}} - \left(\frac{v}{E} \right)^2$$

v^a and v^b are the volume fractions and their summation is equal unity ($v^a + v^b = 1$)

$$v^a = \frac{V^a}{V} = \frac{\text{volume of uncracked zone}}{\text{total volume of the composite}}$$

$$v^b = \frac{V^b}{V} = \frac{\text{volume of cracked zone}}{\text{total volume of the composite}}$$

For example $v^b = \frac{w_f}{h}$ in this Figure.



If $e(\sigma_{22})$ & β (which are regarded as material properties) and v^a & v^b (which are not pure material properties, but they are influenced by the mesh size) are given together with elastic constants, all the variables in the stress-strain relationship are determined.

Yamaguchi and Chen took β as a constant and they reported that β makes no significant difference in the crack propagation process (Their example was a 90 x 90 mm rectangular solid made of mortar with a pre-existing flaw at the center).

When traction-free crack is developed, this cracked but homogenized region loses its load-carrying capacity in the direction perpendicular to the crack. Equation (3.8) becomes:

$$\begin{Bmatrix} d\sigma_{11} \\ d\sigma_{22} \\ d\sigma_{12} \end{Bmatrix} = \begin{bmatrix} E & 0 & 0 \\ 0 & 0 & 0 \\ 0 & 0 & \bar{G} \end{bmatrix} \begin{Bmatrix} d\varepsilon_{11} \\ d\varepsilon_{22} \\ d\gamma_{12} \end{Bmatrix} \quad (3.9)$$

and \bar{G} can be assumed equals zero if the shear transfers across the crack plane is neglected.

In crack band model, crack width and element width are made identical. If w_f assumed to be equal to the width of the cracked region, i.e. $v^b=1$, the model is the same as the crack band model (Bazant and Oh 1983). For more information see Yamaguchi and Chen (1990)

It can be seen that the above crack models (Fictitious crack model, crack band model, and Yamaguchi and Chen model) have focused on the implementation of tension softening of concrete into the crack model based on nonlinear fracture mechanics. Also these models have concentrated the attention on the analysis of crack propagation in fracture tests or localized effects, while no, or little, attention has been paid to analyse the main structure concrete elements (e.g. reinforced concrete beams, slabs, and panels).

3.2.2.3 Tension stiffening

When a reinforced concrete member is subjected to a sufficiently high tensile force, concrete cracks at discrete sections. The concrete between cracks continues to carry tensile stresses and offer stiffness. This phenomenon is called tension stiffening. Modelling of this phenomenon is important in studying the load-deformation characteristics of reinforced concrete structures in the post cracking range. Tension stiffening can be modelled in two ways. In the first method, the stress-strain curve of concrete is modified (Fig. 3.20). In the second method, a modified stress-strain curve for steel is used (Gilbert and Warner 1978, Fig. 3.21).

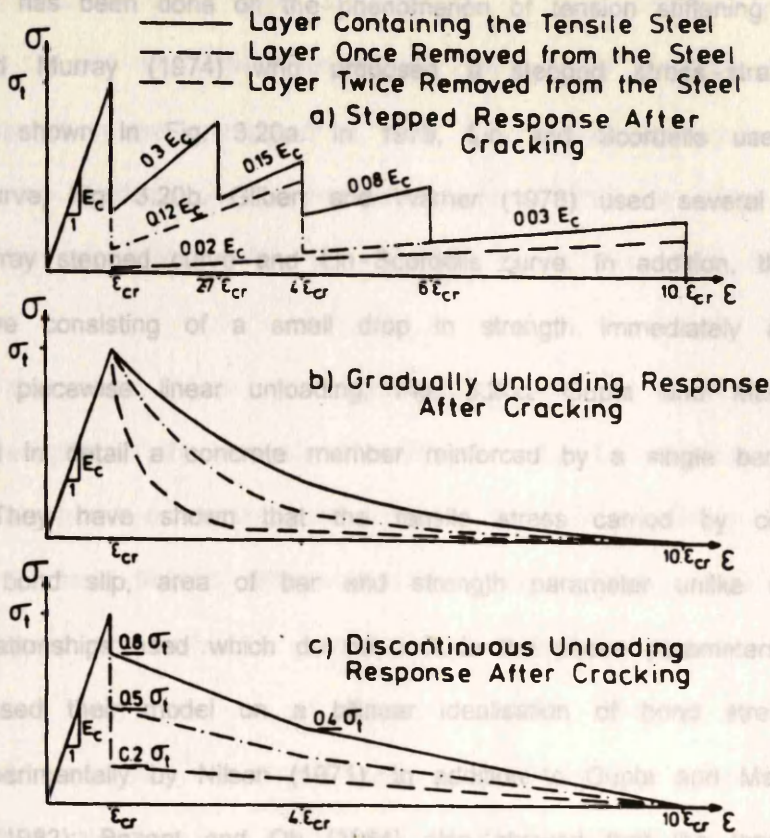
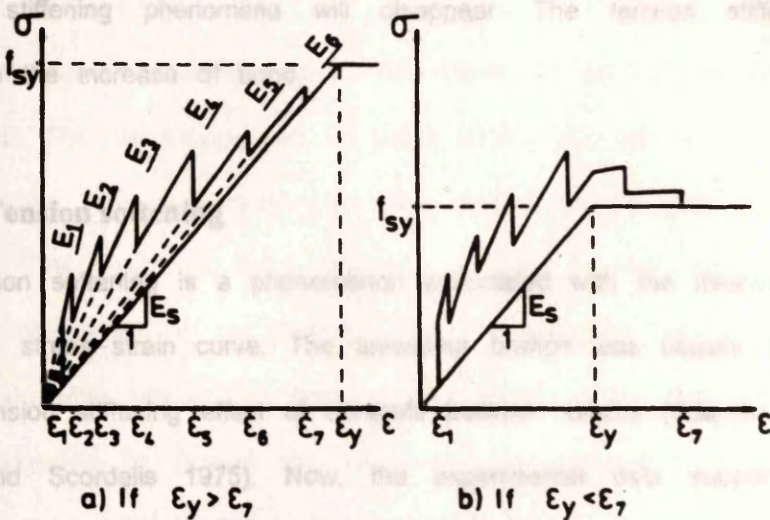


Fig. 3.20 Alternative stress-strain diagrams for concrete in tension.



Material Modelling Law :

E_1	E_2	E_3	E_4	E_5	E_6	E_7
E_{cr}	$1.5 E_{cr}$	$3 E_{cr}$	$5 E_{cr}$	$8 E_{cr}$	$11 E_{cr}$	$14 E_{cr}$

E_1	E_2	E_3	E_4	E_5	E_6
$4.0 E_s$	$27 E_s$	$20 E_s$	$16 E_s$	$11.5 E_s$	$10.5 E_s$

Fig. 3.21 Modified stress-strain diagrams for tension steel after cracking.

Much work has been done on the phenomenon of tension stiffening; starting with Scanlon and Murray (1974) who proposed a stepped stress-strain curve for concrete as shown in Fig. 3.20a. In 1975, Lin and Scordelis used a gradual unloading curve, Fig. 3.20b. Gilbert and Warner (1978) used several variations of Scanlon-Murray stepped curve and Lin-Scordelis curve. In addition, they employed a new curve consisting of a small drop in strength immediately after cracking followed by piecewise linear unloading, Fig. 3.20c. Gupta and Maestrini (1990) have studied in detail a concrete member reinforced by a single bar allowing for bond-slip. They have shown that the tensile stress carried by concrete is a function of bond slip, area of bar and strength parameter unlike many tension stiffening relationships used which do not include the above parameters. Gupta and Maestrini based their model on a bilinear idealisation of bond stress-slip curve obtained experimentally by Nilson (1971). In addition to Gupta and Maestrini, Floegl and Mang (1982); Bazant and Oh (1984) also showed that the tension stiffening is a function of bond slip. If there is no bond between the concrete and steel, the tension stiffening phenomena will disappear. The tension stiffening effect increases with the increase of bond.

3.2.2.4 Tension softening

The tension softening is a phenomenon associated with the descending branch of the tensile stress-strain curve. The unloading branch was usually introduced to model the tension stiffening effect of concrete between cracks (Scanlon and Murray 1974; Lin and Scordelis 1975). Now, the experimental data support the strain softening behaviour of concrete after the recent testing techniques enabled post-peak stress-strain curves to be obtained (Reinhardt 1985; Gopalaratnam and Shah 1985). Tension softening can exist in plain concrete subjected to tensile stress while tension stiffening is absent due to absence of reinforcement.

To derive a stress-strain curve for concrete in direct tension, two parameters are needed; G_f and w_c (Massicotte, et al. 1990). G_f is the fracture energy (the energy dissipated in the opening of a crack in a tension specimen (Fig. 3.22) is defined as the cracking energy per unit of area) which is equal to the area under a stress-elongation curve (Fig. 3.22b). w_c is the width of the fracture process zone.

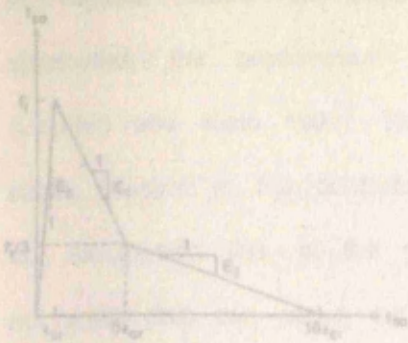
Fig. 3.23 shows some tensile stress-strain curves including tension softening which have been adopted in the analysis of reinforced concrete members. Massicotte, et al. (1990) introduced a stress-strain curve of concrete in tension based on the analysis of 52 tests from 5 different sources. This curve is trilinear with a linear ascending branch and a bilinear softening branch for concrete after cracking (Fig. 3.23a).

Recently, all the newly developed cracking models are including the tension softening in the modelling (e.g. crack-band model, fictitious-crack model; Yamaguchi and Chen model).

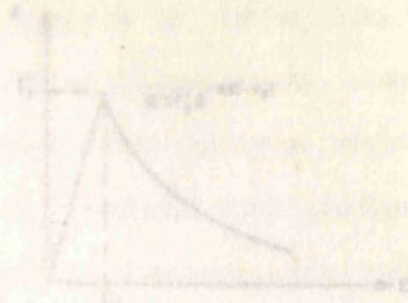
In the present thesis, a tensile stress-strain curve for concrete as shown in Fig. 3.24 is used. The ascending part is linear similar to any tensile stress-strain curve in literature. The descending part is a function of the strain normal to the crack plane. The proposed curve agrees with the trilinear stress-strain curve proposed by Massicotte, et al. (1990). Also the proposed curve has a certain maximum strain after which the tensile stress equals zero. This maximum strain has been suggested by Bazant and Lin (1988) to correspond to a point where the tensile stress normal to the crack reaches to 5% of the tensile strength.

3.2.3 Concrete in shear

Before the cracking of concrete, shear can be transmitted by the concrete continuum. In reinforced concrete structures subjected to shear, various internal mechanisms can be created to resist shear loading.



(a) Massicote, et al. (1990)



(b) L. Ueda, et al. (1987)

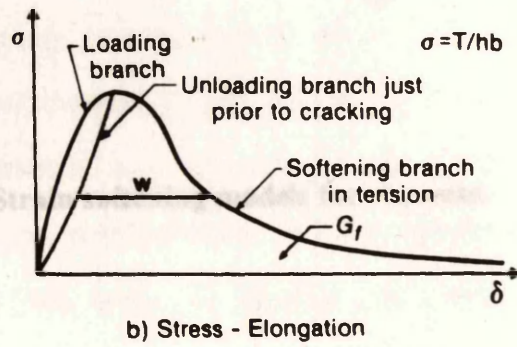
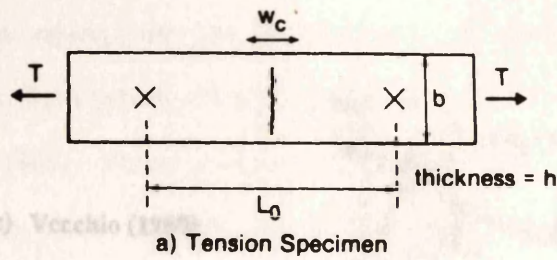


Fig. 3.23 Str

Fig. 3.22 Tension-specimen response

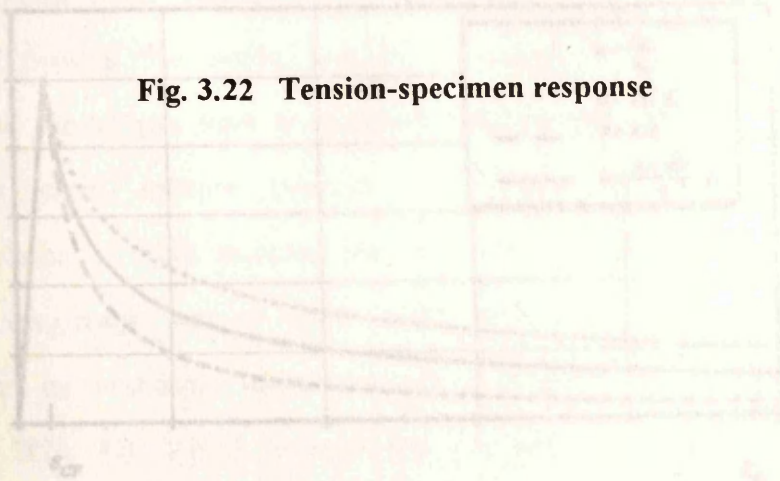
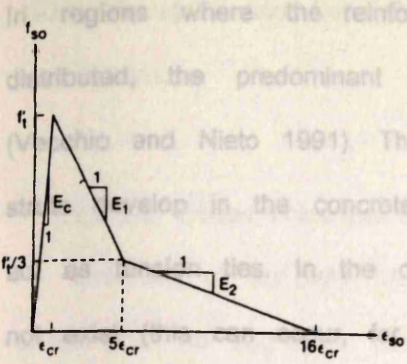
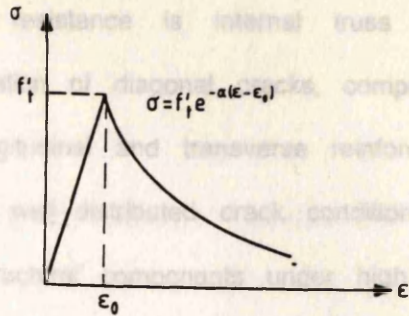


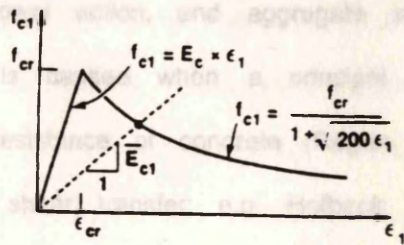
Fig. 3.24 Assumed strain softening model for concrete



(a) Massicte, et al. (1990)



(b) Cervera, et al. (1987)



(c) Vecchio (1989)

Fig. 3.23 Strain softening models for concrete.

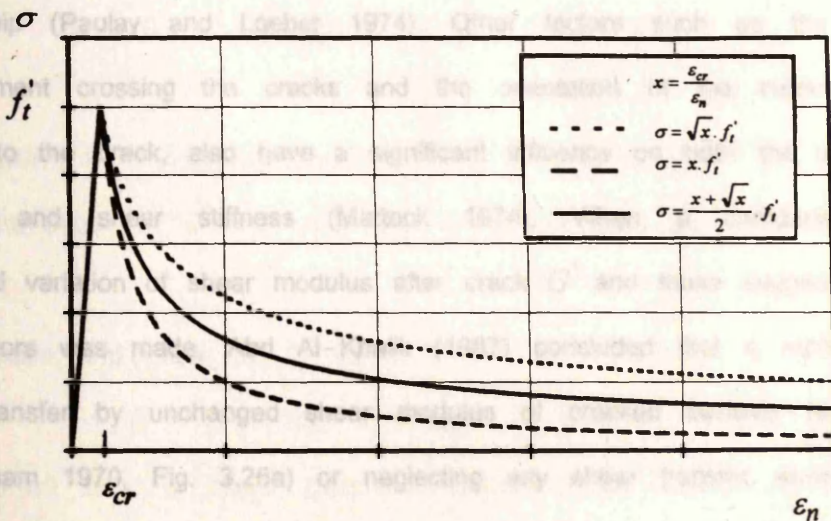


Fig. 3.24 Assumed strain softening model for concrete.

In regions where the reinforcement and ensuring crack conditions are well distributed, the predominant mechanism of resistance is internal truss action (Vecchio and Nieto 1991). Through the formation of diagonal cracks, compression struts develop in the concrete while the longitudinal and transverse reinforcement act as tension ties. In the case where the well-distributed crack condition does not exist (this can occur, for example, in structural components under high direct shear, such as corbels and ledger beams) strength can be governed by behaviour along a single plane or a dominant crack. Here, the mechanism of shear transfer is commonly seen as relying less on the formation of compression fields, and more on contributions from shear friction, dowel action, and aggregate interlock (Vecchio and Nieto 1991). Shear cracking is caused when a principal tensile stress due primarily to shear exceeds the resistance of concrete (Regan 1969). Many experiments have been done on the shear transfer; e.g. Hofbeck, et al. (1969), Taylor (1974), Swamy and Andriopoulos (1974), Mattock (1974), Paulay and Loeber (1974), Millard and Johnson (1984), Abd Al-Khalik (1987), Mphonde (1988). The most important observation from the physical tests is that the crack width has the largest influence on the shear stiffness, and the maximum size and shape of coarse aggregate does not seem to influence the shear stress-shear strain relationship (Paulay and Loeber 1974). Other factors such as the amount of reinforcement crossing the cracks and the orientation of the reinforcement with respect to the crack, also have a significant influence on both the ultimate shear strength and shear stiffness (Mattock 1974). When a comparison between measured variation of shear modulus after crack G' and those suggested by some investigators was made, Abd Al-Khalik (1987) concluded that a representation of shear transfer by unchanged shear modulus of cracked sections (e.g., Isenberg and Adham 1970, Fig. 3.25a) or neglecting any shear transfer across the crack (e.g., Cervenka 1970, Fig. 3.25b) is completely unrealistic. Also, he concluded that constant reduction of shear stiffness after cracking (e.g., Suidan and Schnobrich

1973; Yuzugullu and Schnobrich 1973, Fig. 3.25c) is only an approximation to the real behaviour.

3.2.3.1 Shear retention factor

Cracking of concrete usually occurs along the interface between the cement paste and the aggregate particles. The resulting rough cracks can transfer shear by aggregate interlock. In plain concrete the main shear transfer mechanism is aggregate interlock and in reinforced concrete dowel action will play a significant role. Both mechanisms are controlled by the width of crack, the shear transfer capacity being reduced as the width increases. The above mentioned mechanisms cannot be directly included in finite element analysis of reinforced concrete based on smeared representation of the cracks. In smeared crack model, the reduction in shear modulus across the plane of the crack is usually defined by the shear retention factor β . This factor is clearly associated with the contribution of the aggregate interlock to the shear resistance of the cracked regions.

Many equations have been reported in the literature to define β . For example:

- **Cedolin and DeiPoli (1977)** took the variation of shear modulus after cracking decreasing with the crack width and they assumed a linear dependence.

$$\beta = F (1 - \varepsilon / \varepsilon_c) \quad ; \quad 0 < \varepsilon < \varepsilon_c$$

$$\beta = 0 \quad ; \quad \varepsilon > \varepsilon_c$$

in which F = numerical constant; ε = fictitious strain in the direction normal to the crack; ε_c = limit value after which aggregate interlock becomes zero = 0.005.

- **Arnesen, et al (1980)** took β as

$$\beta = (1 - 0.25 \lambda / \lambda_0)$$

in which λ is a scalar parameter related to the inelastic dilatancy (volume change).

- **Chang, et al. (1987)** took β as

$$\beta = k \cdot \sigma'_n / \sigma_n > \beta_{min} \quad \text{for } \sigma'_n / \sigma_n > -1$$

$$= k \quad \text{for } \sigma'_n / \sigma_n < -1$$

in which k, σ_n = material constants to define shear behaviour; σ'_n = a normal stress acting on the cracked plane (negative value represents compression); β_{min} = a minimum value of β , and they took $\beta_{min} = 0.1$; $\beta_{max} = 0.5$; and $\sigma_n = 0.5 f'_c$.

- **Cervera, Hinton and Hassan (1987)** took the following value

$$\beta = 1 - (\varepsilon / 0.005)^{kl}$$

where ε is the fictitious tensile strain normal to the crack plane, and kl is a parameter in the range of 0.3 - 1.0.

- **Balakrishnan and Murray (1988)** took β as

$$\beta = (\varepsilon_{gt} - \varepsilon) / (\varepsilon_{gt} - \varepsilon_{cr}) > \beta_{min};$$

$$\beta_{min} = 0.05$$

where ε_{cr} = extensional cracking strain; ε_{gt} = strain intercept at zero shear modulus; and ε = average extensional strain.

- Unlike the above, **Bedard and Kotsovos (1985)**, **Yamaguchi and Chen (1990)**, and **Vidosa, et al. (1991)** assumed that aggregate interlock plays a negligible role in load-carrying capacity of a member and this was reflected in their model by taking $\beta = \text{Constant (non-zero)}$ only in order to avoid excessive deterioration of the stiffness matrix.

In this study, the effect of shear retention factor on the prediction will be studied by taking β as a function of the tensile strain normal to the crack as follows

$$\beta = B \varepsilon_{cr} / \varepsilon_n > \beta_{min} \quad (3.10)$$

where ε_{cr} is the tensile crack strain; ε_n is the fictitious tensile strain normal to the crack plane; and B & β_{min} are numerical constants. Four values for these two constants will be studied in this thesis (Fig. 3.25e-h).

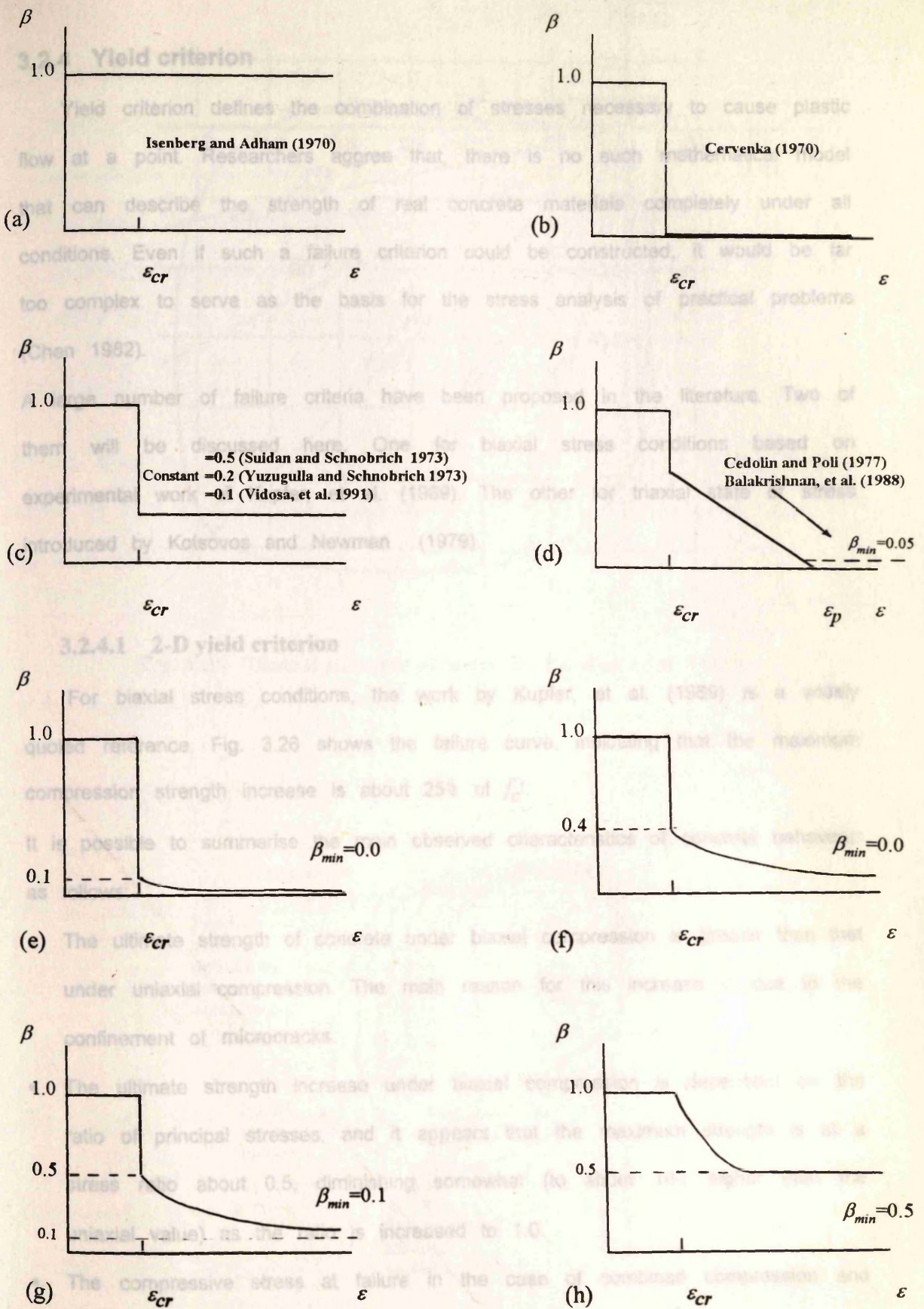


Fig. 3.25 Shear retention factor β .

3.2.4 Yield criterion

Yield criterion defines the combination of stresses necessary to cause plastic flow at a point. Researchers agree that, there is no such mathematical model that can describe the strength of real concrete materials completely under all conditions. Even if such a failure criterion could be constructed, it would be far too complex to serve as the basis for the stress analysis of practical problems (Chen 1982).

A large number of failure criteria have been proposed in the literature. Two of them will be discussed here. One for biaxial stress conditions based on experimental work of Kupfer, et al. (1969). The other for triaxial state of stress introduced by Kotsovos and Newman (1979).

3.2.4.1 2-D yield criterion

For biaxial stress conditions, the work by Kupfer, et al. (1969) is a widely quoted reference. Fig. 3.26 shows the failure curve, indicating that the maximum compression strength increase is about 25% of f_c' .

It is possible to summarise the main observed characteristics of concrete behaviour as follows:

- The ultimate strength of concrete under biaxial compression is greater than that under uniaxial compression. The main reason for this increase is due to the confinement of microcracks.
- The ultimate strength increase under biaxial compression is dependent on the ratio of principal stresses, and it appears that the maximum strength is at a stress ratio about 0.5, diminishing somewhat (to about 16% higher than the uniaxial value) as the ratio is increased to 1.0.
- The compressive stress at failure in the case of combined compression and tension decreases as the tensile stress increases.

Fig. 3.27 Yield surface zones, initial, intermediate and failure envelop.

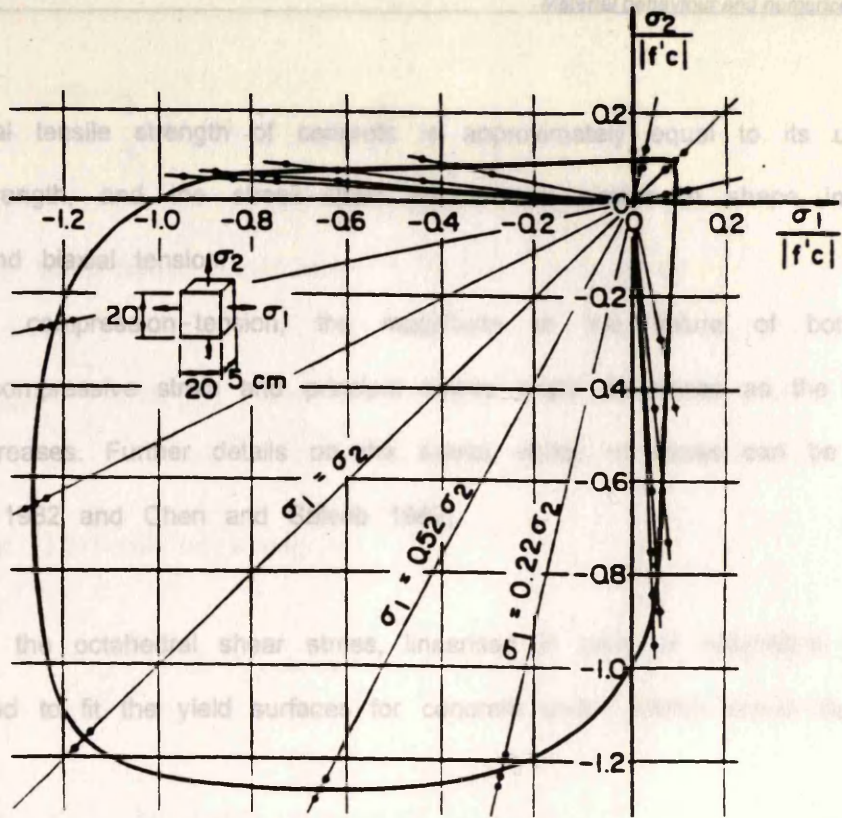


Fig. 3.26 Biaxial strength of concrete (Kupfer, et al. 1969).

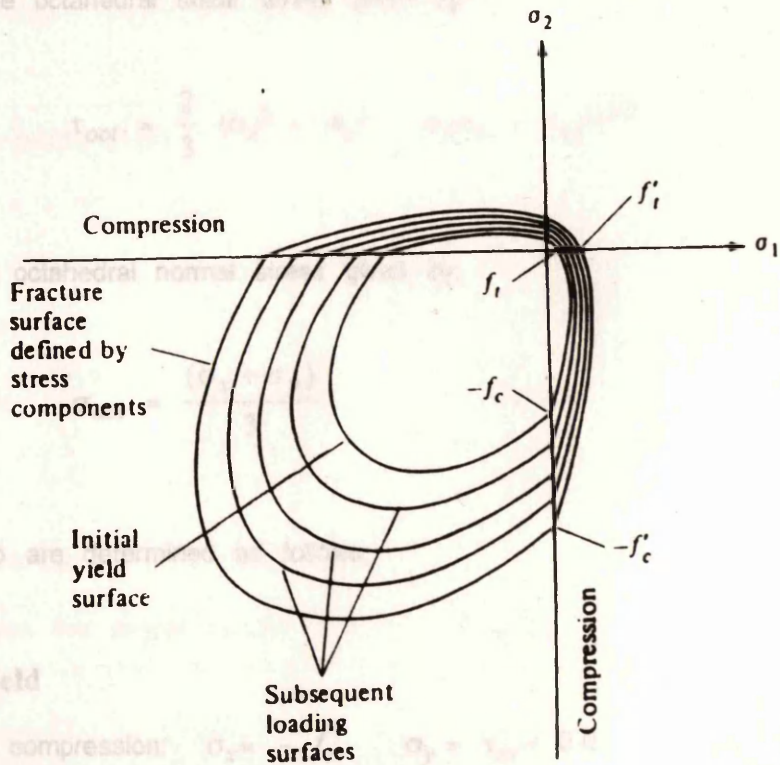


Fig. 3.27 Yield surface zones, initial, intermediate and failure envelop.

- The biaxial tensile strength of concrete is approximately equal to its uniaxial tensile strength, and the stress-strain curves are similar in shape in both uniaxial and biaxial tension.
- In biaxial compression-tension, the magnitude at the failure of both the principal compressive strain and principal tensile strain decreases as the tensile stress increases. Further details on the biaxial states of stress can be found in (Chen 1982 and Chen and Saleeb 1982).

In this study the octahedral shear stress, linearised in term of octahedral normal stress, is used to fit the yield surfaces for concrete under biaxial stress states in the form

$$\tau_{oct} = a + b \sigma_{oct} \quad (3.11)$$

where τ_{oct} is the octahedral shear stress given by:

$$\tau_{oct} = \frac{2}{3} (\sigma_x^2 + \sigma_y^2 - \sigma_x \sigma_y + \tau_{xy}^2)^{1/2}$$

and σ_{oct} is the octahedral normal stress given by:

$$\sigma_{oct} = \frac{(\sigma_x + \sigma_y)}{3}$$

The factors a, b are determined as follows.

Compression yield

1- For uniaxial compression: $\sigma_x = -f_c'$, $\sigma_y = \tau_{xy} = 0.0$

$$\tau_{oct} = \frac{2}{3} f_c' \quad \text{and} \quad \sigma_{oct} = \frac{-f_c'}{3}$$

Substituting in equation (3.11) we get:

To accommodate the change in stiffness of concrete, equation 3.3 is incrementally linearized during loading by assuming intermediate surfaces similar to

2- For biaxial compression: $\sigma_x = \sigma_y = -1.16 f_c'$, $\tau_{xy} = 0.0$ Fig. 3.27. The

first loading surface corresponds to the initial discontinuity in the stress-strain diagrams. The intermediate surfaces are of the same shape of limiting yield surface. Johany (1973) proposes the following equation:

Thus equation (3.11) can be written as:

$$f_{cc} = f_{co} - f_t + (B_d/E_d) f_t \quad (3.10)$$

$$\frac{2}{3}(1.16 f_c') = a - \frac{2}{3}(1.16 f_c') b$$

where f_{cc} = intermediate concrete strength, f_{co} = tensile strength of concrete, E_d = modulus of elasticity of concrete and B_d = instantaneous

Solving for a and b, the biaxial compression yield criterion is given by:

$$\frac{\sigma_x}{f_c'} + \left(0.1714 \frac{\sigma_{oct}}{f_c'} - 0.4143 \right) = 0.0 \quad (3.12)$$

Tension-Compression Yield

$$\sigma_x = -f_c', \quad \sigma_y = f_t = m f_c'$$

Using the same procedure, we obtain:

$$\frac{\tau_{oct}}{f_c'} + \frac{\sqrt{2}(1-m)}{(1+m)} \frac{\sigma_{oct}}{f_c'} - \frac{2\sqrt{2}}{3} \frac{m}{(1+m)} = 0.0 \quad (3.13)$$

3.2.4.2 3-D yield criterion

Tension-Tension Yield

For biaxial tension the simple circular criterion is adopted.

$$\left(\frac{\sigma_1}{f_t'} \right)^2 + \left(\frac{\sigma_2}{f_t'} \right)^2 - 1.0 = 0.0 \quad (3.14)$$

where σ_1 and σ_2 are the principal stresses.

To accommodate the early changes in the stiffness of concrete, equation 3.3 is incrementally linearized during loading by assuming intermediate surfaces similar to that used by Chen and Teng (1980). Such surfaces are shown in Fig. 3.27. The first loading surface corresponds to the initial discontinuity in the stress-strain diagram. The subsequent loading surfaces are assumed to have the same shape of limiting yield surface. Johany (1979) proposed the following equation:

$$f_{cc} = f_{co} - f_t' + (E_c' / E_i) f_t' \quad (3.15)$$

where f_{cc} = intermediate concrete strength, $f_{co} = 0.5 f_c'$, f_t' = tensile strength of concrete, E_c = modulus of elasticity of concrete, and E_i = instantaneous modulus of elasticity of concrete. Up to the peak strain ϵ_p , the concrete instantaneous modulus is computed using equation 3.3 and for strain above this value the following expression is used up to the assumed crushing strain (0.0035).

$$E_i = f_c' / \epsilon_i \quad (3.16)$$

Concrete is considered to be crushed if the failure criteria is violated or, if the principal compressive strain exceeds the ultimate compressive strain $\epsilon_{max} = 0.0035$.

3.2.4.2 3-D yield criterion

Under triaxial loading, experiments indicate that concrete has a fairly consistent failure surface that is a function of the three principal stresses. If isotropy is assumed, the elastic limit (onset of stable crack propagation), the onset of unstable crack propagation, and the failure limit all can be represented as surfaces in three-dimensional principal-stress space (Chen 1982). To reasonable accuracy, constitutive equations (mathematical formulae) for concrete can be incorporated into theoretical models without much difficulty. One of these constitutive equations used

in the 3-D finite element to model concrete compressive triaxial behaviour, is due to Kotsovos, et al. (Kotsovos and Newman 1979; Kotsovos 1979), as shown in Figs. 3.28, 3.29.

Kotsovos developed a mathematical description of the ultimate strength envelope of concrete under axisymmetric stress states by analysing experimental data from a comprehensive programme of investigation into the behaviour of concrete under complex states of stresses. A brief review of this is given below

For the construction of the constitutive equations for concrete, the geometrical representation of the stress state at a point is very useful. Since the stress tensor σ_{ij} has six independent components, it is of course possible to consider these components as positional co-ordinates in a six-dimensional space. However it is too difficult to deal with. The simplest alternative is to take the three principal stresses $\sigma_1, \sigma_2, \sigma_3$ such that $\sigma_1 > \sigma_2 > \sigma_3$ as co-ordinates and represent the stress state at a point in the three dimensional stress space. This orthogonal co-ordinate system $\sigma_1, \sigma_2, \sigma_3$ can be transformed into a cylindrical co-ordinate system z, r, θ and the two system are related by the following equations:

$$z = (\sigma_1 + \sigma_2 + \sigma_3) / \sqrt{3} = \sqrt{3} \sigma_{oct}$$

$$r = \frac{1}{\sqrt{3}} \sqrt{(\sigma_1 - \sigma_2)^2 + (\sigma_2 - \sigma_3)^2 + (\sigma_3 - \sigma_1)^2}$$

$$r = \sqrt{3} \tau_{oct}$$

$$\cos\theta = \frac{1}{r\sqrt{6}} (\sigma_1 + \sigma_2 - 2\sigma_3)$$

where σ_{oct} and τ_{oct} are the normal and shear octahedral stresses, respectively. The variables z and r define the hydrostatic and deviatoric components respectively, of a stress state. The variable θ defines the direction of the deviatoric components on the octahedral plane as shown in Fig.3.28 and varies from

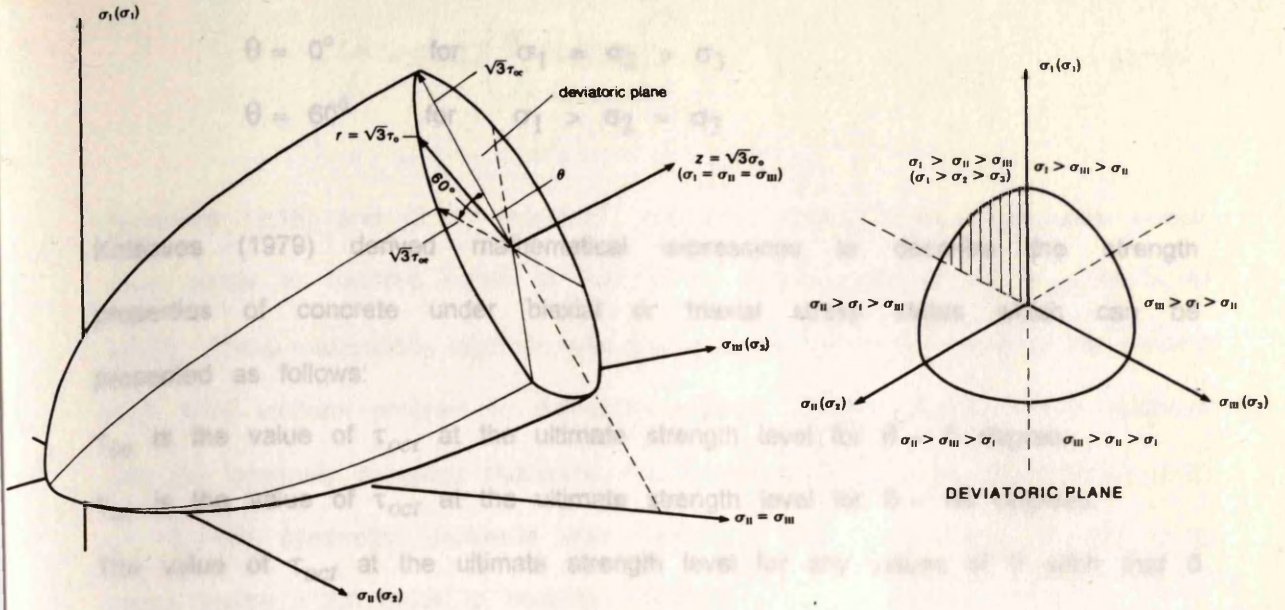


Fig. 3.28 Schematic representation of the ultimate strength surface - definitions.

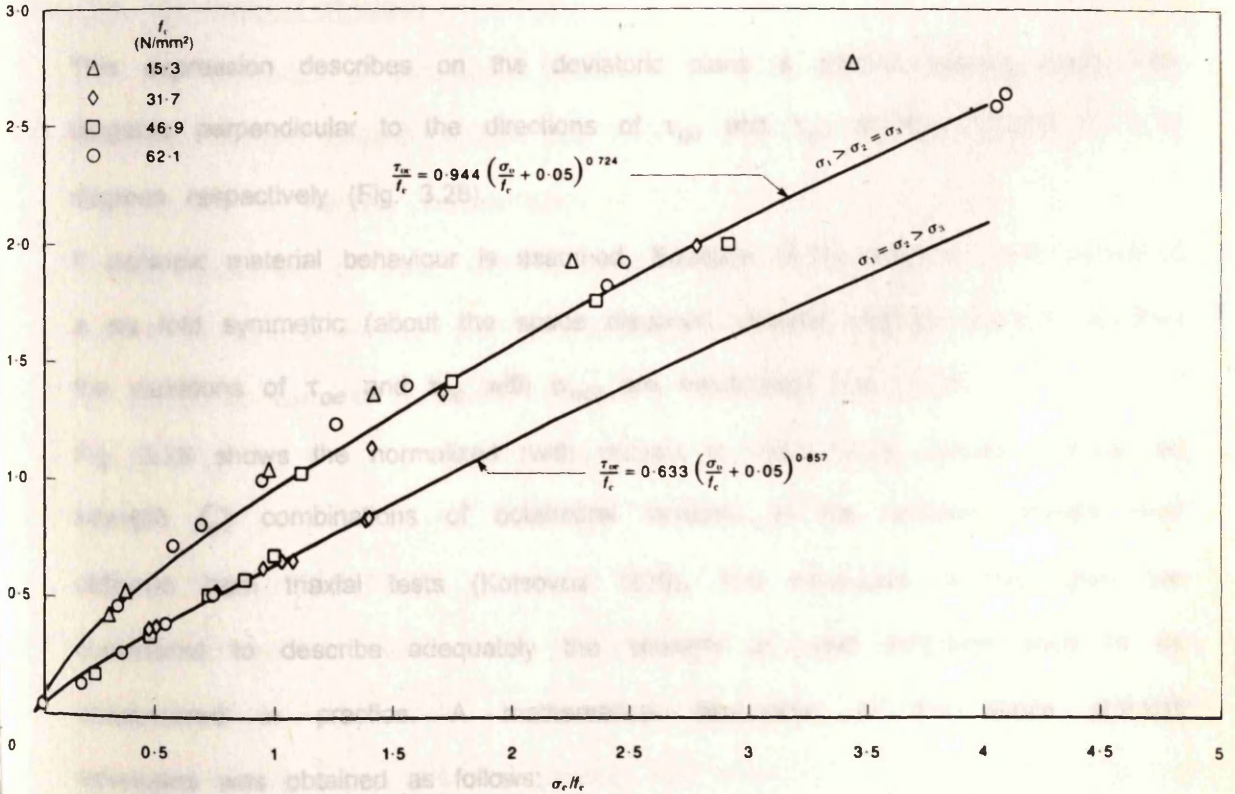


Fig. 3.29 Combinations of octahedral stresses at ultimate strength for concrete under the axisymmetric stress states ($\sigma_1 > \sigma_2 = \sigma_3$ and $\sigma_1 = \sigma_2 > \sigma_3$).

$$\begin{aligned} \theta &= 0^\circ & \text{for } \sigma_1 = \sigma_2 > \sigma_3 \\ \theta &= 60^\circ & \text{for } \sigma_1 > \sigma_2 = \sigma_3 \end{aligned} \quad (3.19)$$

Kotsovos (1979) derived mathematical expressions to describe the strength properties of concrete under biaxial or triaxial stress states which can be presented as follows:

τ_{oe} is the value of τ_{oct} at the ultimate strength level for $\theta = 0$ degree;

τ_{oc} is the value of τ_{oct} at the ultimate strength level for $\theta = 60$ degrees.

The value of τ_{oct} at the ultimate strength level for any values of θ such that $0 < \theta < 60$ degrees may be given by the following expression:

$$\tau_{oct} = \frac{2\tau_{oc}(\tau_{oc}^2 - \tau_{oe}^2)\cos\theta + \tau_{oc}(2\tau_{oe} - \tau_{oc})\sqrt{4(\tau_{oc}^2 - \tau_{oe}^2)\cos^2\theta + 5\tau_{oe}^2 - 4\tau_{oc}\tau_{oe}}}{4(\tau_{oc}^2 - \tau_{oe}^2)\cos^2\theta + (\tau_{oc} - 2\tau_{oe})^2} \quad (3.17)$$

3.3 Modelling of steel

This expression describes on the deviatoric plane a smooth convex curve with tangents perpendicular to the directions of τ_{oe} and τ_{oc} at $\theta = 0$ and $\theta = 60$ degrees respectively (Fig. 3.28).

If isotropic material behaviour is assumed, Equation (3.17) may be used to define a six-fold symmetric (about the space diagonal) ultimate strength surface, provided the variations of τ_{oe} and τ_{oc} with σ_{oct} are established (Fig. 3.28).

Fig. 3.29 shows the normalized (with respect to the uniaxial cylinder compressive strength f_c') combinations of octahedral stresses at the ultimate strength level obtained from triaxial tests (Kotsovos 1979). The envelopes in this figure are considered to describe adequately the strength of most concretes likely to be encountered in practice. A mathematical description of the above strength envelopes was obtained as follows:

$$\frac{\tau_{oc}}{f_c} = 0.944 \left(\frac{\sigma_o}{f_c} + 0.05 \right)^{0.724} \quad (3.18)$$

$$\frac{\tau_{oe}}{f_c} = 0.633 \left(\frac{\sigma_o}{f_c} + 0.05 \right)^{0.857} \quad (3.19)$$

Equations (3.18) and (3.19) represent two open ended convex envelopes whose slope tends to become equal to that of the space diagonal as σ_{oct} tends to infinity. These expressions together with the equation (3.17) are used in the present 3-D finite element program to define an ultimate strength surface which conforms with the generally accepted (Kotsovos and Newman 1979) shape requirements such as six-fold symmetry, convexity with respect to the space diagonal, and open ended shape which tends to become cylindrical as σ_{oct} tends to infinity.

The above mathematical formulae are applicable to a range of concretes with uniaxial cylinder compressive strength f_c' varying from about 15 to 65 MPa.

3.3 Modelling of steel

The derivation of constitutive equations for reinforcing bars is, compared with concrete, straight forward because the material behaviour is essentially uniaxial and well-known. A bilinear representation is fully adequate to simulate the elasto-plastic behaviour of steel with or without strain hardening (Fig. 3.30). Three alternative approaches are used in modelling the reinforcement in a prestressed or a reinforced concrete structure: smeared model, discrete model, and embedded model (Fig. 3.31).

3.3.1 Smeared model:

In this model, reinforcement is assumed to be distributed over the concrete element (Fig. 3.31a). This model is convenient for structures where a large number of reinforcing bars are placed. This model is widely used in reinforced concrete plate and shell structures, in which the structure is divided into layers. This approach was first adopted by Wegmuller (1974).

3.3.2 Discrete model:

In the discrete model, reinforcing bars are modelled as special elements connected to the concrete element by springs to allow for bond-slip (Fig. 3.31b). The reinforcing bar element can be a one-dimensional element. In this case, the bar element is superimposed on the two-dimensional element by assuming that the bar is pin-connected with two degrees of freedom at each end. Alternatively, discrete beam element can be used in which the steel is assumed to be capable of resisting axial force, shear force and bending moment. This case is for heavy bars for which bending is a significant effect. Ngo and Scordelis (1967) used constant strain triangular element for both concrete and steel in the analysis of reinforced concrete beams. Also Cedolin and Polì (1977) used the same element to allow for the longitudinal element to resist the shearing force (dowel action). The discrete model has the advantage of representing material properties more precisely. The finite element method is independent of the finite element mesh, and also different kinds of elements at different nodes can be represented. But the disadvantage is that this model does not consider Cracking, bond-slip, and other aspects related to the concrete behaviour of reinforced concrete.

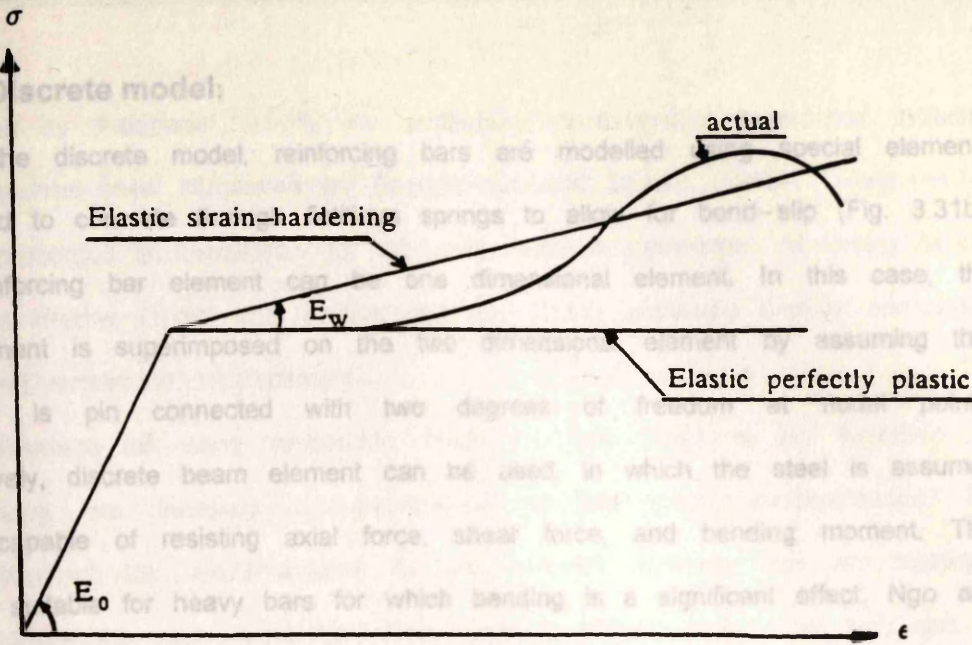
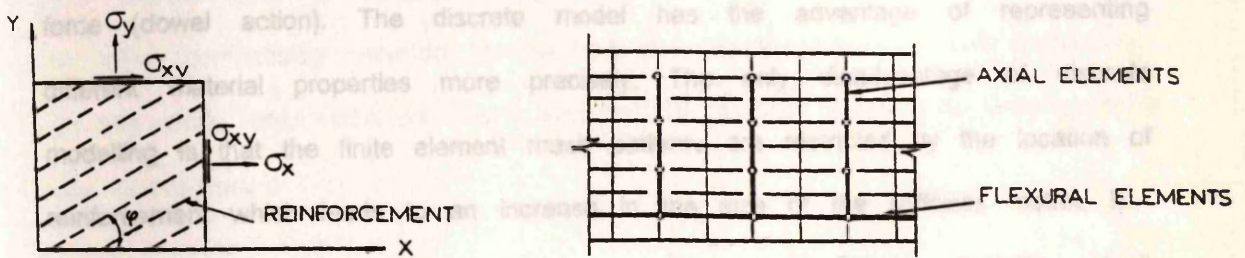
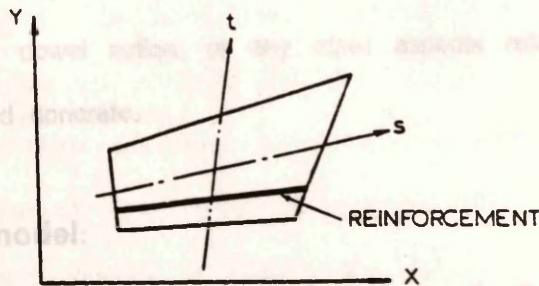


Fig. 3.30 Assumed steel laws.



a) Smearred Approach

b) discrete representation



c) Embedded bars

Fig. 3.31 Alternative representation of steel.

3.3.2 Discrete model:

In the discrete model, reinforcing bars are modelled using special elements connected to concrete through fictitious springs to allow for bond-slip (Fig. 3.31b). The reinforcing bar element can be one dimensional element. In this case, the bar element is superimposed on the two dimensional element by assuming that the bar is pin connected with two degrees of freedom at nodal points. Alternatively, discrete beam element can be used, in which the steel is assumed to be capable of resisting axial force, shear force, and bending moment. This case is suitable for heavy bars for which bending is a significant effect. Ngo and Scordelis (1967) used constant strain triangular element for both concrete and steel in the analysis of reinforced concrete beams. Also Cedolin and Poli (1977) used the same element to allow for the longitudinal reinforcement to resist the shearing force (dowel action). The discrete model has the advantage of representing different material properties more precisely. The only disadvantage of discrete modelling is that the finite element mesh patterns are restricted by the location of reinforcement which leads to an increase in the size of the stiffness matrix. El-Mezaini and Citipitioglu (1991) presented a technique for discrete modelling which allows for the reinforcement of arbitrary type and location to be represented independent of the finite element mesh, and also different bond conditions at different nodes can be represented. But the disadvantage is that this model does not consider Cracking, dowel action, or any other aspects related to the nonlinear behaviour of reinforced concrete.

3.3.3 Embedded model:

To overcome the problem of mesh dependency in the discrete model, a number of embedded formulations were introduced. Phillips and Zienkiewicz (1976) developed an embedded representation provided that the reinforcing bar is aligned with one of the local isoparametric element co-ordinate axes. A model similar to Phillips and Zienkiewicz model, but modified to account for inclined bars has been

introduced by Ranjbaran (1991). An embedded reinforcement formulation including bond-slip has been introduced by Balakrishnan and Murray (1986). Chang, et al. (1987) presented a formulation for arbitrarily oriented embedded reinforcing layers. Elwi and Hrudey (1989) and Phillips and Wu (1990) published another formulation for curved embedded reinforcement.

The advantage of using embedded model is that there is no limitation for representing the locations or distributions of the steel reinforcements. The contribution of the reinforcements to the element stiffness can be evaluated independently for each steel bar. The element stiffness matrix of bar can be introduced using the virtual work principle based on the following assumptions:

- Reinforcing bar has stiffness contribution only in the longitudinal direction.
- Reinforcement is straight and it has a constant cross-section area.
- Full compatibility between the bar and the isoparametric element of concrete.

In this work, only reinforced bars lying parallel to the co-ordinate axes x or y are considered.

3.4 Interaction between concrete and steel

3.4.1 Bond-slip

Bond means transferring of force from the steel bar to the surrounding concrete and vice versa. This bond results from chemical adhesion, friction and mechanical interaction between concrete and reinforced bars. In deformed bars, ribs or lugs add to the bond resistance by bearing on the concrete and thereby minimizing slip considerably (Fig. 3.32). A common way to describe the bond between steel bar and concrete is through the relation between the local bond stress and the relative slip of the bar. Bond stress is the shearing stress on the steel-concrete interface and parallel to the bar axis.

Bond is a complicated phenomena that is influenced by concrete strength, embedment length, concrete cover, bar spacing, stirrups, and associated shear and flexure (Kemp 1986). The location, spacing, and width of cracks; internal

distribution of forces; tensile stiffening contribution of concrete between the primary cracks; and strength of the member relate directly to the characteristics of the interface (Jiang, et al. 1984). Fig. 3.33 shows three types of bond failure in reinforced concrete beams (Kemp 1986).

Many experiments with different approaches have been performed to measure the bond-stress and bond-slip along the steel bar (Perry and Thompson 1966; Abeles 1966; Jiang, et al. 1984; Brettmann, et al. 1986; Kemp 1986; Lahnert, et al. 1986; and Altowajji, et al. 1986). Fig. 3.34 shows an experimental relationship between local bond stress and local bond slip (Houde and Mirza 1974). Also, many attempts to develop an analytical method to determine the bond stress-slip relationship have been done (Jiang, et al. 1984; Yankelevsky 1984; Yannopoulos and Tassios 1991). Not only general agreement is lacking among researchers on the relative influence of various parameters affecting the bond-slip relationship but also the local bond stress-slip relationships obtained by the researches based on tests show considerable scatter.

Using 2-D finite element model, Balakrishnan, et al. (1988) took the bond-slip into account when they predicted the behaviour of five beams without shear reinforcement and they have got some improvement in the prediction (-6, 0, -15, -14, +9% of the experimental failure loads). However, they did not report any result for beams with shear reinforcement despite the fact that they analysed four beams with shear reinforcement.

In this study full bond has been assumed.

3.4.2 Dowel action

When major shear deformations occur after tension cracking has occurred, reinforcing bars passing through this crack act as dowels. As a result, the bars will be subjected to concentrated shear force. The shear deformations are resisted by dowel action of the reinforcing bars and the aggregate interlock between the two rough faces of the interface crack.

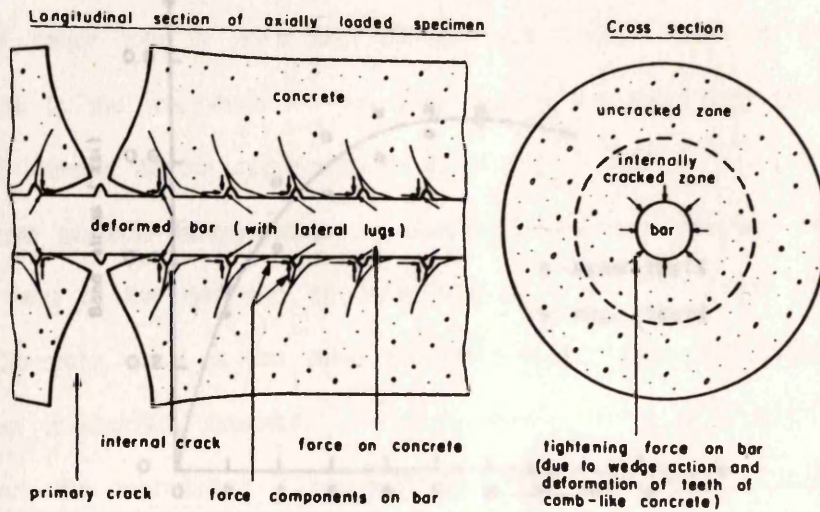


Fig. 3.32 Deformation of concrete around reinforcing bars (after formation of internal cracks).

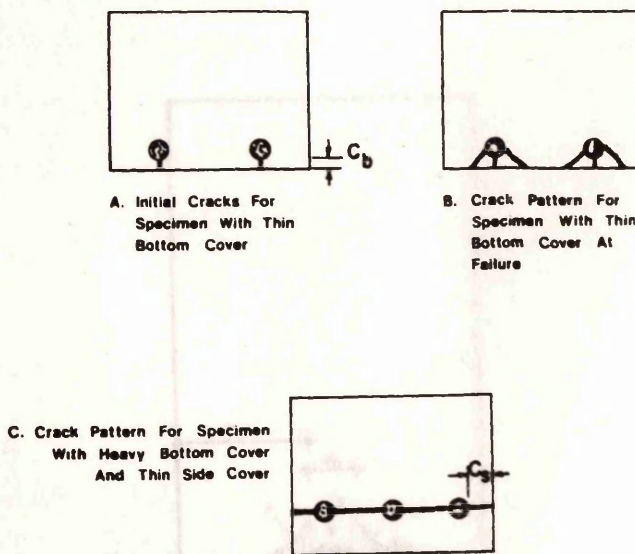


Fig. 3.33 Typical bottom and side bond-splitting cracks (Kemp 1986).

Fig. 3.35 Possible failure modes of bond-splittings (Vintzelev and Tasson 1986)

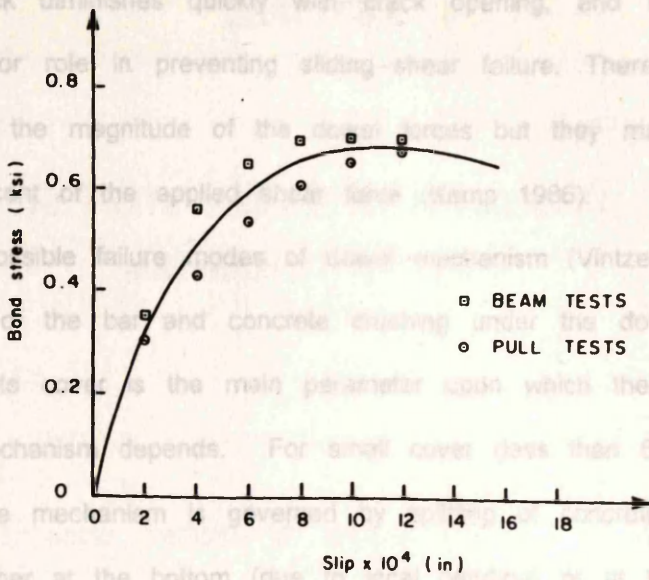


Fig. 3.34 Local bond stress versus local slip.

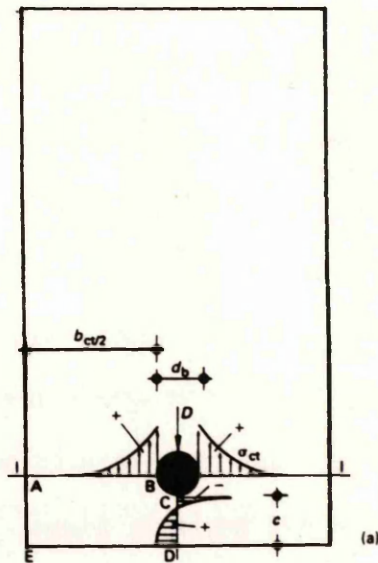


Fig. 3.35 Possible failure modes of dowel mechanism (Vintzeleou and Tassios 1986).

Aggregate interlock diminishes quickly with crack opening, and hence the dowel bars play a major role in preventing sliding-shear failure. There is no common agreement as to the magnitude of the dowel forces but they may amount to as much as 30 percent of the applied shear force (Kemp 1986).

There are two possible failure modes of dowel mechanism (Vintzeleou and Tassios 1986): (1) yield of the bar and concrete crushing under the dowel; (2) concrete splitting. Concrete cover is the main parameter upon which the mode of failure of the dowel mechanism depends. For small cover (less than 6 to 7 times the bar diameter), the mechanism is governed by splitting of concrete, splitting cracks being opened either at the bottom (due to local bending) or at the side faces of a section (due to direct tension), see Fig. 3.35.

The dowel force capacity of a member is increased significantly by increasing the clear cover and the amount of stirrups. If nominal stirrups are used the dowel forces can be carried directly and efficiently by the stirrups (Kemp 1986).

4.3.7 Finite element concept and formulation

The finite element method has been described extensively in the literature (e.g. Zienkiewicz and Owen 1977, Zienkiewicz 1977, Owen and Zienkiewicz 1984). In this chapter, no attempt will be made here to review the literature on the subject. A brief overview of the method will be given in this chapter, drawing on material from several references.

The finite element method starts with an arbitrary structure which is discretized into a mesh of elements. In which a skeletal structure of members is defined. The advantage of one-dimensional elements (axial bending and shear) is that the finite element method for skeletal structures (the elements of an actual structure are discretized together at discrete joints, and equations of equilibrium governing internal forces and member end forces expressed in terms of displacements are formulated at all joints. These equations are solved for joint displacements. The

CHAPTER 4

THE FINITE ELEMENT AND NUMERICAL METHODS OF ANALYSIS

4.1 Introduction

In Chapter 2, some methods of analysis of shear strength of concrete structure were mentioned. None of these methods can be compared with the finite element method. The analysis by the finite element method is more general. By using it in the analysis of reinforced concrete structure, beside the prediction of the failure load, stresses and strains in concrete and steel, deflection at any point, and the mode of failure can be determined.

4.2 Finite element concept and formulation

The finite element method has been described extensively in the literature (e.g.; Hinton and Owen 1977, Zienkiewicz 1977, Owen and Hinton 1980, Bhatt 1986), and no attempt will be made here to review the vast literature in these fields. Instead, a brief review of the method will be presented in the following sections which is selected from several references.

The finite element method started as an extension of the stiffness (or displacement) method, in which a skeletal structure is assumed to be made up of an assemblage of one-dimensional elements (axial, bending and torsional actions). In the stiffness method for skeletal structures the elements of an actual structure are connected together at discrete joints, and equations of equilibrium involving external loads and member end forces expressed in terms of displacements are established at all joints. These equations are solved for joint displacements. The

relationship between the end forces and end displacements of each member is represented by the stiffness matrix which can be derived directly through the solution of differential equations, use of various energy theorems, or the principle of virtual work. However, unlike skeletal structures, in the finite element method, there are no well-defined joints where equilibrium of forces can be established and therefore, the continuum must be discretized into a number of elements of arbitrary shapes and also artificial joints or nodes must be created.

In this way the continuum is approximated by a system with finite degree of freedoms, so that a numerical solution can be achieved.

In recent years the most intensive work has taken place in solving nonlinear problems. The general procedure for solving such problems is to approximate the nonlinear behaviour by a series of linear solutions. The linear solution procedure is therefore a basic and important part of any nonlinear solution method.

4.3 Discretisation by finite element

For structural applications, the governing equilibrium equations can be obtained by minimising the total potential energy of the system. The total potential energy, Π , can be expressed as:

$$\begin{aligned} \Pi = & \frac{1}{2} \int_V \{\sigma\}^T \{\varepsilon\} dV - \int_V \{\delta\}^T \{p\} dV - \int_S \{\delta\}^T \{q\} dS \\ & - \{P\} \{\delta\}^T \end{aligned} \quad (4.1)$$

where σ and ε are the stress and strain vectors respectively, δ is the displacements at any point, p is the body force per unit volume, q is the applied surface tractions, and P is the concentrated forces. Integrations are taken over the volume, V , of the structure and loaded surface areas S .

The first term on the right hand side of equation (4.1) represents the internal strain energy and the second and third terms are the work contributions of the body forces and the distributed surface loads respectively.

In the displacement method, the displacements are assumed to have unknown values at the nodal points so that the variation within any element is described in terms of the nodal values by means of interpolation functions. thus

$$\{\delta\} = [N].\{\delta^e\} \quad (4.2)$$

where N is vector of interpolation functions often termed shape functions, and δ^e is the vector of the nodal displacements of the element. The strains within the elements can be expressed in terms of the element nodal displacements,

$$\{\varepsilon\} = [B].\{\delta^e\} \quad (4.3)$$

where B is the strain matrix generally composed of derivatives of the shape functions. The stresses may be related to the strains by making use of elasticity matrix, D , as follows:

$$\{\sigma\} = [D].\{\varepsilon\} \quad (4.4)$$

Ensuring that the element shape functions have been chosen so that no singularities exist in the integrands of the function, the total potential of the continuum will be the sum of the energy contributions of the individual elements.

Thus:

$$\Pi = \sum_e \pi_e \quad (4.5)$$

where π_e is the total potential of element e , by using equation (4.1), π_e can be written as follows:

$$\pi_e = \frac{1}{2} \int_{V_e} \{\delta^e\}^T [B]^T [D]^T [B] \{\delta^e\} dV - \int_{V_e} \{\delta^e\}^T [N]^T \{p\} dV - \int_{S_e} \{\delta^e\}^T [N]^T \{q\} dS \quad (4.6)$$

where V_e is the element volume and S_e is the loaded surface area of the element.

The performance of the minimisation for element, e , with respect to the nodal displacement, δ^e , of the element results in:

$$\begin{aligned} \frac{d\pi_e}{d\delta^e} &= \int_{V_e} [B]^T [D] [B] \{\delta^e\} dV - \int_{V_e} [N]^T \{p\} dV - \int_{S_e} [N]^T \{q\} dS \\ &= [K^e] \{\delta^e\} - \{F^e\} = 0 \end{aligned} \quad (4.7)$$

where

$$\{F^e\} = \int_{V_e} [N]^T \{p\} dV + \int_{S_e} [N]^T \{q\} dS \quad (4.8)$$

are the equivalent nodal forces for the element and

$$[K^e] = \int_{V_e} [B]^T [D] [B] dV \quad (4.9)$$

is termed the stiffness matrix. The summation of terms in equation (4.7) over all the elements, when equated to zero, results in a system of equilibrium equations for the complete continuum, i.e.

$$\{F\} = [K] \{\delta\} \quad (4.10)$$

where $\{F\}$ is the equivalent nodal forces for the continuum, $[K]$ is the stiffness matrix of continuum and $\{\delta\}$ is the nodal displacements of the continuum.

After the insertion of the necessary boundary equations, these equations are then solved by any standard technique to yield the nodal displacements. Once the

displacements are determined, the strains and thereafter the stresses in each element can be evaluated by using equations (4.3) and (4.4) respectively.

4.4 Isoparametric elements:

The name isoparametric came because the same interpolation function used for defining the displacement variation within the element is also used to define the element geometry.

The basic procedure is to express the element co-ordinates and element displacements by functions expressed in terms of the natural co-ordinates of the element. A natural co-ordinate system is a local system defined by the element geometry and not by the element orientation in the global system. Moreover, these systems are usually arranged such that the natural co-ordinate has unit magnitude at primary external boundaries. Fig. 4.1 shows this type of element and its natural co-ordinate system.

Many reasons encourage one use isoparametric elements, such as:

1. They are far more accurate than simple elements.
2. The simultaneous description of element geometry and displacement variation by the shape functions leads to efficient computing effort.
3. Curved elements can model the curved boundaries of a structure.

In the present investigation, isoparametric elements have been used.

4.4.1 Shape functions:

The fundamental property of the shape (interpolation) function N_i is that its value in the natural co-ordinate system is unity at node i and is zero at all other nodes. A shape function defines the variation of the field variable and its derivatives through an element in terms of its values at the nodes. Therefore, shape functions are closely related to the numbers of nodes and consequently to the type of element. Polynomials are often selected as shape functions because they are relatively easy to manipulate mathematically, particularly with regard to

integration and differentiation. However, the degree of polynomial chosen will clearly depend on the number of nodes and the degree of freedom associated with the element. The shape functions for the eight-noded strain element are given by the following equations in curvilinear co-ordinate ξ and η :

For corner nodes:

$$N_i = \frac{1}{4}(1 + \xi\xi_i)(1 + \eta\eta_i)(\xi\xi_i + \eta\eta_i - 1) \quad (4.11)$$

For midside nodes:

$$N_i = \frac{1}{2}\xi_i(1 + \xi\xi_i)(1 - \eta^2) + \frac{1}{2}\eta_i(1 + \eta\eta_i)(1 - \xi^2) \quad (4.12)$$

where ξ and η are the intrinsic co-ordinates of any point within the element. By definition, ξ and η have values in the interval $[-1,1]$.

These shape functions are part of the so-called serendipity family (Zienkiewicz 1977), and they are shown pictorially in Fig. 4.2. The displacement at any point inside the element, namely u and v , can be expressed in terms of these shape functions as follows:

$$u = \sum_{i=1}^8 N_i(\xi, \eta)u_i \quad (4.13)$$

$$v = \sum_{i=1}^8 N_i(\xi, \eta)v_i \quad (4.14)$$

It should be noted that the displacements u and v are parallel to the x and y , not the ξ and η axes. Similarly, the position of a point within the element in global co-ordinates is given by:

$$x = \sum_{i=1}^8 N_i(\xi, \eta)x_i \quad (4.15)$$

$$y = \sum_{i=1}^8 N_i(\xi, \eta)y_i \quad (4.16)$$

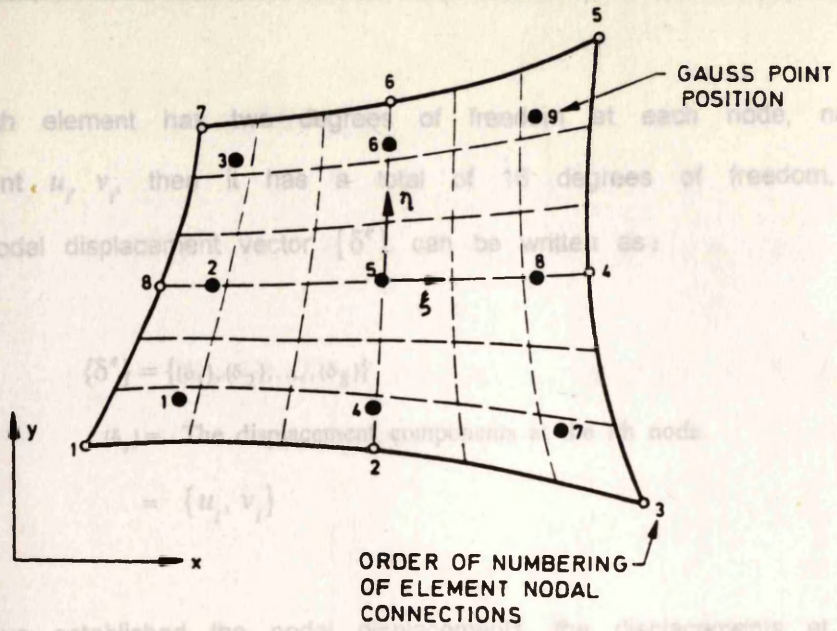
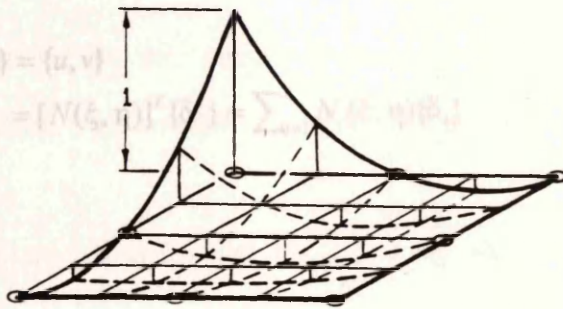


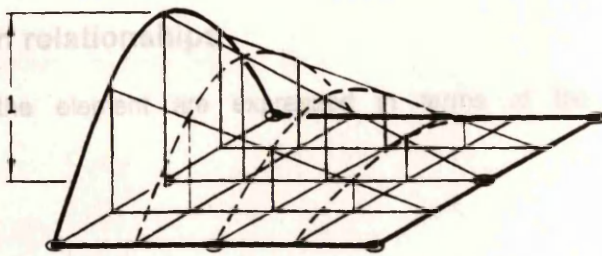
Fig. 4.1 Typical 8-noded isoparametric element.



$$[N(\xi, \eta)]^T = \begin{bmatrix} N_1 & 0 & N_3 & 0 \\ 0 & N_1 & 0 & N_3 \end{bmatrix}$$

corner

= shape function matrix



Midside

Fig. 4.2 Shape function for 8-noded isoparametric element.

Since each element has two degrees of freedom at each node, namely the displacement u_i, v_i , then it has a total of 16 degrees of freedom, and the element nodal displacement vector $\{\delta^e\}$ can be written as:

$$\{\delta^e\} = \{\{\delta_1\}, \{\delta_2\}, \dots, \{\delta_8\}\} \quad (4.17)$$

$\{\delta_i\}$ = The displacement components at the i th node.

$$= \{u_i, v_i\}$$

Having thus established the nodal displacements, the displacements at any point inside the element are expressed in terms of these through the shape functions $[N(\xi, \eta)]$ such as:

$$\{\delta\} = \{u, v\} = [N(\xi, \eta)]^T \{\delta^e\} = \sum_{i=1}^8 N_i(\xi, \eta) \{\delta_i\} \quad (4.18)$$

where well known that the Cartesian and the curvilinear derivatives are related by:

$$[N(\xi, \eta)]^T = \begin{bmatrix} N_1 & 0 & N_2 & 0 & \dots & N_8 & 0 \\ 0 & N_1 & 0 & N_2 & \dots & 0 & N_8 \end{bmatrix} \quad (4.19)$$

= shape function matrix.

4.4.2 Stress-strain relationships

The strains within the element are expressed in terms of the derivations of the displacements:

i.e.

$$\{\varepsilon\} = \{\varepsilon_{xx} \quad \varepsilon_{yy} \quad \gamma_{xy}\}^T \quad (4.20)$$

$$= \left\{ \begin{array}{ccc} \frac{\partial u}{\partial x} & \frac{\partial v}{\partial y} & \left(\frac{\partial u}{\partial y} + \frac{\partial v}{\partial x} \right) \end{array} \right\}^T \quad (4.21)$$

Substituting equations (4.13) and (4.14) into equation (4.21) leads to:

$$\{\varepsilon\} = [B]\{\delta^e\} \quad (4.22)$$

where

$$\{\delta^e\}^T = \{u_1, v_1, u_2, v_2, \dots, u_i, v_i, \dots, u_8, v_8\}$$

and

$$[B] = [B_1(\xi, \eta) \quad B_2(\xi, \eta) \quad \dots \quad B_i(\xi, \eta) \quad \dots \quad B_8(\xi, \eta)]$$

= strain matrix.

in which

$$[B_i(\xi, \eta)] = \begin{bmatrix} \frac{\partial N_i}{\partial x} & 0 \\ 0 & \frac{\partial N_i}{\partial y} \\ \frac{\partial N_i}{\partial y} & \frac{\partial N_i}{\partial x} \end{bmatrix} \quad (4.23)$$

Since the shape functions N_i are defined in terms of the curvilinear co-ordinates ξ and η , a co-ordinate transformation from local to global is required in equation (4.23).

where $[D_i]$ is the tangential elasticity matrix given by:

It is well known that the Cartesian and the curvilinear derivatives are related by:

$$\begin{bmatrix} \frac{\partial}{\partial x} \\ \frac{\partial}{\partial y} \end{bmatrix} = [J]^{-1} \begin{bmatrix} \frac{\partial}{\partial \xi} \\ \frac{\partial}{\partial \eta} \end{bmatrix} \quad (4.24)$$

where J is the Jacobian matrix defined by:

$$[J] = \begin{bmatrix} \frac{\partial x}{\partial \xi} & \frac{\partial y}{\partial \xi} \\ \frac{\partial x}{\partial \eta} & \frac{\partial y}{\partial \eta} \end{bmatrix} \quad (4.25)$$

Differentiating equations (4.15) and (4.16) in accordance with equation (4.24) gives:

$$[J] = \begin{bmatrix} \frac{\partial N_1}{\partial \xi} & \frac{\partial N_1}{\partial \xi} & \dots & \frac{\partial N_1}{\partial \xi} & \dots & \frac{\partial N_1}{\partial \xi} \\ \frac{\partial N_1}{\partial \xi} & \frac{\partial N_1}{\partial \xi} & \dots & \frac{\partial N_1}{\partial \xi} & \dots & \frac{\partial N_1}{\partial \xi} \\ \frac{\partial N_1}{\partial \xi} & \frac{\partial N_1}{\partial \xi} & \dots & \frac{\partial N_1}{\partial \xi} & \dots & \frac{\partial N_1}{\partial \xi} \end{bmatrix} \begin{bmatrix} x_1 & y_1 \\ x_2 & y_2 \\ \cdot & \cdot \\ \cdot & \cdot \\ x_i & y_i \\ \cdot & \cdot \\ \cdot & \cdot \\ x_8 & y_8 \end{bmatrix}$$

For linear analysis of uncracked concrete, and in the absence of initial stresses and strains, the incremental form of stress-strain relationship in global direction in plane stress case is given by the following relationship:

$$\Delta\{\sigma\} = [D_T] \Delta\{\varepsilon\} \quad (4.26)$$

where $[D_T]$ is the tangential elasticity matrix given by:

$$[D_T] = \frac{E}{(1-\nu^2)} \begin{bmatrix} 1 & \nu & 0 \\ \nu & 1 & 0 \\ 0 & 0 & \frac{(1-\nu)}{2} \end{bmatrix} \quad (4.27)$$

For double cracking, where E is Young's modulus of elasticity and ν is Poisson's ratio. The onset of the cracking will introduce orthotropic conditions, and new incremental constitutive relationships will apply for the material parallel to and normal to the cracks. Normal stress across the crack is either reduced to zero in case of tension cut-off criterion, or follows the descending portion of the tensile stress-strain curve when the tension softening is taken into account. A new elasticity matrix in crack directions takes place and is given by:

$$[D_T]^* = \begin{bmatrix} E_n & 0 & 0 \\ 0 & E_t & 0 \\ 0 & 0 & \beta G \end{bmatrix}$$

where β is the shear retention factor, and E_n and E_t are the moduli of elasticity normal and parallel to the crack plane, respectively.

Using tension cut-off criterion, when single crack has occurred then,

$$E_n = 0.0 \quad \text{and} \quad E_t = E$$

Now all the information necessary to evaluate the element stiffness matrix, K^e are

For double cracking, (4.9), i.e.

$$E_n = 0.0 \quad \text{and} \quad E_t = 0.0 \quad (4.28)$$

It is essential, for reasons of numerical stability, to avoid zero values on the diagonals. Thus instead of putting E equal zero it takes a comparatively small value (e.g., $E = 1.E-20$).

When tension softening is taken into account and single crack has occurred, then

$$E_n = \sigma_n / \varepsilon_n \quad \text{and} \quad E_t = E$$

For double cracking, (4.9), i.e.

The displacements $\{u,v\}$ of any point on the bar are

$$E_n = \sigma_n / \varepsilon_n \quad \text{and} \quad E_t = \sigma_t / \varepsilon_t$$

where ε_n and ε_t are the tensile strains normal and tangential to the crack plane, and σ_n and σ_t are the corresponding tensile stresses calculated from the tension softening curve.

To transform the above matrix to the global system (x,y) , the standard displacement vector

transformation matrix $[T]$ can be used as follows:

The virtual work of reinforcing element can be written as

$$[D_r]_{cr} = [T]^T [D] [T] \quad (4.32)$$

where

$$[T] = \begin{bmatrix} C^2 & S^2 & CS \\ S^2 & C^2 & -CS \\ -2CS & 2CS & C^2 - S^2 \end{bmatrix}$$

where $C = \cos \theta$, $S = \sin \theta$, and $\theta =$ the crack angle.

4.4.3 Element stiffness matrix

Now all the information necessary to evaluate the element stiffness matrix, K^e are available. From equation (4.9), i.e.

$$[K^e] = \iiint [B]^T [D] [B] dV \quad (4.28)$$

a typical submatrix K_{ij}^e linking nodes i and j may be evaluated from the expression

$$[K_{ij}^e] = \int_{-1}^{+1} \int_{-1}^{+1} [B_i]^T [D] [B_j] t \cdot \det.J \cdot d\xi \cdot d\eta \quad (4.29)$$

where t is element thickness and the incremental volume dV is given by

$$dV = t \cdot \det.J \cdot d\xi \cdot d\eta \quad (4.30)$$

4.4.4 Stiffness matrix of embedded bar

The displacements $\{u, v\}$ of any point on the bar are obtained from the displacement field of the isoparametric element as:

$$\begin{Bmatrix} u \\ v \end{Bmatrix} = [N(\xi, \eta)] \{\delta\}^e \quad (4.31)$$

where N is the shape function of concrete element and $\{\delta\}^e$ is the nodal displacement vector.

The virtual work of reinforcing element can be written as

$$\delta U = A_s \int_l \delta \varepsilon_l \cdot \sigma_l \cdot dl \quad (4.32)$$

in which δU = internal virtual work in the reinforcement; A_s = cross-sectional area; dl = line segment along the reinforcement; and σ_l, ε_l = the longitudinal stress and strain along line segment, respectively.

For bar parallel to the x-axis,

$$\sigma_l = \sigma_x$$

$$\varepsilon_l = \varepsilon_x$$

$$dl = dx$$

Equation (4.32) becomes

$$\delta U = A_s \int_x \delta \varepsilon_x \cdot \sigma_x \cdot dx \quad (4.33)$$

The strain in the bar can be calculated as follows:

$$\varepsilon_x = \partial u / \partial x = \frac{\partial (N(\xi, \eta) \cdot u_i)}{\partial x}$$

$$\varepsilon_x = \frac{\partial N_i(\xi, \eta)}{\partial x} \cdot u_i$$

$$\begin{Bmatrix} \varepsilon_x \\ \varepsilon_y \end{Bmatrix} = \left[\frac{\partial N_i(\xi, \eta)}{\partial x}, 0 \right] \begin{Bmatrix} u_i \\ v_i \end{Bmatrix}$$

$$\varepsilon = B \delta^e$$

$$\delta \varepsilon = B \delta(\delta^e)$$

where B is the nodal displacement-strain matrix. The relation between the stress and strain in the bar is:

$$\sigma = E_s \varepsilon$$

And the stiffness of the embedded representation can be expressed as

$$K_s = A_s E_s \int_x B^T B dx$$

$$dx = \frac{dx}{d\xi} d\xi = J_s \cdot d\xi$$

$$K_s = A_s E_s \int_{-1}^1 B^T B \frac{d\xi}{J_s} \quad (4.34)$$

where E_s = the bar Young's modulus and J_s = Jacobian for steel element. The same steps can be repeated for a bar parallel to y-axis.

The final expression for the composite element stiffness is simply evaluated by adding the stiffness matrices for concrete and steel together, as follows

$$K_e = K_c + K_s$$

in which K_e is the stiffness matrix for the composite element, K_c and K_s are the element concrete and steel stiffness matrix respectively.

4.4.5 Numerical integration

It is difficult or perhaps impossible to perform the closed form integrations required in evaluating the element matrix and thus numerical integration is essential.

Numerical integration will replace the exact integral by evaluating the integrand at various sampling points and then taking a weighted summation of these values. In

this study Gauss-Legendre quadrature values have been used because of their higher accuracy over other forms of quadrature and the ease with which these

can be implemented. An n th order integration can integrate exactly a polynomial $f(\xi)$ of degree $(2n-1)$.

The general form of the integral using Gauss-Legendre is:

$$\int_{-1}^1 f(\xi) d\xi = \sum_{i=1}^m W_i f(\xi_i) \quad (4.35)$$

where ξ_i is the co-ordinate of the i th integration point, W_i is a weighting factor and m is the total number of integration points.

In two dimensions where a double integral exists, then

$$\begin{aligned}
 \int_{-1}^{+1} \int_{-1}^{+1} f(\xi, \eta) d\xi d\eta &= \int_{-1}^{+1} \left[\int_{-1}^{+1} f(\xi, \eta) d\xi \right] d\eta \\
 &= \int_{-1}^{+1} \left[\sum_{i=1}^m W_i f(\xi_i, \eta) \right] d\eta \\
 &= \int_{-1}^{+1} \left[\sum_{i=1}^m W_i g_i(\eta) \right] d\eta \\
 &= \sum_{i=1}^m \sum_{j=1}^m W_i W_j g(\eta_j) \\
 &= \sum_{i=1}^m \sum_{j=1}^m W_i W_j f(\xi_i, \eta_j) \quad (4.36)
 \end{aligned}$$

where W_i, W_j are the i th and j th weighting factors and ξ_i, η_i are the co-ordinates of the i th integration point.

These Gaussian-Legendre rules are particularly suitable for isoparametric elements since the limits of integration are -1 to $+1$ which coincide with the local co-ordinate system -1 to $+1$ on element boundaries. Table 4.1 shows the symmetrical positions of Gauss points ξ_i and the corresponding weighting factors W_i for $m=1,2,3$, and 4.

4.5 The equation solution technique

There are various equation solution techniques which can be used to solve a given set of linear simultaneous equations. In this study direct Gaussian elimination algorithms have been used in conjunction with the frontal method of equation assembly and reduction, and is applicable here only for symmetric systems of linear equations. The features of this technique are:

1. It assembles the equations and eliminates the variables at the same time, hence the complete structural stiffness is never formed, only the upper triangle of a square matrix containing parts of the equations which are being assembled at a particular time.

2. The frontal solver does not store as many zero coefficients as a banded solver does. Once an equation has been completely assembled and eliminated, it reduces space which can be used for subsequent equations.

Table 4.1 Positions of Gauss points and corresponding weighting factors

m	i	ξ_i	a_i
1	I	0	2
2	I	$+\frac{1}{\sqrt{3}}$	+1
	II	$-\frac{1}{\sqrt{3}}$	+1
3	I	0	$\frac{8}{9}$
	II	$+\sqrt{0.6}$	$\frac{5}{9}$
	III	$-\sqrt{0.6}$	$\frac{5}{9}$
4	I	$+\sqrt{\frac{3+\sqrt{4.8}}{7}}$	$\frac{1}{2} - \frac{\sqrt{30}}{36}$
	II	$-\sqrt{\frac{3+\sqrt{4.8}}{7}}$	$\frac{1}{2} - \frac{\sqrt{30}}{36}$
	III	$+\sqrt{\frac{3-\sqrt{4.8}}{7}}$	$\frac{1}{2} + \frac{\sqrt{30}}{36}$
	IV	$-\sqrt{\frac{3-\sqrt{4.8}}{7}}$	$\frac{1}{2} + \frac{\sqrt{30}}{36}$

(4.37)

$$[K]\{\delta\} - \{F\} = 0 \quad (4.37)$$

in which the assumed linear elastic constitutive law given by eq. (4.36)

$$\{\sigma\} = [D]\{\epsilon\} + \{\sigma_0\} \quad (4.38)$$

where $[D]$ = the constant linear elastic matrix, and $\{\sigma_0\}$ = the initial stress vector

2. The frontal solver does not store as many zero coefficients as a banded solver does. Once an equation has been completely assembled and eliminated, it reduces space which can be used for subsequent equations.
3. The storage allocation in a banded solver is determined by the order in which the nodes are presented for assembly. But, in frontal solver the storage is determined by the order in which the elements are presented. It can handle any order of node numberings. Hence, at any stage, if a mesh of a problem is found to be too coarse in some regions, its modification does not require extensive nodal point renumbering. In this sense, the frontal solver is easier to use than banded solvers.
4. The frontal solver tends to be more economical than banded solvers, especially for higher order elements with midside nodes.

4.6 Numerical methods of analysis

For the solution of nonlinear problems by finite element method, three procedures are usually used:

1. Incremental (Step-wise procedure).
2. Iterative (Newton-Raphson method).
3. Incremental-iterative (mixed procedure).

All these procedures solve the basic linear elastic equations given by equation (4.37)

$$[K]\{\delta\} - \{F\} = 0 \quad (4.37)$$

in which the assumed linear elastic constitutive law given by equation (4.38)

$$[\sigma] = [D]\{\epsilon\} + \{\sigma_0\} \quad (4.38)$$

where $[D]$ = the constant linear elastic matrix, and $\{\sigma_0\}$ = the initial stress vector.

Under nonlinear conditions, equation (4.38) is replaced by a different law of the form:

$$f(\sigma, \varepsilon) = 0 \quad (4.39)$$

which represents the relationship between stress and strain. This procedure has the

The element stiffness matrix is a function of the material properties and can be written as:

$$[K] = [k(\sigma, \varepsilon)] \quad (4.40)$$

The external nodal forces $\{F\}$ are related to the nodal displacements $\{\delta\}$ through the stiffnesses of the element and can be expressed by:

$$\{F\} = [k(\sigma, \varepsilon)] \{\delta\} \quad (4.41)$$

which on inversion becomes:

$$\{\delta\} = [k(\sigma, \varepsilon)]^{-1} \{F\} \quad (4.42)$$

This derivation illustrates the basic nonlinear relationship between $\{\delta\}$ and $\{F\}$, due to influence of the material law on $[K]$.

However, equation (4.42) is solved by a succession of linear approximations, and different methods of applying these linear approximations will lead, in general, to different load-displacement paths influencing the final solution.

4.6.1 Incremental procedure

In this procedure the load is divided into a number of equal or unequal load increments. At each step only one increment of load is added to the structure. At each stage of loading the stiffness of the structure may have a different value

depending on the deformation reached and constitutive law adopted for the material as well as the method for estimating the stiffness at that stage.

The total load and displacement at any stage is given by the sum of the increments of all the loads and displacements of the previous stages. The process is repeated until the ultimate or the total load is reached. This procedure has the advantage that it is simple to apply but the accuracy is rather low unless the load increments are very small. The main disadvantage of this procedure is that it does not account for force redistribution during the application of increment owing to the fact that there is no iteration process to restore equilibrium.

Since in a numerical process, equilibrium conditions are unlikely to be satisfied

4.6.2 Iterative procedure

In this procedure, the load is applied to the structure and then the displacement is adjusted in accordance with the constitutive laws until equilibrium is attained. In this method either the stiffness matrix remains constant or varies throughout the solution. One distinct advantage of this method is that the same stiffness matrix can be used at each of iteration which involves a small amount of computing effort in each subsequent iteration step for the determination of the corresponding displacement. Other methods with variable stiffness matrix $[K]$ such as the secant method and Newton-Raphson method may have a faster convergence rate but only at the expense of having to reassemble and solve a new system of linear equations at each iteration.

4.6.3 Incremental-iterative procedure

In practice, usually a combination of both the increment and iterative procedure is used. The total load is divided into a number of load increments. At every increment of load, iterative procedure is applied until convergence is obtained under that load increment. The constant stiffness procedure can be used. For nonlinear analysis of reinforced concrete structures, experience seems to indicate

that relatively small load increments with fairly frequent updating of the stiffness for just a few iteration steps are required to produce good results.

Developments in numerical analysis and applied mathematics can be used to further improve the efficiency of solution technique at low additional cost. Recently, a number of techniques have been introduced in order to accelerate the rate of convergence, such as the accelerated method and arc length methods.

4.7 Convergence criteria

Since in a numerical process, equilibrium conditions are unlikely to be satisfied exactly, criteria to determine convergence have to be established for objective analysis. The main purpose of reliable convergence criterion is to monitor the gradual elimination of the out-of-balance residual forces until the desired accuracy has been achieved. The convergence criterion, usually used, is based on displacement or out-of-balance force norms and sometimes on internal strain energy. In the present work, convergence criterion is based on out-of-balance force norms. They indicate directly how well equilibrium requirements are met. Since it is difficult and expensive to check the decay of residual forces for every degree of freedom, an overall evaluation of convergence is preferable. This is achieved by using a force norm.

This criterion assumes that convergence is achieved if:

$$\frac{\Delta R_i^*}{F_i^*} \leq Tol \quad (4.43)$$

where:

$$\Delta R_i^* = \sqrt{\{R_i\}^T \{R_i\}}$$

= the norm of the residuals,

$\{R_i\}$ = the residual force vector at i th iteration,

$$F_i^* = \sqrt{\{F_i\}^T \{F_i\}}$$

For nonlinear analysis: $\|F\|$ = the norm of the total applied loads,

1. Check for cracks: $\{F_i\}$ = the total applied load vector,

and Determination of Tol = specified convergence tolerance.

2. Check for convergence.

Fine tolerances are theoretically desirable but can be very expensive to obtain because they quite often require a large number of iterations. Steep discontinuities in material laws (cracks, yielding ...) can cause large residuals and these residuals need to be distributed. However this redistribution will cause more discontinuities in other parts of the structure and hence residuals in subsequent iterations. In such cases the rate of accumulation of residuals can be higher than the rate of distributing them. An intermediate solution is to choose a low tolerance value at initial stages and increase it towards the later part of the load history.

Finally, it should be noted that the rate of convergence depends particularly on the method used in the solution, and it is well known for example that constant stiffness will lead to slow convergence and this leads to many iterations, which is without any doubt a very costly operation.

4.8 Basic steps in nonlinear program

The major steps in the linear and nonlinear analysis of a typical finite element program are:

1. Subdivision of the structure and representing different parts by appropriate types of finite elements.
2. Generation and assembly of load vector $\{F\}$.
3. Generation of the element stiffness $[K^e]$.
4. Assembly of the structure stiffness $[K]$.
5. Solution for the nodal displacements $\{\delta_i\} = [K]^{-1} \{F_i\}$ and hence the strain $\{\varepsilon\} = \int [B]^T \{\delta_i\}$
6. Determination of element stresses $\{\sigma\} = [D]\{\varepsilon\}$

For nonlinear analysis:

7. Check for cracking, yielding, and failure.
8. Determination of unbalanced nodal forces.
9. Check for convergence.
10. This Step depends on the convergence
 - (a) If not converged apply the unbalanced nodal forces again to the structure and go to Step 3 if the stiffness is to updated and to Step 5 if constant stiffness solution is adopted.
 - (b) If converged apply the next load increment and go to Step 2.
11. Stop when failure occurs or when full loading has been applied.

Fig. 4.3 shows the main steps of the finite element nonlinear analysis procedure.

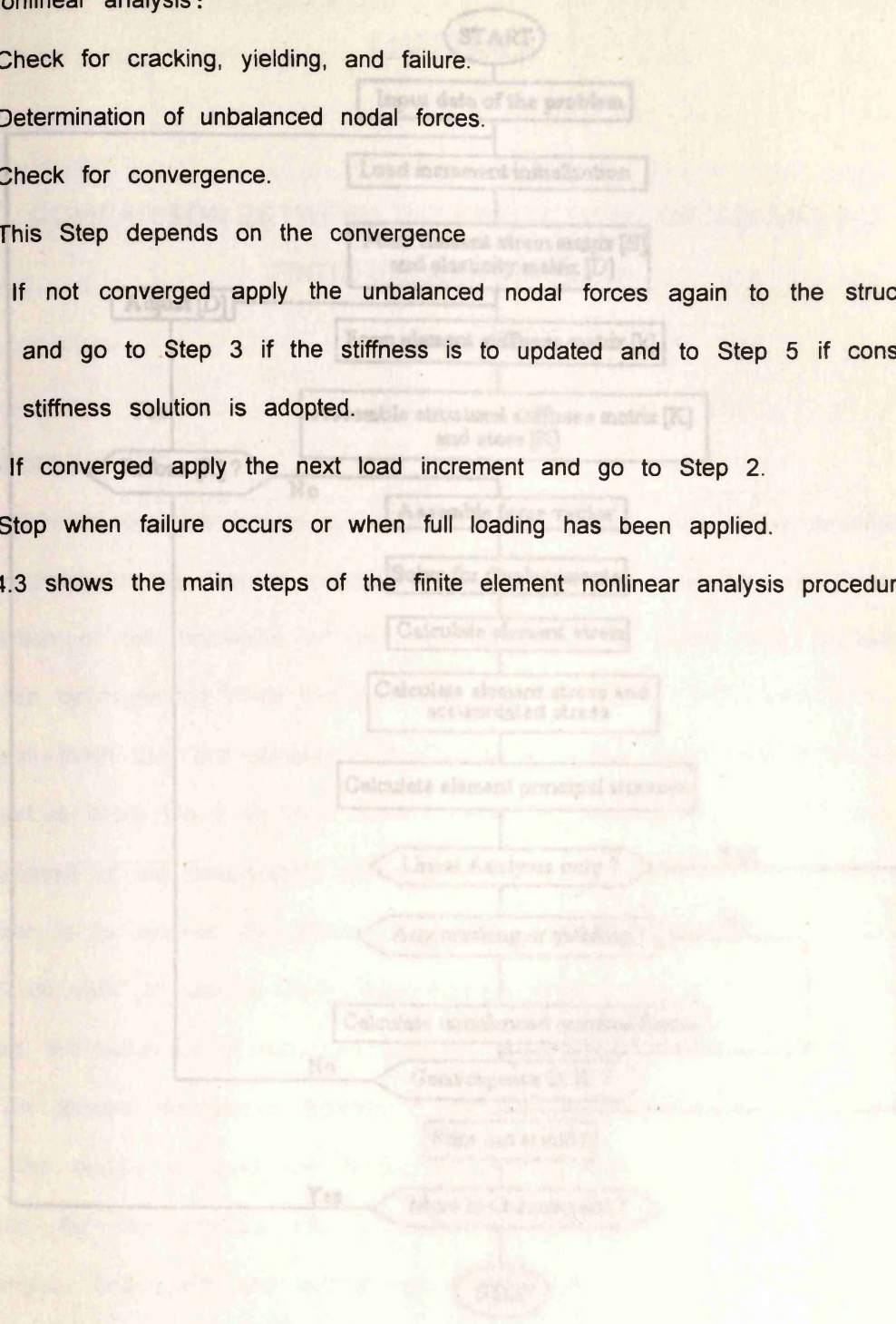


Fig. 4.3 Flow Chart for Linear and Nonlinear Analysis of Structures

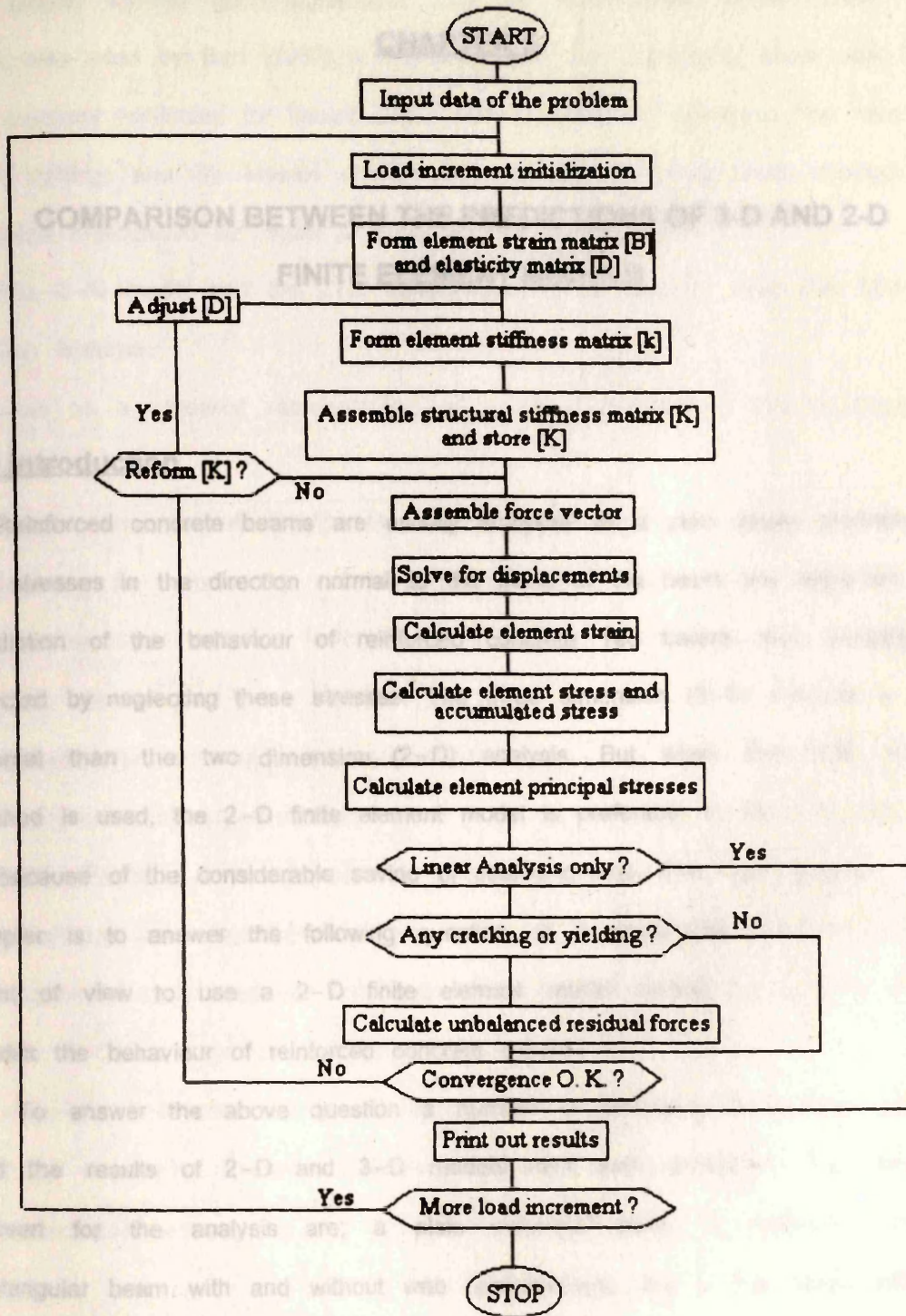


Fig. 4.3 Flow Chart for Linear and Nonlinear Reinforced Concrete Analysis.

CHAPTER 5

COMPARISON BETWEEN THE PREDICTIONS OF 3-D AND 2-D FINITE ELEMENT MODELS

The 3-D model and the 2-D model analysis have the following common features:

- Based on a smeared representation of cracks. Orthogonal cracks approach is

5.1 Introduction

Reinforced concrete beams are usually analysed as a plain stress problem; i.e. the stresses in the direction normal to the plane of the beam are neglected. The prediction of the behaviour of reinforced concrete Tee beams may probably be affected by neglecting these stresses. The three dimension (3-D) analysis is more general than the two dimension (2-D) analysis. But when the finite element method is used, the 2-D finite element model is preferable to the 3-D one. This is because of the considerable saving of cost and time. The main purpose of this chapter is to answer the following question. Is it acceptable from the accuracy point of view to use a 2-D finite element model instead of a 3-D one to predict the behaviour of reinforced concrete beams?

To answer the above question a number of structures have been analysed and the results of 2-D and 3-D models have been compared. The structures chosen for the analysis are; a plain concrete prism, a reinforced concrete rectangular beam with and without web reinforcement, and a Tee beam with web reinforcement.

5.2 Features of the 3-D and 2-D versions used in the analysis

The 3-D finite element model used in the present analysis was developed by Elnounu (1985). This model was used to predict the ultimate loads of rectangular and flanged shear wall-floor slab connections with or without shear reinforcement.

The results showed good agreement with the experimental values. Later, this model was used by Bari (1987) to study the ultimate strength of shear wall-floor slab junctions reinforced for flexure and shear subjected to monotonic and reversed cyclic loading; and by Musavi (1992) to study the punching shear strength of unbonded prestressed flat slabs at edge column junction.

The 3-D model and the 2-D model used in the analysis have the following common features:

- Based on a smeared representation of cracks. Orthogonal cracks approach is adopted.
- Use of tension cut-off criterion for concrete.
- Neglecting the compression softening of concrete.
- Assuming shear retention factor β as a function of the strain normal to the crack plane.
- Deal with the reinforcement as embedded bars.
- Use of force convergence criterion.
- Newton-Raphson method is used in the numerical analysis.
- Use of the same algorithm. Updating the structure stiffness matrix at the second iteration of each increment only and not at every iteration.
- Use of Gauss-Legendre integration method with full integration (3 x 3 Gauss points for 2-D and 3 x 3 x 3 Gauss points for 3-D).
- Use of a constant Poisson's ratio ν (= 0.15).

The differences between the two models are explained below.

3-D Model:

In addition to the common features with the 2-D version mentioned above, the other features of the 3-D model are as follows:

- Based on Kotsovos yield criterion for concrete.
- Assuming the tensile strength of concrete vanishes after tensile stress of $f_t'/2$.

This value has been modified to be f_t' . This is because when the model was

used to analyse an element under uniaxial tensile stress the predicted failure stress was half of the value given in the data as a tensile strength of concrete.

- Assuming the shear retention factor β as a function of the average strain ϵ_m ($=(\epsilon_1 + \epsilon_2 + \epsilon_3)/3$) as follows:

$$\beta = B \frac{\epsilon_{cr}}{\epsilon_m} \geq 0 \quad (5.1)$$

where B is a constant ($=0.4$).

Fig. 5.1a Plain concrete cube under uniaxial compression

2-D model:

The 2-D finite element version used in the present analysis has the following different features :

- Based on Kupfer yield criterion for concrete.
- Assuming the shear retention factor β as a function of the strain normal to the crack ϵ_n as follows:

$$\beta = B \frac{\epsilon_{cr}}{\epsilon_n} \geq 0 \quad (5.2)$$

To see the difference between the assumed uniaxial stress-strain relationship of concrete in the 2-D model and that in the 3-D model, a plain concrete cube element (100 x 100 x 100 mm) was analysed. The assumed uniaxial compressive strength is 30.0 MPa. The cube is analysed with conditions of supports as shown in Fig. 5.1a. The applied load is uniformly distributed on the finite element edge in the 2-D analysis and on the horizontal plane in the 3-D analysis. The stress-strain curves of the cube in this case are shown in Fig. 5.2. From this figure, it can be seen that the difference between the two models is very small up to the peak of stress, after that the 2-D model assumes a perfect plasticity until strain equal 0.0035, while in the 3-D analysis the calculation is stopped at the peak of stress.

Fig. 5.2 Uniaxial stress-strain curve of concrete

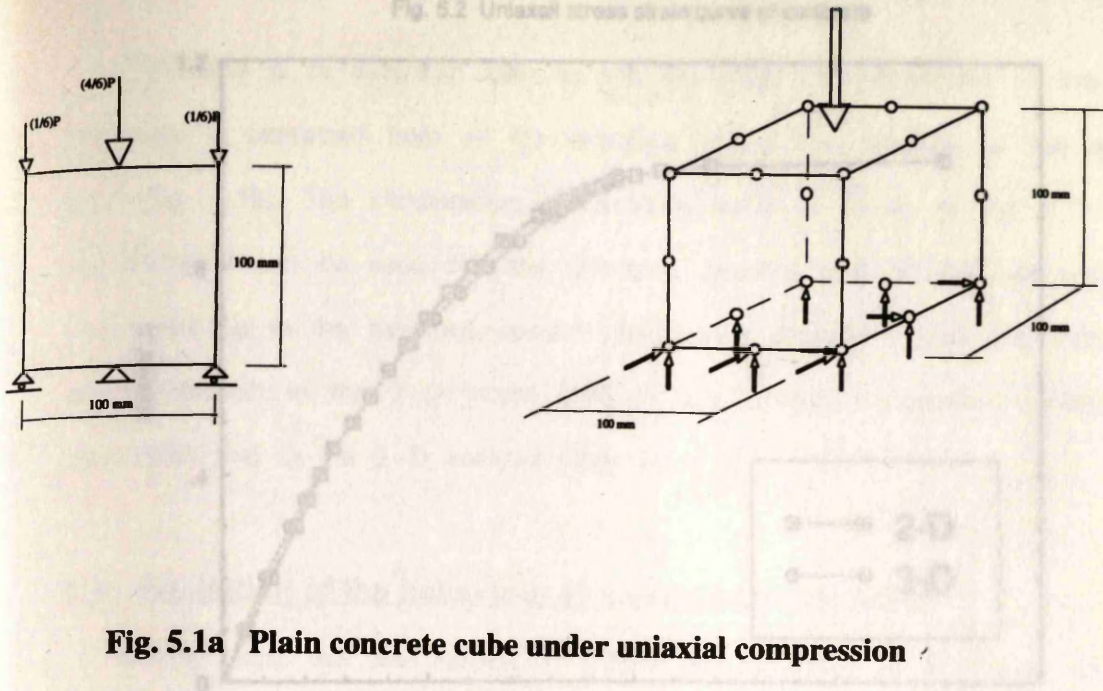


Fig. 5.1a Plain concrete cube under uniaxial compression

Fig. 5.3 Stress-strain curves for concrete (with and without confinement)

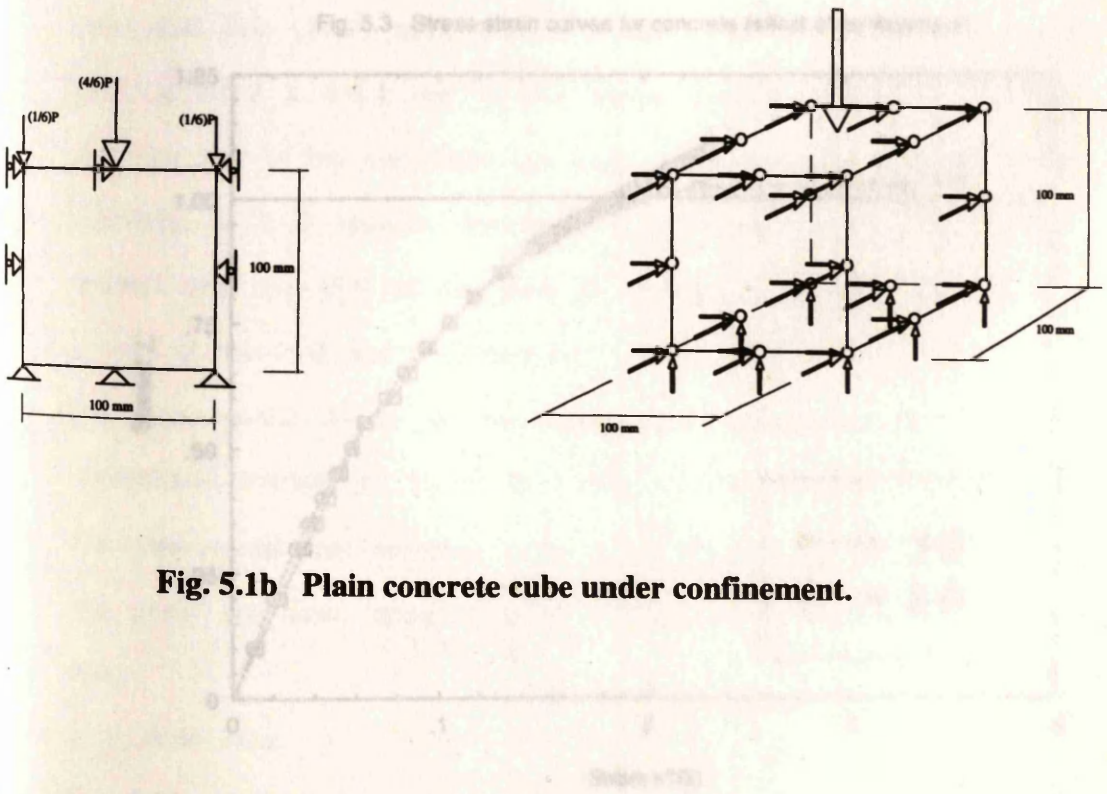


Fig. 5.1b Plain concrete cube under confinement.

Fig. 5.2 Uniaxial stress strain curve of concrete

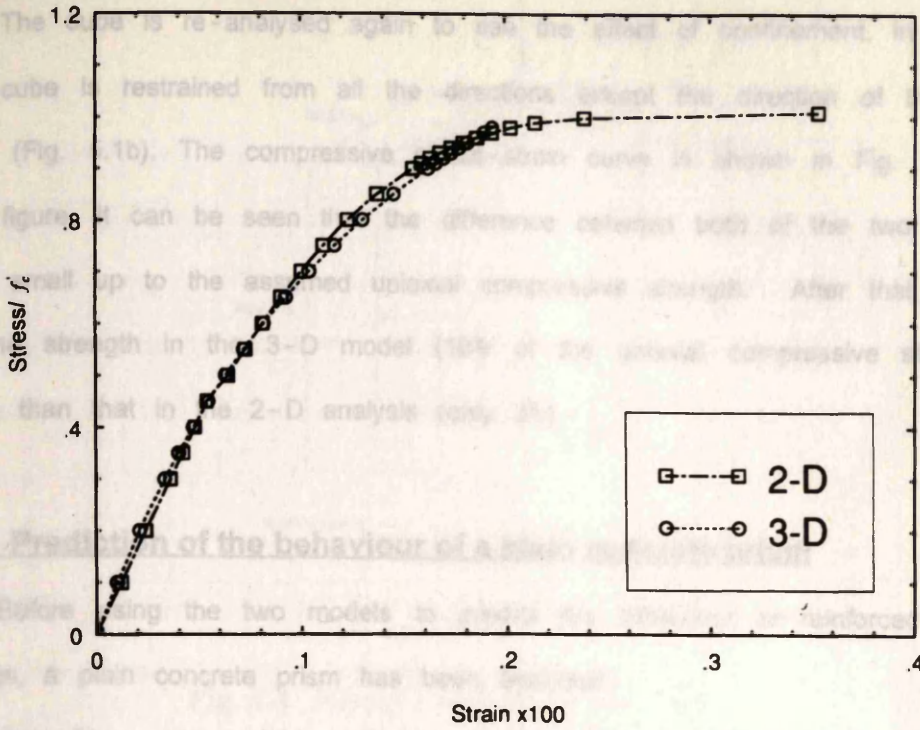
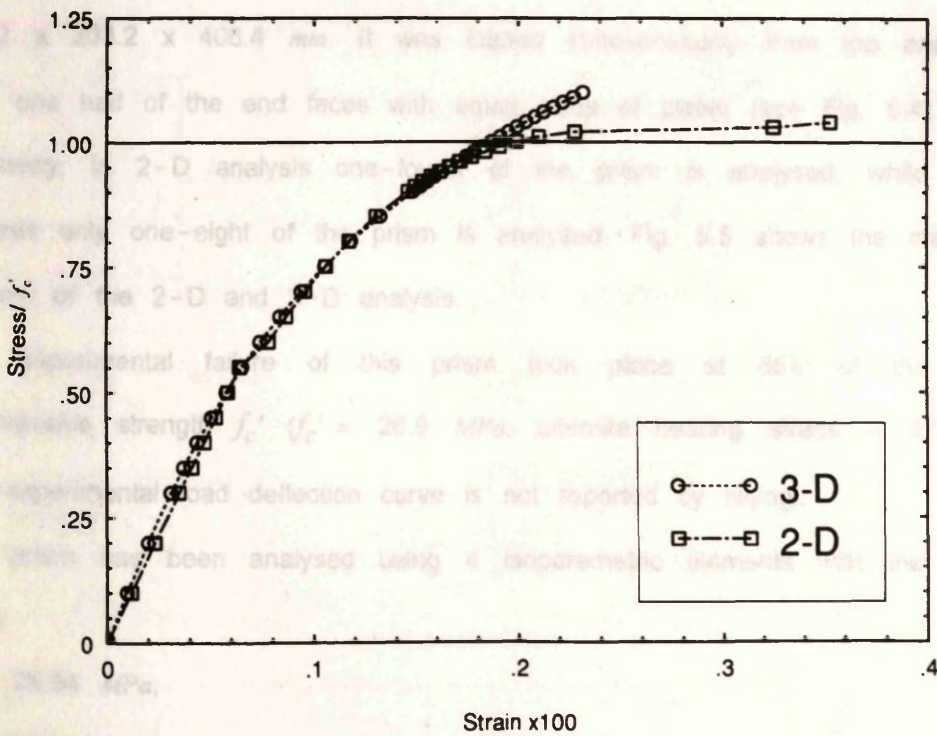


Fig. 5.3 Stress-strain curves for concrete (effect of confinement)



The cube is re-analysed again to see the effect of confinement. In this case the cube is restrained from all the directions except the direction of the applied load (Fig. 5.1b). The compressive stress-strain curve is shown in Fig. 5.3. From this figure, it can be seen that the difference between both of the two curves is very small up to the assumed uniaxial compressive strength. After that, the gain of the strength in the 3-D model (10% of the uniaxial compressive strength) is more than that in the 2-D analysis (only 3%).

5.3 Prediction of the behaviour of a plain concrete prism

Before using the two models to predict the behaviour of reinforced concrete beams, a plain concrete prism has been analysed.

A prism from many plain concrete prisms tested by Niyogi (1974) has been chosen for analysis. This prism has been analysed before by some Authors; e.g. Vidosa, et al. (1991a) using a 3-D model; Bedard and Kotsovos (1986) and Gajer and Dux (1988) using a 2-D model. The dimensions of the prism were 203.2 x 203.2 x 406.4 mm. It was loaded simultaneously from top and bottom over one half of the end faces with equal sizes of plates (see Fig. 5.4). Due to symmetry, in 2-D analysis one-fourth of the prism is analysed, while in 3-D analysis only one-eighth of the prism is analysed. Fig. 5.5 shows the mesh used in both of the 2-D and 3-D analysis.

The experimental failure of this prism took place at 65% of the cylinder compressive strength f_c' ($f_c' = 26.9 \text{ MPa}$, ultimate bearing stress = 17.4 MPa).

The experimental load deflection curve is not reported by Niyogi.

The prism has been analysed using 4 isoparametric elements with the following data:

$$f_c' = 26.94 \text{ MPa,}$$

$$f_t' = 2.80 \text{ MPa,}$$

$$E = 26000 \text{ MPa,}$$

Fig. 5.5 Finite element mesh for Niyogi's plain concrete prism

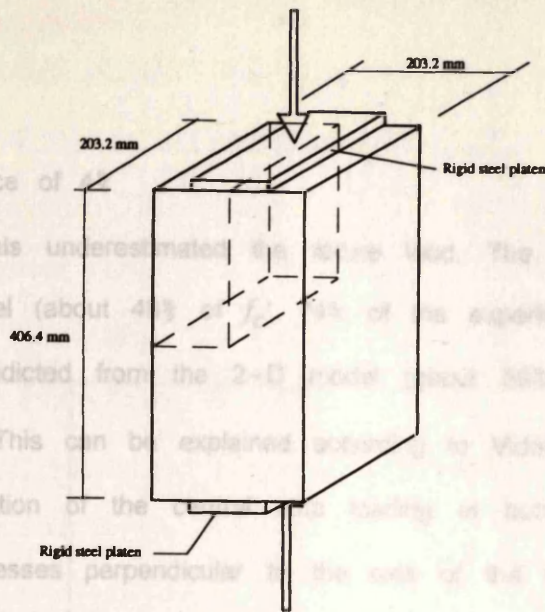
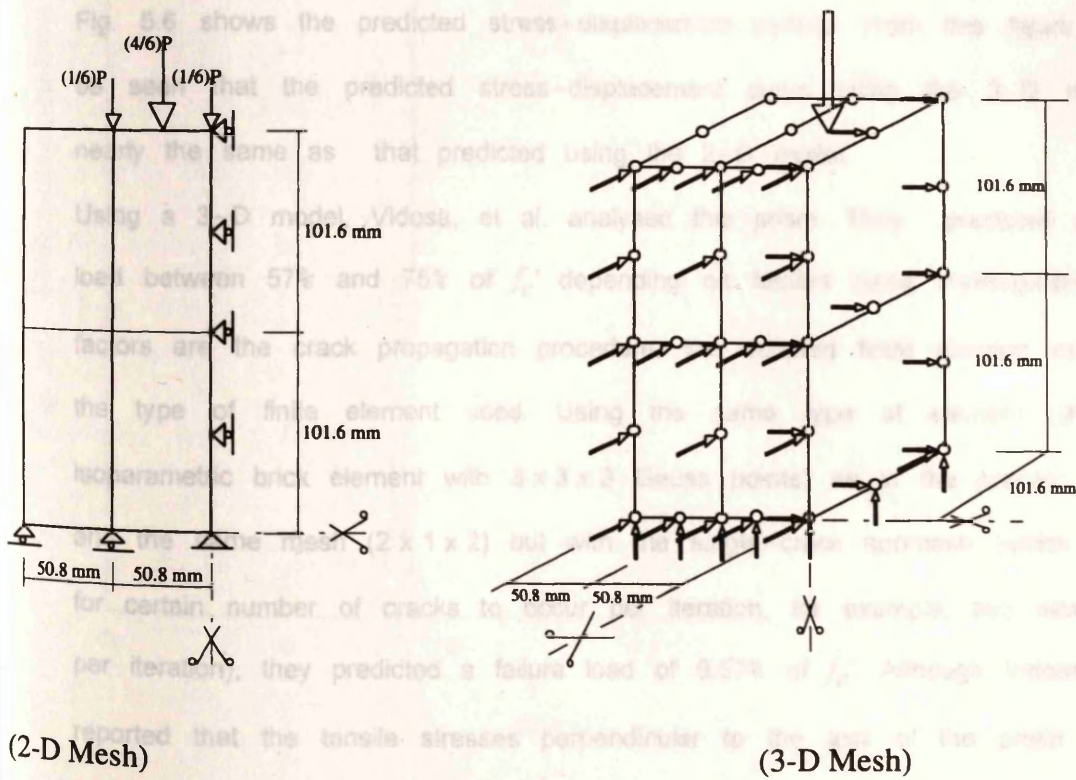


Fig. 5.4 Niyogi's plain concrete prism



(2-D Mesh)

(3-D Mesh)

Fig. 5.5 Finite element mesh for Niyogi's plain concrete prism

$$\nu = 0.15$$

$$B = 0.4$$

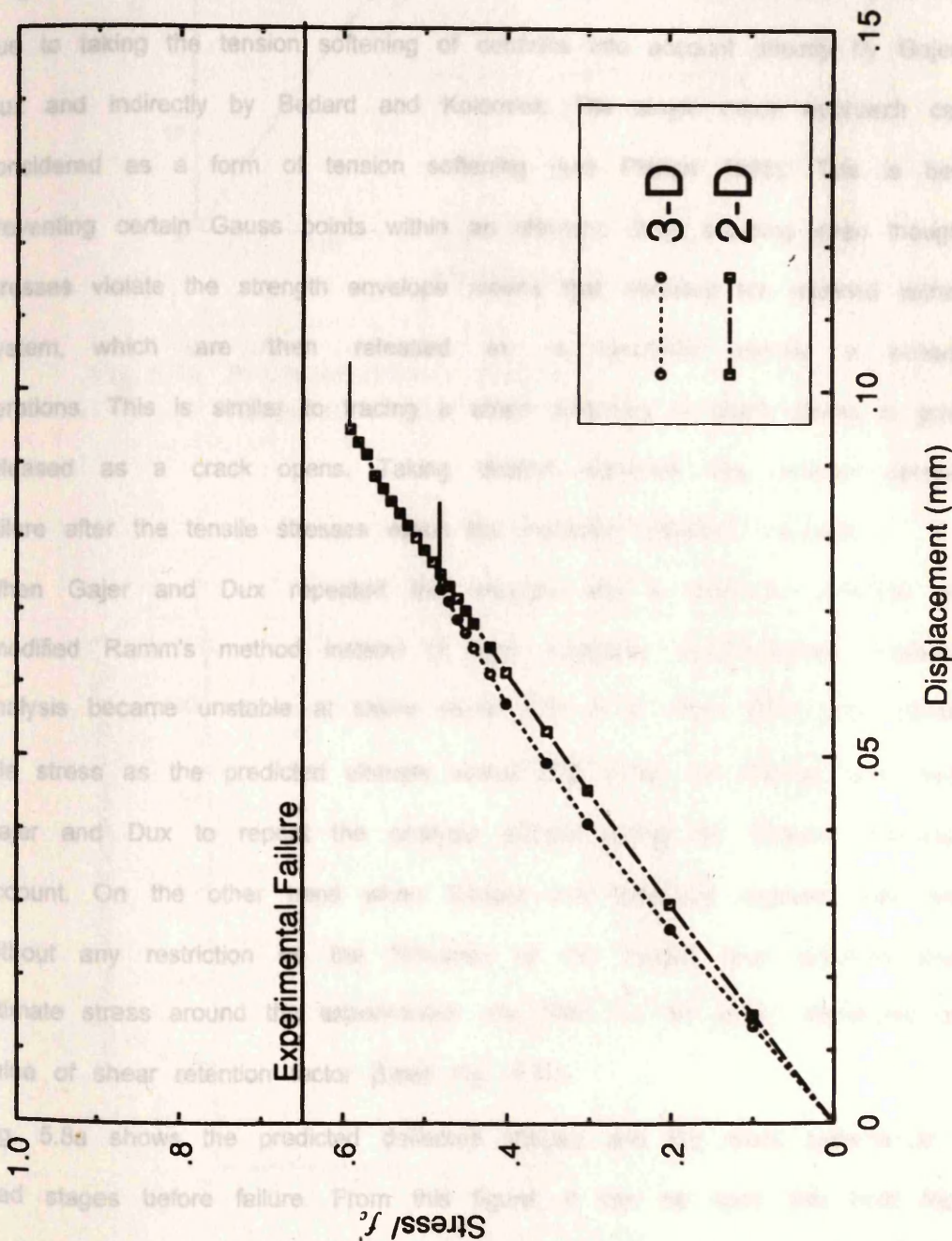
Convergence tolerance of 4%

Both The two models underestimated the failure load. The predicted failure load from the 3-D model (about 48% of f'_c , 74% of the experimental failure load) is lower than that predicted from the 2-D model (about 59% of f'_c , 91% of the experimental load). This can be explained according to Vidosa, et al. (1991c) as follows. The application of the central strip loading at both ends of the prism produces tensile stresses perpendicular to the axis of the structure that have a significant influence on the ultimate load. The 2-D representation allows for some of these stresses, while it neglects those stresses perpendicular to the plane of the prisms. The 3-D representation and triaxial model may remove this shortcoming, and avoid the artificial gain in strength arising through plane-stress modelling.

Fig. 5.6 shows the predicted stress-displacement curves. From this figure, it can be seen that the predicted stress-displacement curve using the 3-D model is nearly the same as that predicted using the 2-D model.

Using a 3-D model, Vidosa, et al. analysed this prism. They predicted a failure load between 57% and 75% of f'_c depending on factors being investigated. These factors are the crack propagation procedure, the adopted finite element mesh and the type of finite element used. Using the same type of element (20-noded isoparametric brick element with $3 \times 3 \times 3$ Gauss points) as in the present analysis and the same mesh ($2 \times 1 \times 2$) but with the single-crack approach (which allowed for certain number of cracks to occur per iteration, for example, two new cracks per iteration), they predicted a failure load of 0.57% of f'_c . Although Vidosa, et al. reported that the tensile stresses perpendicular to the axis of the prism have a significant influence on the ultimate load, in their paper no attempt was made to study the effect of tensile strength of concrete on the prediction. Moreover they did not even mention the value of the tensile strength taken in their analysis.

Fig. 5.6 Stress-displacement curves for Niyogi's prism.



Gajer and Dux (1988) analysed this prism by a 2-D model. Their result confirmed the result of Bedard and Kotsovos (1986) using 2-D model with single crack approach (allowing for the formation of only one new crack per iteration) that failure of the prism began at a stress greater than f_c' and was due to progressive crushing of concrete. One can explain this overestimated prediction as due to taking the tension softening of concrete into account directly by Gajer and Dux and indirectly by Bedard and Kotsovos. The single crack approach can be considered as a form of tension softening (see Phillips 1992). This is because preventing certain Gauss points within an element from cracking even though the stresses violate the strength envelope means that stresses are retained within the system, which are then released in a controlled manner in subsequent iterations. This is similar to tracing a strain softening in which stress is gradually released as a crack opens. Taking tension softening into account delays the failure after the tensile stresses reach the maximum allowable strength.

When Gajer and Dux repeated the analysis with a different numerical method (modified Ramm's method instead of load controlled secant-Newton method) the analysis became unstable at stress about 62% of f_c' from which they considered this stress as the predicted ultimate stress (Fig. 5.7a). No attempt was made by Gajer and Dux to repeat the analysis without taking the tension softening into account. On the other hand when Bedard and Kotsovos repeated their analysis without any restriction on the formation of the cracks, they obtained predicted ultimate stress around the experimental one (56% to 78% of f_c' depending on the value of shear retention factor β , see Fig. 5.7b).

Fig. 5.8a shows the predicted deflected shapes and the crack patterns at some load stages before failure. From this figure, it can be seen that both the two models predict the same type of failure. As in the experiment, the failure starts with the formation of vertical cracks under the applied load at the middle of the prism. A horizontal crack in the outer zone has been observed in the 3-D predicted crack patterns. These cracks occur because of differential vertical

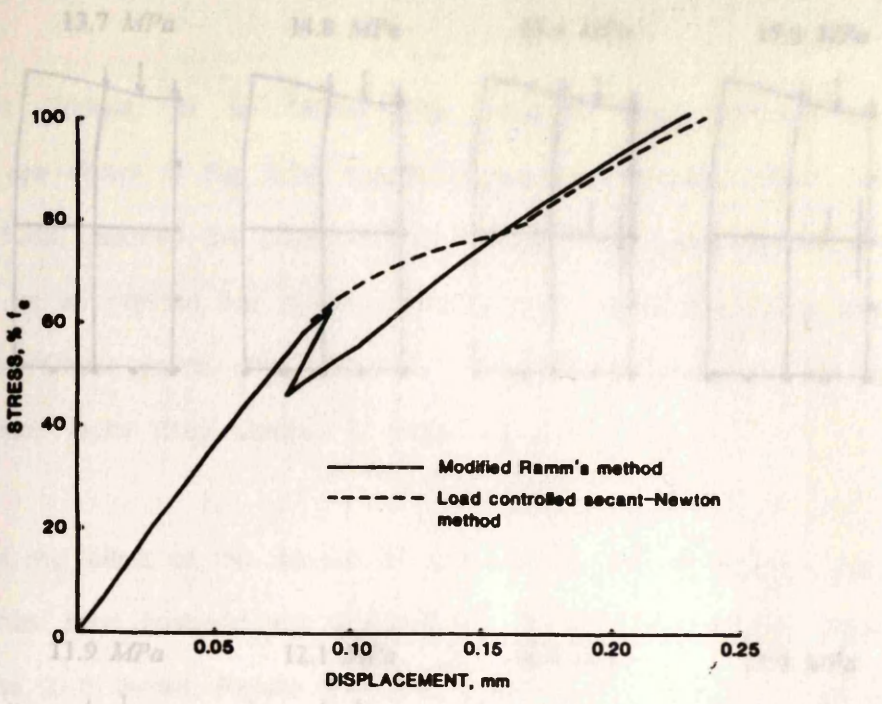


Fig. 5.7a Predicted stress-displacement curves for Niyogi's prism (Gajer and Dux 1988).

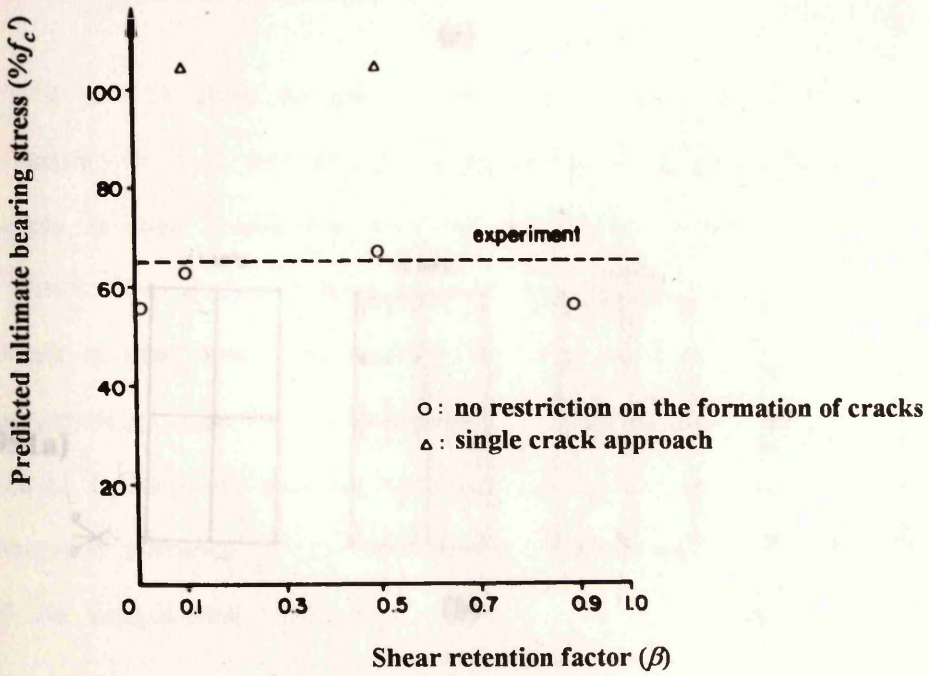


Fig. 5.7b Predicted ultimate bearing stress for Niyogi's prism (Bedard and Kotsovos 1986).

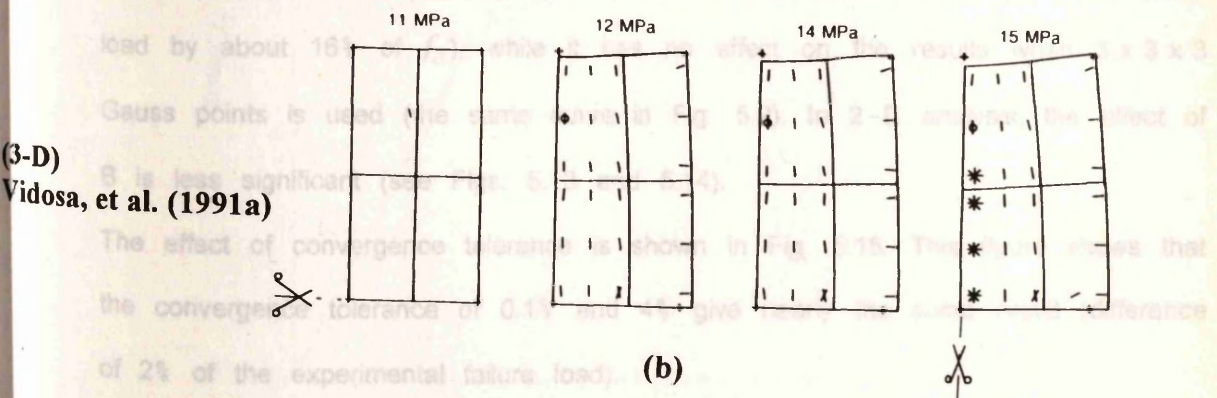
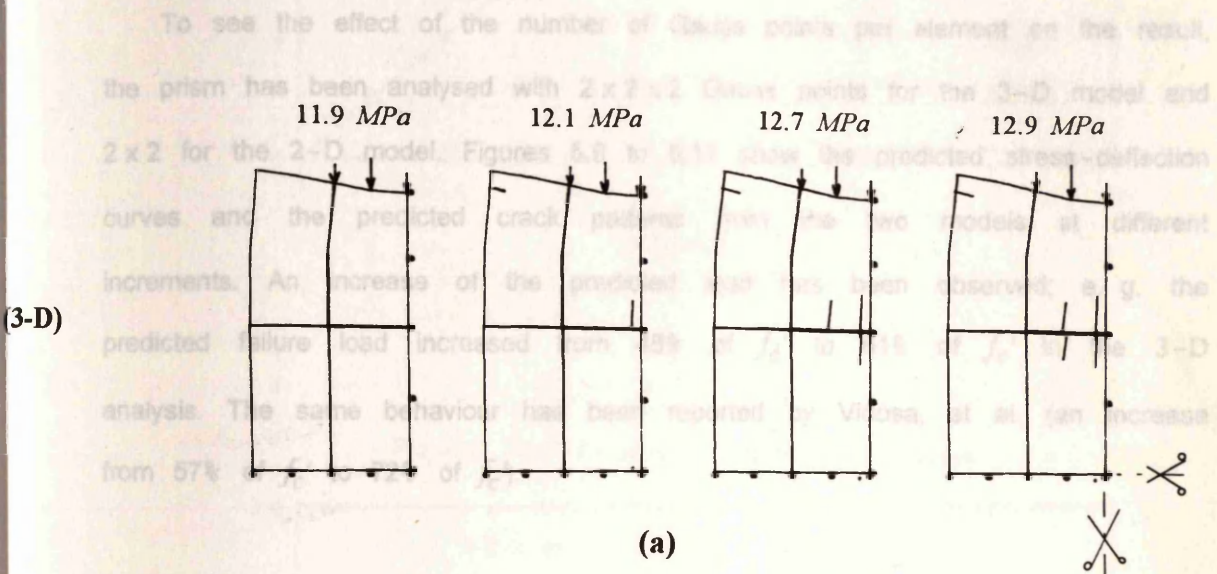
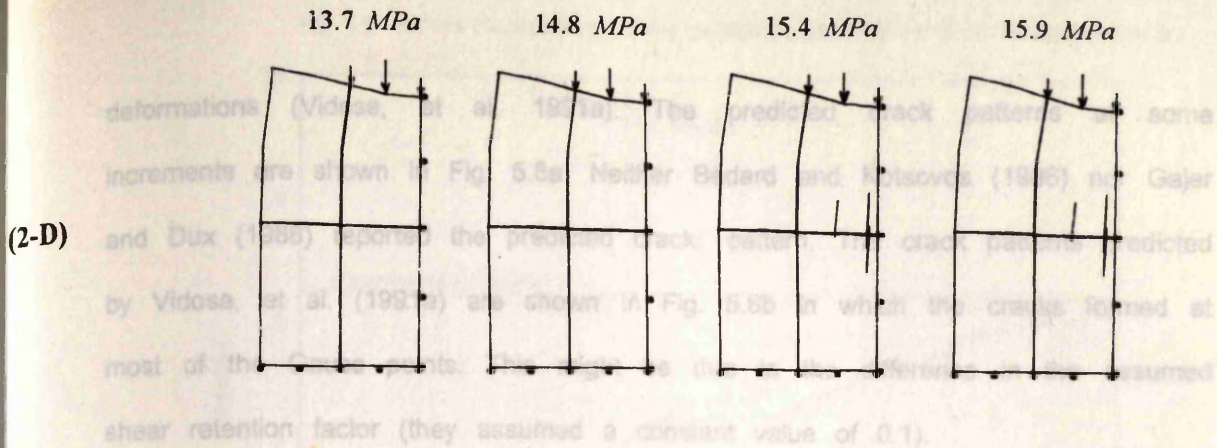


Fig. 5.8 Predicted crack patterns and deformed shapes for Niyogi's prism

deformations (Vidosa, et al. 1991a). The predicted crack patterns at some increments are shown in Fig. 5.8a. Neither Bedard and Kotsovos (1986) nor Gajer and Dux (1988) reported the predicted crack pattern. The crack patterns predicted by Vidosa, et al. (1991a) are shown in Fig. 5.8b in which the cracks formed at most of the Gauss points. This might be due to the difference in the assumed shear retention factor (they assumed a constant value of 0.1).

To see the effect of the number of Gauss points per element on the result, the prism has been analysed with $2 \times 2 \times 2$ Gauss points for the 3-D model and 2×2 for the 2-D model. Figures 5.9 to 5.11 show the predicted stress-deflection curves and the predicted crack patterns from the two models at different increments. An increase of the predicted load has been observed; e. g. the predicted failure load increased from 48% of f_c' to 61% of f_c' in the 3-D analysis. The same behaviour has been reported by Vidosa, et al. (an increase from 57% of f_c' to 72% of f_c').

Figures 5.12 to 5.14 show the effect of the constant B in equations 5.1 and 5.2 on the results. In 3-D analysis, the effect of B is significant when $2 \times 2 \times 2$ Gauss points is used (increase B from 0.4 to 0.99 increases the predicted failure load by about 16% of f_c'), while it has no effect on the results when $3 \times 3 \times 3$ Gauss points is used (the same curve in Fig. 5.9). In 2-D analysis, the effect of B is less significant (see Figs. 5.13 and 5.14).

The effect of convergence tolerance is shown in Fig. 5.15. This figure shows that the convergence tolerance of 0.1% and 4% give nearly the same result (difference of 2% of the experimental failure load).

Fig. 5.9 Stress-displacement curves for Niyogi's prism (effect of No. of Gauss points)

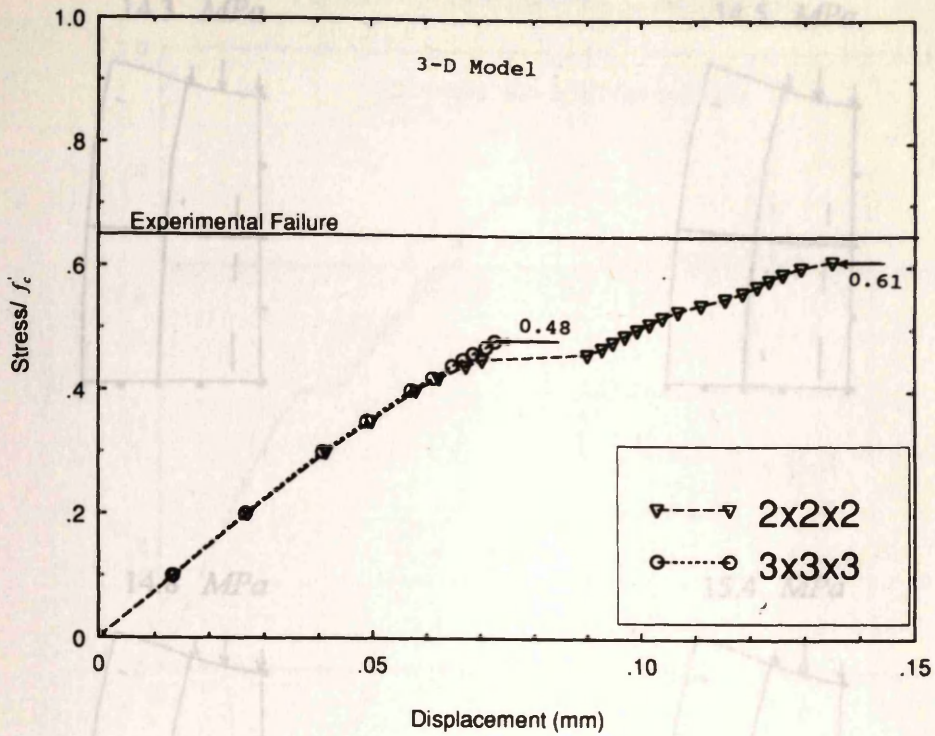


Fig. 5.10 Effect of number of Gauss points in 2-D analysis.

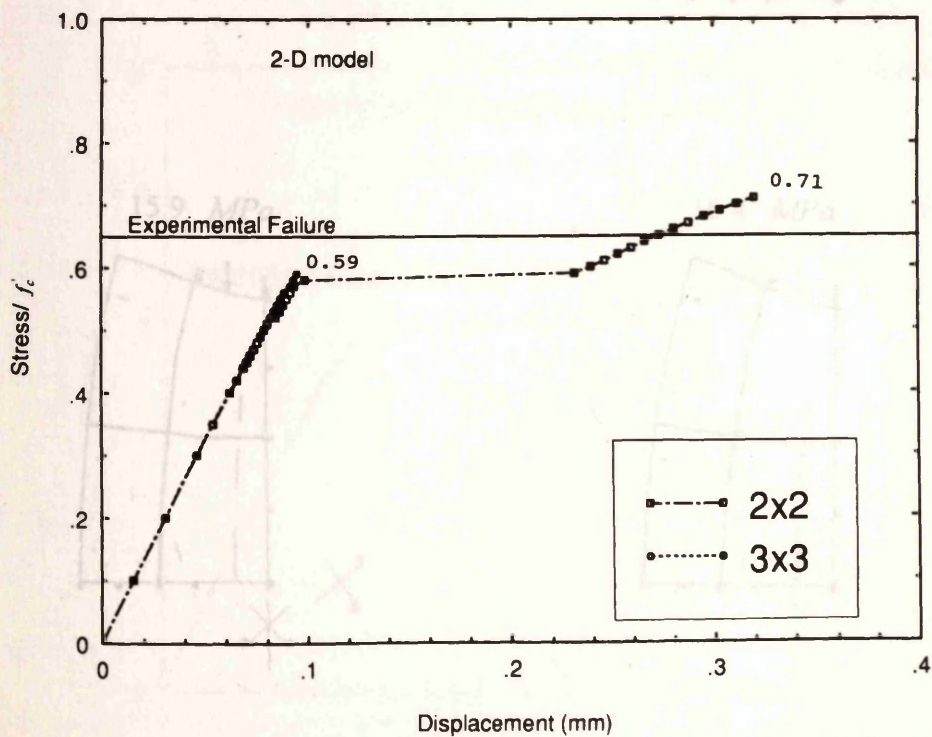


Fig. 5.11 Predicted crack patterns and deformed shapes using 2x2 Gauss points (3-D analysis).

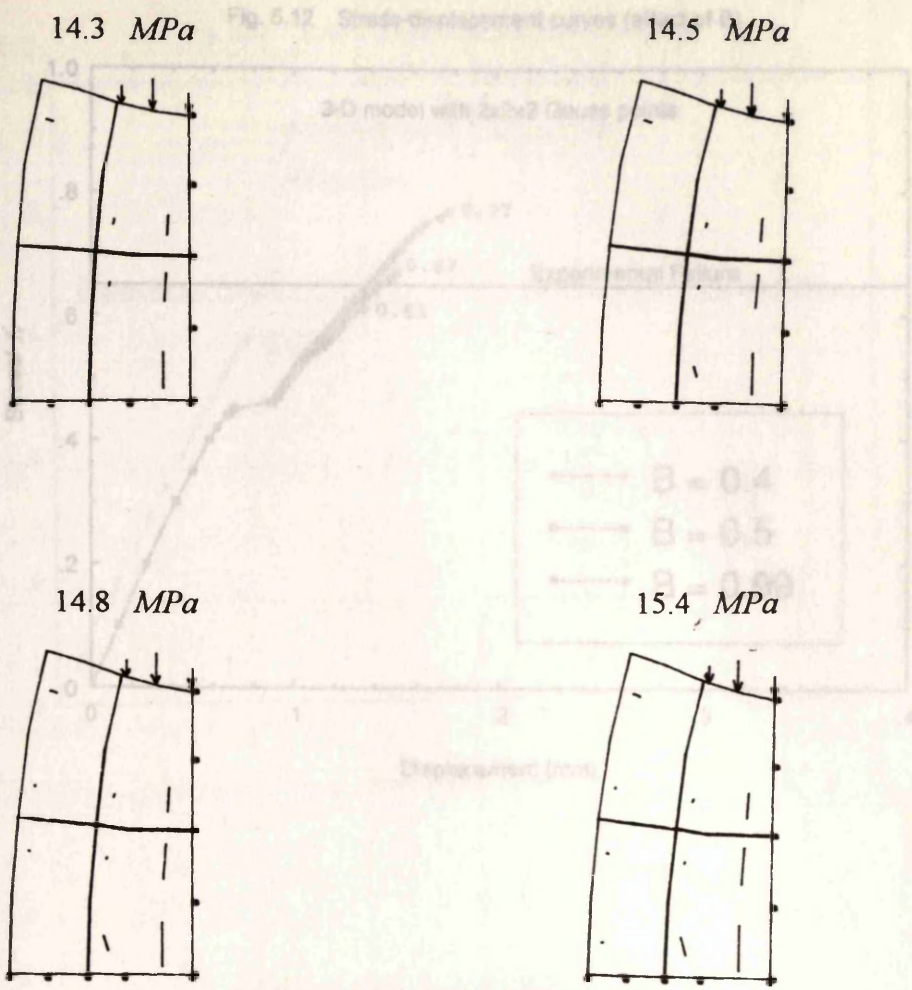


Fig. 5.12 Stress-displacement curves (3-D model with 2x2x2 Gauss points)

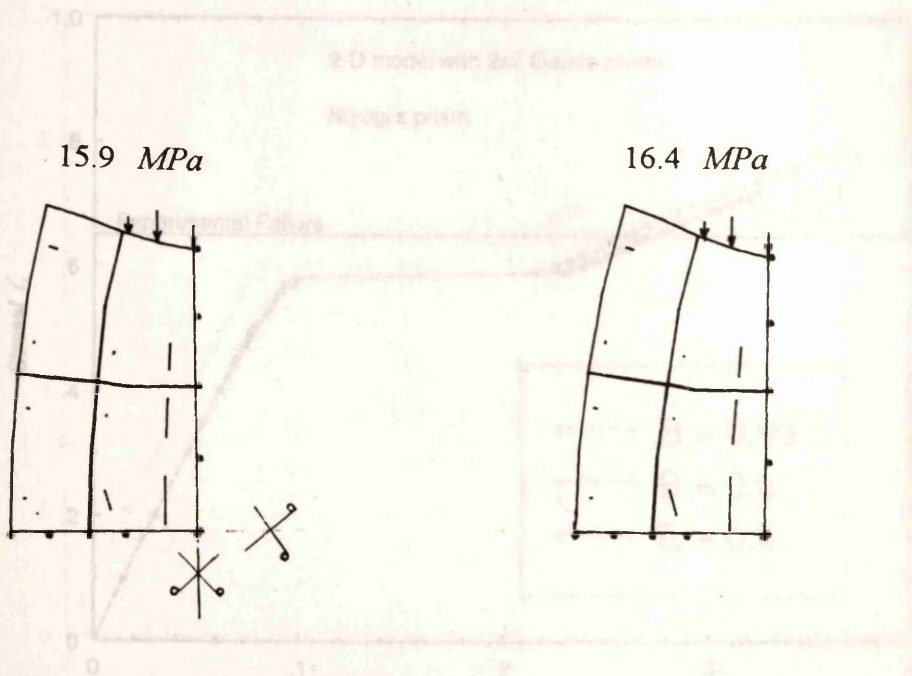


Fig. 5.13 Stress-displacement curves (2-D model with 2x2 Gauss points)

Fig. 5.11 Predicted crack patterns and deformed shapes using 2x2x2 Gauss points (3-D analysis).

Fig. 5.12 Stress-displacement curves (effect of B)

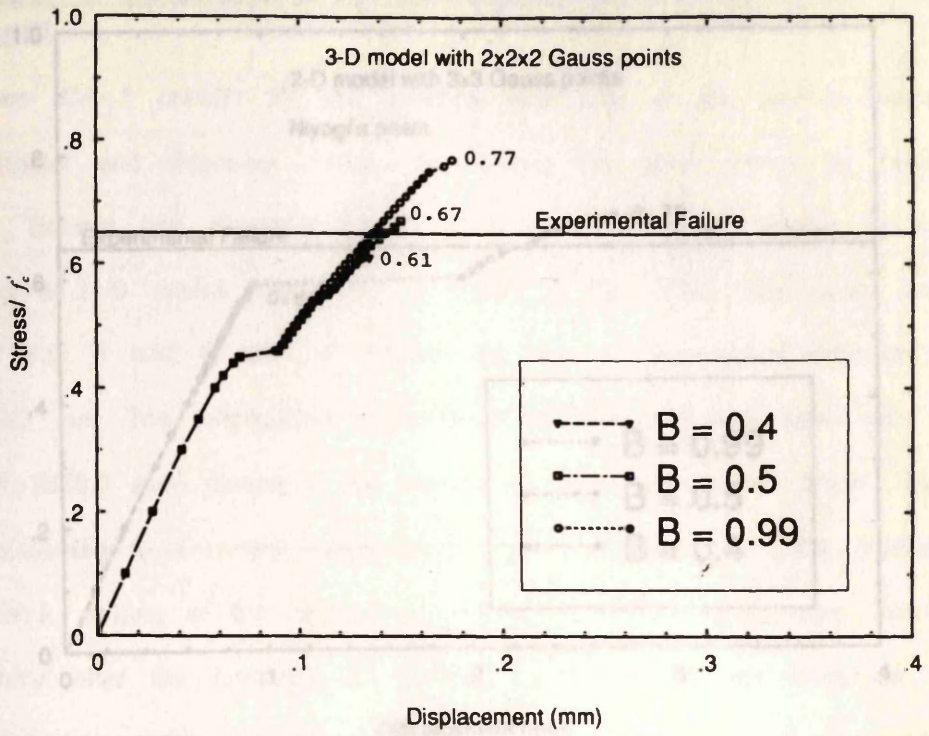


Fig. 5.13 Stress-displacement curves (effect of B)

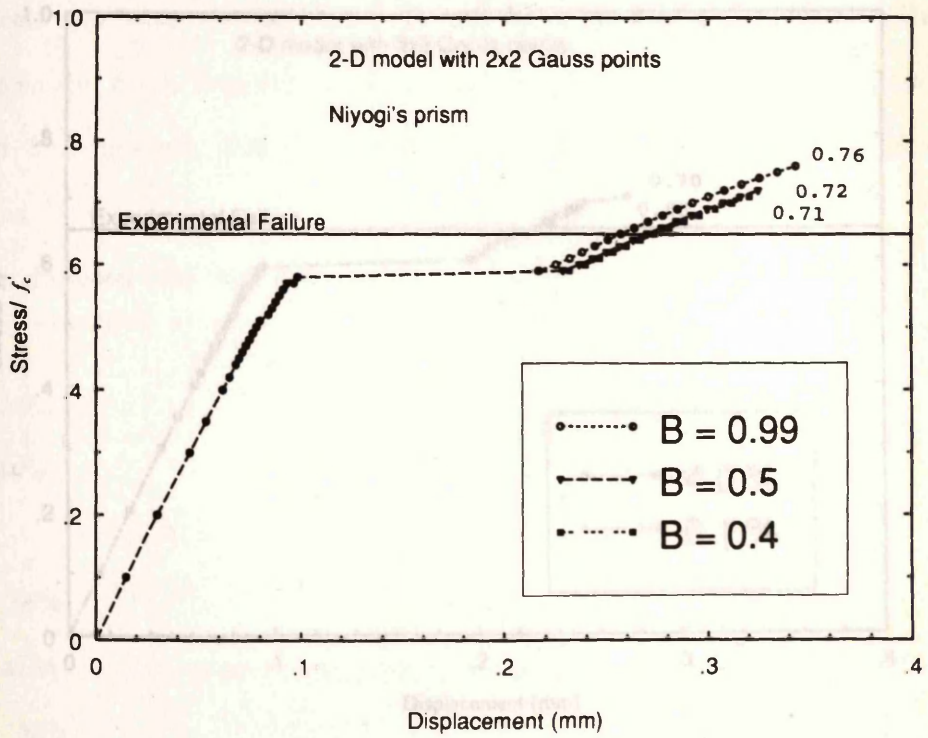


Fig. 5.14 Stress-displacement curves (effect of B)

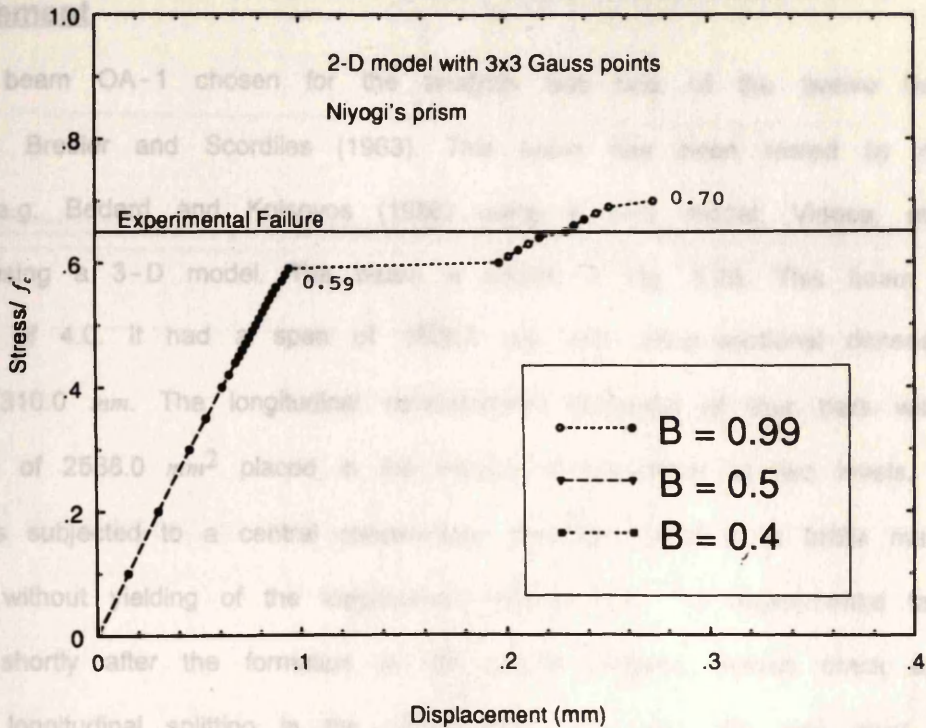
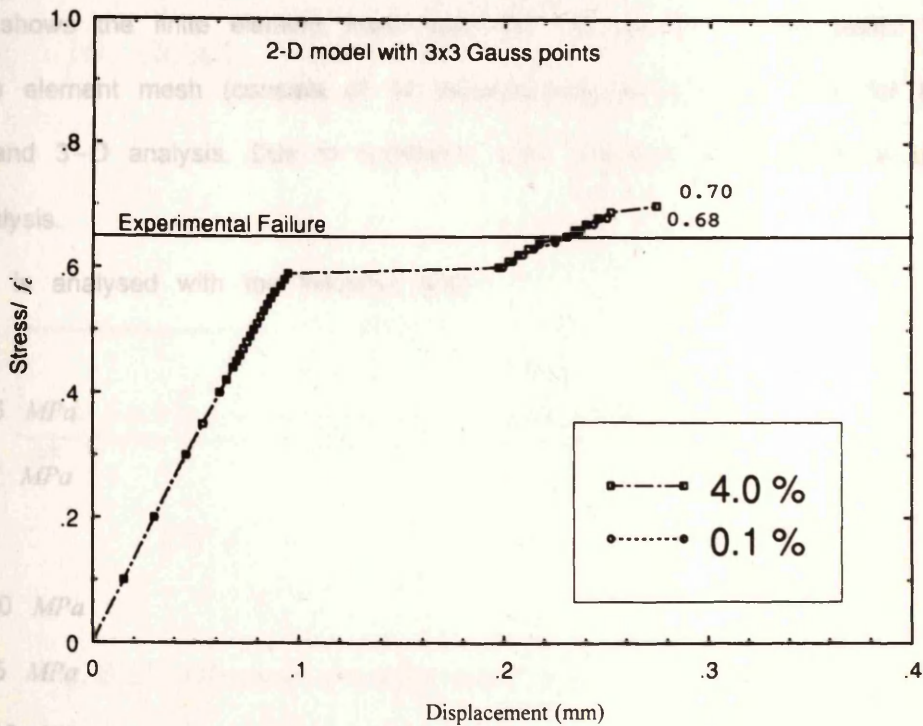


Fig. 5.15 Effect of convergence tolerance.



5.4 Prediction of the behaviour of a rectangular beam without web reinforcement

The beam OA-1 chosen for the analysis was one of the twelve beams tested by Bresler and Scordiles (1963). This beam has been tested by many authors, e.g. Bedard and Kotsovos (1986) using a 2-D model; Vidosa, et al. (1991a) using a 3-D model. The beam is shown in Fig. 5.16. This beam had a/d ratio of 4.0. It had a span of 1828.8 mm with cross-sectional dimensions 556.3 x 310.0 mm. The longitudinal reinforcement consisted of four bars with a total area of 2588.0 mm² placed in the bottom of the beam at two levels. The beam was subjected to a central concentrated load and failed in a brittle manner in shear without yielding of the longitudinal reinforcement. The experimental failure occurred shortly after the formation of the critical diagonal tension crack as a result of longitudinal splitting in the compression zone near the load point and also by horizontal splitting along the tensile reinforcement near the end of the beam. The failure occurred at a load of 333.6 kN with a mid-span deflection of 6.7 mm. Fig. 5.17 shows the crack pattern obtained from the test.

Fig. 5.18 shows the finite element mesh used for the analysis of the beam. The same finite element mesh (consists of 14 isoparametric elements) is used for both the 2-D and 3-D analysis. Due to symmetry, only one-half of the beam is used in the analysis.

The beam is analysed with the following data:

$$f'_c = 22.6 \text{ MPa}$$

$$f'_t = 2.57 \text{ MPa}$$

$$\nu = 0.15$$

$$E = 23800 \text{ MPa}$$

$$f_y = 555.5 \text{ MPa}$$

$$E_s = 218040 \text{ MPa}$$

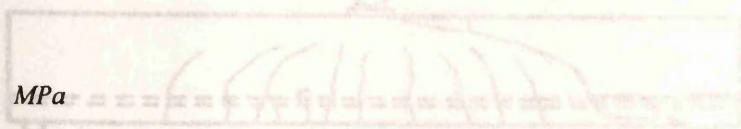
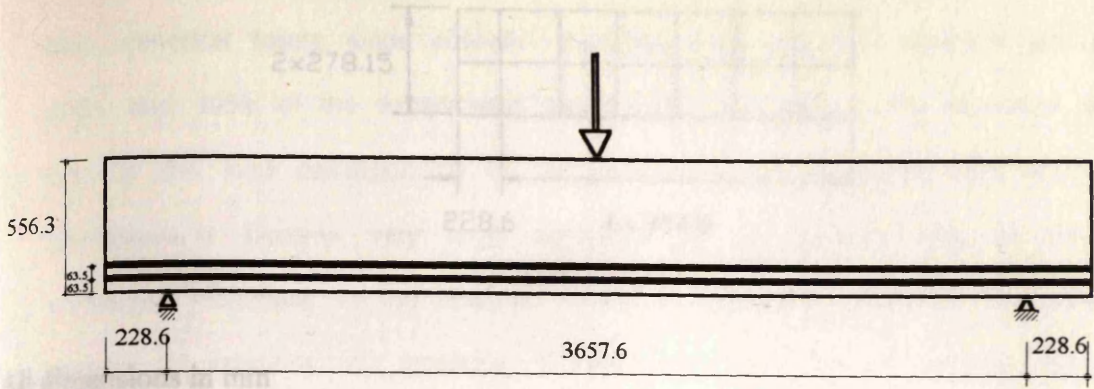


Fig. 5.17 Observed crack pattern for beam OA-1.



All dimensions in mm

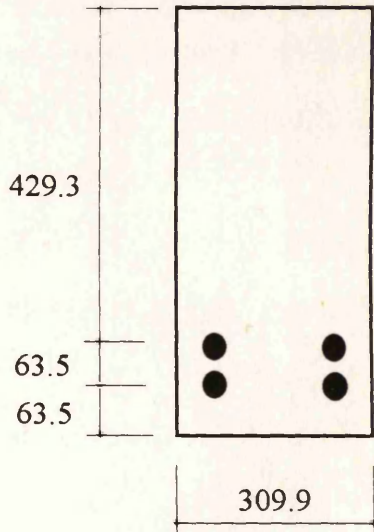


Fig. 5.16 Details of beam OA-1

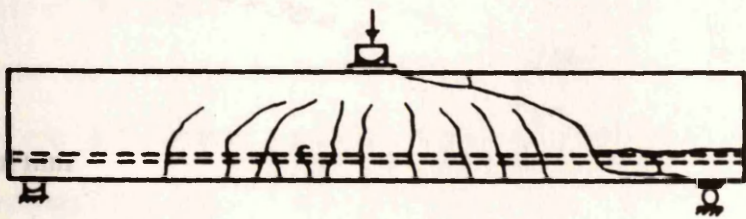


Fig. 5.17 Observed crack pattern for beam OA-1.

The numerical failure loads obtained from the 2-D and 3-D analysis are about 100% and 105% of the experimental failure load, respectively. The numerical failure load is the load corresponding to the last convergent increment after which the displacements become very large compared to the displacements at the last converged increment. In the analysis sometimes at certain increment the maximum number of iterations (50 iterations) reaches while the norm of residual forces is still greater than the convergence tolerance (4%). Despite this, the convergence occurs but at a slow rate such that the norm may reach to about 5% or 6% at the last iteration. Also the displacements are not too large. This should not be considered as a numerical failure.

The predicted load-deflection curves obtained from the 2-D and 3-D analysis are compared with the experimental curve in Fig. 5.19. By comparing the predicted failure loads and the load-deflection curves obtained from the two models it can be concluded that both of the 2-D and 3-D analysis give nearly the same degree of accuracy in predicting the behaviour of the beam under analysis.

The predicted stresses obtained from the two models, at a Gauss point under the applied load near the middle of the beam, are plotted at all increments up to the numerical failure (see Fig. 5.20). From this figure, it can be seen that the stresses obtained from the 3-D model, at all increments, in the direction normal to the plane of the beam (Y-direction) are very small (less than 1.0 MPa) in comparison to the stresses in the other two directions (X and Z). This may explain why the 3-D analysis result did not differ much from that obtained from the 2-D analysis.

In Figs. 5.21 to 5.25, the predicted crack patterns and deformed shapes obtained from the two models are shown at different increments. The displacements are magnified by 20 times. The cracks are plotted at the Gauss points. The crack is represented by a line. Its direction is normal to the maximum principal stress and its length is proportional to the strain normal to the crack at this Gauss point. One line per Gauss point means single crack occurred at this point, two lines

Fig. 5.19 Load-deflection curves of beam OA-1

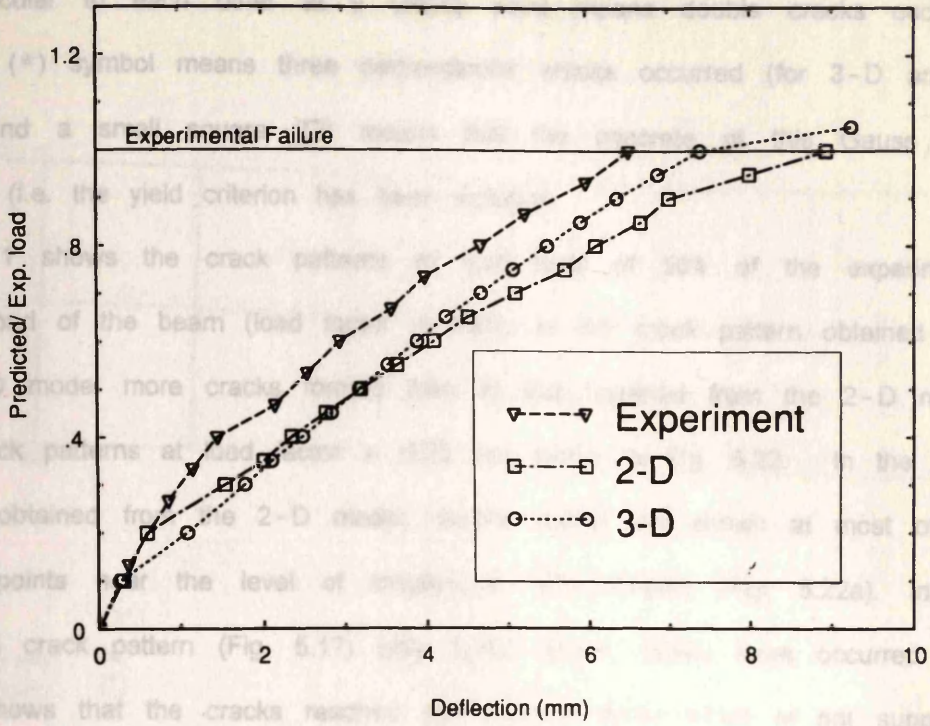
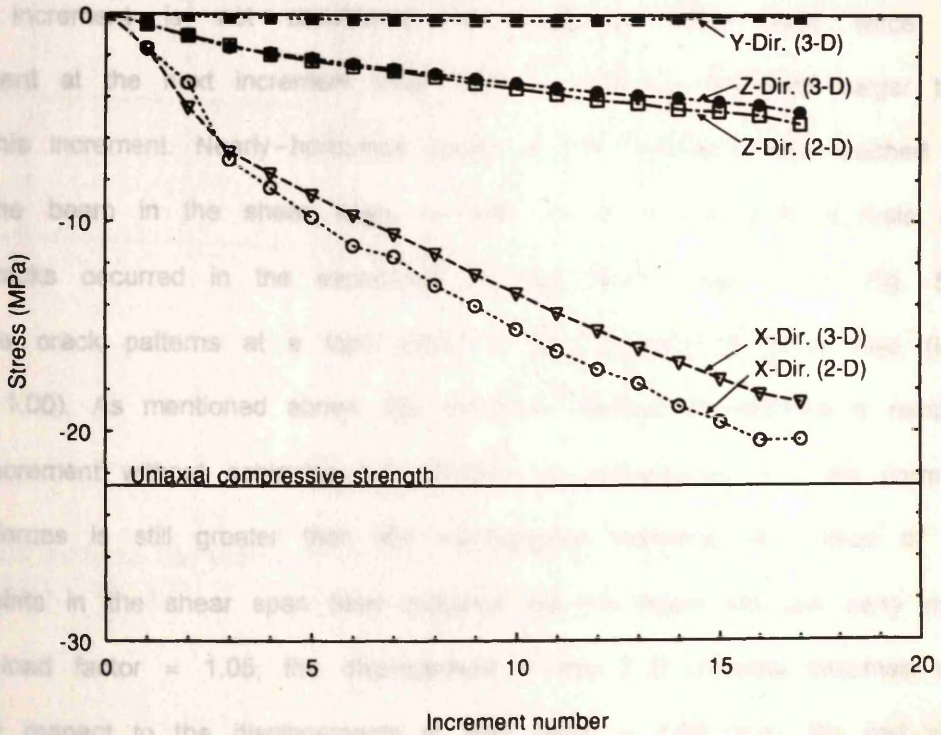
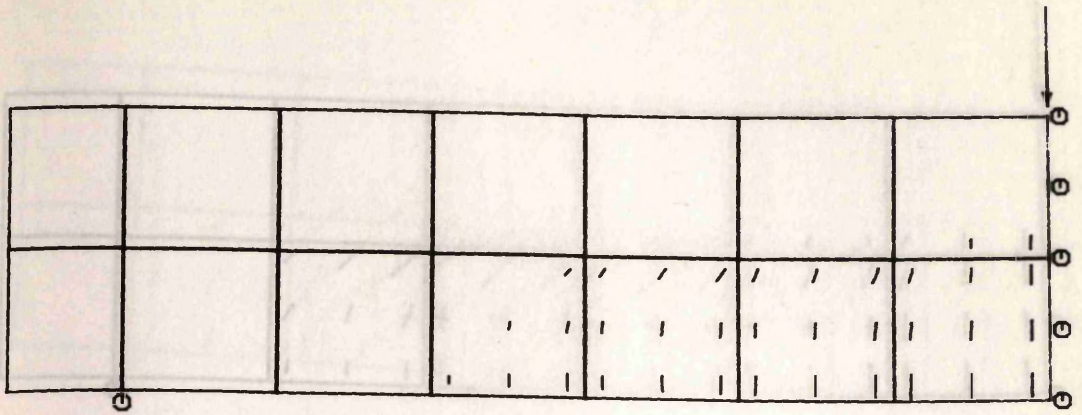


Fig. 5.20 Stresses under the load point at different increments (Beam OA-1)



perpendicular to each other at a Gauss point means double cracks occurred, asterisk (*) symbol means three perpendicular cracks occurred (for 3-D analysis only), and a small square (\square) means that the concrete at this Gauss point crushed (i.e. the yield criterion has been violated).

Fig. 5.21 shows the crack patterns at load level of 50% of the experimental failure load of the beam (load factor = 0.50). In the crack pattern obtained from the 3-D model more cracks formed than in that obtained from the 2-D model. The crack patterns at load factor = 0.75 are shown in Fig. 5.22. In the crack pattern obtained from the 2-D model, double cracks are shown at most of the Gauss points near the level of longitudinal reinforcement (Fig. 5.22a). In the observed crack pattern (Fig. 5.17) only some double cracks have occurred. Fig. 5.22b shows that the cracks reached the support region which is not supported by the observations in the experiment. In Fig. 5.23, the crack patterns obtained from the two models are plotted at a load factor = 0.95. This increment is the last converged increment in both the 2-D and 3-D analysis. Therefore, the load at this increment is not considered the numerical failure load since the displacement at the next increment (load factor = 1.00) is not much larger than that at this increment. Nearly-horizontal cracks at this increment have reached the top of the beam in the shear span, in both the 2-D and 3-D analysis (the critical cracks occurred in the experiment at load factor about 0.80). Fig. 5.24 shows the crack patterns at a load equal to the experimental failure load (load factor = 1.00). As mentioned above, the maximum number of iterations is reached at this increment without achieving the condition of convergence (i.e., the norm of residual forces is still greater than the convergence tolerance, 4%). Most of the Gauss points in the shear span have cracked, but the beam still can carry more load. At load factor = 1.05, the displacement in the 2-D analysis becomes very large with respect to the displacements at load factor = 1.00 (e.g.; the mid-span deflection increased from 8.93 to 145.1 mm). Fig. 5.25 shows the crack patterns and the deformed shapes at a load factor = 1.05 (in Fig. 5.25a displacements



single crack : /
 double crack : //
 triple crack (3-D only): *
 crushing of concrete : □

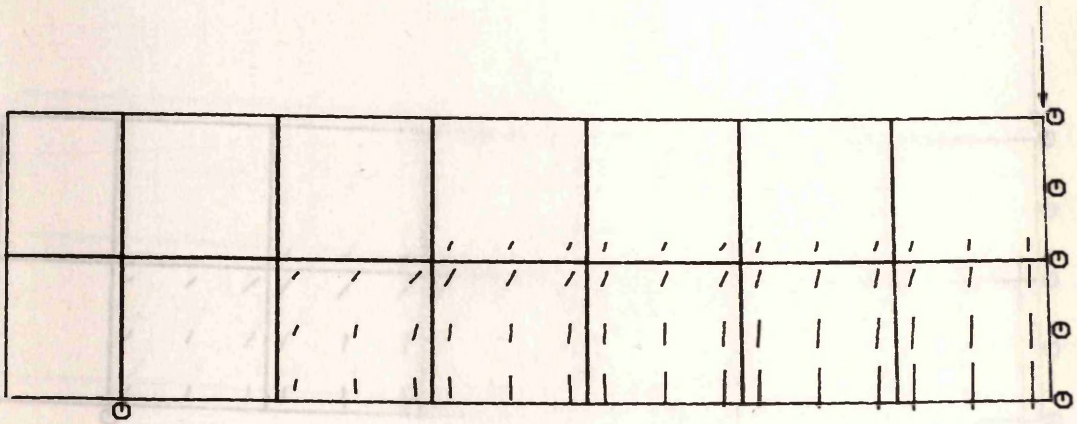
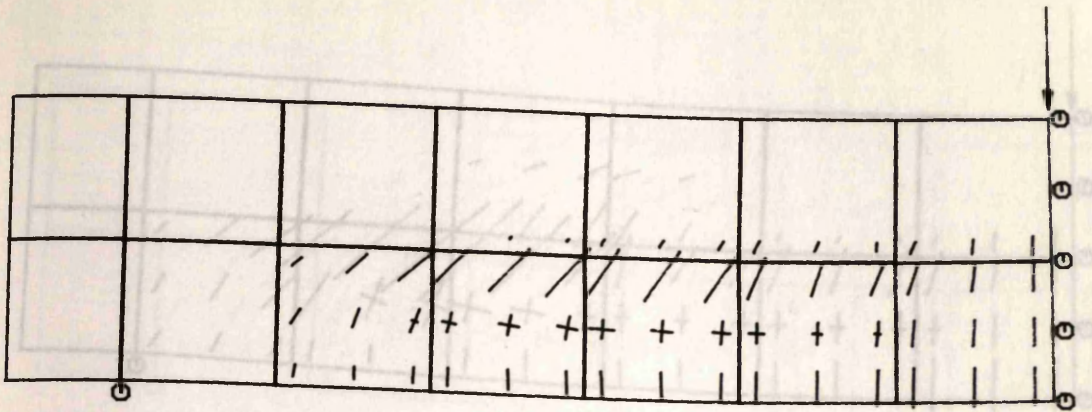


Fig. 5.21 Crack patterns and deformed shapes of beam OA-1 at load factor = 0.50:
 (a) 2-D; (b) 3-D (displacements magnified x 20).



single crack : //
 double crack : X
 triple crack (3-D only): +
 crushing of concrete : □

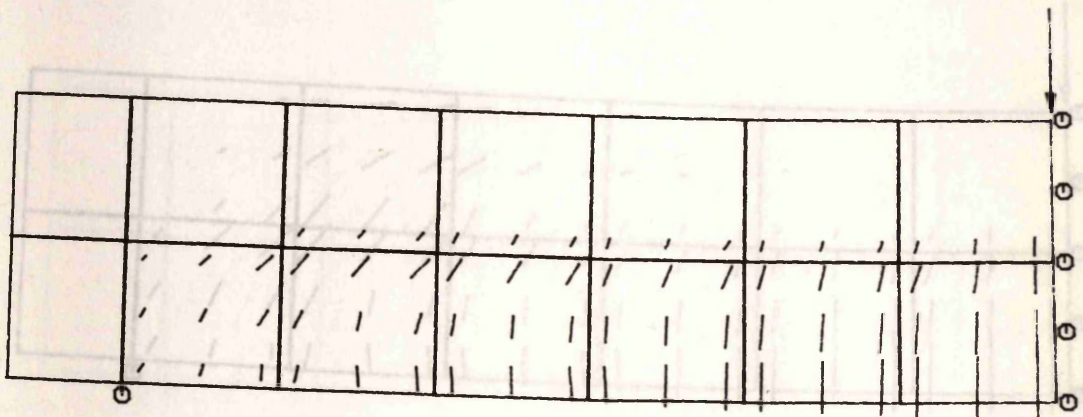


Fig. 5.22 Crack patterns and deformed shapes of beam OA-1 at load factor = 0.75:
 (a) 2-D; (b) 3-D (displacements magnified x 20).

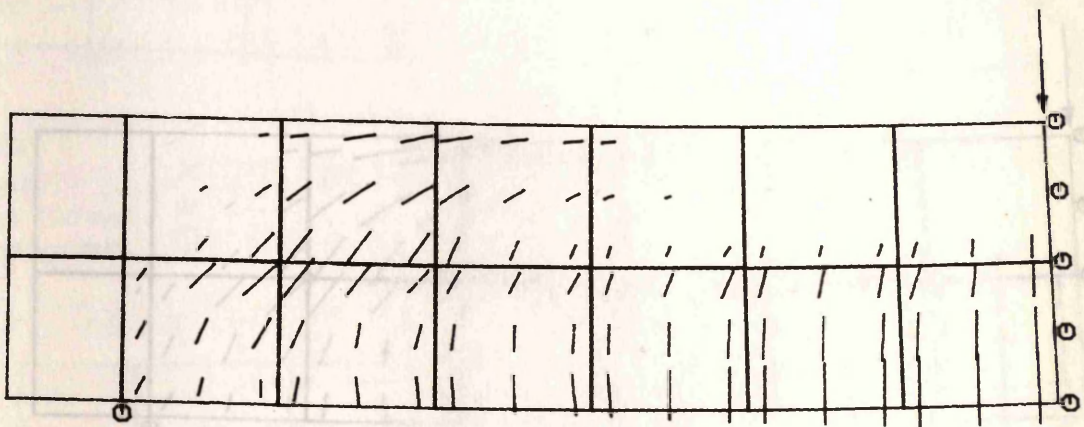
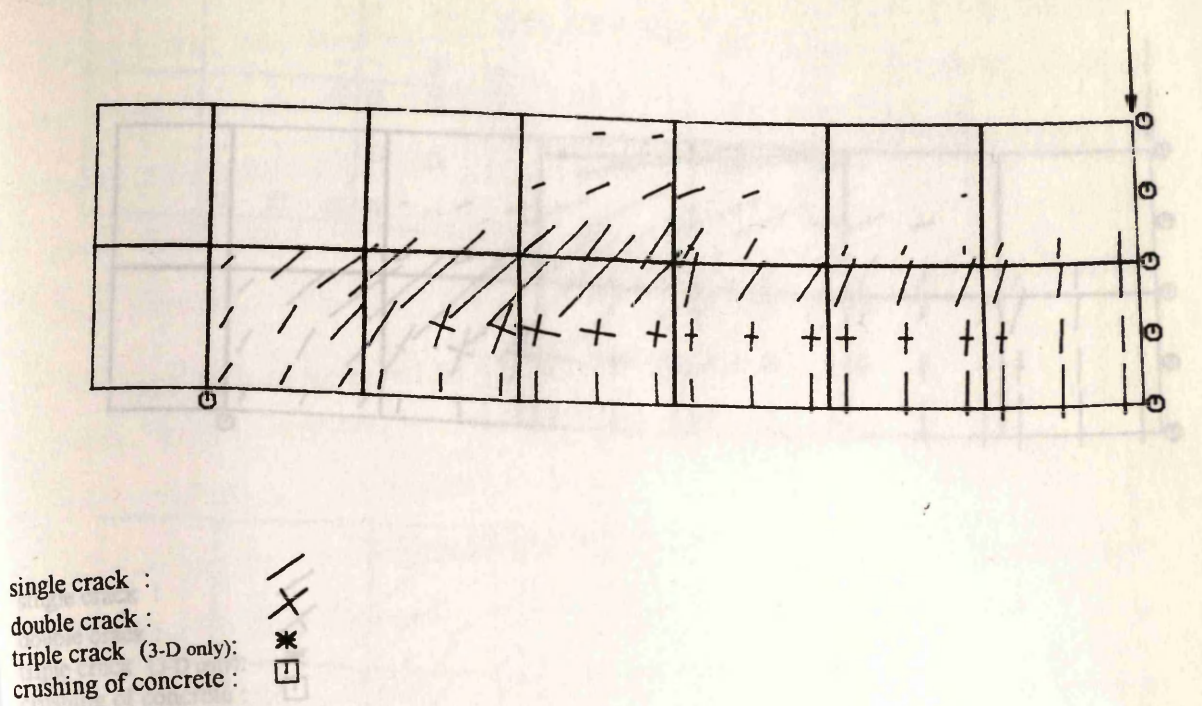


Fig. 5.23 Crack patterns and deformed shapes of beam OA-1 at load factor = 0.95:
 (a) 2-D; (b) 3-D (displacements magnified x 20).

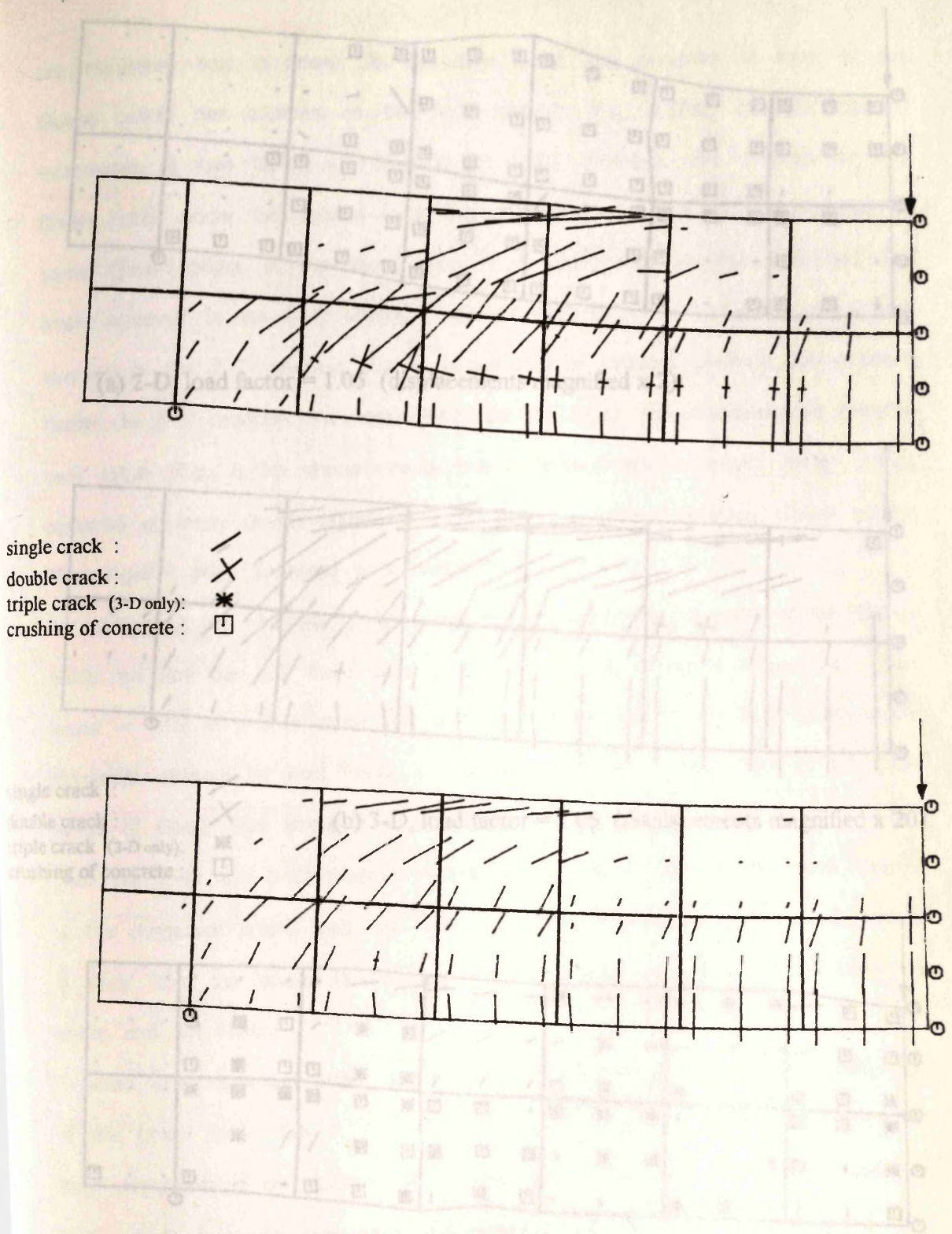
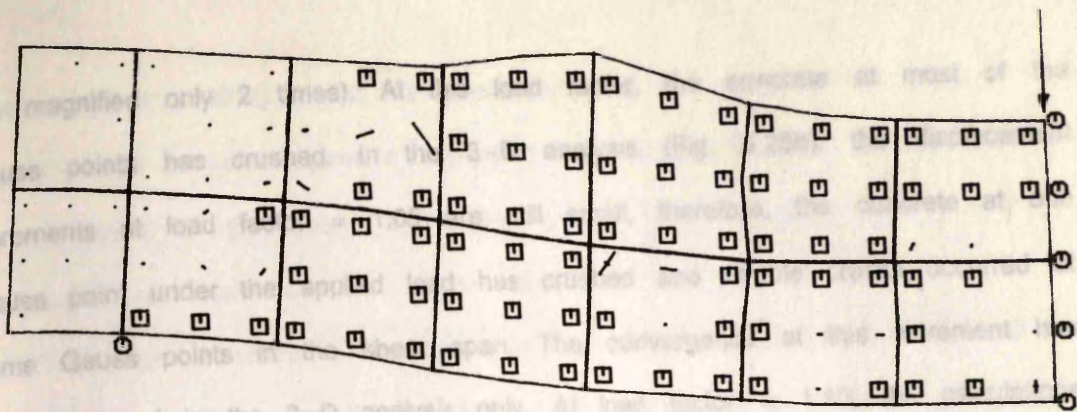
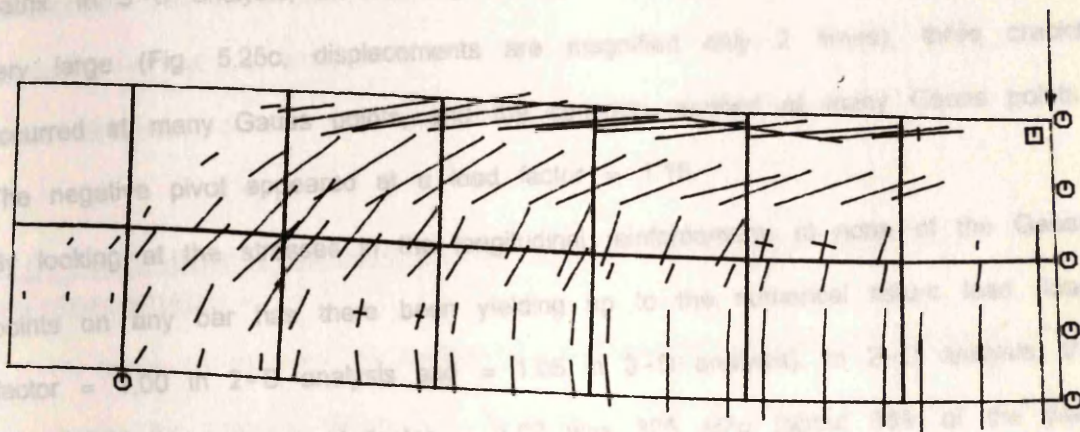


Fig. 5.24 Crack patterns and deformed shapes of beam OA-1 at load factor = 1.00:
 (a) 2-D; (b) 3-D (displacements magnified x 20).

Fig. 5.25 Crack patterns and deformed shapes of beam OA-1

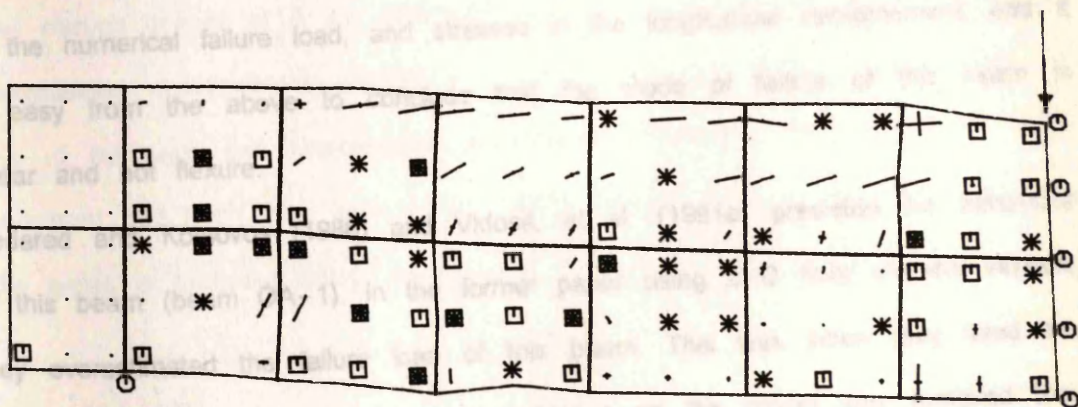


(a) 2-D, load factor = 1.05 (displacements magnified x 2).



(b) 3-D, load factor = 1.05 (displacements magnified x 20).

single crack : /
 double crack : X
 triple crack (3-D only): *
 crushing of concrete : □



(c) 3-D, load factor = 1.10 (displacements magnified x 2).

Fig. 5.25 Crack patterns and deformed shapes of beam OA-1.

are magnified only 2 times). At this load factor, the concrete at most of the Gauss points has crushed. In the 3-D analysis (Fig. 5.25b), the displacement increments at load factor = 1.05 are still small, therefore, the concrete at one Gauss point under the applied load has crushed and double cracks occurred at some Gauss points in the shear span. The convergence at this increment has been achieved in the 3-D analysis only. At load factor = 1.10, the calculations stopped in the 2-D analysis due to appearance of negative pivot in the stiffness matrix. In 3-D analysis, the convergence did not occur, the displacements became very large (Fig. 5.25c, displacements are magnified only 2 times), three cracks occurred at many Gauss points, and the concrete crushed at many Gauss points. The negative pivot appeared at a load factor = 1.15.

By looking at the stresses in the longitudinal reinforcement, at none of the Gauss points on any bar has there been yielding up to the numerical failure load (load factor = 1.00 in 2-D analysis and = 1.05 in 3-D analysis). In 2-D analysis, the maximum stresses at load factor = 1.00 was 325 MPa (about 58% of the yield stress of steel). This stress in 3-D analysis was 356 MPa at load factor = 1.05. Both the 2-D and 3-D models predicted similar crack patterns, deformed shapes at the numerical failure load, and stresses in the longitudinal reinforcement, and it is easy from the above to conclude that the mode of failure of this beam is shear and not flexure.

Bedared and Kotsovos (1986) and Vidosa, et al. (1991a) predicted the behaviour of this beam (beam OA-1). In the former paper using 2-D finite element version, they overestimated the failure load of this beam. This was when they used the single crack approach and when this restriction on the cracks was removed they underestimate the failure load by about 40%. This result was obtained using constant shear retention factor = 0.5. In the second paper using a 3-D finite element version, 7 runs were performed on this beam with different parameters all of them using the single crack approach. The predicted failure load was between 15% to 90% of the experimental failure load. One comment on the analysis by

Vidoso, et al. (1991a) should be mentioned here that despite their using a 3-D model which is very expensive compared to 2-D model, they approximated the representation of the beam by neglecting the concrete cover and putting the longitudinal reinforcement in one layer instead of two.

The large difference in predictions by the 2-D model reported by Bedard and Kotsovos or in those reporting by Vidoso, et al. using a 3-D model may reflect that the problem is not 2-D or 3-D model, but it is how to adjust all parameters that affect the prediction to get the best result, and this cannot be predicted without the analysis of a large number of beams.

More discussion on this beam is presented in the next chapter.

5.5 Prediction of the behaviour of a rectangular beam with web reinforcement

A beam (A-1) from the twelve beams tested by Bresler and Scordiles (1963) is chosen for analysis. Beam A-1 is nearly similar to beam OA-1, that has been analysed in the previous section, except for the use of web and compression reinforcement. The cross-sectional dimensions of the beam are 561.3 x 307.3 mm. The stirrups consist of 6 mm deformed bars with a spacing of 210.0 mm and the compression reinforcement consists of 2 bars of 10 mm diameter (Fig. 5.26). The use of the web and compression reinforcement increased the experimental failure load from 333.3 kN (the experimental failure load of beam OA-1) to 467 kN.

The beam is analysed using the following data:

$$f_c' = 24.1 \text{ MPa}$$

$$f_t' = 2.65 \text{ MPa}$$

$$\nu = 0.15$$

$$E = 23800 \text{ MPa}$$

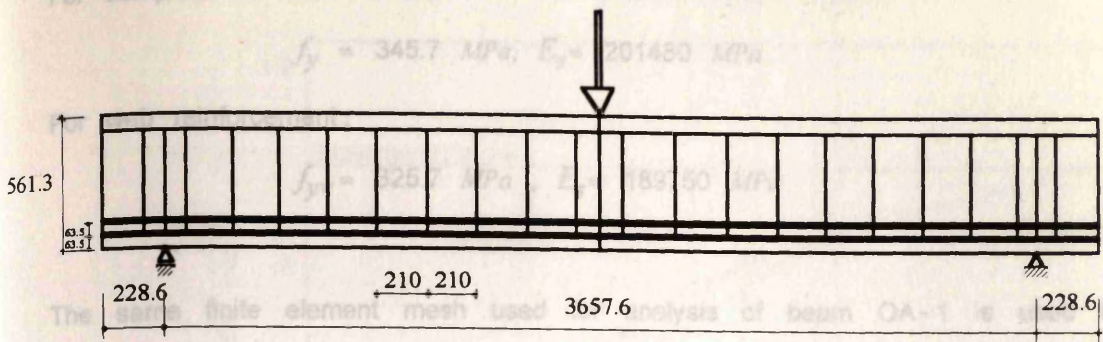
For tension reinforcement:

$$f_y = 555.5 \text{ MPa} , E_s = 218040 \text{ MPa}$$

For compression reinforcement:

$$f_y = 345.7 \text{ MPa}; E_s = 201480 \text{ MPa}$$

$$f_y = 325.7 \text{ MPa}; E_s = 189350 \text{ MPa}$$



All dimensions in mm

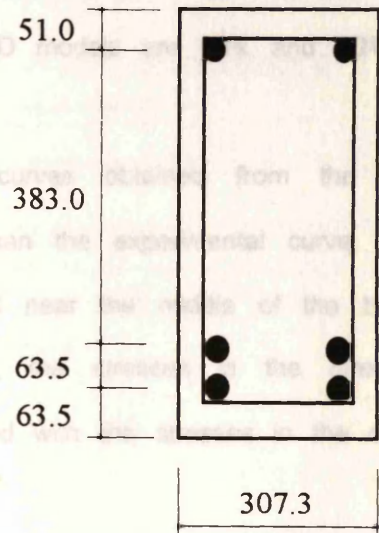


Fig. 5.26a Details of beam A-1

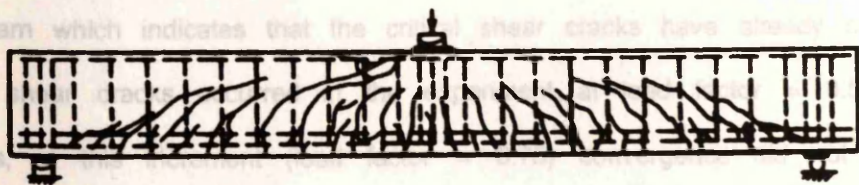


Fig. 5.26b Observed crack pattern for beam A-1.

For compression reinforcement:

$$f_y = 345.7 \text{ MPa}, E_s = 201480 \text{ MPa}$$

For web reinforcement:

$$f_{yv} = 325.7 \text{ MPa}, E_s = 189750 \text{ MPa}$$

The same finite element mesh used for analysis of beam OA-1 is used here (Fig. 5.18). Both of the two models underestimated the failure load of this beam. The predicted failure loads from the 2-D and 3-D models are 90% and 80% of the experimental failure load, respectively.

Fig. 5.27 shows the predicted load-deflection curves obtained from the two models. The predicted curves are more flexible than the experimental curve. The stresses at a Gauss point under the applied load near the middle of the beam are shown in Fig. 5.28. Like the beam OA-1, the stresses in the direction normal to the beam plane are very small compared with the stresses in the other two directions (X and Z directions).

The predicted crack patterns and deformed shapes are plotted in Fig. 5.29 to Fig. 5.32. Fig. 5.29 shows the crack patterns and deformed shapes at load factor = 0.5. The beam behaves at this increment as the beam OA-1 at the same increment, most of the Gauss points at the bottom of the beam have cracked. At load factor = 0.75 (Fig. 5.30), nearly horizontal cracks occurred in the top half of the beam which indicates that the critical shear cracks have already occurred (the critical shear cracks occurred in the experiment at load factor = 0.57). In 3-D analysis, at this increment (load factor = 0.75) convergence did not take place. The rate of convergence was very slow. The norm of residual forces reached 4.76% at the maximum number of iterations allowed (50 iterations).

Fig. 5.31 shows the cracks and the deformed shapes at the numerical failure loads predicted from the 2-D (load factor = 0.90) and 3-D (load factor = 0.80) analysis which clearly indicate that shear is dominant.

Fig. 5.27 Load-deflection curves of beam A-1

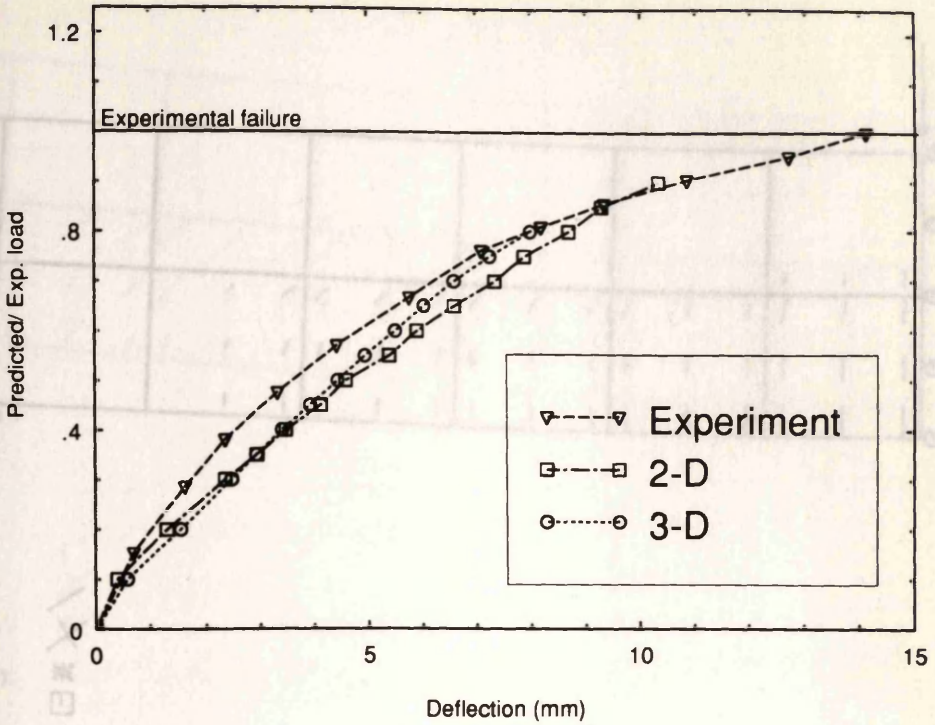
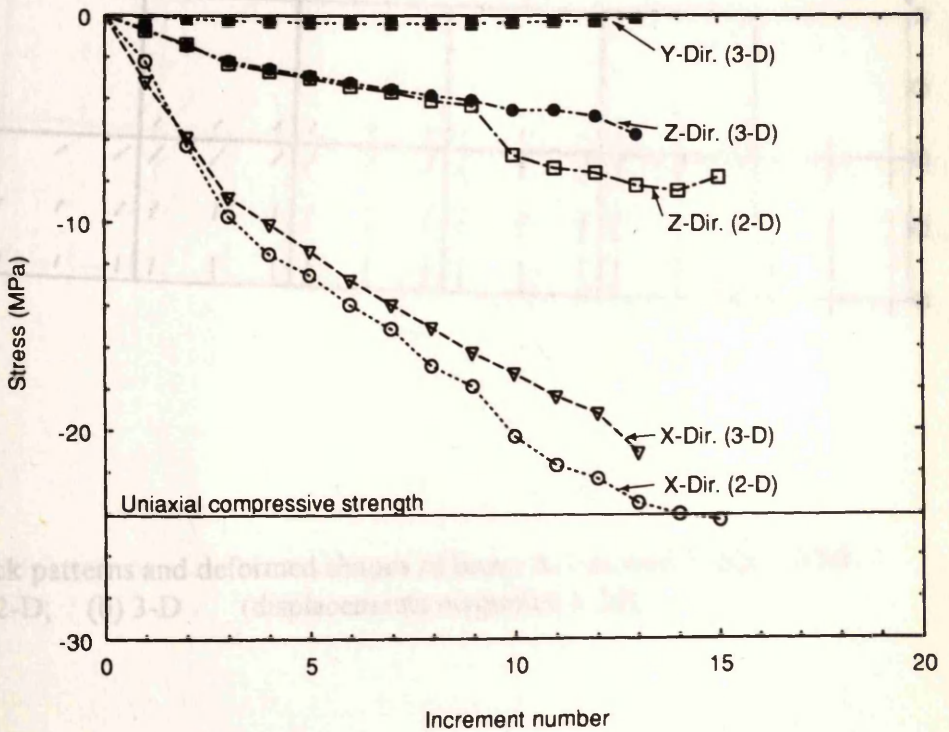
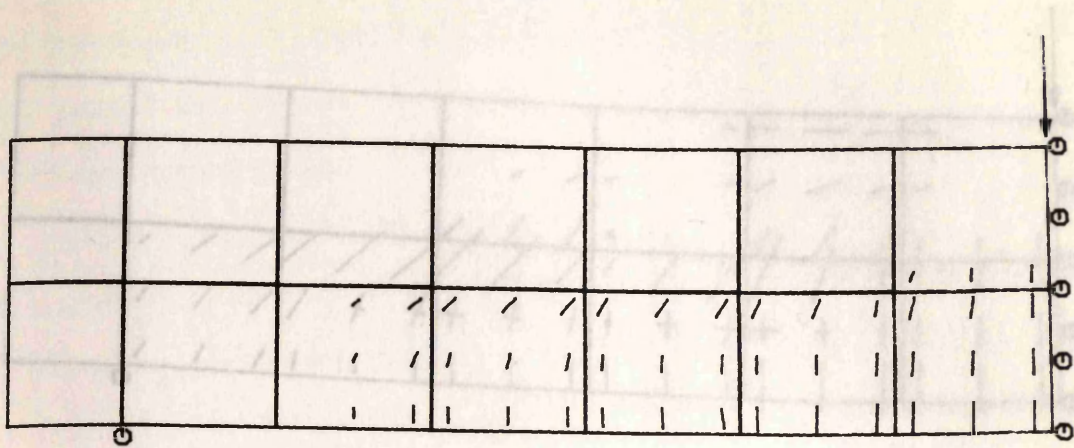


Fig. 5.28 Stresses under the load point at different increments (Beam A-1)





single crack : /
 double crack : X
 triple crack (3-D only): *
 crushing of concrete : □

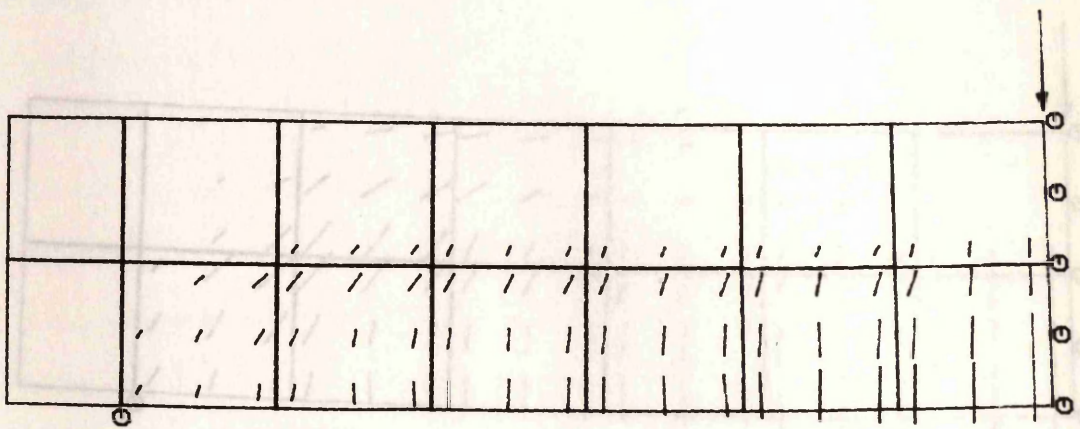
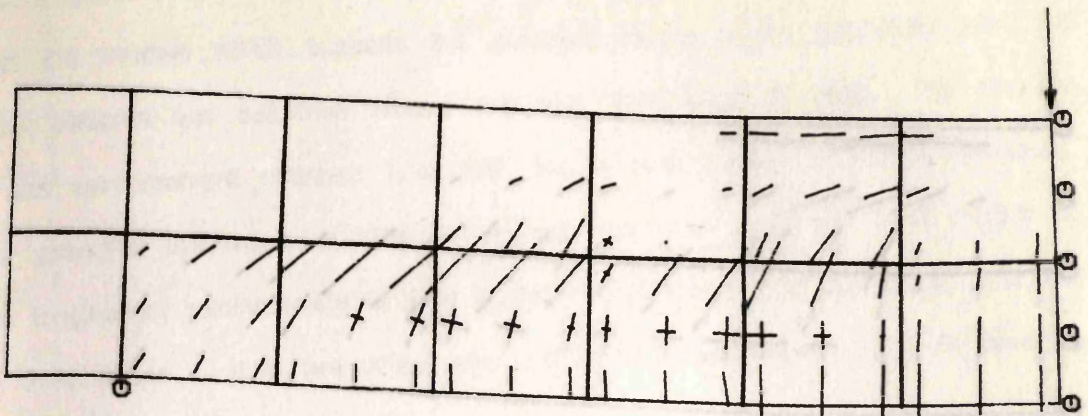


Fig. 5.29 Crack patterns and deformed shapes of beam A-1 at load factor = 0.50:
 (a) 2-D; (b) 3-D (displacements magnified x 20).



single crack : /
 double crack : X
 triple crack (3-D only): *
 crushing of concrete : □

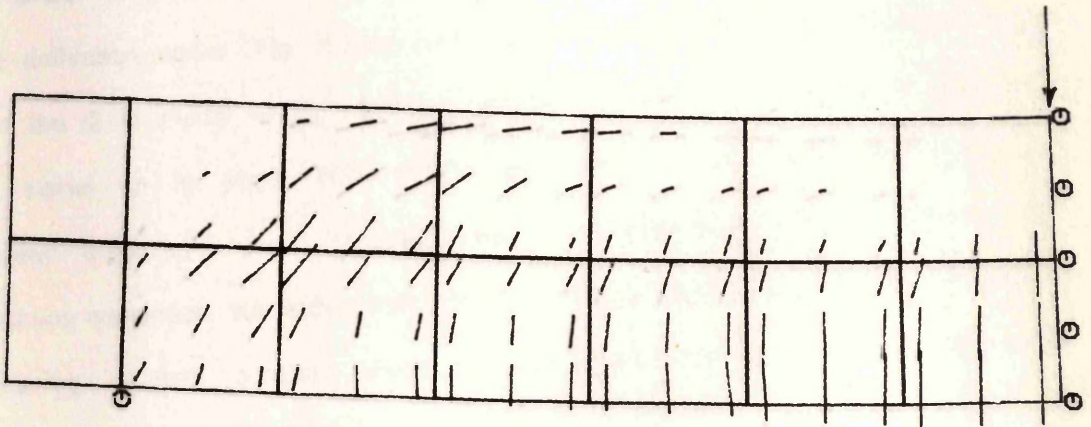
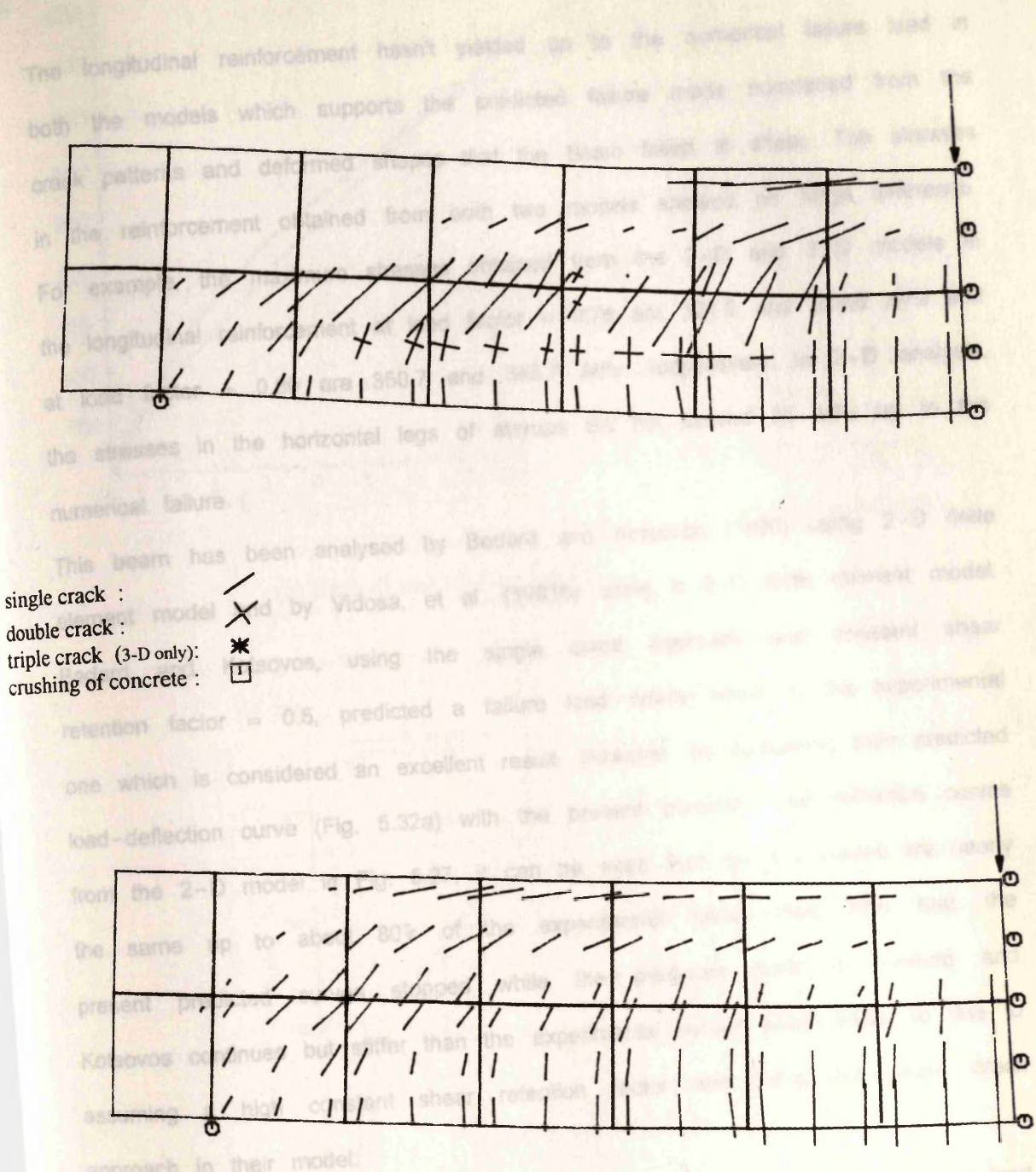


Fig. 5.30 Crack patterns and deformed shapes of beam A-1 at load factor = 0.75:
 (a) 2-D; (b) 3-D (displacements magnified x 20).



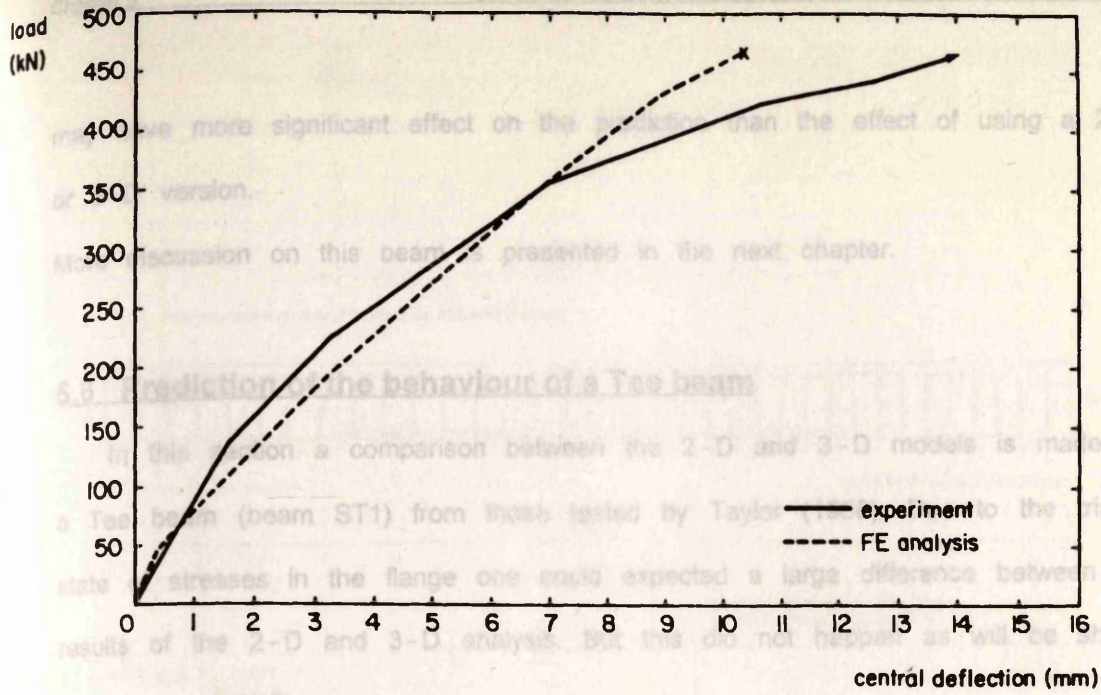
- single crack : /
- double crack : //
- triple crack (3-D only): *
- crushing of concrete : □

Fig. 5.31 Crack patterns and deformed shapes of beam OA-1: (a) 2-D, load factor = 0.90; (b) 3-D, load factor = 0.80 (displacements magnified x 20).

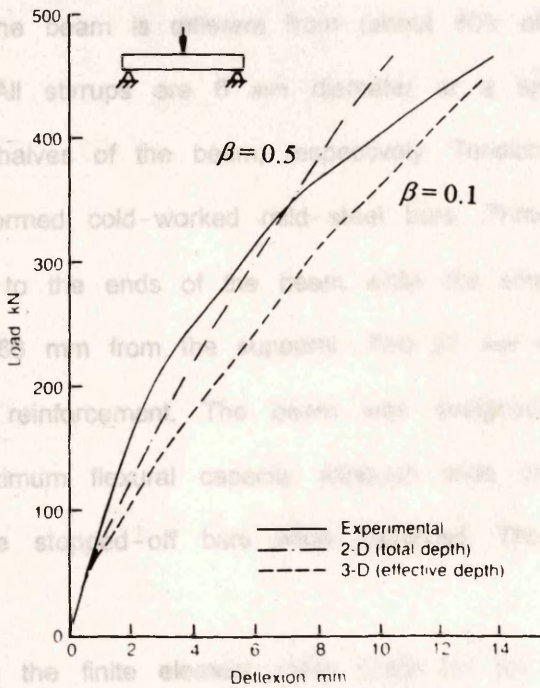
The longitudinal reinforcement hasn't yielded up to the numerical failure load in both the models which supports the predicted failure mode concluded from the crack patterns and deformed shapes that the beam failed in shear. The stresses in the reinforcement obtained from both two models showed no large difference. For example, the maximum stresses obtained from the 2-D and 3-D models in the longitudinal reinforcement at load factor = 0.75 are 321.6 and 328.6 MPa and at load factor = 0.80 are 350.7 and 345.7 MPa, respectively. In 3-D analysis, the stresses in the horizontal legs of stirrups did not exceed 35 MPa up to the numerical failure.

This beam has been analysed by Bedard and Kotsovos (1986) using 2-D finite element model and by Vidosa, et al. (1991b) using a 3-D finite element model. Bedard and Kotsovos, using the single crack approach and constant shear retention factor = 0.5, predicted a failure load nearly equal to the experimental one which is considered an excellent result. However, by comparing their predicted load-deflection curve (Fig. 5.32a) with the present predicted load-deflection curves from the 2-D model in Fig. 5.27, it can be seen that the two curves are nearly the same up to about 80% of the experimental failure load. After that, the present predicted curves stopped while the predicted curve by Bedard and Kotsovos continues but stiffer than the experimental curves which might be due to assuming a high constant shear retention factor and using the single crack approach in their model.

Using a 3-D finite element version, Vidosa, et al. (1991b) predicted a failure load of about 96% of the experimental failure load of this beam. Their predicted load-deflection curve is more flexible than that of Bedard and Kotsovos (Fig. 5.32b). This is because they neglected the concrete cover to the tension reinforcement in their finite element discretization and also due to taking less shear retention factor (0.1). From the above it can be concluded that the assumed value of shear retention factor and the accurate representation of the beam under investigation



(a) Bedard and Kotsovos (1986)



(b) Vedosa, et al. (1991b)

Fig. 5.32 Predicted load-deflection curves for beam A-1.

may have more significant effect on the prediction than the effect of using a 2-D or 3-D version.

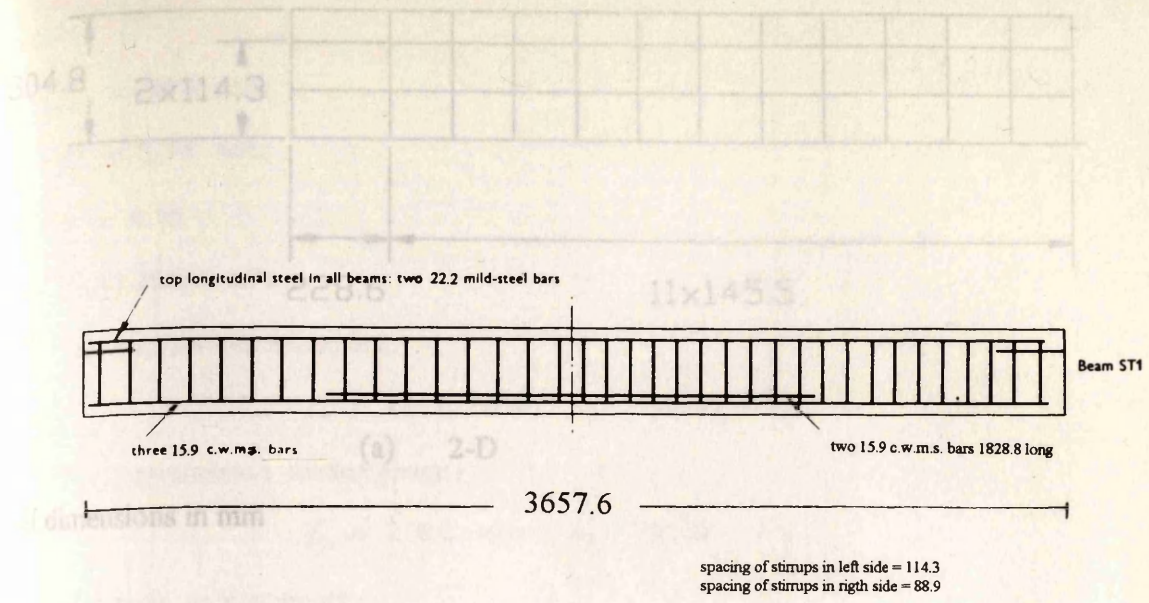
More discussion on this beam is presented in the next chapter.

5.6 Prediction of the behaviour of a Tee beam

In this section a comparison between the 2-D and 3-D models is made on a Tee beam (beam ST1) from those tested by Taylor (1966). Due to the triaxial state of stresses in the flange one could expect a large difference between the results of the 2-D and 3-D analysis. But this did not happen as will be shown below.

The beam has a span of 3099 mm and a cross-section as shown in Fig. 5.33. It is subjected to a central concentrated load. The amount of web reinforcement in one half of the beam is different from (about 80% of) the amount provided in the other half. All stirrups are 6 mm diameter at a spacing of 88.9 and 114.3 mm in the two halves of the beam, respectively. Tension reinforcement consists of five 16 mm deformed cold-worked mild-steel bars. Three of the longitudinal bars were continuous to the ends of the beam while the other two bars were stopped at distance of 686 mm from the supports. Two 22 mm mild-steel bars were used as compression reinforcement. The beam was designed to fail in shear, but it reached its maximum flexural capacity although wide cracks in shear span near the ends of the stopped-off bars were observed. The experimental failure load was 132 kN.

Fig. 5.34 shows the finite element mesh used for the analysis of the beam. In 2-D analysis the mesh consists of 36 elements, while in 3-D analysis 48 elements are used. Due to symmetry, only one-half and one-fourth of the beam are used in 2-D and 3-D analysis, respectively. The beam is analysed using the following data :



All dimensions in mm

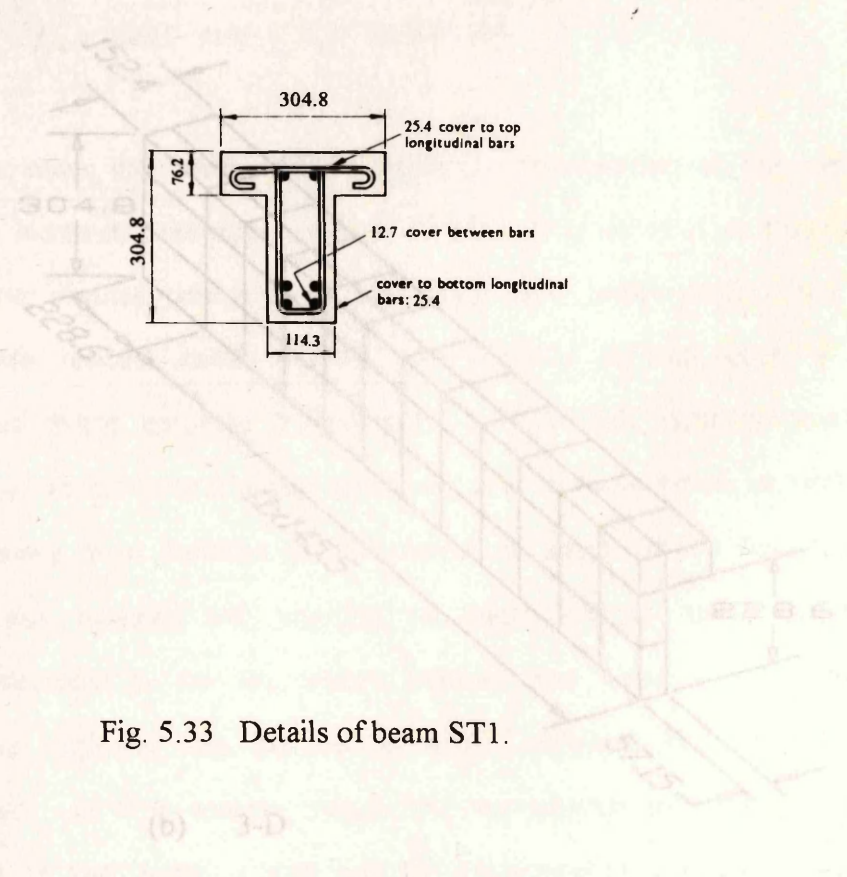
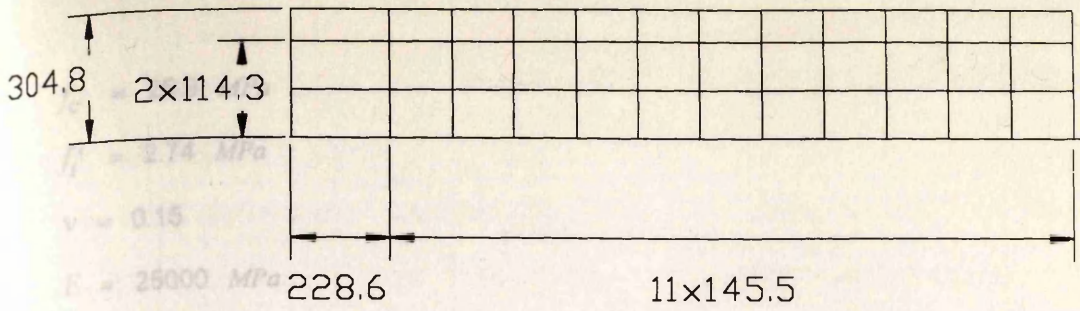


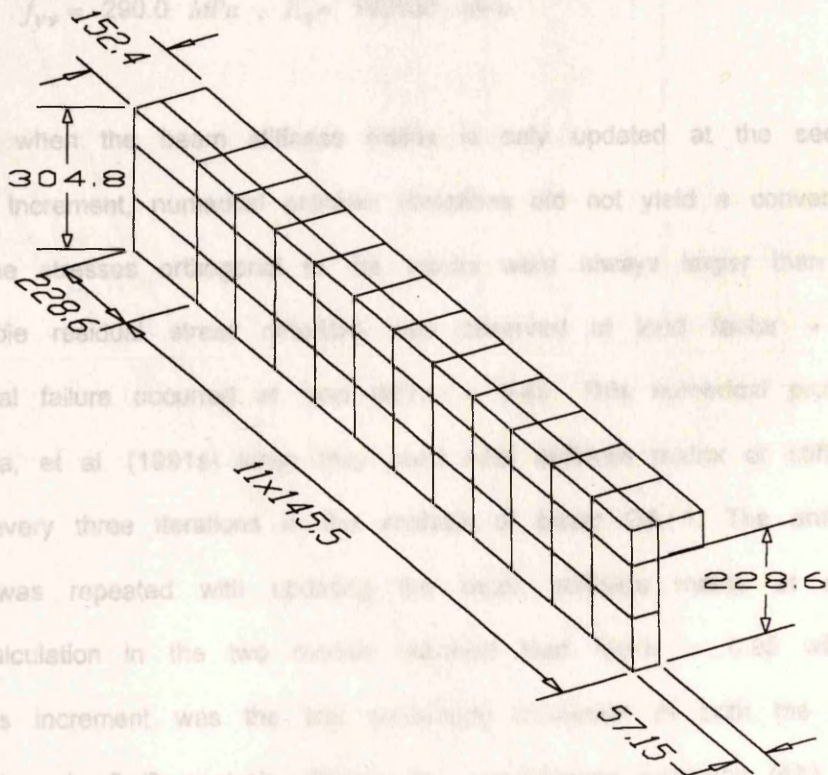
Fig. 5.33 Details of beam ST1.

Fig. 5.34 Finite element mesh for beam ST1



(a) 2-D

All dimensions in mm



(b) 3-D

Fig. 5.34 Finite element mesh for beam ST1.

$$f'_c = 25.9 \text{ MPa}$$

$$f'_t = 2.74 \text{ MPa}$$

$$\nu = 0.15$$

$$E = 25000 \text{ MPa}$$

For tension reinforcement:

$$f_y = 441.6 \text{ MPa} , E_s = 190000 \text{ MPa}$$

For compression reinforcement:

$$f_y = 278.0 \text{ MPa} , E_s = 190000 \text{ MPa}$$

For web reinforcement:

$$f_{yv} = 290.0 \text{ MPa} , E_s = 190000 \text{ MPa}$$

In 2-D analysis when the beam stiffness matrix is only updated at the second iteration of each increment, numerical problem (iterations did not yield a convergent solution, since the stresses orthogonal to the cracks were always larger than the maximum allowable residual stress criterion) was observed at load factor = 0.4 and the numerical failure occurred at load factor = 0.45. This numerical problem also faced Vidosa, et al. (1991a) when they used initial stiffness matrix or stiffness matrix updated every three iterations in the analysis of beam OA-1. The analysis of beam ST1 was repeated with updating the beam stiffness matrix at every iteration. The calculation in the two models reached load factor = 0.95 without any trouble. This increment was the last converged increment in both the 2-D and 3-D analysis. In 3-D analysis, despite the convergence tolerance (4%) was not be achieved at load factor = 1.00 but the displacement increments were not very large and the rate of convergence was very slow (the norm of residual forces reached 10.3% at the last 50th iteration. In 2-D analysis, a negative pivot appeared in the beam stiffness matrix at load factor = 1.00. The predicted failure loads from the 2-D and 3-D analysis are 95% and 100% of the experimental failure load, respectively. The load-deflection curves are shown in Fig. 5.35. As observed in the analysis of the previous two beams (beams OA-1 and A-1), the

predicted load-deflection curve obtained from 3-D model is slightly stiffer than that obtained from 2-D model.

The crack patterns and deformed shapes at load factors = 0.5, 0.75, and 0.95 are shown in Figs. 5.36 to 5.38. Unlike the proposed crack patterns of beams QA-1 and A-1 which failed in shear, the crack patterns of beam ST1 show that

the crack patterns of beam ST1 show that the crack width is proportional to the load applied to the crack area.

The stresses in concrete obtained from the two models at a given point under applied load are shown in Fig. 5.40.

Fig. 5.40 shows the stresses in the range under the load applied in the Y-direction. The maximum compressive load is 3.0 MPa.

The two models predicted nearly the same stresses in the range under the load applied in the Y-direction. The maximum compressive load is 3.0 MPa.

From the comparison between the predicted and experimental load-deflection curves, the maximum compressive load is 3.0 MPa.

From the comparison between the predicted and experimental load-deflection curves, the maximum compressive load is 3.0 MPa.

From the comparison between the predicted and experimental load-deflection curves, the maximum compressive load is 3.0 MPa.

From the comparison between the predicted and experimental load-deflection curves, the maximum compressive load is 3.0 MPa.

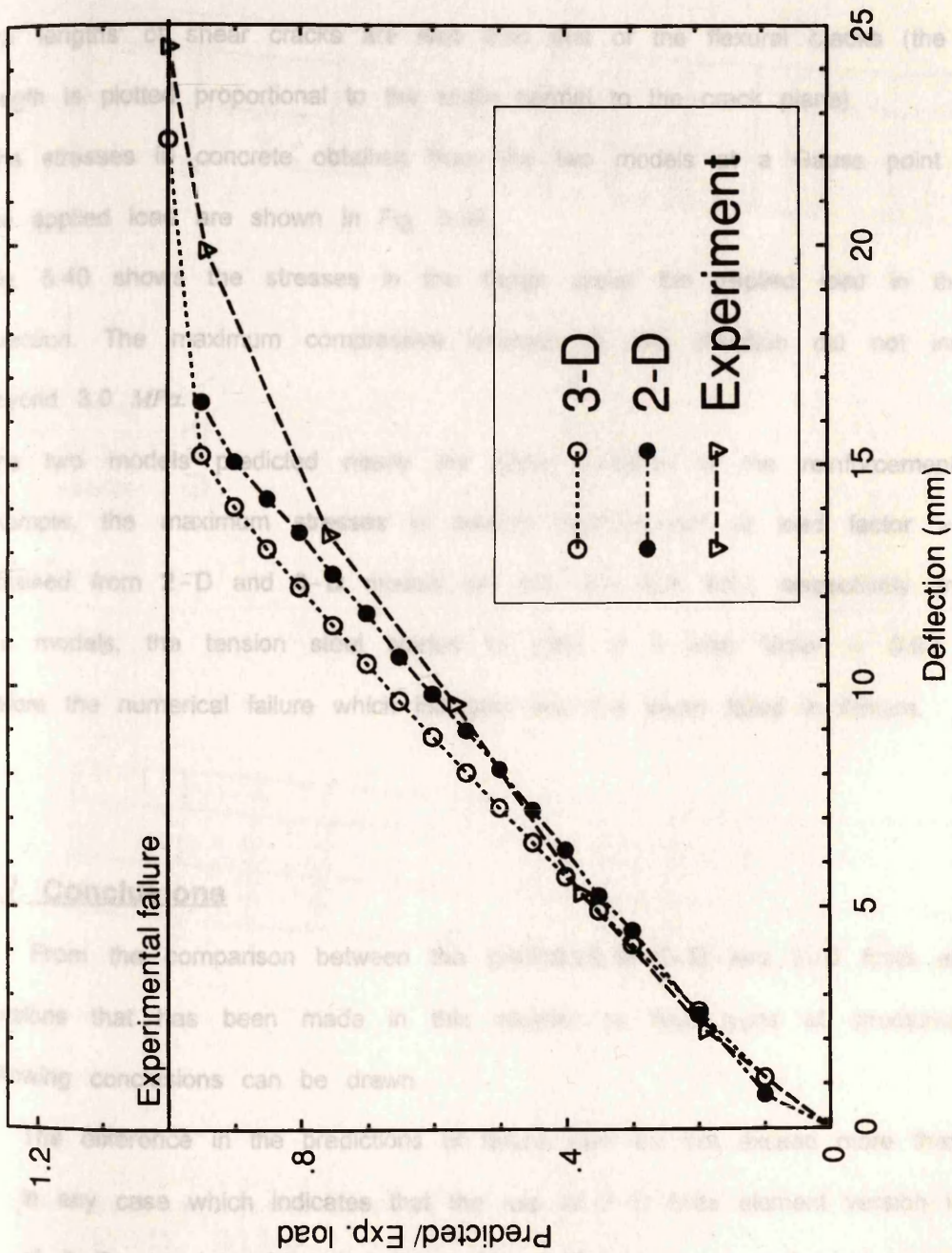
From the comparison between the predicted and experimental load-deflection curves, the maximum compressive load is 3.0 MPa.

From the comparison between the predicted and experimental load-deflection curves, the maximum compressive load is 3.0 MPa.

From the comparison between the predicted and experimental load-deflection curves, the maximum compressive load is 3.0 MPa.

From the comparison between the predicted and experimental load-deflection curves, the maximum compressive load is 3.0 MPa.

Fig. 5.35 Load-deflection curves for beam ST1.



predicted load-deflection curve obtained from 3-D model is slightly stiffer than that obtained from 2-D model.

The crack patterns and deformed shapes at load factors = 0.5, 0.75, and 0.95 are shown in Figs. 5.36 to 5.38. Unlike the predicted crack patterns of beams OA-1 and A-1 which failed in shear, the crack patterns of beam ST1 show that the 'lengths' of shear cracks are less than that of the flexural cracks (the crack length is plotted proportional to the strain normal to the crack plane).

The stresses in concrete obtained from the two models at a Gauss point under the applied load are shown in Fig. 5.39.

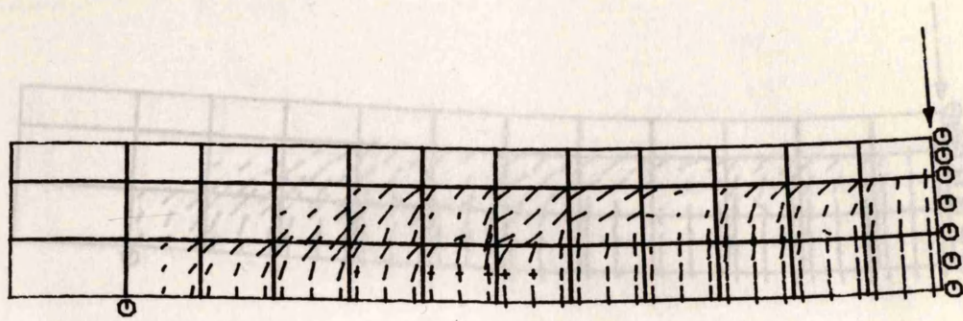
Fig. 5.40 shows the stresses in the flange under the applied load in the Y-direction. The maximum compressive stresses in this direction did not increase beyond 3.0 MPa.

The two models predicted nearly the same stresses in the reinforcement. For example, the maximum stresses in tension reinforcement at load factor = 0.85 obtained from 2-D and 3-D models are 430 and 428 MPa, respectively. In both the models, the tension steel started to yield at a load factor = 0.90, i. e. before the numerical failure which indicates that the beam failed in flexure.

5.7 Conclusions

From the comparison between the predictions of 2-D and 3-D finite element versions that has been made in this chapter on four types of structures, the following conclusions can be drawn.

- The difference in the predictions of failure load did not exceed more than 10% in any case which indicates that the use of 2-D finite element version instead of 3-D one is safely acceptable. The 2-D version is preferable because of the considerable saving of cost and time.



single crack :
 double crack :
 triple crack (3-D only):
 crushing of concrete :

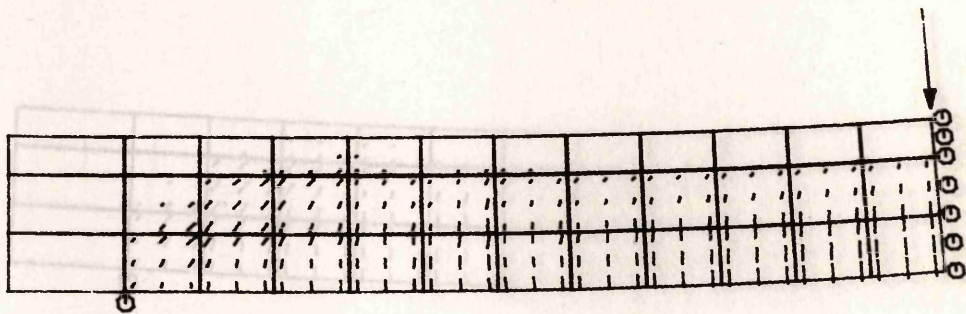
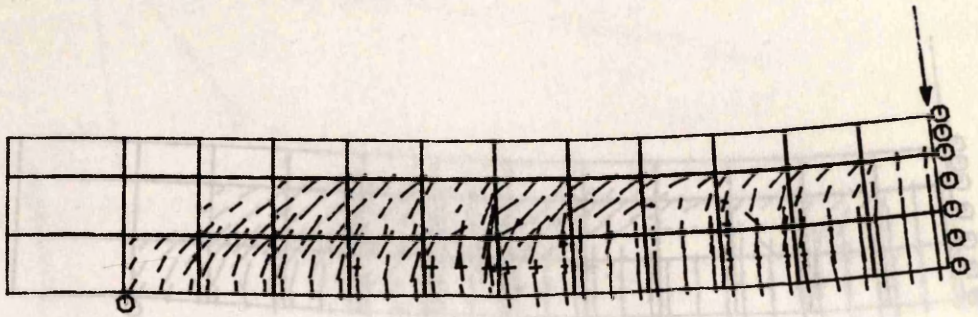


Fig. 5.36 Crack patterns and deformed shapes of beam ST1 at load factor = 0.50:
 (a) 2-D; (b) 3-D (displacements magnified x 20).



single crack : /
double crack : X
triple crack (3-D only): *
crushing of concrete : □

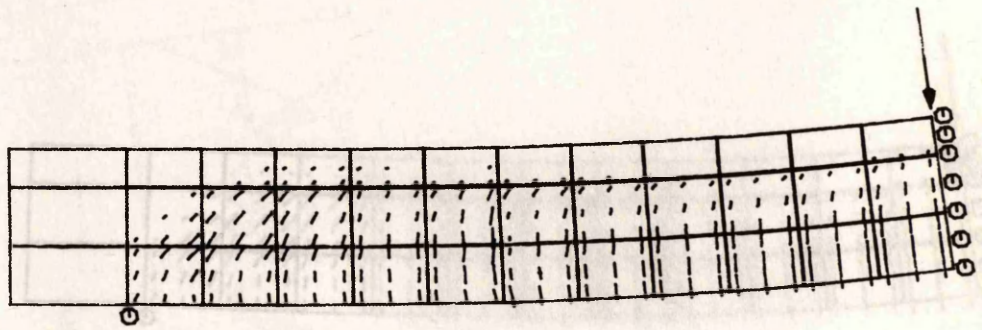
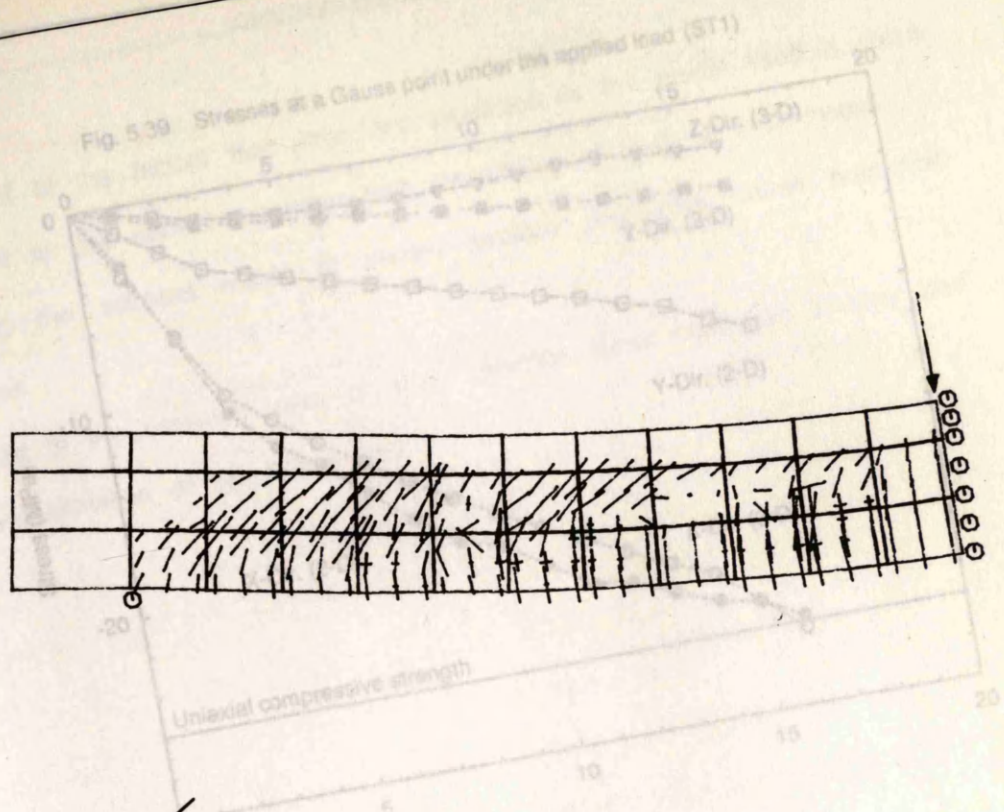


Fig. 5.37 Crack patterns and deformed shapes of beam ST1 at load factor = 0.75:
(a) 2-D; (b) 3-D (displacements magnified x 20).



single crack : 
 double crack : 
 triple crack (3-D only): 
 crushing of concrete : 

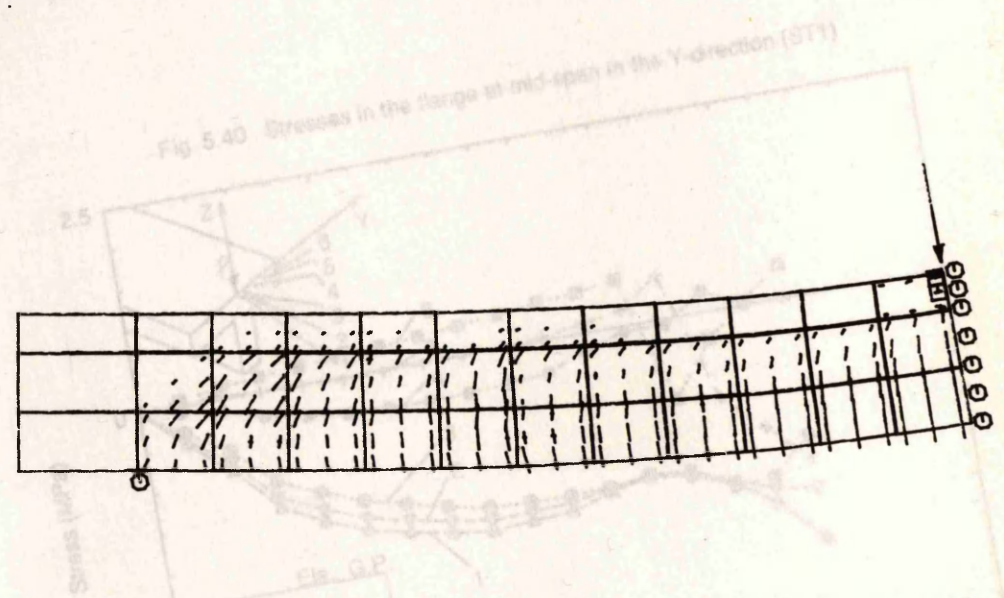


Fig. 5.38 Crack patterns and deformed shapes of beam ST1 at load factor = 0.95:
 (a) 2-D; (b) 3-D (displacements magnified x 20).

Fig. 5.39 Stresses at a Gauss point under the applied load (ST1)

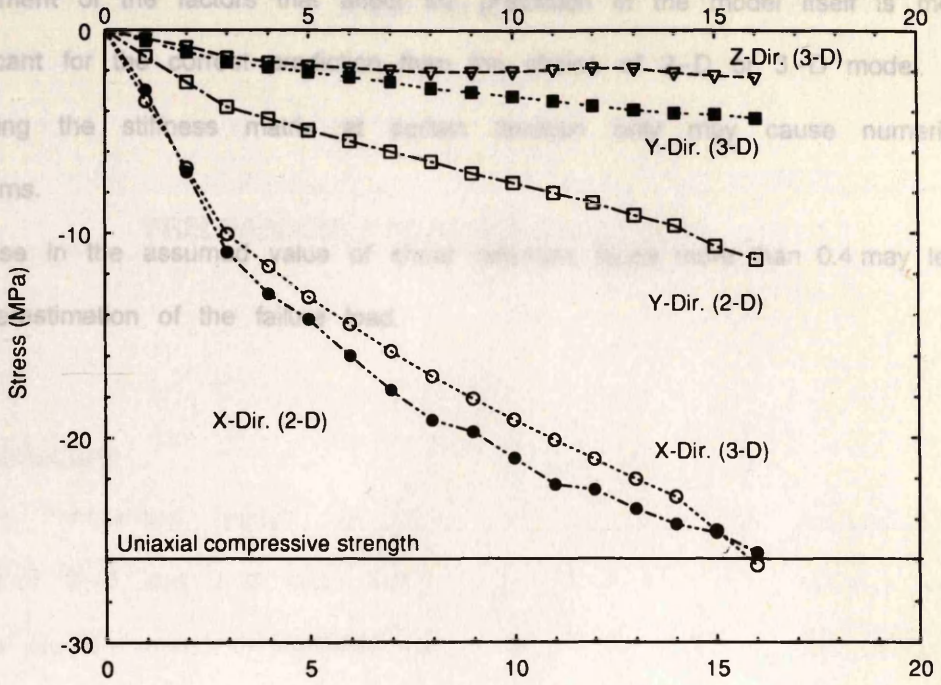
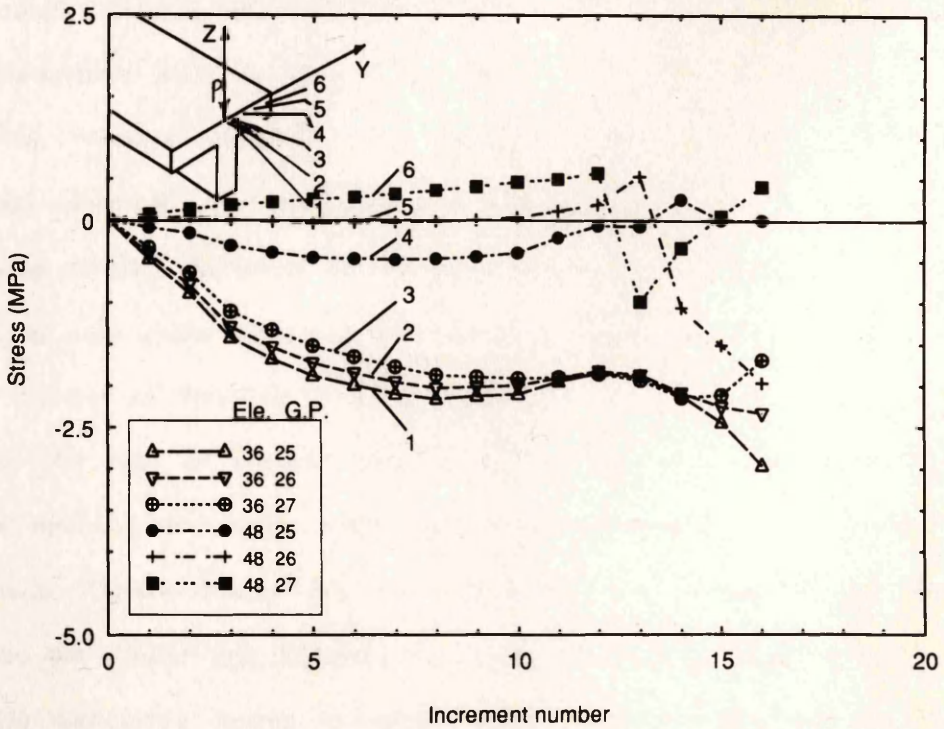


Fig. 5.40 Stresses in the flange at mid-span in the Y-direction (ST1)



- Adjustment of the factors that affect the prediction in the model itself is more significant for the correct prediction than the choice of 2-D or 3-D model.
- Updating the stiffness matrix at certain iteration only may cause numerical problems.
- Increase in the assumed value of shear retention factor more than 0.4 may lead to overestimation of the failure load.

PRELIMINARY PARAMETRIC STUDY

6.1 Introduction

The comparison, which has been made in chapter 5, between the predictions of 2-D and 3-D finite element models led to the conclusion that 2-D finite element model is sufficient for predicting the behaviour of reinforced concrete beams. The aim of this chapter is to find out the features of this 2-D finite element model that gives good prediction of the behaviour of any reinforced concrete rectangular beam. To determine this finite element model, many parameters that affect the prediction should be studied. One can classify the parameters affecting the final results into two classes. The first contains material parameters such as compressive strength of concrete, tensile strength of concrete, Young's modulus, shear modulus, shear retention factor, stress-strain relationships of concrete, and other material parameters. The second class contains numerical parameters such as the number of elements used in calculating strains and stresses, the number of iterations, the maximum number of iterations in each iteration, the number of nodes, the mesh size, the type of element used, the number of nodes per element, and other parameters such as the type of element and applied loads. Twelve beams were analysed in this study. These beams were tested by Bresler and Scordelis in 1968. The main purpose of studying Bresler and Scordelis's beams in this study is to find out the important parameters which have a significant effect on the prediction of their behaviour.

CHAPTER 6

PRELIMINARY PARAMETERIC STUDY

- (i) shear retention factor,
- (ii) tensile strength of concrete,

6.1 Introduction

The comparison, which has been made in chapter 5, between the predictions of 2-D and 3-D finite element models led to the conclusion that 2-D finite element model is sufficient for predicting the behaviour of reinforced concrete beams. The aim of this chapter is to find out the features of this 2-D finite element model that gives good prediction of the behaviour of any reinforced concrete rectangular beam. To determine this finite element model, many parameters that affect the prediction should be studied. One can classify the parameters affecting the final results into two classes. The first contains material parameters such as compressive strength of concrete, tensile strength of concrete, Young's modulus, shear modulus and shear retention factor, stress-strain relationships of concrete, and yield strength of reinforcement. The second class contains numerical parameters such as the numerical method used in calculating strains and stresses, the number and the size of increments, the maximum number of iterations in each increment, the convergence criteria, the mesh size, the type of element used in the analysis, the number of Gauss points per element, and other parameters such as simulation of supports and applied loads. Twelve beams will be analysed in this chapter. These beams were tested by Bresler and Scordelis in 1963. The main purpose of analysing Bresler and Scordelis's beams in great detail is to find out the important parameters which have a significant effect on the prediction of these beams.

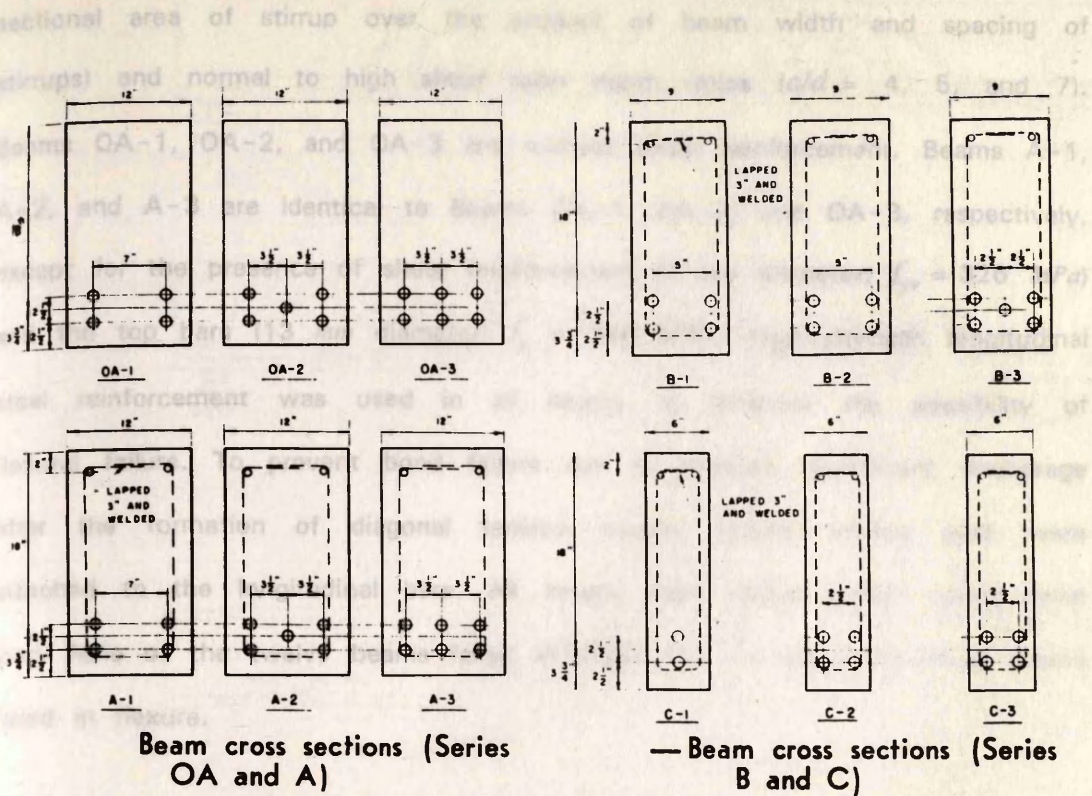
From this preliminary study, it was found that the material parameters have more effect on the prediction than the numerical parameters. Therefore, the concentration in this chapter will be on material parameters. Five parameters which many think have a significant effect on the prediction will be studied. These parameters are:

- (i) shear retention factor,
- (ii) tensile strength of concrete,
- (iii) magnitude of the strain corresponding to the peak stress in the stress-strain curve of concrete in compression,
- (iv) tension softening of concrete, and
- (v) compression softening of concrete.

6.2 Analysis of Bresler and Scordelis's beams

In their famous paper, Bresler and Scordelis (1963) tested a series of 12 beams. These tests were designed to provide (at that time) needed data regarding the shear strength of beams. From these twelve beams, there are four beams which have attracted the attention of investigators during checking the validity of their finite element models. These beams are OA-1, A-1, OA-2, and A-2.

All beams were of rectangular cross section and had the same nominal overall depth of 553 mm (Fig. 6.1). Main longitudinal reinforcement consisted of from two to six 28 mm diameter high strength steel deformed bars ($f_y = 555$ MPa) placed in two or three levels. The nominal effective depth was 457 mm. All stirrups were made from 6 mm intermediate grade steel deformed bars ($f_{yv} = 326$ MPa). Three beam widths 152, 229, and 305 mm and three simple span lengths 3658, 4572, and 6401 mm were used (Table 6.1). All beams were loaded at midspan. The beams have normal to low percentages of web reinforcement ($r f_{yv} = 0, 0.33, 0.48, \text{ and } 0.65$ N/mm², where $r = \frac{A_{sv}}{b.s} =$ cross-



Note: 1. All dimensions shown are nominal; see Table 6.1 for measured dimensions.
 2. Bottom bars are #9, top bars are #4, and stirrups are #2.

Fig. 6.1 Dimensions of cross sections of Bresler and Scordelis's beams

Table 6.1 Data of Bresler and Scordelis's beams

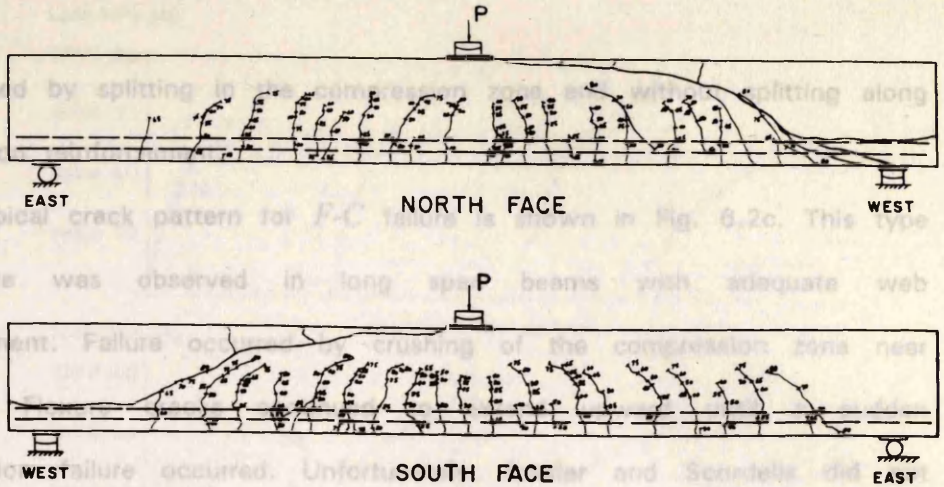
Beam	Length (mm)	Cross-section (mmxmm)	d (mm)	a/d	f'_c (MPa)	ρ (%)	Stirrups		Failure mode	Ultimate shear force (kN)
							Spacing (mm)	r_{fyv} (MPa)		
OA-1	3657.6	310x556	461	3.97	22.56	1.81	-	-	<i>D-T</i>	167.0
OA-2	4572.0	305x561	466	4.90	23.74	2.27	-	-	<i>D-T</i>	178.0
OA-3	6400.8	307x556	462	6.94	37.61	2.74	-	-	<i>D-T</i>	189.0
A-1	3657.6	307x561	466	3.92	24.08	1.80	209.6	0.33	<i>V-C</i>	233.5
A-2	4572.0	305x559	464	4.93	24.29	2.28	209.6	0.33	<i>V-C</i>	244.5
A-3	6400.8	307x561	466	6.91	35.05	2.73	209.6	0.33	<i>F-C</i>	234.0
B-1	3657.6	231x556	461	3.95	24.77	2.43	190.5	0.48	<i>V-C</i>	221.5
B-2	4572.0	229x561	466	4.91	23.18	2.43	190.5	0.48	<i>V-C</i>	200.0
B-3	6400.8	229x556	461	6.95	38.78	3.06	190.5	0.48	<i>F-C</i>	177.0
C-1	3657.6	155x559	464	3.95	29.60	1.80	209.6	0.65	<i>V-C</i>	155.5
C-2	4572.0	152x559	464	4.93	23.81	3.66	209.6	0.65	<i>V-C</i>	162.5
C-3	6400.8	155x554	459	6.98	35.05	3.63	209.6	0.65	<i>F-C</i>	134.5

sectional area of stirrup over the product of beam width and spacing of stirrups) and normal to high shear span depth ratios ($a/d = 4, 5, \text{ and } 7$). Beams OA-1, OA-2, and OA-3 are without shear reinforcement. Beams A-1, A-2, and A-3 are identical to Beams OA-1, OA-2, and OA-3, respectively, except for the presence of shear reinforcement (6 mm diameter; $f_{yv} = 326 \text{ MPa}$) and the top bars (13 mm diameter; $f_y = 346 \text{ MPa}$). High-strength longitudinal steel reinforcement was used in all beams to minimise the possibility of flexural failure. To prevent bond failure due to possible insufficient anchorage after the formation of diagonal tension cracks, special anchor nuts were attached to the longitudinal bars. All beams were tested under centre-point load. Nine of the twelve beams failed in shear and the remaining three beams failed in flexure.

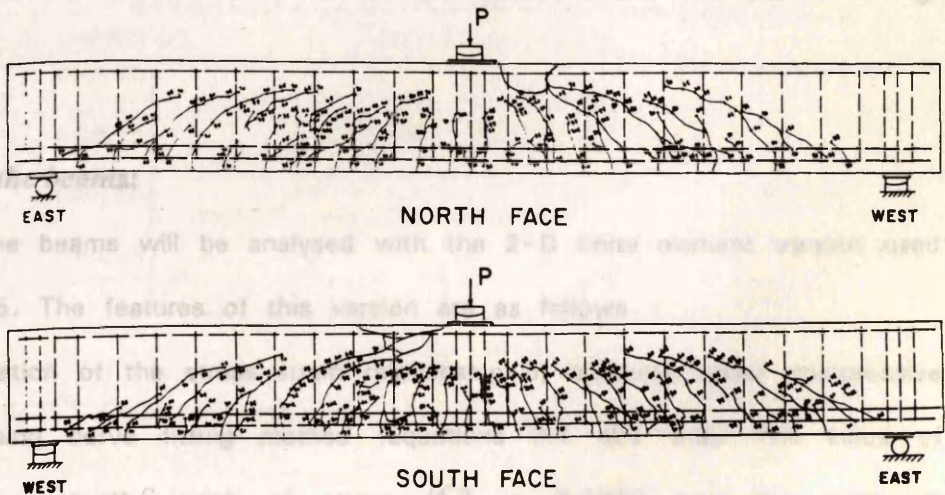
General behaviour of all the twelve beams: Typical flexural cracks appeared first, following by the appearance of diagonal tension cracks, usually in the middle third of the over-all beam depth and at various sections along the span. With further increase in load these diagonal cracks extended both upwards and downwards. The general modes of failure observed in this series of tests were: diagonal tension (*D-T*), shear-compression (*V-C*), and flexure-compression (*F-C*) failures, defined as follows.

- **D-T:** Typical crack pattern for *D-T* failure is shown in Fig. 6.2a. This type of failure was observed in all the beams without shear reinforcement. The failure was sudden and occurred as a result of longitudinal splitting in the compression zone near the load point, and also by horizontal splitting along tensile reinforcement near the end of the beam.
- **V-C:** Typical crack pattern for *V-C* failure is shown in Fig. 6.2b. This type of failure was observed in intermediate span beams with shear reinforcement. Failure developed without extensive propagation of flexural cracks towards the compression zone in the centre portion of the span and

(a) D-T failure



(b) V-C failure



(c) F-C failure

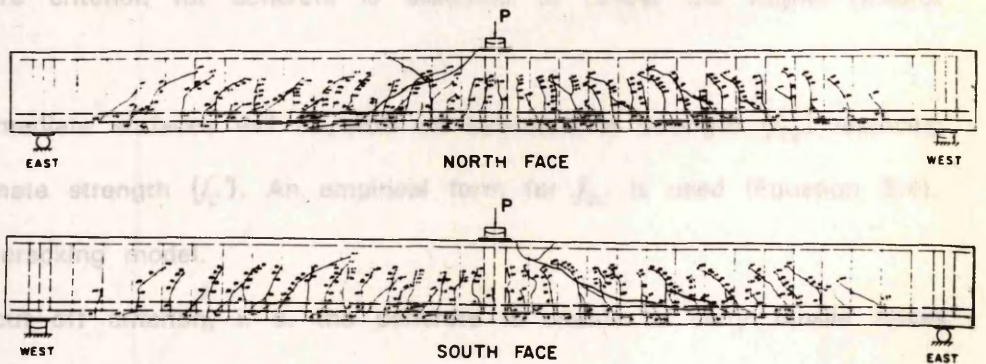


Fig. 6.2 Typical crack patterns of Bresler and Scordelis's beam.

it occurred by splitting in the compression zone and without splitting along the tension reinforcement.

- **F-C:** Typical crack pattern for *F-C* failure is shown in Fig. 6.2c. This type of failure was observed in long span beams with adequate web reinforcement. Failure occurred by crushing of the compression zone near midspan. Flexure cracks continued to extend upward until a sudden compression failure occurred. Unfortunately, Bresler and Scordelis did not measure the strain in the bars.

The observed load-deflection curves for the twelve beams are shown in Fig. 6.3.

Analysis of the beams:

First, the beams will be analysed with the 2-D finite element version used in chapter 5. The features of this version are as follows :

- Representation of the stress-strain relationship of concrete under compressive force using curve fitting method (Equations 3.1 and 3.3). The value of strain ϵ_{cc} at the peak of stress (f_c') is 0.0025 and the maximum compressive strain ϵ_{max} is 0.0035 (Fig. 6.4).
- The failure criterion for concrete is assumed to follow the Kupfer-Hilsdorf criterion
- The intermediate surfaces will be with an intermediate strength (f_{cc}) replacing the ultimate strength (f_c'). An empirical form for f_{cc} is used (Equation 3.4).
- Smearred cracking model.
- Tension cut-off criterion, i. e. the concrete is unable to carry tensile stress after cracking.
- The shear retention factor β is taken as a function of strain normal to the crack plane (see Sec. 6.2.1 for more details).
- Reinforcement is simulated by embedded elements. The bar carries load in its axial direction only. An elastic-perfectly plastic behaviour is assumed.

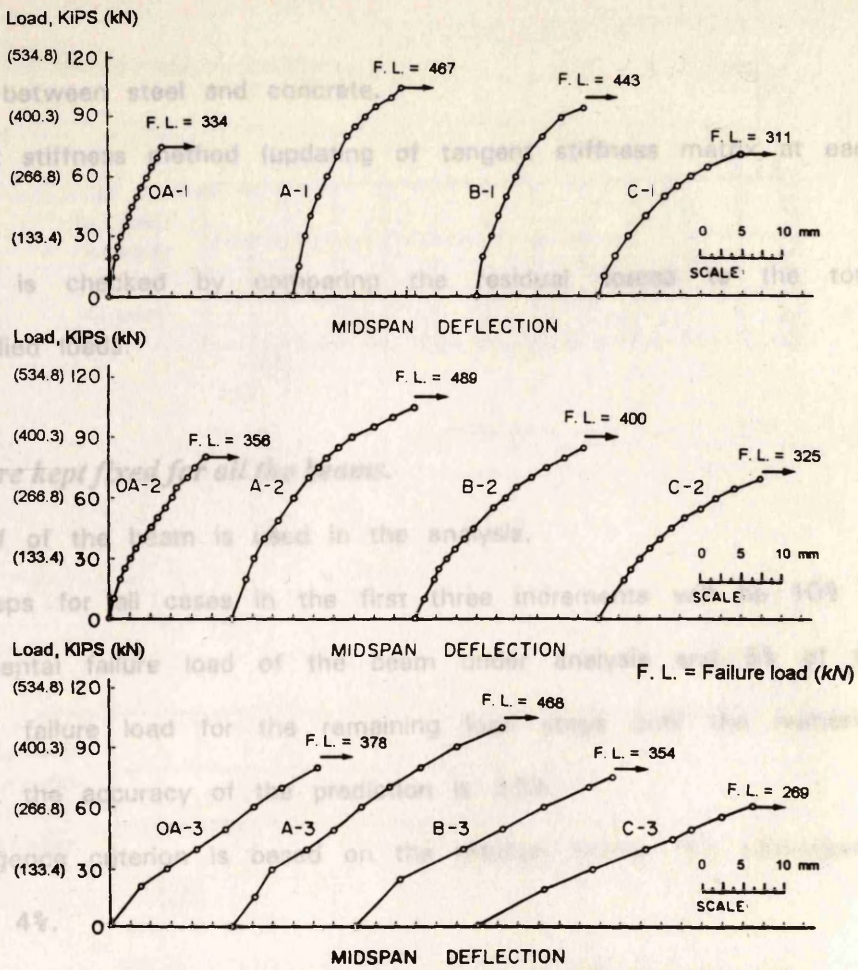


Fig. 6.3 Load-deflection curves of Bresler and Scordelis's beams.

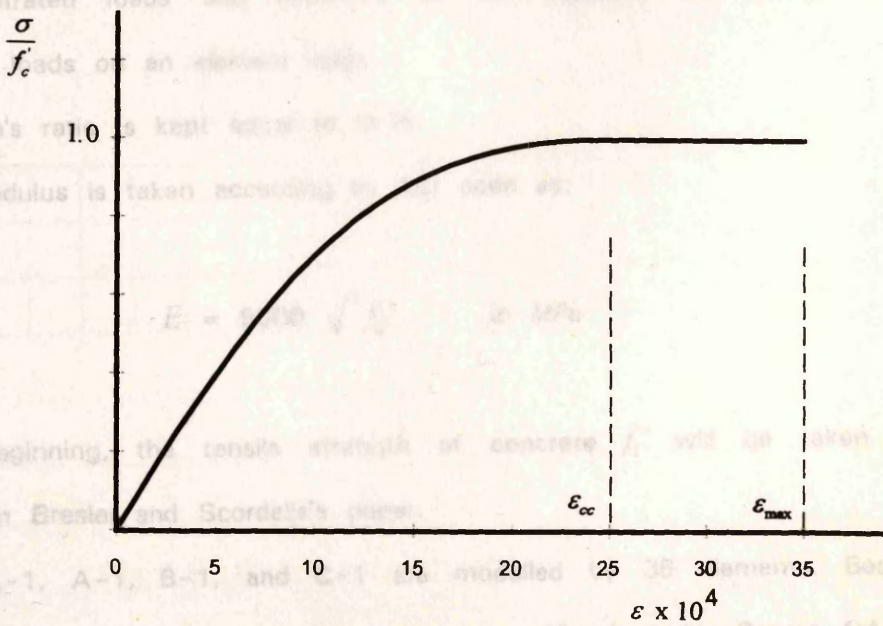


Fig. 6.4 Initial assumption of stress-strain curve of concrete in compression.

- Perfect bond between steel and concrete.
- Using tangent stiffness method (updating of tangent stiffness matrix at each iteration).
- Convergence is checked by comparing the residual forces to the total external applied loads.

The following are kept fixed for all the beams.

- Only one half of the beam is used in the analysis.
- The load steps for all cases in the first three increments will be 10% of the experimental failure load of the beam under analysis and 5% of the experimental failure load for the remaining load steps until the numerical failure, i. e. the accuracy of the prediction is $\pm 5\%$.
- The convergence criterion is based on the residual forces, the convergence tolerance is 4%.
- The predicted failure load is the load at the last converged increment.
- The maximum number of iterations per increment is 50 iterations.
- The concentrated loads and reactions at the supports are simulated as distributed loads on an element edge.
- The poisson's ratio is kept equal to 0.15.
- Young's Modulus is taken according to ACI code as;

$$E = 5000 \sqrt{f_c'} \quad \text{in MPa}$$

- At the beginning, the tensile strength of concrete f_t' will be taken as reported in Bresler and Scordelis's paper.
- Beams OA-1, A-1, B-1, and C-1 are modelled by 36 elements. Beams OA-2, A-2, B-2, and C-2 are modelled by 42 elements. Beams OA-3, A-3, B-3, and C-3 are modelled by 57 elements (see Fig. 6.5).

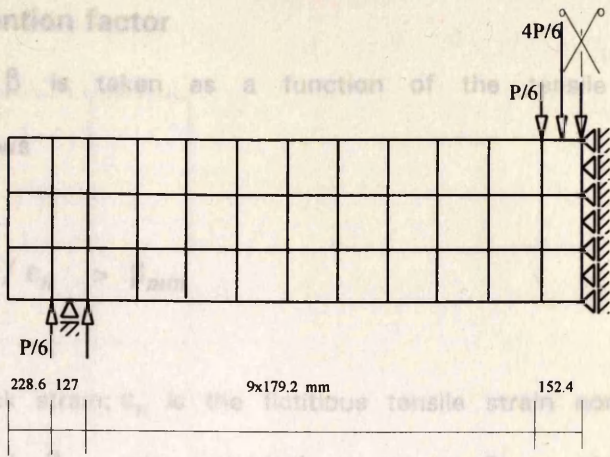
(a)

6.2.1 Effect of shear retention factor

The shear retention factor β is taken as a function of the tensile strain normal to the crack as follows:

- OA-1: 3×185.4
- A-1: 3×187.1
- B-1: 3×185.4
- C-1: 3×186.3

$\beta =$



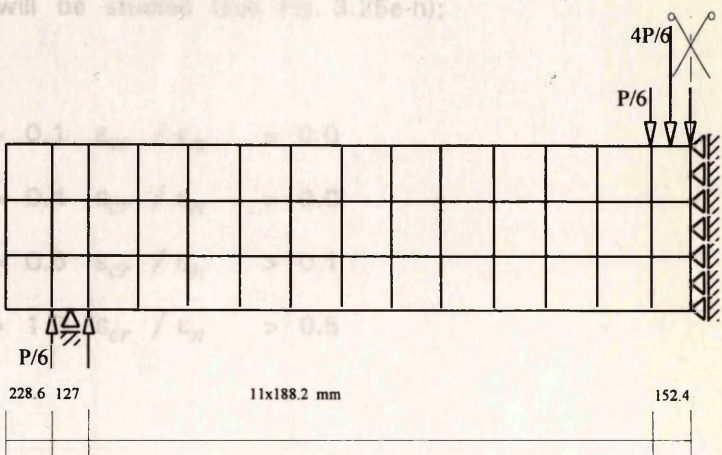
(b)

where ϵ_{cr} is the tensile crack strain; ϵ_s is the instantaneous tensile strain normal to the crack plane; and B and β_{max} are numerical constants. Four values for these two constants will be studied (see Fig. 3.25e-h):

- Case (1) $\beta = 0.1$
- Case (2) $\beta = 0.2$
- Case (3) $\beta = 0.3$
- Case (4) $\beta = 0.5$

- OA-2: 3×187.1
- A-2: 3×186.3
- B-2: 3×187.1
- C-2: 3×186.3

$\beta =$



(c)

6.2.1.1 Beams without shear reinforcement

Figures 6.6 to 6.8 show the load-deflection curves for the four cases of the shear retention factor β for the three beams without shear reinforcement OA-1, OA-2, and OA-3. The results of the parametric study are shown in Table 6.2. It can be seen that the effect of β on the load-carrying capacity is very important. The shear retention factor β used in the prediction of the failure load for these beams is given by Case (1); the mean value of the prediction for the failure load is about 20% of the corresponding experimental failure load. This effective decrease in beam load prediction of the failure load for these beams is given by Case (1); the mean value of the prediction for the failure load is about 20% of the corresponding experimental failure load.

- OA-3: 3×185.4
- A-3: 3×187.1
- B-3: 3×185.4
- C-3: 3×184.6

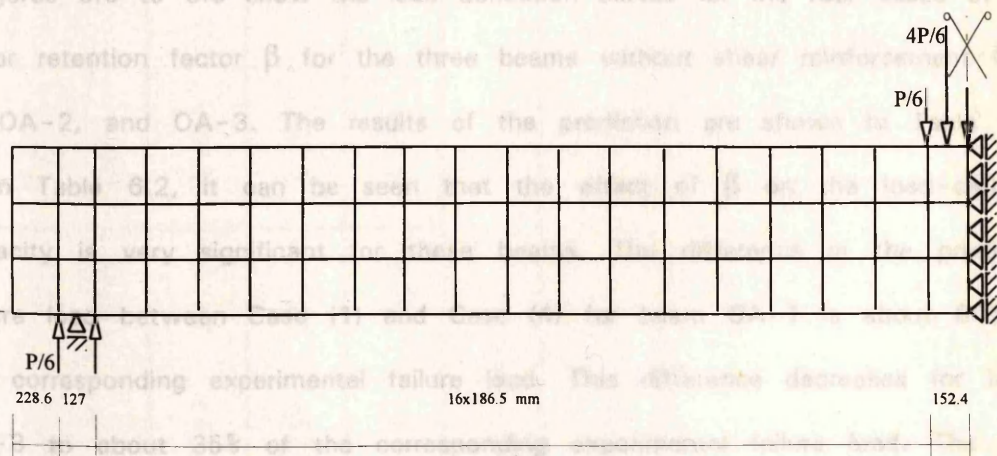


Fig. 6.5 Finite element idealization.

- (a) Beams OA-1, A-1, B-1, and C-1
- (b) Beams OA-2, A-2, B-2, and C-2
- (c) Beams OA-3, A-3, B-3, and C-3

6.2.1 Effect of shear retention factor

The shear retention factor β is taken as a function of the tensile strain normal to the crack as follows

$$\beta = B \varepsilon_{cr} / \varepsilon_n > \beta_{min}$$

where ε_{cr} is the tensile crack strain; ε_n is the fictitious tensile strain normal to the crack plane; and B and β_{min} are numerical constants. Four values for these two constants will be studied (see Fig. 3.25e-h);

Case (1)	$\beta = 0.1$	$\varepsilon_{cr} / \varepsilon_n > 0.0$
Case (2)	$\beta = 0.4$	$\varepsilon_{cr} / \varepsilon_n > 0.0$
Case (3)	$\beta = 0.5$	$\varepsilon_{cr} / \varepsilon_n > 0.1$
Case (4)	$\beta = 1.0$	$\varepsilon_{cr} / \varepsilon_n > 0.5$

6.2.1.1 Beams without shear reinforcement

Figures 6.6 to 6.8 show the load-deflection curves for the four cases of the shear retention factor β for the three beams without shear reinforcement OA-1, OA-2, and OA-3. The results of the prediction are shown in Table 6.2. From Table 6.2, it can be seen that the effect of β on the load-carrying capacity is very significant for these beams. The difference in the predicted failure load between Case (1) and Case (4) for beam OA-1 is about 80% of the corresponding experimental failure load. This difference decreases for beam OA-3 to about 35% of the corresponding experimental failure load. The best prediction of the failure load for these beams is given by Case (1), the mean value of the predicted to the experimental failure loads in this case is about 0.92.

Table 6.2 Effect of shear retention factor in beams without shear reinforcement.

BEAM	a/d	f'_c (MPa)	f'_t (MPa)	* Failure mode	Predicted / Experimental failure load				Difference between Case (4) and Case (1) (% of the experimental failure load)
					Case (1)	Case (2)	Case (3)	Case (4)	
OA-1	3.97	22.60	4.00	D-T	0.95	1.45	1.55	1.75	80
OA-2	4.90	23.70	4.34	D-T	0.95	1.15	1.20	1.40	45
OA-3	6.94	37.60	4.14	D-T	0.85	1.15	1.20	1.20	35
Mean value					0.92	1.25	1.32	1.45	

Case (1): $\beta = 0.1 \frac{\epsilon_{cr}}{\epsilon_n} \geq 0.0$; Case (2): $\beta = 0.4 \frac{\epsilon_{cr}}{\epsilon_n} \geq 0.0$; Case (3): $\beta = 0.5 \frac{\epsilon_{cr}}{\epsilon_n} \geq 0.1$; Case (4): $\beta = 1.0 \frac{\epsilon_{cr}}{\epsilon_n} \geq 0.5$

* From Bresler and Scordelis's paper

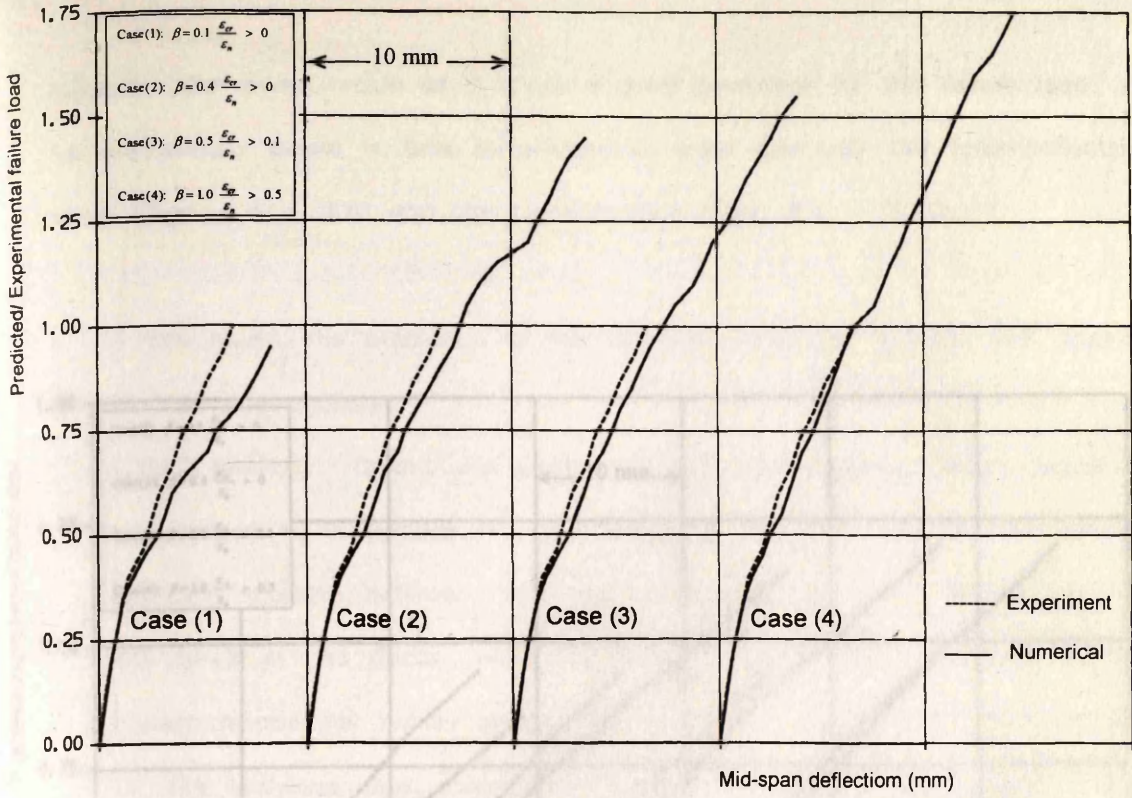


Fig. 6.6 Load-deflection curves for beam OA-1 (effect of shear retention factor β).

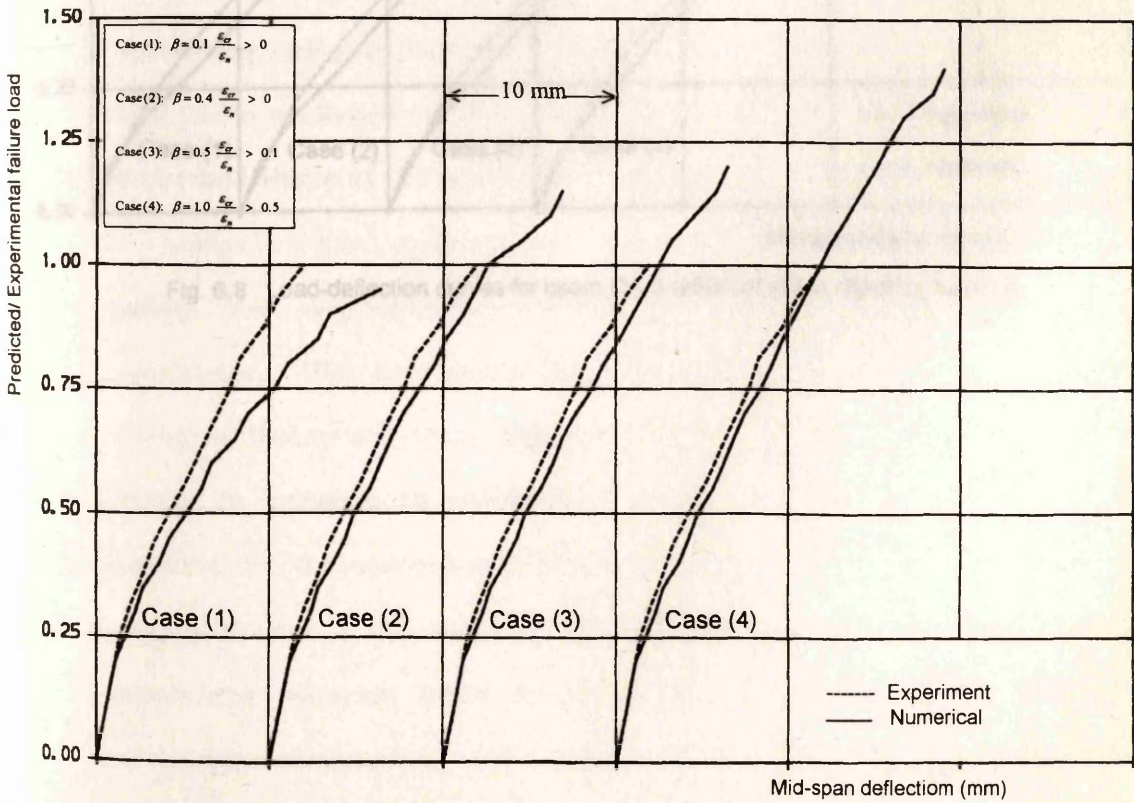


Fig. 6.7 Load-deflection curves for beam OA-2 (effect of shear retention factor β).

Although the lowest value of β gives a good prediction of the failure load, as will be shown below it fails to predict to good accuracy the load-deflection curve (Figs. 6.6 - 6.8) and the crack pattern (Figs. 8.9 - 8.10).

In this study, the prediction of the mode of failure of a beam will depend

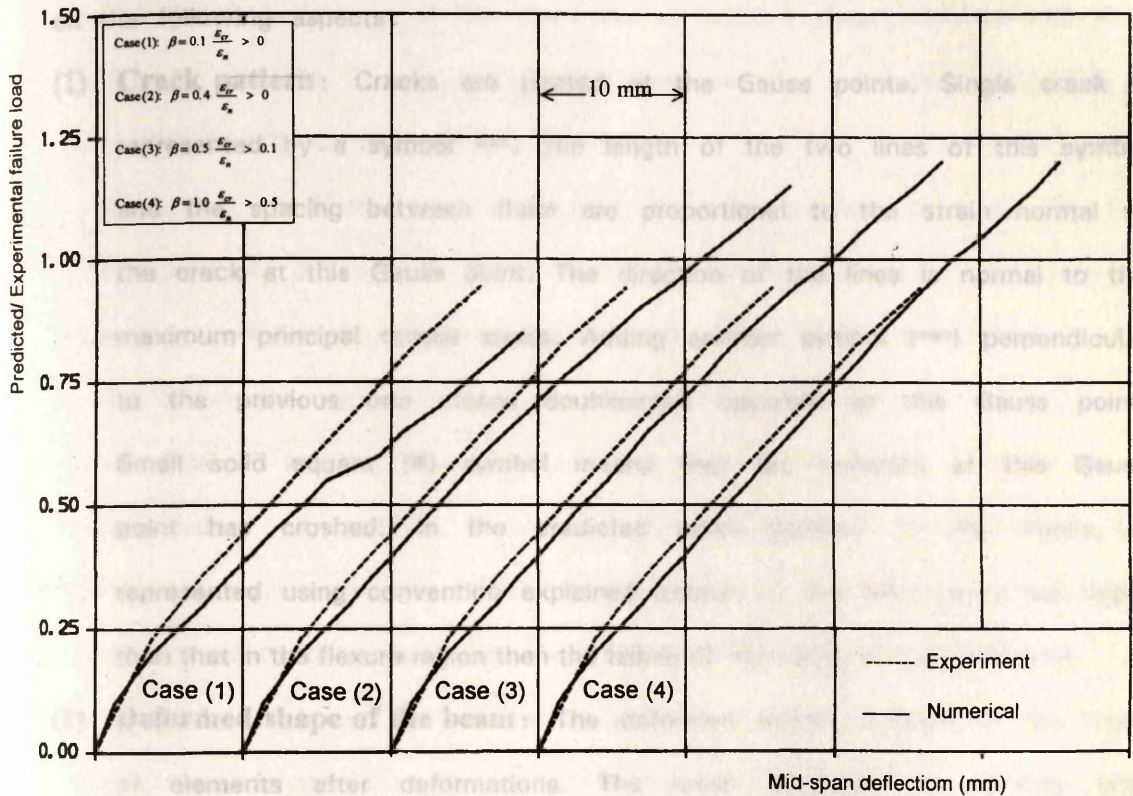


Fig. 6.8 Load-deflection curves for beam OA-3 (effect of shear retention factor β).

Although the lowest value of β gives a good prediction of the failure load, as will be shown below it fails to predict to good accuracy the load-deflection curve (Figs. 6.6 - 6.8) and the crack pattern (Figs. 6.9 - 6.10).

In this study, the prediction of the mode of failure of a beam will depend on the following aspects:

- (1) **Crack pattern:** Cracks are plotted at the Gauss points. Single crack is represented by a symbol \equiv . The length of the two lines of this symbol and the spacing between them are proportional to the strain normal to the crack at this Gauss point. The direction of the lines is normal to the maximum principal tensile stress. Adding another symbol (\equiv) perpendicular to the previous one means doublecrack occurred at this Gauss point. Small solid square (■) symbol means that the concrete at this Gauss point has crushed. In the predicted crack pattern, if the cracks, as represented using convention explained before, in the shear area are larger than that in the flexure region then the failure of the beam is shear dominant.
- (2) **Deformed shape of the beam:** The deformed shape consists of the mesh of elements after deformations. The mesh elements are plotted after adding the displacements (magnified by a suitable factor) to their coordinates. The deformed shape of beams clearly indicates those beams failing in flexure and those failing in shear.
- (3) **Stress in concrete in compression zone:** The stress-strain curve of concrete in the compression zone near mid-span of the beam will be plotted to see if the stress of concrete reached the compressive strength before the numerical failure or not. In beams failing in shear-compression or flexure-compression, this stress should reach to the compressive strength of concrete before or at numerical failure.
- (4) **Stresses in tension steel:** Yielding of tension steel near mid-span of the beam before numerical failure indicates that the beam may fail in flexure.

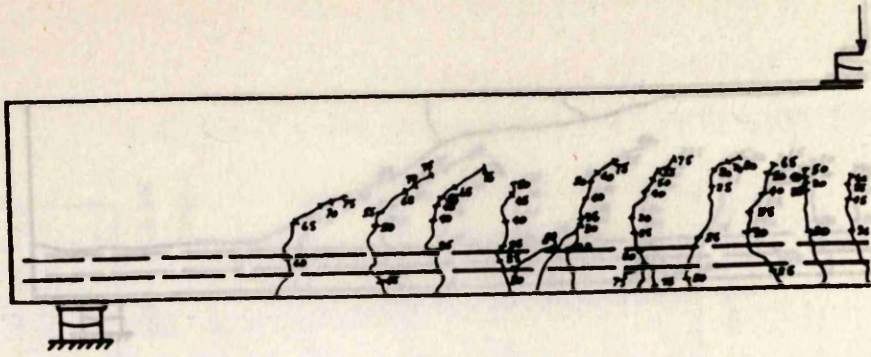
(5) **Stresses in shear and compression reinforcement (if exist):** Yielding of some points of stirrups arranged diagonally from the load point to the support indicates that the beam failed in shear. While yielding of the compression steel before numerical failure indicates that the beam may fail in either shear-compression or flexure-compression.

The predicted behaviours of the three beams without shear reinforcement (OA-1, OA-2, and OA-3) are similar, therefore only the predicted behaviours of beam OA-1 will be discussed.

The effect of β on the prediction of the crack pattern for beam OA-1 is shown in Figs. 6.9 and 6.10. In Fig. 6.9, the crack patterns and deformed shapes are plotted for the four cases of β at the same load factor (L. F.= 0.95). When the value of β is low (Case 1), all the Gauss points in the lower parts of concrete section of the beam crack. Moreover, the number of Gauss points at which double cracking occurs near the longitudinal reinforcement increases. By increasing the value of β , the number of Gauss points at which the cracks occur reduces. By comparing the observed crack pattern (after ignoring the horizontal splitting in the compression zone and along the reinforcement) with the four predicted crack patterns, it can be seen that the crack pattern of Case (2) is the nearest to the observed crack pattern for this beam. In Fig. 6.10, The crack patterns and deformed shapes at the last converged increment are plotted for the four cases of β for beam OA-1. It can be noticed that inspite of the fact that the whole span of the beam has cracked for the higher three cases of β , still the beam carried loads until the compression zone near the mid-span load crushed. This crushing happened due to the compression strain in concrete exceeding the assumed maximum strain (0.0035). The principal compressive stress-strain curve of concrete at a Gauss point, under the load point is shown in Fig. 6.11 for the

Fig. 6.9 Crack patterns and deformed shapes for beam OA-1
(Load factor = 0.95, displacements magnified $\times 10$)

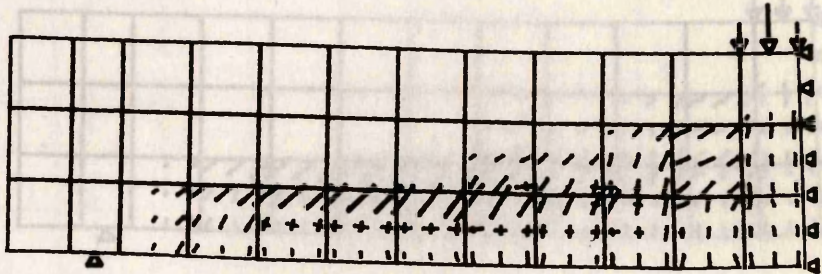
Observed



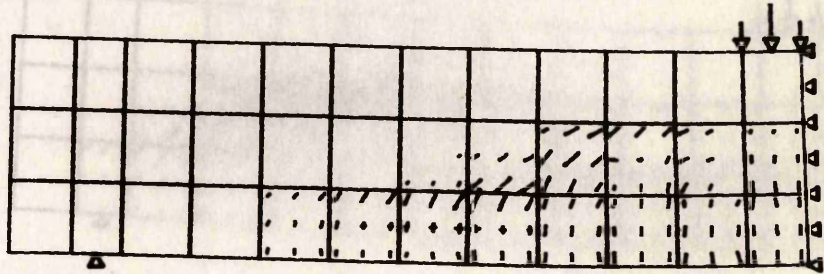
Case (1): $\beta = 0.1 \frac{\epsilon_{\sigma}}{\epsilon_n} > 0$

Single crack /
Double crack X

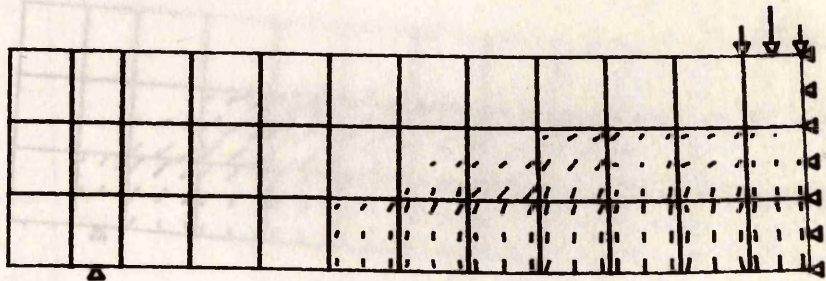
Crushing of concrete ■



Case (2): $\beta = 0.4 \frac{\epsilon_{\sigma}}{\epsilon_n} > 0$



Case (3): $\beta = 0.5 \frac{\epsilon_{\sigma}}{\epsilon_n} > 0.1$



Case (4): $\beta = 1.0 \frac{\epsilon_{\sigma}}{\epsilon_n} > 0.5$

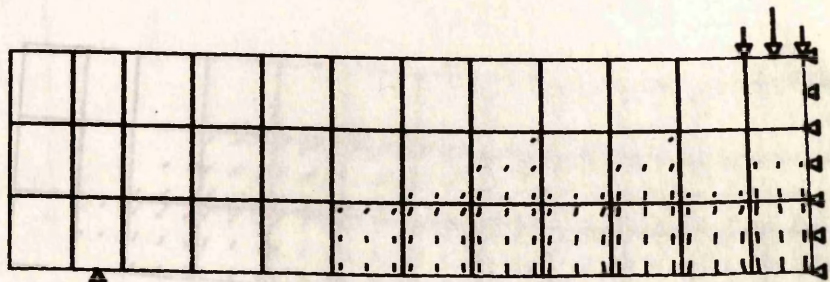


Fig. 6.9 Crack patterns and deformed shapes for beam OA-1 (Load factor = 0.95, displacements magnified x 10).

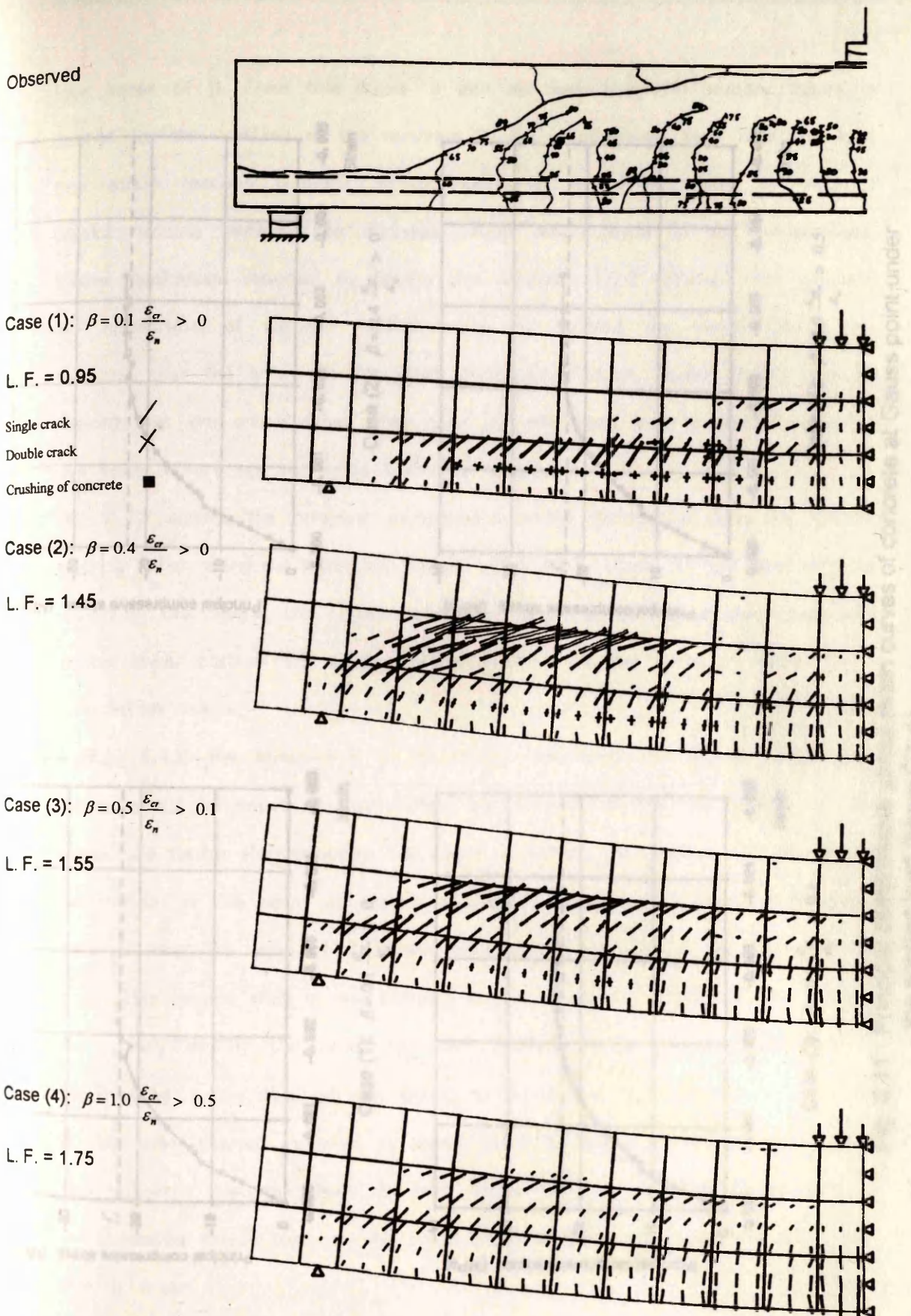


Fig. 6.10 Crack patterns and deformed shapes for beam OA-1 (displacements magnified x 10).

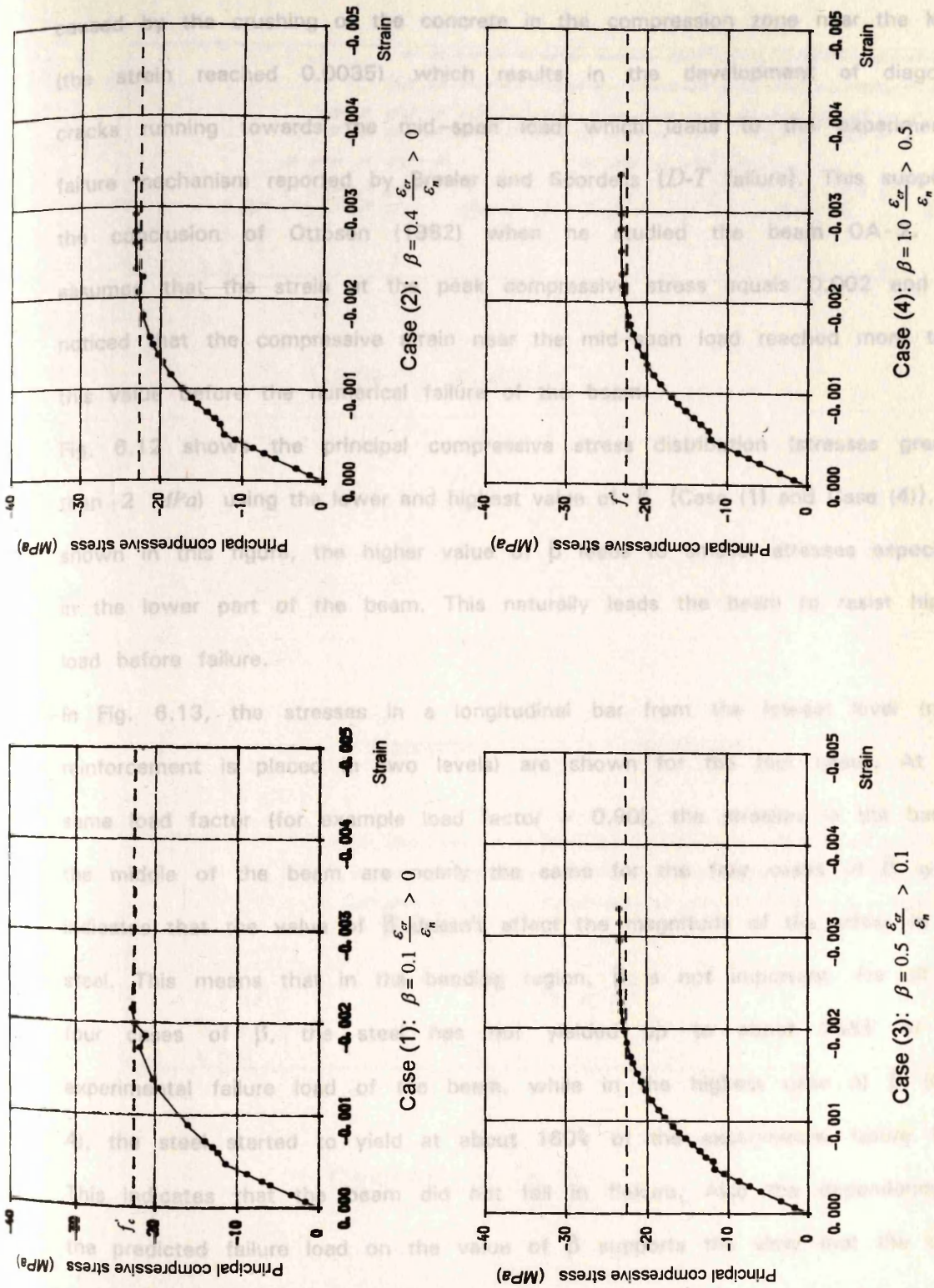


Fig. 6.11 Principal compressive stress-strain curves of concrete at Gauss point under the applied load (beam OA-1).

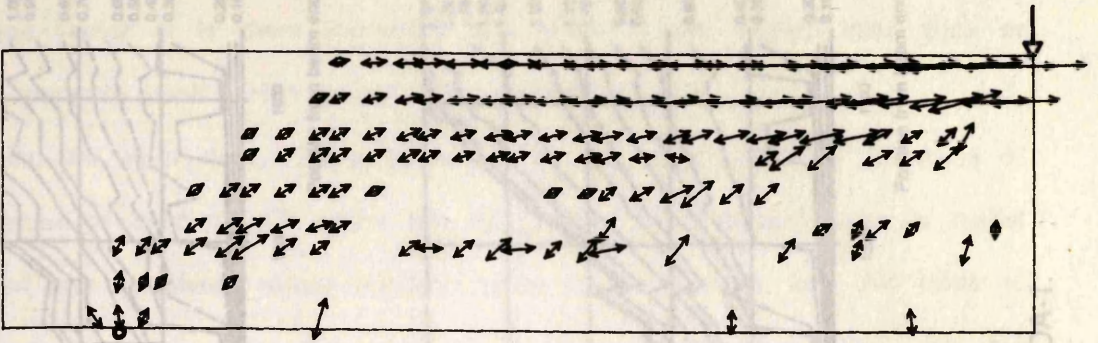
four cases of β . From this figure, it can be seen that the primary failure is caused by the crushing of the concrete in the compression zone near the load (the strain reached 0.0035) which results in the development of diagonal cracks running towards the mid-span load which leads to the experimental failure mechanism reported by Bresler and Scordelis ($D-T$ failure). This supports the conclusion of Ottosen (1982) when he studied the beam OA-2. He assumed that the strain at the peak compressive stress equals 0.002 and he noticed that the compressive strain near the mid-span load reached more than this value before the numerical failure of the beam.

Fig. 6.12 shows the principal compressive stress distribution (stresses greater than 2 MPa) using the lower and highest value of β (Case (1) and Case (4)). As shown in this figure, the higher value of β leads to smaller stresses especially in the lower part of the beam. This naturally leads the beam to resist higher load before failure.

In Fig. 6.13, the stresses in a longitudinal bar from the lowest level (main reinforcement is placed in two levels) are shown for the four cases. At the same load factor (for example load factor = 0.90), the stresses in the bar at the middle of the beam are nearly the same for the four cases of β which indicates that the value of β doesn't affect the magnitude of the stress in the steel. This means that in the bending region, β is not important. For all the four cases of β , the steel has not yielded up to about 155% of the experimental failure load of the beam, while in the highest case of β (Case 4), the steel started to yield at about 160% of the experimental failure load. This indicates that the beam did not fail in flexure. Also the dependency of the predicted failure load on the value of β supports the view that the beam fails in shear.

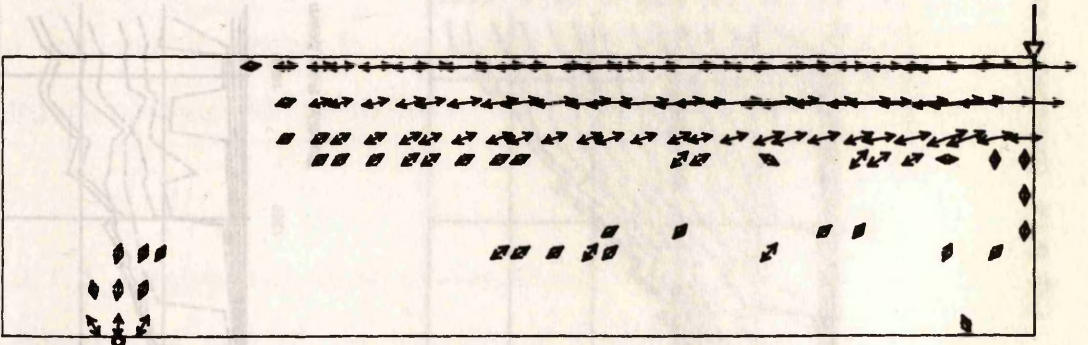
The important question now after this result is why did the prediction overestimate the observed failure loads for these beams especially when a high

Scale (Max.) : ————— = 22.91 MPa



Case (1): $\beta = 0.1 \frac{\epsilon_{cr}}{\epsilon_n} > 0$

Scale (Max.) : ————— = 18.45 MPa



Case (4): $\beta = 1.0 \frac{\epsilon_{cr}}{\epsilon_n} > 0.5$

Fig. 6.12 Principal compressive stress distributions at load factor = 0.95 for beam OA-1 (stresses greater than 2 MPa)

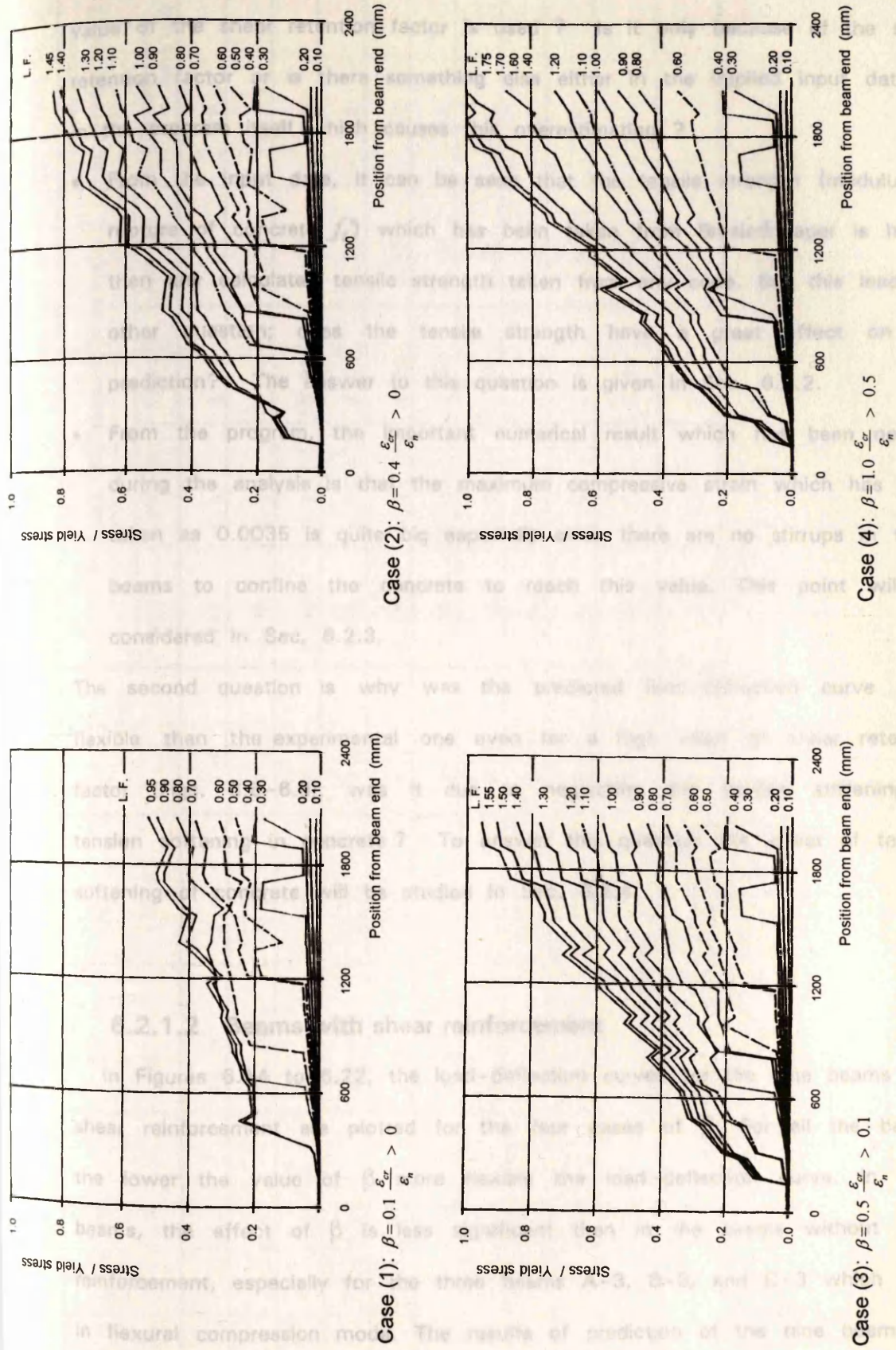


Fig. 6.13 Stresses in tension steel at different load factors for beam OA-1.

value of the shear retention factor is used? Is it only because of the shear retention factor or is there something else either in the implied input data or in the program itself which causes this overestimating?

- From the input data, it can be seen that the tensile strength (modulus of rupture of concrete f_t') which has been taken from Bresler's paper is higher than any calculated tensile strength taken from any code. But this leads to other question; does the tensile strength have a great effect on the prediction? The answer to this question is given in Sec. 6.2.2.
- From the program, the important numerical result which has been noticed during the analysis is that the maximum compressive strain which has been taken as 0.0035 is quite big especially since there are no stirrups in these beams to confine the concrete to reach this value. This point will be considered in Sec. 6.2.3.

The second question is why was the predicted load-deflection curve more flexible than the experimental one even for a high value of shear retention factor (Figs. 6.6-6.8); was it due to neglecting the tension stiffening or tension softening in concrete? To answer this question the effect of tension softening of concrete will be studied in Sec. 6.2.4.

6.2.1.2 Beams with shear reinforcement

In Figures 6.14 to 6.22, the load-deflection curves for the nine beams with shear reinforcement are plotted for the four cases of β . For all the beams, the lower the value of β more flexible the load-deflection curve. In these beams, the effect of β is less significant than in the beams without shear reinforcement, especially for the three beams A-3, B-3, and C-3 which failed in flexural compression mode. The results of prediction of the nine beams are shown in Table 6.3. The difference between the mean values of the ratios of the predicted to the observed failure load for Case (1) and Case (4) is about

Table 6.3 Effect of shear retention factor in beams with shear reinforcement

Beam	a/d	f'_c (MPa)	f'_t (MPa)	Failure mode	Predicted / Experimental failure load				Difference between Case (4) and Case(1) (% of the experimental failure load)
					Case (1)	Case (2)	Case (3)	Case (4)	
A-1	3.92	24.08	3.86	V-C	0.85	1.10	1.20	1.35	50
A-2	4.93	24.29	3.73	V-C	0.70	0.90	1.00	1.05	35
A-3	6.91	35.05	4.34	F-C	0.80	0.90	0.95	1.00	20
B-1	3.95	24.77	3.99	V-C	0.75	0.95	1.05	1.15	40
B-2	4.91	23.18	3.76	V-C	0.65	0.85	0.90	0.95	30
B-3	6.95	38.78	4.22	F-C	0.85	1.00	1.00	1.05	20
C-1	3.95	29.60	4.22	V-C	0.80	1.05	1.05	1.05	25
C-2	4.93	23.81	3.93	V-C	0.65	0.80	0.85	0.85	20
C-3	6.98	35.05	3.86	F-C	0.75	0.85	0.90	0.95	20
Mean value					0.76	0.93	0.99	1.04	
Standard deviation (%)					7.7	10.0	10.5	14.2	

Case (1): $\beta = 0.1 \frac{\epsilon_{cr}}{\epsilon_n} \geq 0.0$; Case (2): $\beta = 0.4 \frac{\epsilon_{cr}}{\epsilon_n} \geq 0.0$; Case (3): $\beta = 0.5 \frac{\epsilon_{cr}}{\epsilon_n} \geq 0.1$; Case (4): $\beta = 1.0 \frac{\epsilon_{cr}}{\epsilon_n} \geq 0.5$

* From Bresler and Scordelis's paper

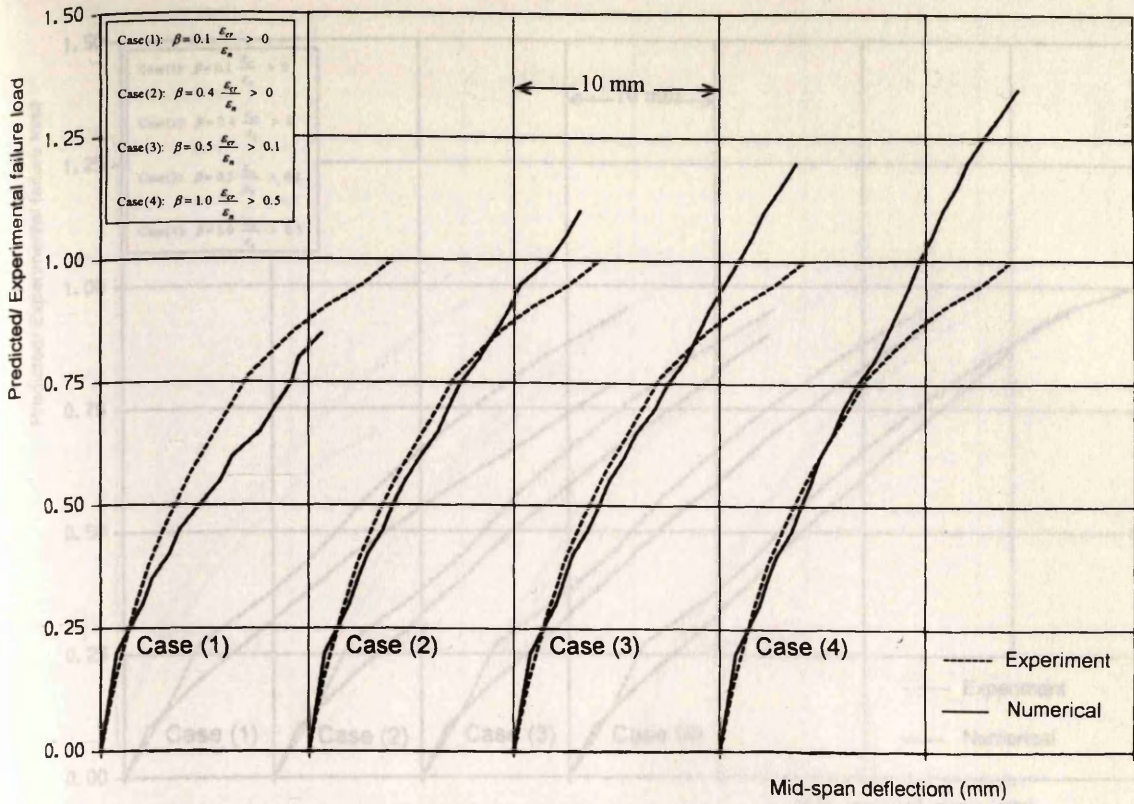


Fig. 6.14 Load-deflection curves for beam A-1 (effect of shear retention factor β).

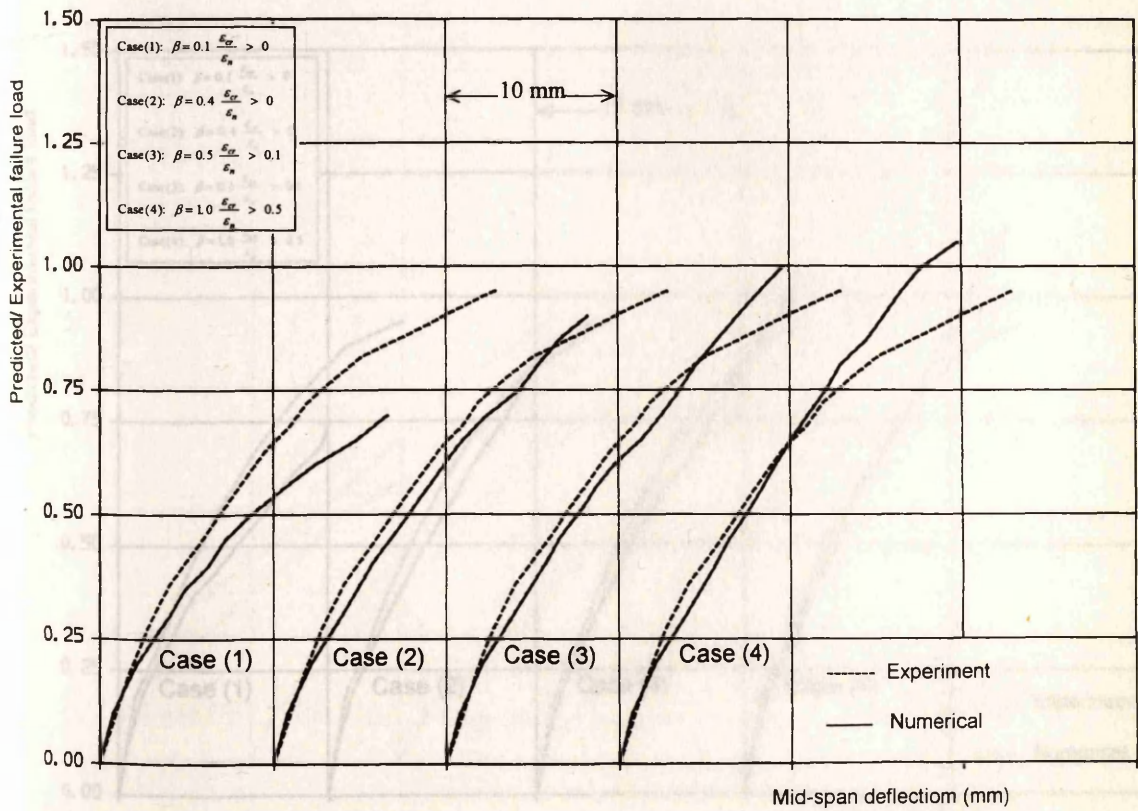


Fig. 6.15 Load-deflection curves for beam A-2 (effect of shear retention factor β).

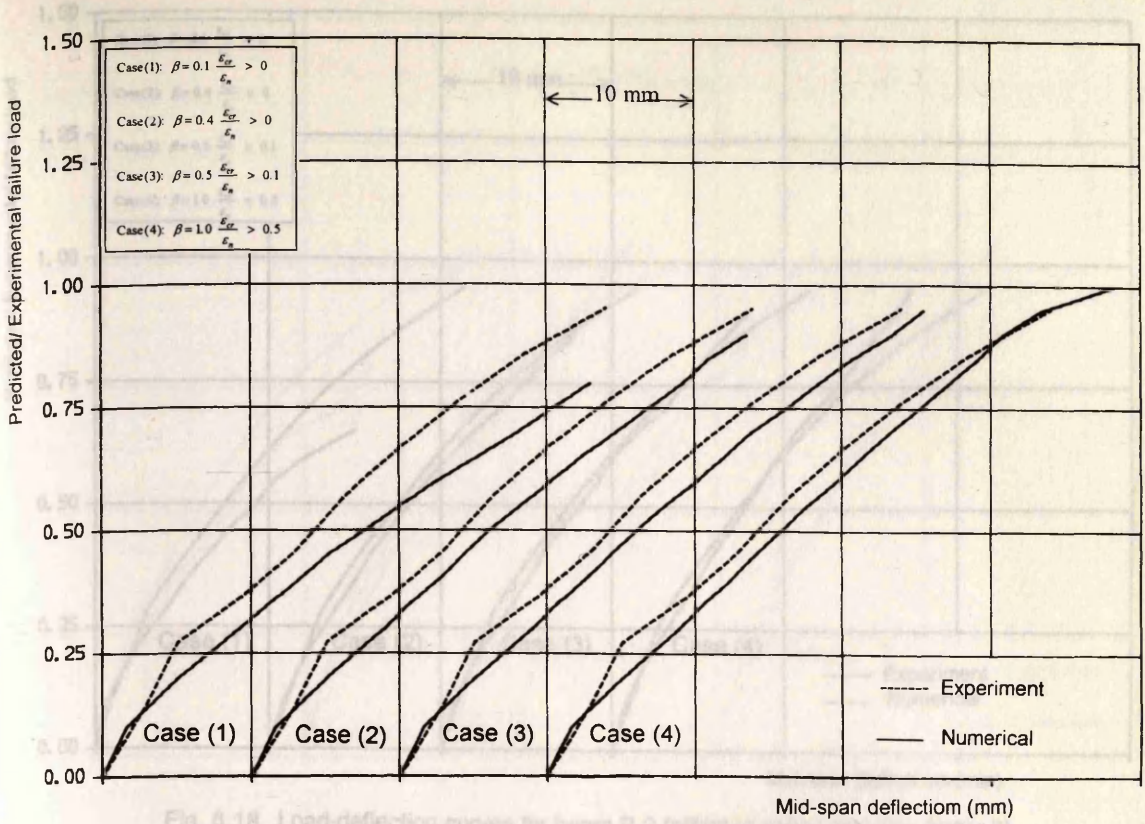


Fig. 6.16 Load-deflection curves for beam A-3 (effect of shear retention factor β).

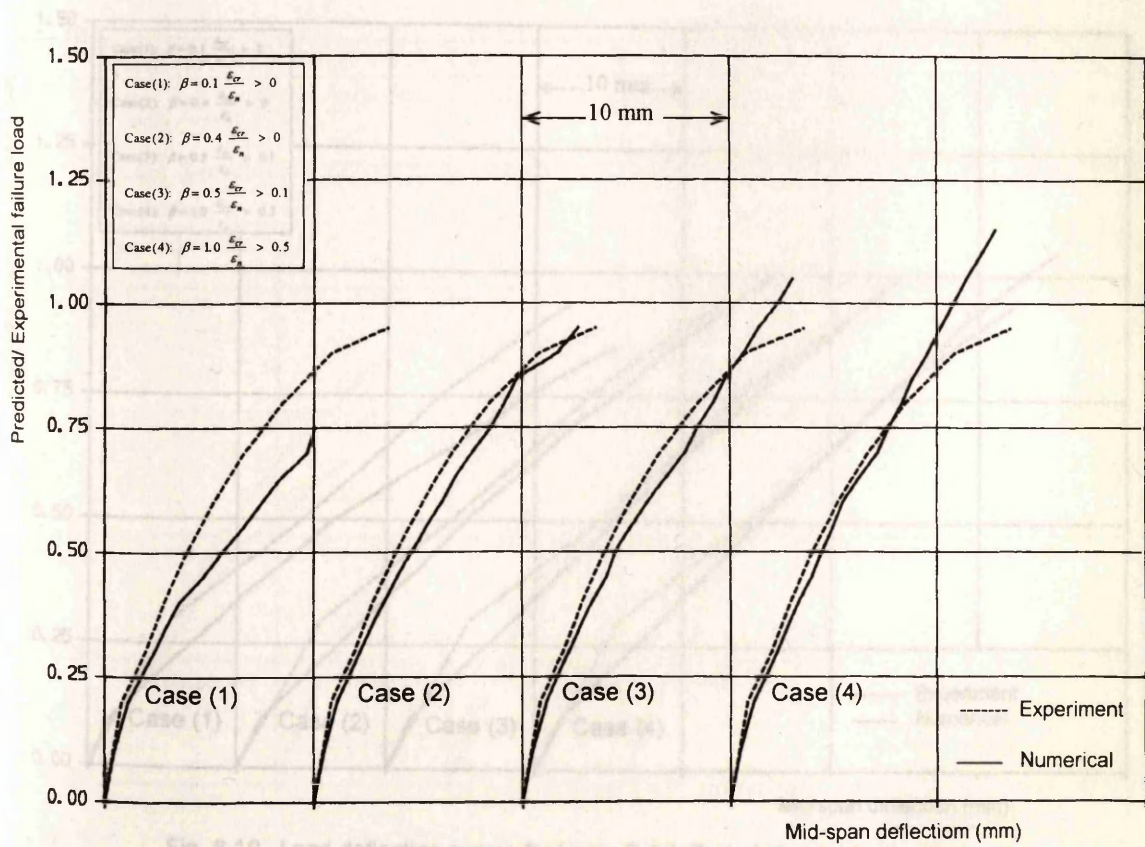


Fig. 6.17 Load-deflection curves for beam B-1 (effect of shear retention factor β).

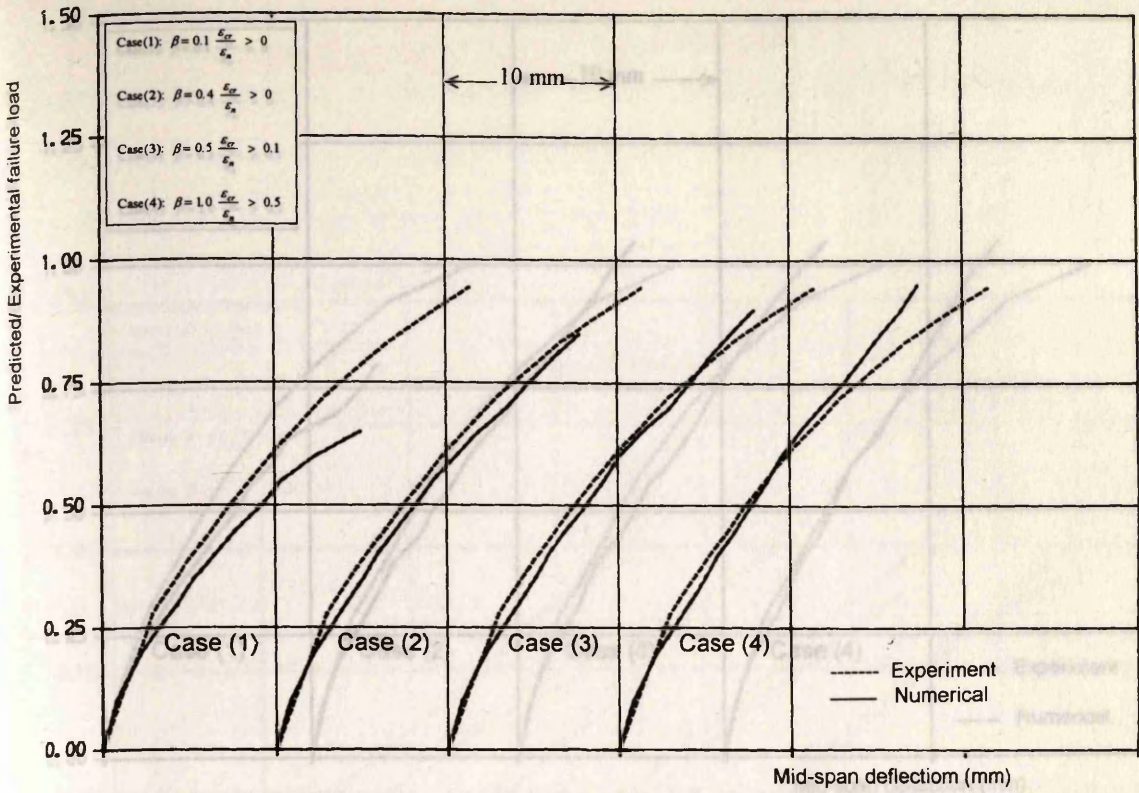


Fig. 6.18 Load-deflection curves for beam B-2 (effect of shear retention factor β).

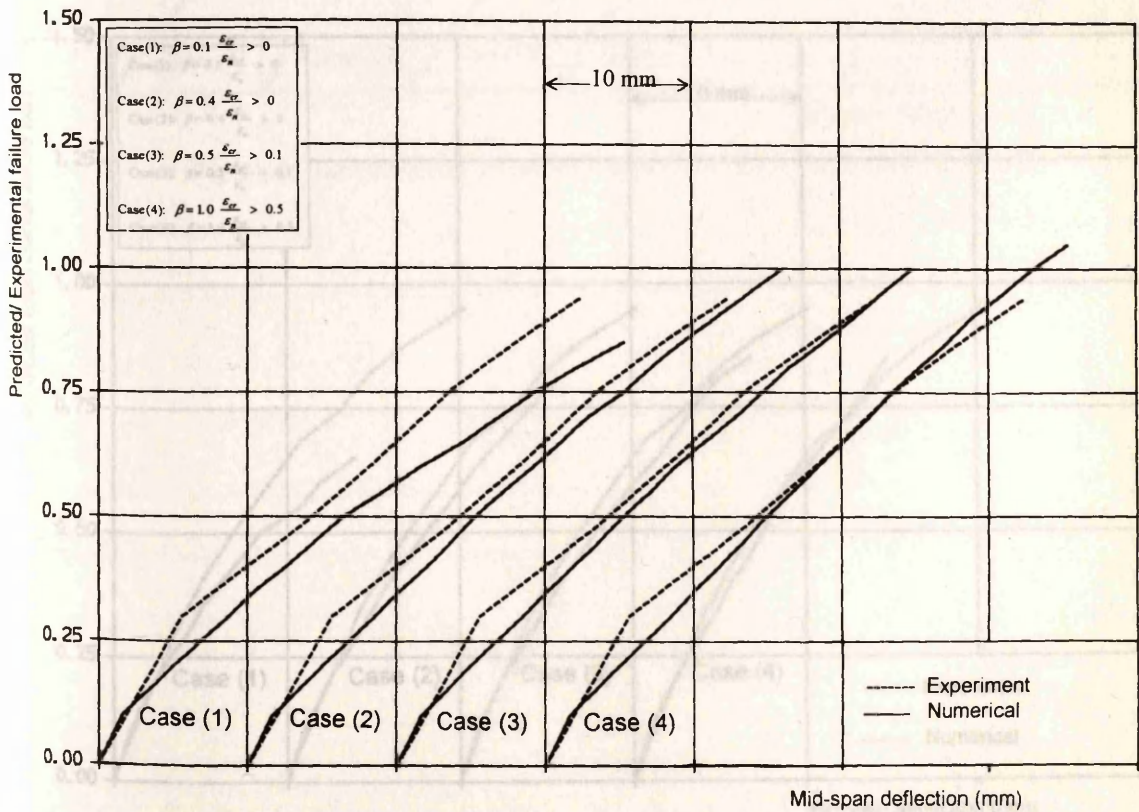


Fig. 6.19 Load-deflection curves for beam B-3 (effect of shear retention factor β).

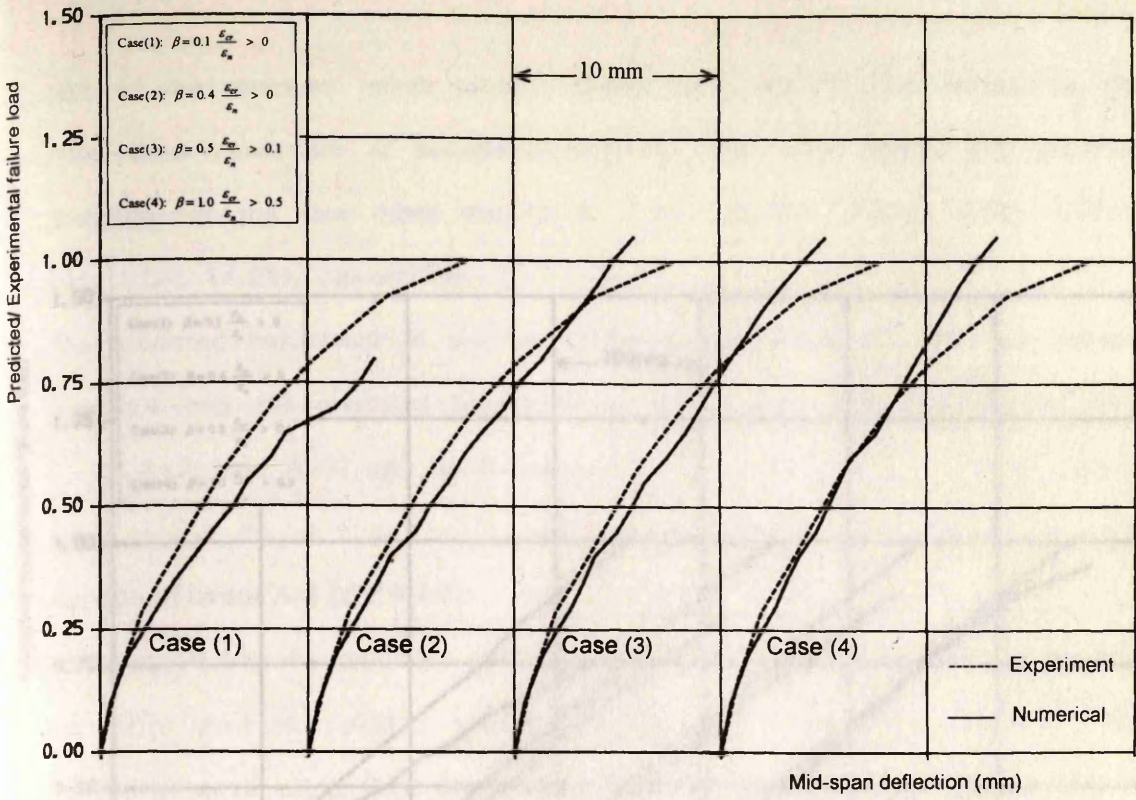


Fig. 6.20 Load-deflection curves for beam C-1 (effect of shear retention factor β).

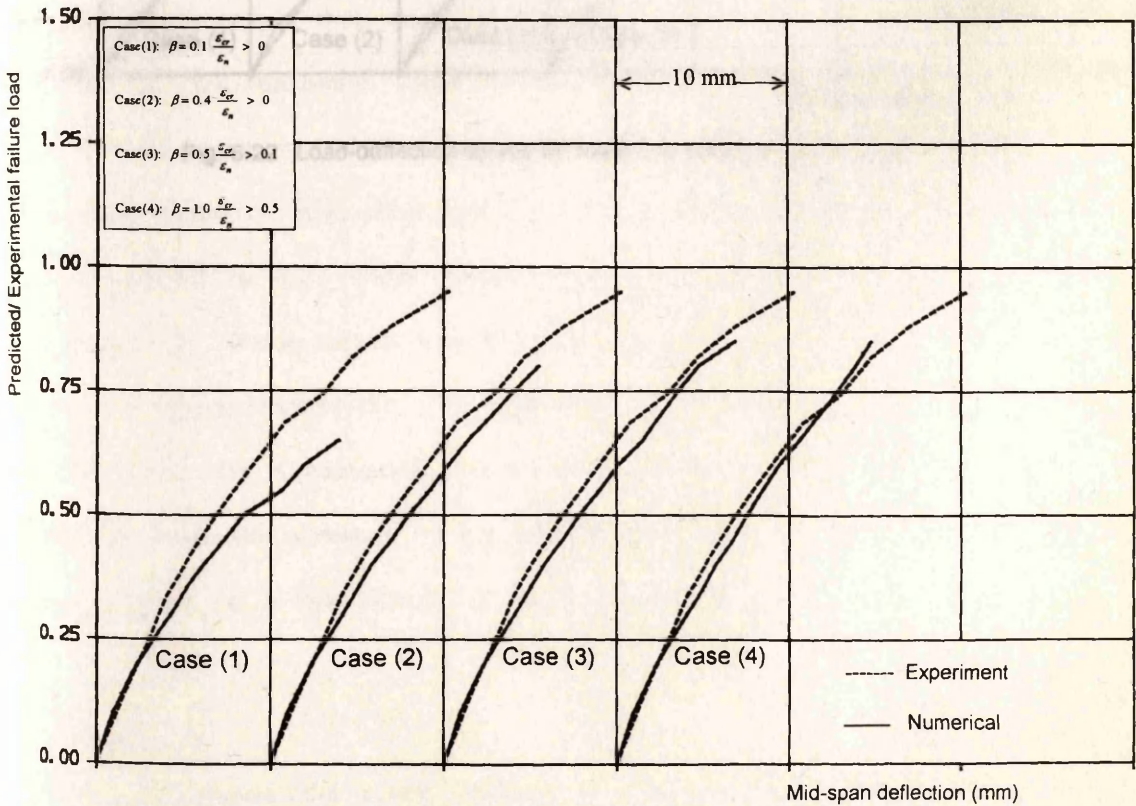


Fig. 6.21 Load-deflection curves for beam C-2 (effect of shear retention factor β).

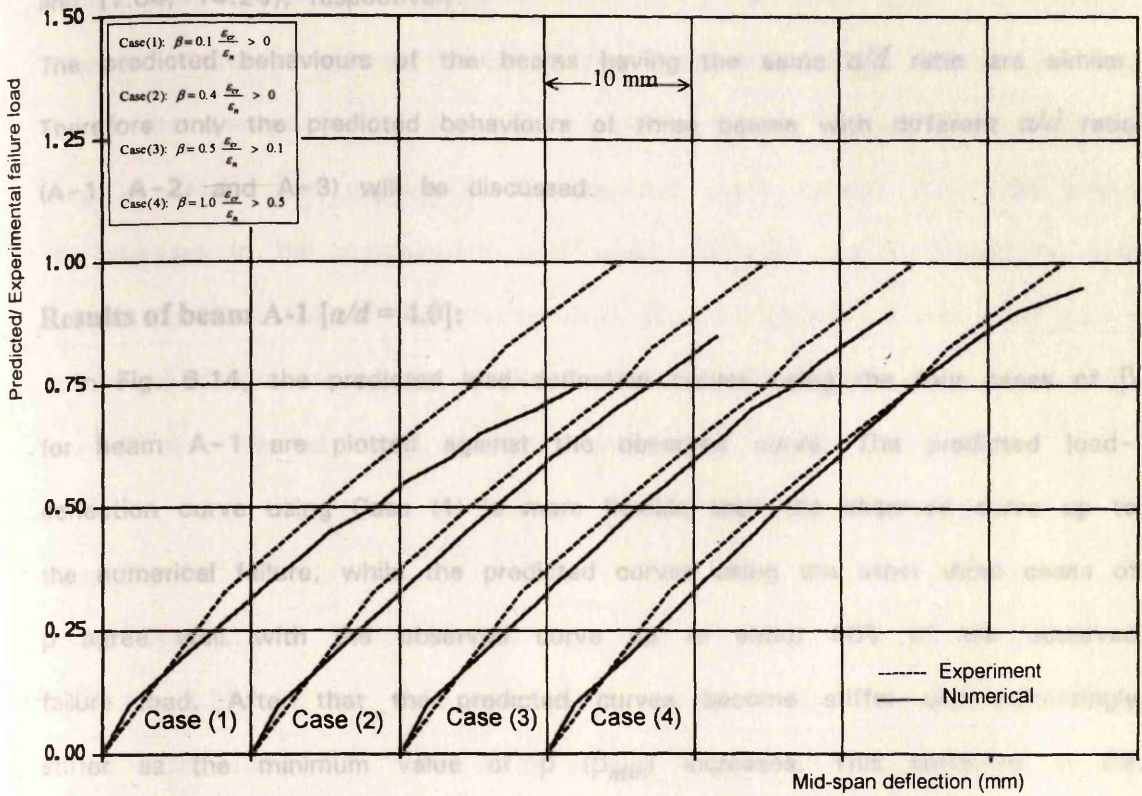


Fig. 6.22 Load-deflection curves for beam C-3 (effect of shear retention factor β).

28% of the observed failure loads. Except for Case (1), the results for the other three cases are of acceptable accuracy. The mean values and standard deviation for the four cases are (0.76, 7.7%), (0.93, 10.0%), (0.99, 10.5%), and (1.04, 14.2%), respectively.

The predicted behaviours of the beams having the same a/d ratio are similar. Therefore only the predicted behaviours of three beams with different a/d ratio (A-1, A-2, and A-3) will be discussed.

Results of beam A-1 [$a/d = 4.0$]:

In Fig. 6.14, the predicted load-deflection curves using the four cases of β for beam A-1 are plotted against the observed curve. The predicted load-deflection curve using Case (1) is more flexible than the observed curve up to the numerical failure, while the predicted curves using the other three cases of β agree well with the observed curve up to about 80% of the observed failure load. After that the predicted curves become stiffer and increasingly stiffer as the minimum value of β (β_{min}) increases. This stiffening in the predicted curves might be due to assuming a minimum value of β (which remains constant) even after reaching a very large width of the crack.

Figures 6.23 to 6.27 show some numerical results for beam A-1 for the four cases of β . These results are; the crack patterns and deformed shapes at the last converged increments, the stresses in the stirrups at the last converged increments, the stress-strain curves of concrete at a Gauss point under the applied load, the stresses in the compression steel for several increments, and the stresses in a longitudinal bar from the tension steel.

Case (1):

Fig. 6.23 shows the crack patterns at the last converged increments. The crack pattern of Case (1) agrees to a certain extent with the observed crack pattern at failure in that some cracks penetrated the compression zone at the

middle of the beam and some horizontal cracks appeared in this zone (this indicates that failure starts in compression zone). However, the predicted crack pattern of Case (1) disagrees with the observed crack pattern in that except near the load, no cracks occurred above the lower third. The predicted stresses in the stirrups are shown in Fig. 6.24; the position of the points at which the stirrups yielded does not correspond to the correct position of the diagonal cracks that appears in the observed crack pattern. Fig. 6.26 shows the stresses in the compression steel which indicates that it started to yield before numerical failure. The tension steel has not yielded at any point (which means no flexure failure, Fig. 6.27). From the above, it can be concluded that the failure is nearest to be Shear-Compression.

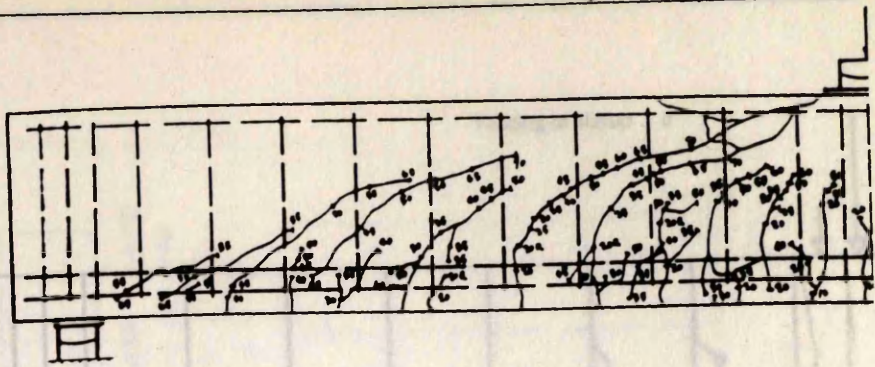
Case (2):

Using Case (2) of β , the results for beam A-1 are also shown in Figures 6.23 to 6.27. In this case, the program overestimated the failure load by about 10% (Table 6.3). The crack pattern and deformed shape at the last converged increment (L.F. = 1.10) are shown in Fig. 6.23. From the figure, it can be seen that the diagonal cracks dominate and penetrated the compression zone up to the top of the beam although the beam can still carry load. Many points in the stirrups yielded in the shear span (Fig. 6.24). The compression steel started to yield at L.F.= 1.0 (Fig. 6.26), and the main steel has not yielded (Fig. 6.27). This leads one to conclude that the predicted failure mode is Shear-Compression.

Case (3):

Figures 6.23 to 6.27 show the results of Case (3) for the same beam A-1. Nearly the same results as for Case (2) but with overestimating of the failure load by about 20% (Table 6.3).

Observed



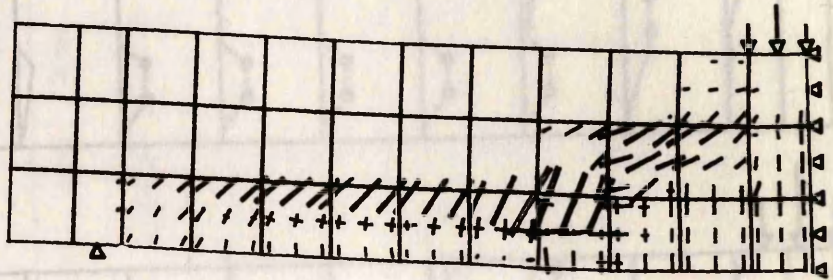
Case (1): $\beta = 0.1 \frac{\epsilon_{cr}}{\epsilon_n} > 0$

L. F. = 0.85

Single crack

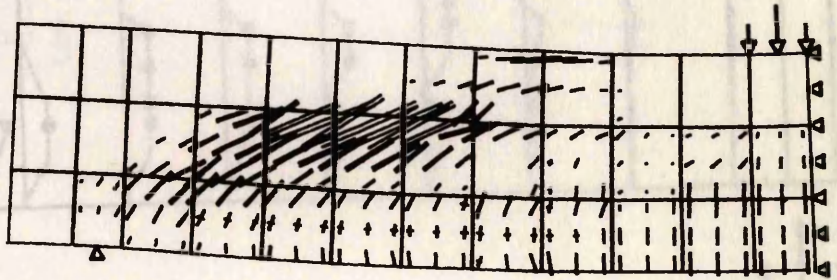
Double crack

Crushing of concrete



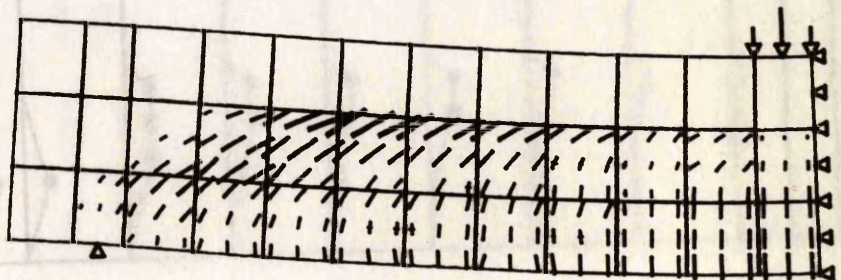
Case (2): $\beta = 0.4 \frac{\epsilon_{cr}}{\epsilon_n} > 0$

L. F. = 1.10



Case (3): $\beta = 0.5 \frac{\epsilon_{cr}}{\epsilon_n} > 0.1$

L. F. = 1.20



Case (4): $\beta = 1.0 \frac{\epsilon_{cr}}{\epsilon_n} > 0.5$

L. F. = 1.35

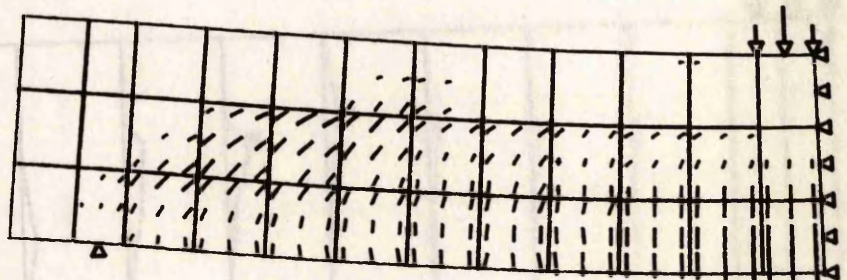
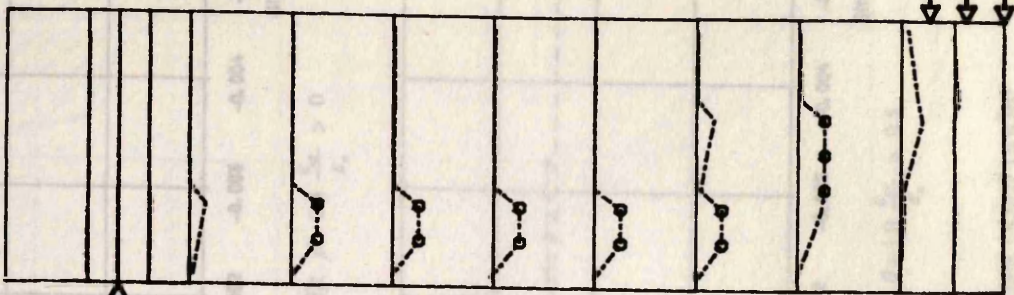


Fig. 6.23 Crack patterns and deformed shapes for beam A-1 (displacements magnified x 10).

Yielding of stirrup o

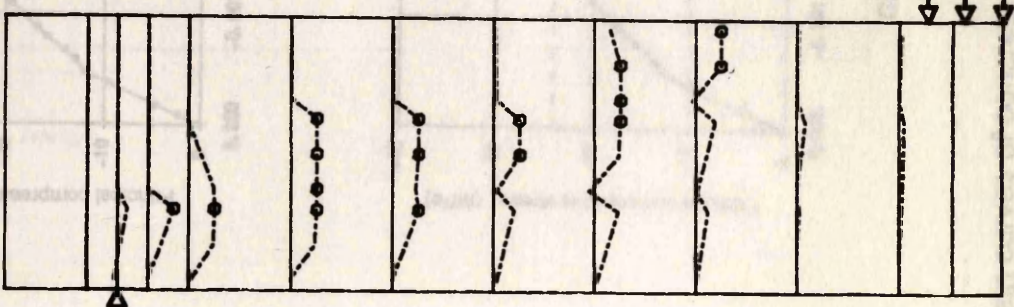
Case (1): $\beta = 0.1 \frac{\epsilon_{cr}}{\epsilon_n} > 0$

L. F. = 0.85



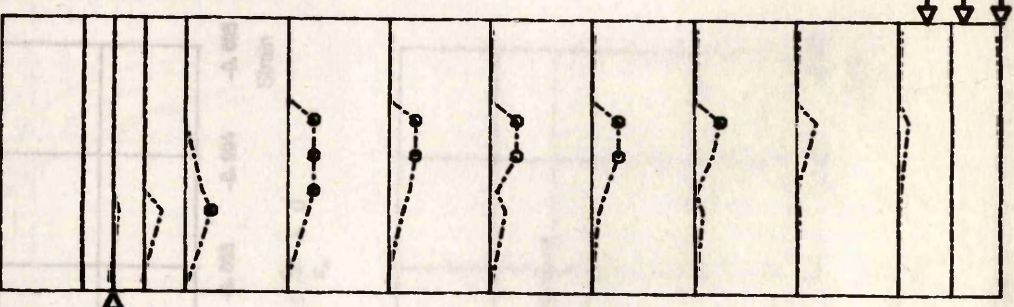
Case (2): $\beta = 0.4 \frac{\epsilon_{cr}}{\epsilon_n} > 0$

L. F. = 1.10



Case (3): $\beta = 0.5 \frac{\epsilon_{cr}}{\epsilon_n} > 0.1$

L. F. = 1.20



Case (4): $\beta = 1.0 \frac{\epsilon_{cr}}{\epsilon_n} > 0.5$

L. F. = 1.35

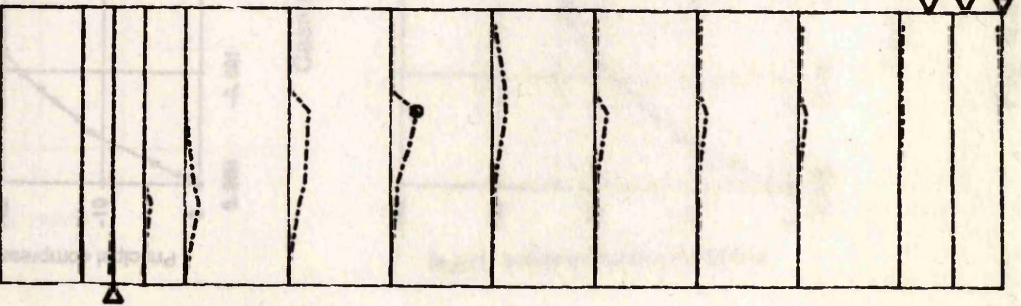


Fig. 6.24 Stresses in shear reinforcement (beam A-1).

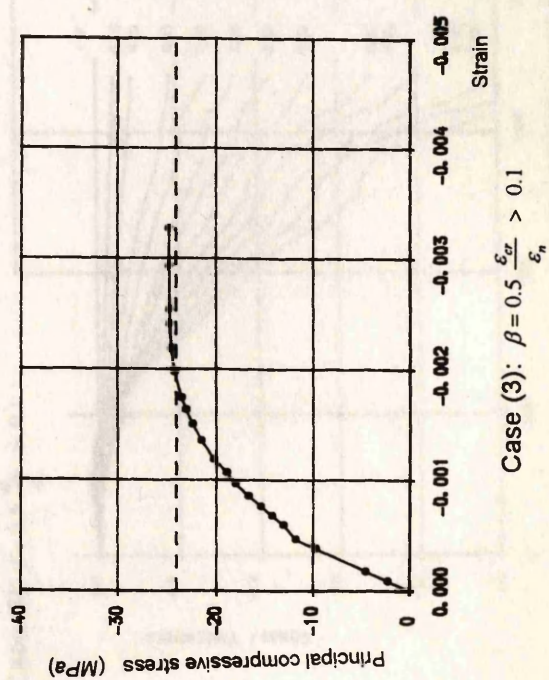
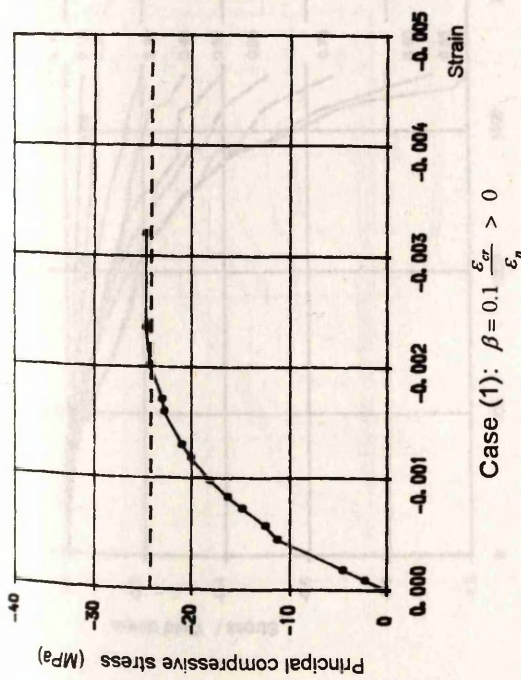
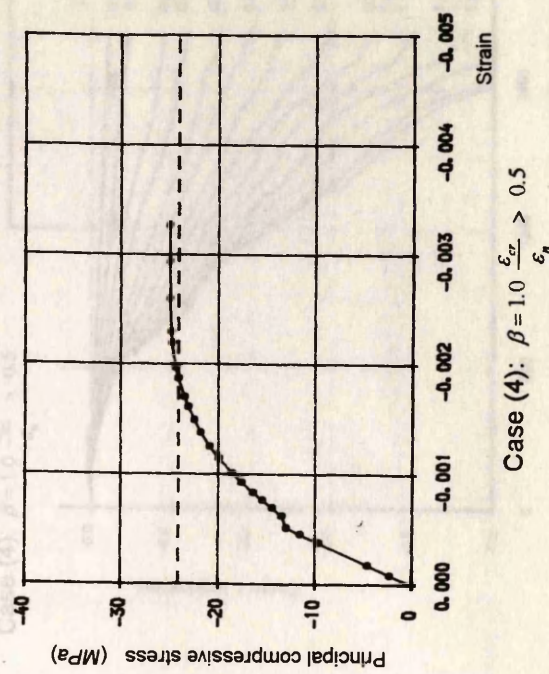
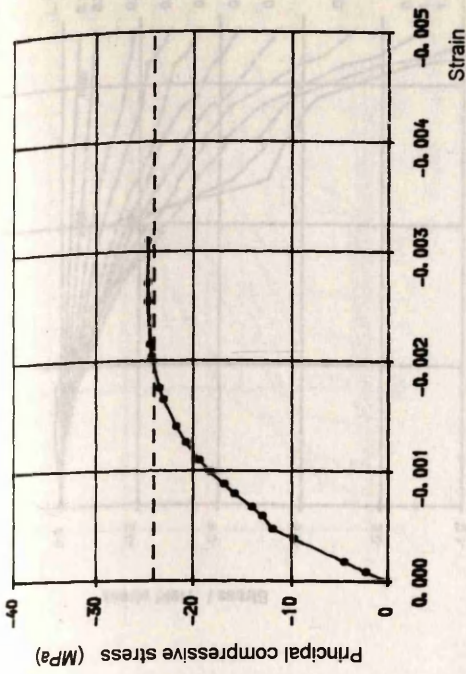


Fig. 6.25 Principal compressive stress-strain curves of concrete at Gauss point under the applied load (beam A-1).

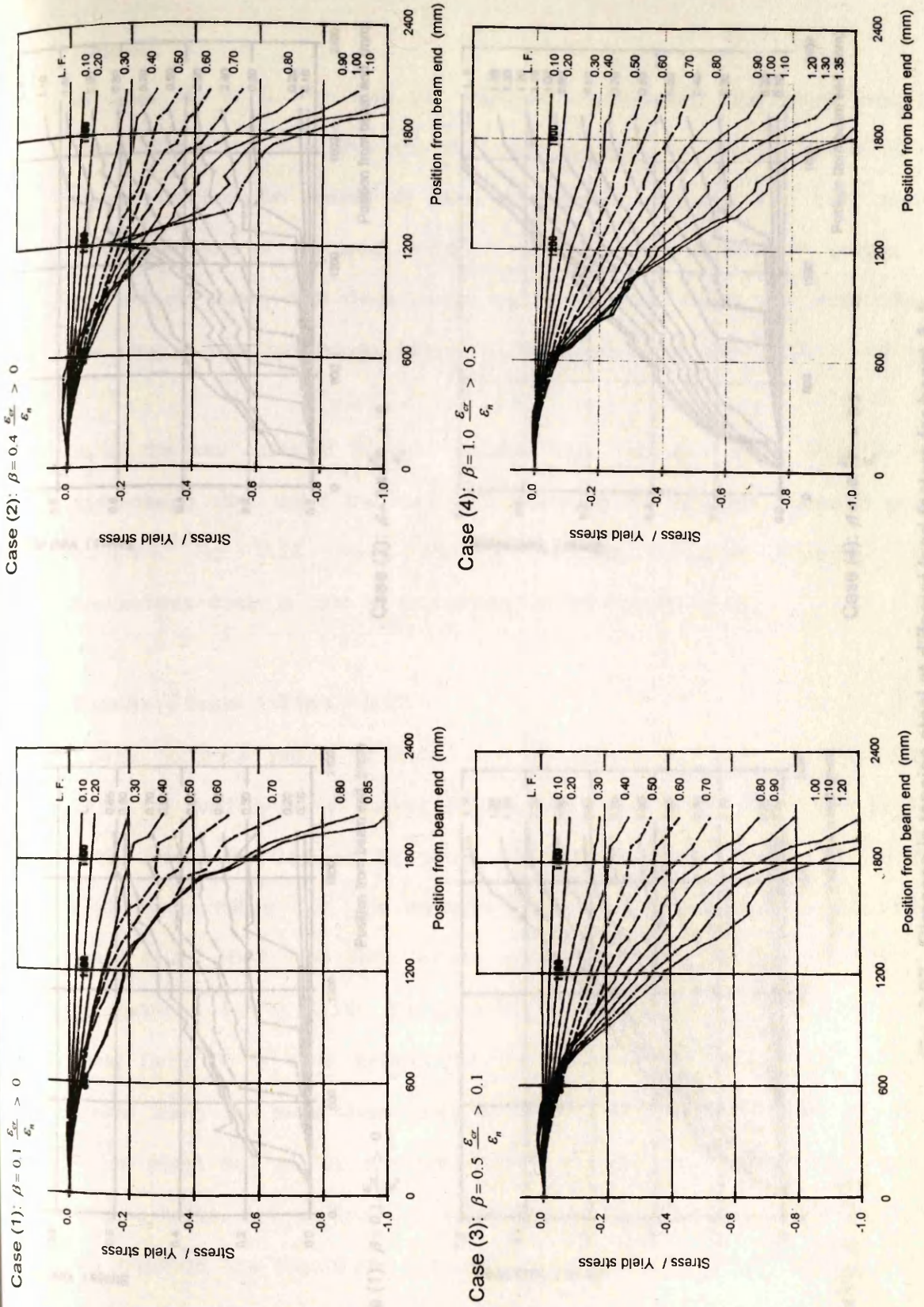
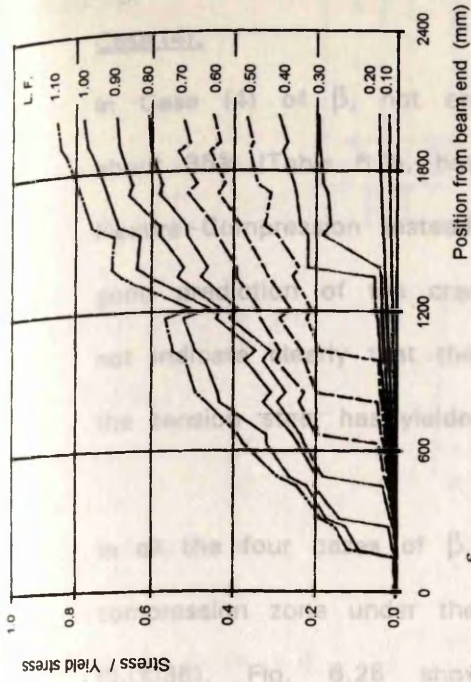
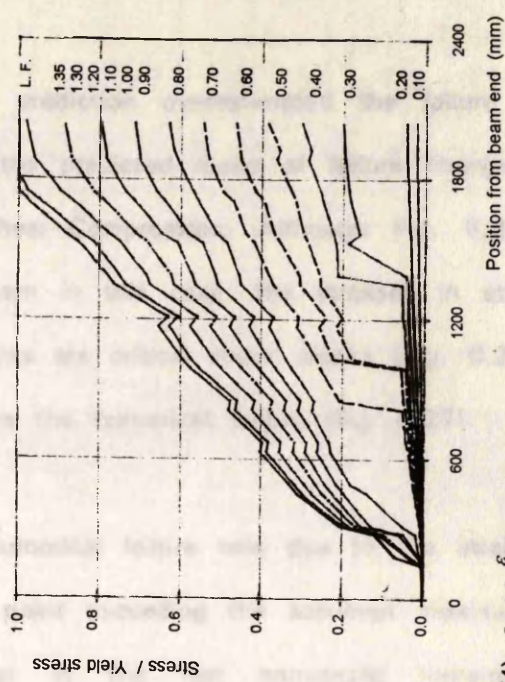


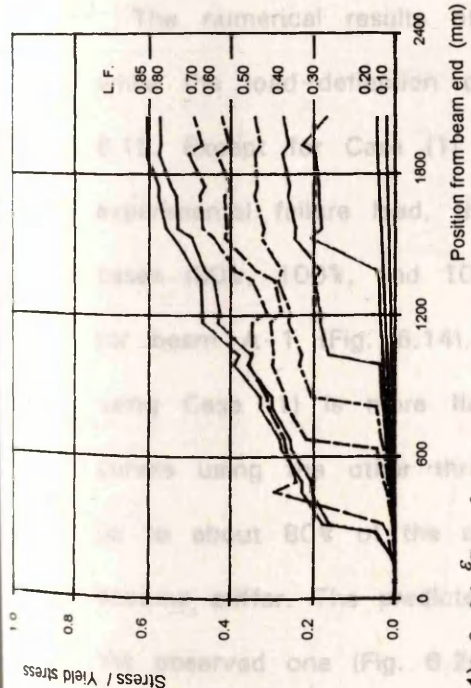
Fig. 6.26 Stresses in compression steel at different load factors for beam A-1.



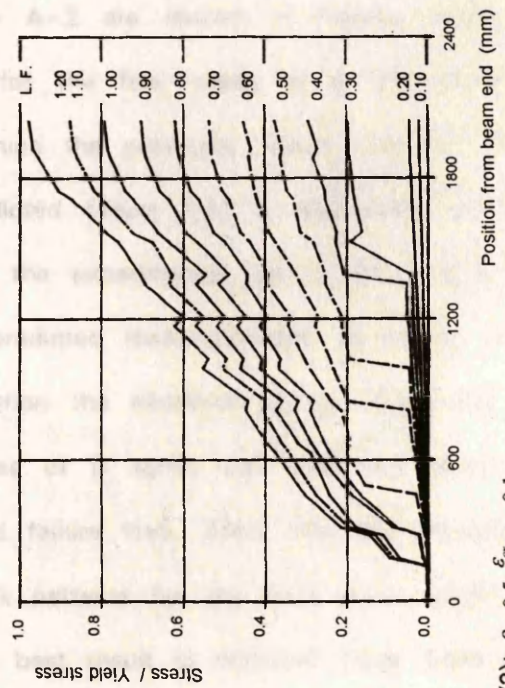
Case (2): $\beta = 0.4 \frac{\epsilon_{cr}}{\epsilon_n} > 0$



Case (4): $\beta = 1.0 \frac{\epsilon_{cr}}{\epsilon_n} > 0.5$



Case (1): $\beta = 0.1 \frac{\epsilon_{cr}}{\epsilon_n} > 0$



Case (3): $\beta = 0.5 \frac{\epsilon_{cr}}{\epsilon_n} > 0.1$

Fig. 6.27 Stresses in tension steel at different load factors for beam A-1.

Case (4):

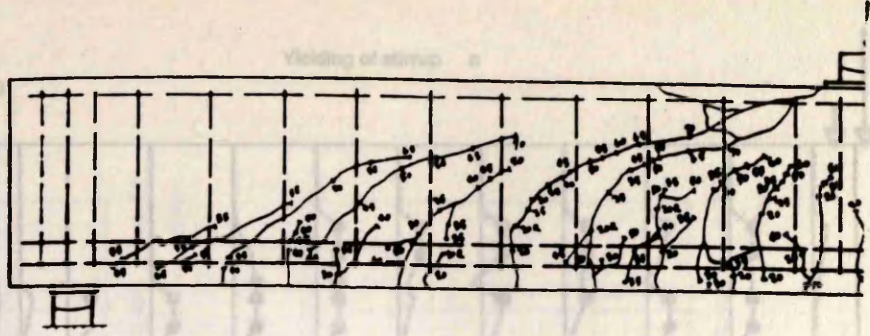
In Case (4) of β , not only the prediction overestimated the failure load by about 35% (Table 6.3), but also the predicted mode of failure changed to be Flexure-Compression instead of Shear-Compression. Although Fig. 6.23 shows good prediction of the crack pattern in this case, the stresses in stirrups do not indicate clearly that these cracks are critical shear cracks (Fig. 6.24). Also, the tension steel has yielded before the numerical failure (Fig. 6.27).

In all the four cases of β , the numerical failure was due to the strain in the compression zone under the load point exceeding the assumed maximum strain (0.0035). Fig. 6.25 shows that at the last converged increment, the compressive strain is near to 0.0035 for the four cases of β .

Results of beam A-2 [$a/d = 5.0$]:

The numerical results of beam A-2 are shown in Figures 6.28 to 6.32, while the load-deflection curves for the four cases of β are shown in Fig. 6.15. Except for Case (1) for which the predicted failure load is 70% of the experimental failure load, the predicted failure load is reasonable for the other cases (90%, 100%, and 105% of the experimental failure load, Table 6.3). As for beam A-1 (Fig. 6.14), the predicted load-deflection curve for beam A-2 using Case (1) is more flexible than the observed curve, while the predicted curves using the other three cases of β agree well with the observed curve up to about 80% of the observed failure load. After that the predicted curves become stiffer. The predicted crack patterns for the four cases agree well with the observed one (Fig. 6.28), the best result is obtained using Case (2) which predicted both the horizontal cracks in the compression zone near the load and the double cracks at the level of tension steel near the middle of the beam and near the support. The shear cracks are clear in the predicted crack patterns, many points on the stirrups have yielded in the shear span (except

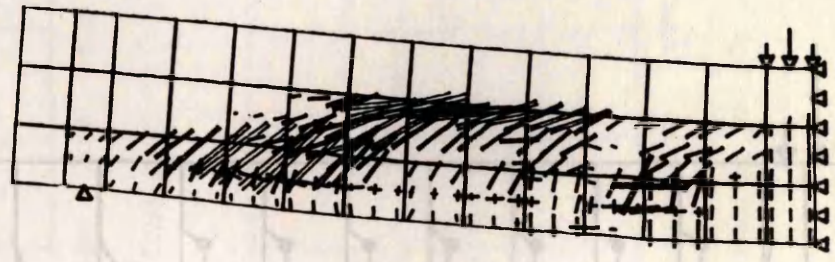
Observed



Case (1): $\beta = 0.1 \frac{\epsilon_{cr}}{\epsilon_n} > 0$

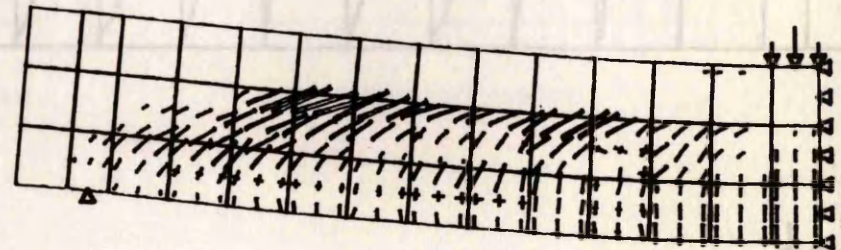
L. F. = 0.70

- Single crack /
- Double crack X
- Crushing of concrete ■



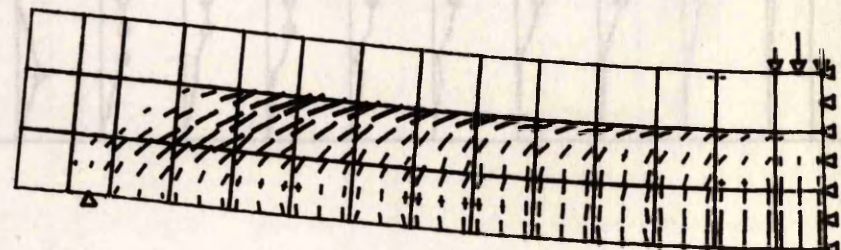
Case (2): $\beta = 0.4 \frac{\epsilon_{cr}}{\epsilon_n} > 0$

L. F. = 0.90



Case (3): $\beta = 0.5 \frac{\epsilon_{cr}}{\epsilon_n} > 0.1$

L. F. = 1.00



Case (4): $\beta = 1.0 \frac{\epsilon_{cr}}{\epsilon_n} > 0.5$

L. F. = 1.05

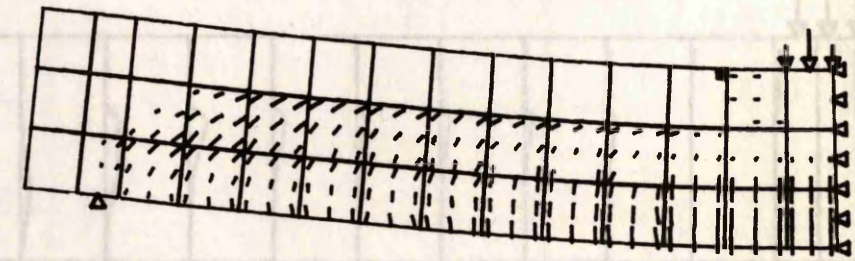


Fig. 6.28 Crack patterns and deformed shapes for beam A-2 (displacements magnified x 10).

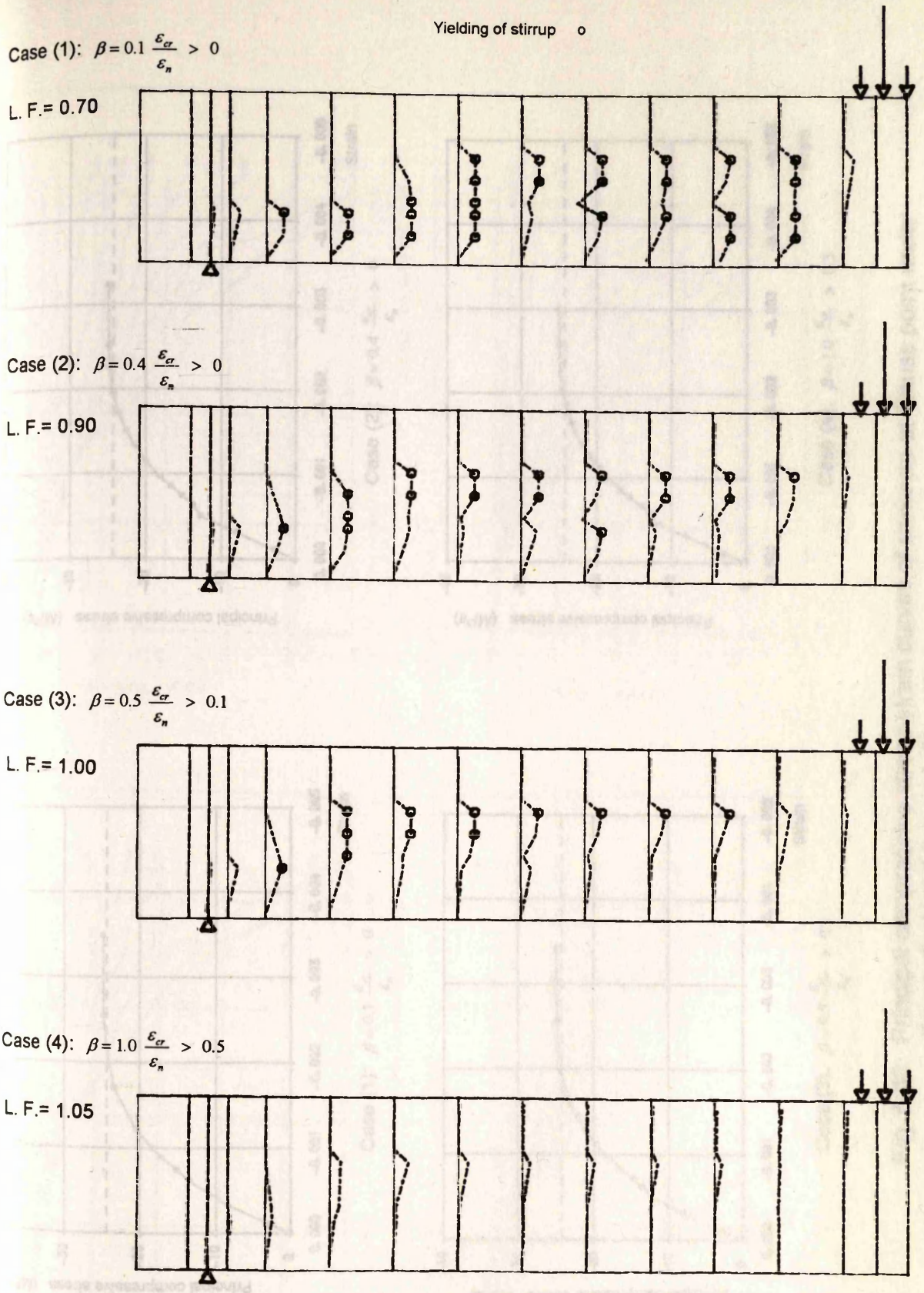


Fig. 6.29 Stresses in shear reinforcement (beam A-2).

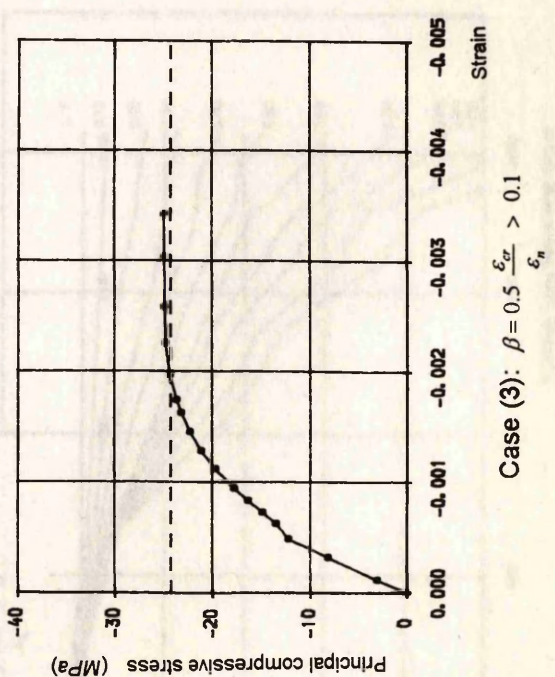
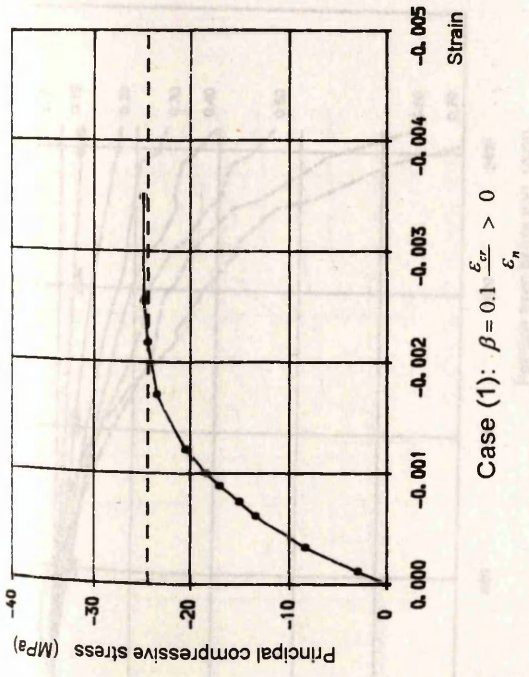
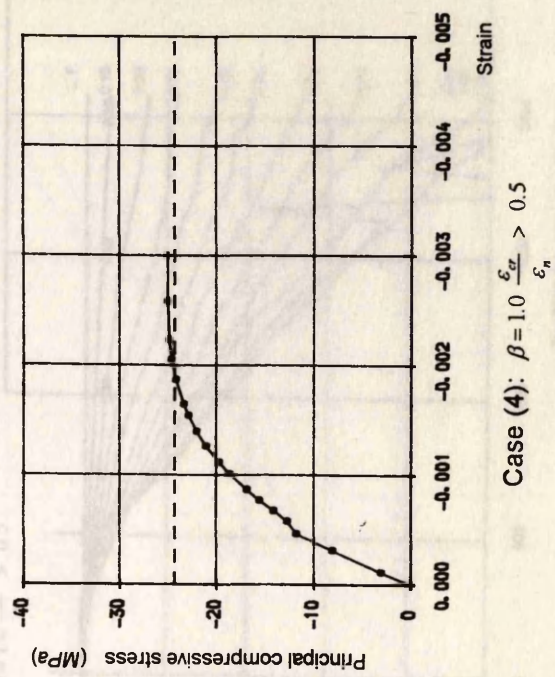
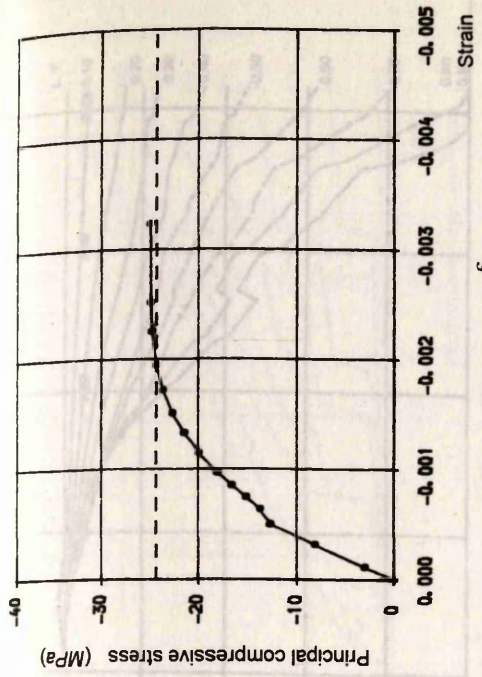


Fig. 6.30 Principal compressive stress-strain curves of concrete at Gauss point under the applied load (beam A-2).

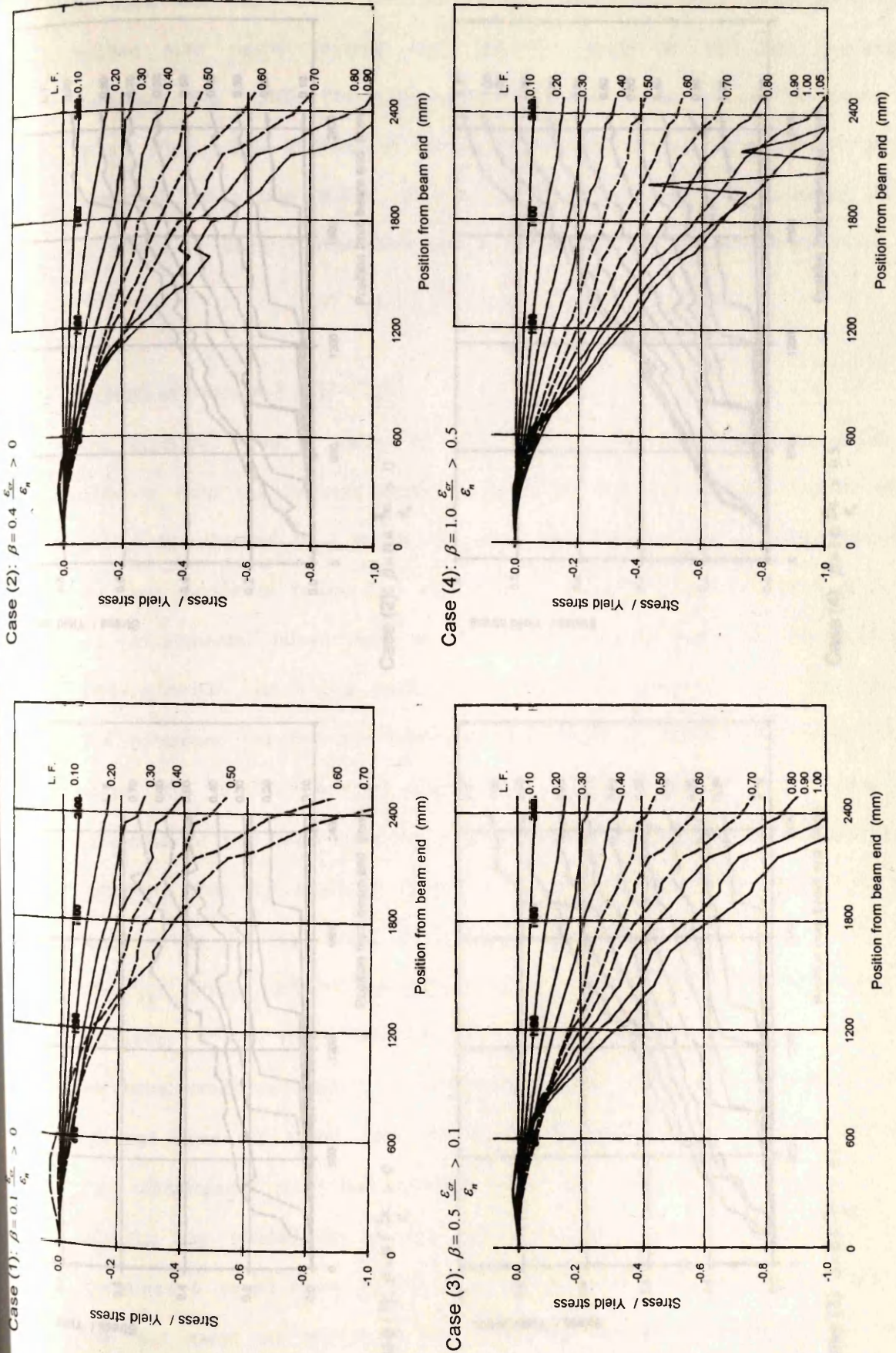
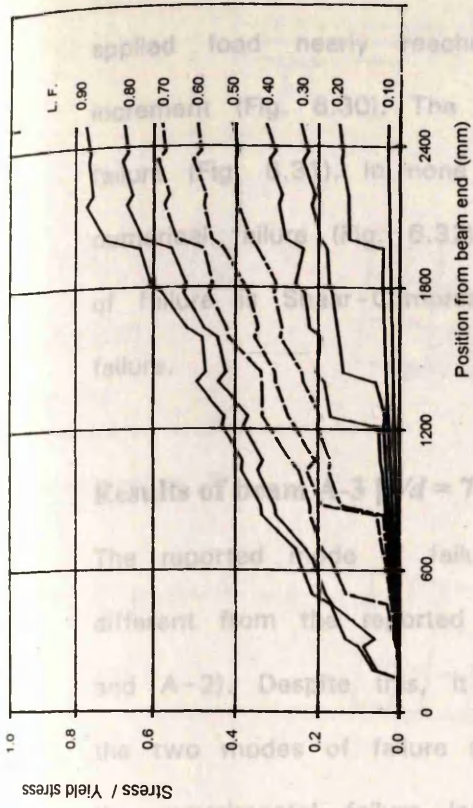
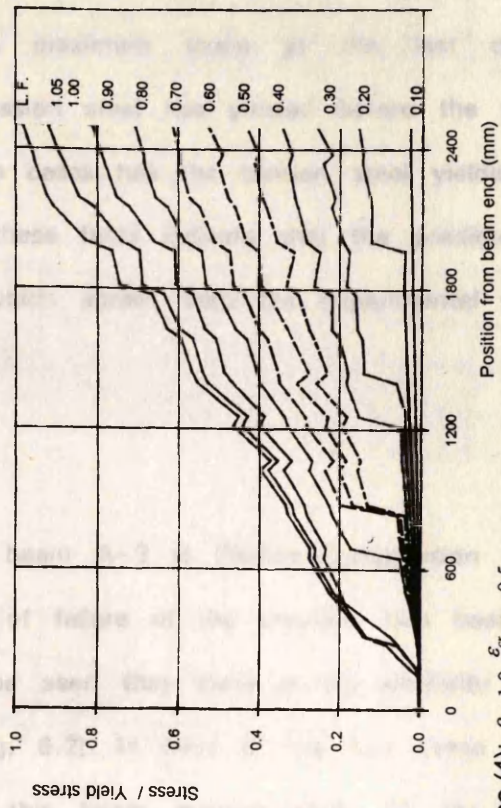


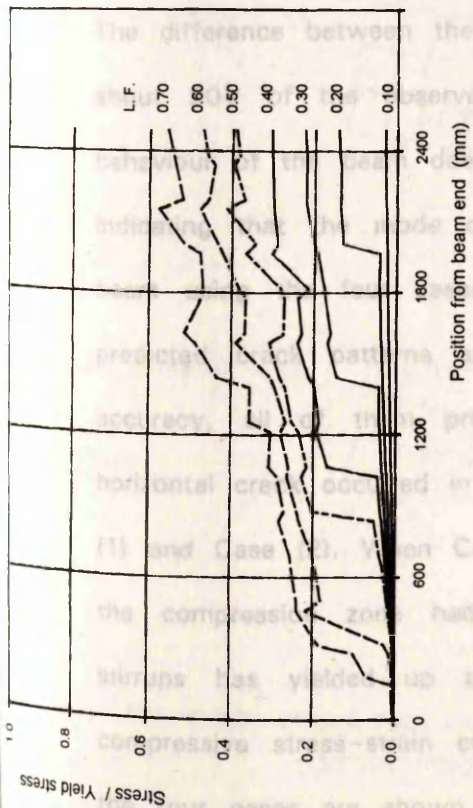
Fig. 6.31 Stresses in compression steel at different load factors for beam A-2.



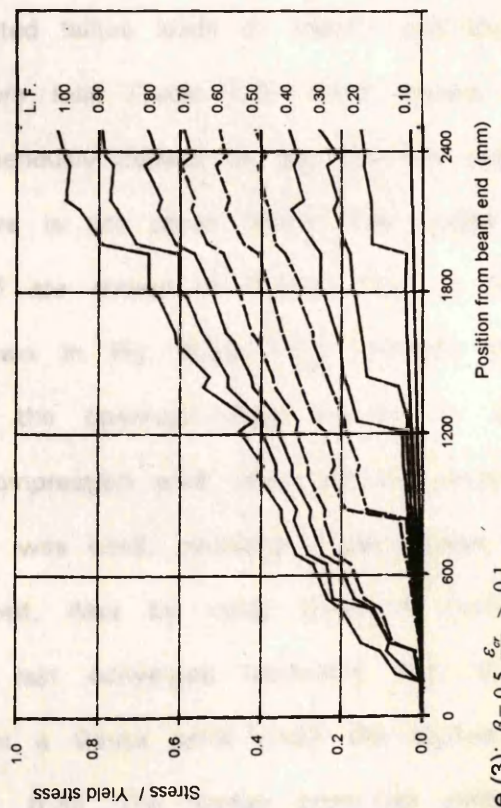
Case (2): $\beta = 0.4 \frac{\epsilon_{xz}}{\epsilon_n} > 0$



Case (4): $\beta = 1.0 \frac{\epsilon_{xz}}{\epsilon_n} > 0.5$



Case (1): $\beta = 0.1 \frac{\epsilon_{xz}}{\epsilon_n} > 0$



Case (3): $\beta = 0.5 \frac{\epsilon_{xz}}{\epsilon_n} > 0.1$

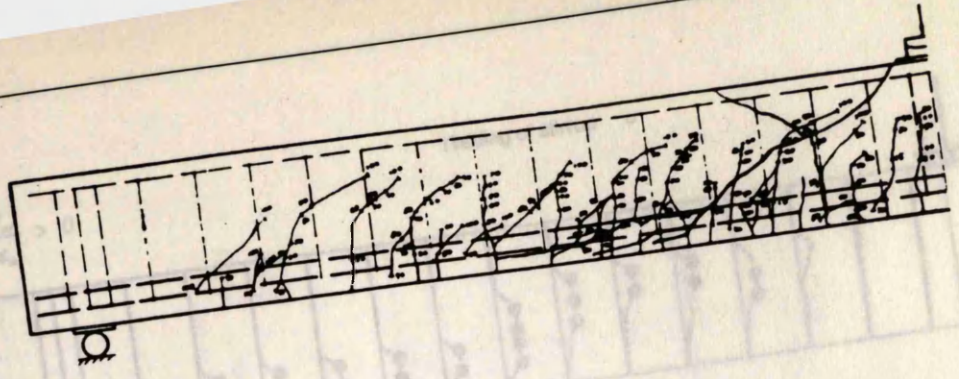
Fig. 6.32 Stresses in tension steel at different load factors for beam A-2.

in Case (4), Fig. 6.29). The compressive strain at Gauss point under the applied load nearly reached the maximum strain at the last converged increment (Fig. 6.30). The compression steel has yielded before the numerical failure (Fig. 6.31). In none of the cases has the tension steel yielded before numerical failure (Fig. 6.32). All these facts indicate that the predicted mode of failure is Shear-Compression which agrees with the experimental mode of failure.

Results of beam A-3 [$a/d = 7.0$]:

The reported mode of failure of beam A-3 is Flexure-Compression which is different from the reported mode of failure of the previous two beams (A-1 and A-2). Despite this, it can be seen that there is big similarity between the two modes of failure (see Fig. 6.2). In none of the four cases of β , is the experimental failure load of this beam overestimated. All the predicted load-deflection curves are more flexible than the observed curve (Fig. 6.16). The difference between the predicted failure loads of Case(1) and Case (4) is about 20% of the observed failure load (Table 6.3) which means that the behaviour of the beam does not seriously depend on the assumed value of β , indicating that the mode of failure is not shear failure. The results for this beam using the four cases of β are shown in Figures 6.33 to 6.37. The predicted crack patterns are shown in Fig. 6.33. With different degree of accuracy, all of them predicted the observed crack pattern. In Case (3), horizontal crack occurred in the compression zone which did not occur in Case (1) and Case (2). When Case (4) was used, concrete at two Gauss points in the compression zone had crushed. Also by using Case (4) none of the stirrups has yielded up to the last converged increment (Fig. 6.34). The compressive stress-strain curves at a Gauss point under the applied load for the four cases are shown in Fig. 6.35. The tension steel has yielded before the numerical failure only by using Case (4) (Figs. 6.36).

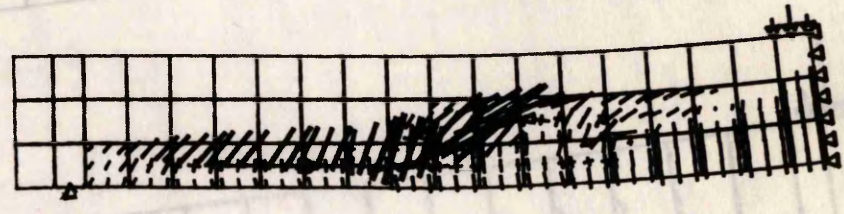
Observed



Case (1): $\beta = 0.1 \frac{\epsilon_{\sigma}}{\epsilon_n} > 0$

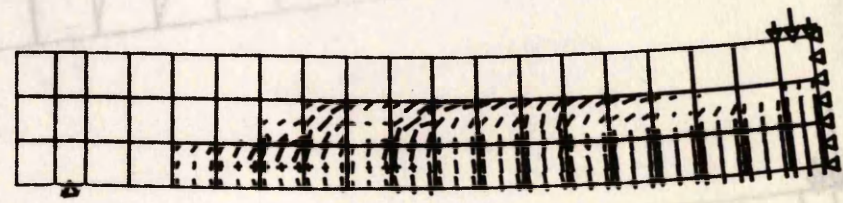
L. F. = 0.80

Single crack /
 Double crack X
 Crushing of concrete ■



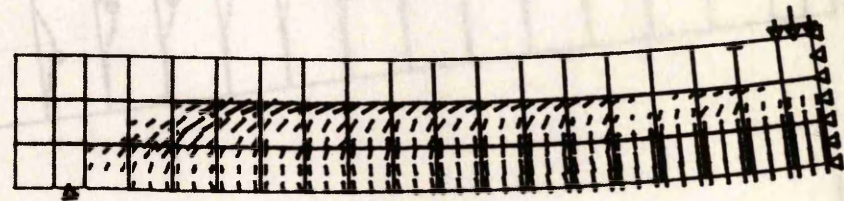
Case (2): $\beta = 0.4 \frac{\epsilon_{\sigma}}{\epsilon_n} > 0$

L. F. = 0.90



Case (3): $\beta = 0.5 \frac{\epsilon_{\sigma}}{\epsilon_n} > 0.1$

L. F. = 0.95



Case (4): $\beta = 1.0 \frac{\epsilon_{\sigma}}{\epsilon_n} > 0.5$

L. F. = 1.00

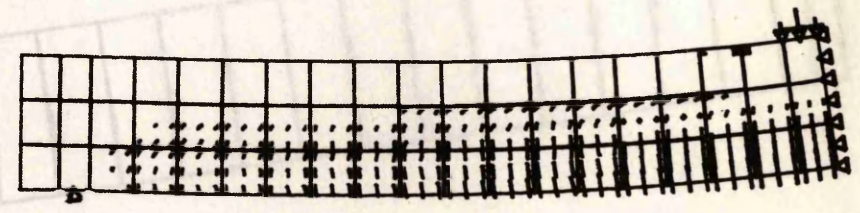
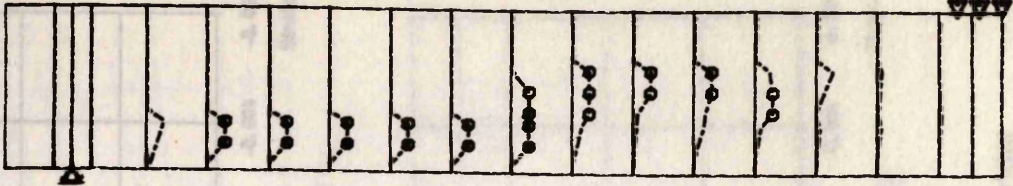


Fig. 6.33 Crack patterns and deformed shapes for beam A-3 (displacements magnified x 10).

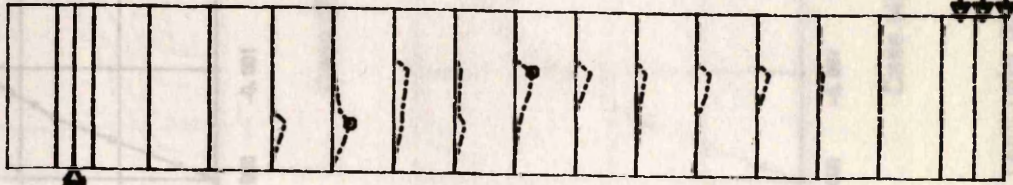
Case (1): $\beta = 0.1 \frac{\epsilon_{cr}}{\epsilon_n} > 0$

L. F. = 0.80



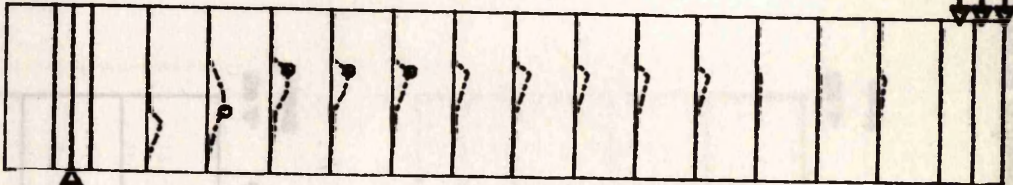
Case (2): $\beta = 0.4 \frac{\epsilon_{cr}}{\epsilon_n} > 0$

L. F. = 0.90



Case (3): $\beta = 0.5 \frac{\epsilon_{cr}}{\epsilon_n} > 0.1$

L. F. = 0.95



Case (4): $\beta = 1.0 \frac{\epsilon_{cr}}{\epsilon_n} > 0.5$

L. F. = 1.00

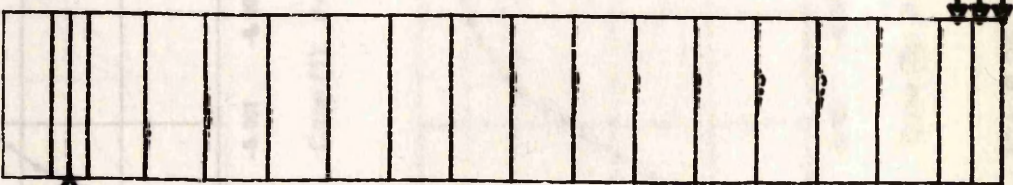


Fig. 6.34 Stresses in shear reinforcement (beam A-3).

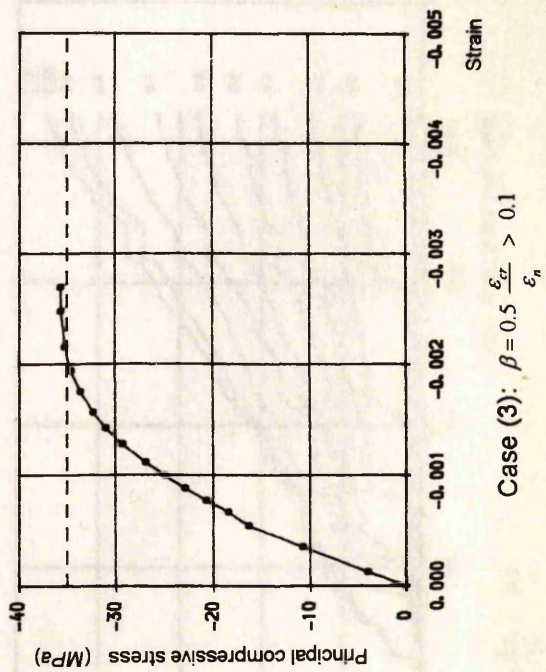
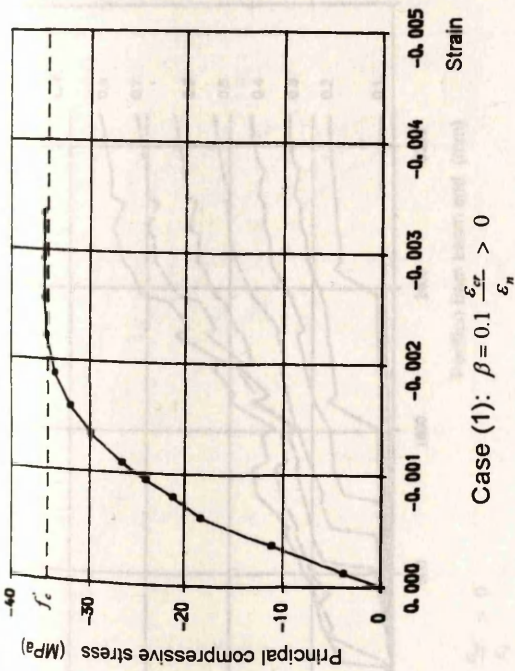
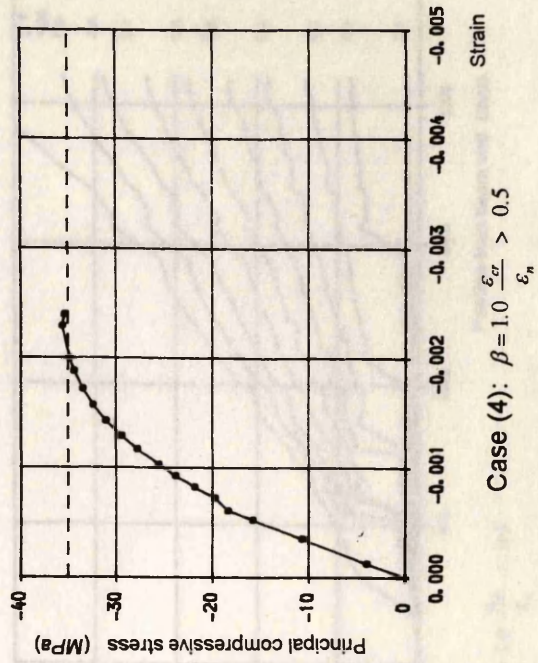
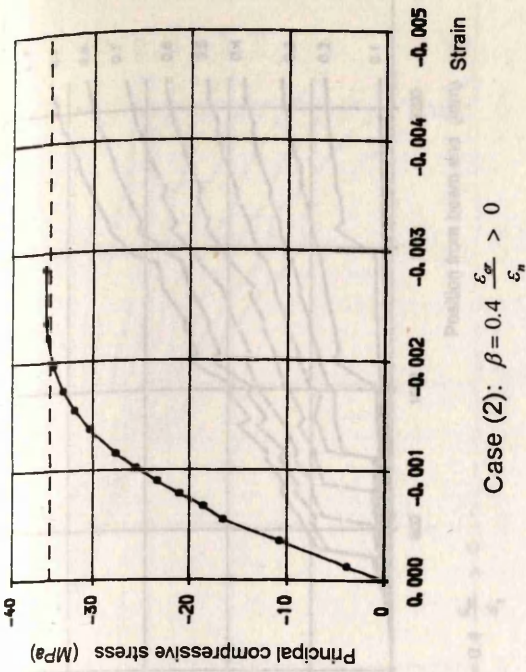
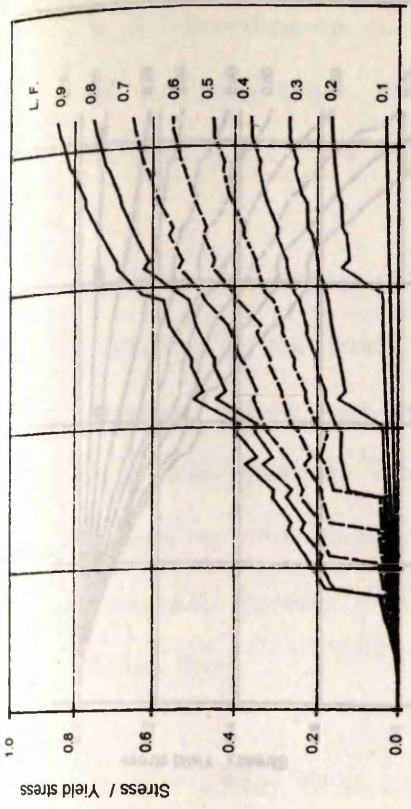
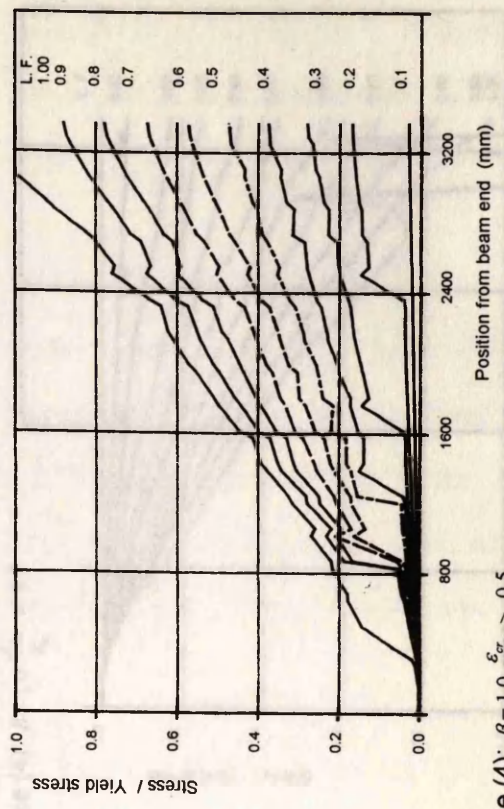


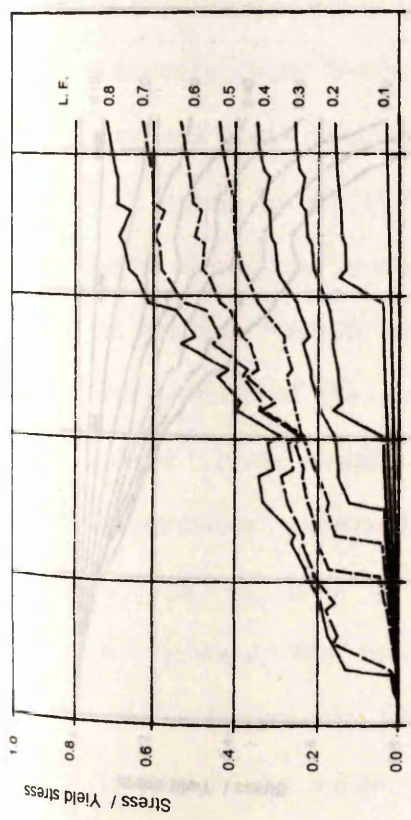
Fig. 6.35 Principal compressive stress-strain curves of concrete at Gauss point under the applied load (beam A-3).



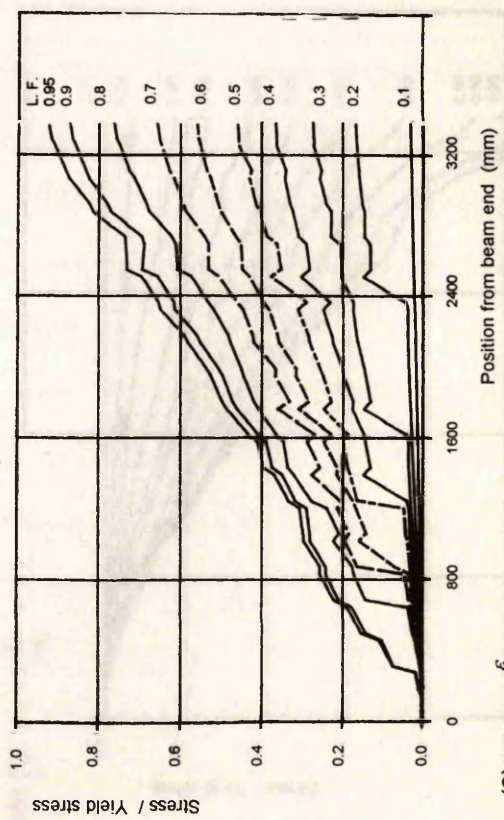
Case (2): $\beta = 0.4 \frac{\epsilon_{cr}}{\epsilon_n} > 0$



Case (4): $\beta = 1.0 \frac{\epsilon_{cr}}{\epsilon_n} > 0.5$



Case (1): $\beta = 0.1 \frac{\epsilon_{cr}}{\epsilon_n} > 0$



Case (3): $\beta = 0.5 \frac{\epsilon_{cr}}{\epsilon_n} > 0.1$

Fig. 6.36 Stresses in tension steel at different load factors for beam A-3.

Fig. 6.37 Stresses in compression steel at different load factors for beam A-3.

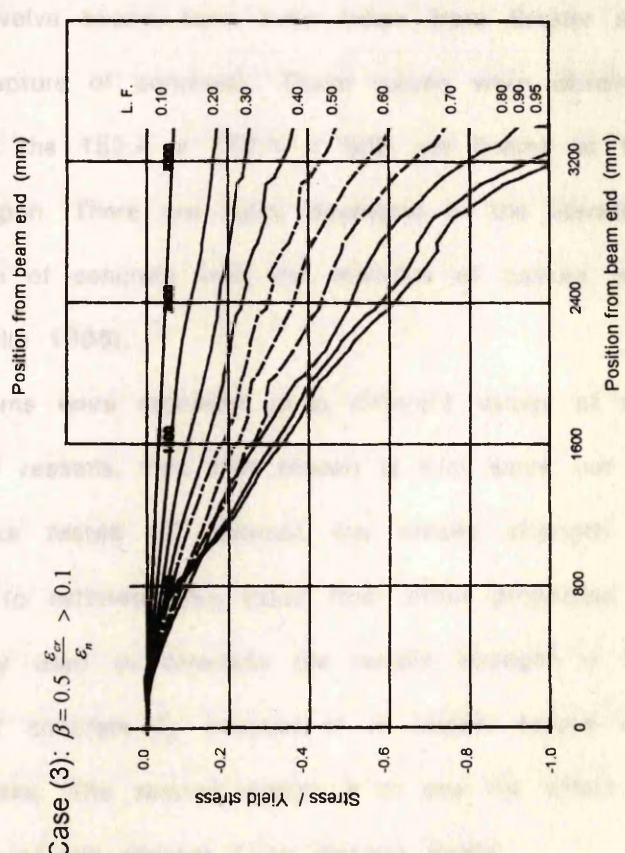
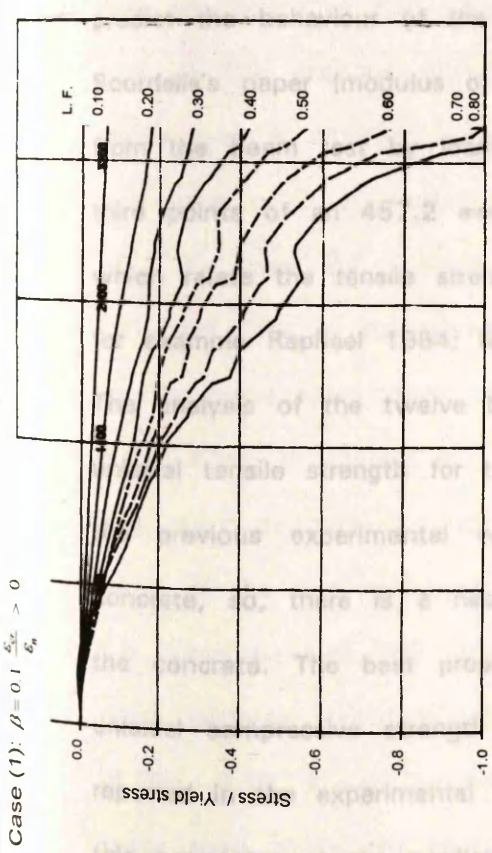
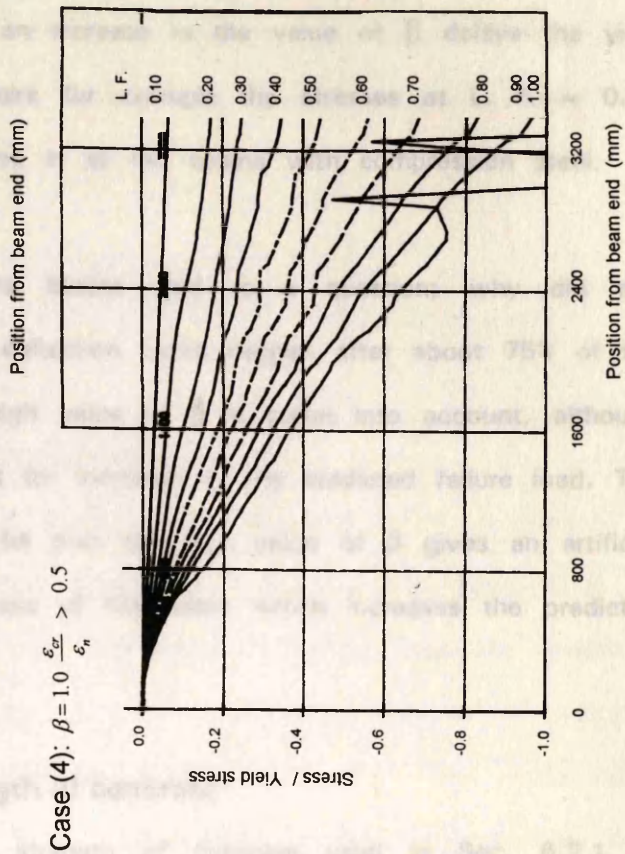
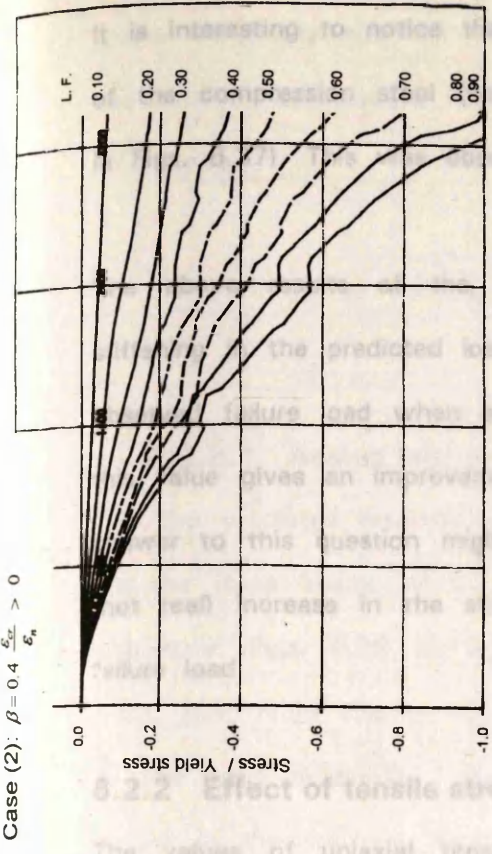


Fig. 6.37 Stresses in compression steel at different load factors for beam A-3.

It is interesting to notice that an increase in the value of β delays the yield of the compression steel (compare for example the stresses at L. F. = 0.80 in Figs. 6.37). This was observed in all the beams with compression steel.

The above results of the nine beams lead to a question; why did this stiffening in the predicted load-deflection curve happen after about 75% of the observed failure load when a high value of β is taken into account, although this value gives an improvement (or increase) in the predicted failure load. The answer to this question might be that the high value of β gives an artificial (not real) increase in the stiffness of the beam which increases the predicted failure load.

6.2.2 Effect of tensile strength of concrete

The values of uniaxial tensile strength of concrete used in Sec. 6.2.1 to predict the behaviour of the twelve beams have been taken from Bresler and Scordelis's paper (modulus of rupture of concrete). These values were obtained from the beam test by loading the 152.4 x 152.4 x 508 mm beams at the third points of an 457.2 mm span. There are many equations in the literature which relate the tensile strength of concrete with the modulus of rupture (see for example Raphael 1984; Neville 1986).

The analysis of the twelve beams were repeated using different values of the uniaxial tensile strength for two reasons. The first reason is that since not all the previous experimental works tested or reported the tensile strength of concrete, so, there is a need to estimate this value from other properties of the concrete. The best property used to calculate the tensile strength is the uniaxial compressive strength of concrete f_c' because it is usually tested and reported in the experimental works. The second reason is to see the effect of this parameter on the prediction of the present finite element model.

There are many empirical equations which estimate the tensile strength from the cylinder compressive strength f_c' . One from these equations is taken from *ACI Code*.

$$f_t' = 0.54 \sqrt{f_c'} \quad \text{MPa}$$

6.2.2.1 Beams without shear reinforcement

The predicted load-deflection curves using the value of $f_t' = 0.54 \sqrt{f_c'}$ for the three beams without shear reinforcement for the four cases of β are shown in Figs. 6.38 to 6.40, and the predicted failure loads are shown in Table 6.4. From Figures, as expected, that for all beams and for all cases of β the load-deflection curves become more flexible than the corresponding values in the previous results, This is because all values of f_t' used in these runs are less than that used in the previous runs (mean value of f_t' is about 68% of the previous one). The effect of change of f_t' on the predicted failure load is different from one beam to another and also from the case of one value of β to another. For example, the effect of using a lower value of f_t' on beam OA-1 using Case (1) of β decreases the predicted failure load by about 10% of the observed failure load, this decrease becomes about 35% for the same beam when Case (2) of β is used. While for beam OA-3, there is no effect of change of f_t' on the prediction using cases (2) & (4).

The crack patterns and deformed shapes for the beam OA-1 for three cases of β at the last converged increment are shown in Fig. 6.41. By comparing the crack patterns and deformed shapes of Fig. 6.41 with the corresponding crack patterns and deformed shapes (using value of f_t' reported in the paper) of Fig. 6.10, it can be seen that in Case (1), more cracks occurred in the shear span above the bottom third of the over-all beam depth. In Case (2), the cracks formed at the top of the beam in the whole shear span and the

Table 6.4 Effect of tensile strength of concrete f'_t in beams without shear reinforcement

Beam	f'_c MPa	f'_t MPa reported in Bresler and Scordelis's paper (a)	$f'_t = 0.54\sqrt{f'_c}$ MPa (b)	(b) / (a)	shear retention factor β	Predicted / Exp. failure load		Decrease in prediction after using f'_t in column (b)
						Using f'_t as reported in Bresler and Scordelis's paper	Using $f'_t =$ $0.54\sqrt{f'_c}$	
OA-1	22.6	4.00	2.57	0.64	Case (1)	0.95	0.85	10%
					Case (2)	1.45	1.10	35%
					Case (3)	1.55	1.45	10%
					Case (4)	1.75	1.60	15%
OA-2	23.7	4.34	2.63	0.61	Case (1)	0.95	0.70	25%
					Case (2)	1.15	0.90	25%
					Case (3)	1.20	1.15	5%
					Case (4)	1.40	1.35	5%
OA-3	37.6	4.14	3.31	0.80	Case (1)	0.85	0.75	10%
					Case (2)	1.15	1.15	0%
					Case (3)	1.20	1.15	5%
					Case (4)	1.20	1.20	0%
Mean	value				Case (1)	0.92	0.77	15%
					Case (2)	1.25	1.05	20%
					Case (3)	1.32	1.25	7%
					Case (4)	1.45	1.38	7%

Case (1): $\beta = 0.1 \frac{\epsilon_{cr}}{\epsilon_n} \geq 0.0$; Case (2): $\beta = 0.4 \frac{\epsilon_{cr}}{\epsilon_n} \geq 0.0$; Case (3): $\beta = 0.5 \frac{\epsilon_{cr}}{\epsilon_n} \geq 0.1$; Case (4): $\beta = 1.0 \frac{\epsilon_{cr}}{\epsilon_n} \geq 0.5$

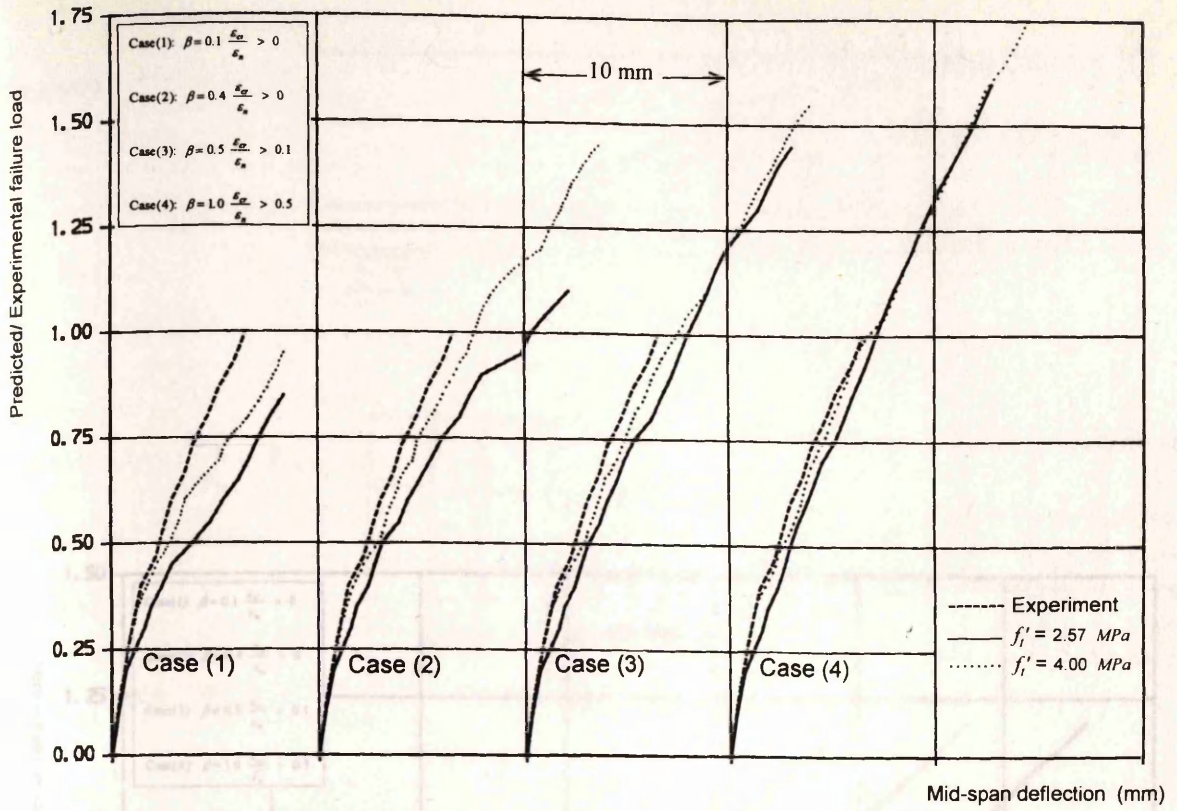


Fig. 6.38 Load-deflection curves for beam OA-1 (effect of tensile strength of concrete f_t').

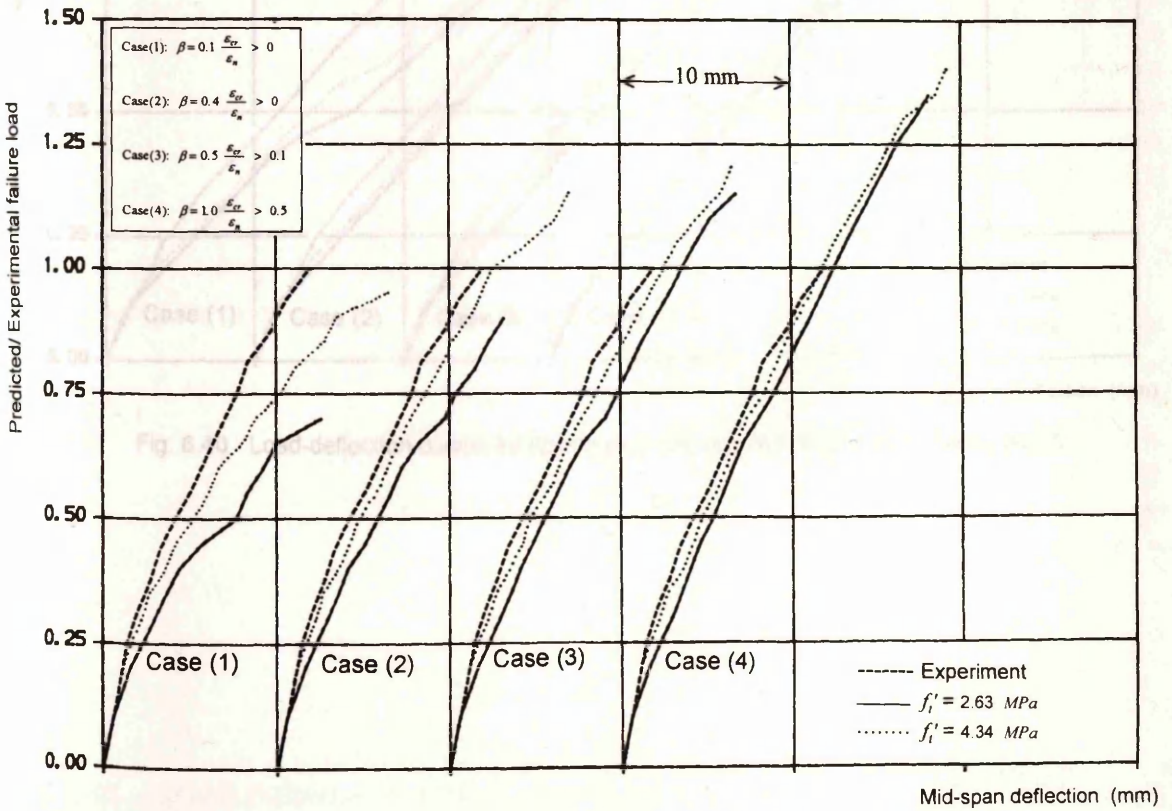


Fig. 6.39 Load-deflection curves for beam OA-2 (effect of tensile strength of concrete f_t').

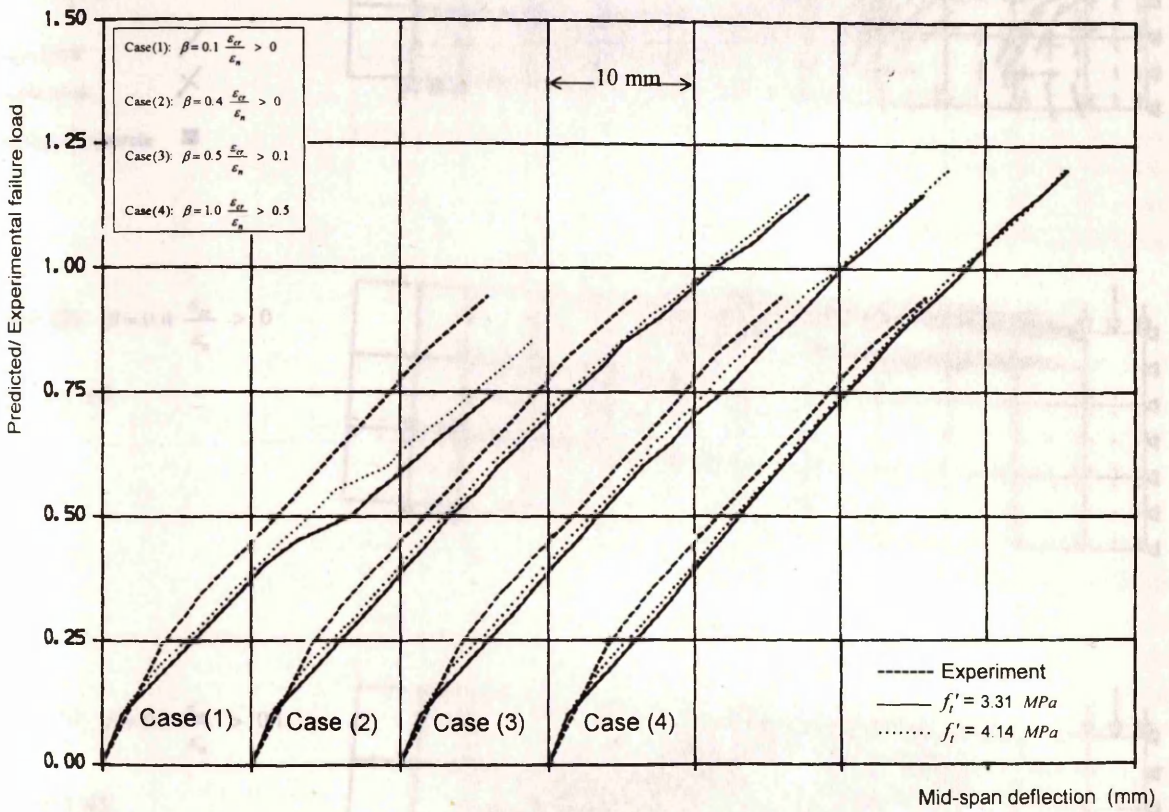
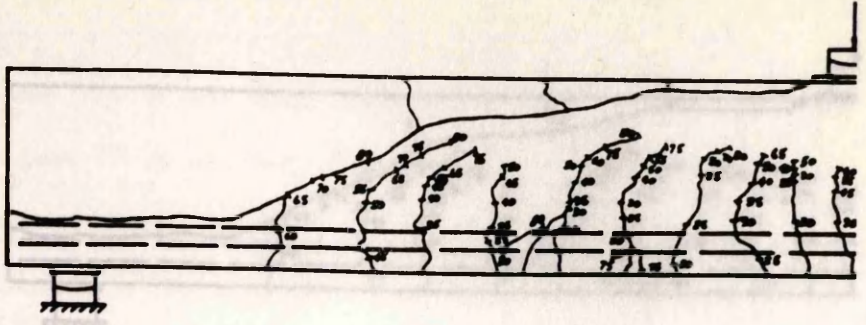


Fig. 6.40 Load-deflection curves for beam OA-3 (effect of tensile strength of concrete f_t').

Observed



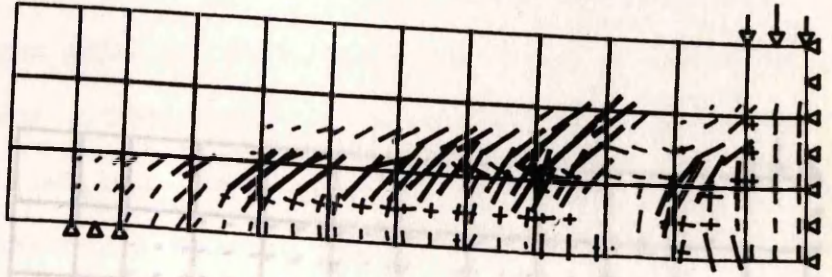
Case (1): $\beta = 0.1 \frac{\epsilon_{cr}}{\epsilon_n} > 0$

L. F. = 0.85

Single crack /

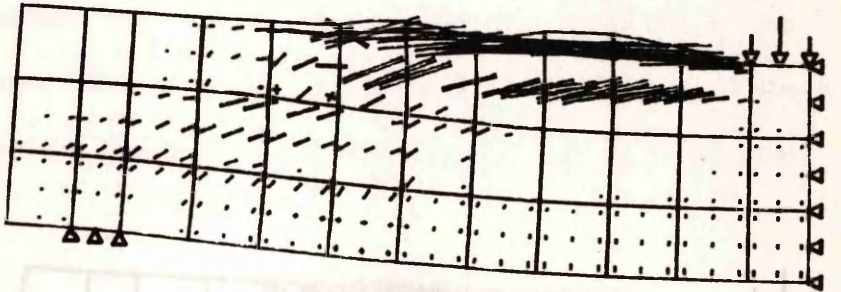
Double crack X

Crushing of concrete ■



Case (2): $\beta = 0.4 \frac{\epsilon_{cr}}{\epsilon_n} > 0$

L. F. = 1.10



Case (3): $\beta = 0.5 \frac{\epsilon_{cr}}{\epsilon_n} > 0.1$

L. F. = 1.45

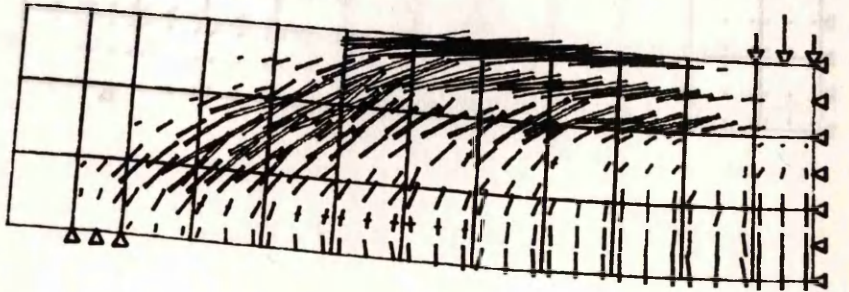
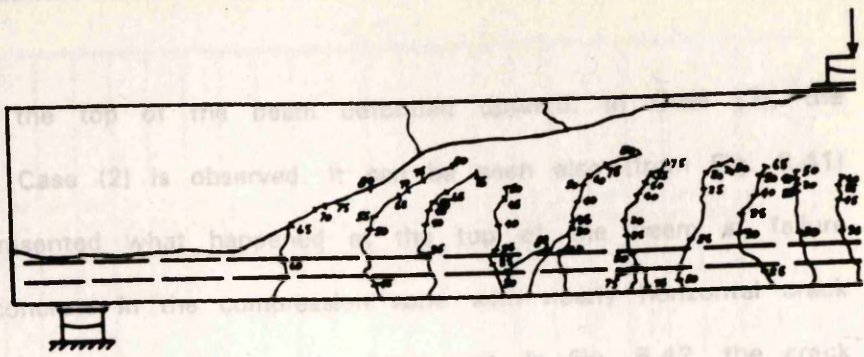
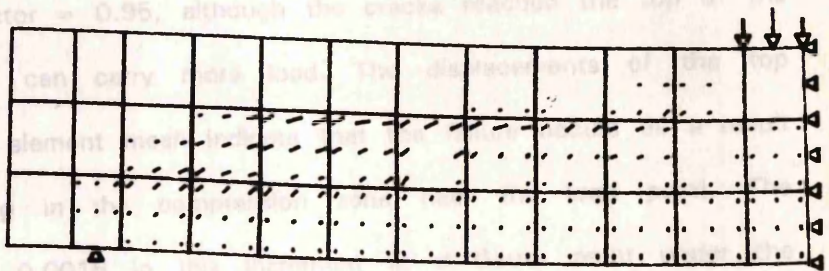


Fig. 6.41 Crack patterns and deformed shapes for beam OA-1 after reduction in f'_c (displacements magnified x 10).

Observed



L. F. = 0.90

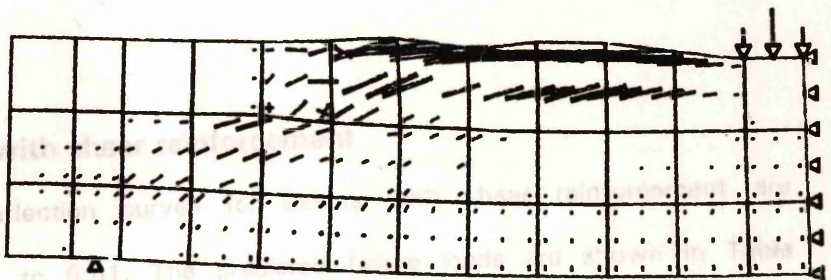


Single crack

Double crack

Crushing of concrete

L. F. = 0.95



6.2.2.2 Beams with...

The predicted load-deflection...

shown in figures 6.43 to 6.5.

In general, the predicted load-deflection curves using the calculated values...

of J_c are more flexible than that presented using the value of J_c reported in...

Trasler and Scordelis's paper. Also, the effect of variation of J_c on the...

predicted failure load is insignificant for values of J_c ranging from 0.8 to 1.2.

In the prediction for any beam at any stage of loading, J_c should not exceed more than...

10% of the observed failure load. Although the mean value of the reduction in...

J_c was about 1-4% of the observed failure loads.

$$\text{Case (2): } \beta = 0.4 \frac{\epsilon_{cr}}{\epsilon_n} > 0$$

Fig. 6.42 Crack patterns and deformed shapes using Case (2) of β (beam OA-1) (displacements magnified x 10).

mesh elements at the top of the beam deformed upward. In Case (3), the same behaviour as Case (2) is observed. It can be seen also (from Fig. 6.41) that case (2) represented what happened at the top of the beam at failure (Buckling of the concrete in the compression zone with nearly horizontal crack above the longitudinal steel reached to the beam end. In Fig. 6.42, the crack patterns and deformed shapes are shown for Case (2) at two load factors (0.90 and 0.95). At load factor = 0.90, no cracks has formed at the top of the beam. At load factor = 0.95, although the cracks reached the top of the beam, still the beam can carry more load. The displacements of the top elements of the finite element mesh indicate that the failure occurs as a result of longitudinal splitting in the compression zone near the load point. The compressive strain of 0.0016 in this increment at a Gauss point under the load point did not exceed the assumed maximum strain of 0.0035. If one remembers that the main reason of failure of this beam is the crushing of the compression zone, this may explain why the beam did not fail by these large shear cracks.

6.2.2.2 Beams with shear reinforcement

The predicted load-deflection curves for beams with shear reinforcement are shown in figures 6.43 to 6.51. The predicted failure loads are shown in Table 6.5. In general, the predicted load-deflection curves using the calculated values of f_t' are more flexible than that predicted using the values of f_t' reported in Bresler and Scordelis's paper. Also, the effect of change of f_t' on the predicted failure load is insignificant for these beams. The maximum difference in the prediction for any beam at any case of β does not exceed more than 10% of the observed failure load. Although the mean value of the reduction in f_t' was about 38%, the mean value of the reduction in the predicted failure loads is about 1-4% of the observed failure loads.

Table 6.5 Effect of tensile strength of concrete f_t' in beams with shear reinforcement.

Beam	f_c' MPa	f_t' MPa reported in Bresler and Scordelis's paper	$f_t' = 0.54\sqrt{f_c'}$ MPa (b)	(b) / (a)	shear retention factor β	Predicted / Exp. failure load		Decrease in prediction after using f_t' in column (b)
						Using f_t' as reported in Bresler and Scordelis's paper	Using $f_t' =$ $0.54\sqrt{f_c'}$	
A-1	24.08	3.86	2.65	0.69	Case (1)	0.85	0.75	10%
					Case (2)	1.10	1.05	5%
					Case (3)	1.20	1.15	5%
					Case (4)	1.35	1.25	10%
A-2	24.29	3.73	2.66	0.71	Case (1)	0.70	0.65	5%
					Case (2)	0.90	0.85	5%
					Case (3)	1.00	0.95	5%
					Case (4)	1.05	1.05	0%
A-3	35.05	4.34	3.20	0.74	Case (1)	0.80	0.70	10%
					Case (2)	0.90	0.90	0%
					Case (3)	0.95	0.95	0%
					Case (4)	1.00	0.95	5%
B-1	24.77	3.86	2.65	0.67	Case (1)	0.75	0.70	5%
					Case (2)	0.95	0.95	0%
					Case (3)	1.05	1.00	0%
					Case (4)	1.15	1.05	10%
B-2	23.18	3.73	2.66	0.69	Case (1)	0.65	0.65	0%
					Case (2)	0.85	0.85	0%
					Case (3)	0.90	0.90	0%
					Case (4)	0.95	0.95	0%
B-3	38.78	4.34	3.20	0.86	Case (1)	0.85	0.85	0%
					Case (2)	1.00	0.95	5%
					Case (3)	1.00	1.05	5%
								(increase)

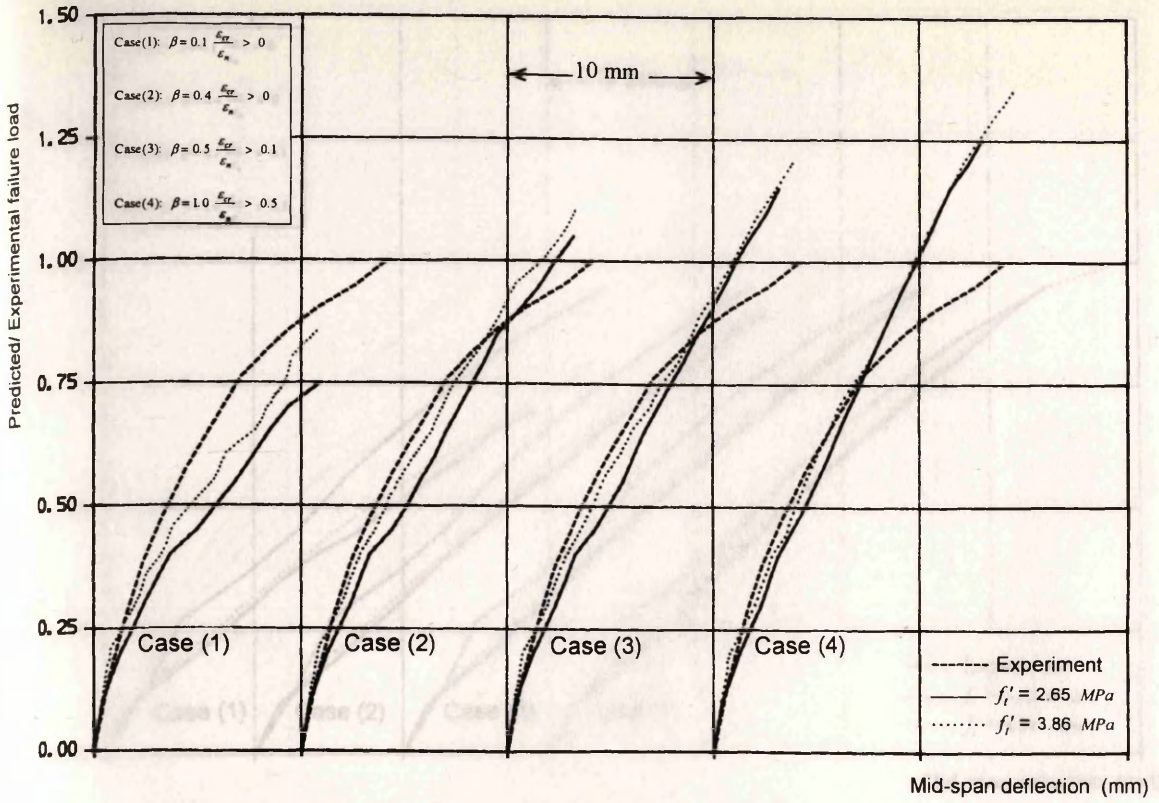


Fig. 6.43 Load-deflection curves for beam A-1 (effect of tensile strength of concrete f'_t).

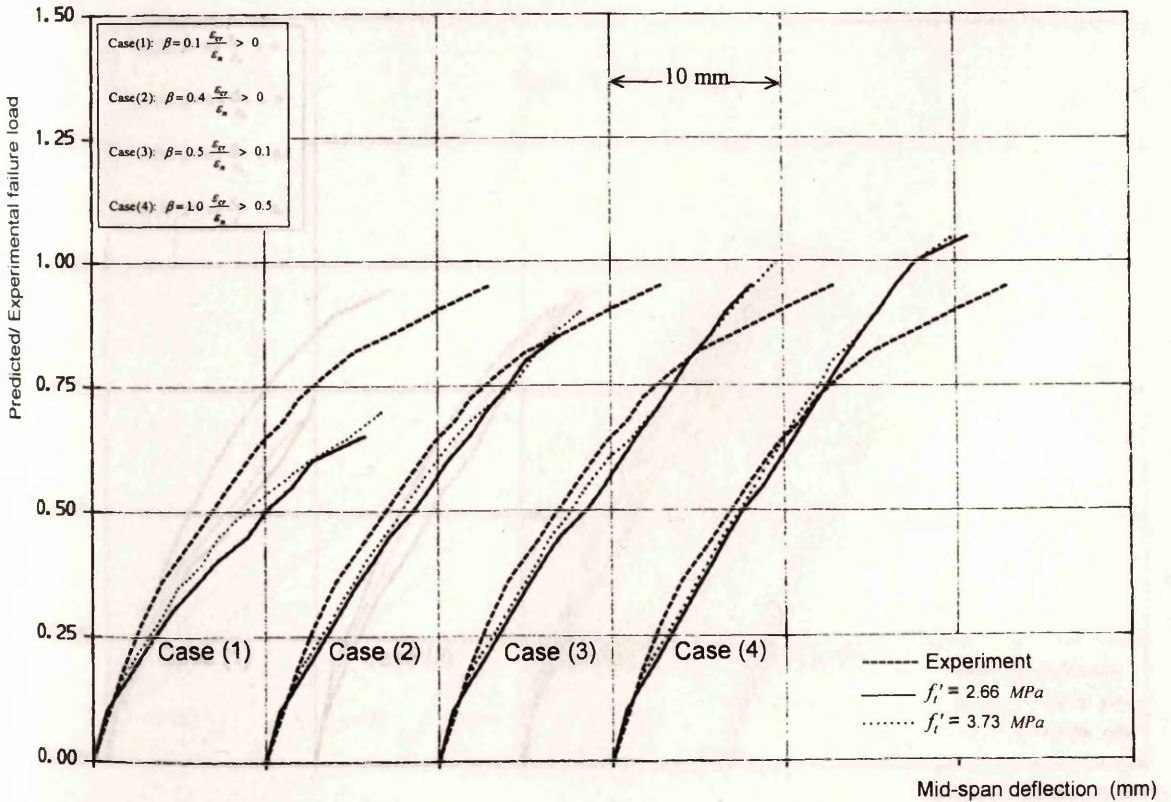


Fig. 6.44 Load-deflection curves for beam A-2 (effect of tensile strength of concrete f'_t).

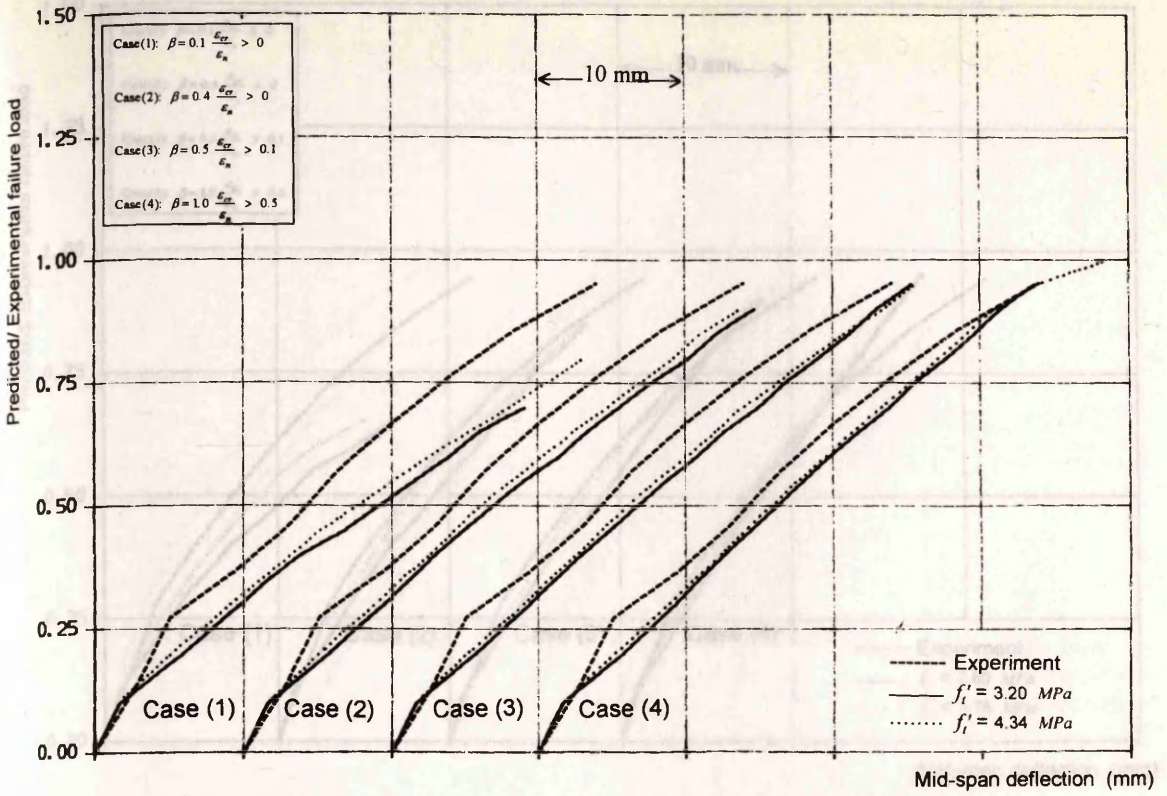


Fig. 6.45 Load-deflection curves for beam A-3 (effect of tensile strength of concrete f_t').

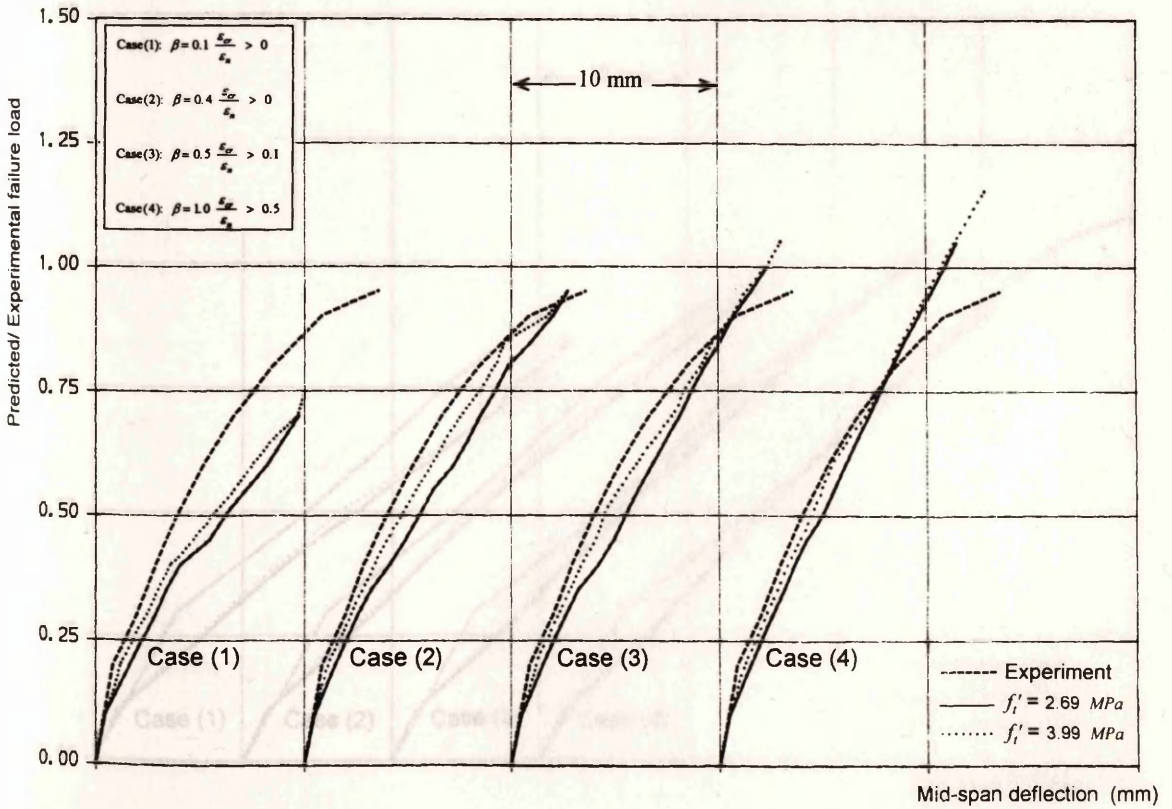


Fig. 6.46 Load-deflection curves for beam B-1 (effect of tensile strength of concrete f_t').

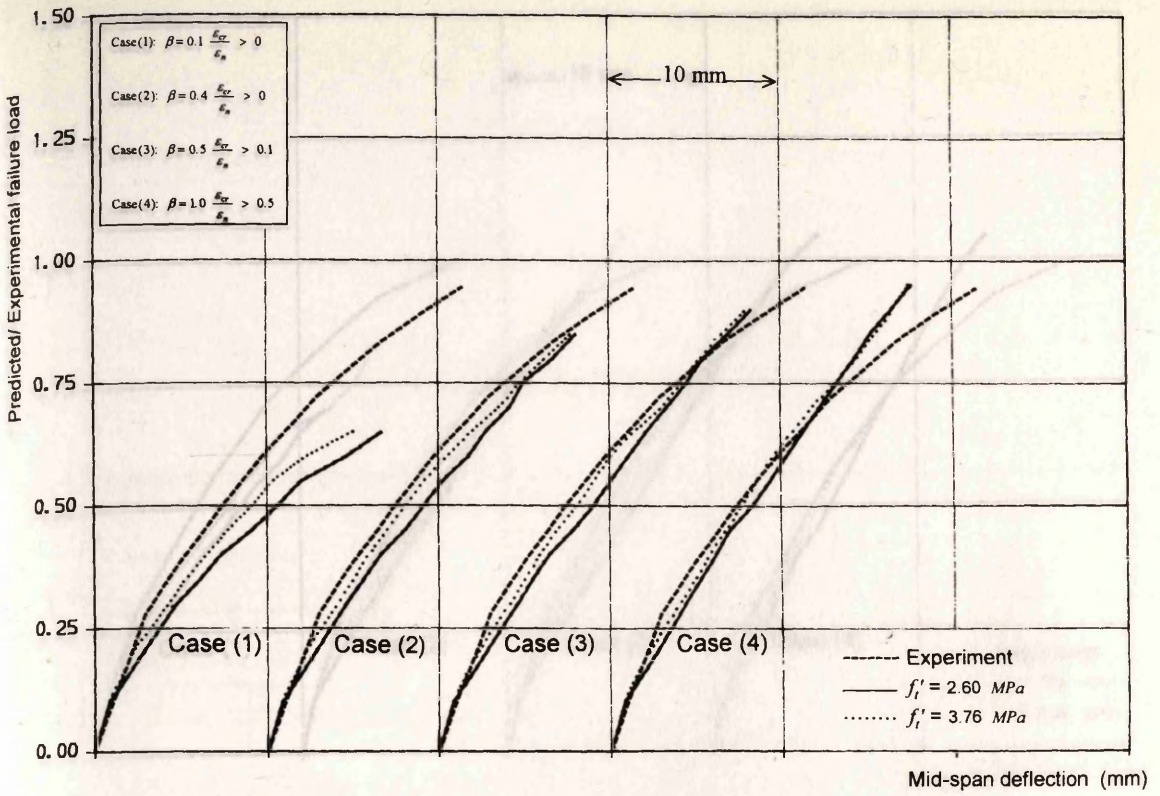


Fig. 6.47 Load-deflection curves for beam B-2 (effect of tensile strength of concrete f'_t).

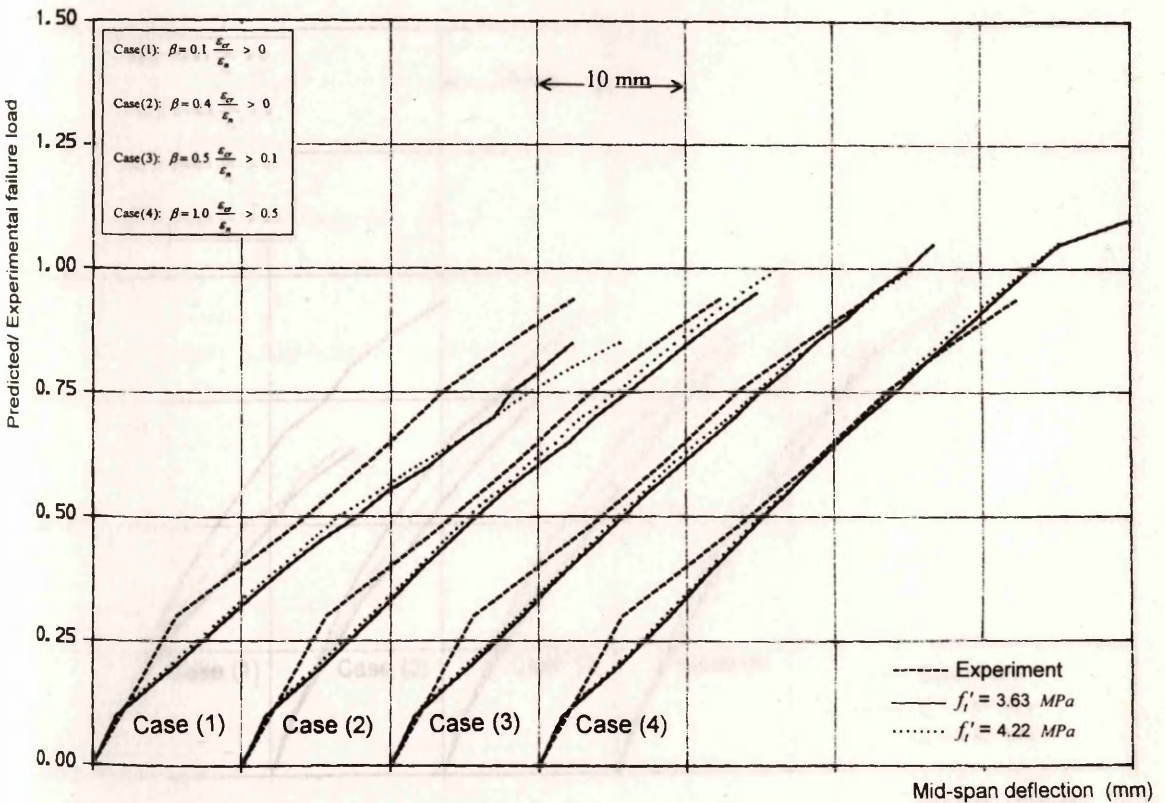


Fig. 6.48 Load-deflection curves for beam B-3 (effect of tensile strength of concrete f'_t).

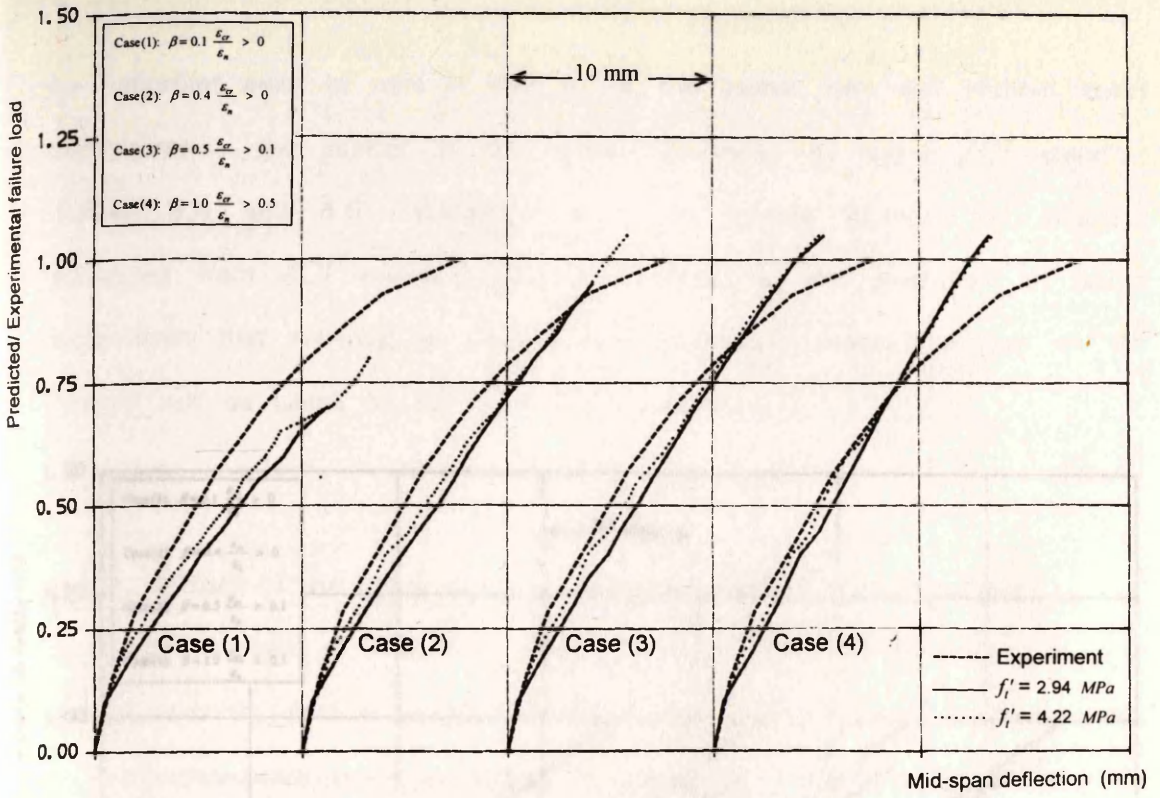


Fig. 6.49 Load-deflection curves for beam C-1 (effect of tensile strength of concrete f_t').

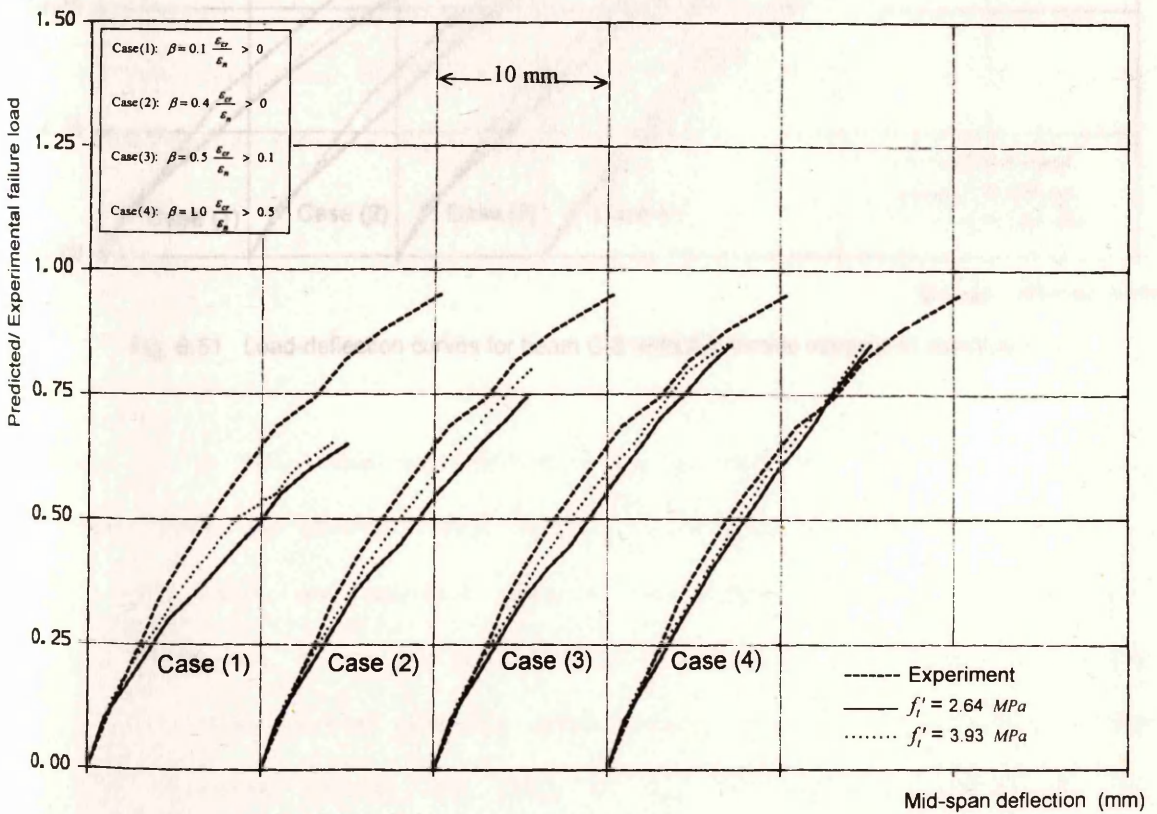


Fig. 6.50 Load-deflection curves for beam C-2 (effect of tensile strength of concrete f_t').

An important point to note is that for all the beams with and without shear reinforcement, the scatter in the results decreases by using *ACI* equation (Tables 6.4 and 6.5). Therefore, since the tensile strength of concrete calculated from *ACI* equation gives less scatter in the prediction of failure loads than that reported in Brosler and Kormanik's paper, the rest of the analysis will be based on this equation in subsequent chapters.

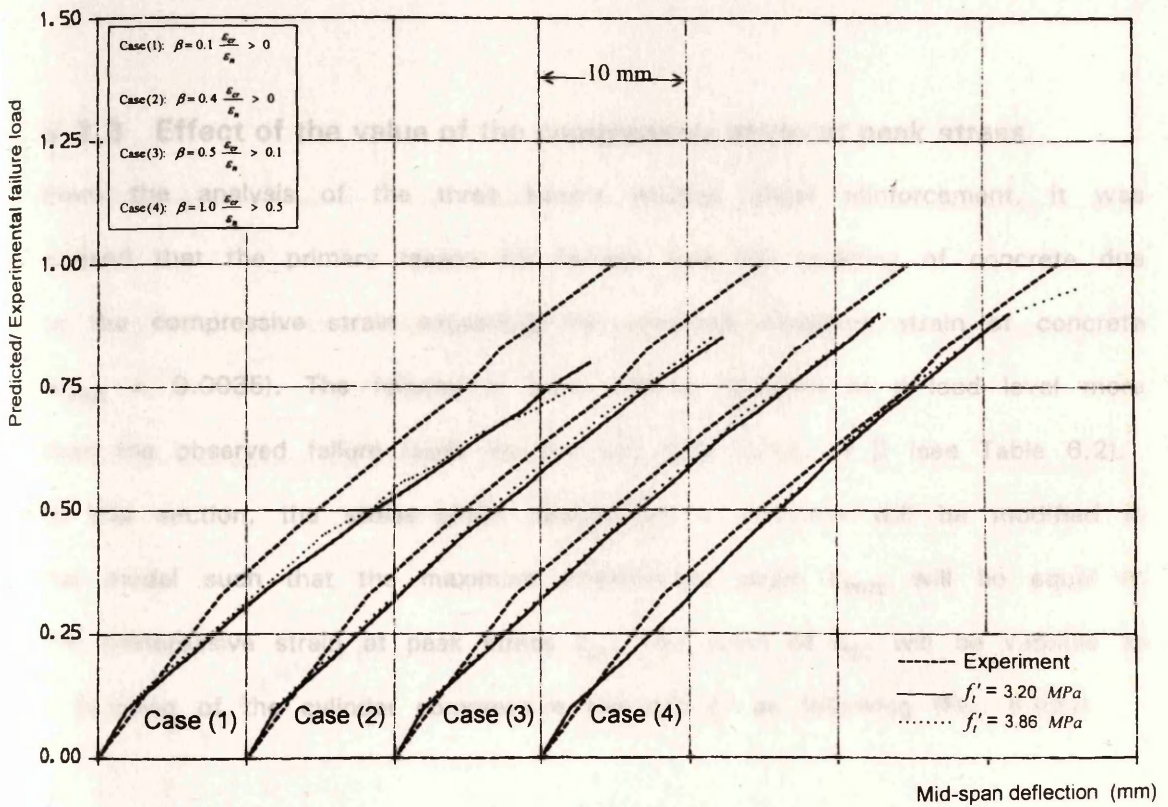


Fig. 6.51 Load-deflection curves for beam C-3 (effect of tensile strength of concrete f_t').

An important point to note is that for all the beams with and without shear reinforcement, the scatter in the results decreases by using *ACI* equation (Tables 6.4 and 6.5). Therefore, since the tensile strength of concrete calculated from *ACI* equation gives less scatter in the prediction of failure loads than that reported in Bresler and Scordelis's paper, the rest of the analysis will be based on this equation in calculating f_t' .

6.2.3 Effect of the value of the compressive strain at peak stress

From the analysis of the three beams without shear reinforcement, it was noticed that the primary reason for failures was the crushing of concrete due to the compressive strain exceeding the assumed maximum strain of concrete ($\epsilon_{max} = 0.0035$). The failures of these beams occurred at a load level more than the observed failure loads for the last three cases of β (see Table 6.2). In this section, the stress-strain relationship of concrete will be modified in the model such that the maximum compressive strain ϵ_{max} will be equal to the compressive strain at peak stress ϵ_{cc} . The value of ϵ_{cc} will be variable as a function of the cylinder compressive strength f_c' as following (Fig. 6.52a).

$$\epsilon_{max} = \epsilon_{cc} = \sqrt{f_c'} / 2500$$

where f_c' in *MPa*. The load-deflection curves after this modification for the twelve beams are shown in Figs. 6.53 to 6.64 and the predicted failure loads, the mean value, and standard deviation are shown in Tables 6.6 and 6.7. From the figures, it can be seen that the predicted load-deflection curves are nearly the same as that predicted using constant ϵ_{cc} (0.0025) for most of the beams. However, change the value of ϵ_{cc} has significant effect on the predicted failure loads. Table 6.6 shows the change in the predicted failure

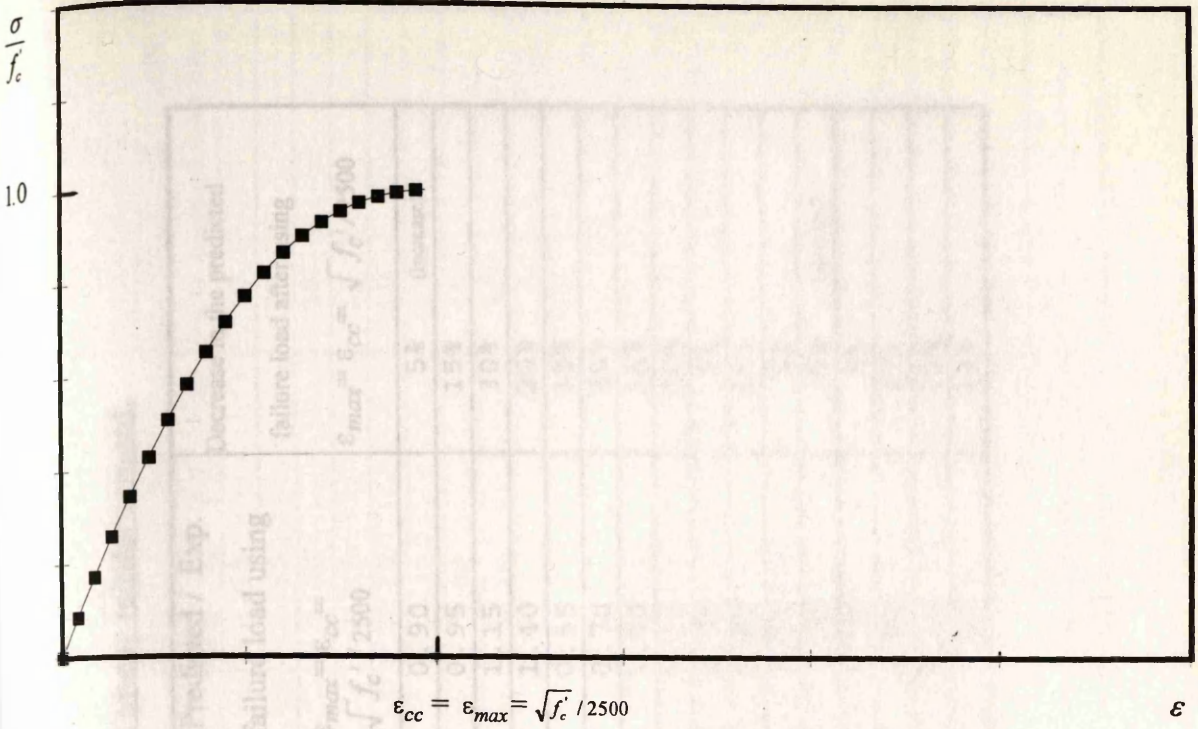


Fig. 6.52a Stress-strain curve of concrete in compression without softening.

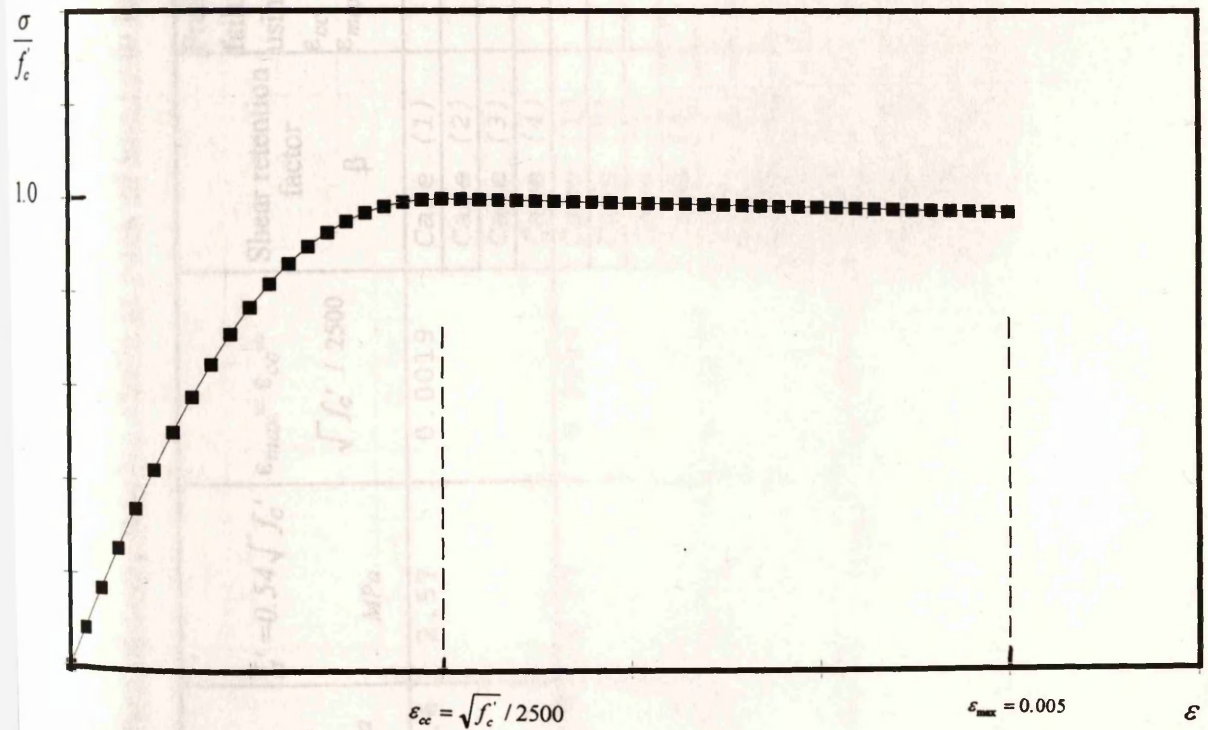


Fig. 6.52b Stress-strain curve of concrete in compression with softening.

Table 6.6 Effect of compressive strain at peak of stress in beam without shear reinforcement.

Beam	f'_c MPa	$f'_i = 0.54\sqrt{f'_c}$ MPa	$\epsilon_{max} = \epsilon_{cc} = \sqrt{f'_c} / 2500$	Shear retention factor β	Predicted / Exp. failure load using $\epsilon_{cc} = 0.0025$ $\epsilon_{max} = 0.0035$	Predicted / Exp. failure load using $\epsilon_{max} = \epsilon_{cc} = \sqrt{f'_c} / 2500$	Decrease in the predicted failure load after using $\epsilon_{max} = \epsilon_{cc} = \sqrt{f'_c} / 2500$
OA-1	22.6	2.57	0.0019	Case (1)	0.85	0.90	5% (increase)
				Case (2)	1.10	0.95	15%
				Case (3)	1.45	1.15	30%
				Case (4)	1.60	1.40	20%
OA-2	23.7	2.63	0.0020	Case (1)	0.70	0.55	15%
				Case (2)	0.90	0.70	20%
				Case (3)	1.15	1.00	15%
				Case (4)	1.35	1.15	20%
OA-3	37.6	3.31	0.0025	Case (1)	0.75	0.70	5%
				Case (2)	1.15	0.85	30%
				Case (3)	1.15	1.15	0%
				Case (4)	1.20	1.25	5% (increase)
Mean value							
				Case (1)	0.77	0.72	5%
				Case (2)	1.05	0.83	22%
				Case (3)	1.25	1.10	15%
				Case (4)	1.38	1.27	11%

Table 6.7 Effect of compressive strain at peak of stress in beams with shear reinforcement.

Beam	f_c' MPa	$f_t' = 0.54\sqrt{f_c'}$ MPa	$\epsilon_{cc} = \frac{\epsilon_{cc}'}{2500}$	Shear retention factor β	Predicted / Exp. failure load using $\epsilon_{cc} = 0.0025$ $\epsilon_{cc} = 0.0035$	Predicted / Exp. failure load using $\epsilon_{cc} = 0.0025$ $\epsilon_{cc} = 0.0035$	Decrease in the predicted failure load after using $\epsilon_{cc} = \epsilon_{cc}' = \sqrt{f_c' / 2500}$ % of the experimental failure load)
A-1	24.08	2.65	0.0020	Case (1)	0.75	0.75	0
				Case (2)	1.05	0.85	20
				Case (3)	1.15	0.95	20
				Case (4)	1.25	1.15	10
A-2	24.29	2.66	0.0020	Case (1)	0.65	0.55	10
				Case (2)	0.85	0.70	15
				Case (3)	0.95	0.80	15
				Case (4)	1.05	0.90	15
A-3	35.05	3.20	0.0024	Case (1)	0.70	0.65	5
				Case (2)	0.90	0.80	10
				Case (3)	0.95	0.85	10
				Case (4)	0.95	0.95	0
B-1	24.77	2.69	0.0020	Case (1)	0.70	0.55	15
				Case (2)	0.95	0.70	15
				Case (3)	1.00	0.85	15
				Case (4)	1.05	0.95	10
B-2	23.18	2.60	0.0019	Case (1)	0.65	0.55	10
				Case (2)	0.85	0.60	25
				Case (3)	0.90	0.70	20
				Case (4)	0.95	0.80	15
B-3	38.78	3.63	0.0025	Case (1)	0.85	0.70	15
				Case (2)	0.95	0.85	10
				Case (3)	1.05	0.95	10
				Case (4)	1.10	1.05	5

Table 6.7 Effect of compressive strain at peak of stress in beams with shear reinforcement (continued).

Beam	f_c' MPa	$f_t' = 0.54\sqrt{f_c}$ MPa	$\epsilon_{max} = \epsilon_{cc} = \sqrt{f_c' / 2500}$	Shear retention factor β	Predicted / Exp. failure load using $\epsilon_{cc} = 0.0025$ $\epsilon_{max} = 0.0035$	Predicted / Exp. failure load using $\epsilon_{max} = \epsilon_{cc} = \sqrt{f_c' / 2500}$	Decrease in the predicted failure load after using $\epsilon_{max} = \epsilon_{cc} = \sqrt{f_c' / 2500}$ (% of the experimental failure load)
C-1	29.60	2.94	0.0022	Case (1)	0.70	0.65	5
				Case (2)	0.95	0.75	20
				Case (3)	1.05	0.85	20
				Case (4)	1.05	1.00	5
C-2	23.81	2.64	0.0020	Case (1)	0.65	0.55	10
				Case (2)	0.75	0.65	10
				Case (3)	0.85	0.65	20
				Case (4)	0.85	0.80	5
C-3	35.05	3.20	0.0024	Case (1)	0.80	0.65	15
				Case (2)	0.85	0.75	10
				Case (3)	0.90	0.80	10
				Case (4)	0.90	0.90	0
		<i>Mean value</i>					
				Case (1)	0.72	0.62	10
				Case (2)	0.90	0.74	16
				Case (3)	0.98	0.82	16
				Case (4)	1.02	0.94	8
		<i>Standard deviation (%)</i>					
				Case (1)	7.1	7.6	
				Case (2)	8.7	8.6	
				Case (3)	9.4	10.0	
				Case (4)	12.0	11.3	

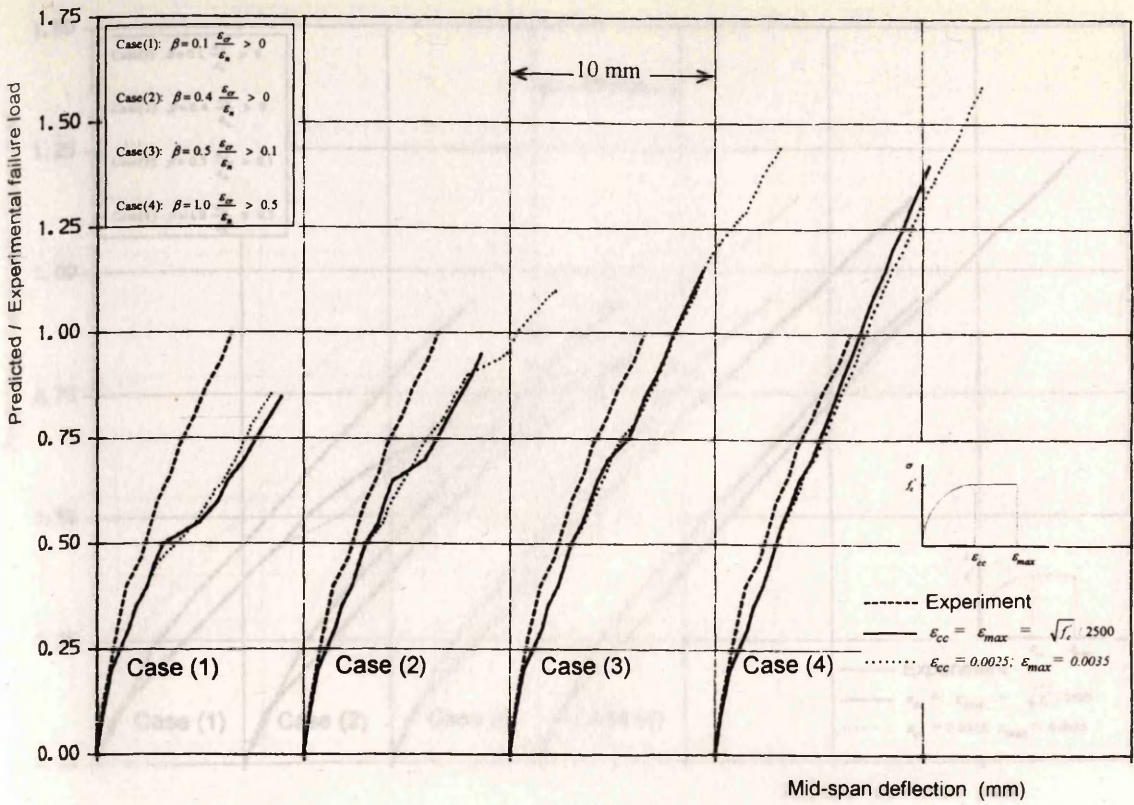


Fig. 6.53 Load-deflection curves for beam OA-1 (effect of ϵ_{cc} , ϵ_{max}).

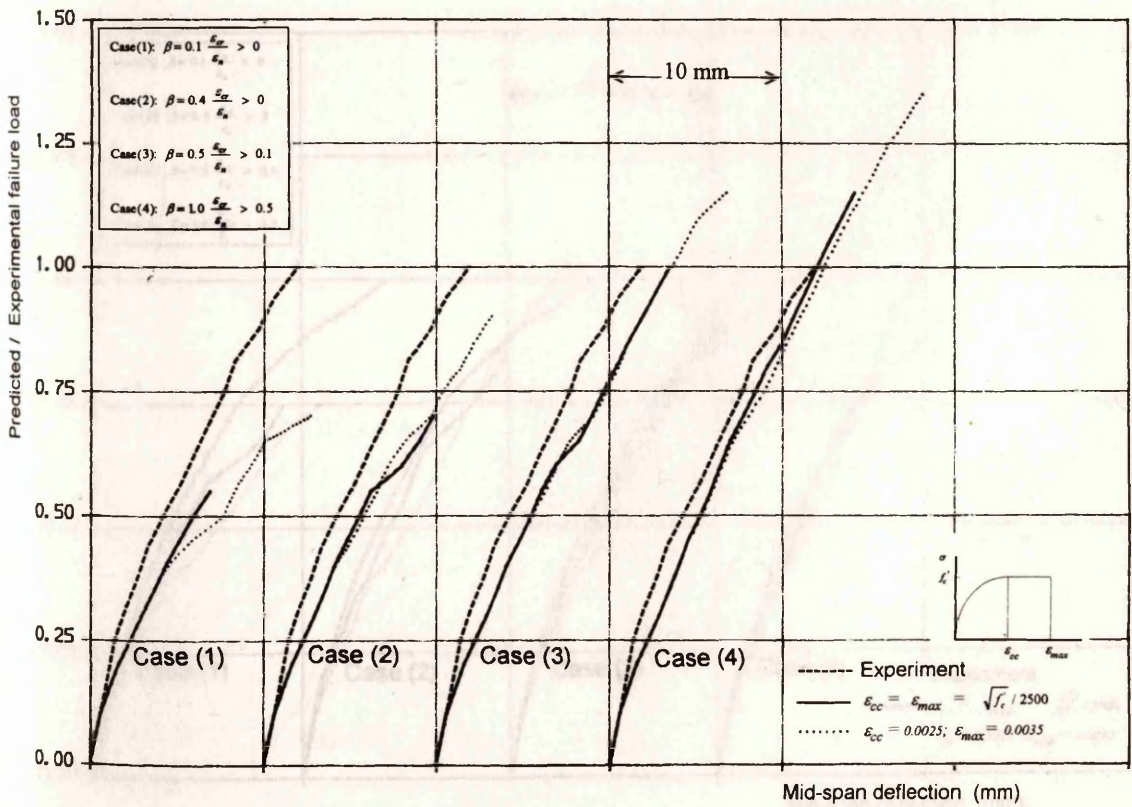


Fig. 6.54 Load-deflection curves for beam OA-2 (effect of ϵ_{cc} , ϵ_{max}).

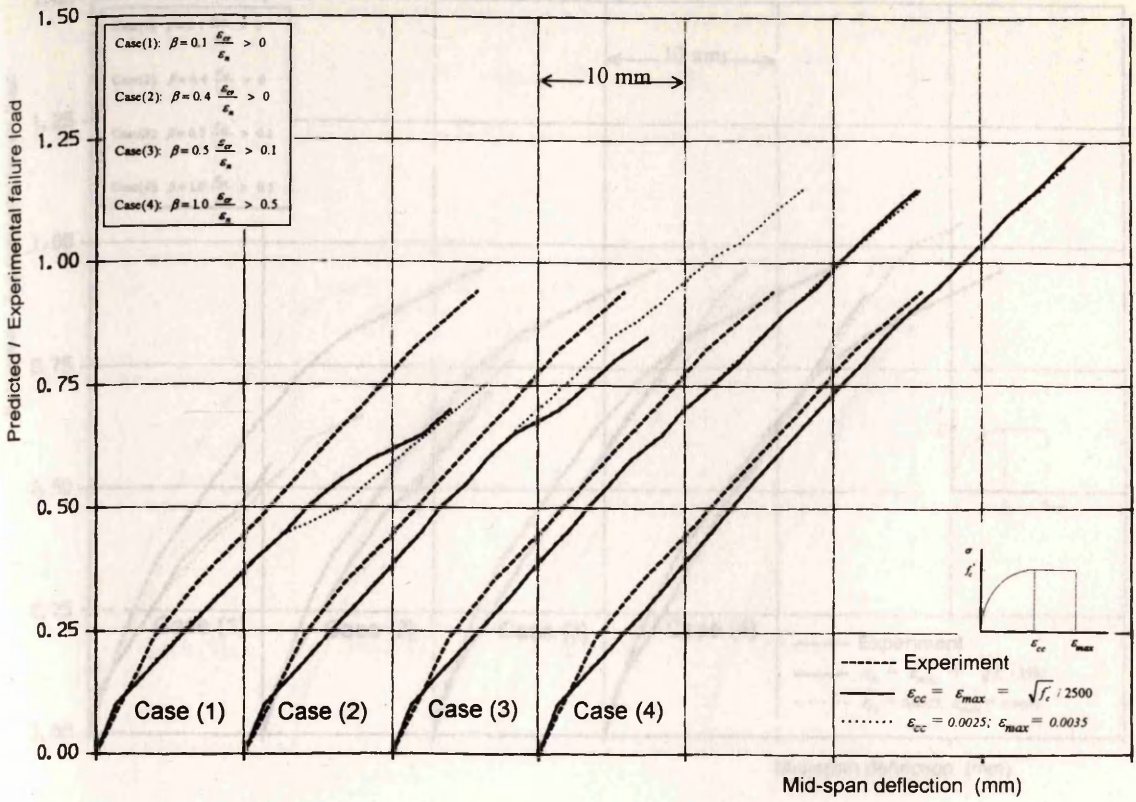


Fig. 6.55 Load-deflection curves for beam OA-3 (effect of ϵ_{cc} , ϵ_{max}).

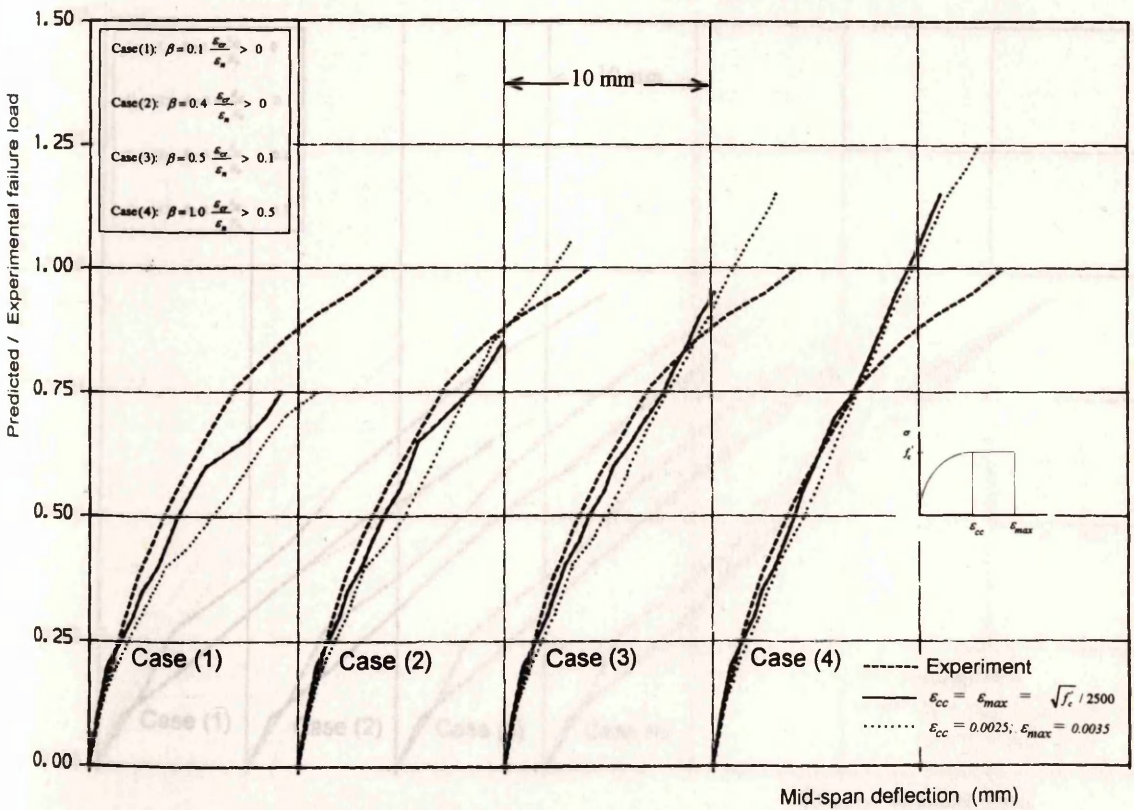


Fig. 6.56 Load-deflection curves for beam A-1 (effect of ϵ_{cc} , ϵ_{max}).

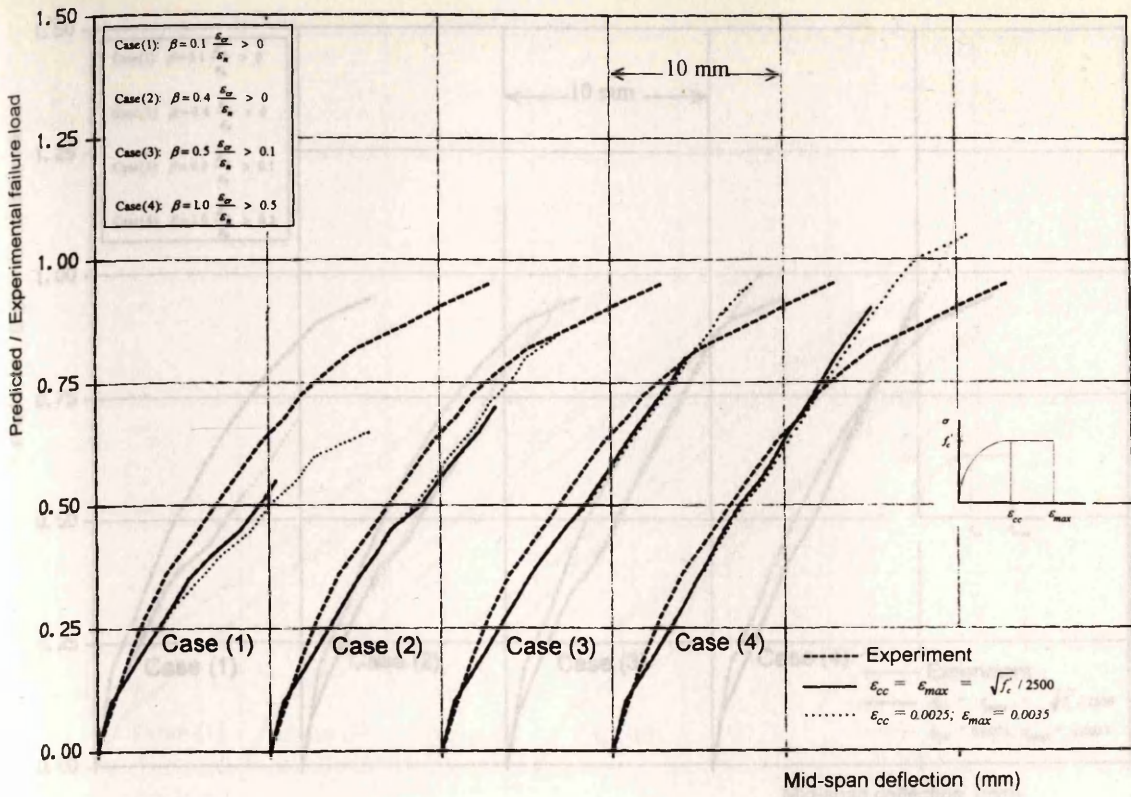


Fig. 6.57 Load-deflection curves for beam A-2 (effect of ϵ_{cc} , ϵ_{max}).

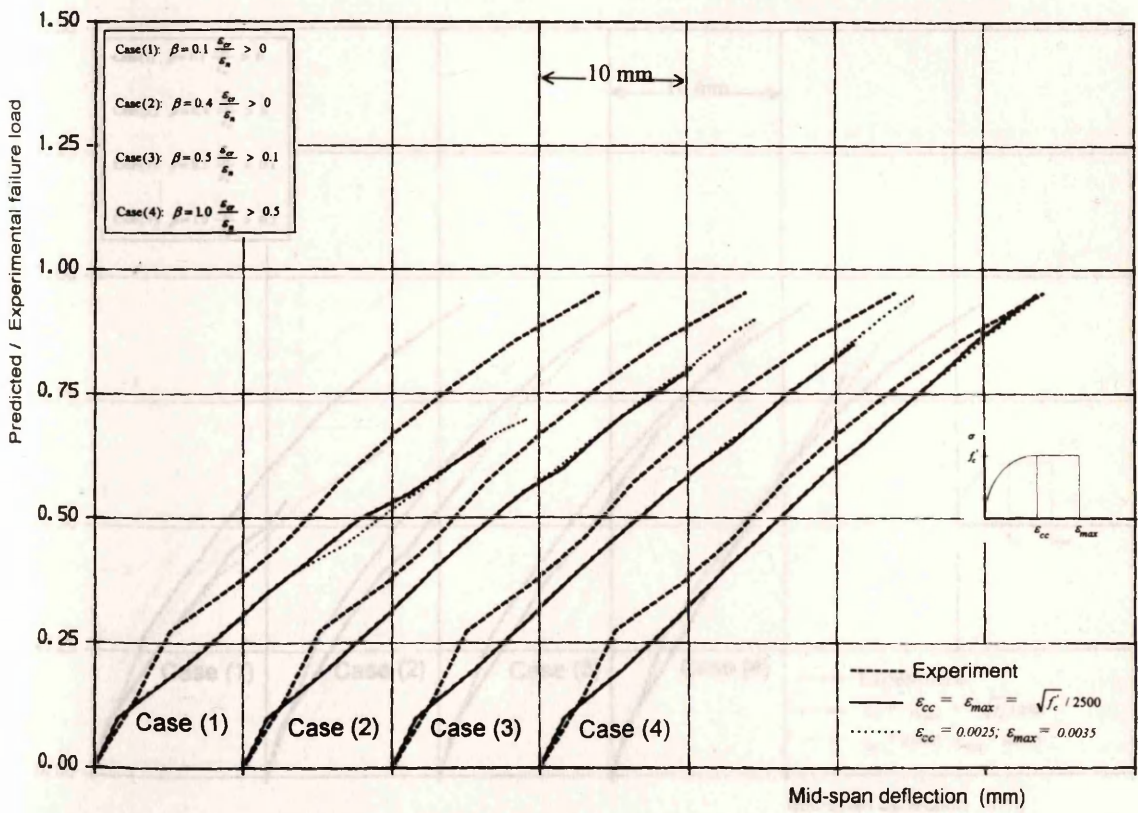


Fig. 6.58 Load-deflection curves for beam A-3 (effect of ϵ_{cc} , ϵ_{max}).

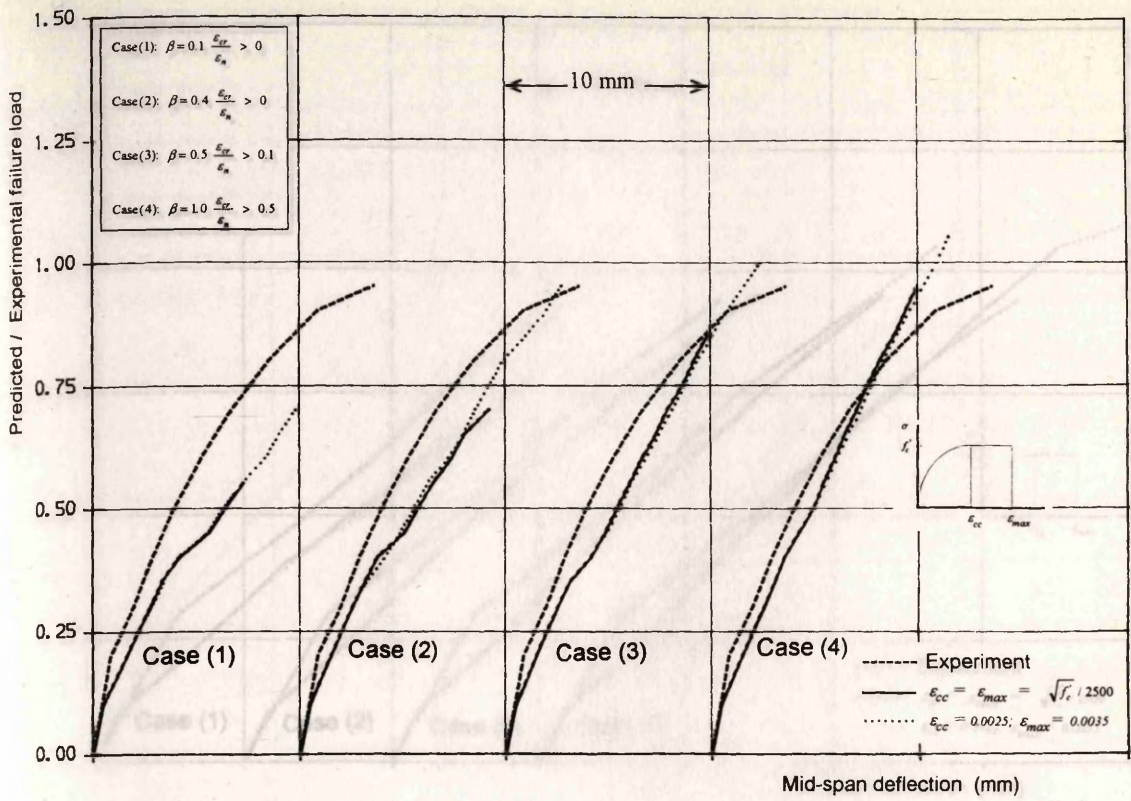


Fig. 6.59 Load-deflection curves for beam B-1 (effect of ϵ_{cc} , ϵ_{max}).

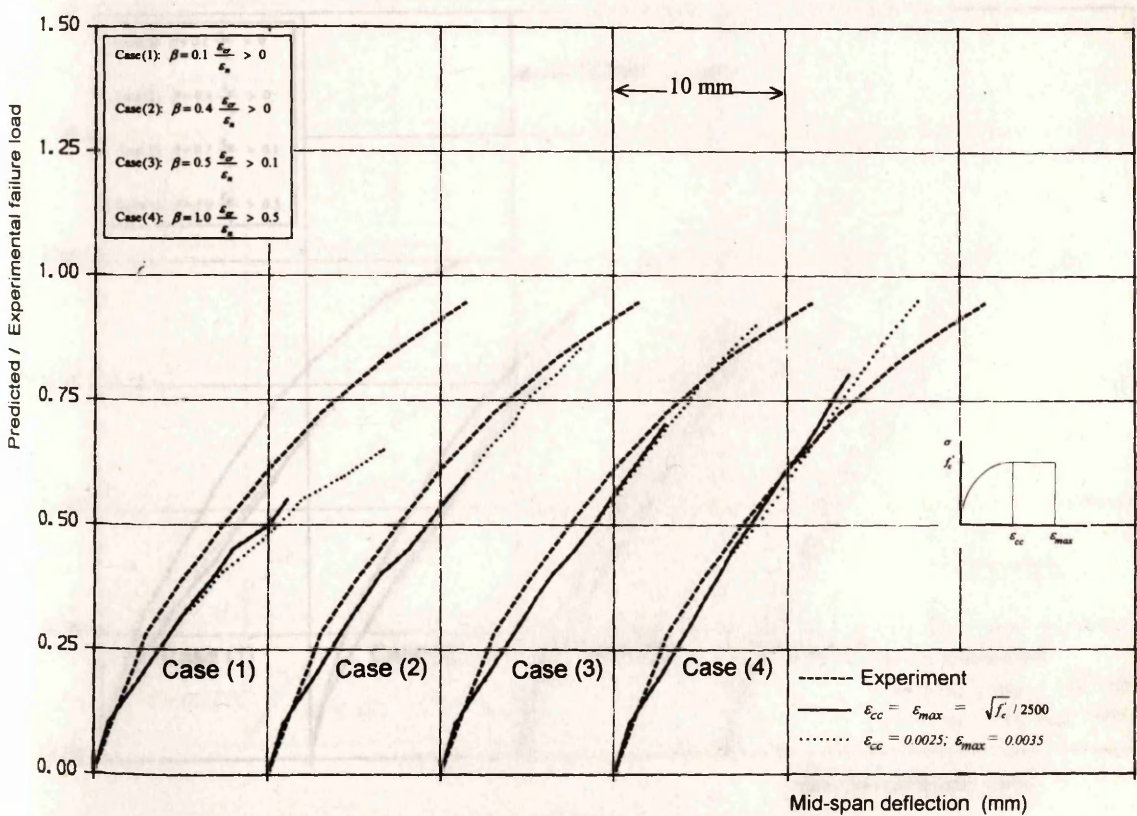


Fig. 6.60 Load-deflection curves for beam B-2 (effect of ϵ_{cc} , ϵ_{max}).

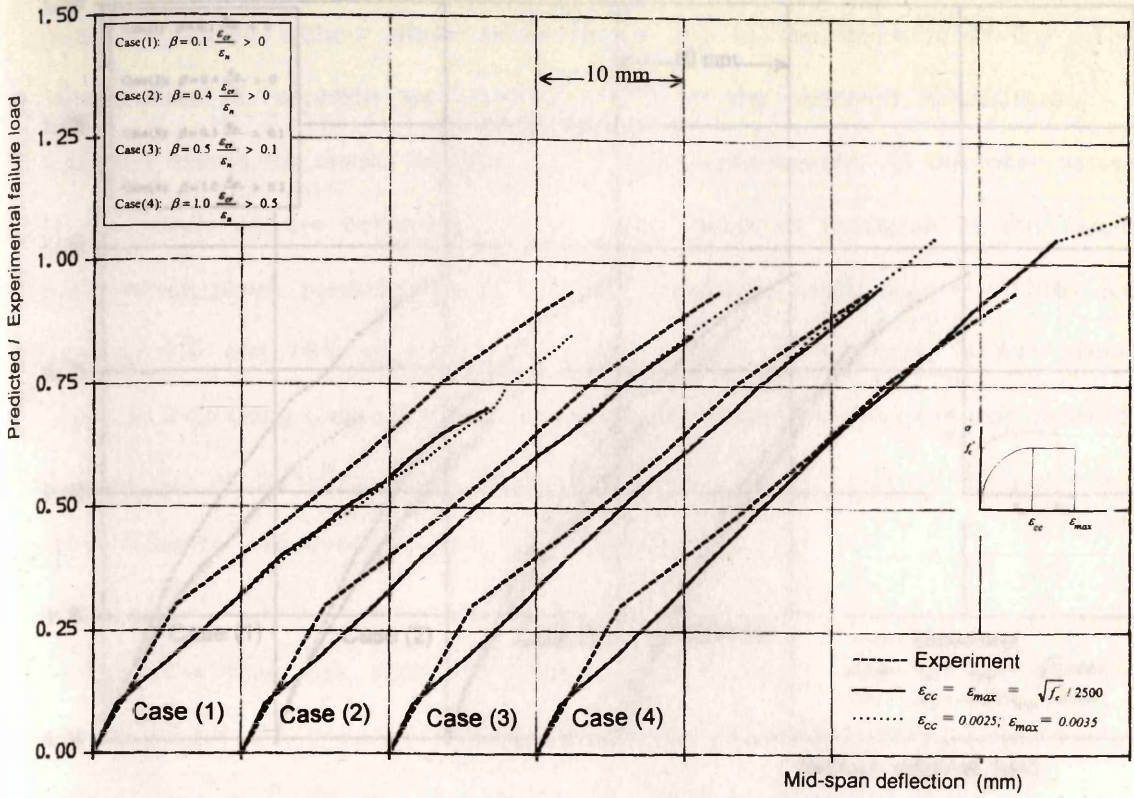


Fig. 6.61 Load-deflection curves for beam B-3 (effect of ϵ_{cc} , ϵ_{max}).

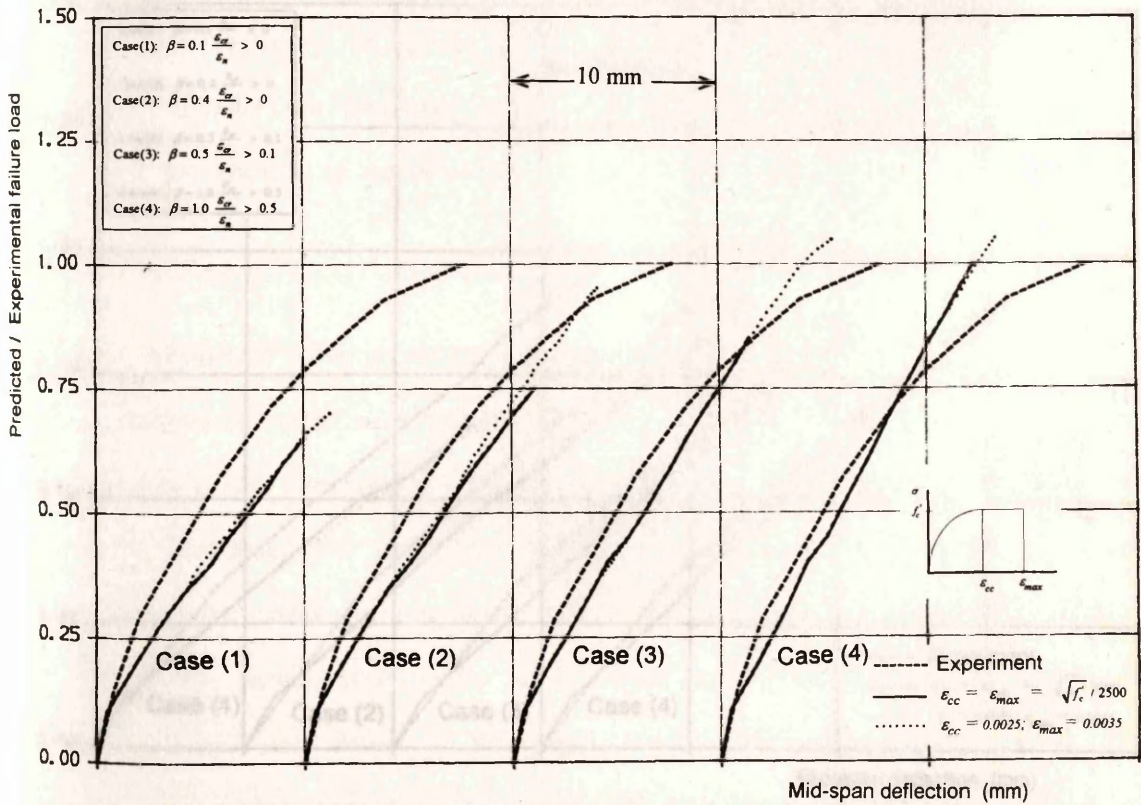


Fig. 6.62 Load-deflection curves for beam C-1 (effect of ϵ_{cc} , ϵ_{max}).

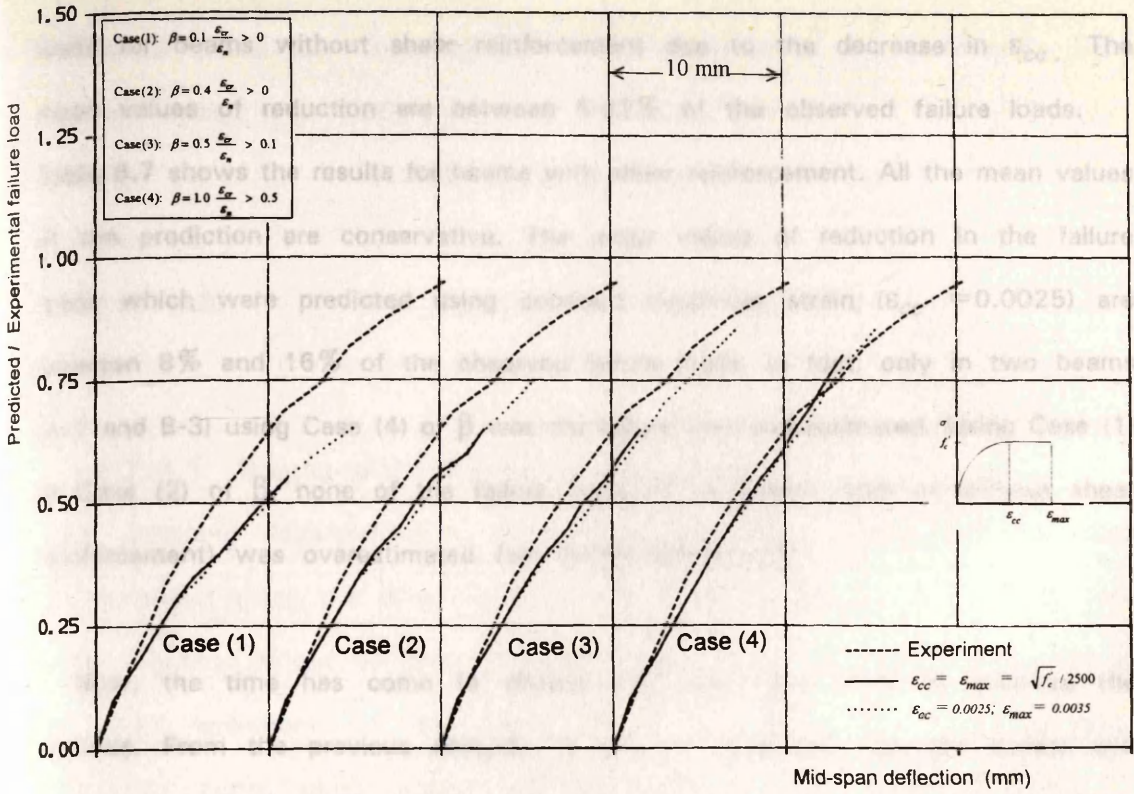


Fig. 6.63 Load-deflection curves for beam C-2 (effect of ϵ_{cc} , ϵ_{max}).

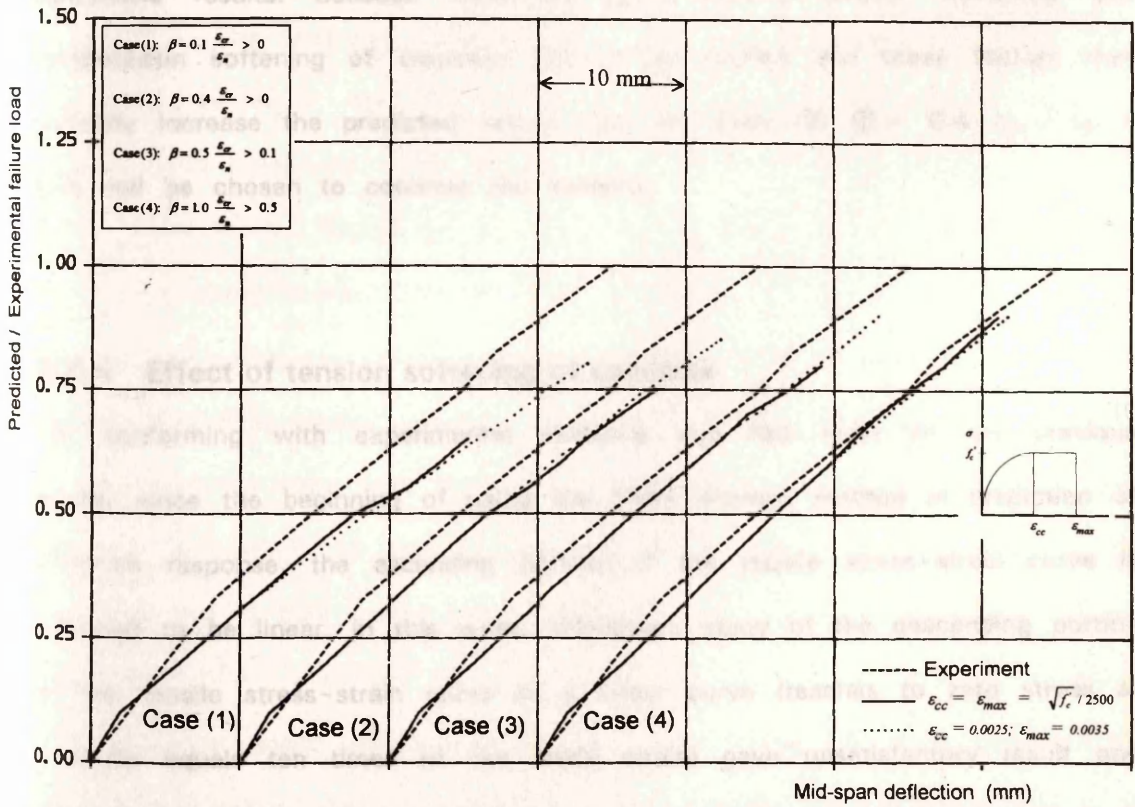


Fig. 6.64 Load-deflection curves for beam C-3 (effect of ϵ_{cc} , ϵ_{max}).

loads for beams without shear reinforcement due to the decrease in ϵ_{cc} . The mean values of reduction are between 5-22% of the observed failure loads. Table 6.7 shows the results for beams with shear reinforcement. All the mean values of the prediction are conservative. The mean values of reduction in the failure loads which were predicted using constant maximum strain ($\epsilon_{cc} = 0.0025$) are between 8% and 16% of the observed failure loads. In fact, only in two beams (A-1 and B-3) using Case (4) of β was the failure load overestimated. Using Case (1) or Case (2) of β , none of the failure loads of all beams (with or without shear reinforcement) was overestimated (see Tables 6.6 and 6.7).

Now, the time has come to choose only one case of β to continue the analysis. From the previous analysis, it can be concluded that the lowest and highest case of β did not give reasonable results either in predicting the load-deflection curve or the failure load while the remaining two cases gave an acceptable results. Because there are some factors (tension softening and compression softening of concrete) still to be studied and these factors may probably increase the predicted failure load, so, Case (2) ($\beta = 0.4 \epsilon_{cr} / \epsilon_n > 0.0$) will be chosen to continue the analysis.

6.2.4 Effect of tension softening of concrete

In conforming with experimental evidence and like most of the previous works, since the beginning of using the finite element method in prediction of structure response, the ascending portion of the tensile stress-strain curve is assumed to be linear. In this work, preliminary study of the descending portion of the tensile stress-strain curve as a linear curve (reaches to zero stress at a strain equals ten times of the crack strain) gave unsatisfactory result and so, the descending portion will be taken as a function of the strain normal to

the crack plane (non-linear curve). Three equations of the descending curve will be studied (Fig. 6.65)

Equation (A) $\sigma = (\epsilon_{cr} / \epsilon_n) f_t'$

Equation (B) $\sigma = \sqrt{(\epsilon_{cr} / \epsilon_n)} f_t'$

Equation (AB) $\sigma = (\epsilon_{cr} / \epsilon_n + \sqrt{(\epsilon_{cr} / \epsilon_n)}) f_t' / 2$

6.2.4.1 Beams without shear reinforcement

The predicted load-deflection curves for the three beams without shear reinforcement using the three equations are shown in Figs. 6.66 to 6.68. From these Figures, it can be seen that all the predicted load-deflection curves are in good agreement for the three beams. In general, the predicted load-deflection curve using equation B to represent the tension softening of concrete is stiffer than that using the other two equations (A and AB). Also, the predicted load-deflection curve using equation AB is stiffer than that using equation A. The predicted failure loads are also in good agreement (Table 6.8); the mean values of the ratio of the predicted failure loads to the observed failure loads using the three equations (A, AB, and B) are 0.97, 1.0, and 1.02, respectively. Neglecting the compression softening of concrete did not make the result worse. This may be explained as follow. Since there are no stirrups to confine the concrete and the failures of these beams are brittle and sudden, the compression softening of concrete does not take place.

It can also be seen that there is an increase in the predicted failure load because of taking the tension softening into account. This increase in the predicted failure load varies from 5-25% of the experimental failure load (see Table 6.8).

The predicted crack pattern and deformed shape using the three equations are nearly the same. In Fig. 6.69, the crack pattern and deformed shape for beam OA-2 (using Eq. AB) are shown at three different load factors (L.F.=

0.50, 0.95, and 1.00). At L.F.= 0.50, the crack pattern is in good agreement with the observed; the quarter span of the beam near the support has no cracks. The crack pattern at L.F.= 0.95 shows that the flexural cracks reach the centre line of the beam in the shear span; no cracks occur near the supports. At the last increment at which numerical instability occurred (L.F.= 1.00), a crushing in the compression zone under the load point occurred while a large nearly horizontal cracks appear above the middle of the beam. This indicates that the main reason for failure is the crushing of concrete in compression zone under the load point. This can be seen from the stress-strain relationship at a Gauss point in the compression zone and close to the load point (Fig. 6.70). Fig. 6.71 shows the stresses in the longitudinal steel; the maximum stress in the bar at the last converged increment (L.F.= 0.95) does not exceed 55% of the yield stress.

These satisfactory results for these three beams without shear reinforcement makes it possible to conclude that further investigation of shear failure of beams without shear reinforcement is not required.

6.2.4.2 Beams with shear reinforcement

Figs. 6.72 to 6.80 show the predicted load-deflection curves of the beams with shear reinforcement. It can be seen from these figures that the predicted load-deflection curves agree well with the observed load-deflection curves up to the numerical failure which occurs at a load level less than the observed failure load. As for beams without shear reinforcement, the predicted load-deflection curve for these beams using equation B to represent the tension softening of concrete is stiffer than that using the other two equations (A and AB). Also, the predicted load-deflection curve using equation AB is stiffer than that using equation A. The mean values of the predicted to the observed

Fig. 6.65 Assumed stress-strain curve of concrete in tension

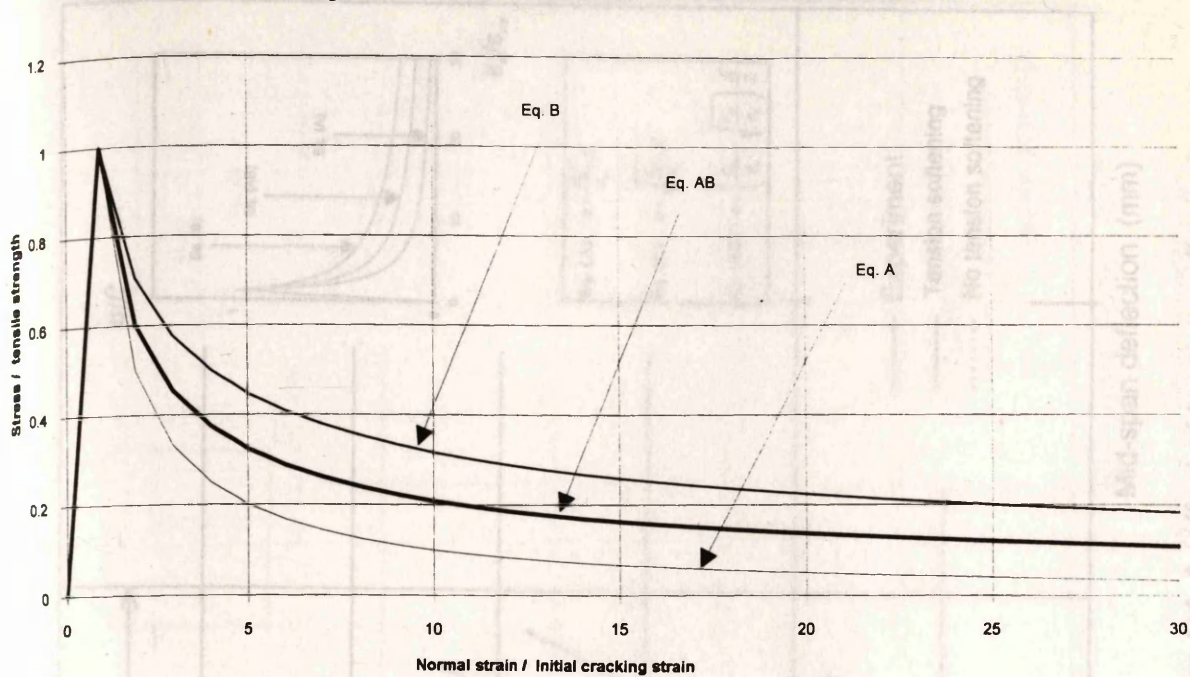


Table 6.8 Effect of tension softening of concrete in beams without shear reinforcement

Beam	f_c' MPa	$f_t' = 0.54\sqrt{f_c'}$ MPa	$\epsilon_{max} = \epsilon_{cc} = \sqrt{f_c'}/2500$	Without tension softening	Predicted / Experimental failure load		
					EQUATION (A)	EQUATION (AB)	EQUATION (B)
OA-1	22.6	2.57	0.0019	0.95	1.10	1.05	1.00
OA-2	23.7	2.63	0.0020	0.70	0.95	0.95	0.95
OA-3	37.6	3.31	0.0025	0.85	1.00	1.00	0.95
Mean	value			0.83	0.97	1.00	1.02

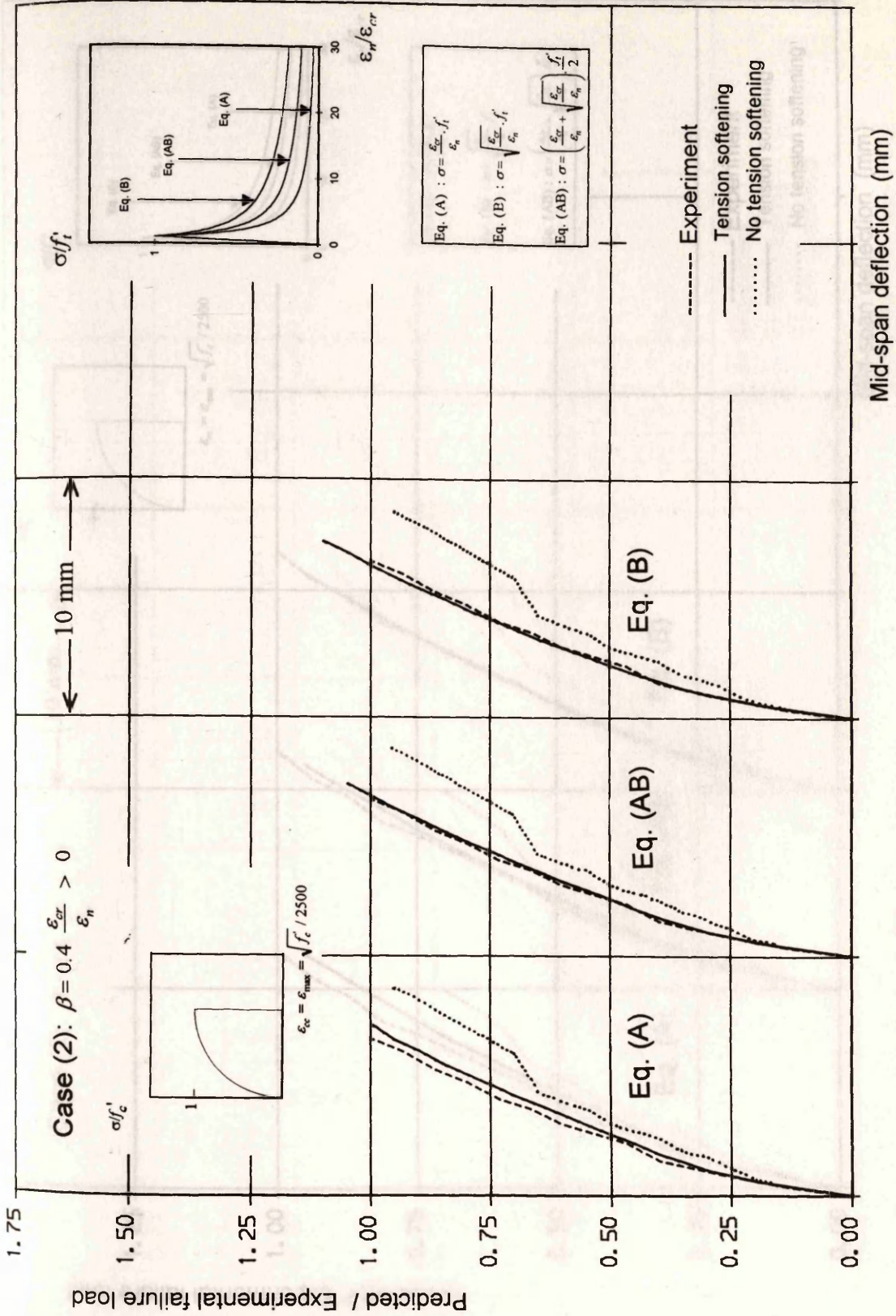


Fig. 6.66 Load-deflection curves for beam OA-1 (effect of tension softening).

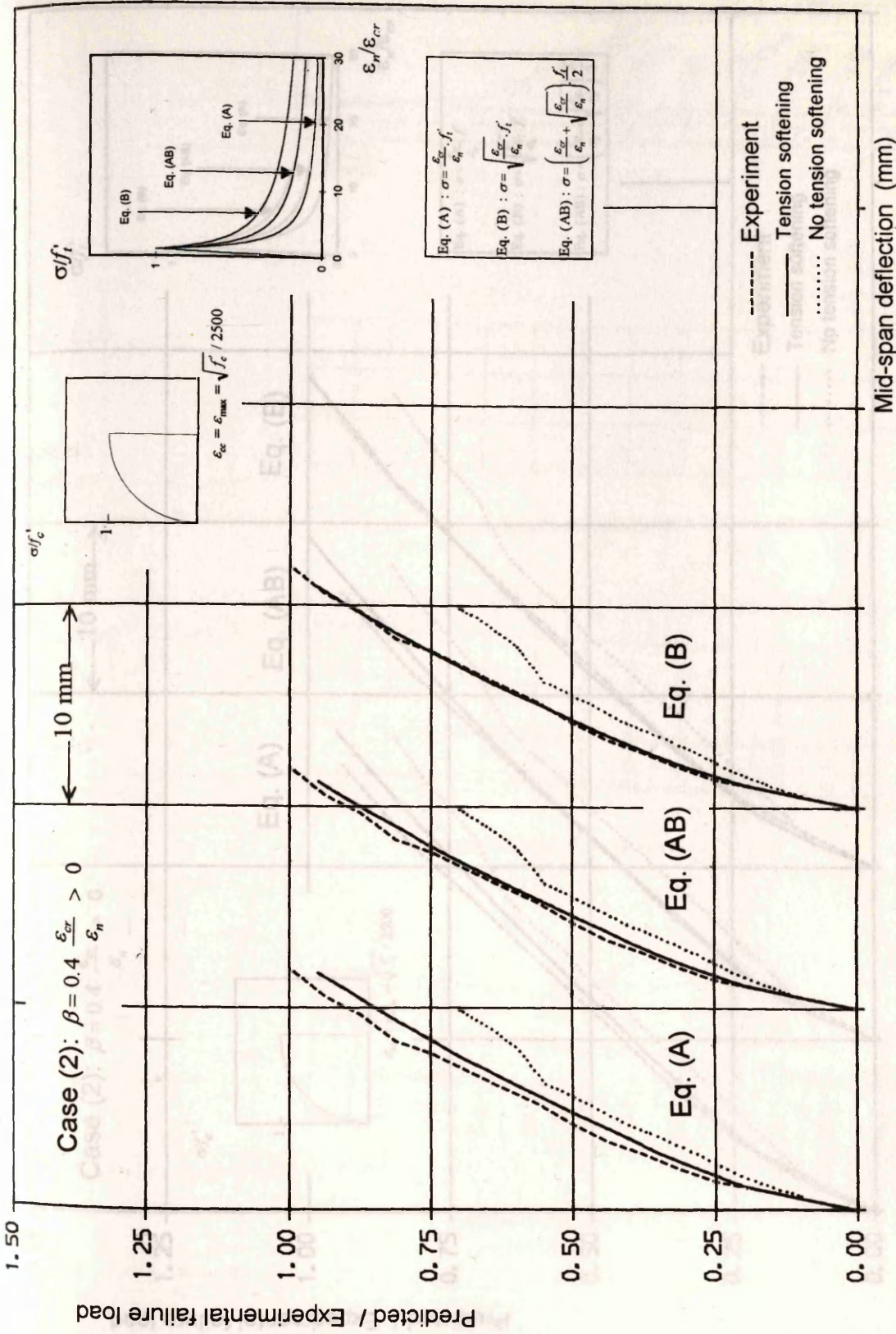


Fig. 6.67 Load-deflection curves for beam OA-2 (effect of tension softening).

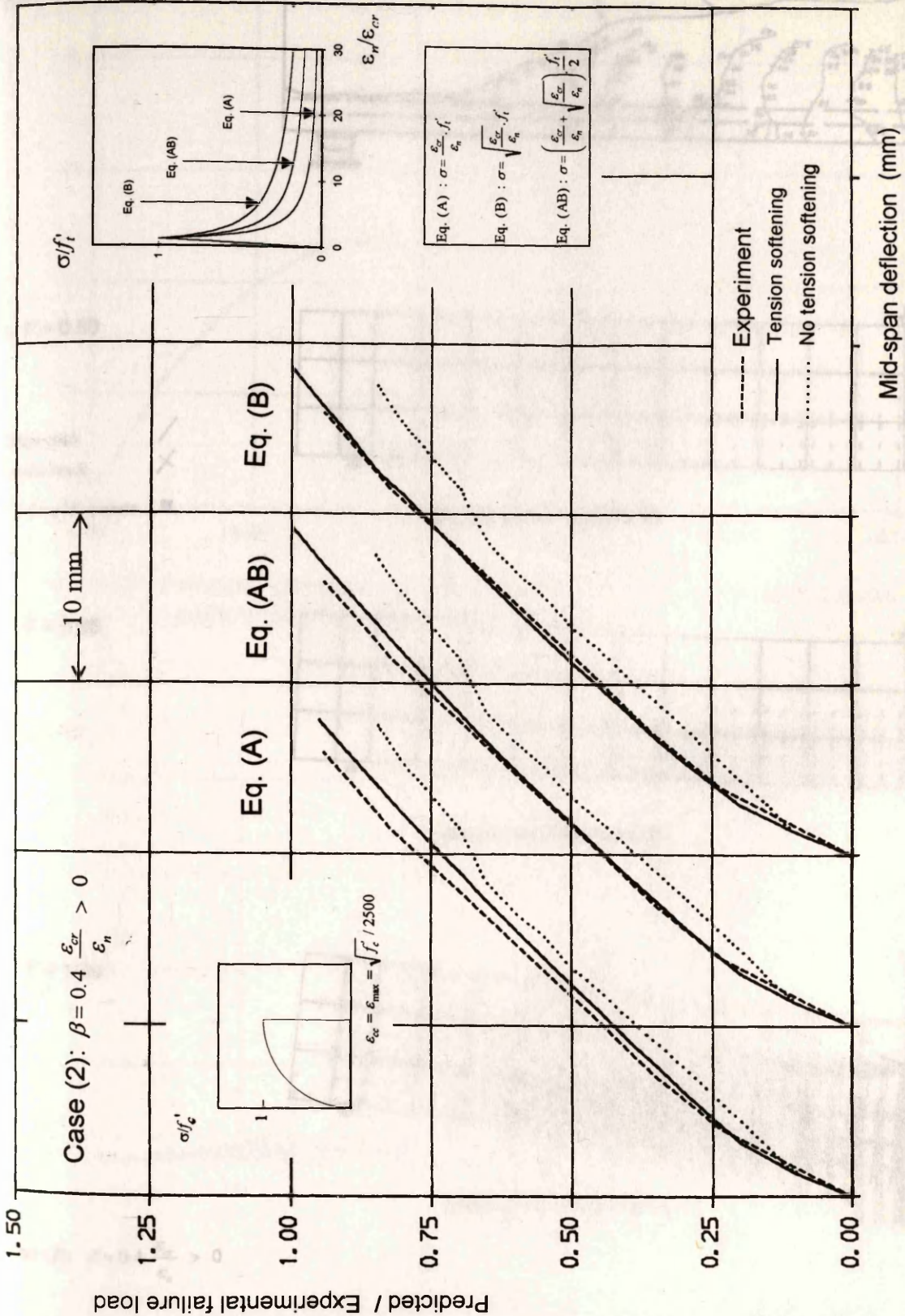


Fig. 6.68 Load-deflection curves for beam OA-3 (effect of tension softening).

Predicted / Experimental failure load

Fig. 6.69 Crack patterns and deformed shapes of beam OA-3

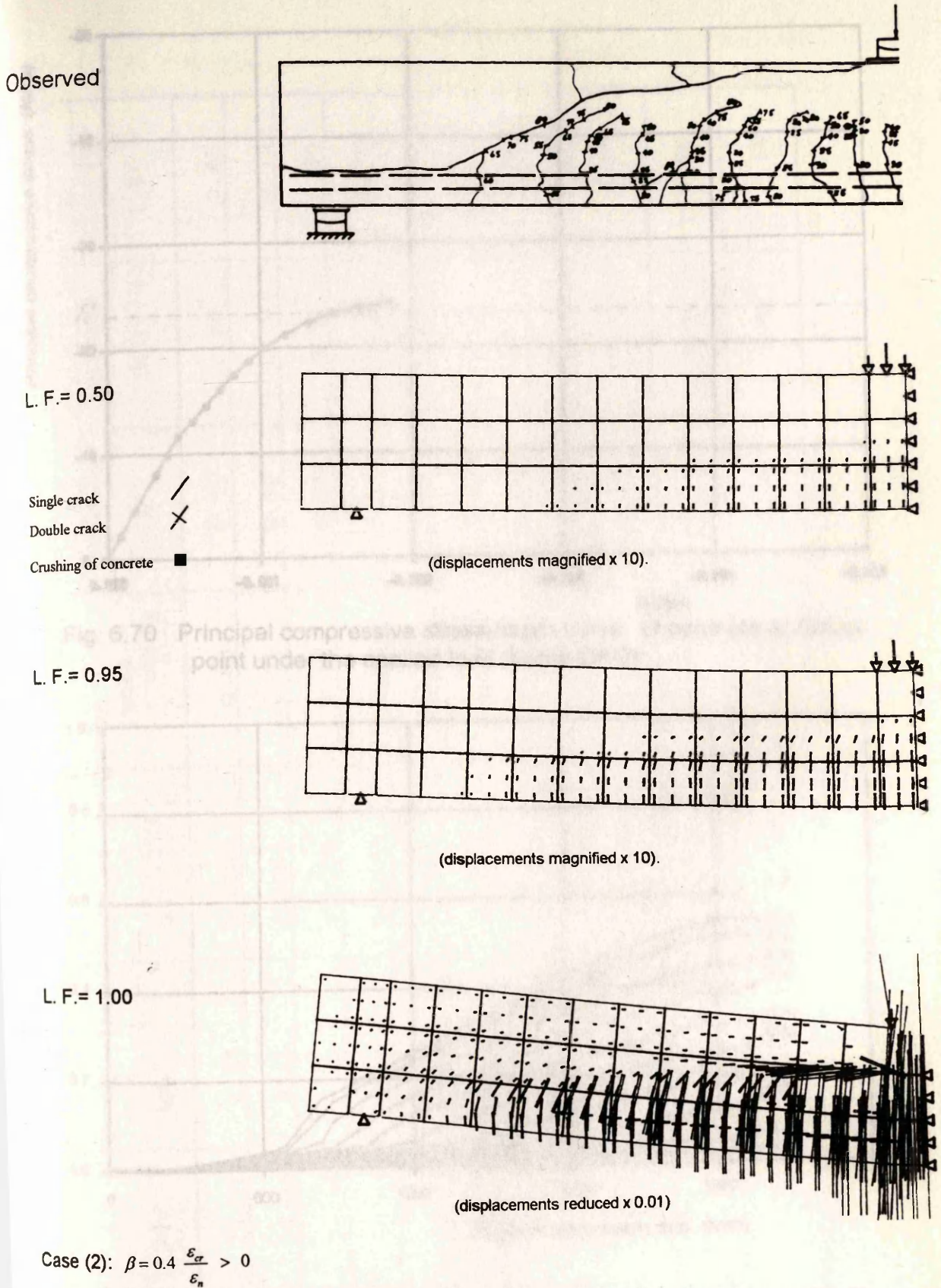


Fig. 6.69 Crack patterns and deformed shapes for beam OA-2

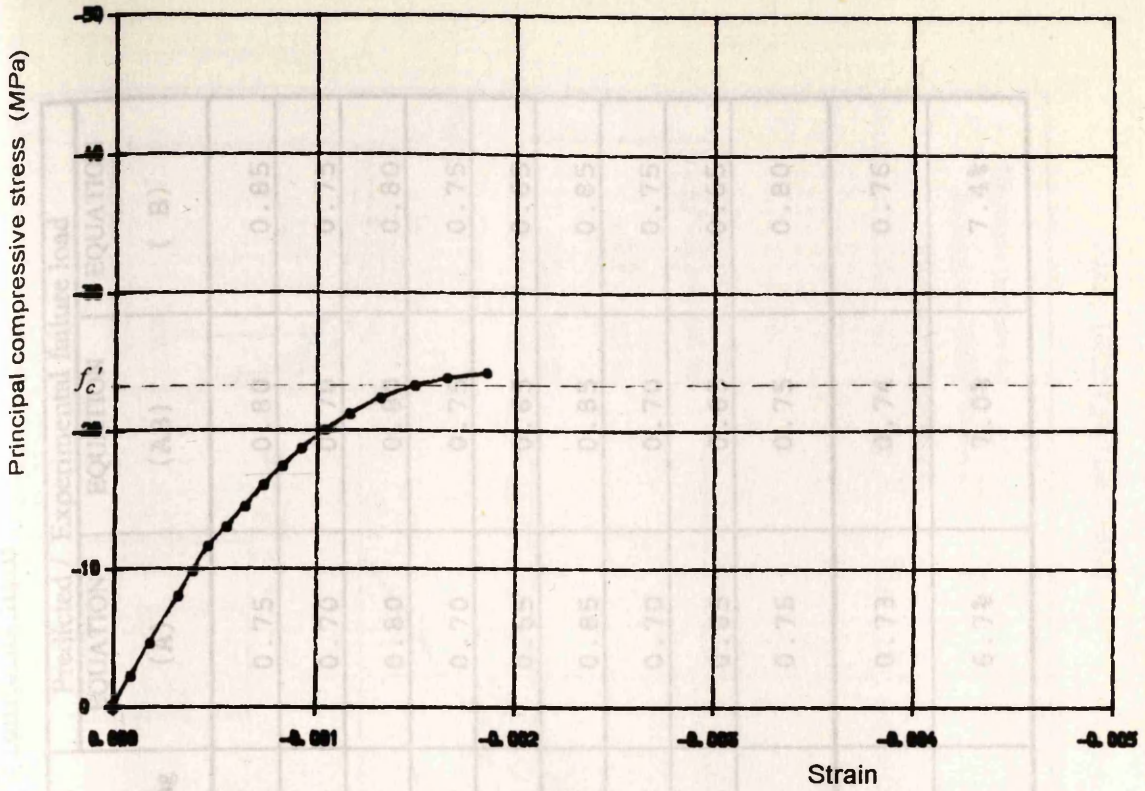


Fig. 6.70 Principal compressive stress-strain curve of concrete at Gauss point under the applied load (beam OA-2).

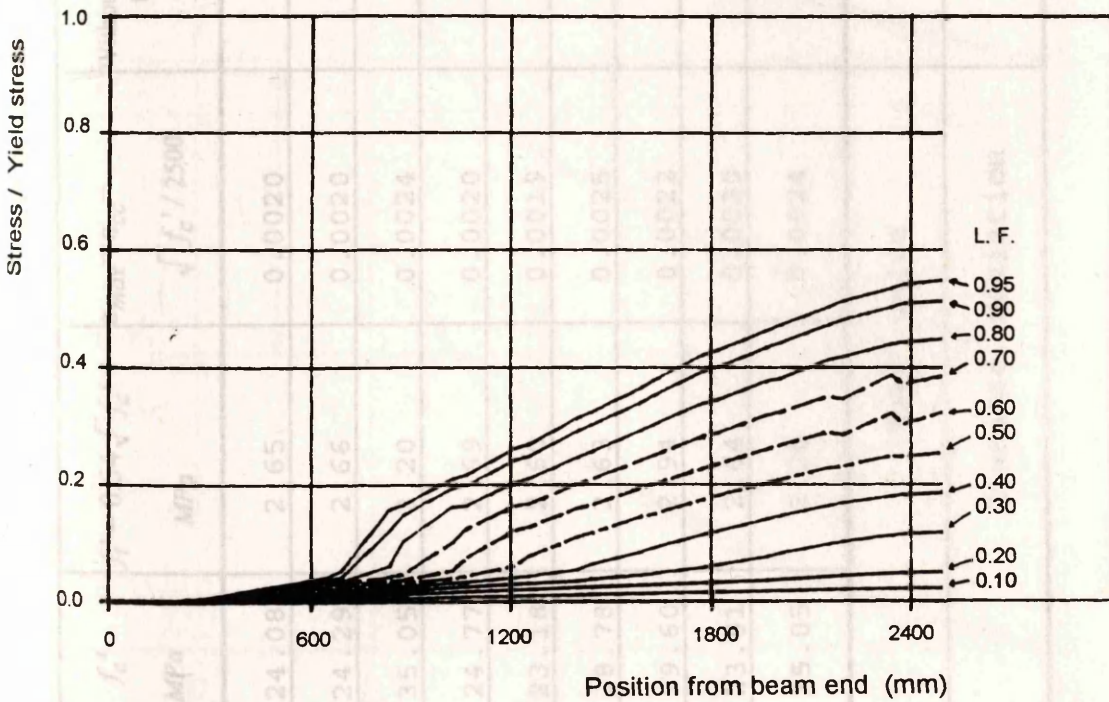


Fig. 6.71 Stresses in tension steel at different load factors (beam OA-2).

Table 6.9 Effect of tension softening of concrete in beams with shear reinforcement

Beam	f'_c MPa	$f'_t = 0.54\sqrt{f'_c}$ MPa	$\epsilon_{max} = \epsilon_{cc} = \sqrt{f'_c} / 2500$	Without tension softening	Predicted / Experimental failure load	
					EQUATION (A)	EQUATION (AB) (B)
A-1	24.08	2.65	0.0020	0.85	0.75	0.80 0.85
A-2	24.29	2.66	0.0020	0.70	0.70	0.70 0.75
A-3	35.05	3.20	0.0024	0.80	0.80	0.80 0.80
B-1	24.77	2.69	0.0020	0.70	0.70	0.75 0.75
B-2	23.18	2.60	0.0019	0.60	0.65	0.65 0.65
B-3	38.78	3.63	0.0025	0.85	0.85	0.85 0.85
C-1	29.60	2.94	0.0022	0.75	0.70	0.70 0.75
C-2	23.81	2.64	0.0020	0.65	0.65	0.65 0.65
C-3	35.05	3.20	0.0024	0.75	0.75	0.75 0.80
Mean value				0.74	0.73	0.74 0.76
Standard deviation				8.6%	6.7%	7.0% 7.4%

Mid-span deflection (mm)

Fig. 6.72 Load-deflection curves for beam A-1 (effect of tension softening)

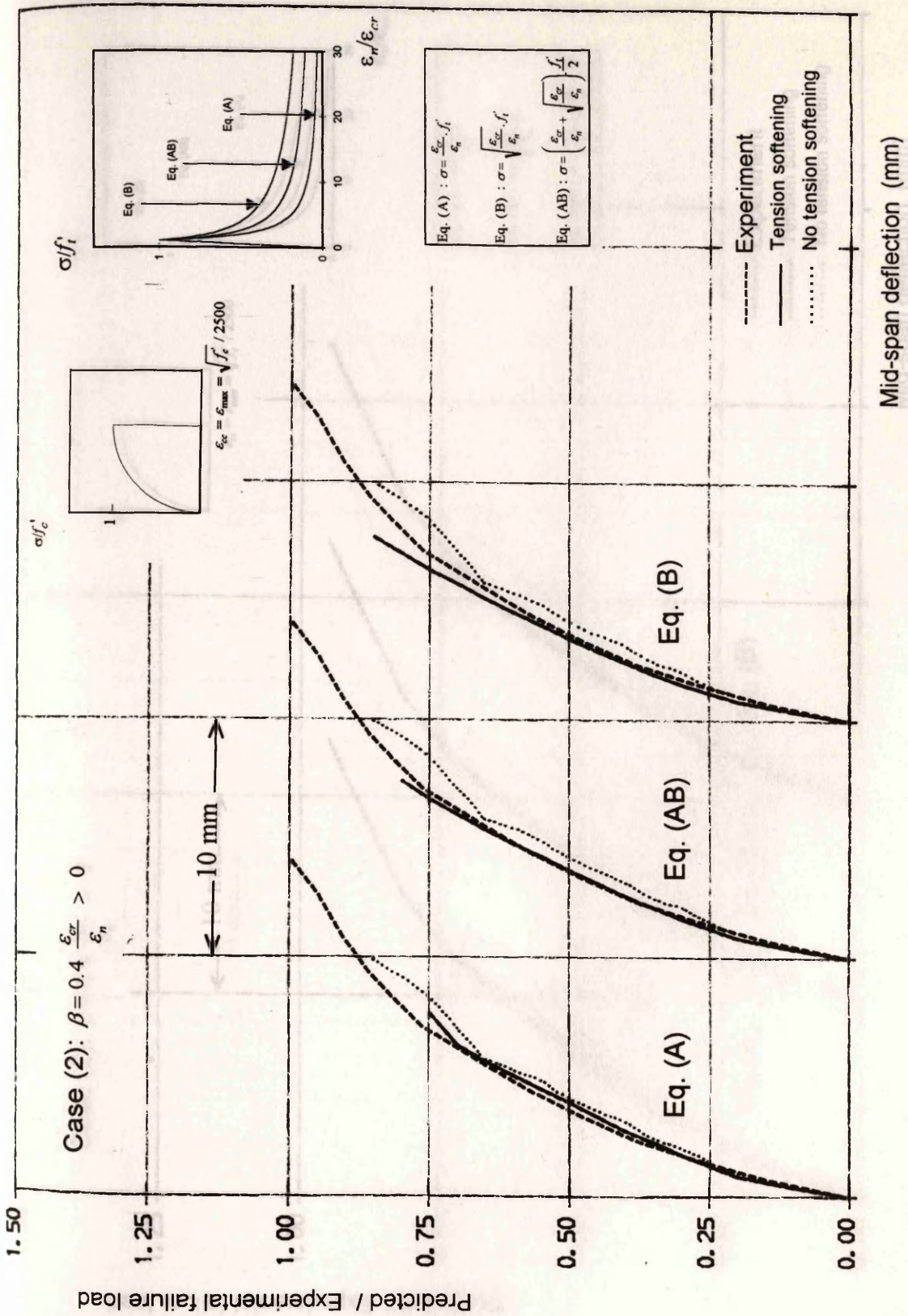


Fig. 6.72 Load-deflection curves for beam A-1 (effect of tension softening).

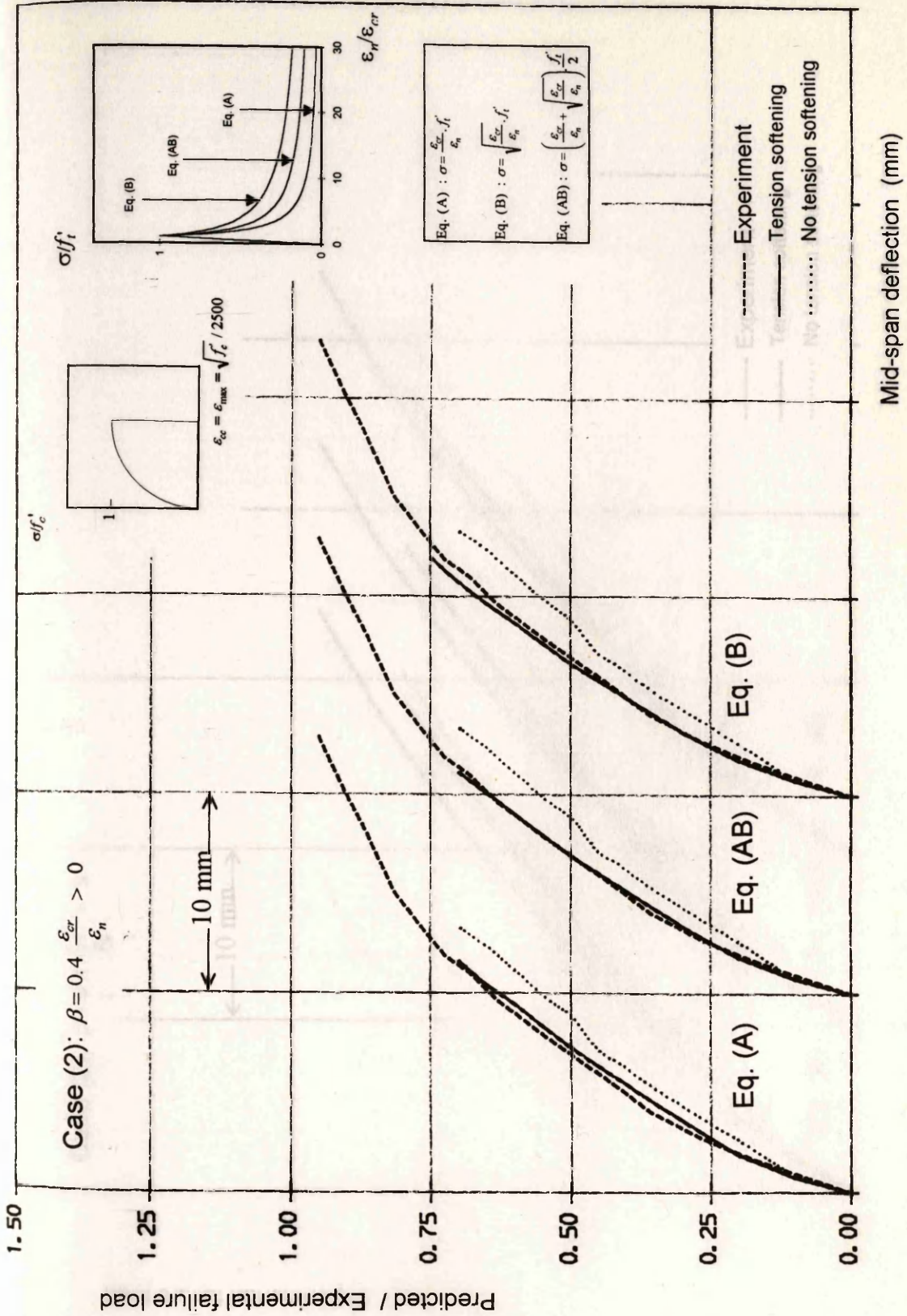


Fig. 6.73 Load-deflection curves for beam A-2 (effect of tension softening).

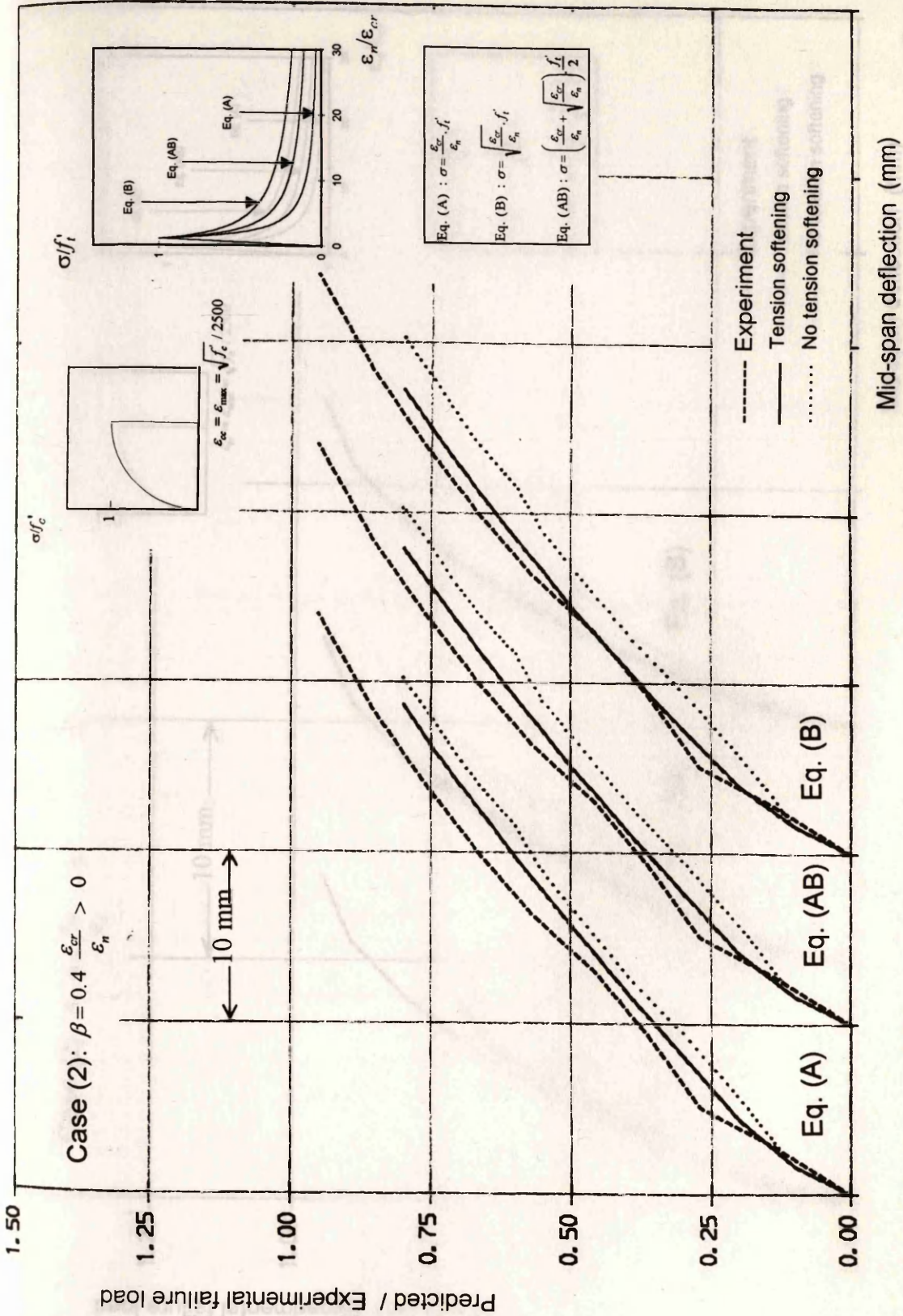


Fig. 6.74 Load-deflection curves for beam A-3 (effect of tension softening).

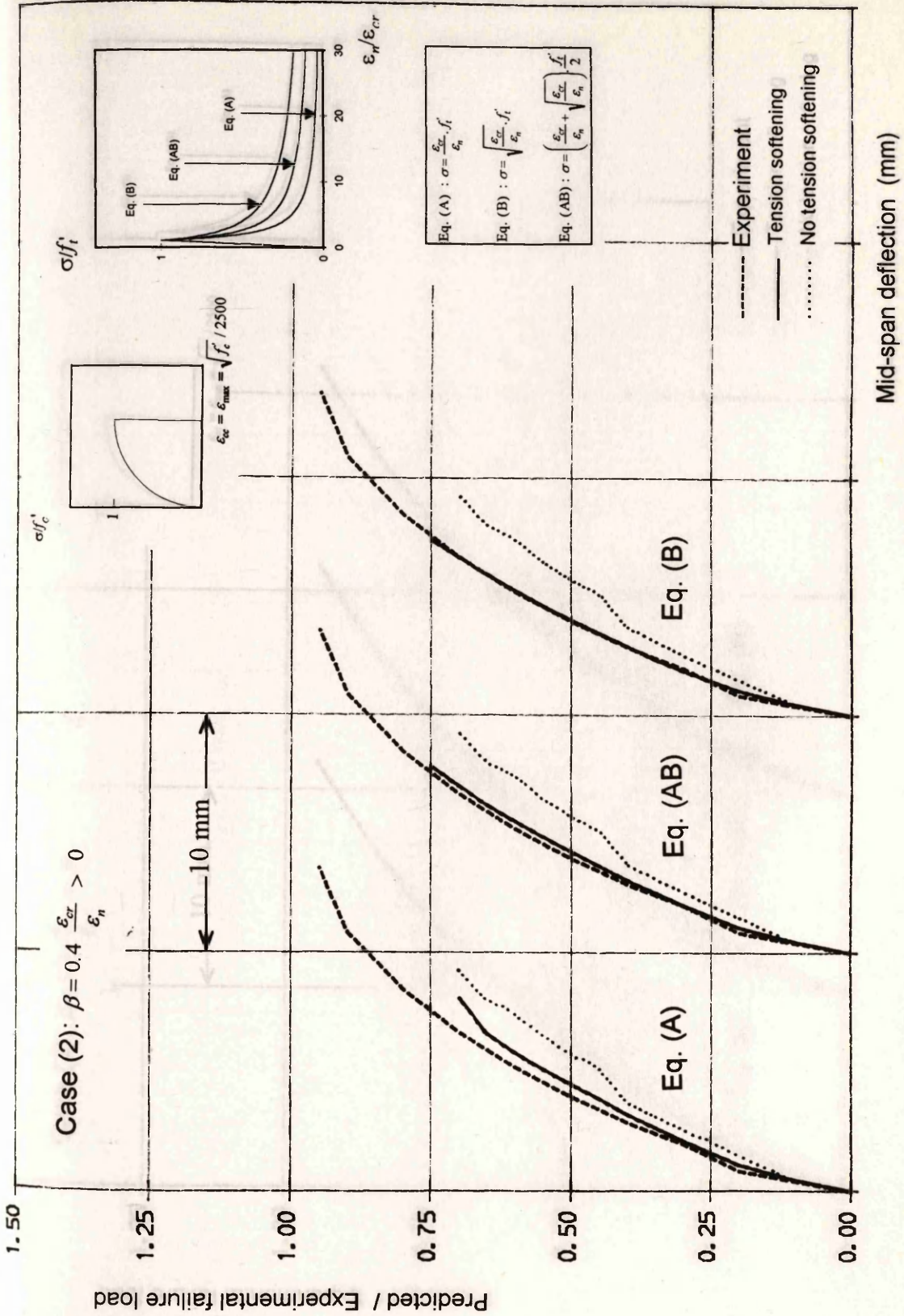


Fig. 6.75 Load-deflection curves for beam B-1 (effect of tension softening).

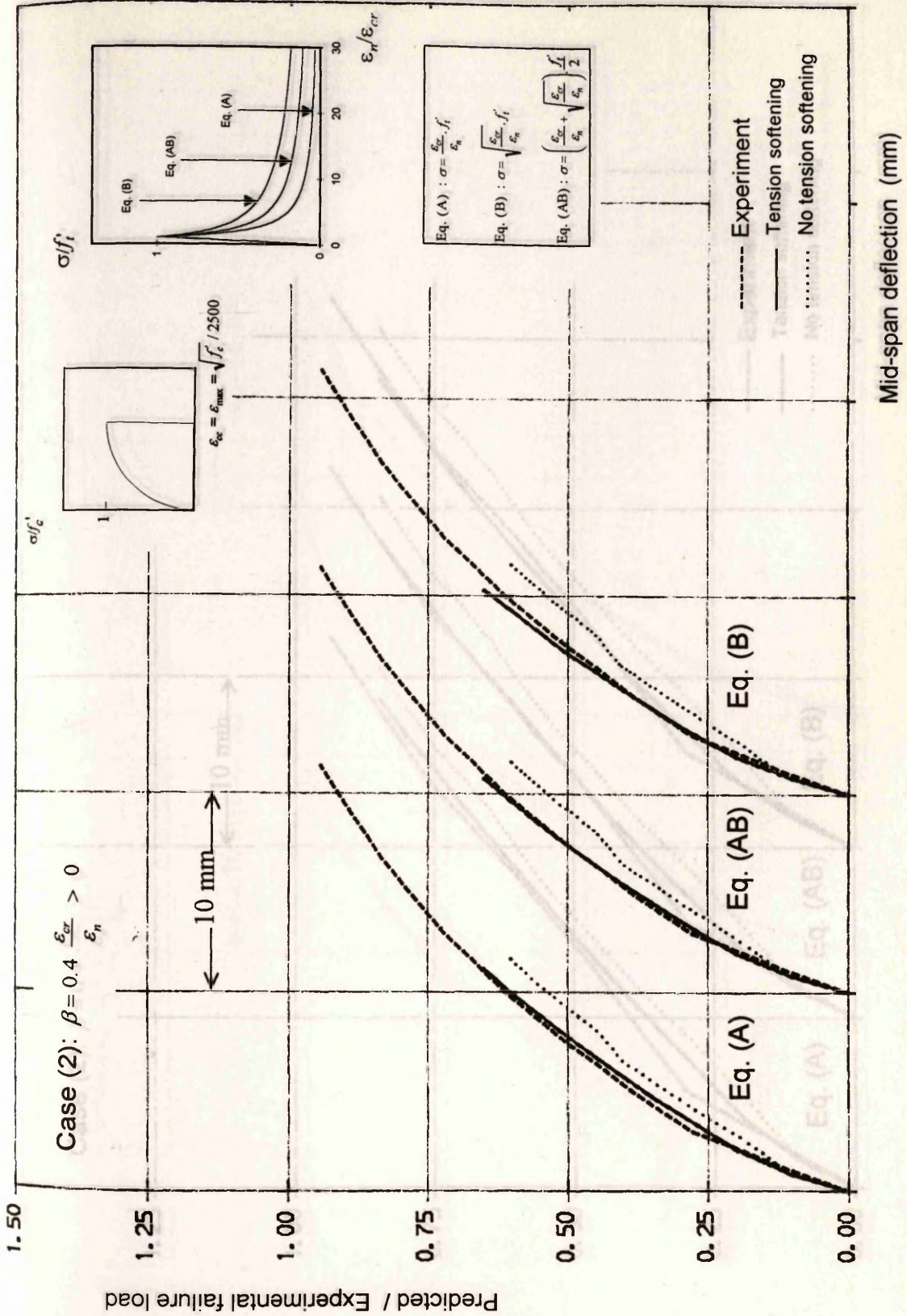


Fig. 6.76 Load-deflection curves for beam B-2 (effect of tension softening).

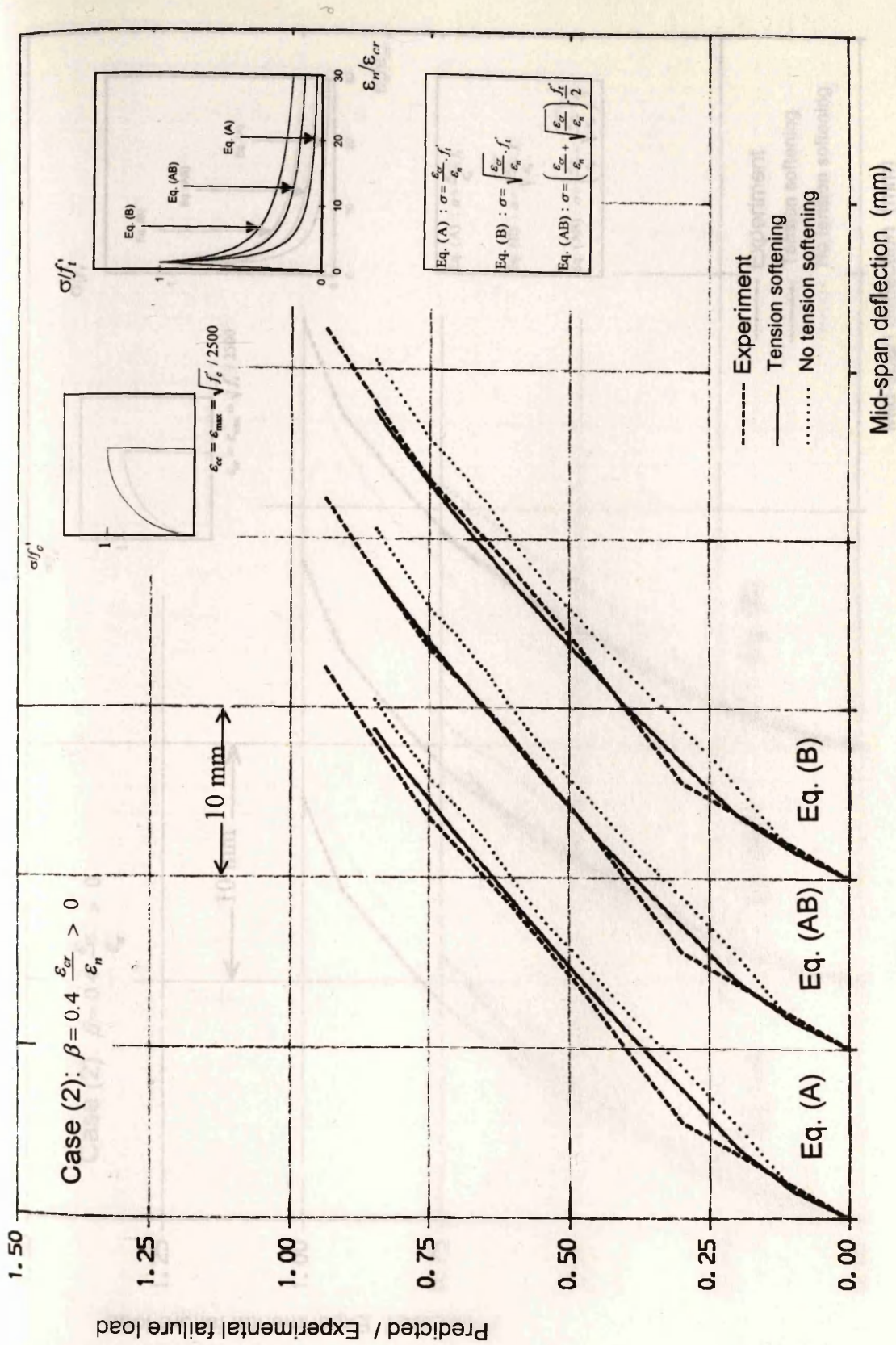


Fig. 6.77 Load-deflection curves for beam B-3 (effect of tension softening).

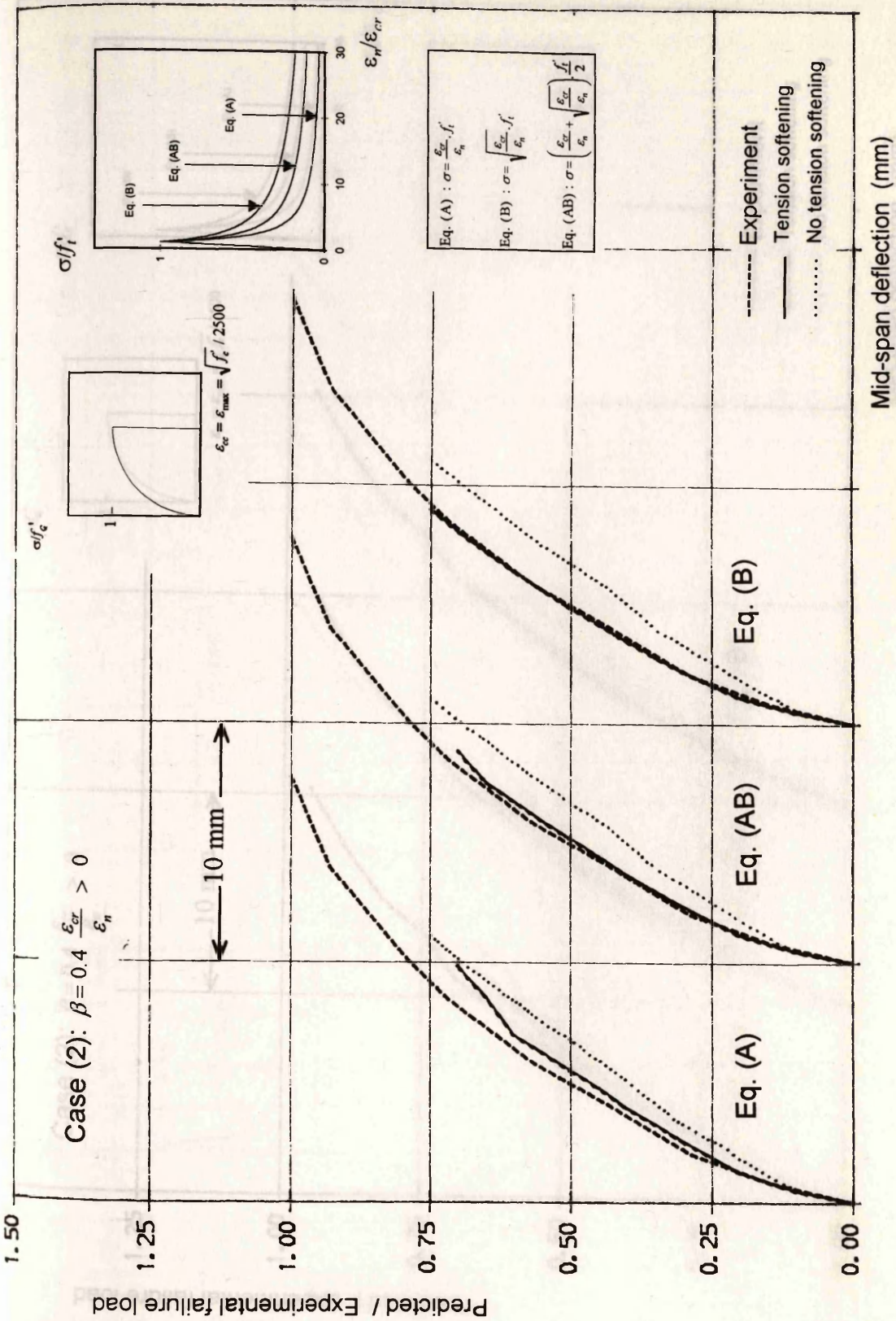


Fig. 6.78 Load-deflection curves for beam C-1 (effect of tension softening).

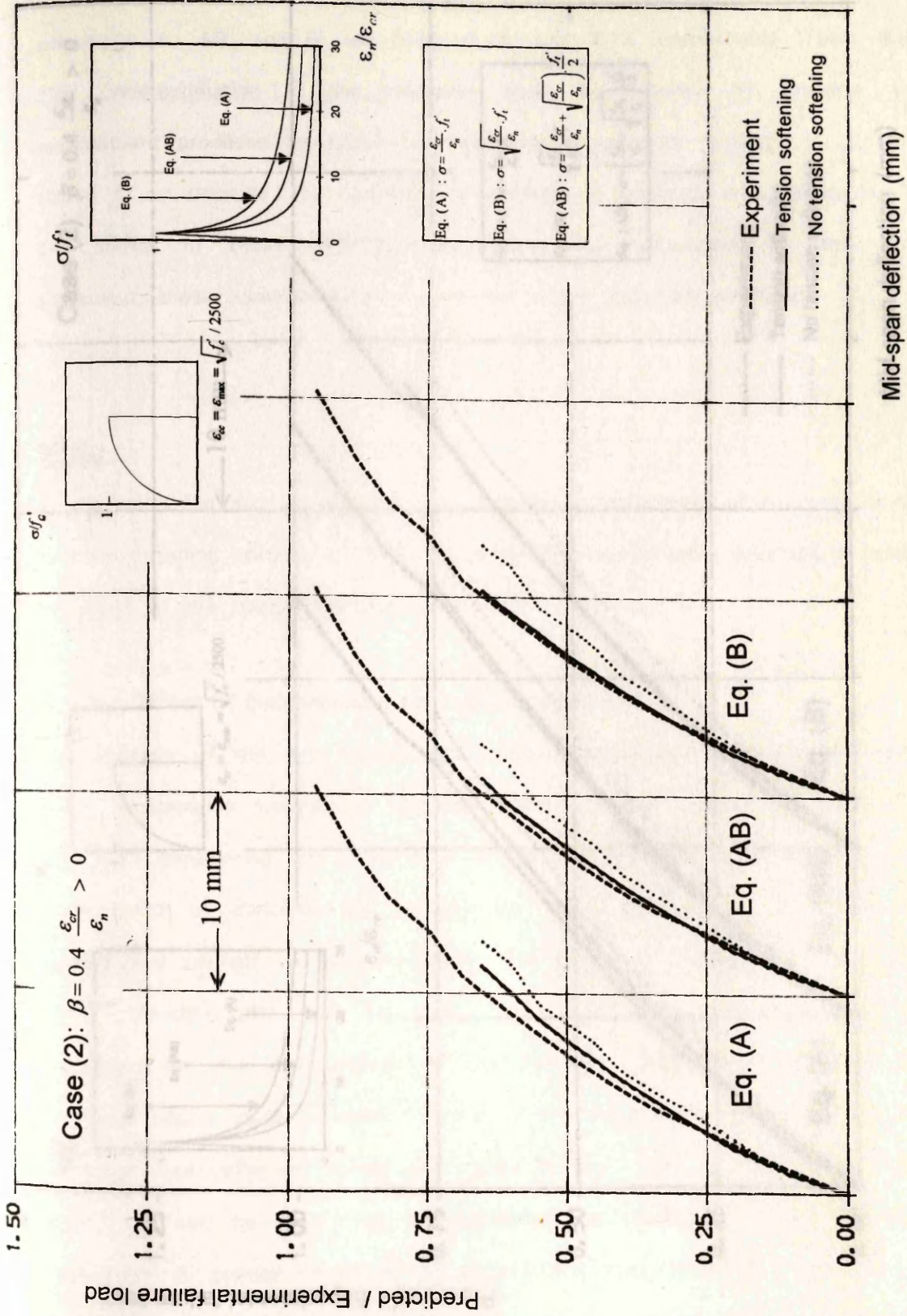


Fig. 6.79 Load-deflection curves for beam C-2 (effect of tension softening).

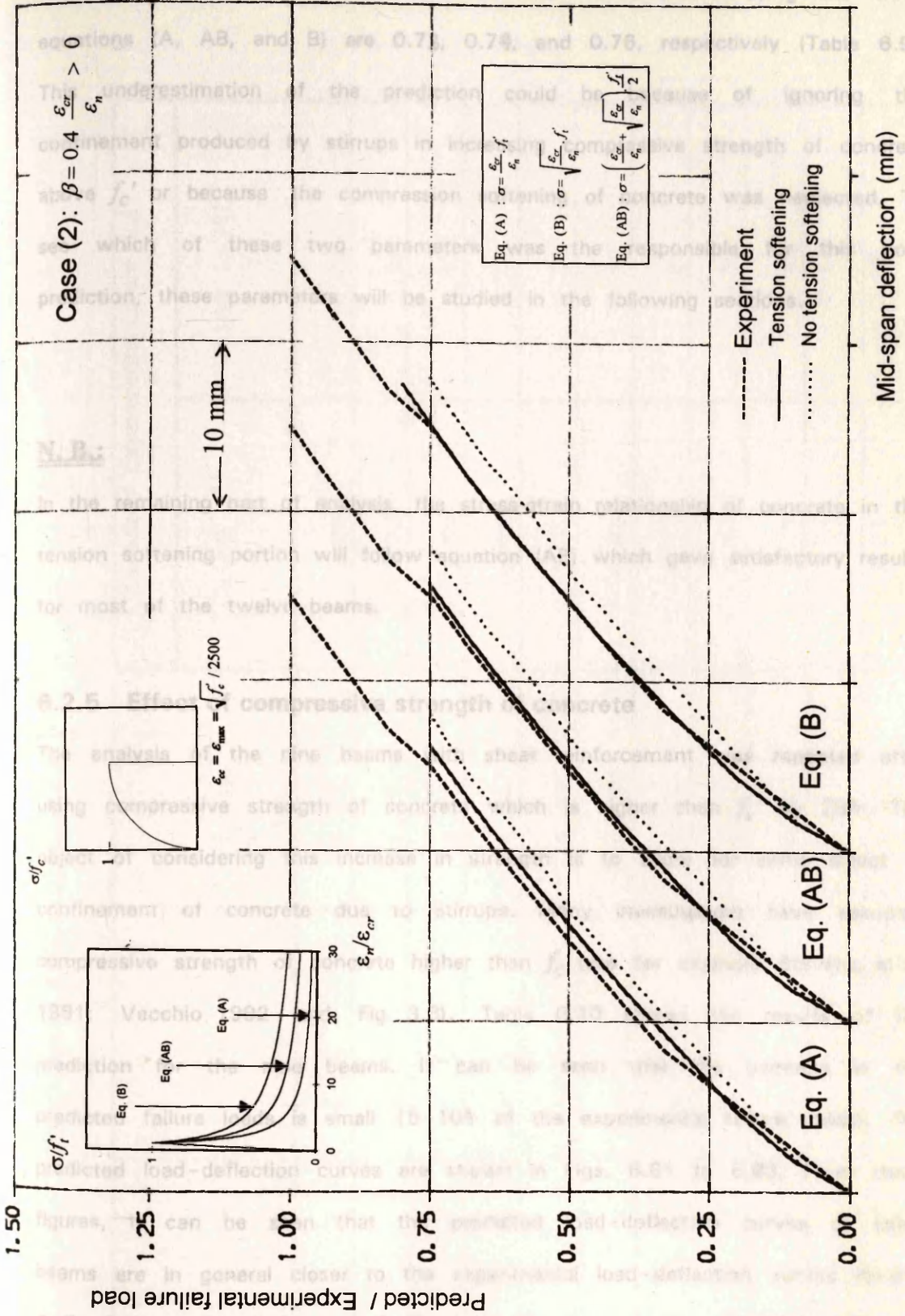


Fig. 6.80 Load-deflection curves for beam C-3 (effect of tension softening).

failure loads of the nine beams with shear reinforcement using the three equations (A, AB, and B) are 0.73, 0.74, and 0.76, respectively (Table 6.9). This underestimation of the prediction could be because of ignoring the confinement produced by stirrups in increasing compressive strength of concrete above f_c' or because the compression softening of concrete was neglected. To see which of these two parameters was the responsible for this poor prediction, these parameters will be studied in the following sections.

N. B.:

In the remaining part of analysis, the stress-strain relationship of concrete in the tension softening portion will follow equation (AB) which gave satisfactory results for most of the twelve beams.

6.2.5 Effect of compressive strength of concrete

The analysis of the nine beams with shear reinforcement was repeated after using compressive strength of concrete which is higher than f_c' by 28%. The object of considering this increase in strength is to allow for some effect of confinement of concrete due to stirrups. Many investigators have assumed compressive strength of concrete higher than f_c' (see for example Stevens, et al. 1991; Vecchio 1992 and Fig. 3.6). Table 6.10 shows the results of the prediction for the nine beams. It can be seen that the increase in the predicted failure loads is small (5-10% of the experimental failure loads). The predicted load-deflection curves are shown in Figs. 6.81 to 6.83. From these figures, it can be seen that the predicted load-deflection curves of some beams are in general closer to the experimental load-deflection curves (beams A-3, B-1, C-1, C-2, and C-3) while in some beams the load-deflection curve became stiffer than the experimental curve (beams A-1, A-2, B-2, and B-3).

Table 6.10 Effect of compressive strength of concrete.

BEAM	f_c' MPa	$1.28f_c'$ MPa	Predicted / Experimental failure load	
			Using f_c'	Using $1.28f_c'$
A-1	24.08	30.87	0.80	0.85
A-2	24.29	31.14	0.70	0.80
A-3	35.05	44.94	0.80	0.90
B-1	24.77	31.76	0.75	0.75
B-2	23.18	29.72	0.65	0.70
B-3	38.78	49.72	0.85	0.95
C-1	29.60	37.95	0.70	0.80
C-2	23.81	30.53	0.65	0.70
C-3	35.05	44.94	0.75	0.85
Mean value			0.74	0.81
Standard deviation			7.0%	8.6%

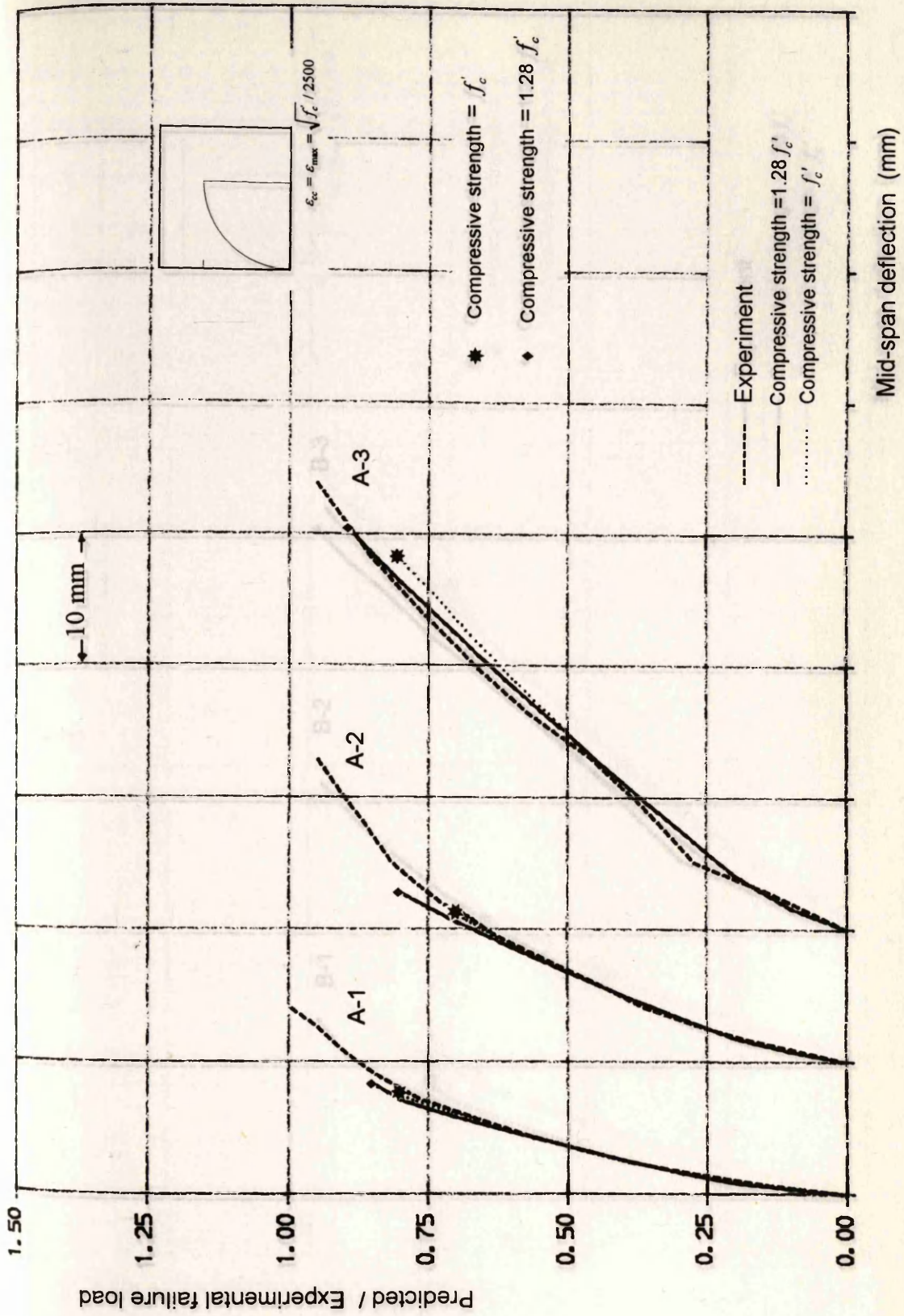


Fig. 6.81 Load-deflection curves for beams A-1, A-2, and A-3 (effect of compressive strength of concrete).

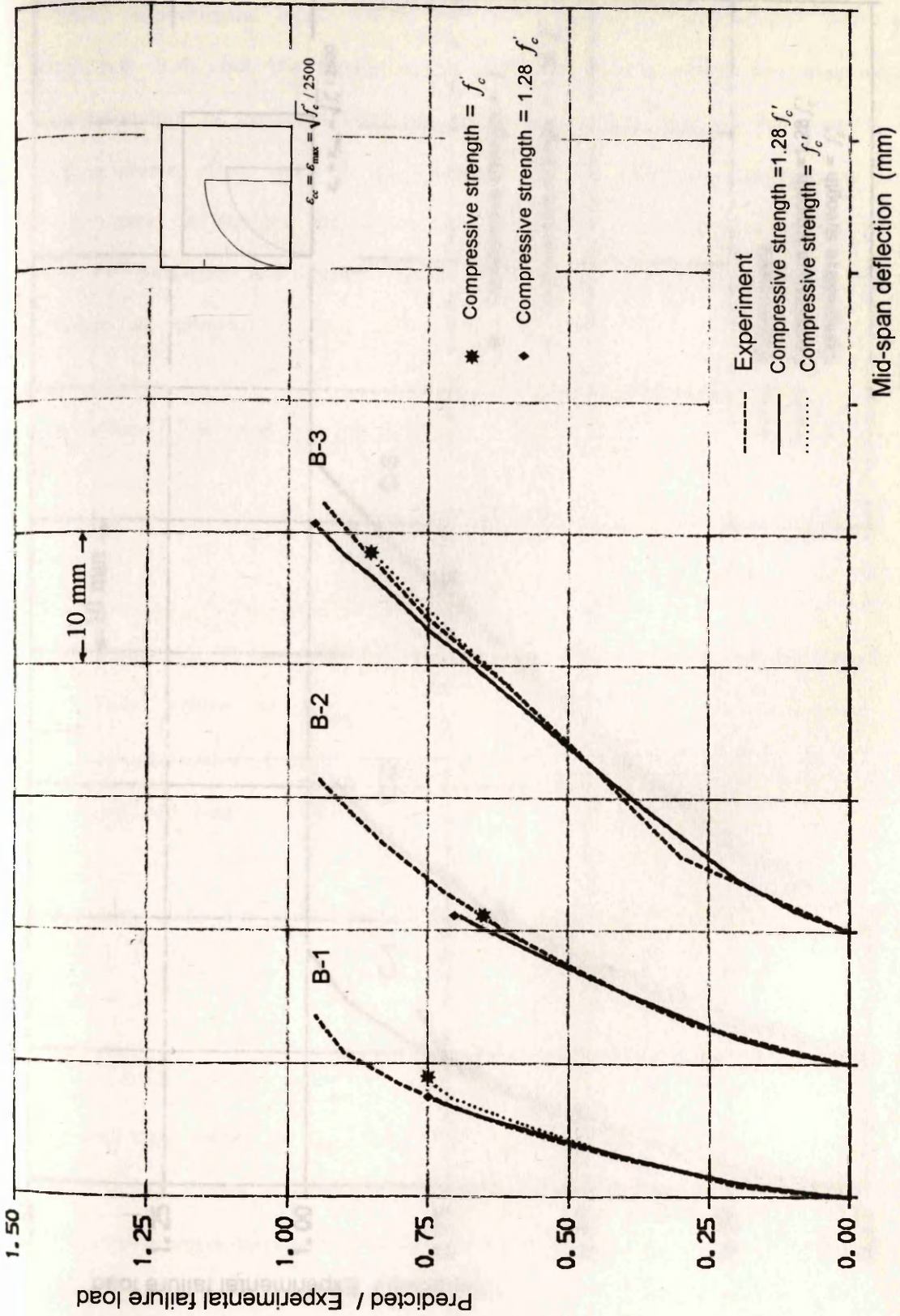


Fig. 6.82 Load-deflection curves for beams B-1, B-2, and B-3 (effect of compressive strength of concrete).

6.2.6 Effect of compression softening of concrete

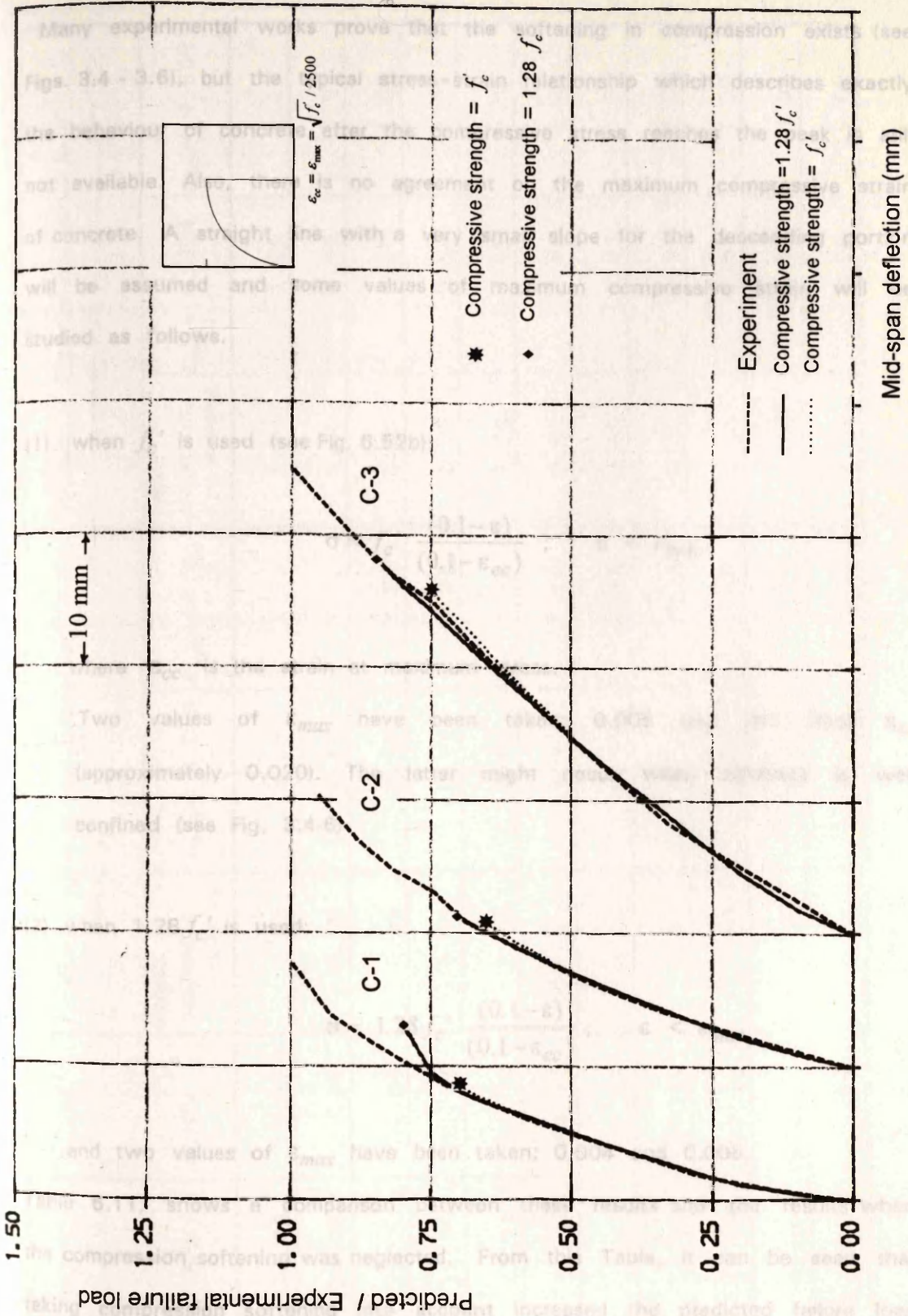


Fig. 6.83 Load-deflection curves for beams C-1, C-2, and C-3 (effect of compressive strength of concrete).

6.2.6 Effect of compression softening of concrete

Many experimental works prove that the softening in compression exists (see Figs. 3.4 - 3.6), but the typical stress-strain relationship which describes exactly the behaviour of concrete after the compressive stress reaches the peak is still not available. Also, there is no agreement on the maximum compressive strain of concrete. A straight line with a very small slope for the descending portion will be assumed and some values of maximum compressive strain will be studied as follows.

(1) when f_c' is used (see Fig. 6.52b):

$$\sigma = f_c' \frac{(0.1 - \epsilon)}{(0.1 - \epsilon_{cc})} ; \quad \epsilon < \epsilon_{max}$$

where ϵ_{cc} is the strain at maximum stress.

Two values of ϵ_{max} have been taken; 0.005 and ten times ϵ_{cc} (approximately 0.020). The latter might occur when concrete is well confined (see Fig. 3.4-6)

(2) when $1.28 f_c'$ is used:

$$\sigma = 1.28 f_c' \frac{(0.1 - \epsilon)}{(0.1 - \epsilon_{cc})} ; \quad \epsilon < \epsilon_{max}$$

and two values of ϵ_{max} have been taken; 0.004 and 0.005.

Table 6.11, shows a comparison between these results and the results when the compression softening was neglected. From this Table, it can be seen that taking compression softening into account increased the predicted failure load by about 10 - 50% of the corresponding experimental failure load. An increase of

Table 6.11 Effect of compression softening of concrete

BEAM	f_c' MPa	$1.28f_c'$ MPa	Predicted / Experimental failure load using f_c'			Predicted / Experimental failure load using $1.28 f_c'$		
			Without compression softening	$\epsilon_{max} = 0.005$	$\epsilon_{max} = 1.0 \cdot \epsilon_{cc}$	Without compression softening	$\epsilon_{max} = 0.004$	$\epsilon_{max} = 0.005$
A-1	24.08	30.87	0.80	1.05	1.30	0.85	1.05	1.10
A-2	24.29	31.14	0.70	0.85	1.10	0.80	0.90	0.95
A-3	35.05	44.94	0.80	0.90	1.05	0.90	1.00	1.05
B-1	24.77	31.76	0.75	0.85	0.95	0.75	0.90	0.95
B-2	23.18	29.72	0.65	0.80	1.00	0.70	0.85	0.90
B-3	38.78	49.72	0.85	1.00	1.15	0.95	1.05	1.15
C-1	29.60	37.95	0.70	0.90	1.00	0.80	0.90	0.95
C-2	23.81	30.53	0.65	0.75	0.85	0.70	0.80	0.80
C-3	35.05	44.94	0.75	0.85	1.05	0.85	0.95	1.00
	Mean	value	0.74	0.88	1.05	0.81	0.93	0.98
	Standard	deviation	7.0%	9.4%	12.8%	8.6%	8.7%	10.6%

ϵ_{max} from 0.004 to 0.005, increased the mean value by 5%. When ϵ_{max} increased from 0.005 to $10.\epsilon_{cc}$ (about 0.020) the mean value increased by 17%. The best mean value (0.98) was obtained by using compressive strength of concrete = $1.28 f'_c$ and $\epsilon_{max} = 0.005$, although the standard deviation was not the best (10.6%). The mean value and the standard deviation using compressive strength = f'_c and $\epsilon_{max} = 0.005$ are (0.88, 9.4%). In this case it can be seen that all the predicted failure loads except for beam A-1 are conservative. Using compressive strength = f'_c and $\epsilon_{max} = 10.\epsilon_{cc}$, the mean values and standard deviation become (1.05, 12.8%). These results of Table 6.11 show that there is an interaction between the maximum compressive strength and the maximum compressive strain and any increase in one of them leads to an increase in the predicted failure load.

The predicted load-deflection curves are shown in Figs. 6.84-85. From these figures, it can be seen that assuming high value of maximum compressive strain ϵ_{max} (even 10 times the strain at the peak of stress ϵ_{cc} , Fig. 6.84a-c) makes most of the predicted load-deflection curves continue in the same trend as the experimental curves and delays failure which means that the reason of failure of these beams is the crushing of compression zone.

In the following, the predicted behaviours of some beams using compressive strength of concrete = $1.28 f'_c$ and $\epsilon_{max} = 0.005$, which gave the best mean value, are presented.

Figs 6.86 to 6.90 show the predicted crack pattern and the stresses in stirrups, compression, and tension reinforcement for beam A-1. The crack patterns at two load factors are shown in Fig. 6.86 which show good agreement with the observed crack pattern. The principal compressive stress-strain curve of concrete at Gauss points under the applied load is shown in Fig. 6.87, in which the compressive strain nearly reached the value of ϵ_{max} (=0.005). The points at which the stirrups have yielded are arranged diagonally in the shear span from the support to the load point (Fig. 6.88). The

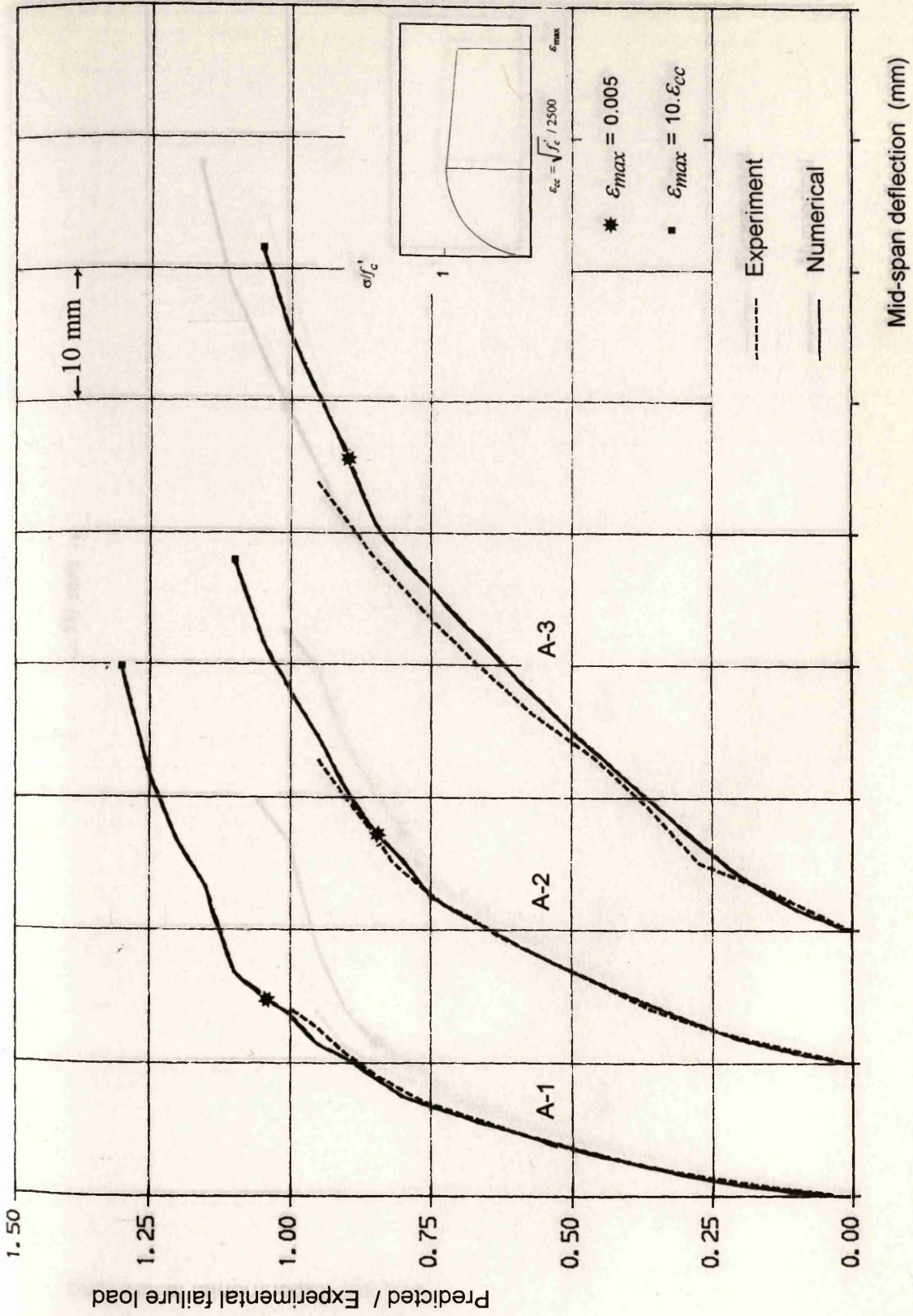


Fig. 6.84a Load-deflection curves for beams A-1, A-2, and A-3 (effect of ϵ_{max}).

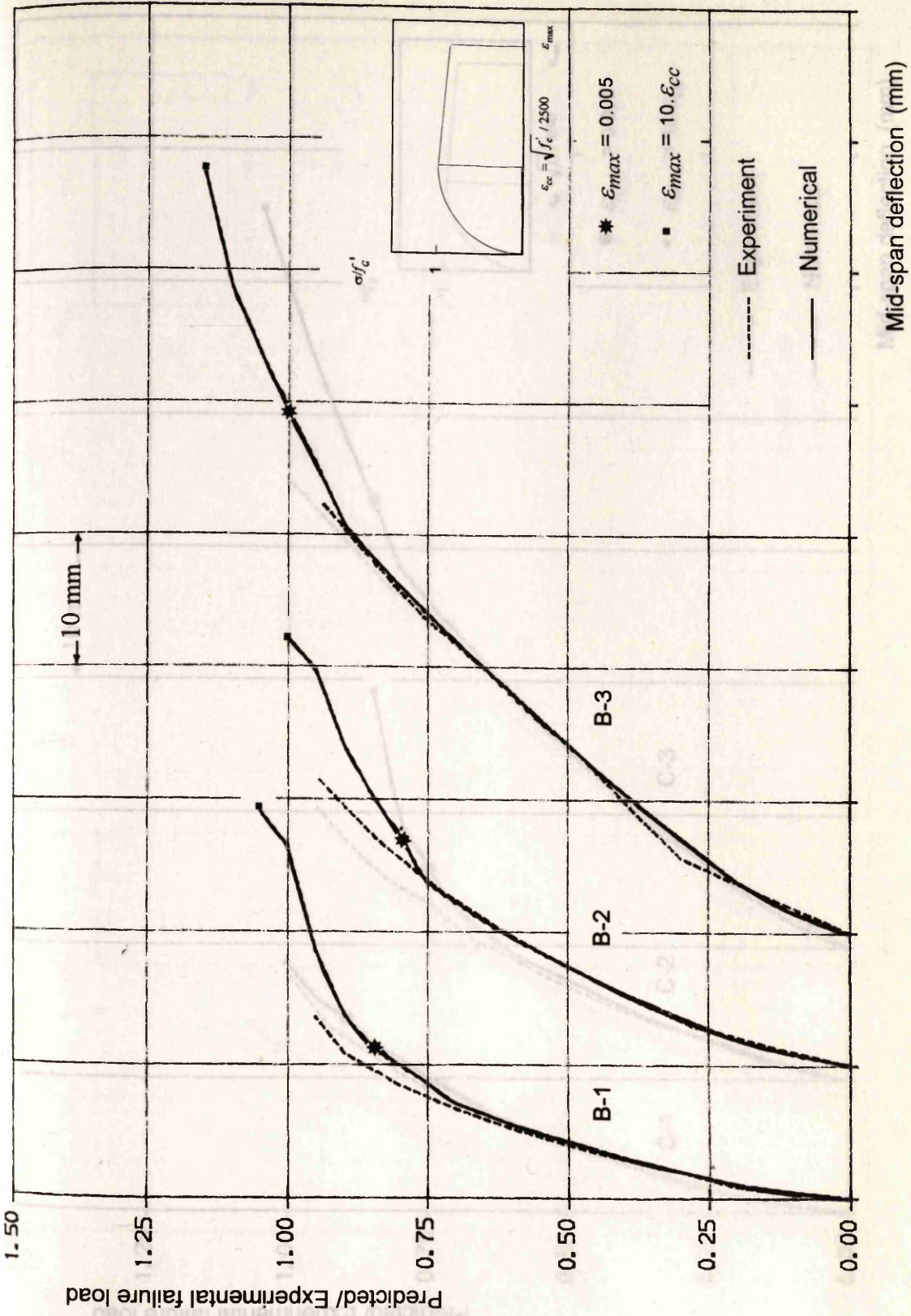


Fig. 6.84b Load-deflection curves for beams B-1, B-2, and B-3 (effect of ϵ_{max}).

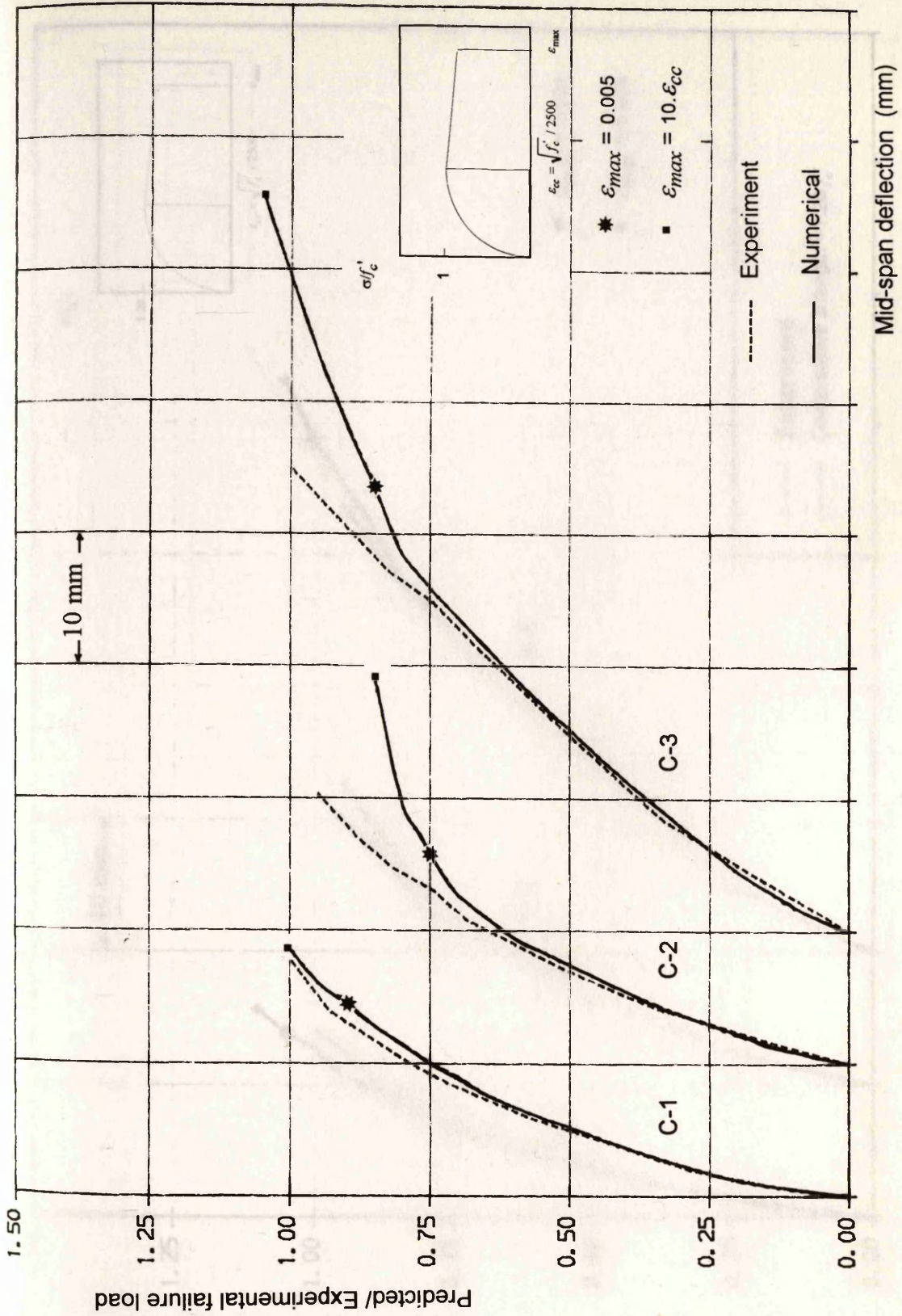


Fig. 6.84c Load-deflection curves for beams C-1, C-2, and C-3 (effect of ϵ_{max}).

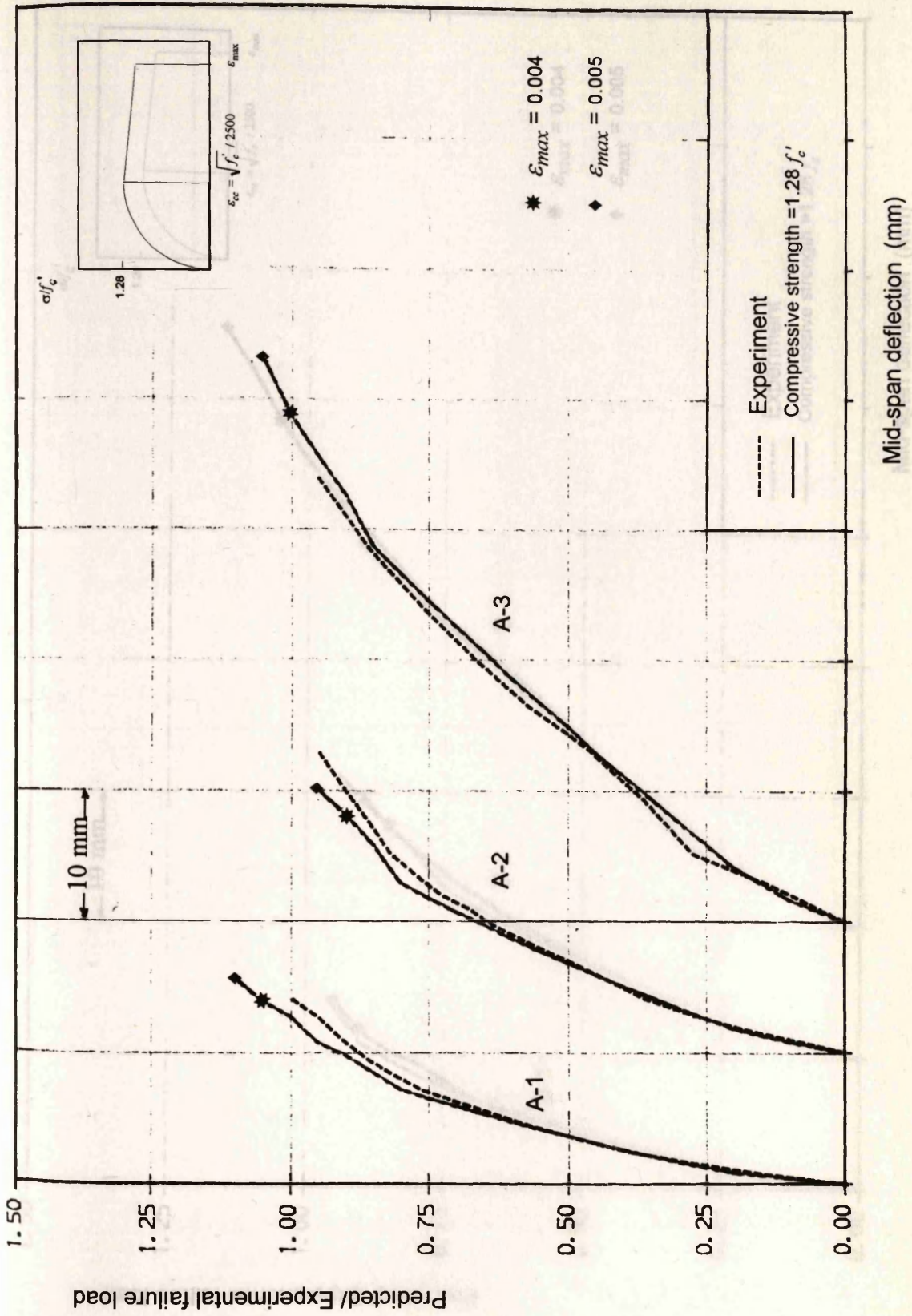


Fig. 6.85a Load-deflection curves for beams A-1, A-2, and A-3 (effect of ϵ_{max}).

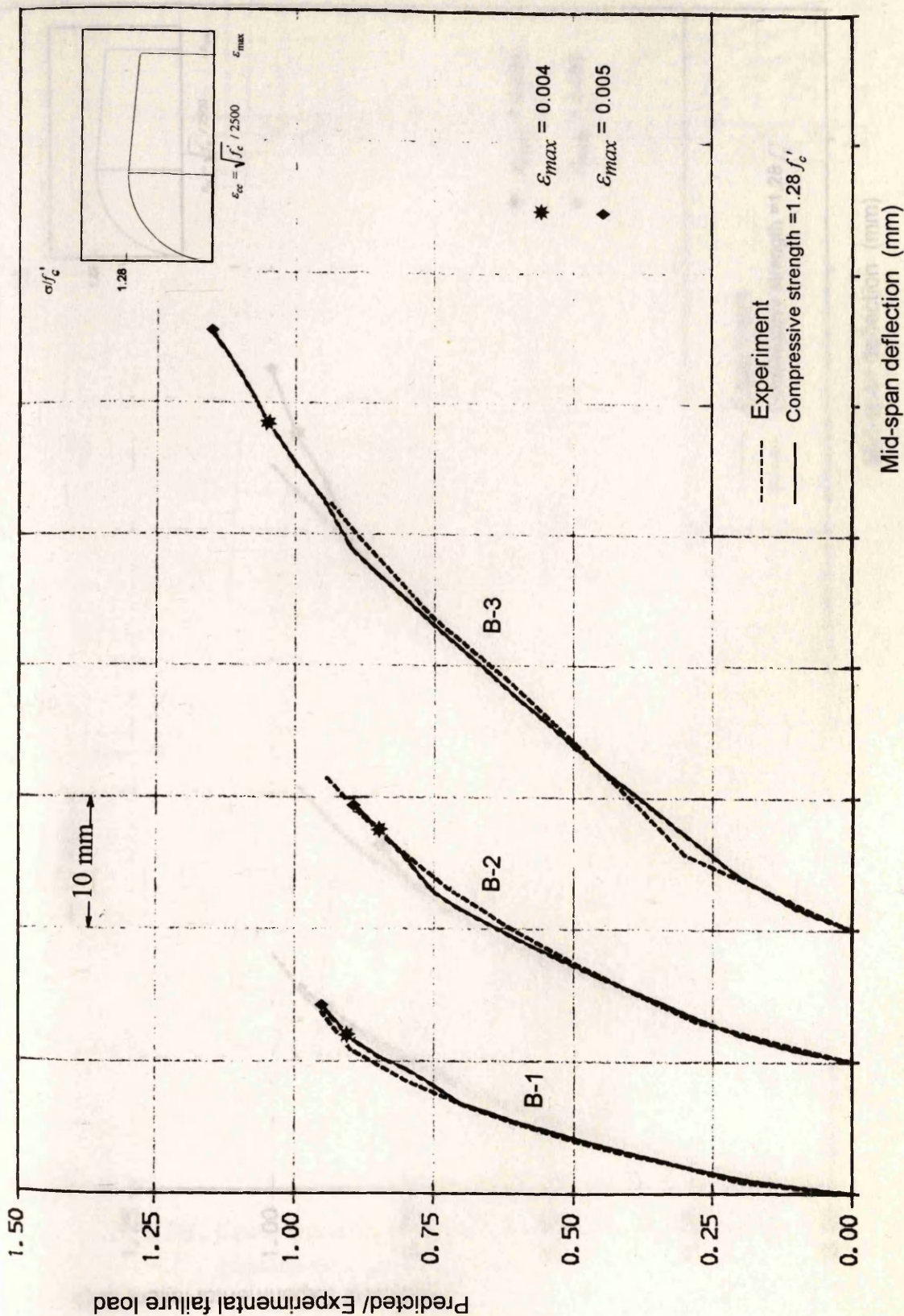


Fig. 6.85b Load-deflection curves for beams B-1, B-2, and B-3 (effect of ϵ_{max}).

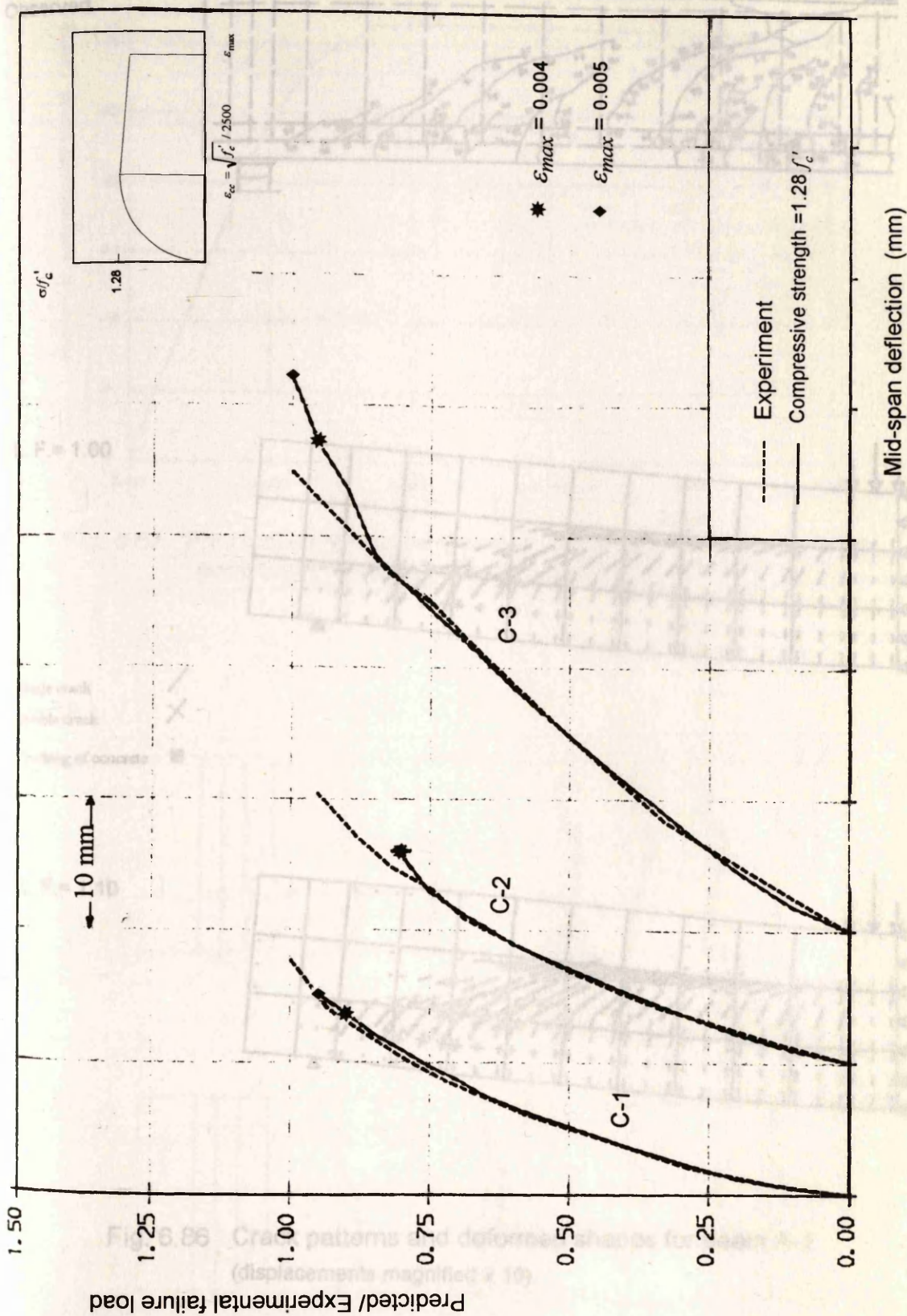


Fig. 6.85c Load-deflection curves for beams C-1, C-2, and C-3 (effect of ϵ_{max}).

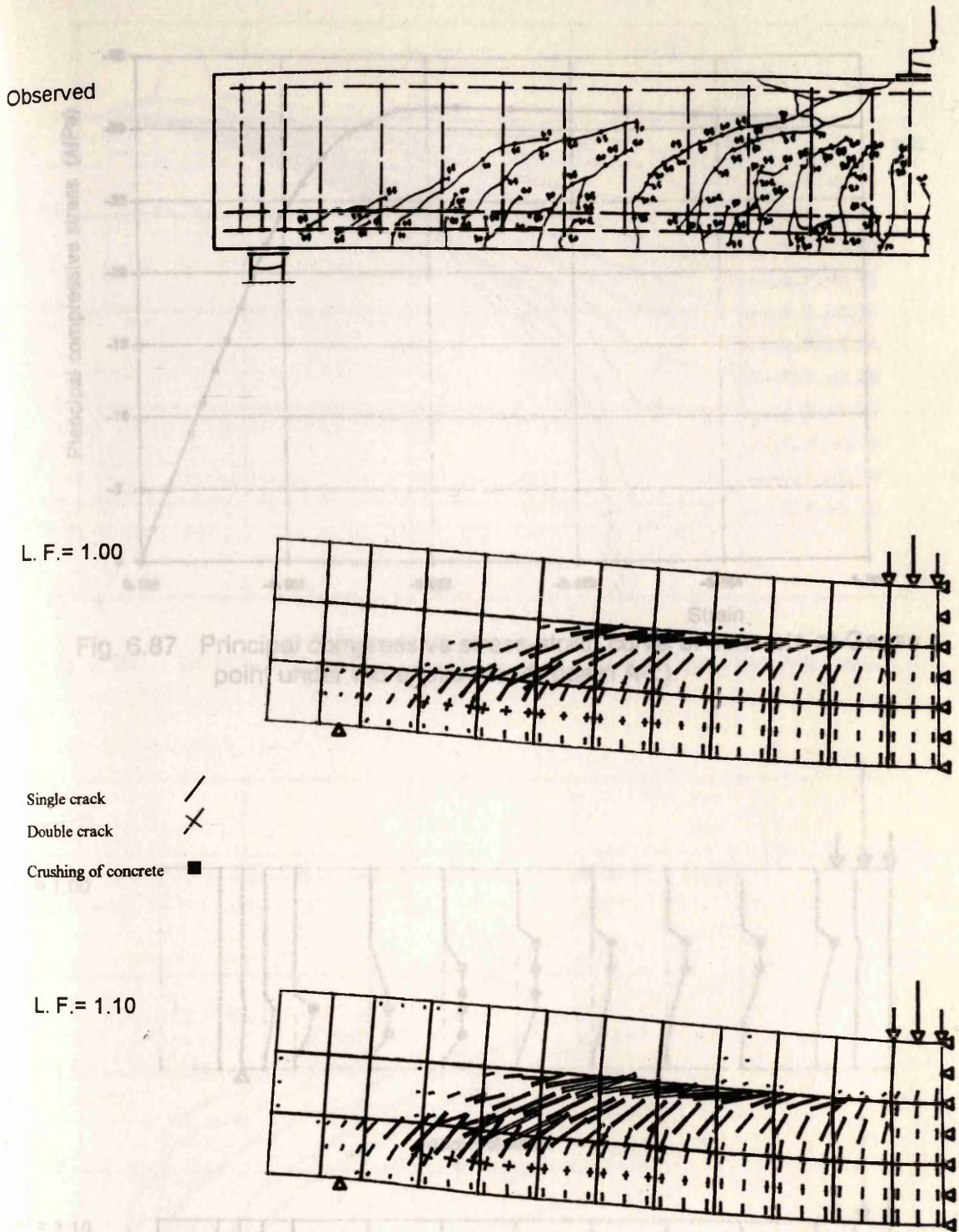


Fig. 6.86 Crack patterns and deformed shapes for beam A-1 (displacements magnified x 10).

Fig. 6.88 Stresses in shear reinforcement (beam A-1)

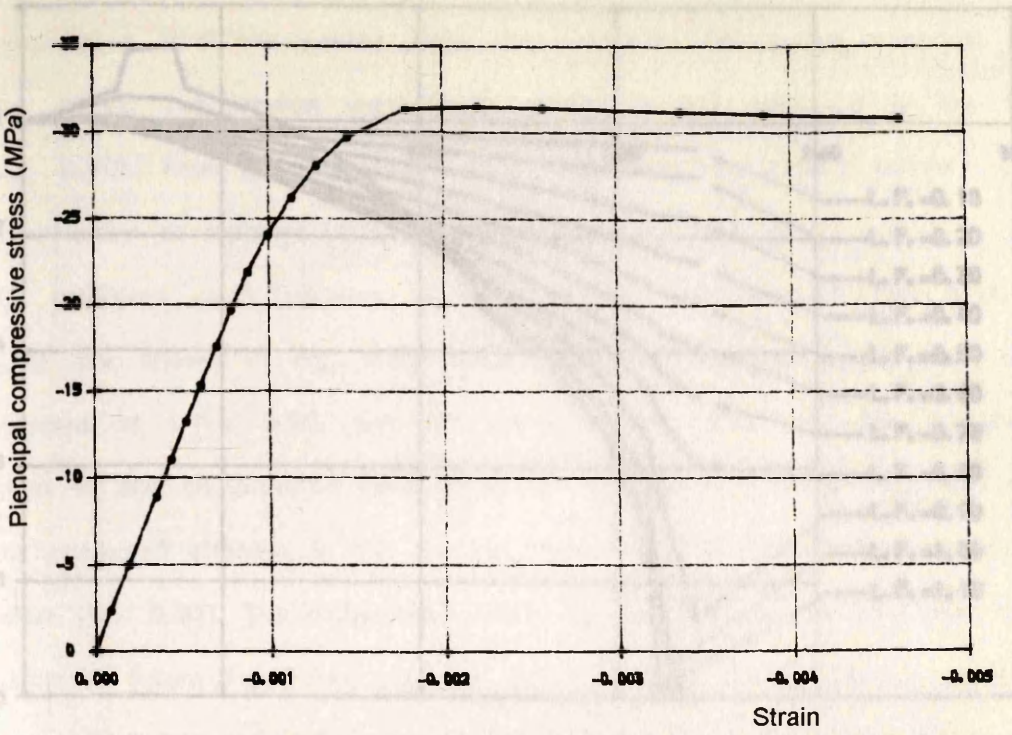


Fig. 6.87 Principal compressive stress-strain curve of concrete at Gauss point under the applied load (beam A-1).

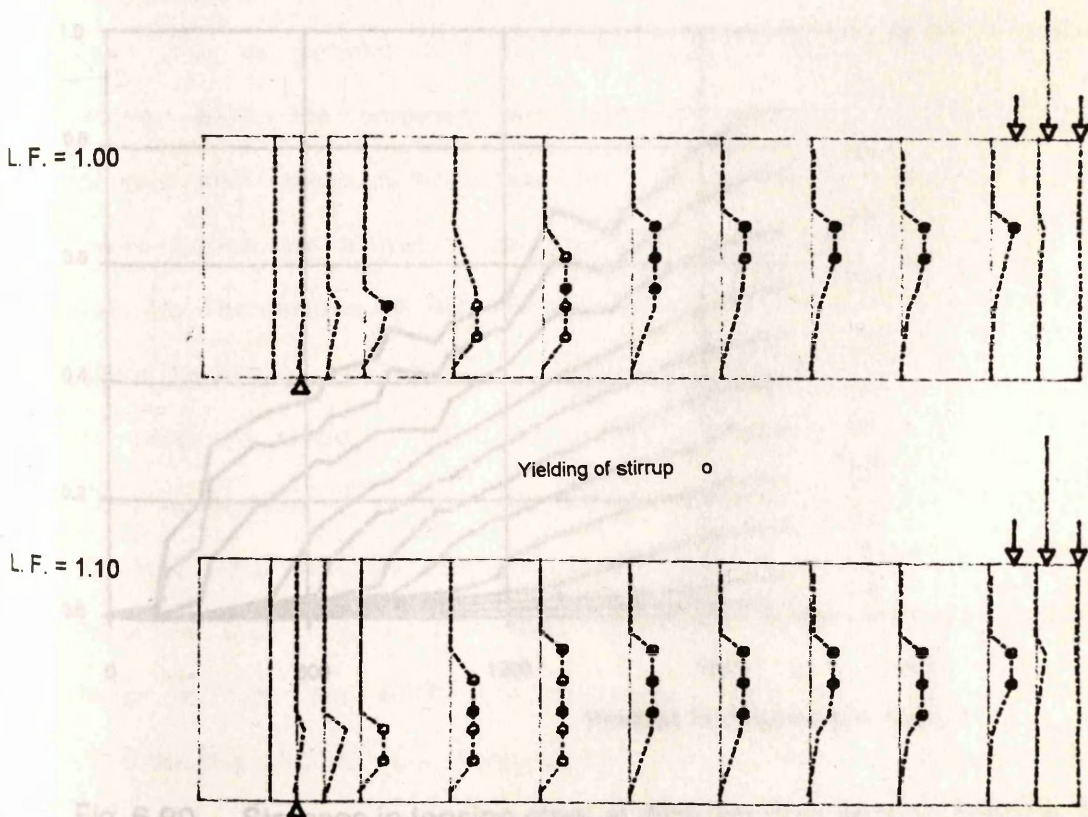


Fig. 6.88 Stresses in shear reinforcement (beam A-1).

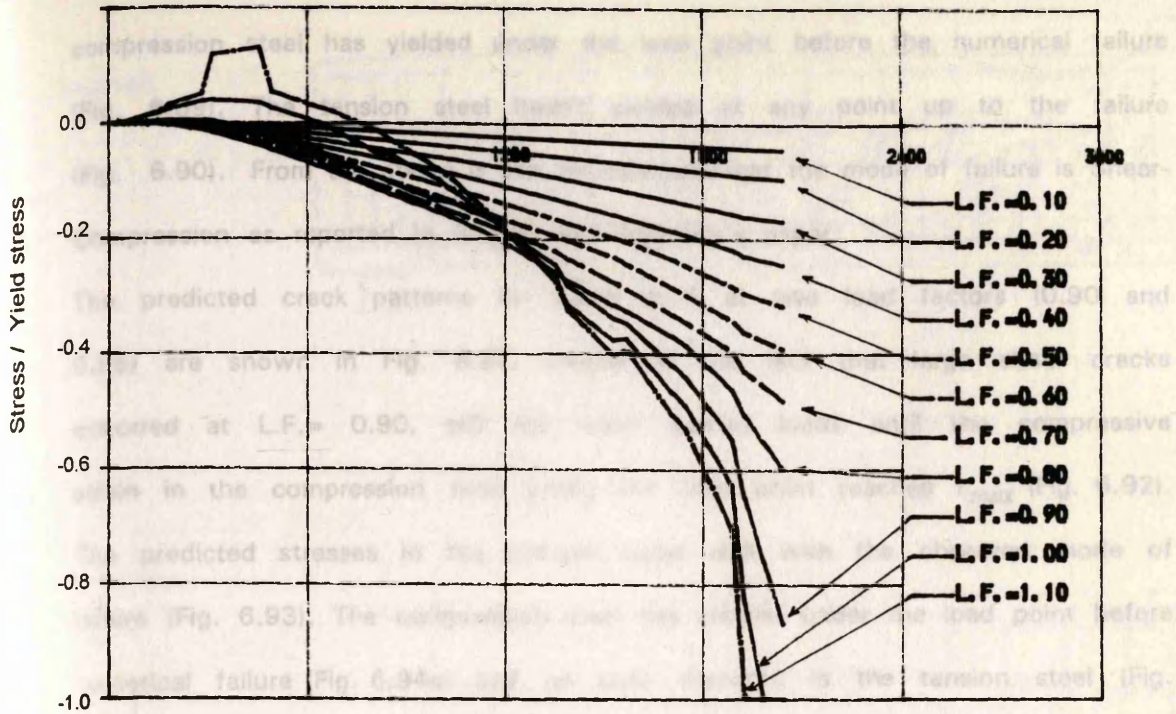


Fig. 6.89 Stresses in compression steel at different load factors (beam A-1).

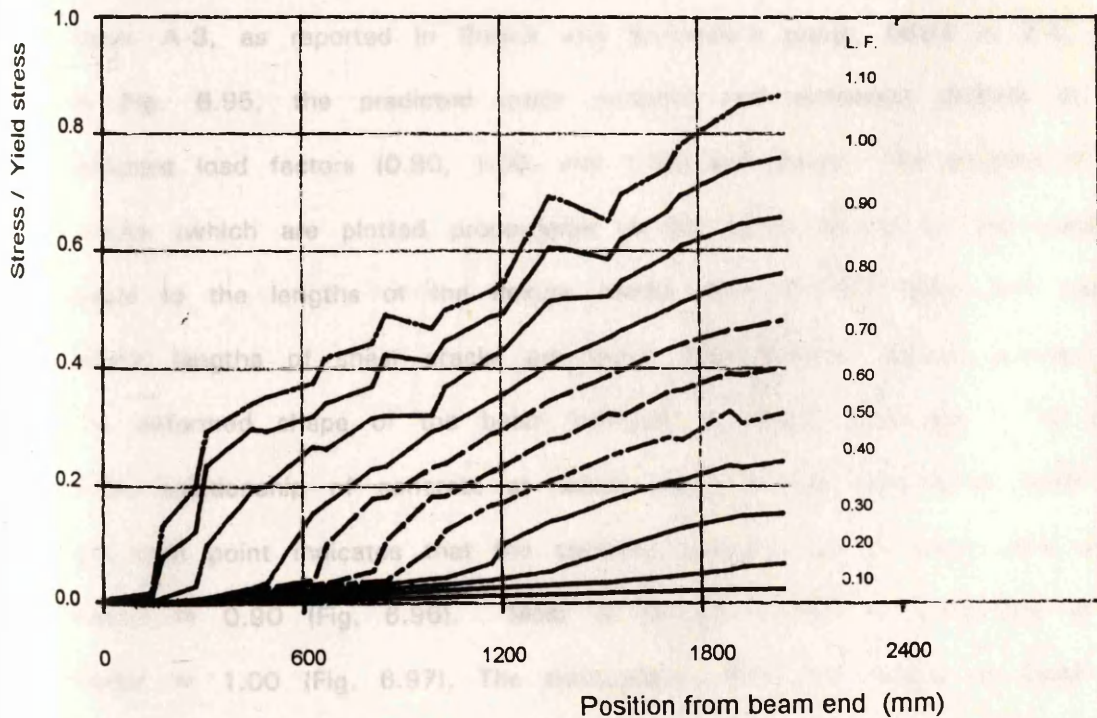


Fig. 6.90 Stresses in tension steel at different load factors (beam A-1).

compression steel has yielded under the load point before the numerical failure (Fig. 6.89). The tension steel hasn't yielded at any point up to the failure (Fig. 6.90). From the above it can be concluded that the mode of failure is Shear-Compression as reported in Bresler and Scordelis's paper.

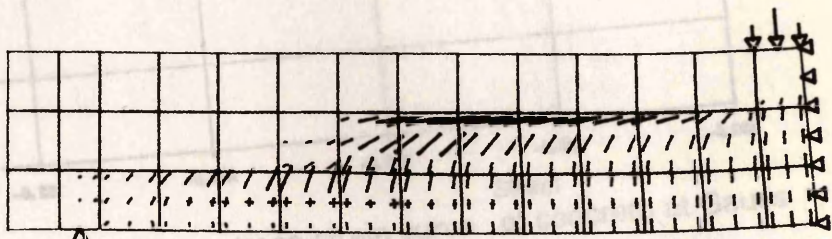
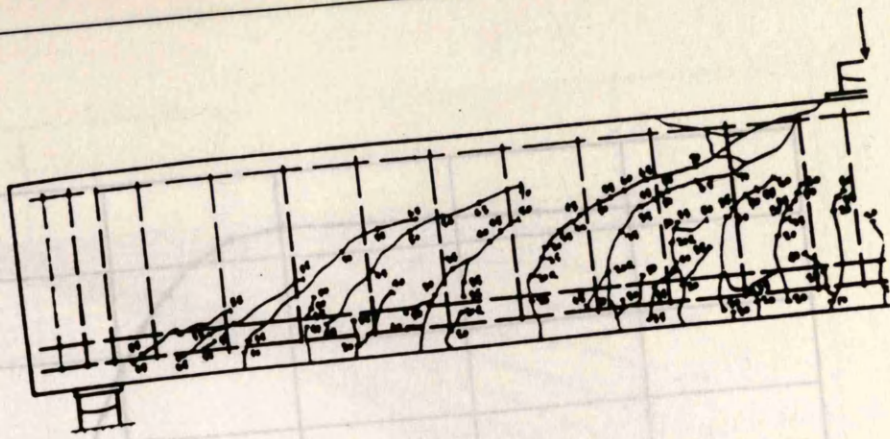
The predicted crack patterns for beam A-2 at two load factors (0.90 and 0.95) are shown in Fig. 6.91. In spite of the fact that large shear cracks occurred at L.F.= 0.90, still the beam carried loads until the compressive strain in the compression zone under the load point reaches ϵ_{max} (Fig. 6.92). The predicted stresses in the stirrups agree well with the observed mode of failure (Fig. 6.93). The compression steel has yielded under the load point before numerical failure (Fig. 6.94a) and no yield occurred in the tension steel (Fig. 6.94b). The predicted failure mode for this beam is Shear-Compression. The main reason of failure is, like beam A-1, the crushing of concrete in the compression zone under the load point.

Beam A-3, as reported in Bresler and Scordelis's paper, failed in *F-C* mode. In Fig. 6.95, the predicted crack patterns and deformed shapes at three different load factors (0.90, 1.00, and 1.05) are shown. The lengths of shear cracks (which are plotted proportional to the strain normal to the crack) are equal to the lengths of the flexure cracks (and not like beam A-1 and A-2 where lengths of shear cracks are larger than that of flexure cracks). Also, the deformed shape of the beam indicates a ductile behaviour. The stress-strain relationship of concrete at Gauss point in the compression zone under the load point indicates that the concrete entered the softening zone at load factor = 0.90 (Fig. 6.96). Most of stirrups started to yield late at Load factor = 1.00 (Fig. 6.97). The compression steel has yielded at Load factor = 0.90 (Fig. 6.98a). The stress in tension steel nearly reached yield stress at the last converged increment (Fig. 6.98b). The reason for failure is the crushing of concrete due to increase in the compressive strain of more than ϵ_{max} (=0.005). The predicted failure mode is nearer to Flexure-Compression.

Observed

Principal compressive stress (MPa)

L. F. = 0.90



- Single crack /
- Double crack X
- Crushing of concrete ■

Fig. 6.92 Principal compressive stress point under the applied load (beam A-2)

L. F. = 0.95

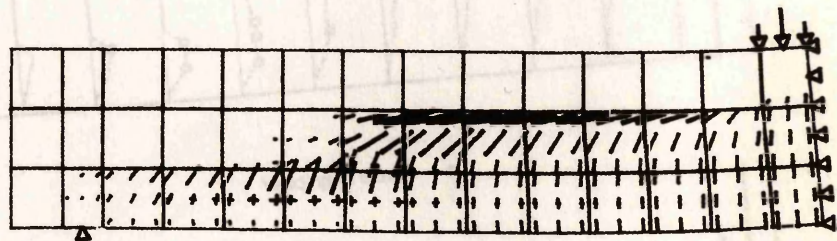


Fig. 6.91 Crack patterns and deformed shapes for beam A-2 (displacements magnified x 10).

Fig. 6.93 Stresses in shear (beam A-2)

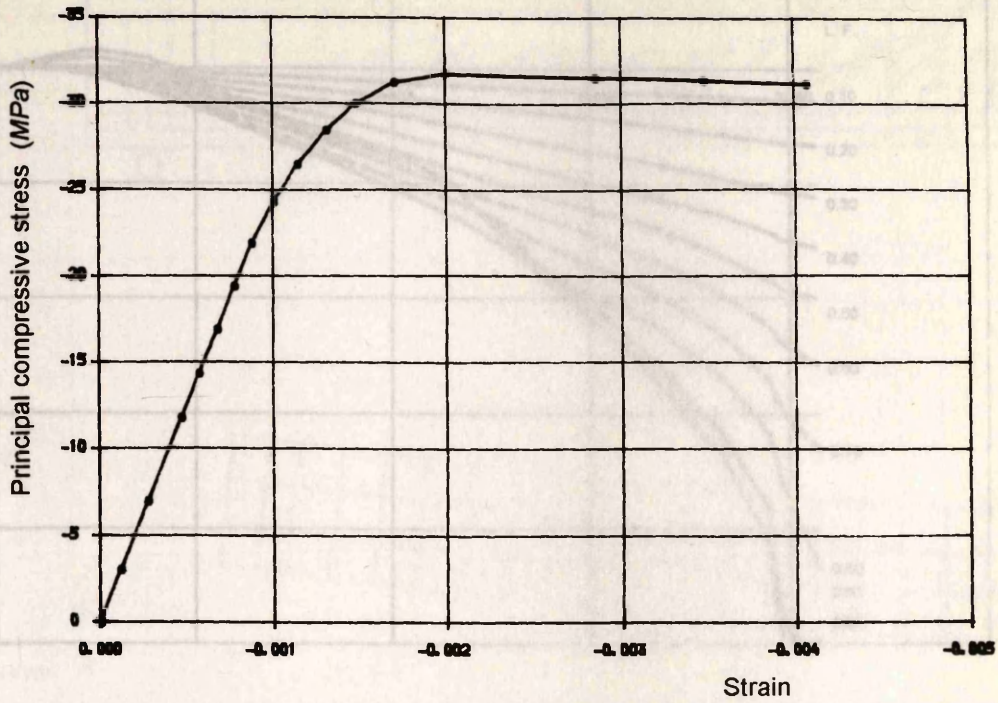


Fig. 6.92 Principal compressive stress-strain curve of concrete at Gauss point under the applied load (beam A-2).

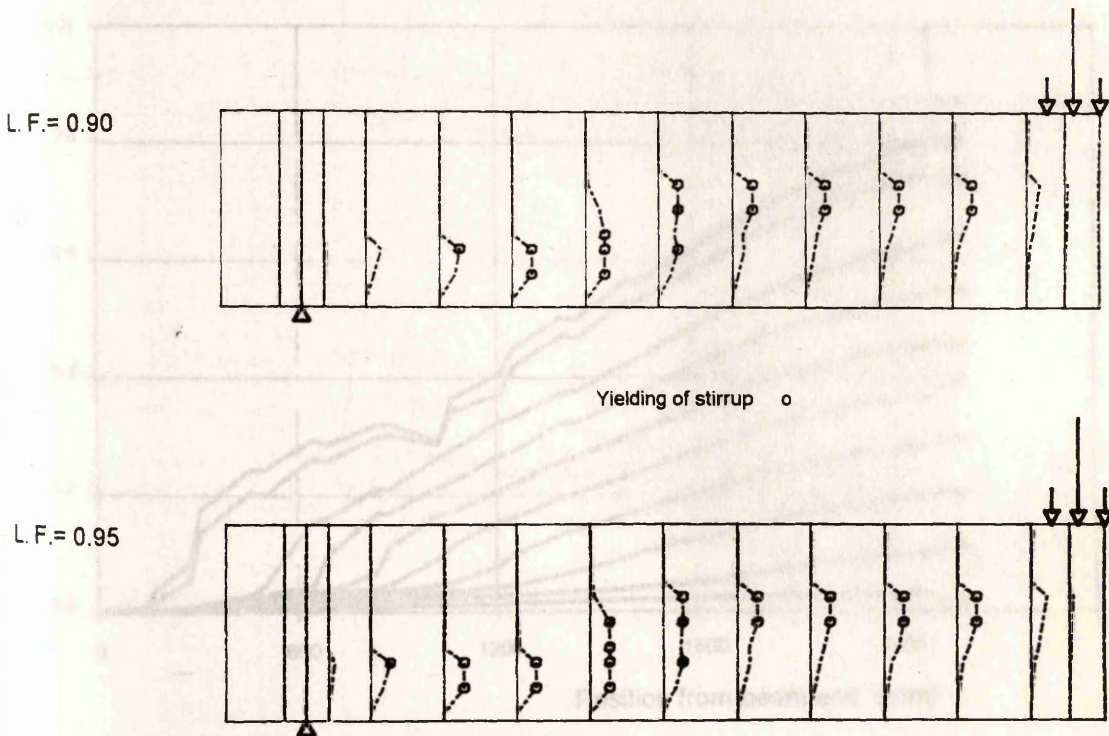


Fig. 6.93 Stresses in shear reinforcement (beam A-2).

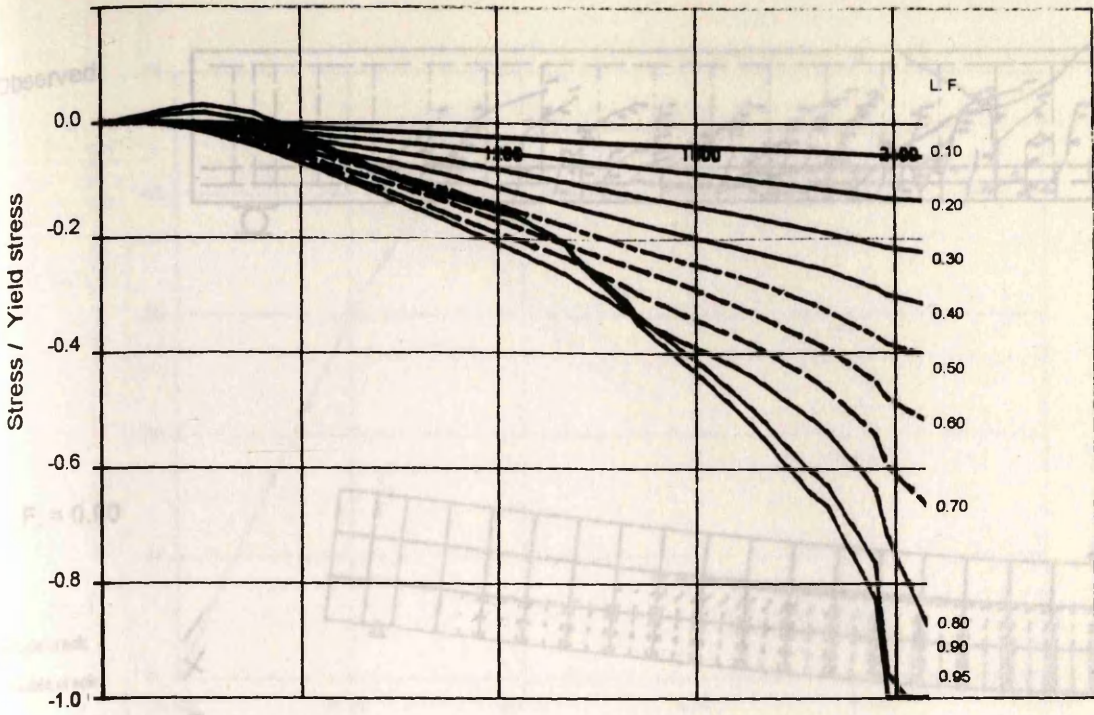


Fig. 6.94a Stresses in compression steel at different load factors (beam A-2).

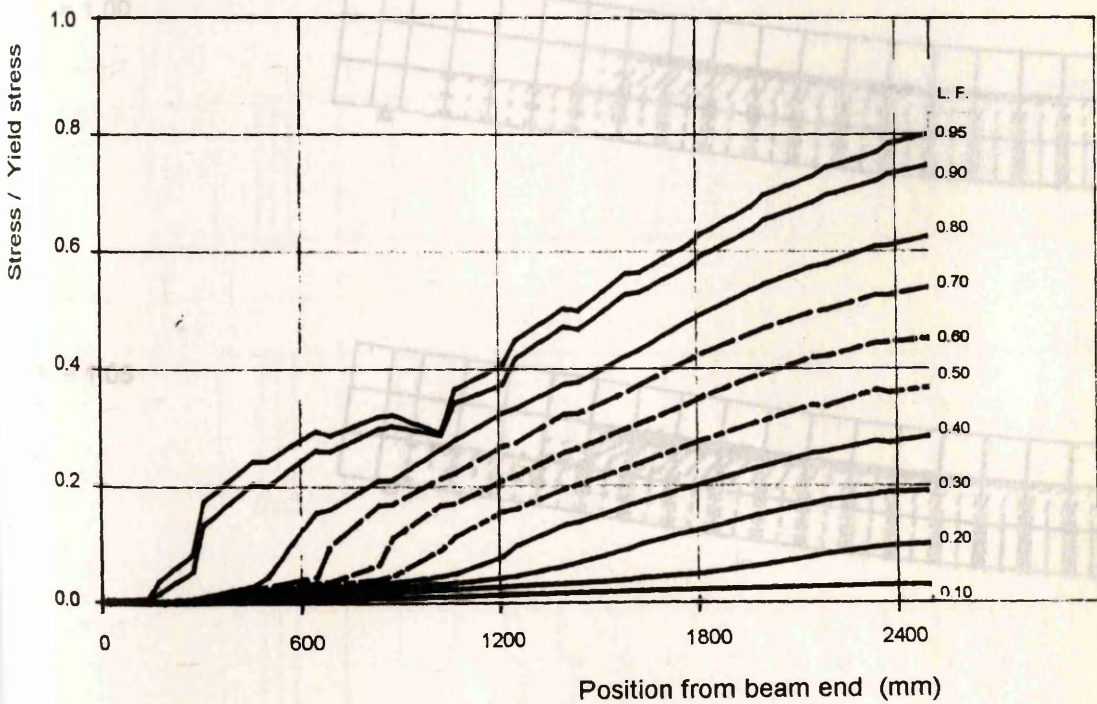


Fig. 6.94b Stresses in tension steel at different load factors (beam A-2).

Fig. 6.95 Crack patterns and deformed shapes for beam A-3 (displacements magnified x 10)

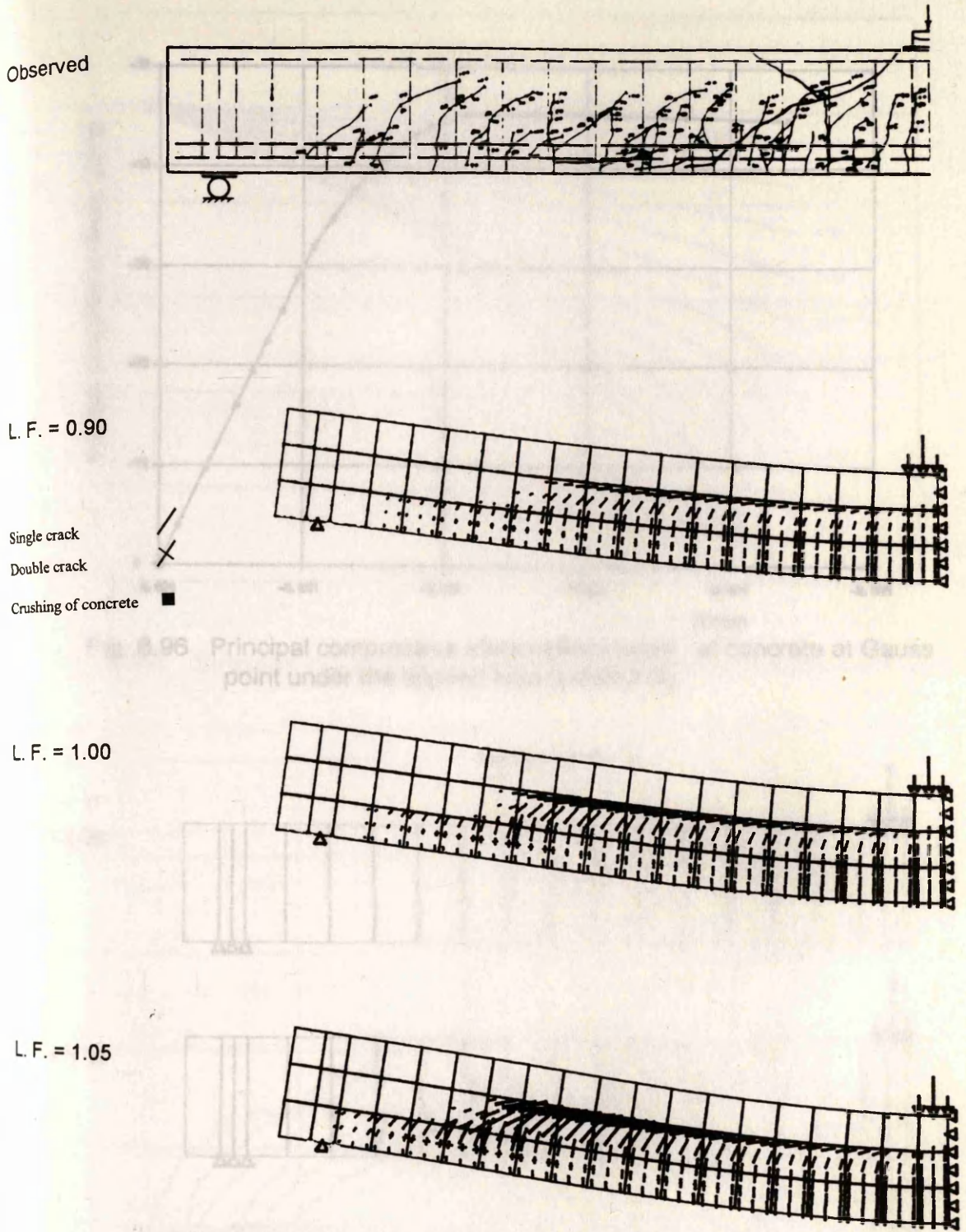


Fig. 6.95 Crack patterns and deformed shapes for beam A-3 (displacements magnified x 10).

Fig. 6.97 Stresses in beam A-3

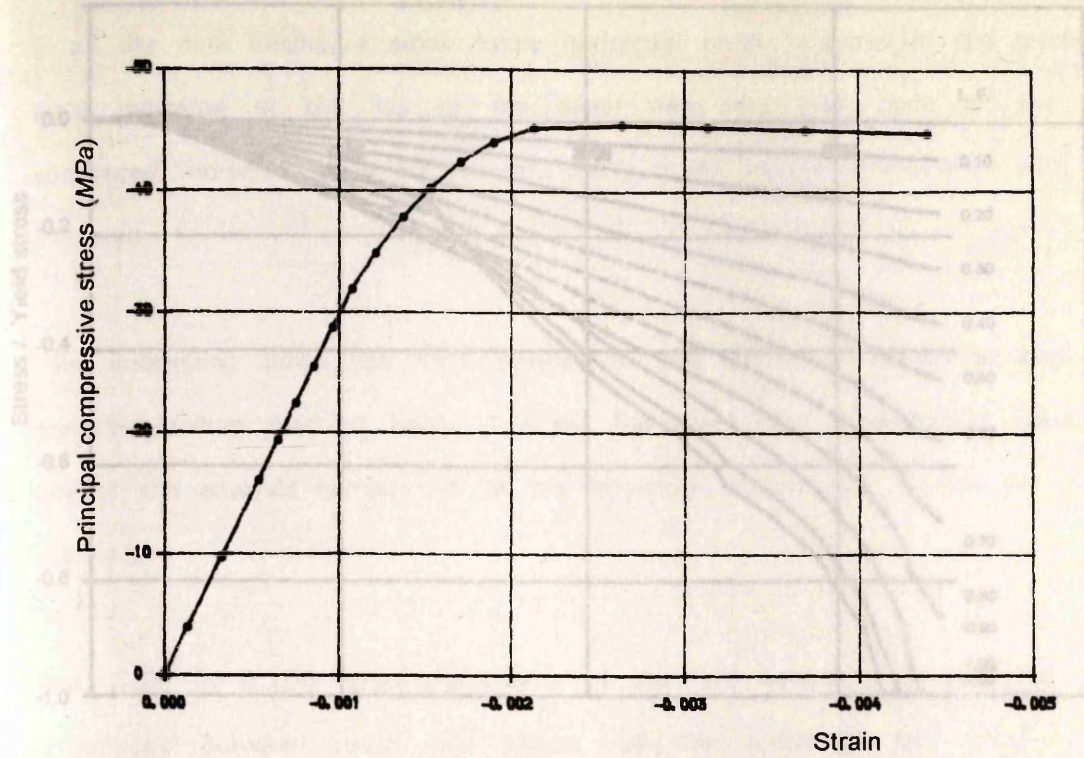


Fig. 6.96 Principal compressive stress-strain curve of concrete at Gauss point under the applied load (beam A-3).

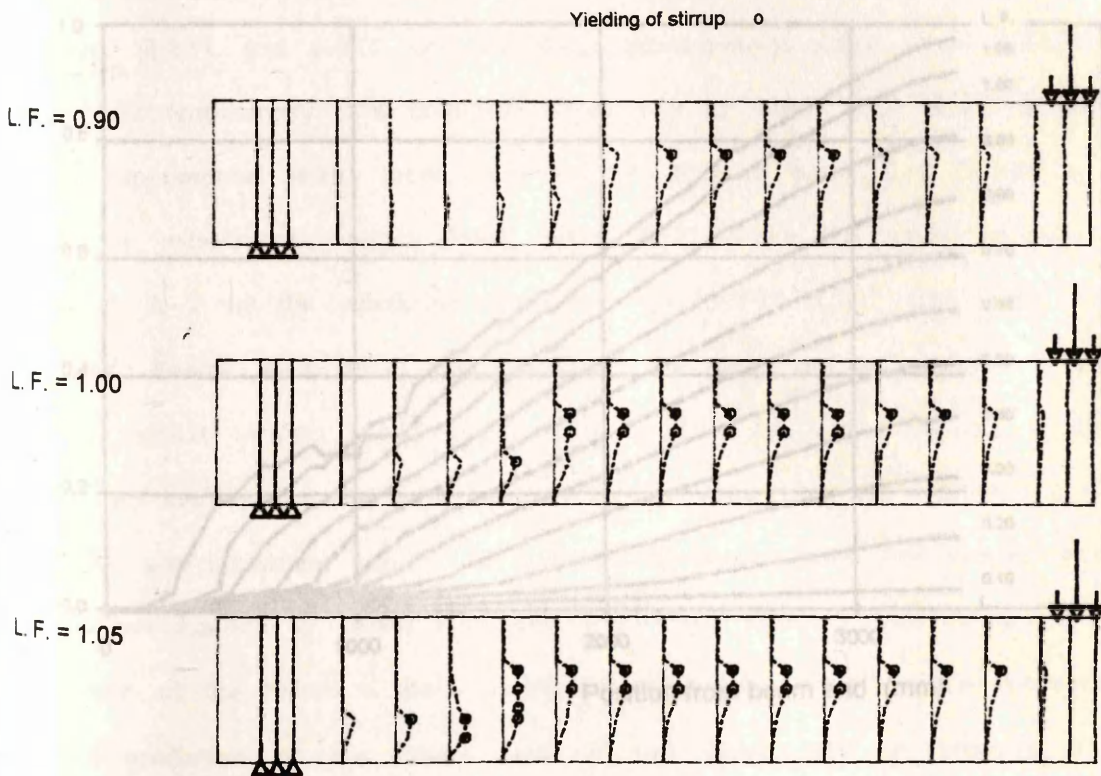


Fig. 6.98b Stresses in tension steel at different load factors (beam A-3).

Fig. 6.97 Stresses in shear reinforcement (beam A-3).

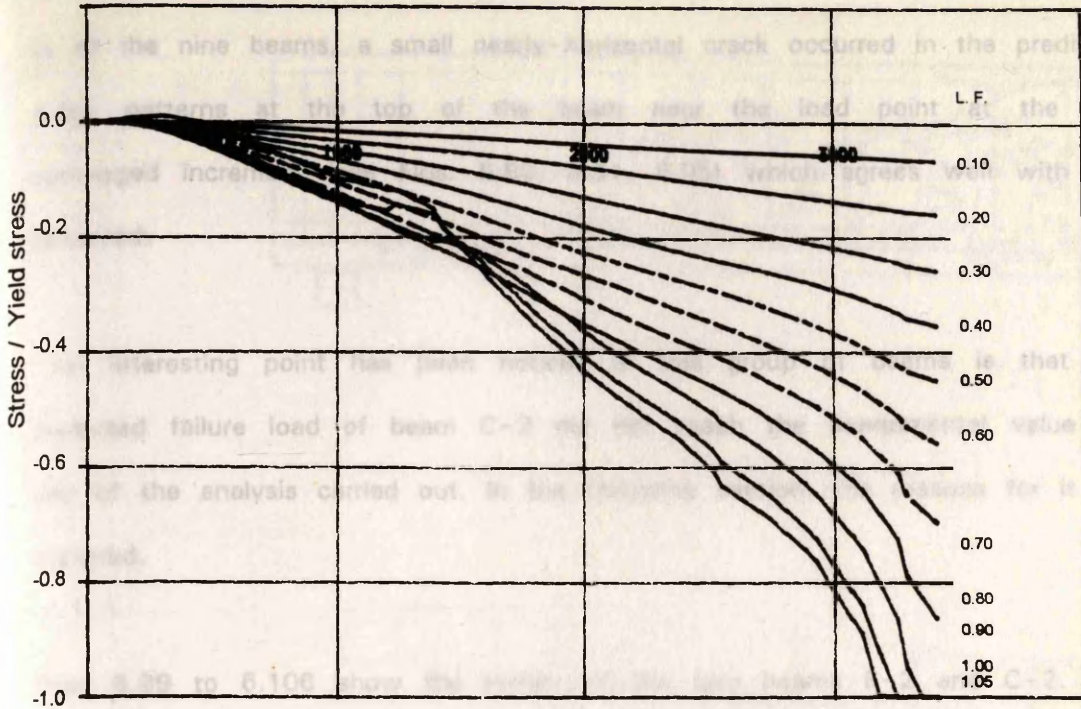


Fig. 6.98a Stresses in compression steel at different load factors (beam A-3).

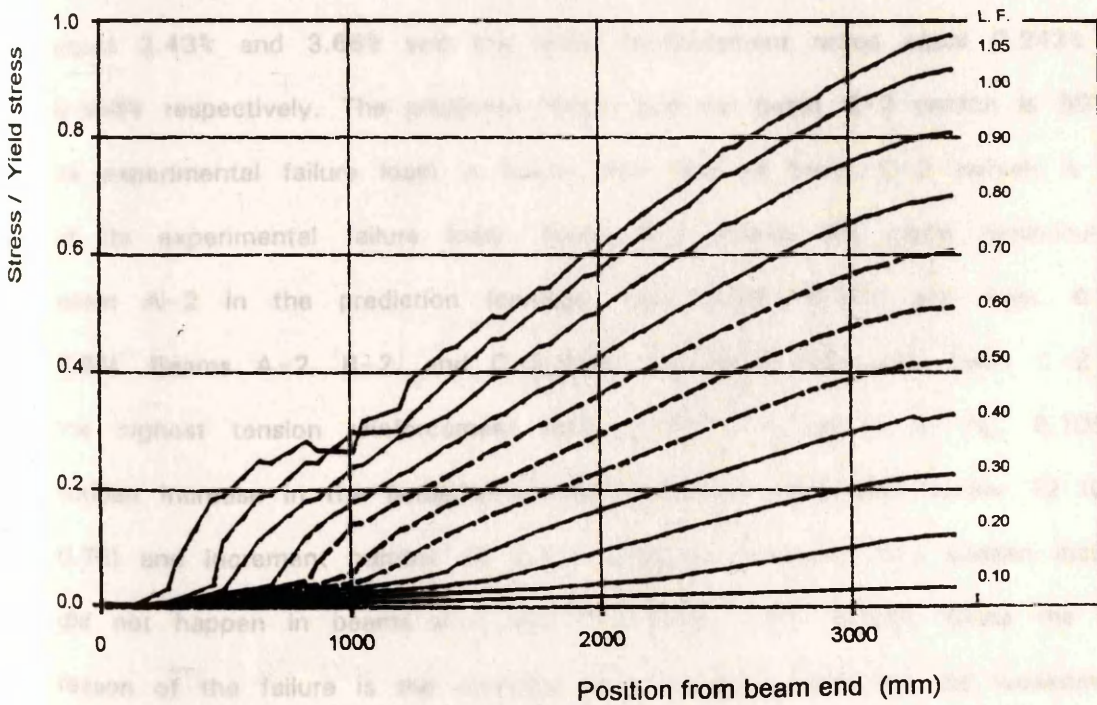


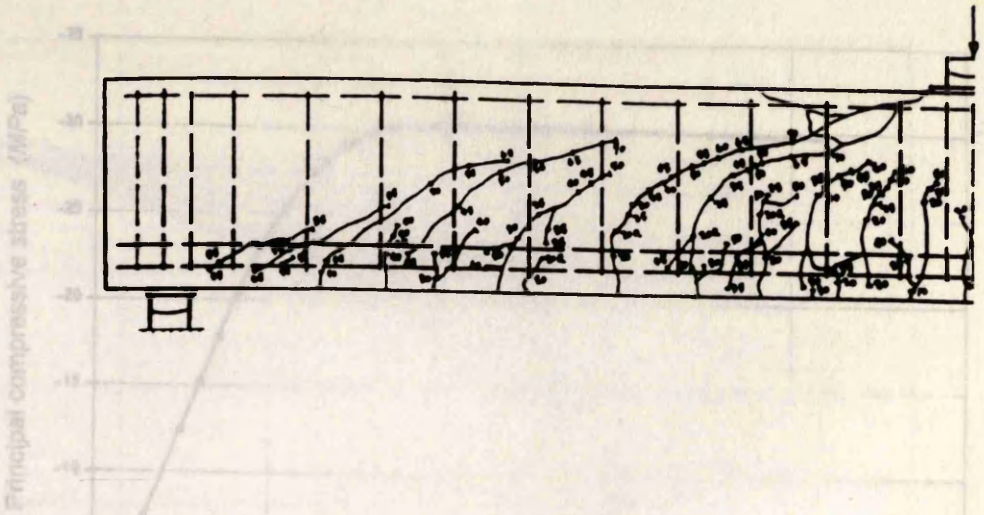
Fig. 6.98b Stresses in tension steel at different load factors (beam A-3).

In all the nine beams, a small nearly-horizontal crack occurred in the predicted crack patterns at the top of the beam near the load point at the last converged increment (see Figs. 6.86, 6.91, 6.95) which agrees well with the observed.

An interesting point has been noticed in this group of beams is that the predicted failure load of beam C-2 did not reach the experimental value for any of the analysis carried out. In the following section, the reasons for it are explored.

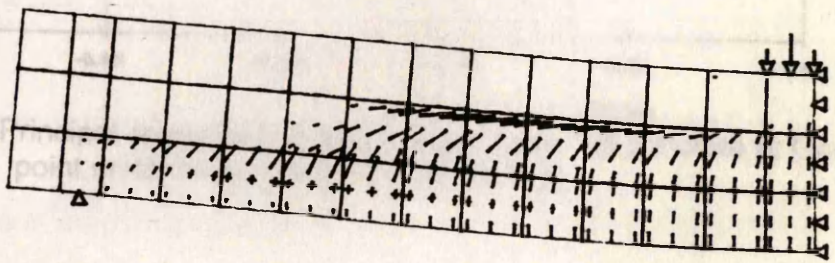
Figs. 6.99 to 6.106 show the results of the two beams B-2 and C-2. The differences between these two beams are the width of the cross-section (228.6, 152.4 mm respectively) and the spacing between the stirrups (190.5, 209.6 mm respectively). These differences make the tension reinforcement ratios equal 2.43% and 3.66% and the shear reinforcement ratios equal 0.243% and 0.366% respectively. The predicted failure load for beam B-2 (which is 90% of its experimental failure load) is better than that of beam C-2 (which is 80% of its experimental failure load). Beam B-2 shows the same behaviour as beam A-2 in the prediction (compare Figs. 6.99 - 6.102 with Figs. 6.91 - 6.94). Beams A-2, B-2, and C-2 have the same a/d ratio. Beam C-2 has the highest tension reinforcement ratio (3.66%). As shown in Fig. 6.105, a sudden increase in the compressive strain between increment number 12 (L.F.= 0.75) and increment number 13 (L.F.= 0.80) is observed. This sudden increase did not happen in beams A-2 and B-2 (Figs. 6.92, 6.100). Since the main reason of the failure is the crushing of compression zone so, the weakness in the prediction of the failure load of this beam may be because of the assumed stress-strain curve of concrete.

Observed



L. F. = 0.85

- Single crack /
- Double crack X
- Crushing of concrete ■



L. F. = 0.90

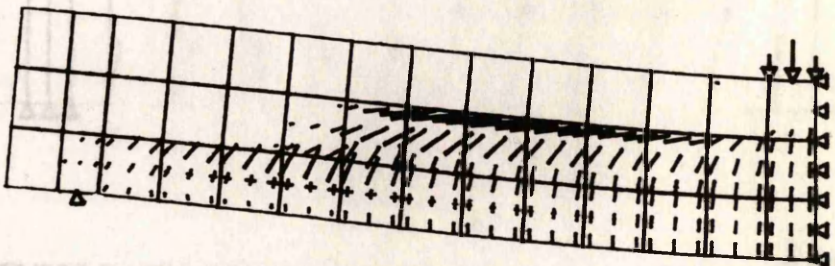


Fig. 6.99 Crack patterns and deformed shapes for beam B-2 (displacement magnified x 10)

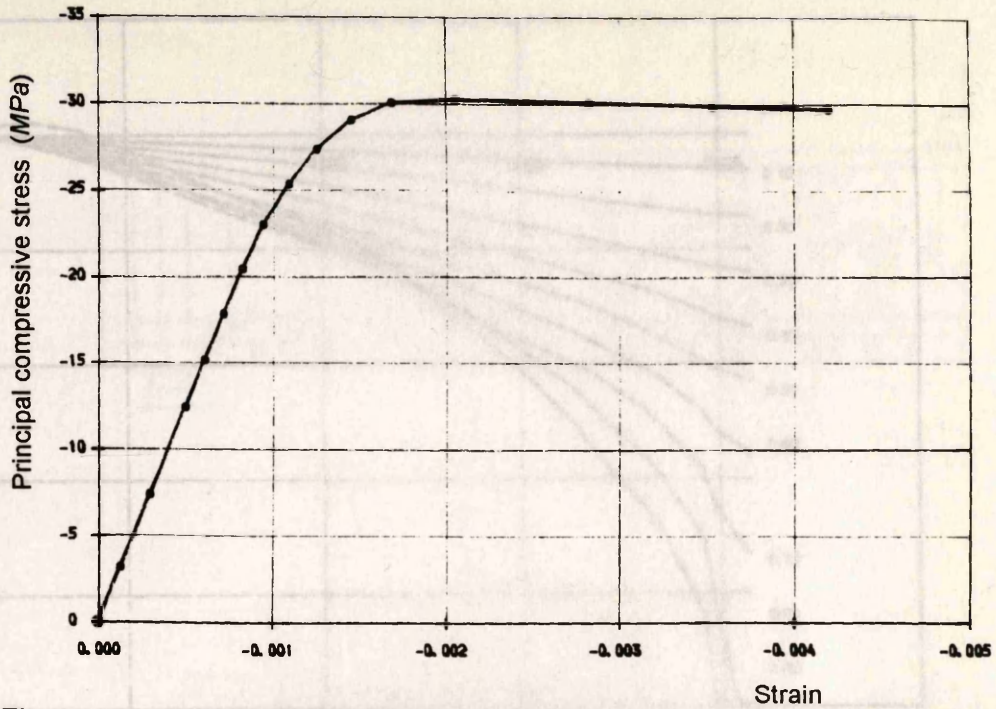


Fig. 6.100 Principal compressive stress-strain curve of concrete at Gauss point under the applied load (beam B-2).

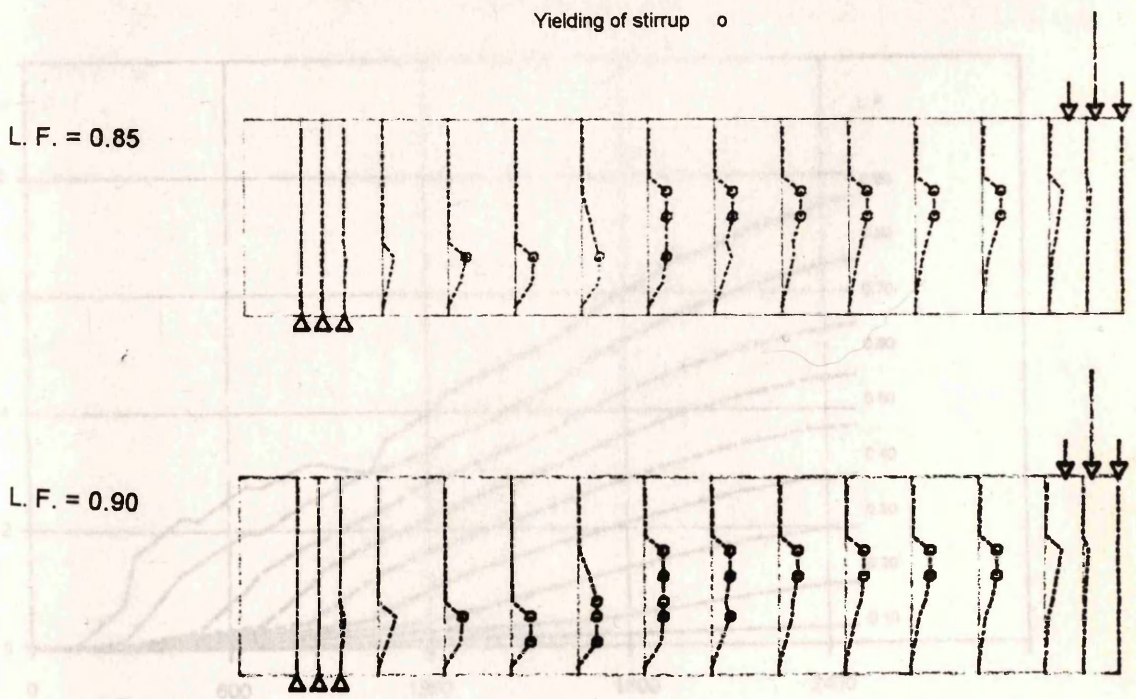


Fig. 6.101 Stresses in shear reinforcement (beam B-2).

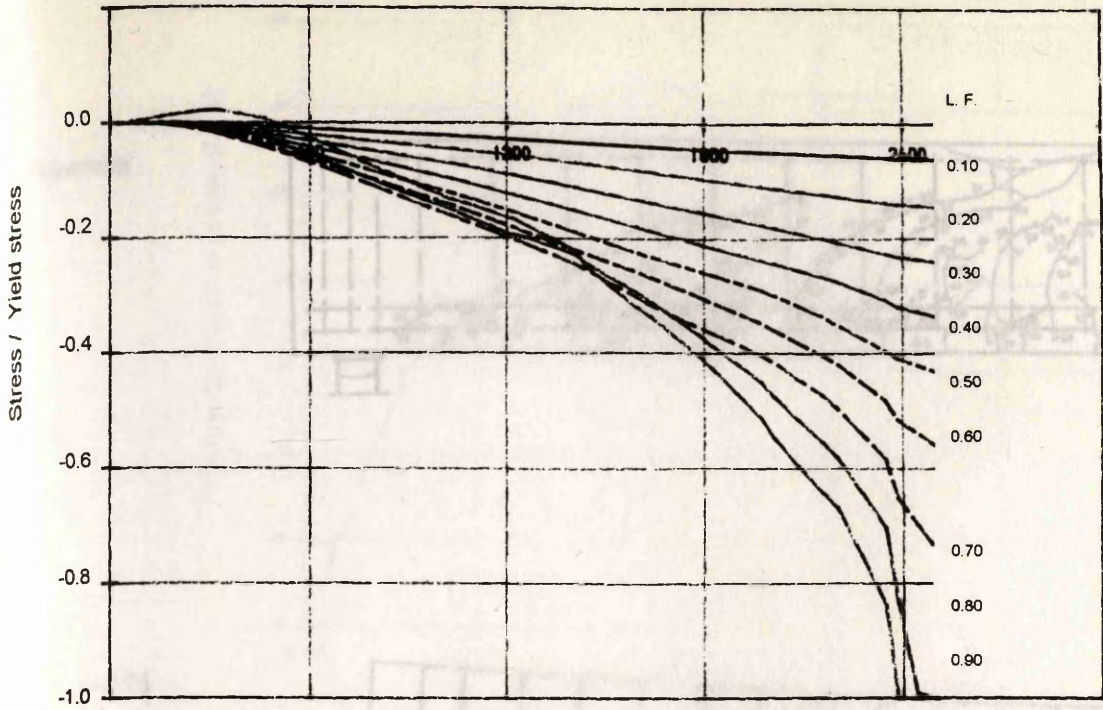


Fig. 6.102a Stresses in compression steel at different load factors (beam B-2).

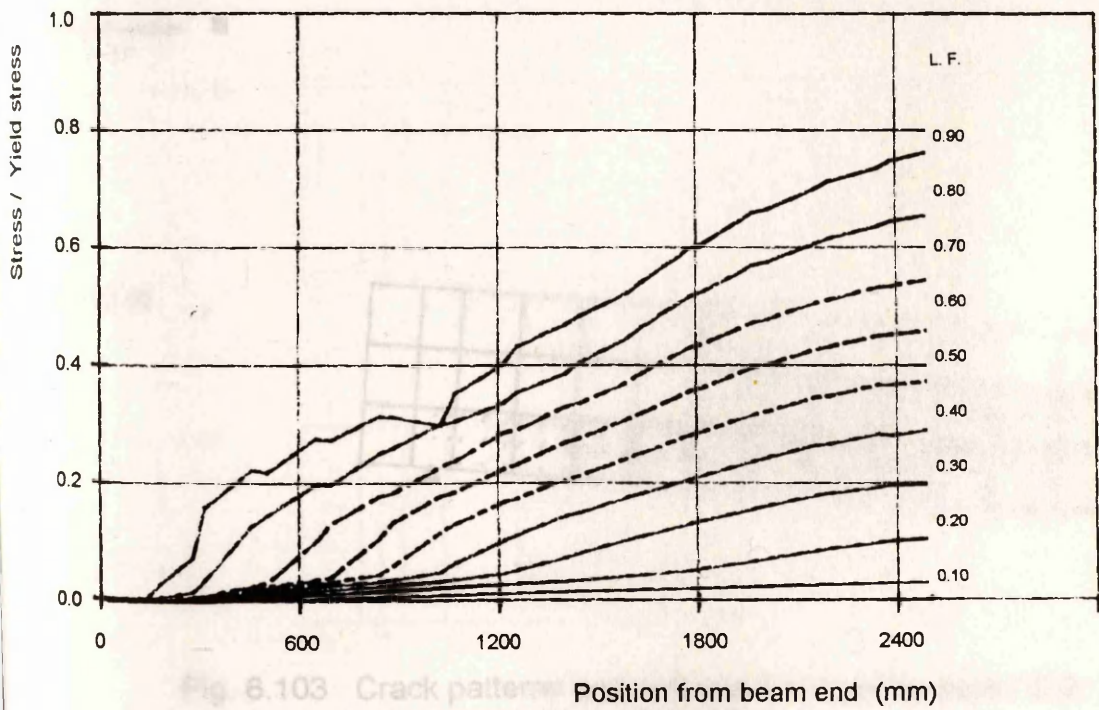
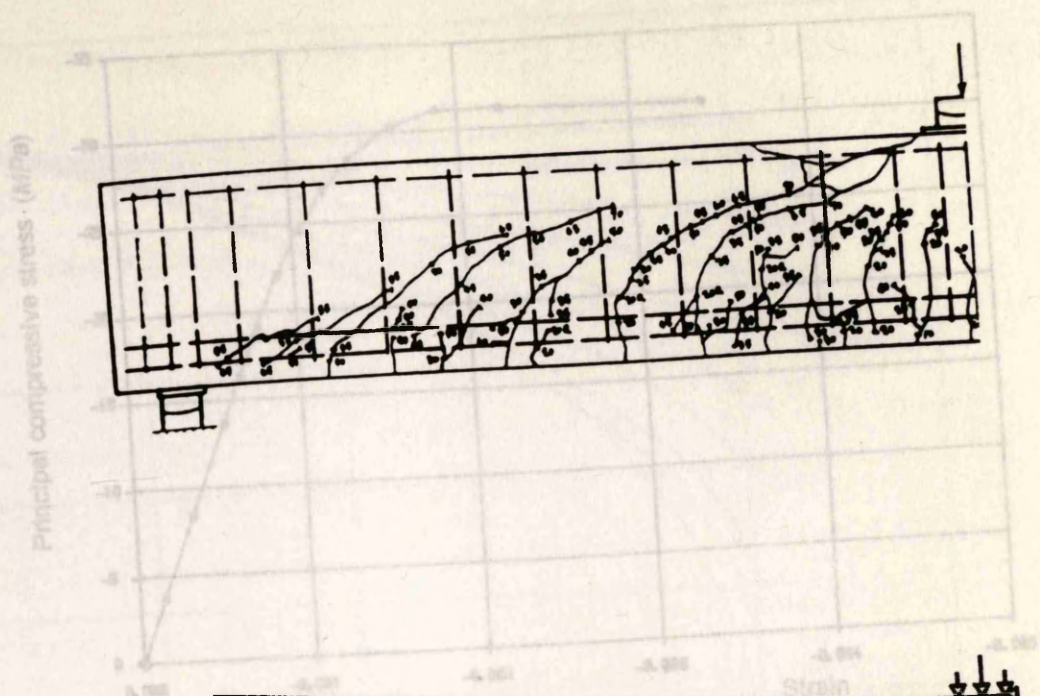


Fig. 6.103 Crack patterns (displacement) magnified

Fig. 6.102b Stresses in tension steel at different load factors (beam B-2).

Observed

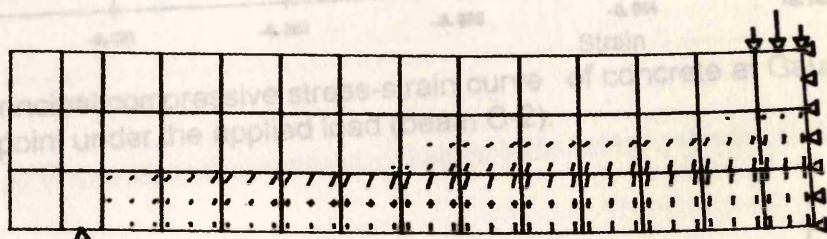


L. F. = 0.75

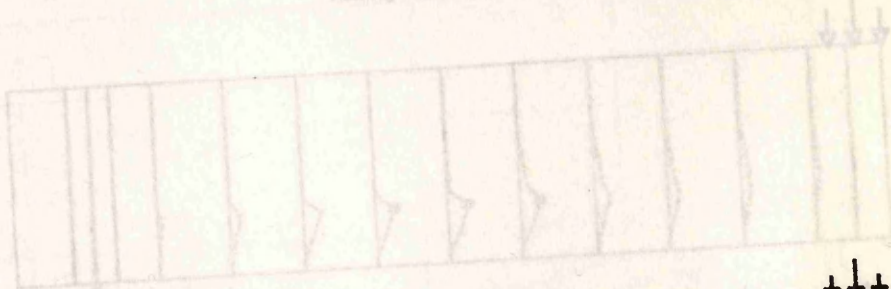
Single crack

Double crack

Crushing of concrete



L. F. = 0.75



L. F. = 0.80

L. F. = 0.80

Fig. 6.103 Crack patterns and deformed shapes for beam C-2 (displacements magnified x 10).

Fig. 6.105 Stresses in shear reinforcement (beam C-2)

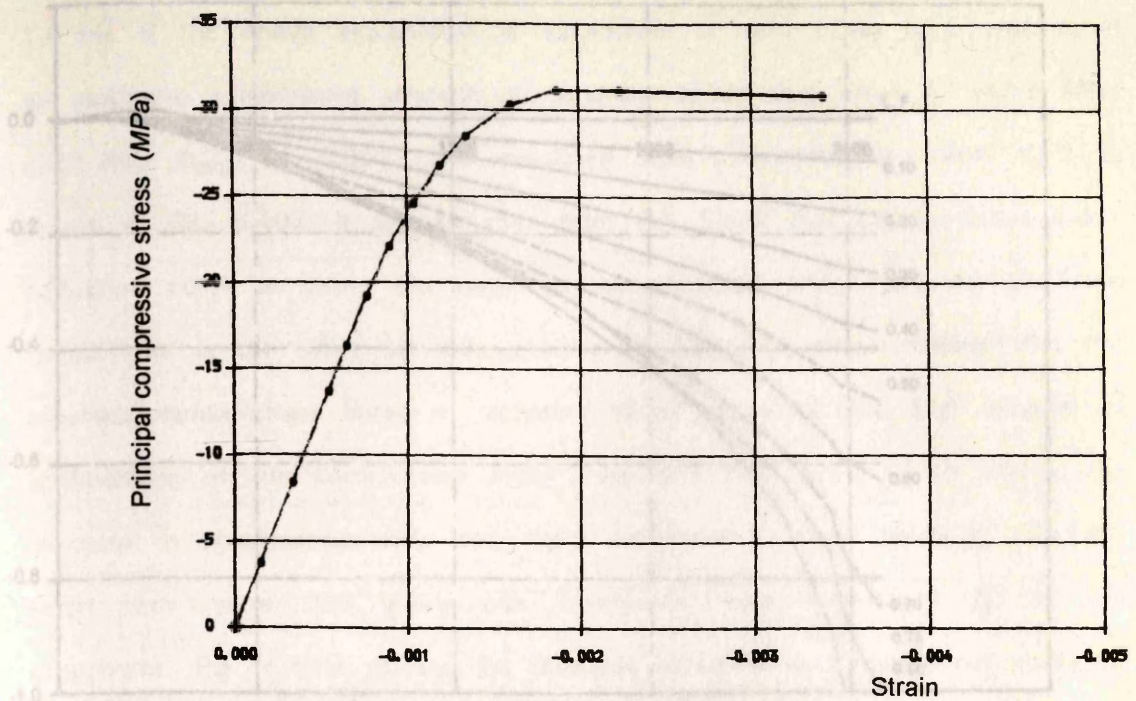


Fig. 6.104 Principal compressive stress-strain curve of concrete at Gauss point under the applied load (beam C-2).

Fig. 6.106a Stresses in compression steel at different load factors (beam C-2).

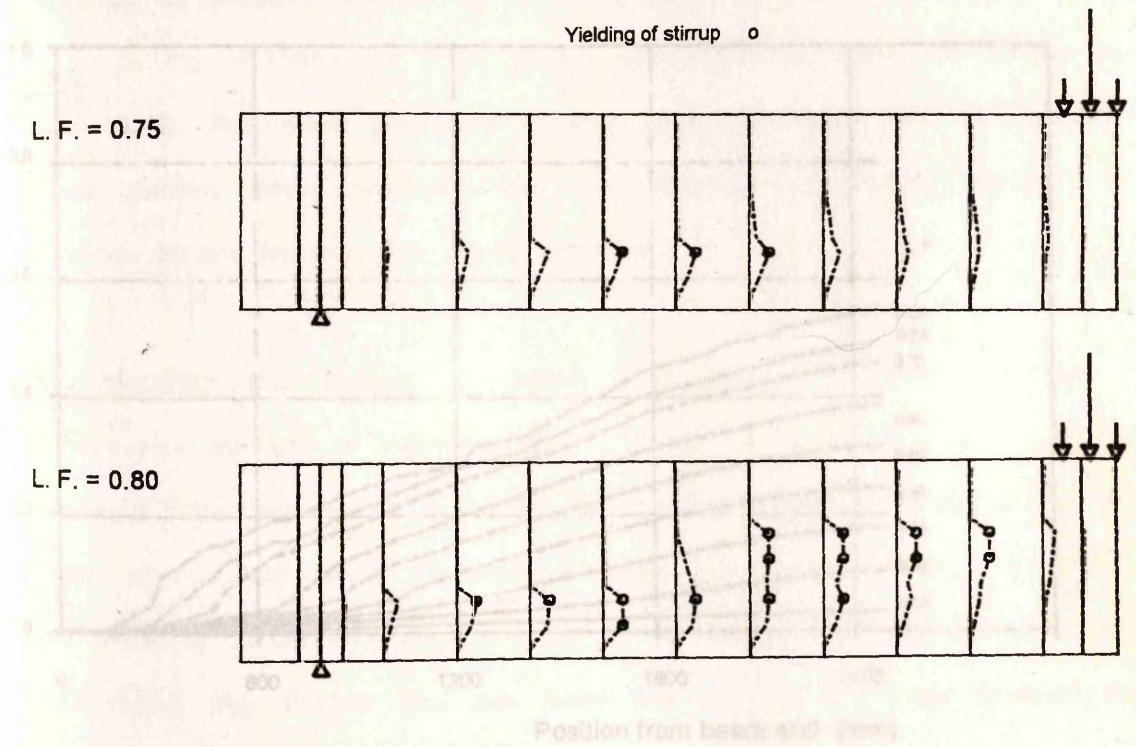


Fig. 6.105 Stresses in shear reinforcement (beam C-2).

Fig. 6.106b Stresses in tension steel at different load factors (beam C-2).

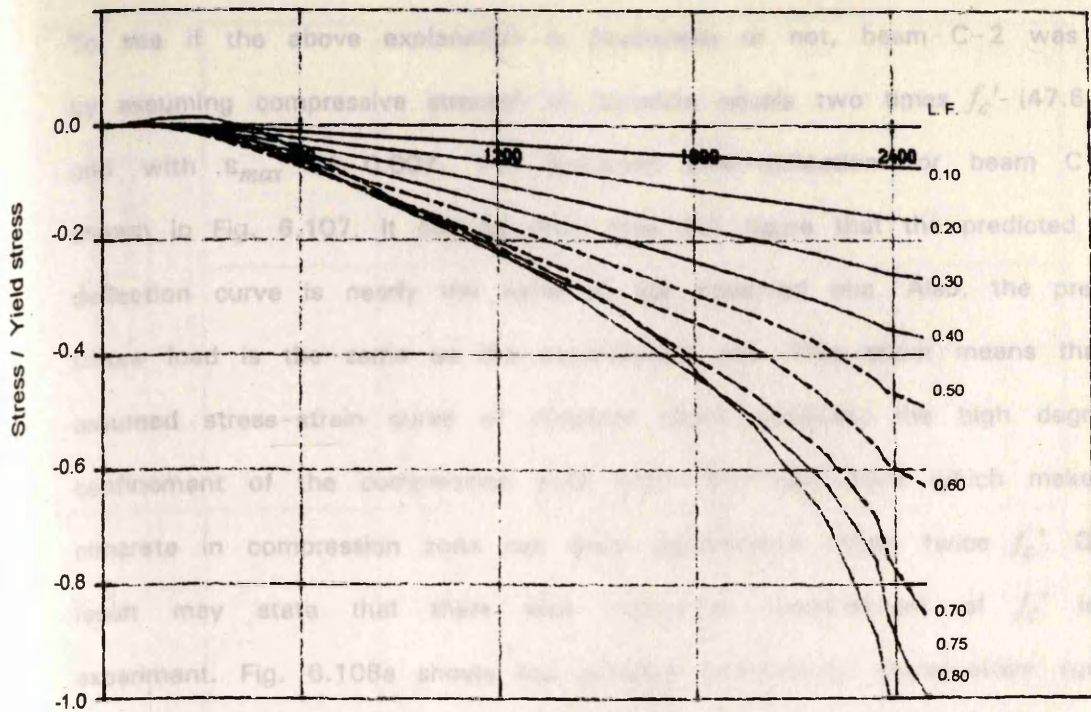


Fig. 6.106a Stresses in compression steel at different load factors (beam C-2).

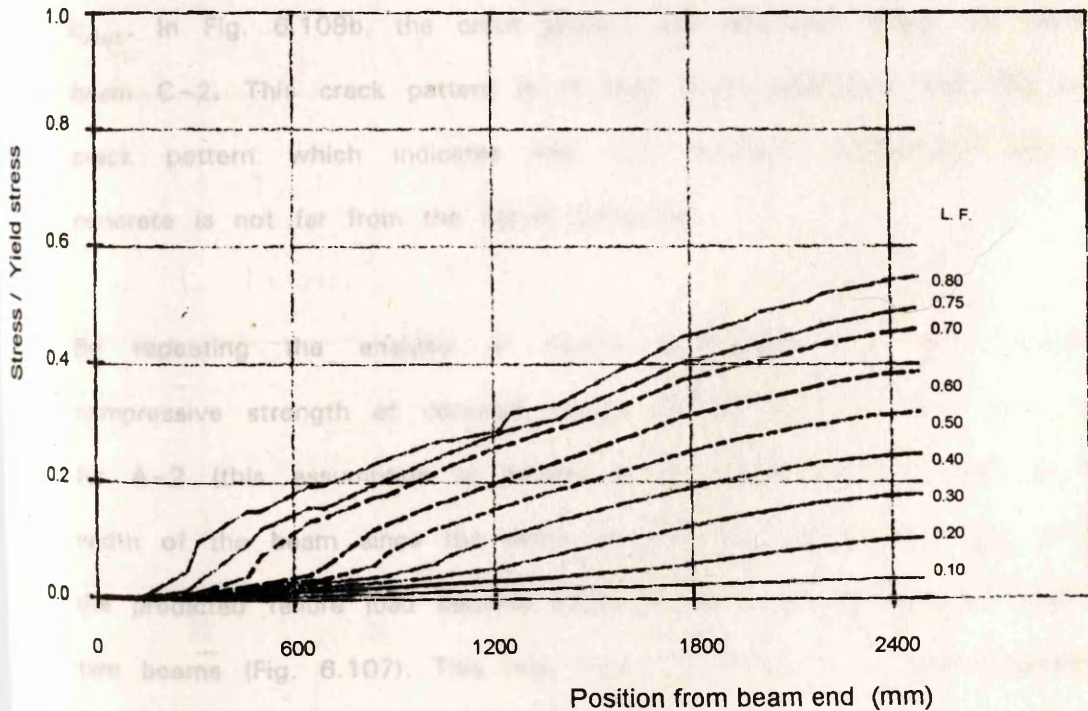


Fig. 6.106b Stresses in tension steel at different load factors (beam C-2).

To see if the above explanation is acceptable or not, beam C-2 was rerun by assuming compressive strength of concrete equals two times f'_c (47.6 MPa) and with ϵ_{max} of 0.007. The predicted load-deflection for beam C-2 is shown in Fig. 6.107. It can be seen from this figure that the predicted load-deflection curve is nearly the same as the observed one. Also, the predicted failure load is the same as the experimental one. This result means that the assumed stress-strain curve of concrete might represent the high degree of confinement of the compression zone under the load point which makes the concrete in compression zone can carry compressive stress twice f'_c . Or this result may state that there was inaccurate measurement of f'_c in the experiment. Fig. 6.108a shows the principal compressive stress-strain curve of concrete at a Gauss point in the compression zone under the load point. From this figure, it is clear that the stresses in the compression zone reached the assumed compressive strength up to the assumed maximum compressive strain ϵ_{max} . In Fig. 6.108b, the crack pattern and deformed shape are plotted for beam C-2. This crack pattern is in very good agreement with the observed crack pattern which indicates that the assumed compressive strength of concrete is not far from the actual behaviour.

By repeating the analysis of beams B-2 and A-2 after assuming a compressive strength of concrete equals 1.5 f'_c for beam B-2 and 1.25 f'_c for A-2 (this assumption is related to the cross-sectional area, or to the width of the beam since the depth is nearly the same) with ϵ_{max} of 0.007, the predicted failure load became equal to the experimental failure load in the two beams (Fig. 6.107). This may mean that there is a relation between the stress-strain curve of concrete or the degree of confinement and the cross-sectional dimensions.

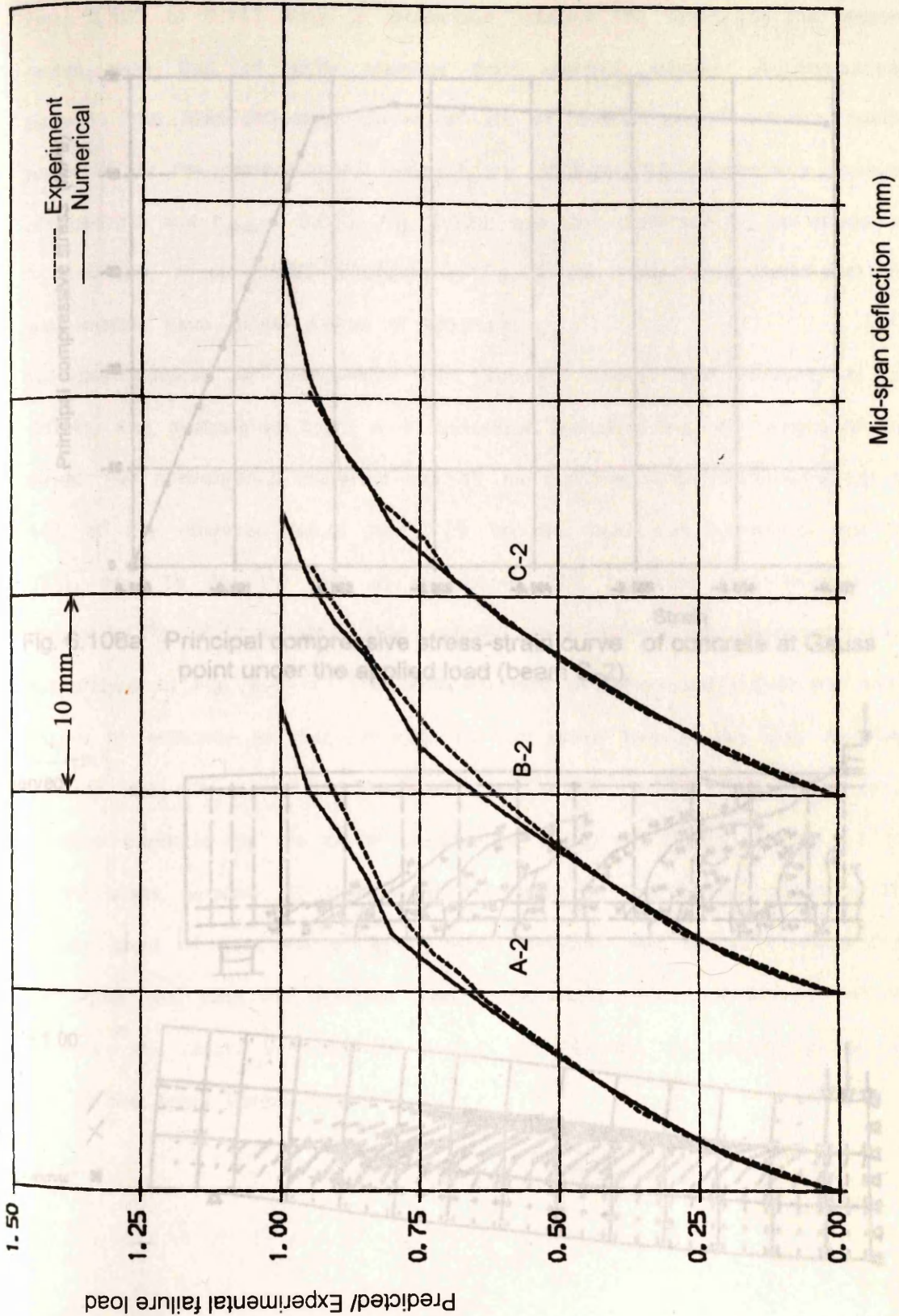


Fig. 6.107 Load-deflection curves for beams A-2, B-2, and C-2.

Predicted/ Experimental failure load

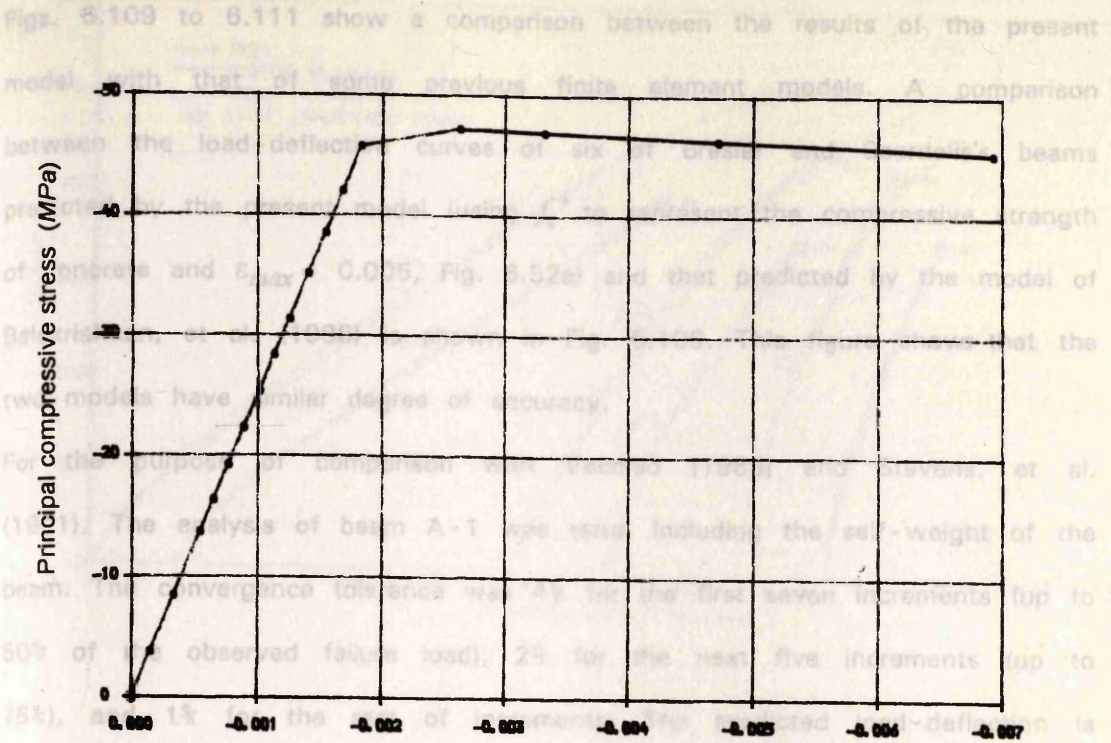
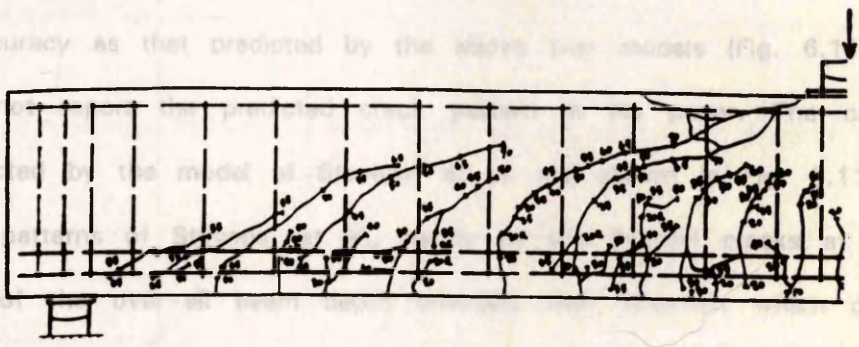


Fig. 6.108a Principal compressive stress-strain curve of concrete at Gauss point under the applied load (beam C-2).

Observed



L. F. = 1.00

- Single crack /
- Double crack X
- Crushing of concrete ■

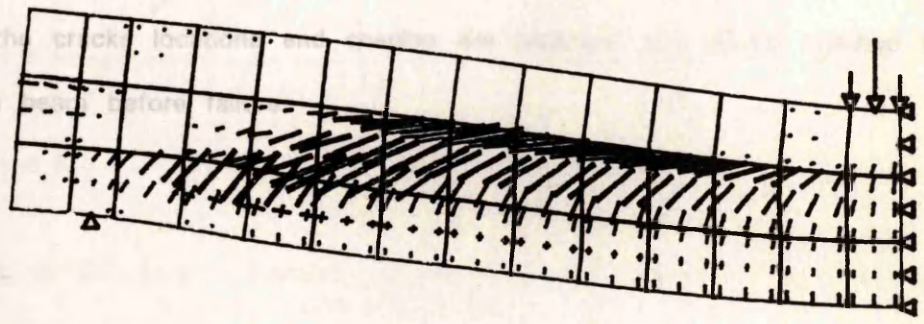


Fig. 6.108b Crack pattern and deformed shape for beam C-2 (Load factor = 1.00, displacements magnified x 10).

Figs. 6.109 to 6.111 show a comparison between the results of the present model with that of some previous finite element models. A comparison between the load-deflection curves of six of Bresler and Scordelis's beams predicted by the present model (using f'_c to represent the compressive strength of concrete and $\varepsilon_{max} = 0.005$, Fig. 6.52a) and that predicted by the model of Balakrishnan, et al. (1988) is shown in Fig. 6.109. This figure shows that the two models have similar degree of accuracy.

For the purpose of comparison with Vecchio (1989) and Stevens, et al. (1991), The analysis of beam A-1 was rerun including the self-weight of the beam. The convergence tolerance was 4% for the first seven increments (up to 50% of the observed failure load), 2% for the next five increments (up to 75%), and 1% for the rest of increments. The predicted load-deflection is shown in Fig. 6.110b, while the predicted crack pattern and deformed shape are shown in Fig. 6.111c. The predicted load-deflection curve has the same degree of accuracy as that predicted by the above two models (Fig. 6.110a). Vecchio did not report the predicted crack pattern in his paper. The crack patterns predicted by the model of Stevens, et al. are shown in Fig. 6.111b. In the crack patterns of Stevens, et al., nearly all the flexural cracks at the bottom third of the over-all beam depth changed their direction which does not agree well with the observed, also in the crack pattern of Stevens, et al., in which the cracks locations and spacing are arbitrary, the cracks reached the top of the beam before failure.

Fig. 6.109 Load-deflection curves for six of Bresler and Scordelis's beams.
(a) Balakrishnan, et al. (1988)

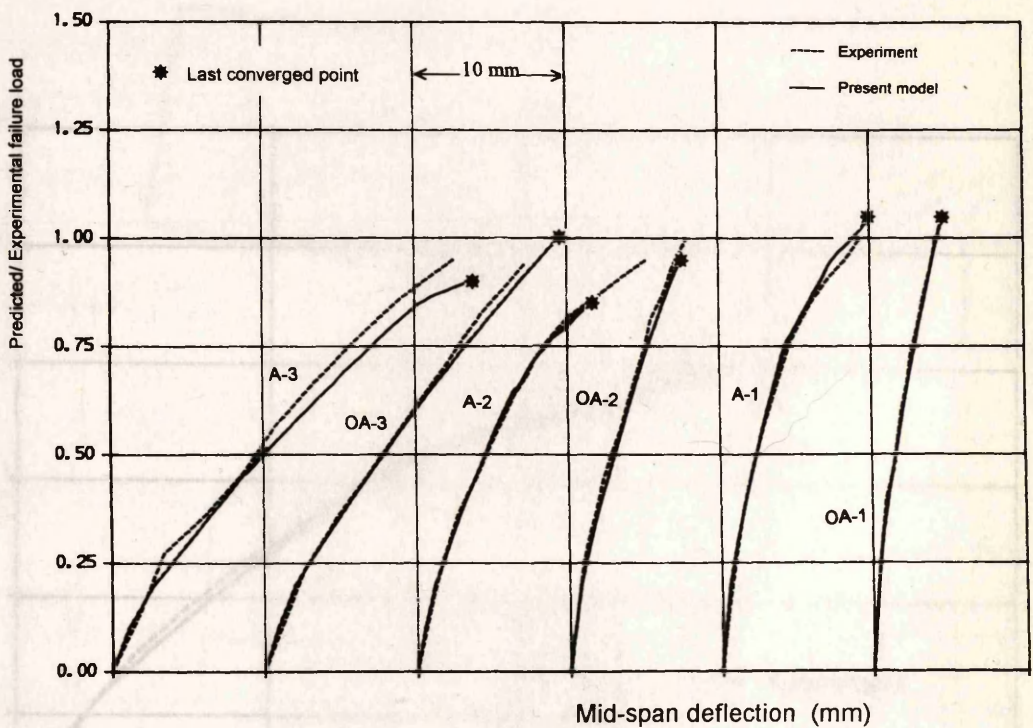
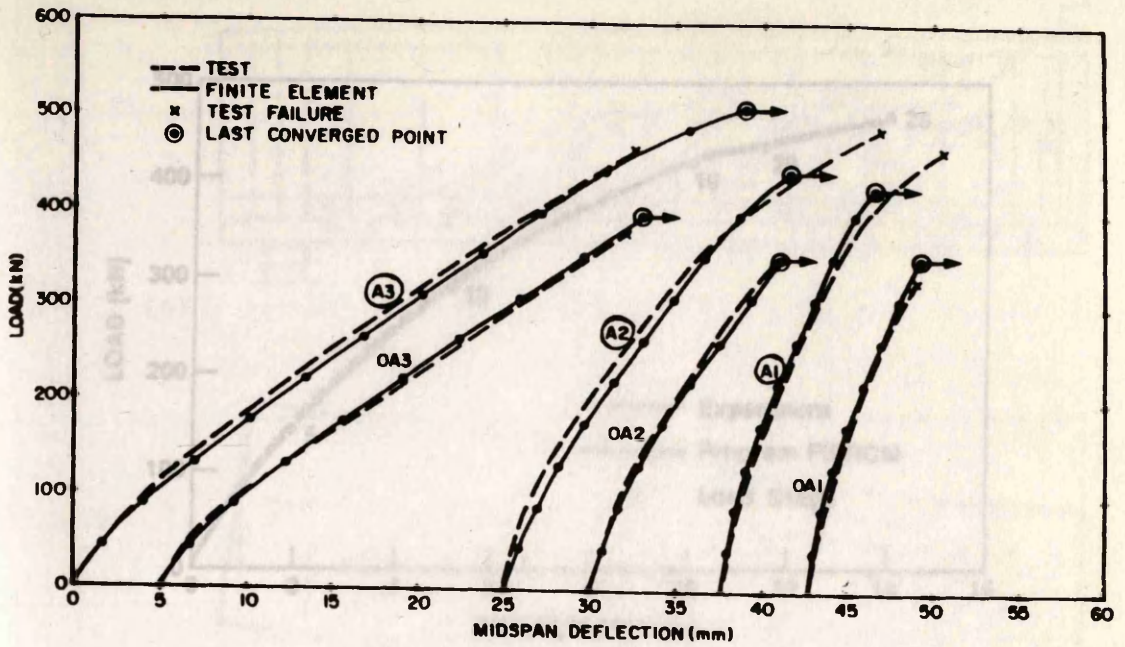


Fig. 6.109 Load-deflection curves for six of Bresler and Scordelis's beams.
 (a) Balakrishnan, et al. (1988b) (b) Present model

Fig. 6.110 Load-deflection curves for beam A-1
 (a) Vecchio (1989) (b) Present model

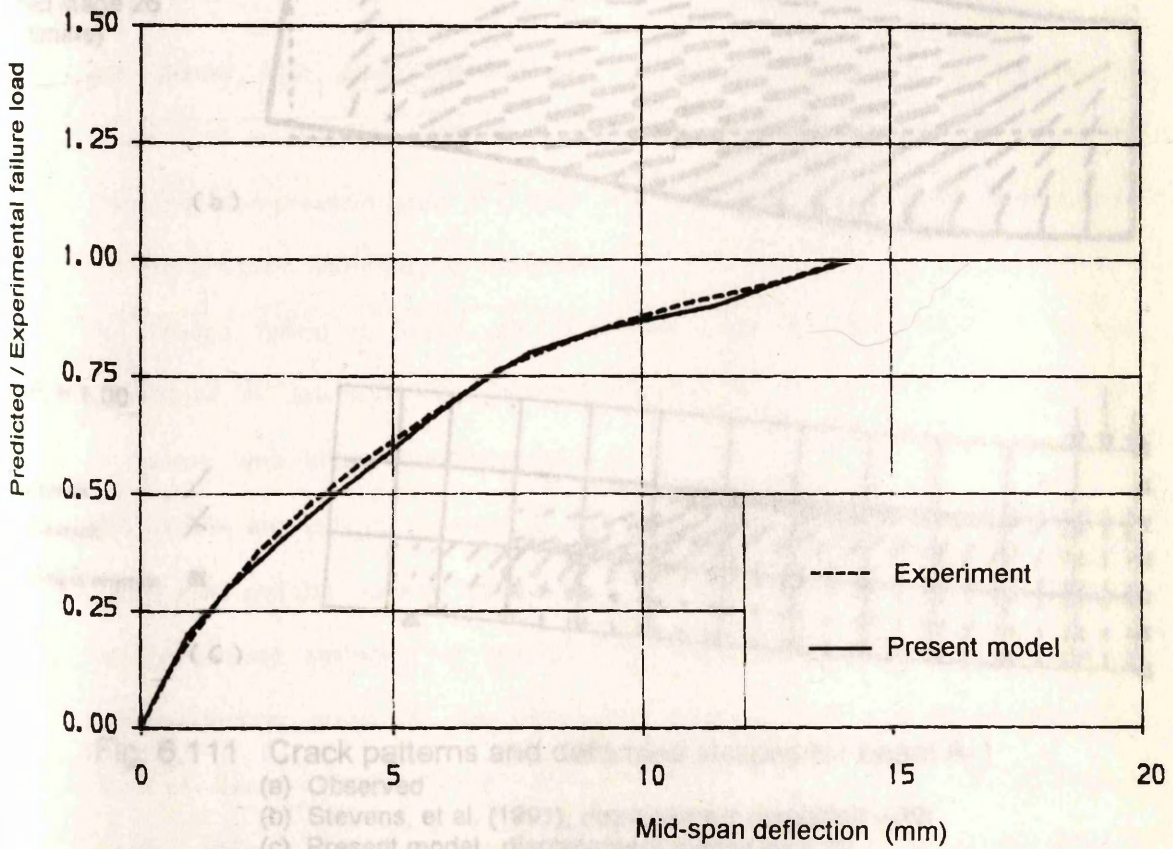
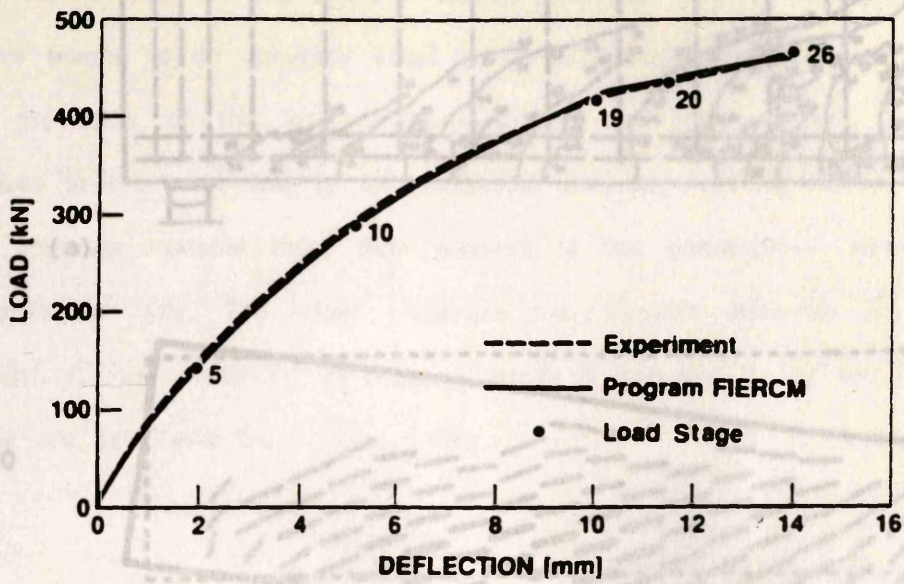
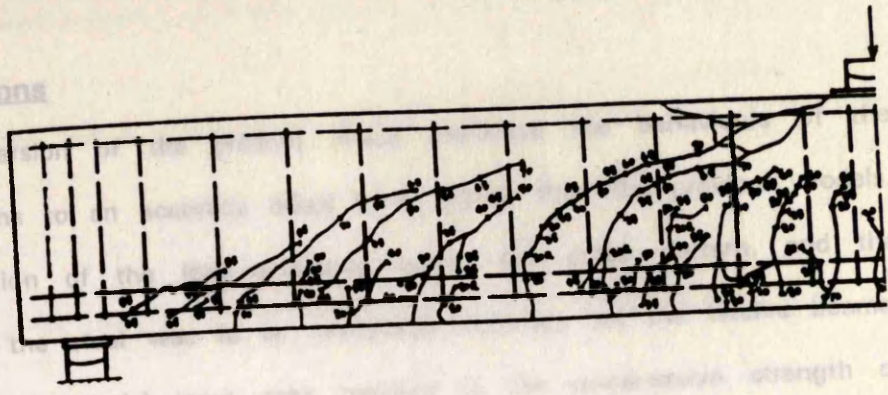


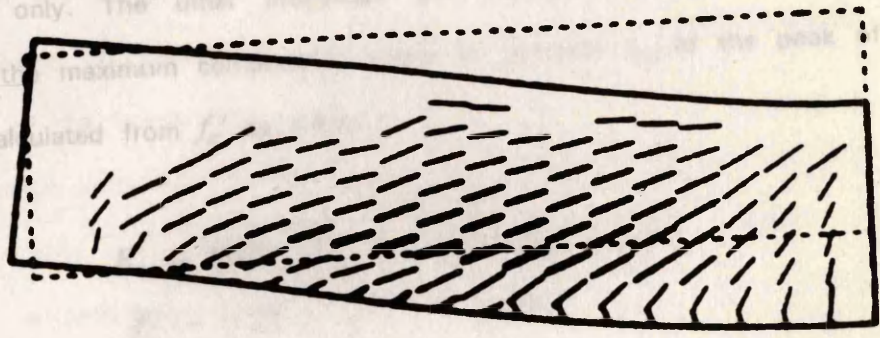
Fig. 6.110 Load-deflection curves for beam A-1
 (a) Vecchio (1989) (b) Present model.

Observed

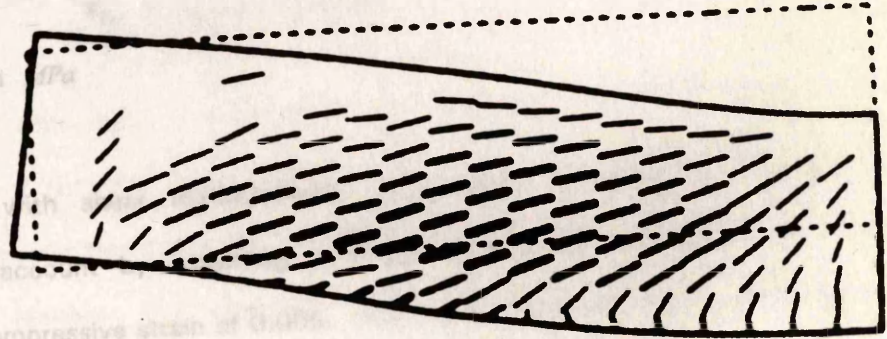


(a)

Load stage 20



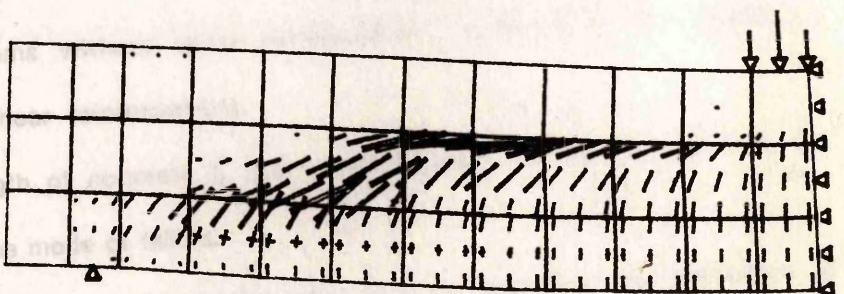
Load stage 26 (ultimate)



(b)

L. F. = 1.00

- Single crack /
- Double crack X
- Crushing of concrete ■



(c)

Fig. 6.111 Crack patterns and deformed shapes for beam A-1

- (a) Observed
- (b) Stevens, et al. (1991), displacement magnified x 20
- (c) Present model, displacement magnified x 10

6.3 Conclusions

- The last version of the present model predicted the behaviours of the twelve beams to an accuracy equal to or better than the previous models. The prediction of the load-deflection curve, the crack pattern, and the stresses in the steel was to an acceptable accuracy for the twelve beams. The concrete material input data required is the compressive strength of concrete f_c' only. The other properties viz. Young's modulus E , tensile strength f_t' , the maximum compressive strain of concrete ϵ_{cc} at the peak of stress are calculated from f_c' as follow:

$$E = 5000 \sqrt{f_c'} \quad \text{MPa}$$

$$f_t' = 0.54 \sqrt{f_c'} \quad \text{MPa}$$

$$\epsilon_{cc} = \sqrt{f_c'} / 2500$$

where f_c' in MPa

- For beams with shear reinforcement, compression softening of concrete is taken into account by assuming a straight line with very small slope and maximum compressive strain of 0.005. For beams without shear reinforcement no compression softening is assumed.
- For beams failing in shear, the effect of shear retention factor β is very significant in beams without shear reinforcement, while it is less significant in beams with shear reinforcement.
- The tensile strength of concrete f_t' has a small effect on the prediction of the failure load and the mode of failure.
- Taking tension softening of concrete into account improves the prediction of load-deflection curve. It has significant effect on the prediction of failure load of beams without shear reinforcement (10-25% of the failure load of beam) while it has insignificant effect on the prediction of failure load of beams with shear reinforcement. The following equation for the descending

portion of the stress-strain curve of concrete in tension gave satisfactory results.

$$\sigma = (\epsilon_{cr} / \epsilon_n + \sqrt{(\epsilon_{cr} / \epsilon_n)}) f_t' / 2 \text{ in MPa}$$

- The value of the compressive strain at the peak of stress in the stress-strain relationship of concrete ϵ_{cc} has a significant effect on the prediction (up to 25% of the failure load of beam).
- The compression softening of concrete has a significant effect on the load-carrying capacity of beams with shear reinforcement. Taking the compression softening into account increased the predicted failure loads of the nine beams with shear reinforcement by 15-20% of their load-carrying capacity.
- For beams with shear reinforcement with small spacing of stirrups, i.e. well confinement of concrete, assuming compressive strength of concrete ($=kf_c'$, where k is factor greater than 1.0) which is higher than f_c' gave good results for most of the beams. However, the failure load of some beams became overestimated by about 15%. For beams without shear reinforcement and for beams with shear reinforcement with spacing of stirrups greater than half of the effective depth of beam, assuming compressive strength of concrete of f_c' gave good results.

7.2 Data of beams

7.2.1 Krefeld and Thurston's beams

Krefeld and Thurston (1968b) tested over 200 reinforced concrete beams subjected to concentrated and distributed loads, among them there were 45 beams with shear reinforcement. All the beams with shear reinforcement in addition to 4 beams which have the same properties as the beams with shear reinforcement but

CHAPTER 7

PARAMETRIC STUDY CONTINUED

7.1 Introduction

In chapter 6, a 2-D finite element model was developed to predict the behaviour of reinforced concrete beams. The model was adjusted to get the best prediction of the behaviours of twelve beams tested by Bresler and Scordelis (1963). In this chapter, an attempt is made to investigate the model further by studying beams from other sources. Only reinforced concrete rectangular beams have been studied in this chapter. A study of other types of beams will be presented in the next two chapters. More than one hundred and fifty beams have been analysed. The beams studied were taken from three previous experimental works; Krefeld and Thurston (1966b), Clark (1951), and Mphonde and Frantz (1984). These beams covered important variables affecting the shear strength of reinforced concrete beams such as: shear span to depth ratio a/d , amount of shear reinforcement, effective depth and width of beam, and compressive strength of concrete. Most of the beams failed in shear. The beams which failed in flexure were studied for the purpose of comparison.

7.2 Data of beams

7.2.1 Krefeld and Thurston's beams

Krefeld and Thurston (1966b) tested over 200 reinforced concrete beams subjected to concentrated and distributed loads, among them there were 44 beams with shear reinforcement. All the beams with shear reinforcement, in addition to 4 beams which have the same properties as the beams with shear reinforcement but

without shear reinforcement have been analysed. Also, the first 27 beams without shear reinforcement reported in the paper have been analysed. There was no specific reason for selecting these as opposed to others. The dimensions of the beams and the methods of loads application are shown in Fig. 7.1. Table 7.1 shows the data required for the analysis of beams without shear reinforcement. These beams had a range of a/d ratio from 2.35 to 6.0, a range of f_c' from 16.5 to 30.2 N/mm^2 , and a range of tension reinforcement ratio ρ from 0.8 to 5.1%. The data required for the analysis of beams with shear reinforcement are shown in Table 7.2. These beams had a range of a/d ratio from 3.89 to 6.0, a range of f_c' from 15.7 to 48.5 N/mm^2 , and a range of ρ from 2.22 to 3.41%. The spacing of stirrups s was from 88.9 to 533.4 mm and the product of the percentage of shear reinforcement r ($=A_{sv}/b.s$) and the yield stress of stirrups f_{yv} was from 0.21 to 1.67 N/mm^2 .

The experimental load-deflection curves of the beams have not been reported in the paper. Six types of failures have been reported by Krefeld and Thurston as follows (see Fig. 2.9):

- DT:** Failure occurred due to a diagonal crack at nearly constant slope to the top surface of the beam.
- DT-S:** A sliding type failure along a diagonal plane above or at the end of a horizontal crack in the compression zone.
- DT-C:** A crushing disintegration failure above or at the end of a horizontal crack in the compression zone.
- DT-R:** A failure associated with a relative rotation of adjacent segments at the end of horizontal portion of diagonal tension crack in the compression zone which has extended close to the top surface. In many cases a thin layer of concrete above the horizontal crack buckles upward.
- F-C:** Flexure-Compression.
- F-T:** Flexure-Tension.

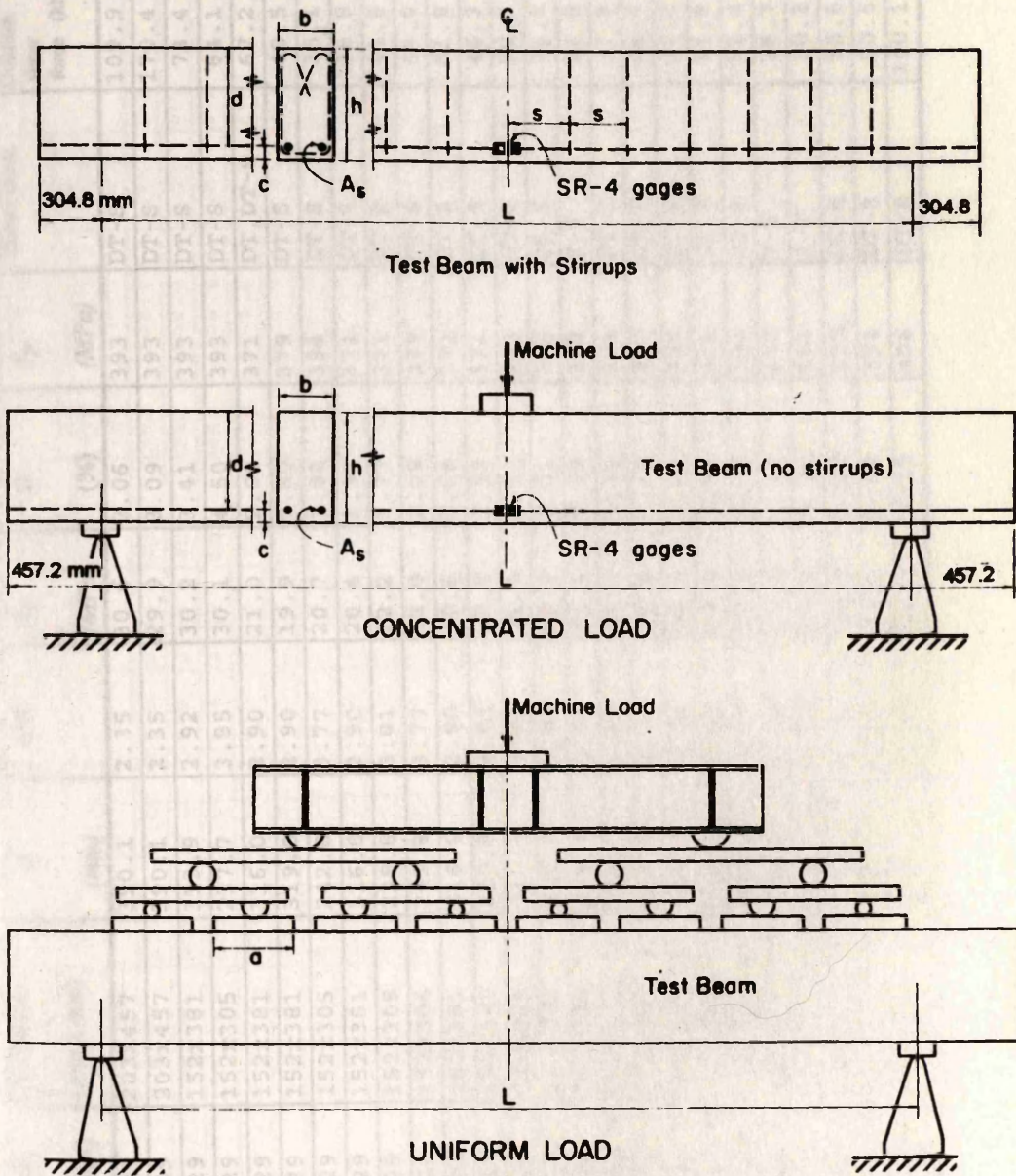


Fig. 7.1 Krefeld and Thurston's beams and type of loading.

Table 7.1 Data of Krefeld and Thurston's beams without shear reinforcement

No.	Beams	No. of Beams	Length (mm)	Cross-section (mm x mm)	d (mm)	a/d	f'_c (MPa)	ρ (%)	f_y (MPa)	Failure mode	Ultimate shear force (kN)	Mesh type
1	4A3	1	1829	203x457	390.1	2.35	30.6	2.06	393	DT-S	109.9	I
2	5A3	1	1829	203x457	390.1	2.35	29.9	3.09	393	DT-S	170.4	I
3	11A2	1	1829	152x381	313.9	2.92	30.2	3.41	393	DT-S	73.4	II
4	12A2	1	1829	152x305	237.7	3.85	30.1	4.50	393	DT-S	64.1	III
5-8	18A2-D2	4	1829	152x381	316.0	2.90	21.0	2.68	371	DT, DT-S	67.2	II
9	13A2	1	1829	152x381	319.0	2.90	19.9	0.80	379	DT-S	48.5	II
10	14A2	1	1829	152x305	242.8	3.77	20.7	1.05	394	DT-S	35.1	III
11-12	15A2, B2	2	1829	152x381	316.0	2.90	20.4	1.34	371	DT-S	48.9	II
13	16A2	1	1829	152x305	239.8	3.81	22.2	1.77	371	DT-R	41.8	III
14	17A2	1	1829	152x305	242.8	3.77	22.0	2.09	379	DT-S	44.0	III
15	18E2	1	1829	152x381	316.0	2.90	19.8	2.68	371	DT-S	81.8	II
16	19A2	1	1829	152x305	239.8	3.81	20.6	3.53	371	DT-S	46.3	III
17	20A2	1	1829	152x305	237.7	3.85	21.0	4.52	393	DT-S	50.7	III
18	21A2	1	1829	203x305	237.7	3.85	19.9	5.01	393	DT-S	76.5	III
19	1AC	1	2438	152x305	255.5	4.77	21.9	0.99	379	F-T	32.9	IV
20	2AC	1	2438	152x305	254.0	4.80	23.0	1.32	394	DT-C	37.8	IV
21	3AC	1	2438	152x305	255.5	4.77	20.8	1.99	379	DT-R	44.0	IV
22	4AC	1	2438	152x305	254.0	4.80	16.5	2.63	394	DT-R	37.8	IV
23	5AC	1	2438	152x305	252.5	4.83	18.4	3.35	371	DT-S	41.8	IV
24	6AC	1	2438	152x305	250.4	4.87	22.8	4.30	393	DT-R	53.4	IV
25	1CC	1	3048	152x305	255.5	5.96	19.0	1.00	379	F-T	26.7	V
26	2CC	1	3048	152x305	254.0	6.00	20.8	1.32	394	F-T	30.2	V
27	3CC	1	3048	152x305	255.5	5.96	20.5	1.99	379	DT-R	35.6	V
28-29	OCabs-I	2	3048	152x305	254.0	6.00	37.4	2.63	394	DT-R	50.5	VI
30-31	OCabs-II	2	3658	254x508	455.7	4.02	38.3	2.22	406	DT-R	140.1	VII

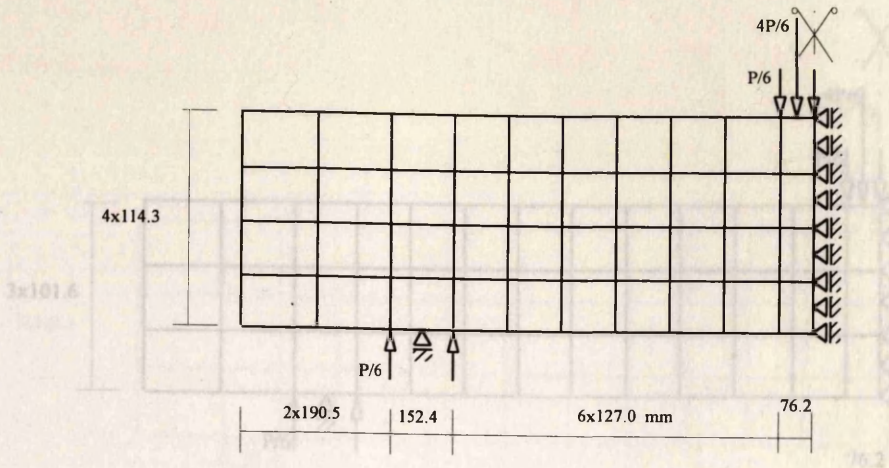
Table 7.2 Data of Krefeld and Thurston's beams with shear reinforcement

No.	Beams	No. of Beams	Length (mm)	Cross-section (mm x mm)	d (mm)	a/d	f _c ' (MPa)	ρ (%)	f _y (MPa)	Stirrups			Failure mode	Ultimate shear force (kN)	Mesh type
										f _{yv} (MPa)	Spacing (mm)	s (s)			
1	23.5	1	3048	152x305	254.0	6.00	38.5	2.63	394	342	88.9	1.64	F-T	60.9	VI
2-3	26a, b	2	3048	152x305	254.0	6.00	34.8	2.63	394	342	152.4	0.95	F-T	60.9	VI
4-6	210a-c	3	3048	152x305	254.0	6.00	38.4	2.63	394	342	254.0	0.58	F-T	63.5	VI
7-8	212a, b	2	3048	152x305	254.0	6.00	39.5	2.63	394	342	304.8	0.48	F-T	66.9	VI
9	24-1	1	3658	254x508	455.7	4.02	37.3	2.22	406	342	101.6	0.82	F-T	244.6	VII
10	26-1	1	3658	254x508	455.7	4.02	40.2	2.22	406	342	152.4	0.55	DT-R	206.8	VII
11-12	29a-1, b-1	2	3658	254x508	455.7	4.02	38.3	2.22	406	342	228.6	0.37	DT-R	159.9	VII
13	213.5-1	1	3658	254x508	455.7	4.02	38.9	2.22	406	342	342.9	0.24	DT-R	148.1	VII
14	24.5-2	1	3658	254x508	455.7	4.02	37.6	2.22	406	373	114.3	0.86	F-T	243.8	VII
15	29a-2	1	3658	254x508	455.7	4.02	37.2	2.22	406	373	228.6	0.43	DT-C	216.6	VII
16-17	29b-2, f-2	2	3658	254x508	455.7	4.02	41.6	2.22	406	373	228.6	0.43	DT-C, F-T, DT-R	218.4	VII
18	29c-2	1	3658	254x508	455.7	4.02	24.2	2.22	406	373	228.6	0.43	DT-C	161.5	VII
19	29d-2	1	3658	254x508	455.7	4.02	30.4	2.22	406	373	228.6	0.43	DT-C	165.0	VII
20	29e-2	1	3658	254x508	455.7	4.02	48.5	2.22	406	373	228.6	0.43	DT-R	206.4	VII
21	29g-2	1	3658	254x508	455.7	4.02	15.7	2.22	406	373	228.6	0.43	DT-C	149.9	VII
22	213.5a-2	1	3658	254x508	455.7	4.02	37.0	2.22	406	373	342.9	0.29	DT-C	161.5	VII
23	218a-2	1	3658	254x508	455.7	4.02	37.6	2.22	406	373	457.2	0.21	DT-R	164.1	VII
24	24.5-3	1	3658	254x508	455.7	4.02	35.5	2.22	406	237	114.3	0.55	F-C	232.6	VII
25	29-3	1	3658	254x508	455.7	4.02	34.3	2.22	406	237	228.6	0.28	DT-C	177.9	VII
26	39-1	1	3658	254x508	455.7	4.02	37.3	2.22	406	518	228.6	1.28	F-T	248.2	VII
27	313.5-1	1	3658	254x508	455.7	4.02	37.3	2.22	406	518	342.9	0.85	F-T	251.3	VII
28	318-1	1	3658	254x508	455.7	4.02	40.6	2.22	406	518	457.2	0.64	DT-C	220.2	VII

Table 7.2 Data of Krefeld and Thurston's beams with shear reinforcement (continued)

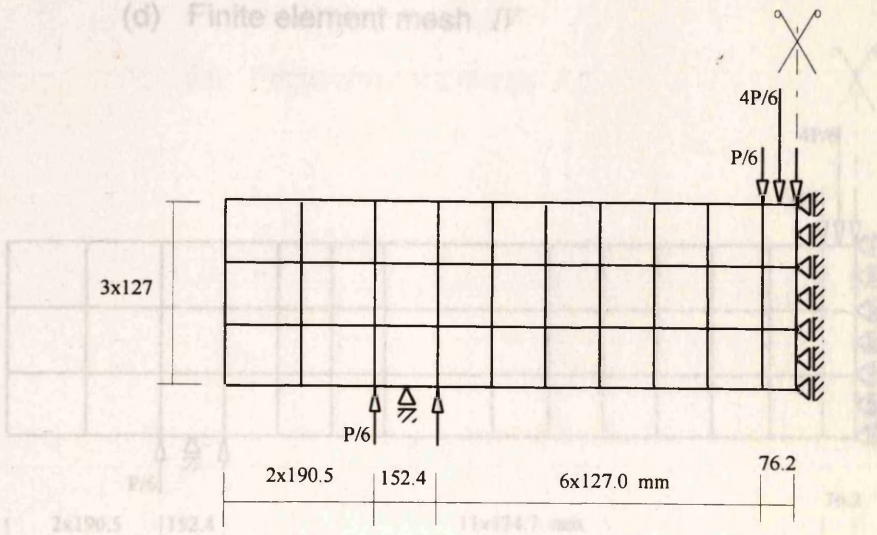
No.	Beams	No. of Beams	Length (mm)	Cross-section (mm x mm)	d (mm)	a/d	f'_c (MPa)	ρ (%)	f_y (MPa)	Stirrups			Failure mode	Ultimate shear force (kN)	Mesh type
										f_{yv} (MPa)	Spacing (mm)	$r f_{yv}$ (MPa)			
29	321-1	1	3658	254x508	455.7	4.02	38.8	2.22	406	518	533.4	0.55	DT-R	163.7	VII
30	39-2	1	3658	254x508	455.7	4.02	37.1	2.22	406	352	228.6	0.88	F-T	248.6	VII
31	313.5-2	1	3658	254x508	455.7	4.02	39.7	2.22	406	352	342.9	0.59	F-T,DT-C	234.9	VII
32	318-2	1	3658	254x508	455.7	4.02	38.9	2.22	406	352	457.2	0.44	DT-C	177.0	VII
33	321-2	1	3658	254x508	455.7	4.02	38.0	2.22	406	352	533.4	0.38	DT-R	166.8	VII
34	39-3	1	3658	254x508	455.7	4.02	42.7	2.22	406	276	228.6	0.67	F-T,DT-C	239.7	VII
35	313.5-3	1	3658	254x508	455.7	4.02	42.7	2.22	406	276	342.9	0.45	DT-C	213.5	VII
36	318-3	1	3658	254x508	455.7	4.02	43.1	2.22	406	276	457.2	0.33	DT-R	174.8	VII
37	321-3	1	3658	254x508	455.7	4.02	43.1	2.22	406	276	533.4	0.29	DT-R	140.6	VII
38-39	6A1, B1 *	2	2438	152x381	313.9	3.89	29.9	3.41	393	388	203.2	1.57	F-C	258.0	VIII
40	9A1 *	1	3048	152x381	313.9	4.86	30.8	3.41	393	388	190.5	1.67	F-C	203.7	IX
41	9B1 *	1	1829	152x381	313.9	2.92	29.9	3.41	393	388	190.5	1.67	F-C	350.5	X
42	23.5U *	1	3048	152x305	254.0	6.00	38.5	2.63	394	342	88.9	1.64	F-T	113.4	XI
43	213.5b-2*	1	3658	254x508	455.7	4.02	33.0	2.22	406	373	342.9	0.29	F-T	466.6	XII
44	218b-2 *	1	3658	254x508	455.7	4.02	34.6	2.22	406	373	457.2	0.21	DT-C	341.2	XII

* Beams subjected to distributed loads



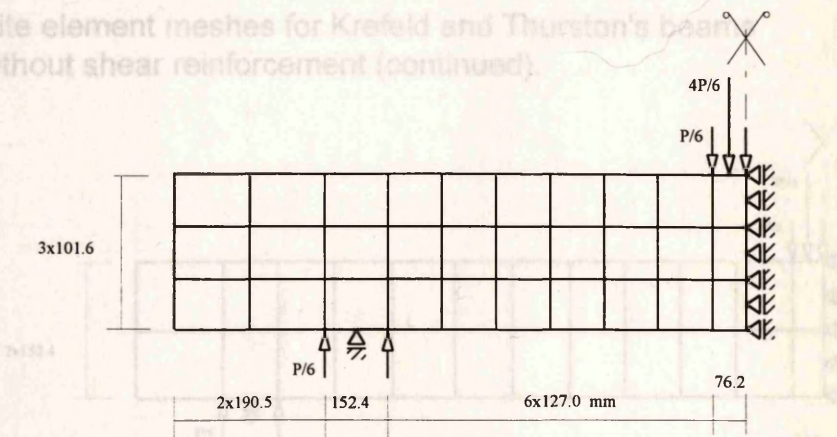
(a) Finite element mesh I

(d) Finite element mesh II



(b) Finite element mesh II

Fig. 7.2 Finite element meshes for Krefeld and Thurston's beams without shear reinforcement (continued).



(c) Finite element mesh III

(a) Finite element mesh II

Fig. 7.2 Finite element meshes for Krefeld and Thurston's beams without shear reinforcement.

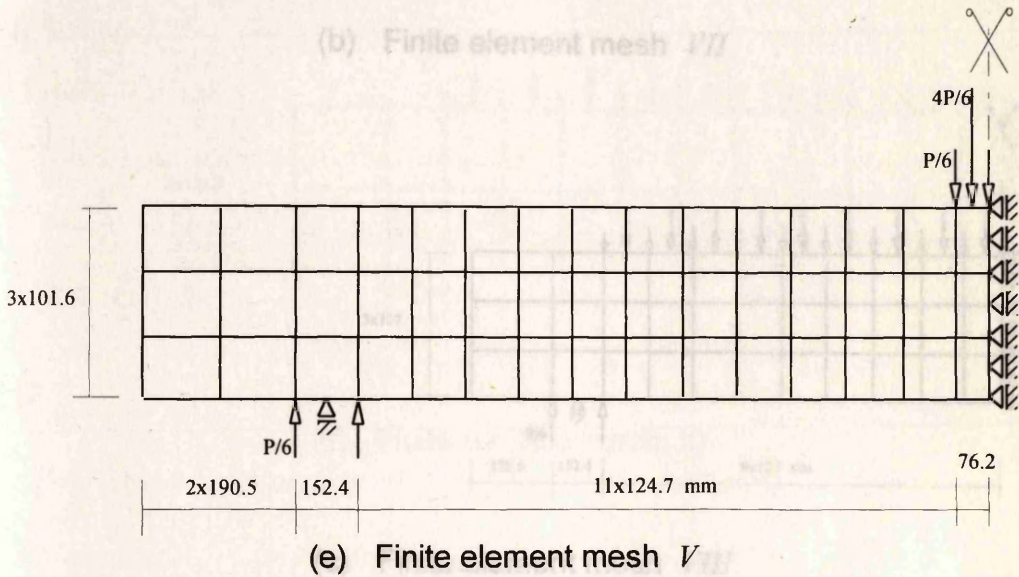
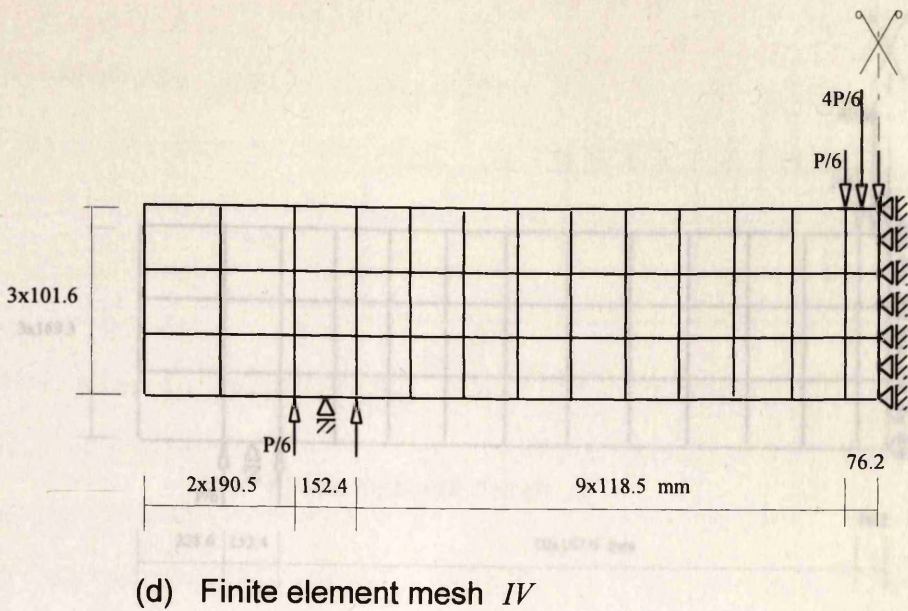


Fig. 7.2 Finite element meshes for Krefeld and Thurston's beams without shear reinforcement (continued).

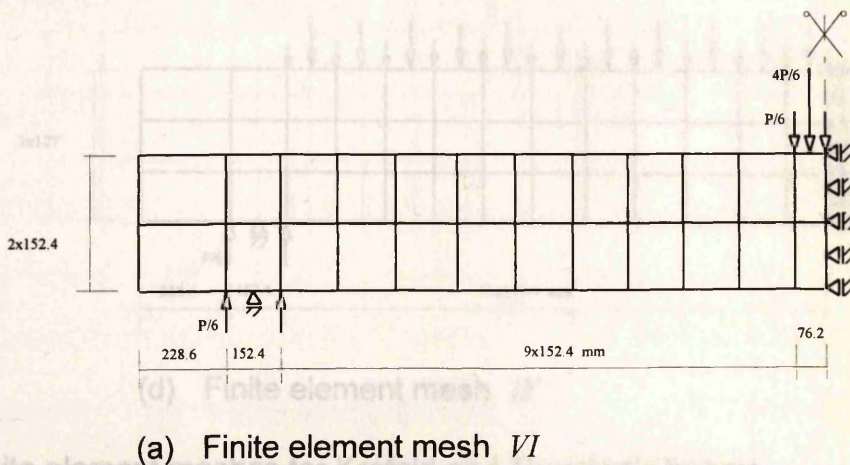
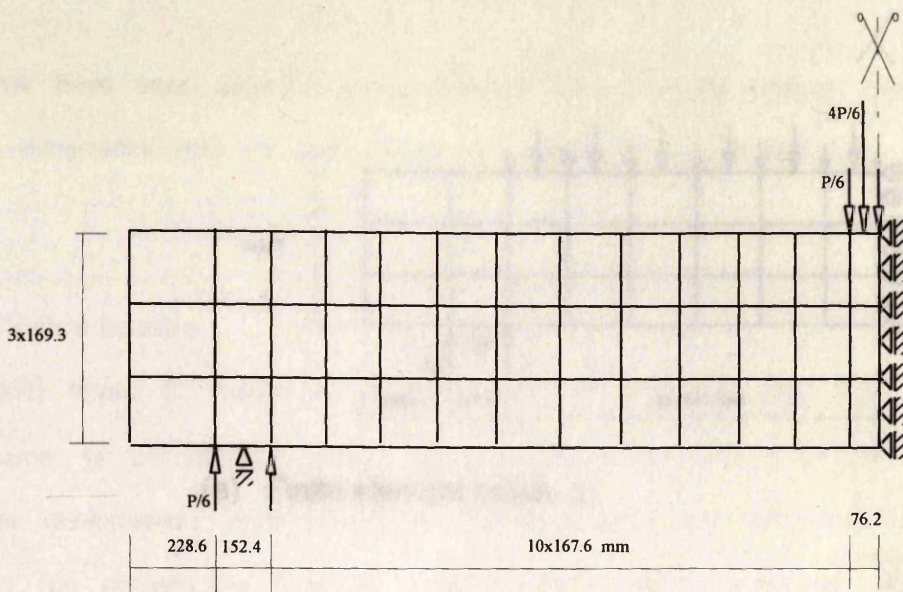
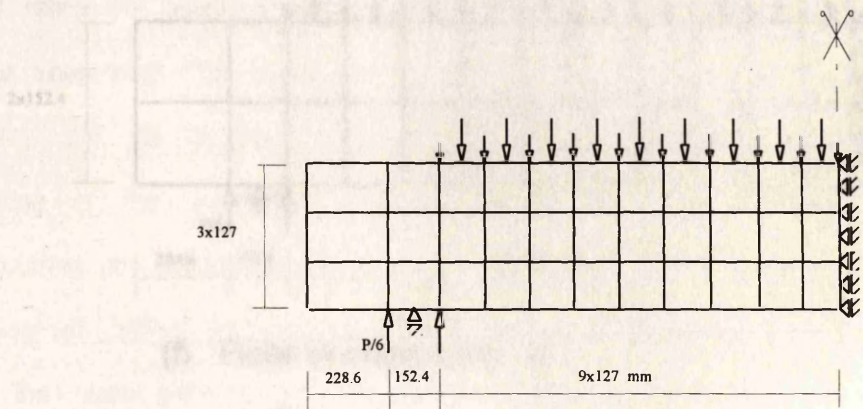


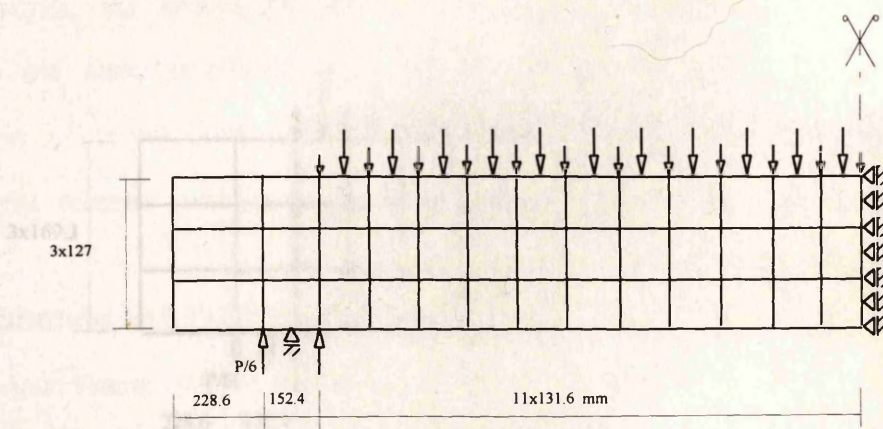
Fig. 7.3 Finite element meshes for Krefeld and Thurston's beams with shear reinforcement.



(b) Finite element mesh VII

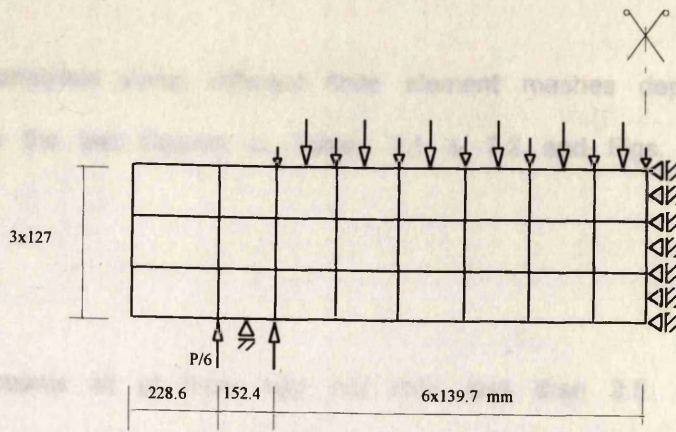


(c) Finite element mesh VIII

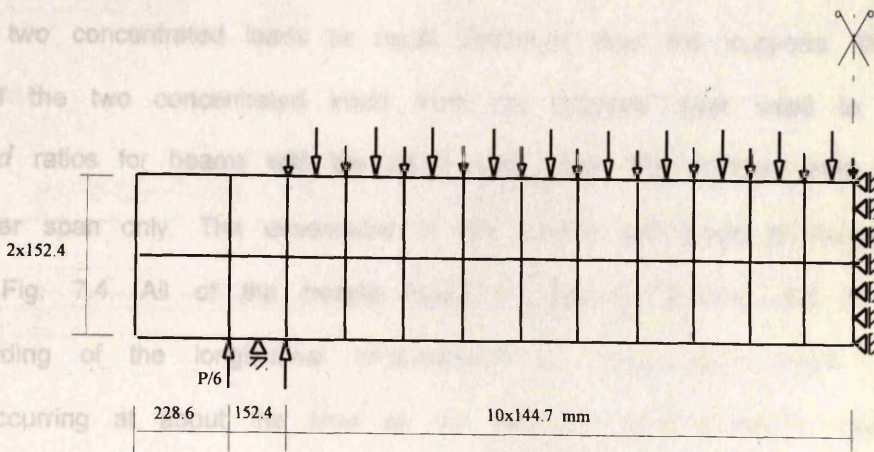


(d) Finite element mesh IX

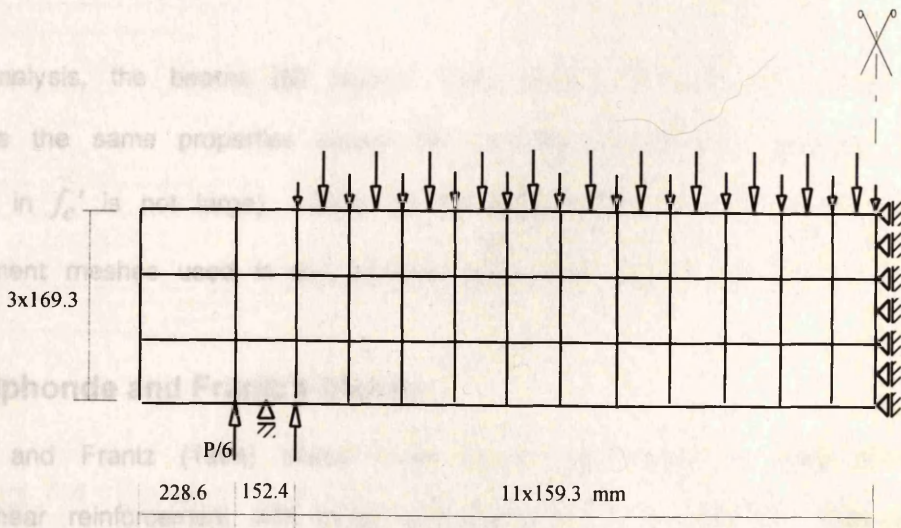
Fig. 7.3 Finite element meshes for Krefeld and Thurston's beams with shear reinforcement (continued).



(e) Finite element mesh *X*



(f) Finite element mesh *XI*



(g) Finite element mesh *XII*

Fig. 7.3 Finite element meshes for Krefeld and Thurston's beams with shear reinforcement (continued).

The beams have been analysed using different finite element meshes depending on beam dimensions (see the last Column in Tables 7.1 & 7.2 and Figs. 7.2 & 7.3).

7.2.2 Clark's beams

Clark (1951) tested 62 beams all of them had a/d ratio less than 2.5. Among these beams, 12 beams were without shear reinforcement. Only 4 of the beams with shear reinforcement were loaded by mid-span loads, the other beams were loaded by two concentrated loads at equal distances from the supports. Different positions of the two concentrated loads from the supports were used to obtain different a/d ratios for beams with the same total span. The stirrups were placed in the shear span only. The dimensions of the beams and types of loading are shown in Fig. 7.4. All of the beams failed in diagonal tension, but in some beams yielding of the longitudinal reinforcement or compressive failure of the concrete occurring at about the time as the diagonal tension failure made the primary cause of failure difficult to determine. The experimental load-deflection curves and the crack patterns of some beams have been reported (Figs. 7.5 & 7.6).

In the analysis, the beams (62 beams) have been divided to 22 groups. Each group has the same properties except the concrete compressive strength f_c' (the difference in f_c' is not large). Data for the beams are shown in Table 7.3. The finite element meshes used in the analysis are shown in Fig. 7.7.

7.2.3 Mphonde and Frantz's beams

Mphonde and Frantz (1984) tested three series (19 beams in total) of beams without shear reinforcement with three a/d ratios; 1.5, 2.5, and 3.6. They studied the effect of a very wide range of concrete compressive strength (designed to be between 21 and 103 MPa). All beams except one had the same tension reinforcement ratio ($\rho = 3.36\%$). This high ratio was used to ensure that a shear

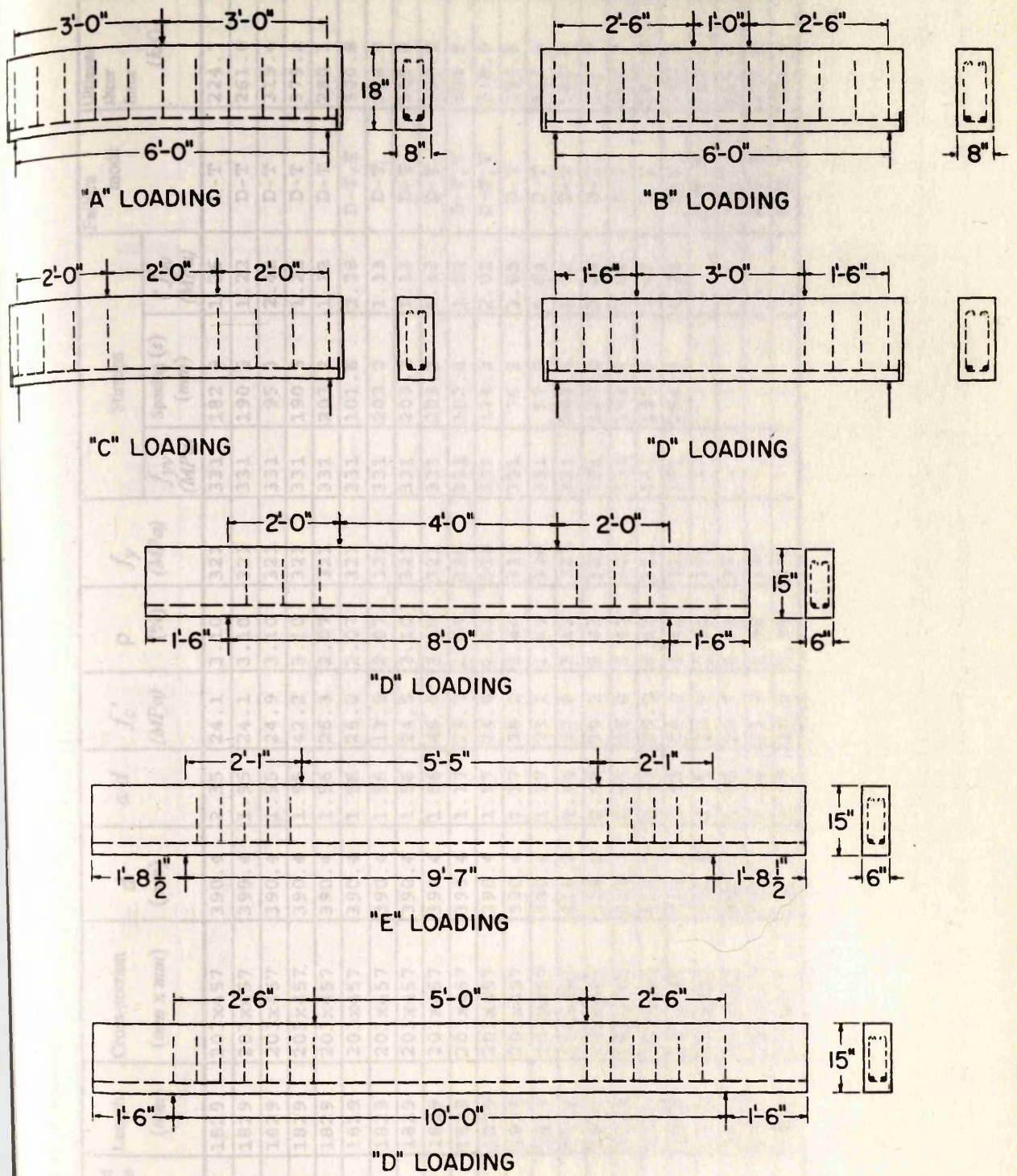


Fig. 7.4 Dimensions of Clark's beams and type of loading.

1 in. = 25.4 mm

Table 7.3 Data of Clark's beams

No.	Beams	No. of Beams	Length (mm)	Cross-section (mm x mm)	d (mm)	a/d	f _c ' (MPa)	ρ (%)	f _y (MPa)	Stirrups			Failure mode	Ultimate shear force (kN)	Mesh type
										f _{yv} (MPa)	Spacing (mm)	r f _{yv} (MPa)			
1-4	A1 1-4	4	1829	203x457	390.4	2.35	24.1	3.10	321	331	182.9	1.26	D-T	224.7	I
5-9	B1 1-5	5	1829	203x457	390.4	1.95	24.1	3.10	321	331	190.5	1.22	D-T	261.0	II
10-12	B2 1-3	3	1829	203x457	390.4	1.95	24.9	3.10	321	331	95.3	2.42	D-T	319.4	II
13	B6 1	1	1829	203x457	390.4	1.95	42.2	3.10	321	331	190.5	1.22	D-T	379.2	II
14-17	C1 1-4	4	1829	203x457	390.4	1.56	26.3	2.07	321	331	203.2	1.13	D-T	280.1	III
18-21	C2 1-4	4	1829	203x457	390.4	1.56	25.0	2.07	321	331	101.6	2.28	D-T,T	300.8	III
22-24	C3 1-3	3	1829	203x457	390.4	1.56	13.9	2.07	321	331	203.2	1.13	D-T	204.0	III
25	C4 1	1	1829	203x457	390.4	1.56	24.5	3.10	321	331	203.2	1.13	D-T	309.0	III
26-28	C6 2-4	3	1829	203x457	390.4	1.56	45.9	3.10	321	331	203.2	1.13	D-T	429.0	III
29-31	D1 1-3	3	1829	203x457	390.4	1.17	25.7	1.63	336	331	152.4	1.52	D-T,T	304.8	IV
32-35	D2 1-4	4	1829	203x457	390.4	1.17	24.8	1.63	336	331	114.3	2.02	D-T,T	318.0	IV
36	D3 1	1	1829	203x457	390.4	1.17	28.2	2.44	336	331	76.2	3.05	D-T	394.8	IV
37	D4 1	1	1829	203x457	390.4	1.17	23.1	1.63	336	331	57.2	4.04	D-T	312.0	IV
38-40	D1 6-8	3	2438	152x381	314.2	1.94	27.8	3.42	321	331	203.2	1.52	D-T	180.0	V
41	E1 1	1	2921	152x381	314.2	2.02	30.2	3.42	321	331	127.0	2.42	D-T	221.7	VI
42-44	D2 6-8	3	3048	152x381	314.2	2.43	28.0	3.42	321	331	152.4	2.02	D-T	164.7	VII
45-47	D4 1-3	3	3048	152x381	314.2	2.43	25.0	3.42	321	331	190.5	1.62	D-T	163.5	VII
48-50	D5 1-3	3	3048	152x381	314.2	2.43	28.0	3.42	321	331	254.0	1.22	D-T	153.6	VII
51-53	AO 1-3	3	1829	203x457	390.4	2.35	23.8	0.98	371	-	-	-	D-T,T	105.0	I
54-56	BO 1-3	3	1829	203x457	390.4	1.95	23.7	0.98	371	-	-	-	D-T	114.4	II
57-59	CO 1-3	3	1829	203x457	390.4	1.56	23.9	0.98	371	-	-	-	D-T,T	173.0	III
60-62	DO 1-3	3	1829	203x457	390.4	1.17	26.0	0.98	371	-	-	-	D-T,T	234.9	IV

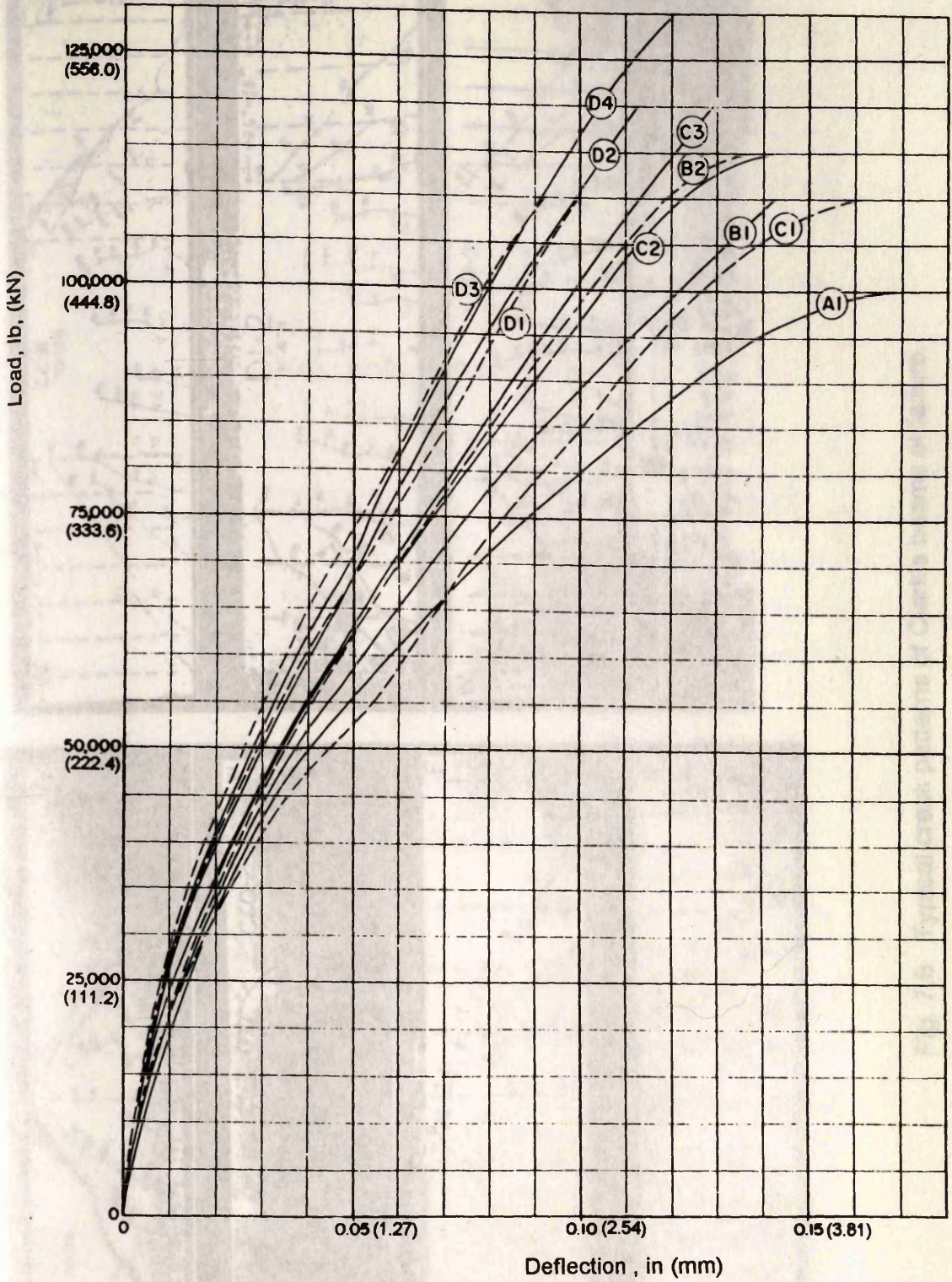


Fig. 7.5 Load-deflection curves of Clark's beams
 (1 in. = 25.4 mm, 1 lb = 4.448 N)

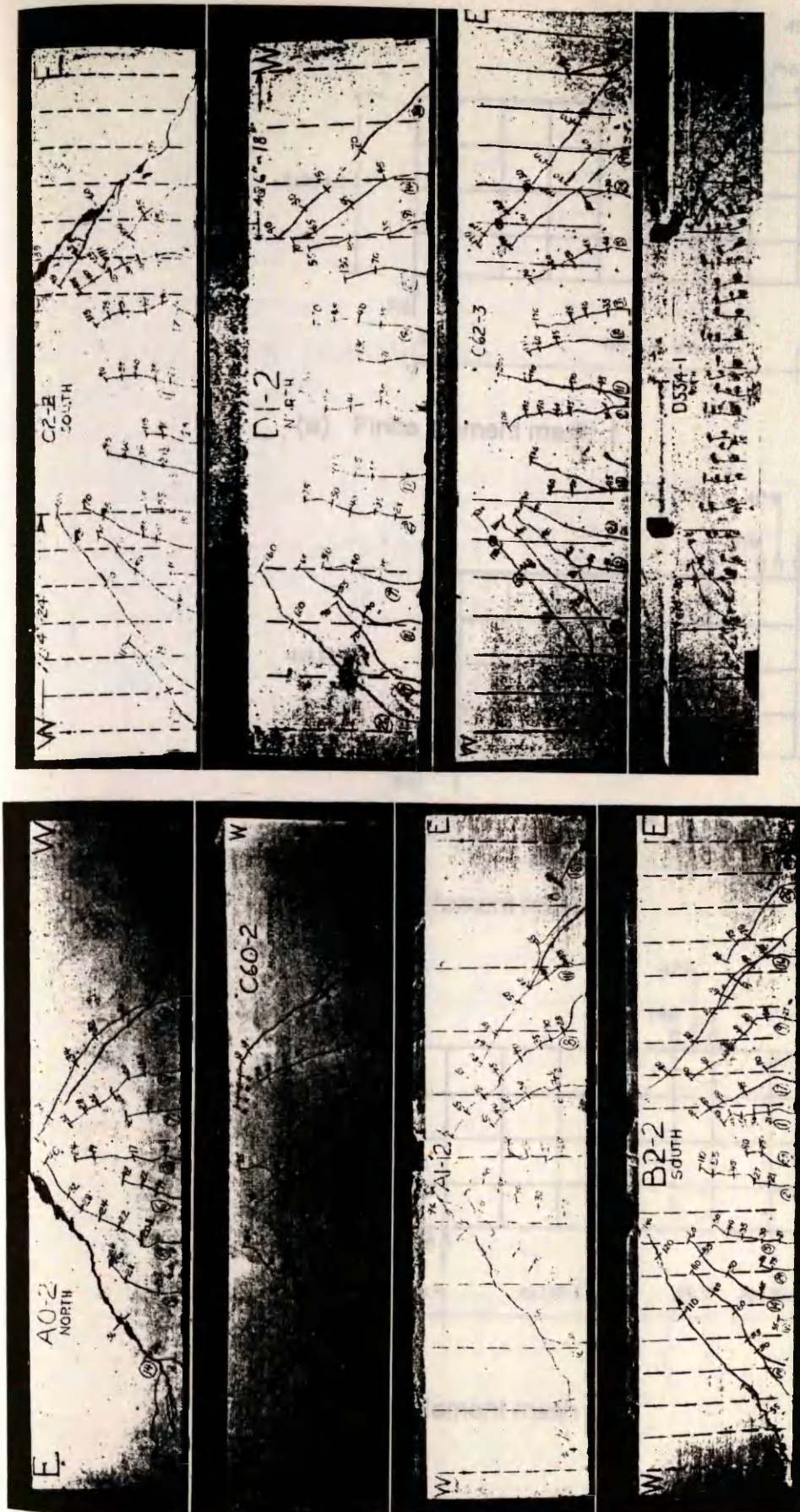
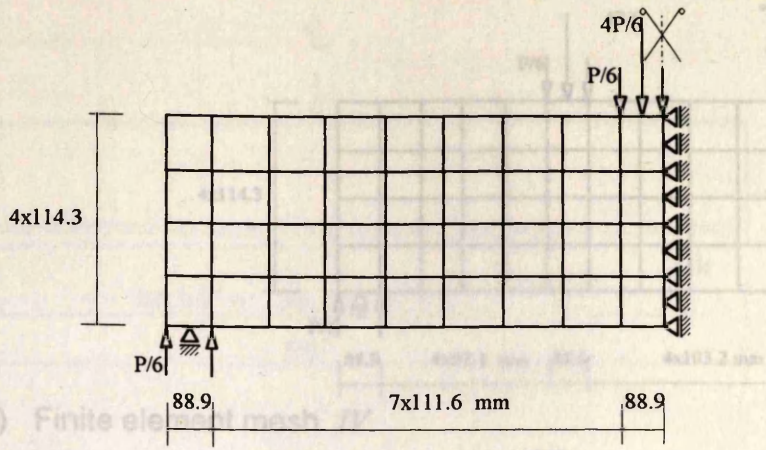
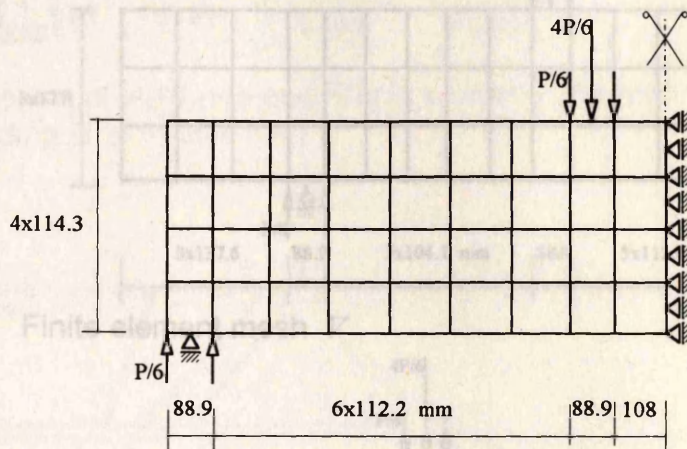


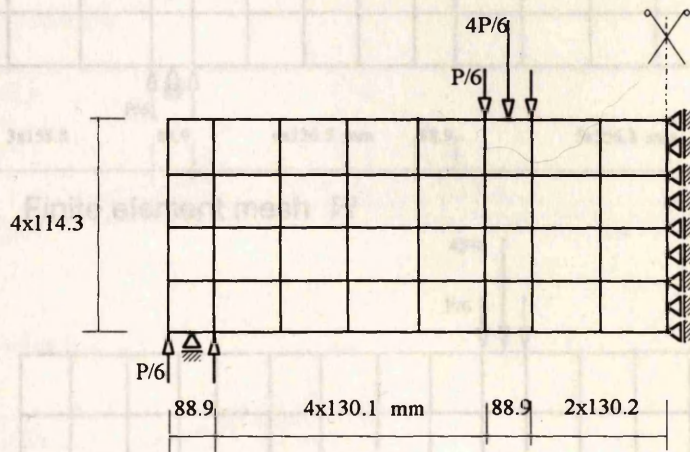
Fig. 7.6 Typical crack patterns of Clark's beams at failure.



(a) Finite element mesh I

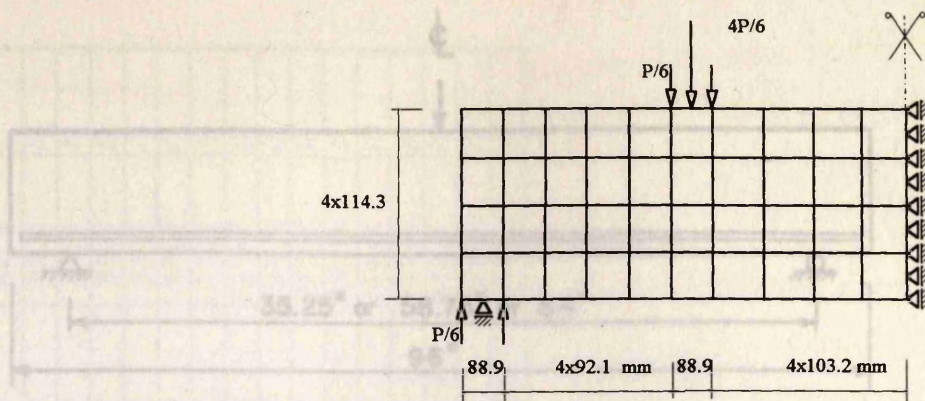


(b) Finite element mesh II

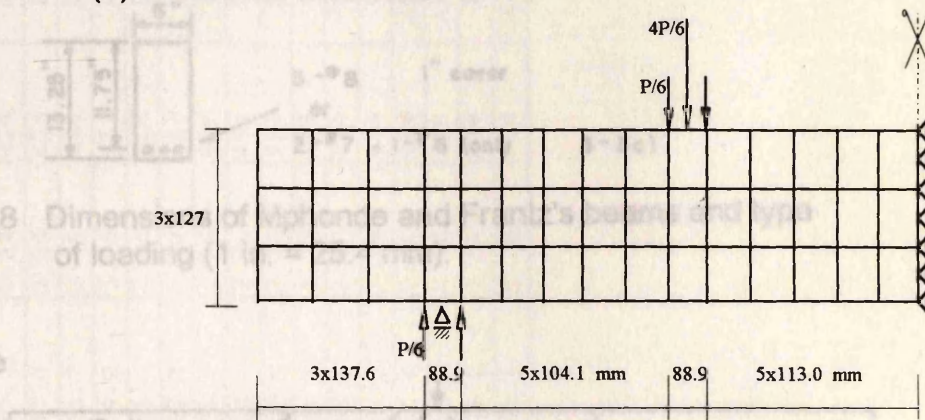


(c) Finite element mesh III

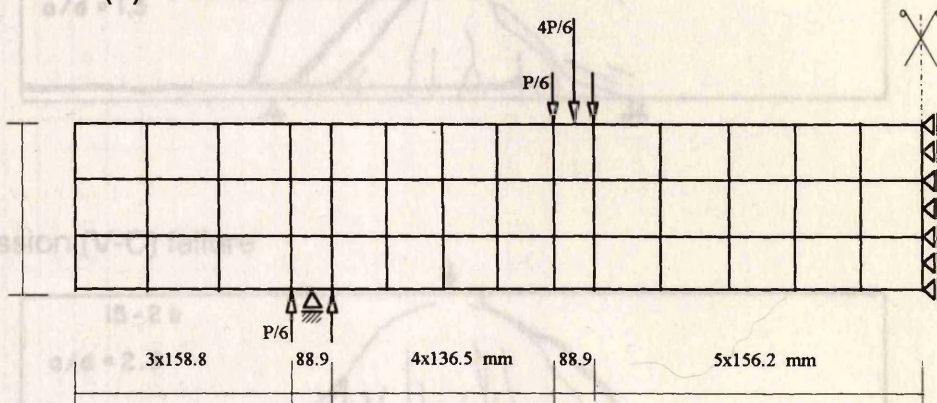
Fig. 7.7 Finite element meshes for Clark's beams.



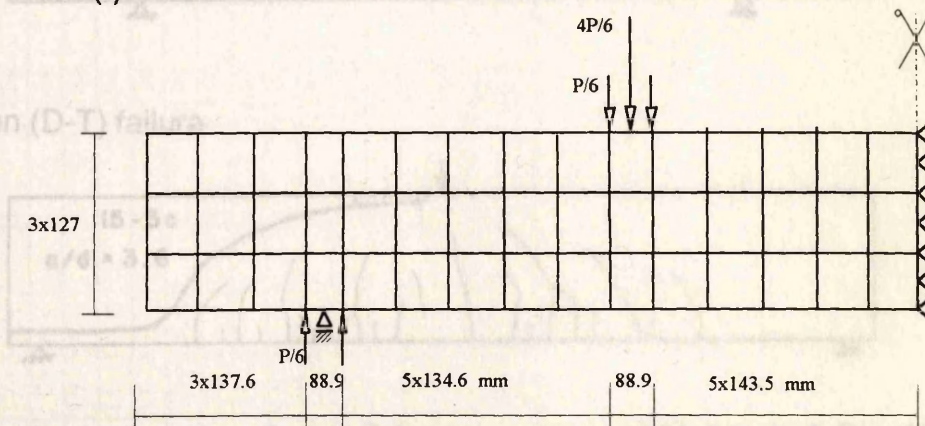
(d) Finite element mesh IV



(e) Finite element mesh V



(f) Finite element mesh VI



(g) Finite element mesh VII

Fig. 7.7 Finite element meshes for Clark's beams (continued).

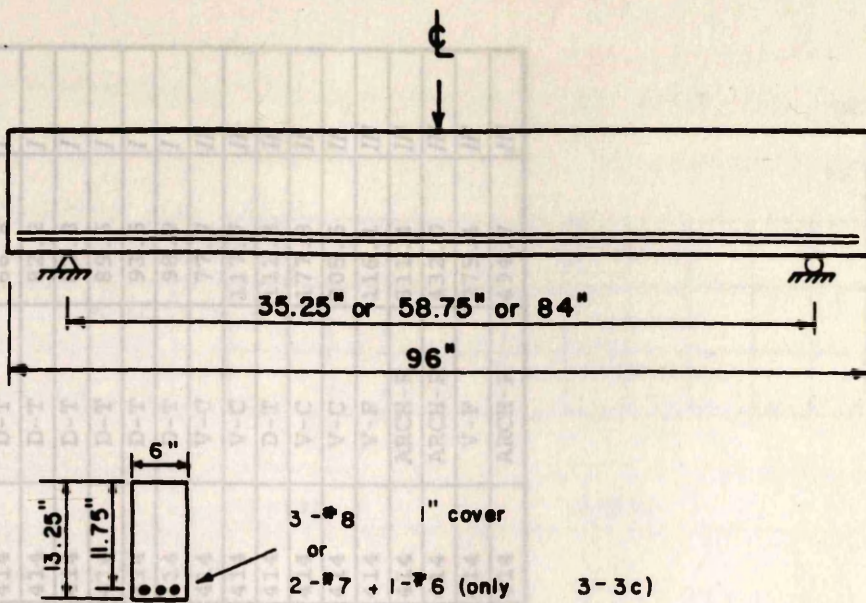
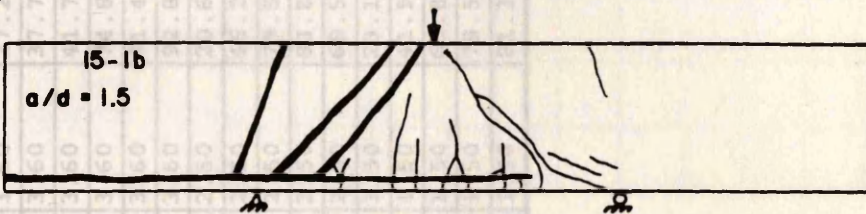
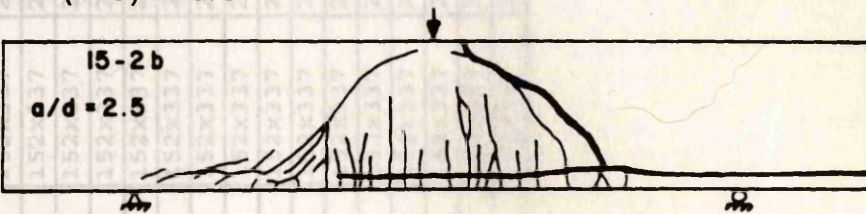


Fig. 7.8 Dimensions of Mphonde and Frantz's beams and type of loading (1 in. = 25.4 mm).

Arch rib failure



Shear compression (V-C) failure



Diagonal tension (D-T) failure

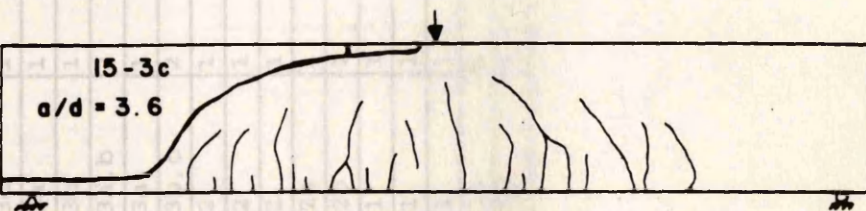


Fig. 7.9 Typical crack patterns of the three series of Mphonde & Frantz's beams.

Table 7.4 Data of Mphonde and Frantz's beams

No.	Beams	No. of Beams	Length (mm)	Cross-section (mmxmm)	d (mm)	a/d	f'_c (MPa)	ρ (%)	f_y (MPa)	Failure mode	Ultimate shear force (kN)	Mesh type
1	3-3b	1	2134	152x337	298.5	3.60	20.8	3.36	414	D-T	64.7	I
2	3-3c	1	2134	152x337	298.5	3.60	27.2	2.32	414	D-T	66.8	I
3	7-3a	1	2134	152x337	298.5	3.60	37.7	3.36	414	D-T	82.2	I
4	7-3b	1	2134	152x337	298.5	3.60	41.7	3.36	414	D-T	82.8	I
5-6	11-3a, b	2	2134	152x337	298.5	3.60	74.8	3.36	414	D-T	89.6	I
7	15-3a	1	2134	152x337	298.5	3.60	81.4	3.36	414	D-T	93.5	I
8-9	15-3b, c	2	2134	152x337	298.5	3.60	92.8	3.36	414	D-T	98.9	I
10	3-2	1	1492	152x337	298.5	2.50	20.6	3.36	414	V-C	77.7	II
11	7-2	1	1492	152x337	298.5	2.50	45.2	3.36	414	V-C	117.7	II
12	11-2	1	1492	152x337	298.5	2.50	79.5	3.36	414	D-T	111.3	II
13	15-2a	1	1492	152x337	298.5	2.50	83.8	3.36	414	V-C	177.8	II
14	15-2b	1	1492	152x337	298.5	2.50	69.5	3.36	414	V-C	205.5	II
15	3-1	1	895	152x337	298.5	1.50	23.1	3.36	414	V-F	116.1	III
16	7-1	1	895	152x337	298.5	1.50	41.9	3.36	414	ARCH-R	311.4	III
17	11-1	1	895	152x337	298.5	1.50	65.8	3.36	414	ARCH-R	432.0	III
18	15-1a	1	895	152x337	298.5	1.50	79.5	3.36	414	V-F	275.4	III
19	15-1b	1	895	152x337	298.5	1.50	81.3	3.36	414	ARCH-R	494.7	III

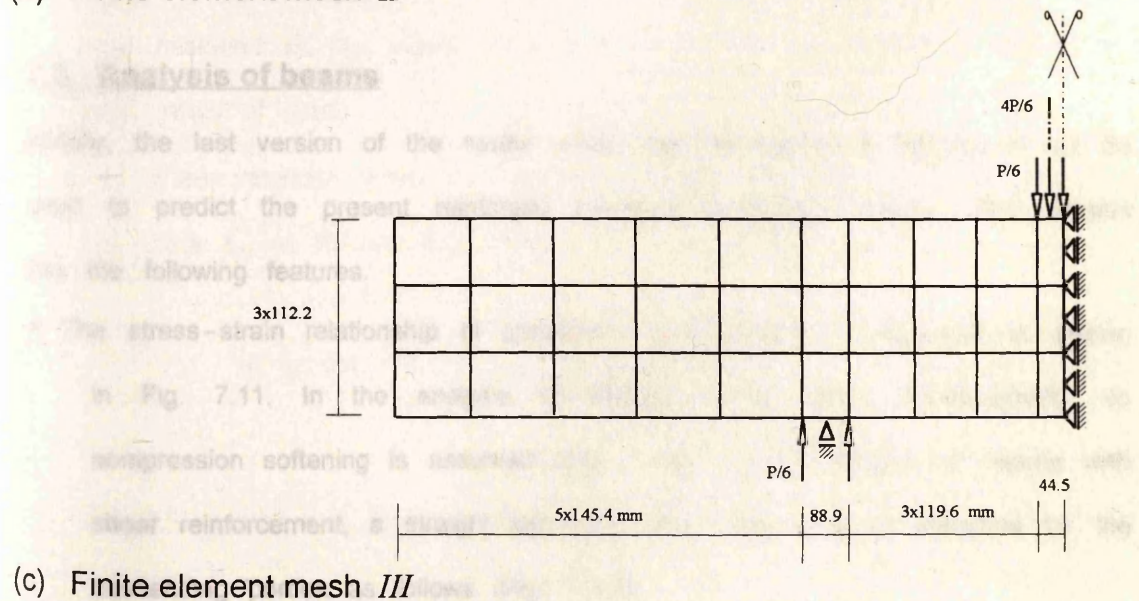
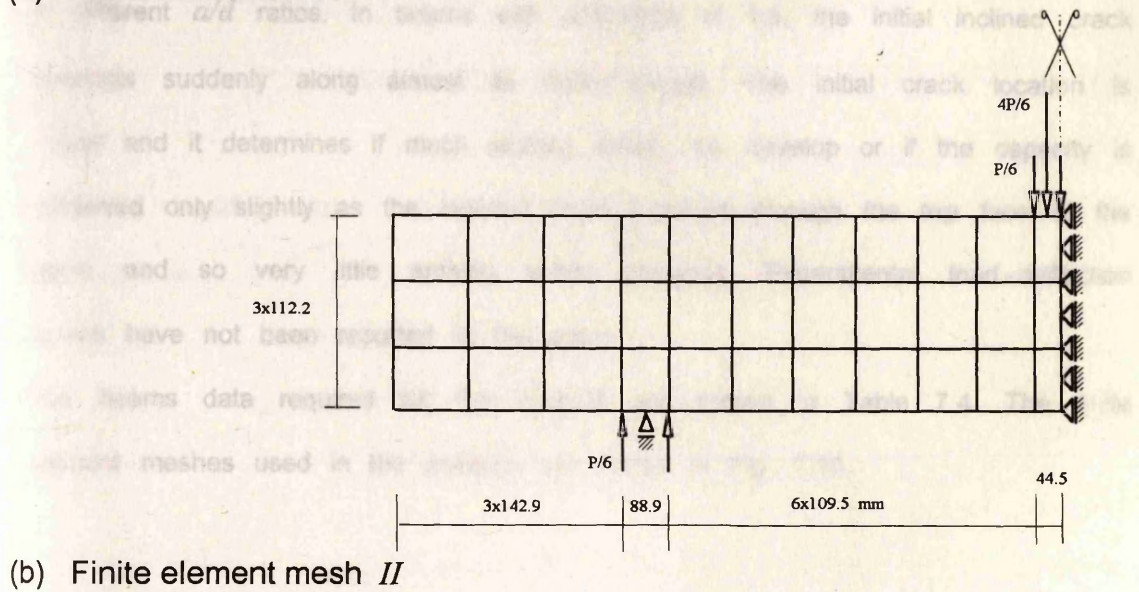
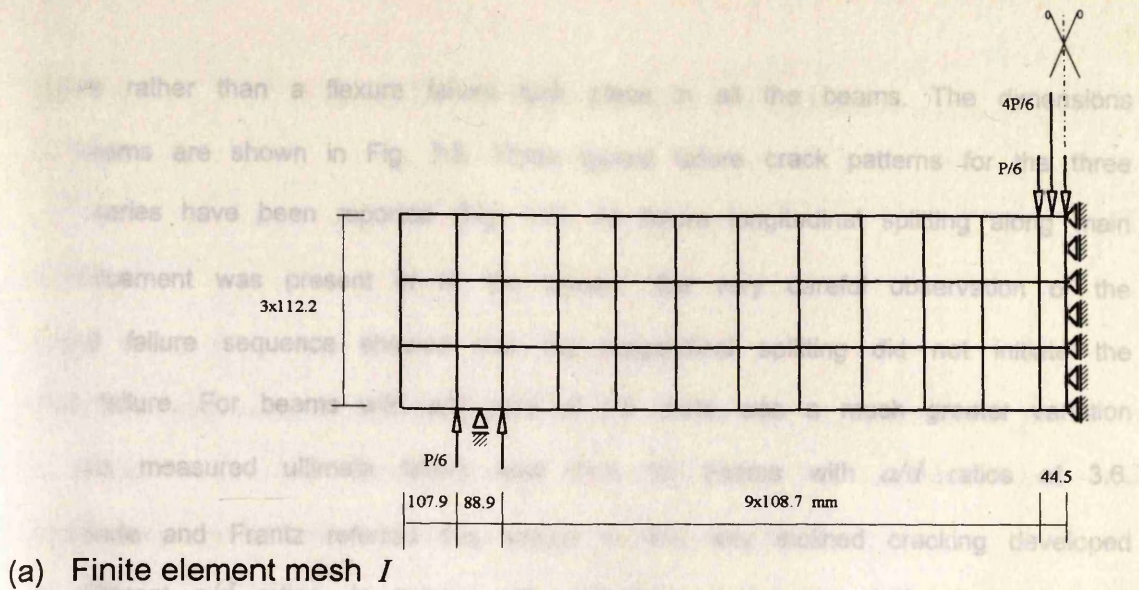


Fig. 7.10 Finite element meshes for Mphonde and Frantz's beams

failure rather than a flexure failure took place in all the beams. The dimensions of beams are shown in Fig. 7.8. Three typical failure crack patterns for the three a/d series have been reported (Fig. 7.9). At failure longitudinal splitting along main reinforcement was present in all the beams. But very careful observation of the actual failure sequence showed that the longitudinal splitting did not initiate the final failure. For beams with a/d ratio of 1.5 there was a much greater variation in the measured ultimate failure load than for beams with a/d ratios of 3.6. Mhponde and Frantz referred this scatter to the way inclined cracking developed at different a/d ratios. In beams with a/d ratio of 1.5, the initial inclined crack develops suddenly along almost its entire length. The initial crack location is critical and it determines if much arching action can develop or if the capacity is increased only slightly as the inclined crack punches through the top face of the beam and so very little arching action develops. Experimental load-deflection curves have not been reported in the paper.

The beams data required for the analysis are shown in Table 7.4. The finite element meshes used in the analysis are shown in Fig. 7.10.

7.3 Analysis of beams

Initially, the last version of the model which was developed in chapter 6 will be used to predict the present reinforced concrete rectangular beams. This version has the following features.

- The stress-strain relationship of concrete in compression is assumed as shown in Fig. 7.11. In the analysis of beams without shear reinforcement, no compression softening is assumed (Fig. 7.11a). In the analysis of beams with shear reinforcement, a straight line with very small slope is assumed for the descending portion as follows (Fig. 7.11b).

$$\sigma = f_c' (0.1 - \varepsilon) / (0.1 - \varepsilon_{cc}); \quad \varepsilon < \varepsilon_{max} \quad (7.1)$$

$$\varepsilon_{cc} = \sqrt{f_c'} / 2500; \quad \varepsilon_{max} = 0.005.$$

where f_c' in MPa

- The stress-strain relationship of concrete in tension is assumed as shown in Fig. 7.12. The tensile strength of concrete f_t' is estimated from the compressive strength of concrete f_c' as follows (Fig. 7.13).

$$f_t' = 0.54 \sqrt{f_c'} \quad \text{MPa} \quad (7.2)$$

The equation which represents the descending portion of the stress-strain curve is.

$$\sigma = \frac{1}{2} \left(\frac{\varepsilon_{cr}}{\varepsilon_n} + \sqrt{\frac{\varepsilon_{cr}}{\varepsilon_n}} \right) f_t'; \quad \varepsilon_n < \varepsilon_{tmax} \quad (7.3)$$

Two values of ε_{tmax} will be studied in this chapter; a very large value (which was assumed in the model of chapter 6) and $20 \varepsilon_{cr}$ (which is around the yield strain of steel).

- The shear retention factor β is assumed as a function of the strain normal to the crack ε_n as follows (Fig. 7.14).

$$\beta = 0.4 \frac{\varepsilon_{cr}}{\varepsilon_n} > \beta_{min}; \quad \beta_{min} = 0.0 \quad (7.4)$$

- Young's modulus is taken as follows.

$$E = 5000 \sqrt{f_c'} \quad \text{MPa}$$

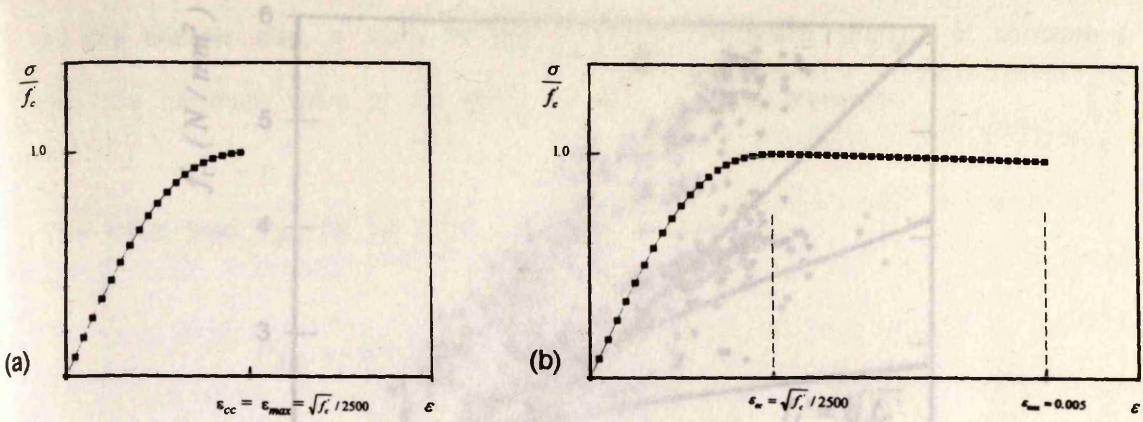


Fig. 7.11 Assumed stress-strain curve of concrete in compression
 (a) for beams without shear reinforcement
 (b) for beams with shear reinforcement

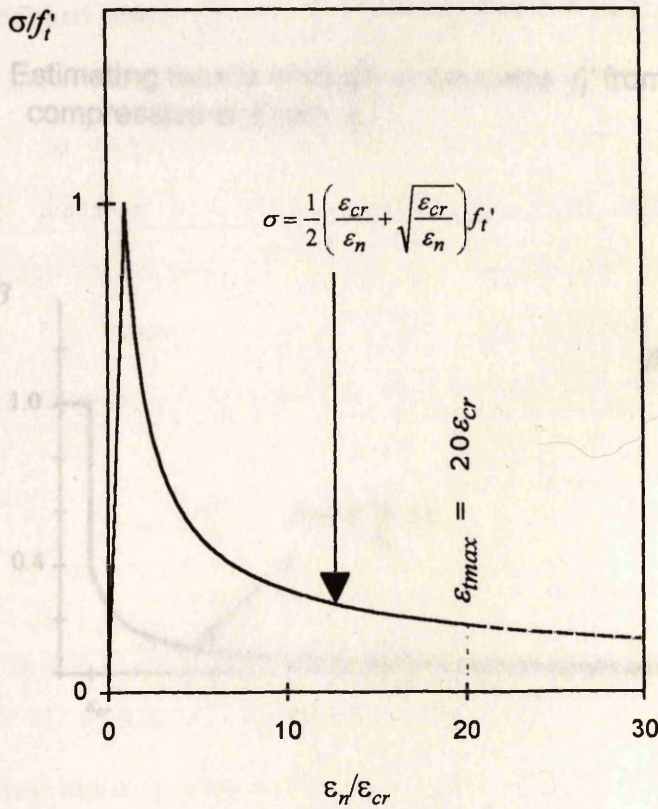


Fig. 7.12 Assumed stress-strain curve of concrete in Tension

7.3.1.1 Results of Krefeld and Thurston's beams: Table 7.5
 In this chapter also, a study on the effect of the tensile strength of concrete f_t' and the minimum value of the shear retention β_{min} is presented.

The results of Krefeld and Thurston's beams without shear reinforcement are shown in Table 7.5. The results in Column A of this Table are obtained from the model of chapter 6. The results are acceptable for all the beams except for three beams (4A3, 11A2, and OCake-R) in which the experimental failure load is overestimated by more than 20%. The mean value of the results and the standard deviation are 1.06 and 15.9%, respectively when ϵ_{tmax} was taken = $20\epsilon_{cr}$, nearly the same

$$P_{ini} = 0.6 f_y A_s / (a/d)$$

This initial load is about 70% (0.6/0.87) of the flexure capacity of the beam (for two point loading, Moment = Pa , P = load, a = shear span, flexure capacity $\cong f_y A_s (0.87d)$, d = effective depth). The beam which reaches its full flexure capacity takes about 26 increments (1.45 of the initial load).

7.3.1 Beams without shear reinforcement: Tables 7.5 to 7.7.

The results of prediction for beams without shear reinforcement are presented in Tables 7.5 to 7.7. In these tables, there are four basic sets of runs. In Column (A), the ratios of predicted to the experimental failure load using the model of chapter 6 are presented. Column (B) shows the results after assuming $\epsilon_{tmax} = 20\epsilon_{cr}$ (Fig. 7.12). In Column (C), the analysis was repeated after taking the tensile strength of concrete f_t' from the following equation (Fig. 13).

$$f_t' = \sqrt[4]{f_c'} \quad \text{MPa} \quad (7.5)$$

The object of using this equation is to obtain lower values of tensile strength than the given by Eq. 7.2 ($f_t' = 0.54 \sqrt{f_c'}$) because analysis has shown that obtaining f_t' from Eq. 7.2 gave higher prediction than the experiment. Column (D) shows the results after assuming that the minimum value of shear retention factor β_{min} (see equation 7.4) is equal 0.05.

7.3.1.1 Results of Krefeld and Thurston's beams: Table 7.5

The results of Krefeld and Thurston's beams without shear reinforcement are shown in Table 7.5. The results in Column A of this Table are obtained from the model of chapter 6. The results are acceptable for all the beams except for three beams (4A3, 11A2, and OCabs-II) in which the experimental failure load is overestimated by more than 30%. The mean value of the results and the standard deviation are 1.06 and 15.8%, respectively. When ϵ_{tmax} was taken $= 20\epsilon_{cr}$, nearly the same results as of Column A were obtained (Column B). The beams which were slightly affected by the value of ϵ_{tmax} were those having a/d ratio less than 4.0. The mean value and standard deviation in this case are 1.04 and 13.7%, respectively. When the tensile strength was calculated from equation (7.5), a decrease of about 10% in the mean value was obtained with standard deviation 9.4% rather than 13.7% (compare Columns B and C). The strength of one of the beams was overestimated by more than 10%. The results in Column D are obtained by assuming minimum value of shear retention factor ($\beta_{min} = 0.05$). As shown in this column, this small value of β increased the predicted failure load of some beams by more than 25% (beams 4A3 and OCabs-II).

7.3.1.2 Clark's beams: Table 7.6

Table 7.6 shows the results of Clark's beams without shear reinforcement. As for Krefeld and Thurston's beams (Table 7.5), the more conservative result for Clark's beams was obtained by using equation (7.5) for estimating f'_t . Also less scatter in the results was obtained by using this equation. By comparing Column C and D it can be seen that increasing β_{min} from zero to 0.05 increased the mean value of the predicted failure loads by 15%.

7.3.1.3 Mphonde and Frantz's beams: Table 7.7

The results of Mphonde and Frantz's beams (without shear reinforcement) are shown in Table 7.7. In this Table there are six sets of runs. To see clearly the effect of f'_t and β on the results, in addition to the basic four sets of runs

Table 7.5 Results of Krefeld and Thurston's beams without shear reinforcement

No.	Beams	a/d	f'_c (MPa)	Failure mode	Ultimate shear force (kN)	Predicted / Experimental failure load			
						(A) $\epsilon_{tmax} = \text{very large}$ $\beta_{min} = 0.0$ $f'_t = 0.54\sqrt{f'_c}$	(B) $\epsilon_{tmax} = 20 \epsilon_{cr}$ $\beta_{min} = 0.0$ $f'_t = 0.54\sqrt{f'_c}$	(C) $\epsilon_{tmax} = 20 \epsilon_{cr}$ $\beta_{min} = 0.0$ $f'_t = 4\sqrt{f'_c}$	(D) $\epsilon_{tmax} = 20 \epsilon_{cr}$ $\beta_{min} = 0.05$ $f'_t = 4\sqrt{f'_c}$
1	4A3	2.35	30.6	DT-S	109.9	1.49	1.43	1.05	1.30
2	5A3	2.35	29.9	DT-S	170.4	1.02	0.96	0.72	0.84
3	11A2	2.92	30.2	DT-S	73.4	1.34	1.27	1.04	1.19
4	12A2	3.85	30.1	DT-S	64.1	1.04	1.04	0.84	1.04
5-8	18A2-D2	2.90	21.0	DT, DT-S	67.2	1.10	1.04	0.92	1.04
9	13A2	2.90	19.9	DT-S	48.5	1.03	1.00	0.95	1.05
10	14A2	3.77	20.7	DT-S	35.1	1.07	1.04	0.98	1.07
11-12	15A2, B2	2.90	20.4	DT-S	48.9	1.18	1.14	1.10	1.27
13	16A2	3.81	22.2	DT-R	41.8	1.09	1.09	1.02	1.13
14	17A2	3.77	22.0	DT-S	44.0	1.10	1.10	0.92	1.10
15	18E2	2.90	19.8	DT-S	81.8	0.85	0.85	0.75	0.80
16	19A2	3.81	20.6	DT-S	46.3	1.15	1.15	1.02	1.08
17	20A2	3.85	21.0	DT-S	50.7	1.07	1.07	0.99	1.07
18	21A2	3.85	19.9	DT-S	76.5	0.96	0.96	0.88	0.88
19	1AC	4.77	21.9	F-T	32.9	0.93	0.93	0.91	0.91
20	2AC	4.80	23.0	DT-C	37.8	1.00	1.00	1.00	1.03
21	3AC	4.77	20.8	DT-R	44.0	0.94	0.94	0.90	0.94
22	4AC	4.80	16.5	DT-R	37.8	0.94	0.94	0.94	0.94
23	5AC	4.83	18.4	DT-S	41.8	0.94	0.94	0.94	0.94
24	6AC	4.87	22.8	DT-R	53.4	0.87	0.87	0.80	0.87
25	1CC	5.96	19.0	F-T	26.7	0.92	0.90	0.87	0.87
26	2CC	6.00	20.8	F-T	30.2	1.00	1.00	0.97	1.03
27	3CC	5.96	20.5	DT-R	35.6	0.93	0.93	0.93	0.97
28-29	OCabs-I	6.00	37.4	DT-R	50.5	1.07	1.07	0.95	1.15
30-31	OCabs-II	4.02	38.3	DT-R	140.1	1.39	1.28	1.06	1.50
	Mean	value				1.06	1.04	0.94	1.04
	Standard deviation					15.8%	13.7%	9.3%	16.0%

Table 7.6 Results of Clark's beams without shear reinforcement

No.	Beams	a/d	f'_c (MPa)	Failure mode	Range of ultimate shear force (kN)	Ultimate shear force (kN)	Predicted / Experimental failure load			
							(A) $\epsilon_{max} = \text{very large}$ $\beta_{min} = 0.0$ $f'_s = 0.54V'_c$	(B) $\epsilon_{max} = 20 \epsilon_{cr}$ $\beta_{min} = 0.0$ $f'_s = 0.54V'_c$	(C) $\epsilon_{max} = 20 \epsilon_{cr}$ $\beta_{min} = 0.0$ $f'_s = 4V'_c$	(D) $\epsilon_{max} = 20 \epsilon_{cr}$ $\beta_{min} = 0.05$ $f'_s = 4V'_c$
4	AO 1-3	2.35	23.8	D-T, T	89.0-119.1	105.0	1.09	0.98	0.84	1.09
5	BO 1-3	1.95	23.7	D-T	94.2-128.0	114.4	1.16	1.08	0.89	1.04
6	CO 1-3	1.56	23.9	D-T, T	166.9-175.8	173.0	0.83	0.80	0.77	0.86
7	DO 1-3	1.17	26.0	D-T, T	221.6-259.9	234.9	0.94	0.85	0.82	0.91
	Mean						1.01	0.93	0.83	0.98
	Standard deviation						14.8%	12.7%	5.0%	10.8%

(Column A, B, C, and D), there are two other sets; one by assuming $f_t' = 0.1 f_c'$ (Column B0, Fig. 7.13) and the other (Column E) by assuming constant shear retention factor ($\beta = \beta_{min} = 0.4$).

In these beams the effect of limiting the tension softening of concrete at strain $\epsilon_{tmax} = 20\epsilon_{cr}$ was significant (compare Column A and B). A decrease in the mean value of about 9% was obtained. In beam 15-3a a decrease in the predicted failure load of 28% of the experimental failure load was obtained.

Comparing the results of Columns B0, B, and C, in which the only difference was in the assumed values of f_t' , it can be seen that the effect of f_t' on the predicted failure load was very significant. For example in beams 11-3b,c the predicted failure load decreased from 1.88 to 0.88 of the experimental failure load by changing the value of f_t' from $0.1 f_c'$ (7.48 MPa) to $\sqrt[4]{f_c'}$ (2.94 MPa). Also, it can be seen that the lower the assumed value of f_t' , less the scatter in the results. In beams which failed in diagonal tension and having a/d ratio of 3.6, the higher the value of compressive strength of concrete f_c' , higher the predicted failure load. This high prediction reduced as the values of f_t' decreased. This can be seen in the first five rows of table 7.7. In Column A, the predicted failure load varied from 0.81 for beam 3-3b to 1.85 for beams 11-3a,b, while in column C for the same beams the predicted failure load is around 0.85.

With regard to β , in general, the results of all beams were seriously affected by its value. An increase in the value of β_{min} from zero to 0.05 increased the mean value of the results by about 38% (compare Columns C and D). In beam 11-3a,b, the predicted failure load increased by 100% of the experimental failure load when β_{min} changed from 0.0 to 0.4 (Columns C and E). Although high value of β_{min} generally overestimate the predicted failure load, for three beams the predicted failure loads were underestimated (7-1, 11-1, and 15-1b). The reported mode of failure of these three beams was arch-rib (see Fig.7.9). This type of failure occurred in beams with a small a/d ratio (1.5) and it does not

always occurs. Mphonde and Frantz tested two beams with the same properties but one (beam 15-1a) failed in shear flexure mode at a low load while the other beam (15-1b) failed in arch-rib mode at a load which is greater by 80%. As mentioned earlier, this type of failure depends on the location and the direction of inclined critical crack. It seems that from the numerical point of view that, unlike the other types of failures, higher the assumed value of β more accurate the predicted failure load for those beams.

7.3.2 Beams with shear reinforcement: Tables 7.8 and 7.9.

7.3.2.1 Krefeld and Thurston's beams: Table 7.8.

Table 7.8 shows the results of Krefeld and Thurston's beams with shear reinforcement. In these beams the effect of limiting the tension softening of concrete at strain $\varepsilon_{tmax} = 20\varepsilon_{cr}$ was insignificant (compare Column A and B). Column C shows the results after using equation (7.5) for f'_t . The results improved for most of the beams which failed in shear. The mean value decreased from 1.14 to 0.97 with standard deviation 11.9% rather than 20.1%. Only for three beams were the failure load overestimated by more than 20%. By increasing β_{min} from zero to 0.05, the results became the worst results for these beams. The mean value increased to 1.16 with standard deviation of 23.1%.

7.3.2.2 Clark's beams: Table 7.9.

Table 7.9 shows the results of Clark's beams with shear reinforcement. Column A shows the results using the model of chapter 6. The mean value and standard deviation 0.97 and 9.4%, respectively. Column B shows that the effect of limiting the tension softening of concrete at strain $\varepsilon_{tmax} = 20\varepsilon_{cr}$ was very small, a reduction of only 4% in the mean value was obtained. Columns B and C show that the effect of f'_t was very small. The results were good for all cases. The best result was with using equation 7.5 for f'_t and assuming $\beta_{min} = 0.05$, the

Table 7.8 Results of Krefred and Thurston's beams with shear reinforcement

No.	Beams	a/d	f'_c (MPa)	Failure mode	Ultimate shear force (kN)	Predicted / Experimental failure load			
						(A) $\epsilon_{max} = \text{very large}$ $\beta_{min} = 0.0$ $f'_t = 0.54v_f'$	(B) $\epsilon_{max} = 20 \epsilon_{cr}$ $\beta_{min} = 0.0$ $f'_t = 0.54v_f'$	(C) $\epsilon_{max} = 20 \epsilon_{cr}$ $\beta_{min} = 0.0$ $f'_t = 4v_f'$	(D) $\epsilon_{max} = 20 \epsilon_{cr}$ $\beta_{min} = 0.05$ $f'_t = 4v_f'$
1	23.5	6.00	38.5	F-T	60.9	0.99	0.99	0.99	0.99
2-3	26a,b	6.00	34.8	F-T	60.9	0.99	0.99	0.92	0.95
4-6	210a-c	6.00	38.4	F-T	63.5	0.95	0.95	0.92	0.95
7-8	212a,b	6.00	39.5	F-T	66.9	0.99	0.99	0.87	0.99
9	24-1	4.02	37.3	F-T	244.6	0.99	0.99	0.89	0.99
10	26-1	4.02	40.2	DT-R	206.8	1.17	1.17	0.98	1.17
11-12	29a-1,b-1	4.02	38.3	DT-R	159.9	1.51	1.46	1.22	1.51
13	213.5-1	4.02	38.9	DT-R	148.1	1.58	1.53	1.16	1.63
14	24.5-2	4.02	37.6	F-T	243.8	0.99	0.99	0.86	0.99
15	29a-2	4.02	37.2	DT-C	216.6	1.12	1.12	0.86	1.12
16-17	29b-2,f-2	4.02	41.6	DT-C,F,T,DT-R	218.4	1.11	1.11	0.89	1.11
18	29c-2	4.02	24.2	DT-C	161.5	1.11	1.11	1.01	1.21
19	29d-2	4.02	30.4	DT-C	165.0	1.32	1.32	1.09	1.42
20	29e-2	4.02	48.5	DT-R	206.4	1.20	1.20	0.98	1.17
21	29g-2	4.02	15.7	DT-C	149.9	0.89	0.89	0.89	0.94
22	213.5a-2	4.02	37.0	DT-C	161.5	1.40	1.40	1.11	1.50
23	218a-2	4.02	37.6	DT-R	164.1	1.33	1.33	1.00	1.42
24	24.5-3	4.02	35.5	F-C	232.6	1.04	1.04	0.84	1.04
25	29-3	4.02	34.3	DT-C	177.9	1.23	1.23	0.97	1.36
26	39-1	4.02	37.3	F-T	248.2	0.97	0.97	0.91	0.97
27	313.5-1	4.02	37.3	F-T	251.3	0.96	0.96	0.87	0.96
28	318-1	4.02	40.6	DT-C	220.2	1.10	1.10	0.92	1.10
29	321-1	4.02	38.8	DT-R	163.7	1.48	1.43	1.19	1.48
30	39-2	4.02	37.1	F-T	248.6	0.97	0.97	0.88	0.97
31	313.5-2	4.02	39.7	F-T,DT-C	234.9	1.03	1.03	0.90	1.03
32	318-2	4.02	38.9	DT-C	177.0	1.32	1.32	1.06	1.37

Table 7.8 Results of Kreferd and Thurston's beams with shear reinforcement (continued)

No.	Beams	a/d	f'_c (MPa)	Failure mode	Ultimate shear force (kN)	Predicted / Experimental failure load			
						(A) ϵ_{max} = very large β_{min} = 0.0 $f'_l = 0.54v'_c$	(B) $\epsilon_{max} = 20 \epsilon_{cr}$ $\beta_{min} = 0.0$ $f'_l = 0.54v'_c$	(C) $\epsilon_{max} = 20 \epsilon_{cr}$ $\beta_{min} = 0.0$ $f'_l = 4v'_c$	(D) $\epsilon_{max} = 20 \epsilon_{cr}$ $\beta_{min} = 0.05$ $f'_l = 4v'_c$
33	321-2	4.02	38.0	DT-R	166.8	1.40	1.40	1.08	1.45
34	39-3	4.02	42.7	F-T,DT-C	239.7	1.04	1.04	0.91	1.01
35	313.5-3	4.02	42.7	DT-C	213.5	1.17	1.13	0.95	1.13
36	318-3	4.02	43.1	DT-R	174.8	1.38	1.38	1.07	1.38
37	321-3	4.02	43.1	DT-R	140.6	1.66	1.66	1.28	1.72
38-39	6A1, B1 *	3.89	29.9	F-C	258.0	0.92	0.92	0.92	0.92
40	9A1 *	4.86	30.8	F-C	203.7	0.97	0.97	0.97	0.97
41	9B1 *	2.92	29.9	F-C	350.5	0.86	0.86	0.79	0.90
42	23.5U *	6.00	38.5	F-T	113.4	0.99	0.99	0.99	0.99
43	213.5b-2 *	4.02	33.0	F-T	466.6	0.94	0.90	0.74	0.94
44	218b-2 *	4.02	34.6	DT-C	341.2	1.19	1.28	0.91	1.33
	Mean	value				1.14	1.14	0.97	1.16
	Standard deviation	deviation				21.0%	20.1%	11.9%	23.1%

* Beams subjected to distributed loads

Table 7.9 Results of Clark's beams with shear reinforcement

No.	Beams	a/d	f'_c (MPa)	Failure mode	Range of ultimate shear force (kN)	Ultimate shear force (kN)	Predicted / Experimental failure load			
							(A) $\epsilon_{max} = \text{very large}$ $\beta_{min} = 0.0$ $f'_i = 0.54vf'_c$	(B) $\epsilon_{max} = 20 \epsilon_{cr}$ $\beta_{min} = 0.0$ $f'_i = 0.54vf'_c$	(C) $\epsilon_{max} = 20 \epsilon_{cr}$ $\beta_{min} = 0.0$ $f'_i = 4vf'_c$	(D) $\epsilon_{max} = 20 \epsilon_{cr}$ $\beta_{min} = 0.05$ $f'_i = 4vf'_c$
57	A1 1-4	2.35	24.1	D-T	209.1-244.7	224.7	0.94	0.90	0.85	0.94
58	B1 1-5	1.95	24.1	D-T	241.4-284.8	261.0	0.93	0.88	0.84	0.98
59	B2 1-5	1.95	24.9	D-T	301.1-334.8	319.4	0.87	0.87	0.84	0.91
60	B6 1	1.95	42.2	D-T	-----	379.2	0.86	0.80	0.74	0.93
61	C1 1-4	1.56	26.3	D-T	245.9-311.1	280.1	0.97	0.94	0.87	1.05
62	C2 1-4	1.56	25.0	D-T, T	288.1-323.7	300.8	1.01	0.97	0.97	0.97
63	C3 1-3	1.56	13.9	D-T	188.1-223.6	204.0	0.94	0.89	0.89	0.94
64	C4 1	1.56	24.5	D-T	-----	309.0	0.88	0.83	0.78	0.98
65	C6 2-4	1.56	45.9	D-T	423.8-434.9	429.0	0.88	0.81	0.78	1.02
66	D1 1-3	1.17	25.7	D-T, T	256.6-356.7	304.8	1.13	1.06	1.02	1.13
67	D2 1-4	1.17	24.8	D-T, T	289.9-334.8	318.0	1.08	1.08	0.96	1.08
68	D3 1	1.17	28.2	D-T	-----	394.8	1.14	1.09	1.09	1.18
69	D4 1	1.17	23.1	D-T	-----	312.0	1.10	1.07	1.10	1.07
70	D1 6-8	1.94	27.8	D-T	174.7-185.8	180.0	1.04	1.04	0.99	1.08
71	E1 1	2.02	30.2	D-T	-----	221.7	0.88	0.88	0.84	0.95
72	D2 6-8	2.43	28.0	D-T	157.3-168.4	164.7	0.98	0.94	0.90	1.02
73	D4 1-3	2.43	25.0	D-T	157.3-168.4	163.5	0.87	0.83	0.83	0.91
73	D5 1-3	2.43	28.0	D-T	146.2-157.3	153.6	0.93	0.93	0.84	1.01
	Mean			value			0.97	0.93	0.90	1.01
	Standard deviation			deviation			9.4%	9.7%	10.4%	7.7%

mean value and standard deviation are 1.01 and 7.7%, respectively. Unlike Krefeld and Thurston's beams, it can be seen that increasing β_{min} from zero to 0.05 improved the results of Clark's beams.

The predicted failure loads are plotted against the experimental failure loads for all beams in Figs. 7.15–17. Fig. 7.15a shows the results using the model of chapter 6. Fig. 7.15b shows the results after taking $\epsilon_{tmax} = 20\epsilon_{cr}$ in the stress strain curve of concrete (see Fig. 7.12). The results after taking f'_t as from equation 7.5 are shown in Fig. 7.16. In this case if the predicted failure load is assumed to be 80% of the numerical failure load, all the predicted failure loads will be conservative. After increasing β_{min} to be 0.05, the results are shown in Fig. 7.17.

7.4 Prediction of failure mode

Ten types of failure have been reported by Krefeld and Thurston, Clark, and Mphonde and Frantz. In the following some of these types of failure have been analysed to see how accurately the present finite element model predicts the mode of failure. The prediction of the mode of failure depends on the following (see Sec. 6.2.1.1):

- the deformed shape of the beam,
- the crack pattern,
- the stresses of concrete in the compression zone, and
- the stresses in the reinforcement.

Beams OCa.bs-I (DT-R failure)

Beams OCa and OCb were two of Krefeld and Thurston's beams (series S-I) which failed in DT-R failure type. These two beams were without shear reinforcement and similar in everything except for a slight difference in the cylinder compressive strength f'_c and the reported failure load. There were eight beams

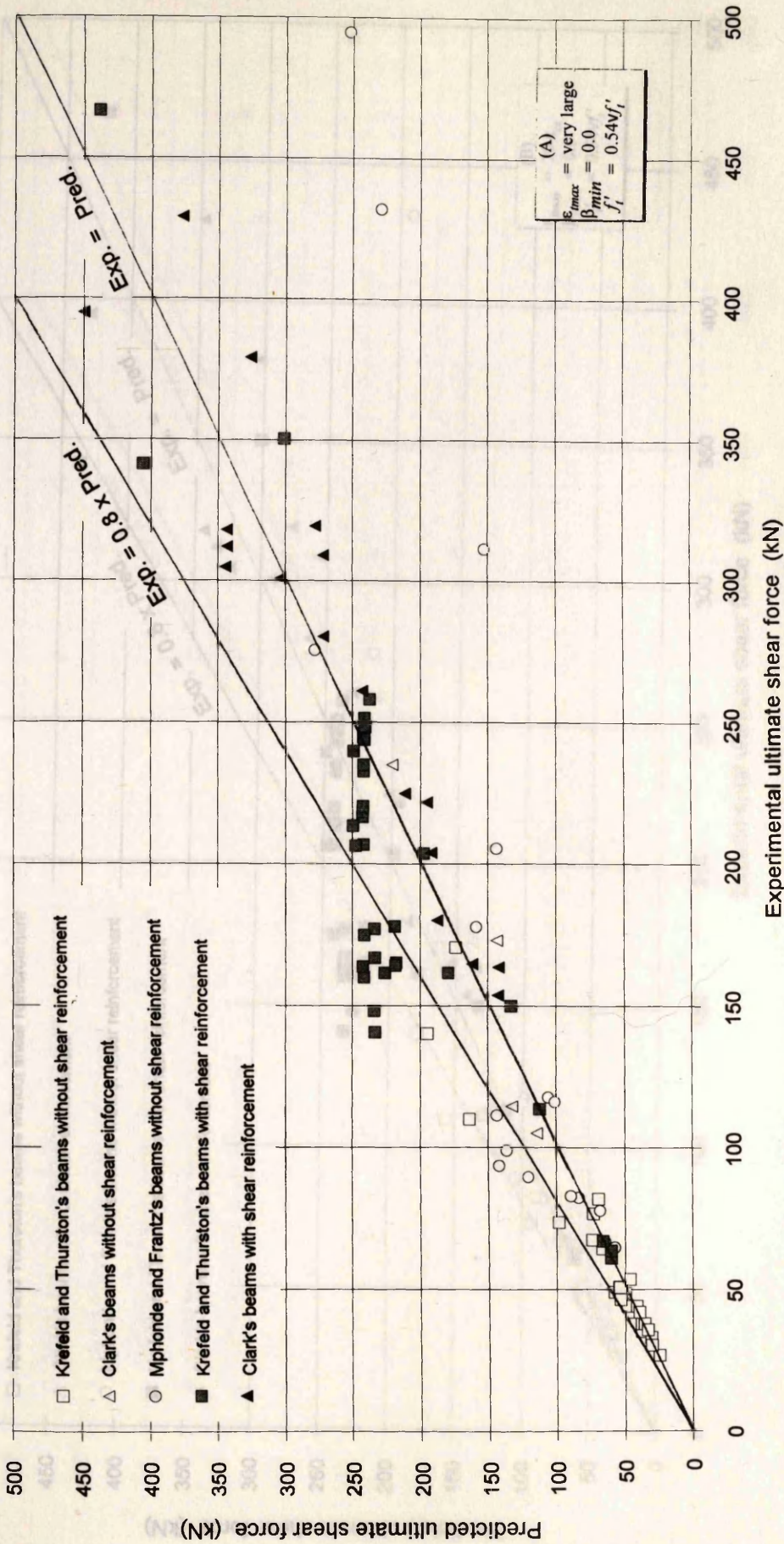


Fig. 7.15a Results of prediction of reinforced concrete rectangular beams with and without shear reinforcement using the model of chapter 6 (results of Column A in Tables 7.5-9)

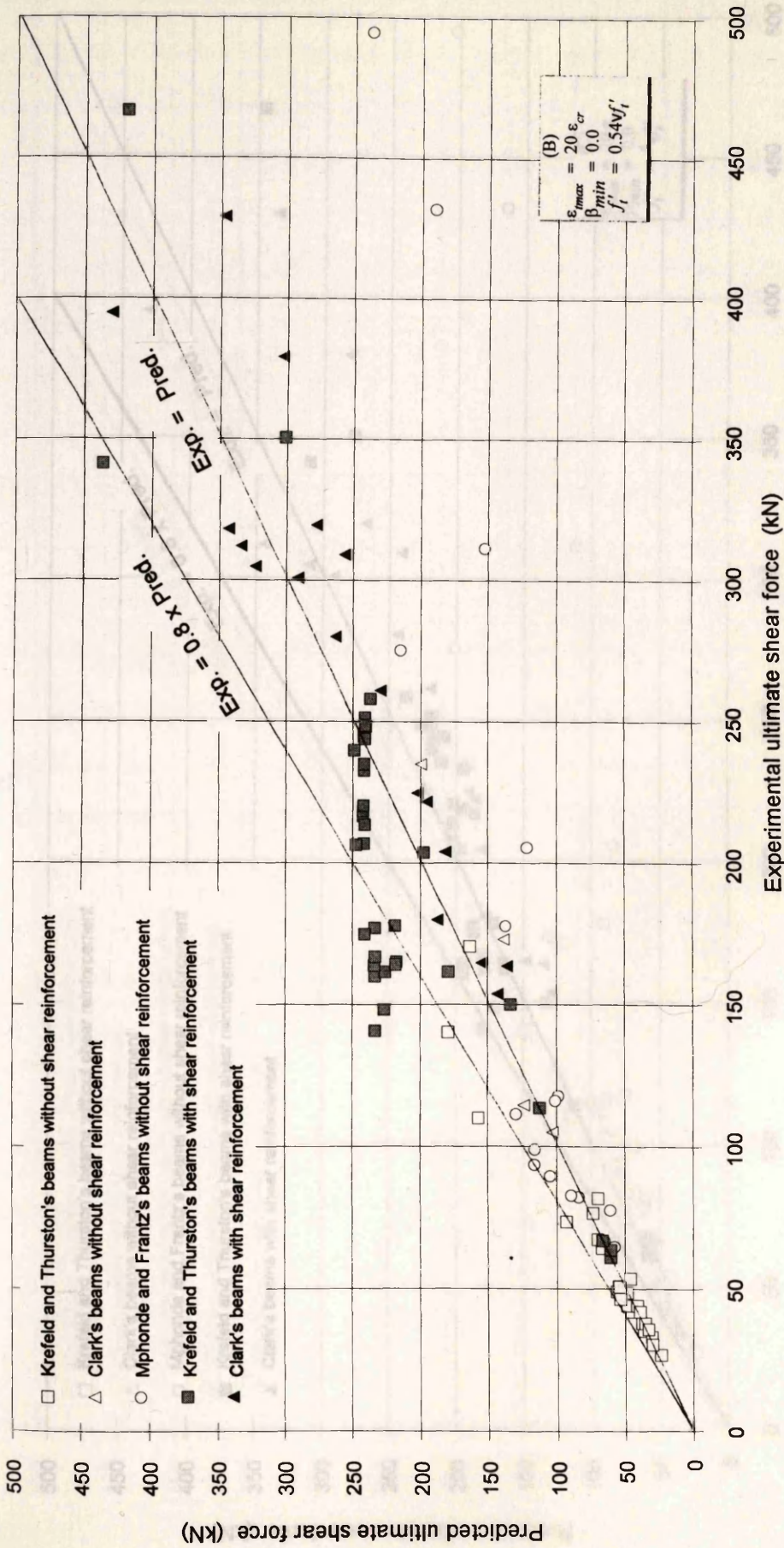


Fig. 7.15b Results of prediction of reinforced concrete rectangular beams with and without shear reinforcement after assuming $\epsilon_{max} = 20 \epsilon_{cr}$ (results of Column B in Tables 7.5-9)

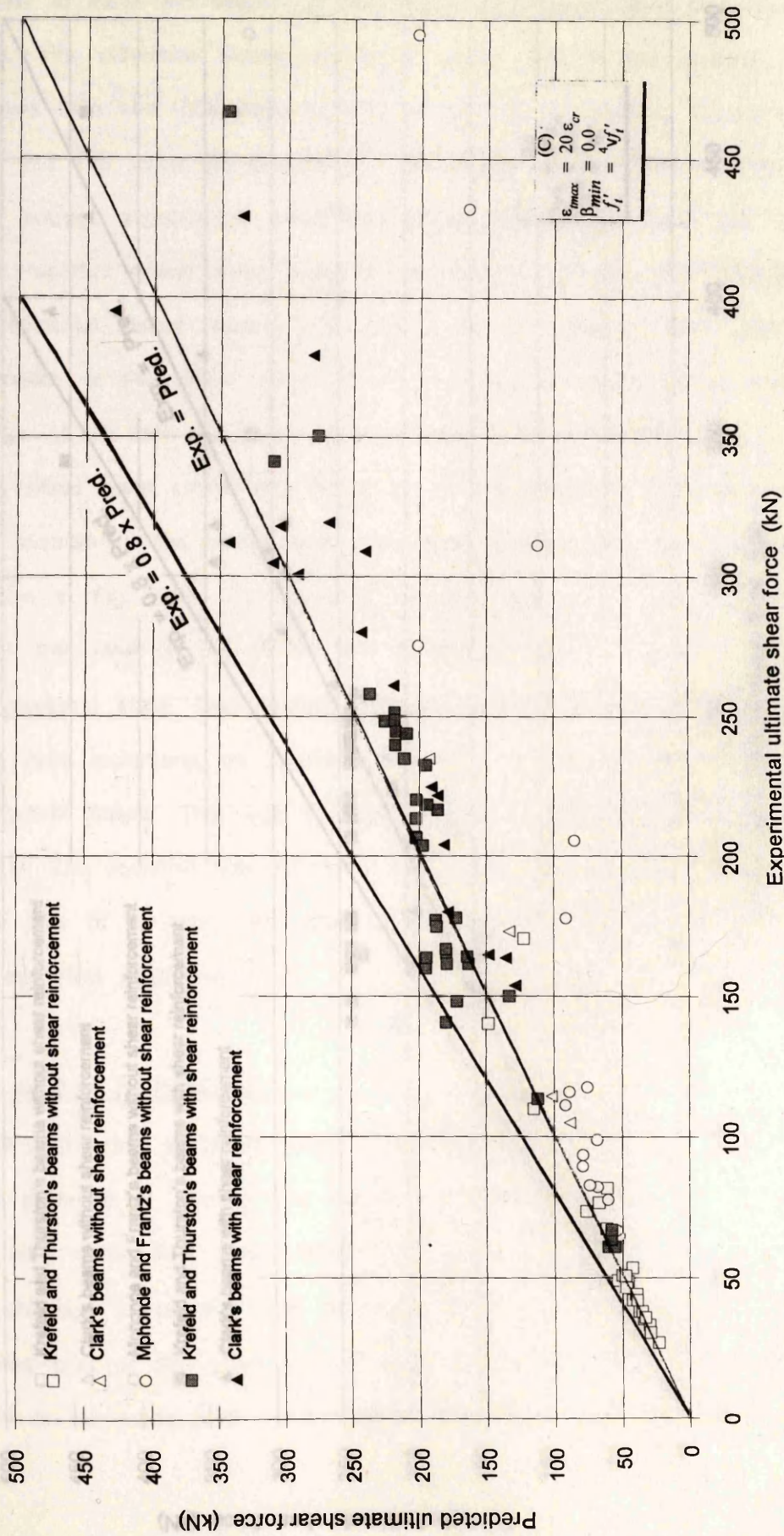


Fig. 7.16 Results of prediction of reinforced concrete rectangular beams with and without shear reinforcement after using $f_t' = 4\sqrt{f_c'}$ (results of Column C in Tables 7.5-9)

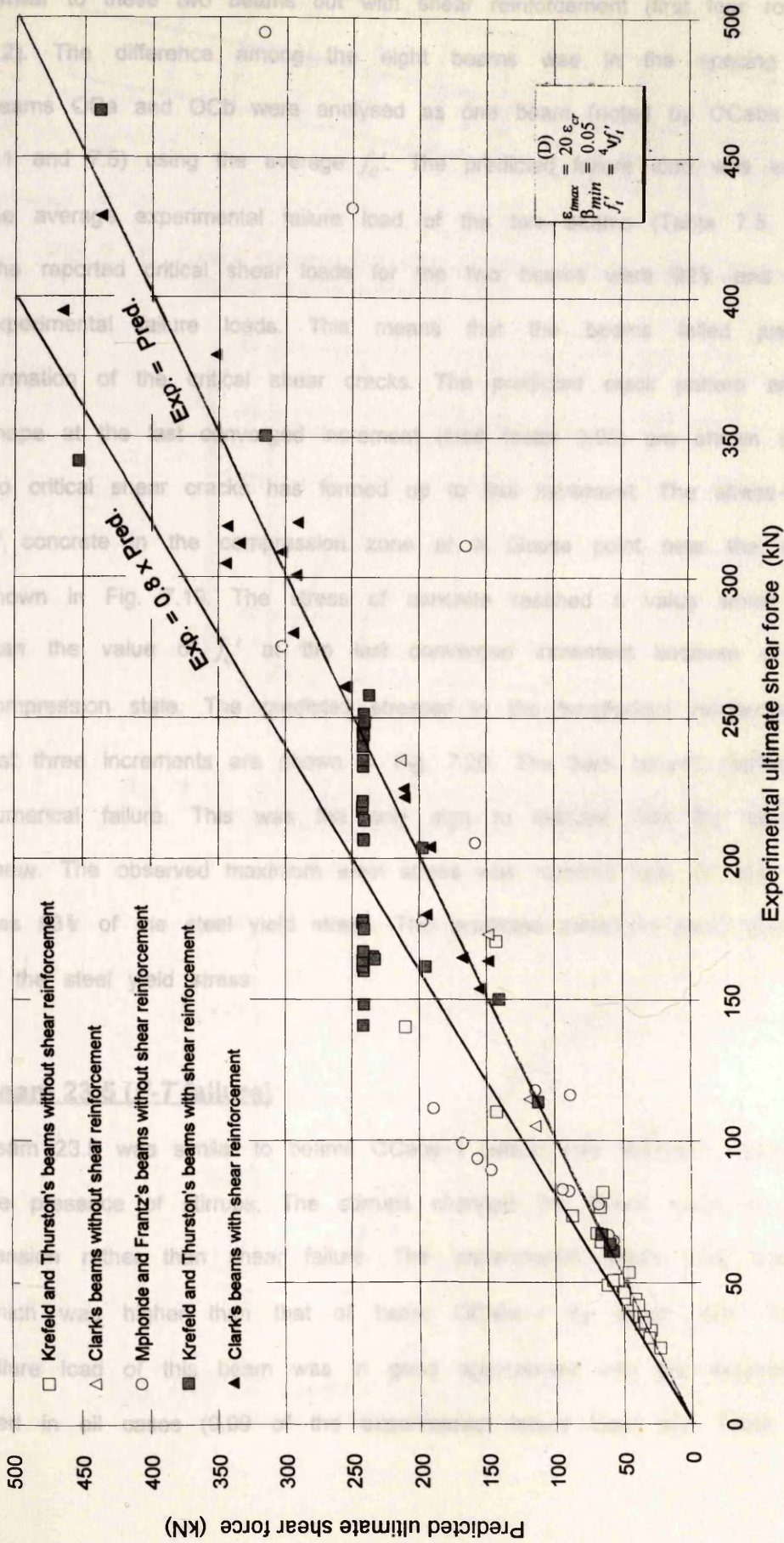


Fig. 7.17 Results of prediction of reinforced concrete rectangular beams with and without shear reinforcement after using $\beta_{min} = 0.05$ (results of Column D in Tables 7.5-9)

similar to these two beams but with shear reinforcement (first four rows in Table 7.2). The difference among the eight beams was in the spacing of stirrups. Beams OCa and OCb were analysed as one beam (noted by OCabs-I in Tables 7.1 and 7.5) using the average f_c' . The predicted failure load was equal 95% of the average experimental failure load of the two beams (Table 7.5, Column C). The reported critical shear loads for the two beams were 92% and 97% of the experimental failure loads. This means that the beams failed just after the formation of the critical shear cracks. The predicted crack pattern and deformed shape at the last converged increment (load factor 0.95) are shown in Fig. 7.18. No critical shear cracks has formed up to this increment. The stress-strain curve of concrete in the compression zone at a Gauss point near the mid-span is shown in Fig. 7.19. The stress of concrete reached a value which was higher than the value of f_c' at the last converged increment because of the biaxial compression state. The predicted stresses in the longitudinal reinforcement at the last three increments are shown in Fig. 7.20. The bars haven't yielded up to the numerical failure. This was the only sign to indicate that the beam failed in shear. The observed maximum steel stress was reported only for one beam which was 93% of the steel yield stress. The predicted maximum steel stress was 79% of the steel yield stress.

Beam 23.5 (F-T failure)

Beam 23.5 was similar to beams OCabs-I (which was analysed above) except for the presence of stirrups. The stirrups changed the failure mode to be Flexure-Tension rather than shear failure. The experimental failure load was 121.9 kN which was higher than that of beam OCabs-I by about 20%. The predicted failure load of this beam was in good agreement with the experimental failure load in all cases (0.99 of the experimental failure load, see Table 7.8) which

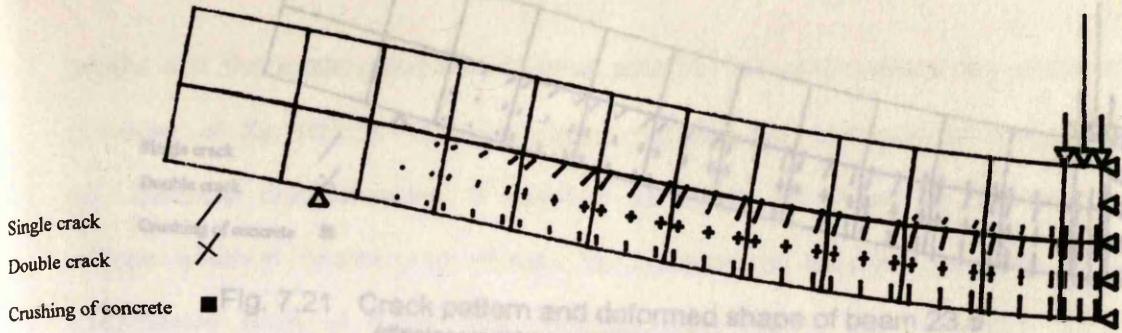


Fig. 7.18 Crack pattern and deformed shape of beam OCabs-I (displacements magnified x 20)

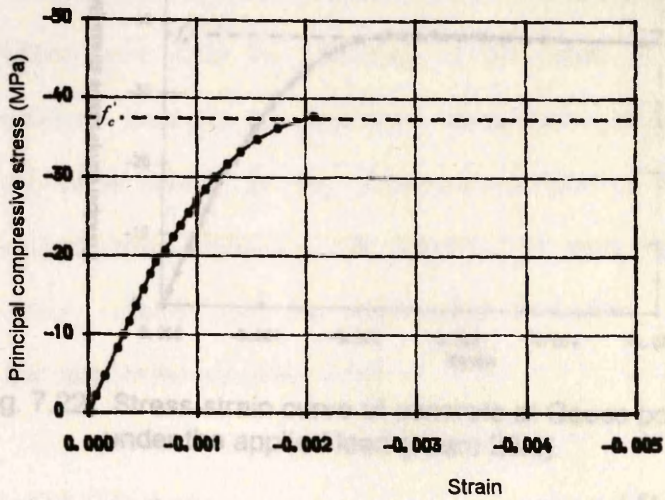


Fig. 7.19 Stress-strain curve of concrete at Gauss point under the applied load (beam OCabs-I)

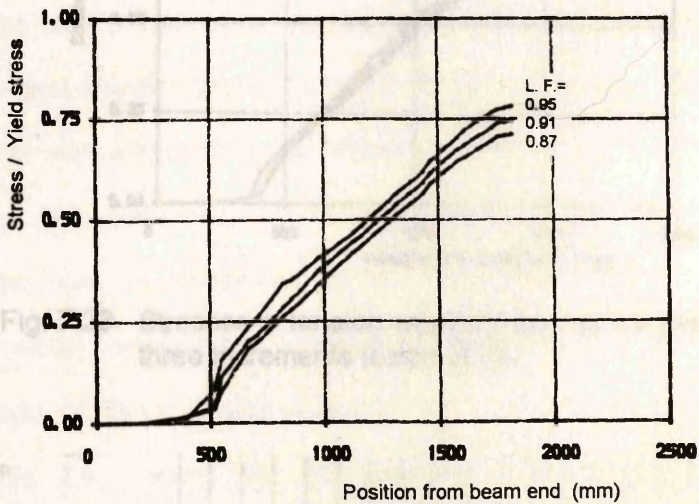


Fig. 7.20 Stresses in tension reinforcement at the last three increments (beam OCabs-I)

Fig. 7.24 Stresses in stirrups at the last three increments (beam OCabs-I)

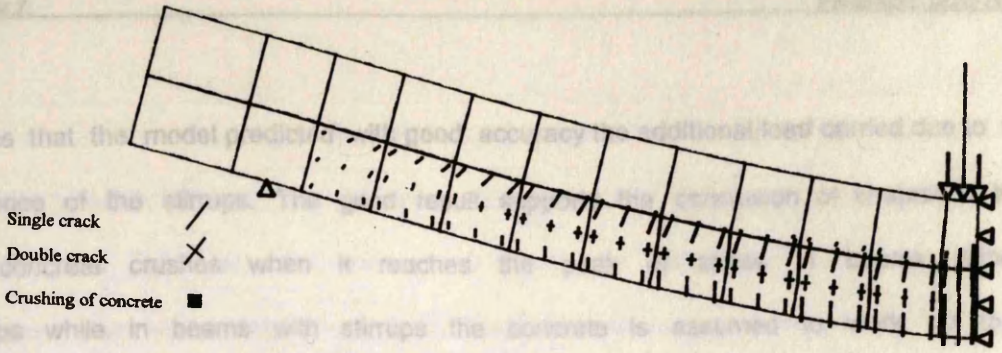


Fig. 7.21 Crack pattern and deformed shape of beam 23.5 (displacements magnified x 20)

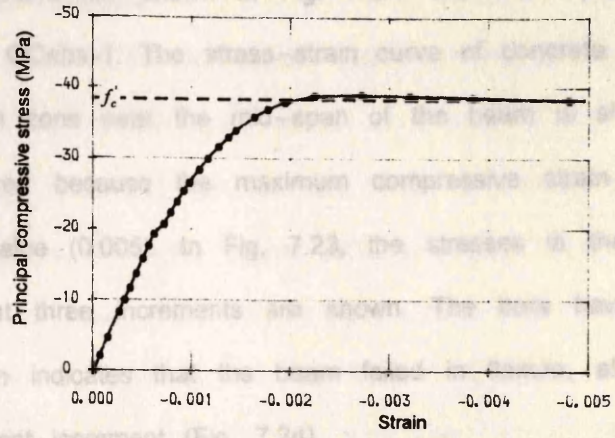


Fig. 7.22 Stress-strain curve of concrete at Gauss point under the applied load (beam 23.5)

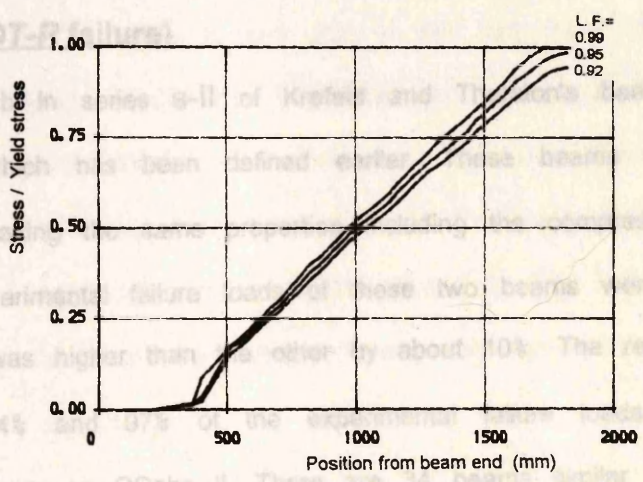


Fig. 7.23 Stresses in tension reinforcement at the last three increments (beam 23.5)

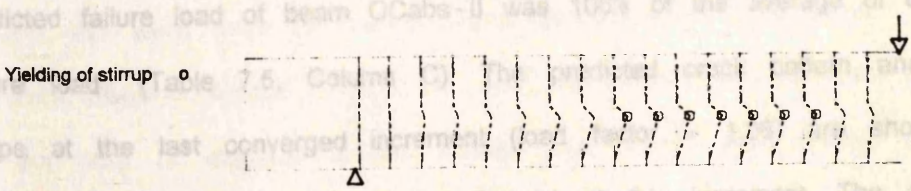


Fig. 7.24 Stresses in stirrups at the last increment (beam 23.5)

means that the model predicted with good accuracy the additional load carried due to the existence of the stirrups. The good result supports the conclusion of chapter 6 that the concrete crushes when it reaches the peak of stress in beams without stirrups while in beams with stirrups the concrete is assumed to work up to a compressive strain of 0.005. The predicted crack pattern and deformed shape at the last converged increment are shown in Fig. 7.21. The crack pattern is very similar to that of beam OCabs-I. The stress-strain curve of concrete at a Gauss point in the compression zone near the mid-span of the beam is shown in Fig. 7.22. The failure occurred because the maximum compressive strain of concrete reached the assumed value (0.005). In Fig. 7.23, the stresses in the longitudinal reinforcement at the last three increments are shown. The bars have yielded at the last increment which indicates that the beam failed in flexure, although some stirrups yielded at the last increment (Fig. 7.24).

Beams OCa.bs-II (DT-R failure)

Beams OCa and OCb in series S-II of Krefeld and Thurston's beams failed in DT-R failure type which has been defined earlier. These beams were without shear reinforcement having the same properties including the compressive strength of concrete. The experimental failure loads of these two beams were 293.6 and 266.9 kN; i.e., one was higher than the other by about 10%. The reported critical shear loads were 94% and 97% of the experimental failure loads. These two beams are denoted here as OCabs-II. There are 34 beams similar to these two beams but with shear reinforcement (beams number 9-37 in Table 7.2). The predicted failure load of beam OCabs-II was 106% of the average of experimental failure load (Table 7.5, Column C). The predicted crack pattern and deformed shape at the last converged increment (load factor = 1.06) are shown in Fig. 7.25. The critical shear cracks have formed at this increment. The stress-strain curve of concrete at a Gauss point near the mid-span is shown in Fig. 7.26.

The stresses in the longitudinal bars at the last three increments are shown in Fig. 7.27 which shows that the bars did not yield up to the numerical failure. The reported maximum steel stresses for these two beams were 61% and 58% of the steel yield stress which has been predicted very well as shown in Fig. 7.27.

Beams 29a-1,b-1 (DT-R failure)

Beams 29a-1 and 29b-1 were two of Krefeld and Thruston's beams which failed in DT-R failure type. These beams were similar to beams OCabs-II except for the stirrups. The stirrups increased the ultimate load by about 14% but didn't change the mode of failure. The two beams were analysed as one beam. The predicted failure load for this beam was higher than the average of the experimental failure loads by 22% (Table 7.8, Column C). The predicted crack pattern and deformed shape are shown in Fig. 7.28 which shows clearly that the beam failed in shear. The stress-strain curve of concrete near mid-span is shown in Fig. 7.29. The stresses in one bar at the last three increments are shown in Fig. 7.30 which shows that the steel did not yield. The measured maximum steel stresses for these two beams were 51% and 83% of the steel yield stress. The predicted one was about 78% of the steel yield stress. The stresses in the stirrups at the last increment are shown in Fig. 7.31 which shows that the Gauss points at which the stirrups have yielded are arranged diagonally from the load point to the support.

Beams AO (D-T failure)

Beams AO were three of Clark's beams without shear reinforcement which failed in pure diagonal tension (*D-T*); i.e., the tensile reinforcement hadn't yielded up to the time of diagonal tension failure. The beams were similar in everything except for small differences in the values of f_c' (21.5, 26.0, and 23.7 MPa). The reported failure loads for these beams were 178.1, 215.9, and 238.1 kN,

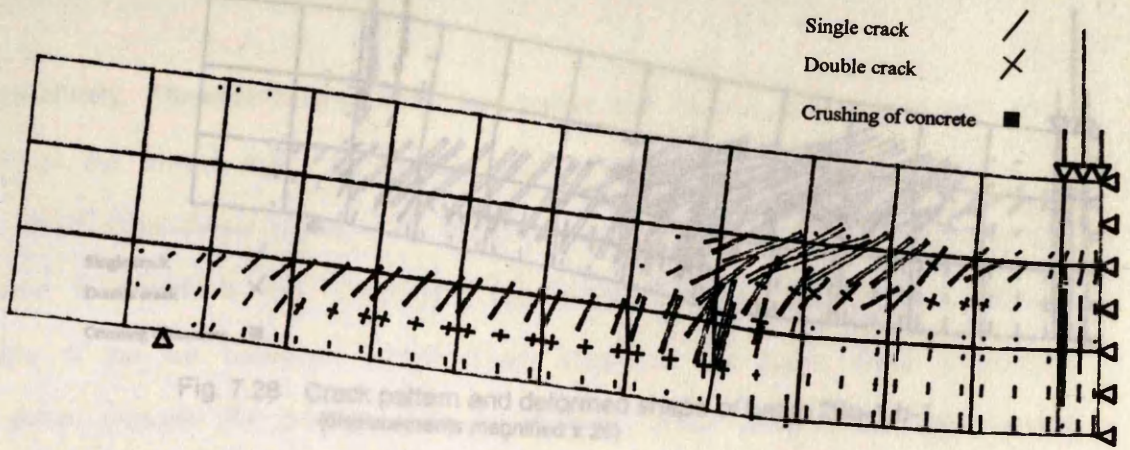


Fig. 7.25 Crack pattern and deformed shape of beam OCabs-II (displacements magnified x 20)

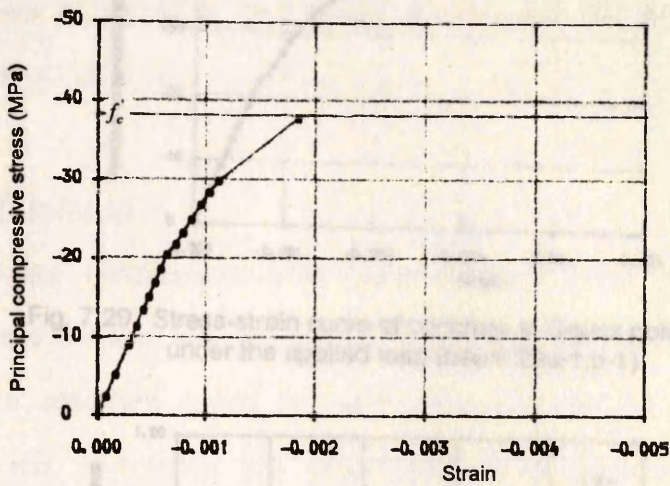


Fig. 7.26 Stress-strain curve of concrete at Gauss point under the applied load (beam OCabs-II)

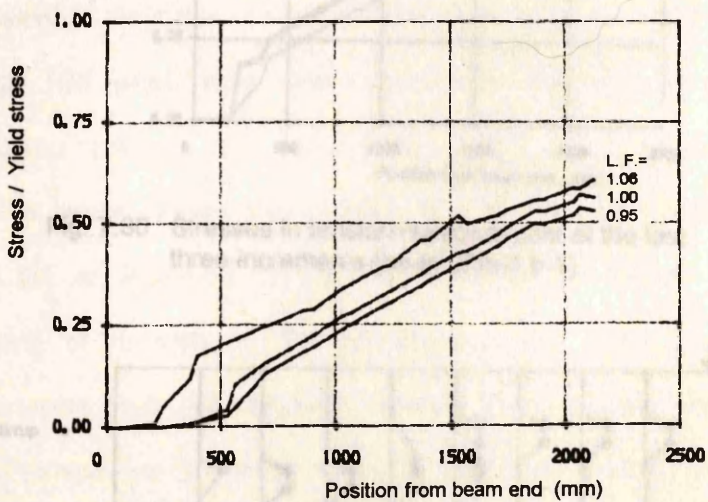


Fig. 7.27 Stresses in tension reinforcement at the last three increments (beam OCabs-II)

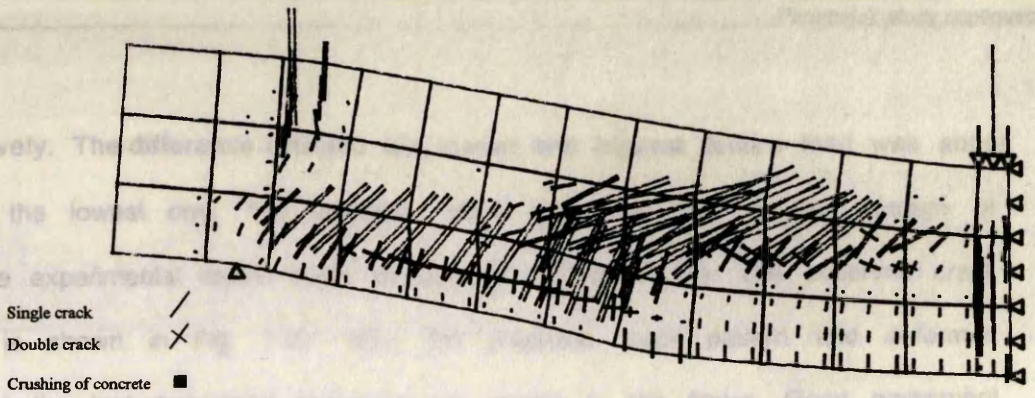


Fig. 7.28 Crack pattern and deformed shape of beam 29a-1,b-1 (displacements magnified x 20)

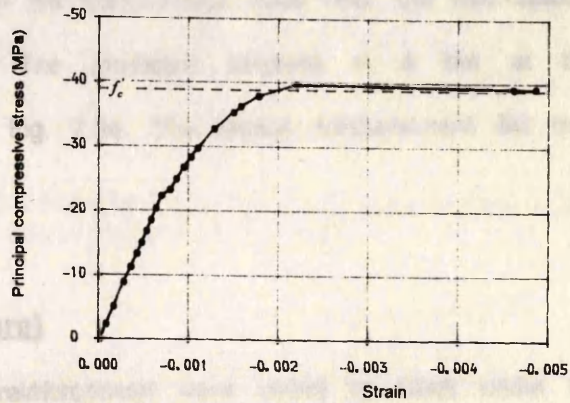


Fig. 7.29 Stress-strain curve of concrete at Gauss point under the applied load (beam 29a-1,b-1)

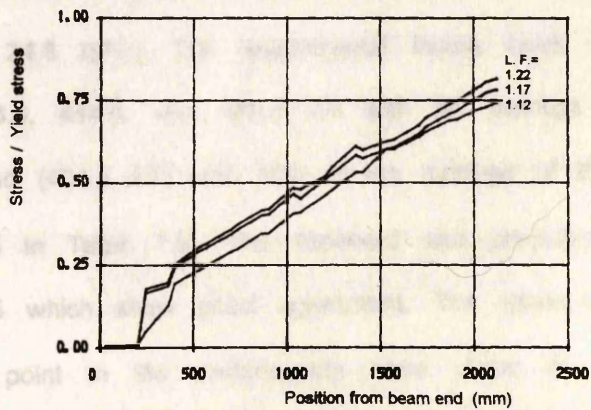


Fig. 7.30 Stresses in tension reinforcement at the last three increments (beam 29a-1,b-1)

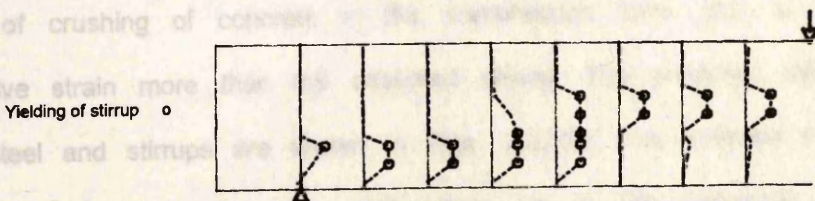


Fig. 7.31 Stresses in stirrups at the last increment (beam 29a-1,b-1)

respectively. The difference between the lowest and highest failure load was about 34% of the lowest one. The predicted failure load was 98% of the average of the three experimental failure loads (Column B in Table 7.15). The observed crack pattern is shown in Fig. 7.32. Also, the predicted crack pattern and deformed shape at the last converged increment are shown in this figure. Good agreement is shown between the predicted and the observed crack pattern. The stress-strain curve at a Gauss point in the compression zone near the mid-span of the beam is shown in Fig. 7.33. The predicted stresses in a bar at the last three increments are shown in Fig. 7.34. The tensile reinforcement did not yield up to the numerical failure.

Beams A1 (D-T failure)

Four beams with shear reinforcement were tested by Clark under the designation A1. The beams failed in pure diagonal tension at different levels of load although they had the same properties except for slight differences in the values of f_c' (24.7, 23.7, 23.4, and 24.8 MPa). The experimental failure loads for these four beams were 444.9, 418.3, 444.9, and 489.4 kN with an average of 449.4 kN. The predicted failure load (404.5 kN) was 90% of the average of the experimental failure loads (Column B in Table 7.9). The observed and predicted crack pattern are shown in Fig. 7.35 which show good agreement. The stress-strain curve of concrete at a Gauss point in the compression zone under the load point is shown in Fig. 7.36 which shows that without the compression softening portion, the beam could fail at increment 14 (about 75% of the ultimate failure load) because of crushing of concrete in the compression zone (due to increase the compressive strain more than the assumed strain). The predicted stresses in the tension steel and stirrups are shown in Figs. 7.37,38. The stresses in the tension steel were much less than the yield stress up to the numerical failure which indicates that the beam failed in shear.

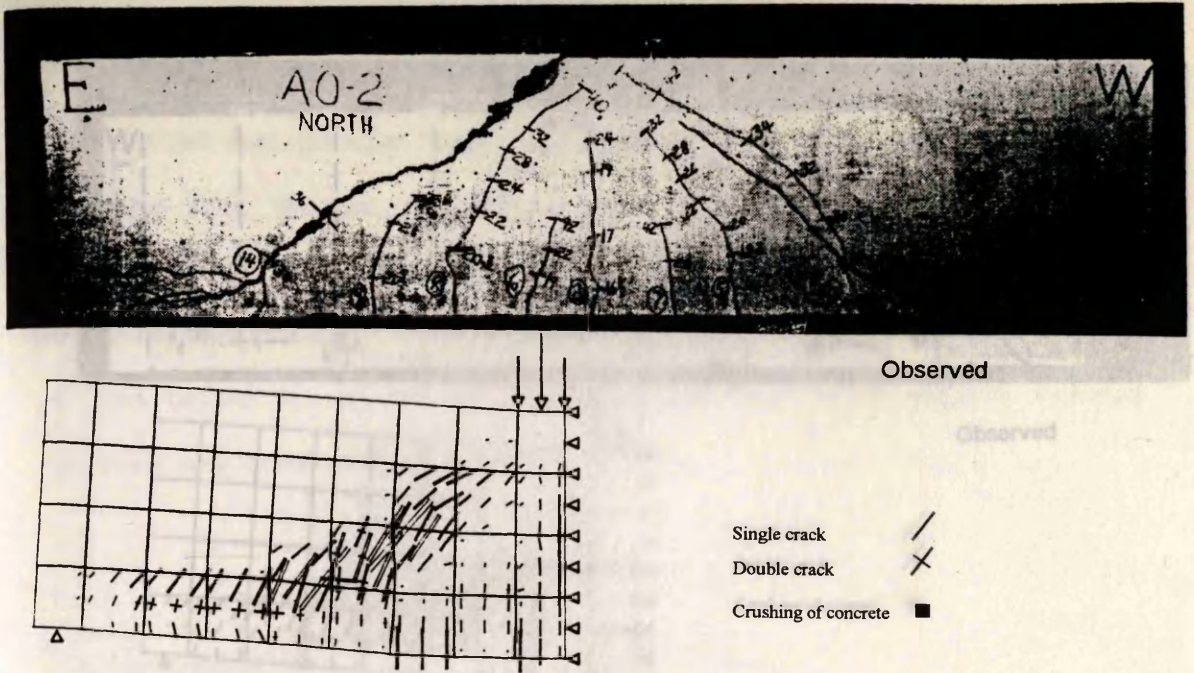


Fig. 7.32 Crack pattern and deformed shape of beam AO (displacements magnified x 20)

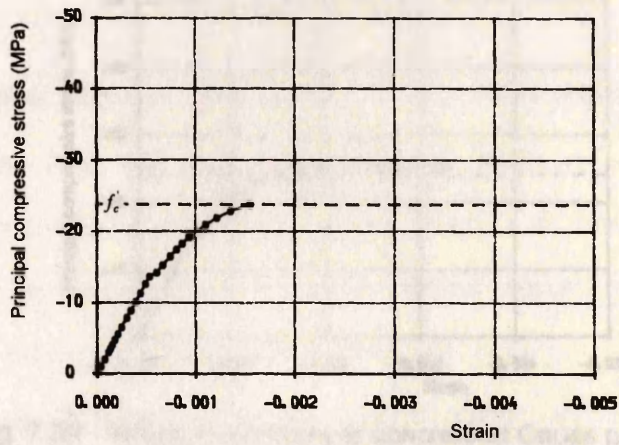


Fig. 7.33 Stress-strain curve of concrete at Gauss point under the applied load (beam AO)

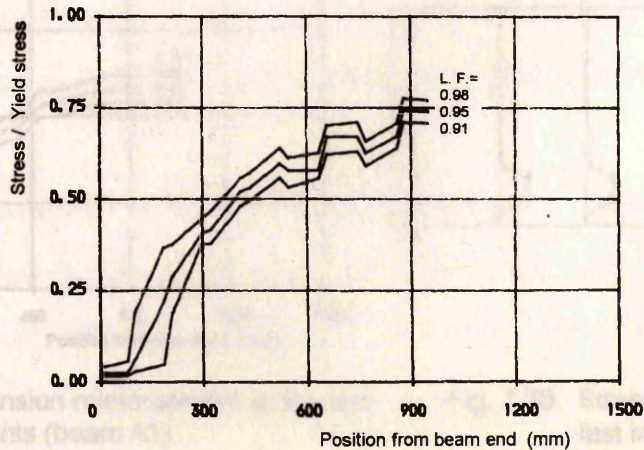


Fig. 7.34 Stresses in tension reinforcement at the last three increments (beam AO)

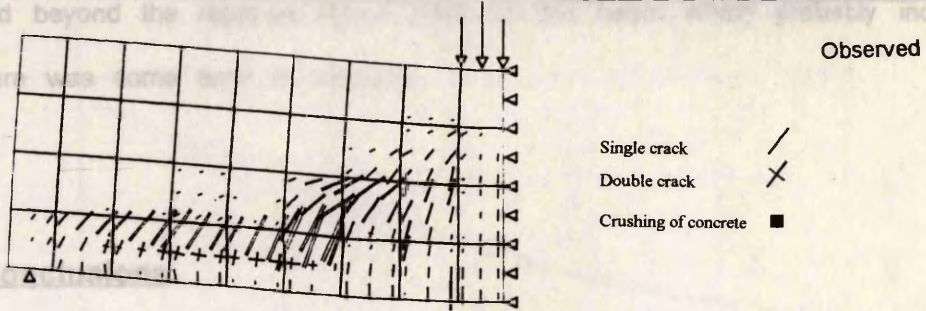
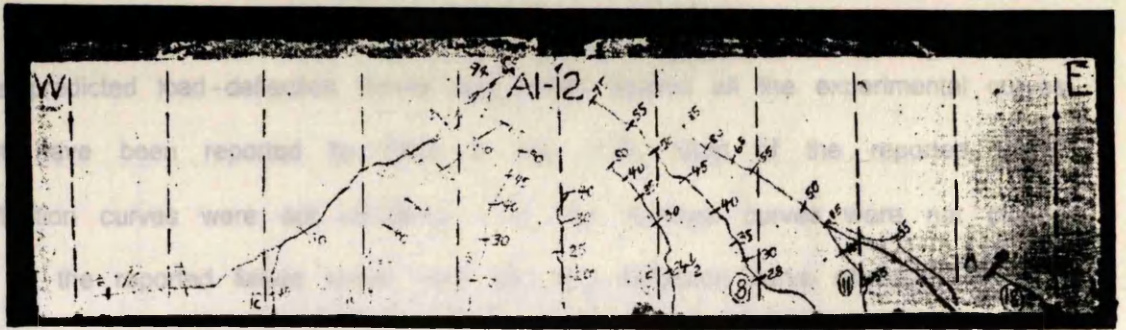


Fig. 7.35 Crack pattern and deformed shape of beam A1 (displacements magnified x 20)

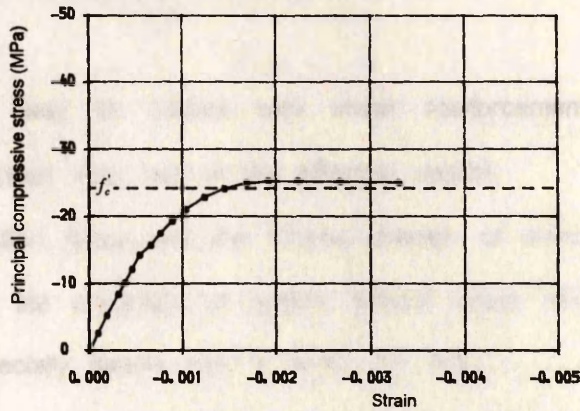


Fig. 7.36 Stress-strain curve of concrete at Gauss point under the applied load (beam A1)

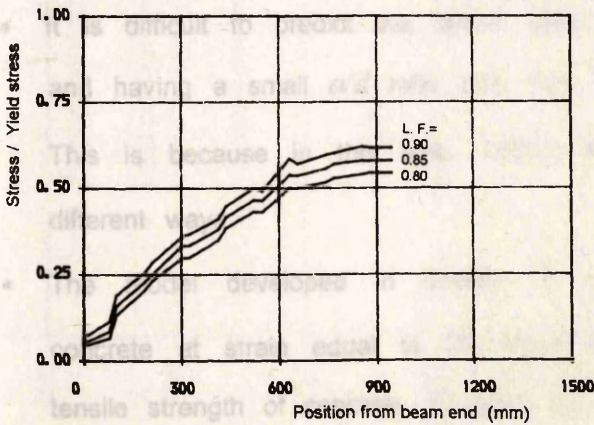


Fig. 7.37 Stresses in tension reinforcement at the last three increments (beam A1)

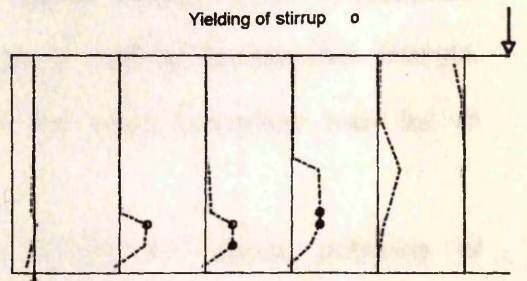


Fig. 7.38 Stresses in stirrups at the last increment (beam A1)

The predicted load-deflection curves are plotted against all the experimental curves that have been reported by Clark in Fig. 7.39. Most of the reported load-deflection curves were not complete; i. e., the reported curves were not plotted up to the reported failure loads. Also, the load-deflection curve of beam C3 was extended beyond the reported failure loads of this beam which probably indicated that there was some error in reporting.

7.5 Conclusions

In this chapter, an attempt is made to establish the generality of the 2-D finite element model which was developed in chapter 6 and the following conclusions can be drawn:

- The best prediction was for beams with shear reinforcement with a small spacing of stirrups (less than half of the effective depth).
- Both the shear retention factor and the tensile strength of concrete had a very significant effect on the prediction of beams without shear reinforcement which failed in shear, especially beams with a small a/d ratio.
- Increasing the assumed value of shear retention factor improved the predicted failure loads of beams with shear reinforcement and having a small a/d ratio.
- It is difficult to predict the failure load of beams without shear reinforcement and having a small a/d ratio and high value of cylinder compressive strength. This is because in this type, beams with the same properties may fail in different ways.
- The model developed in chapter 6 with limiting the tension softening of concrete at strain equal to 20 times the initial crack strain and taking the tensile strength of concrete f_t' equal $\sqrt[4]{f_c'}$ (in MPa) gave good results.

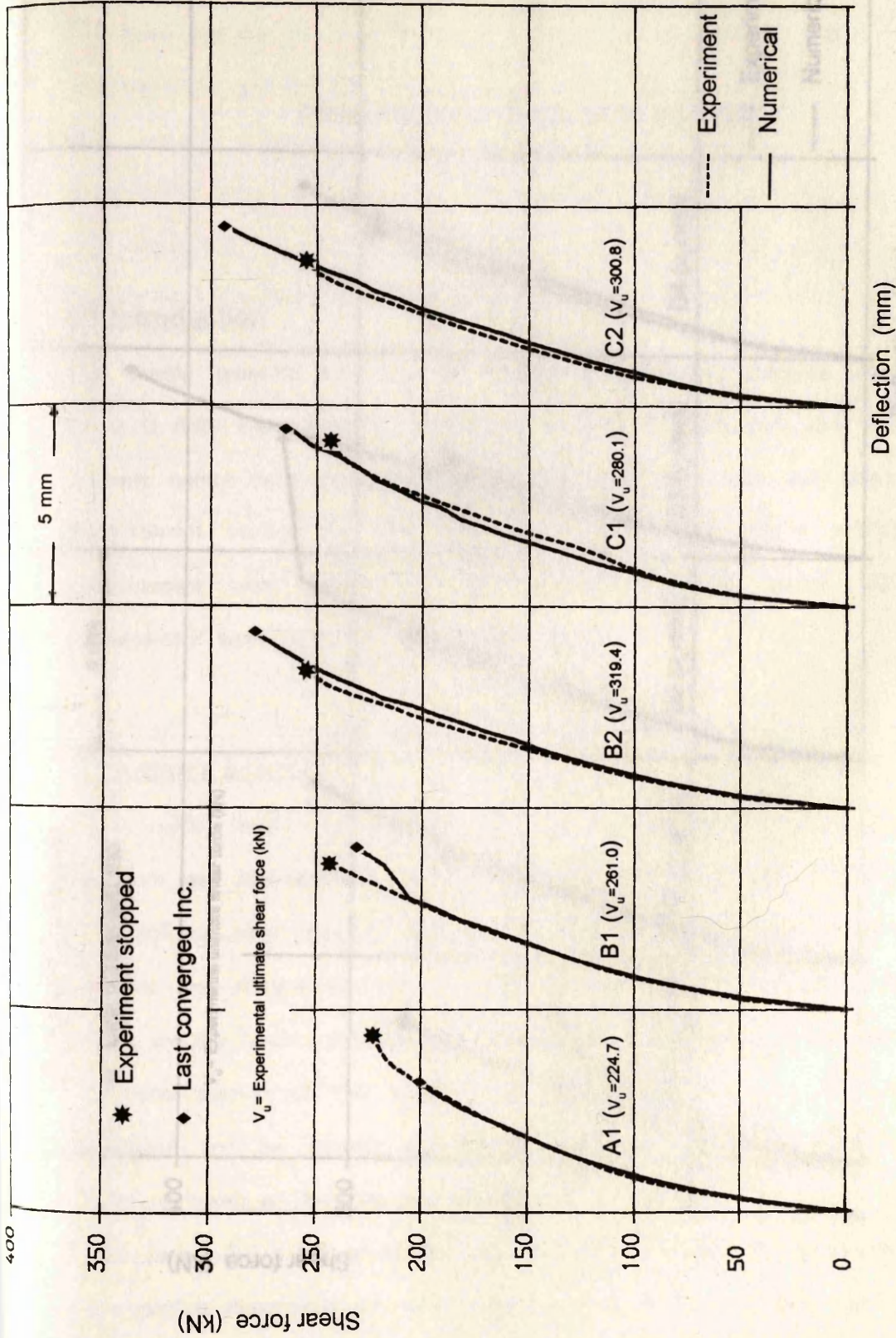


Fig. 7.39a Load-deflection curves of Clark's beams (A1, B1, B2, C1, and C2)

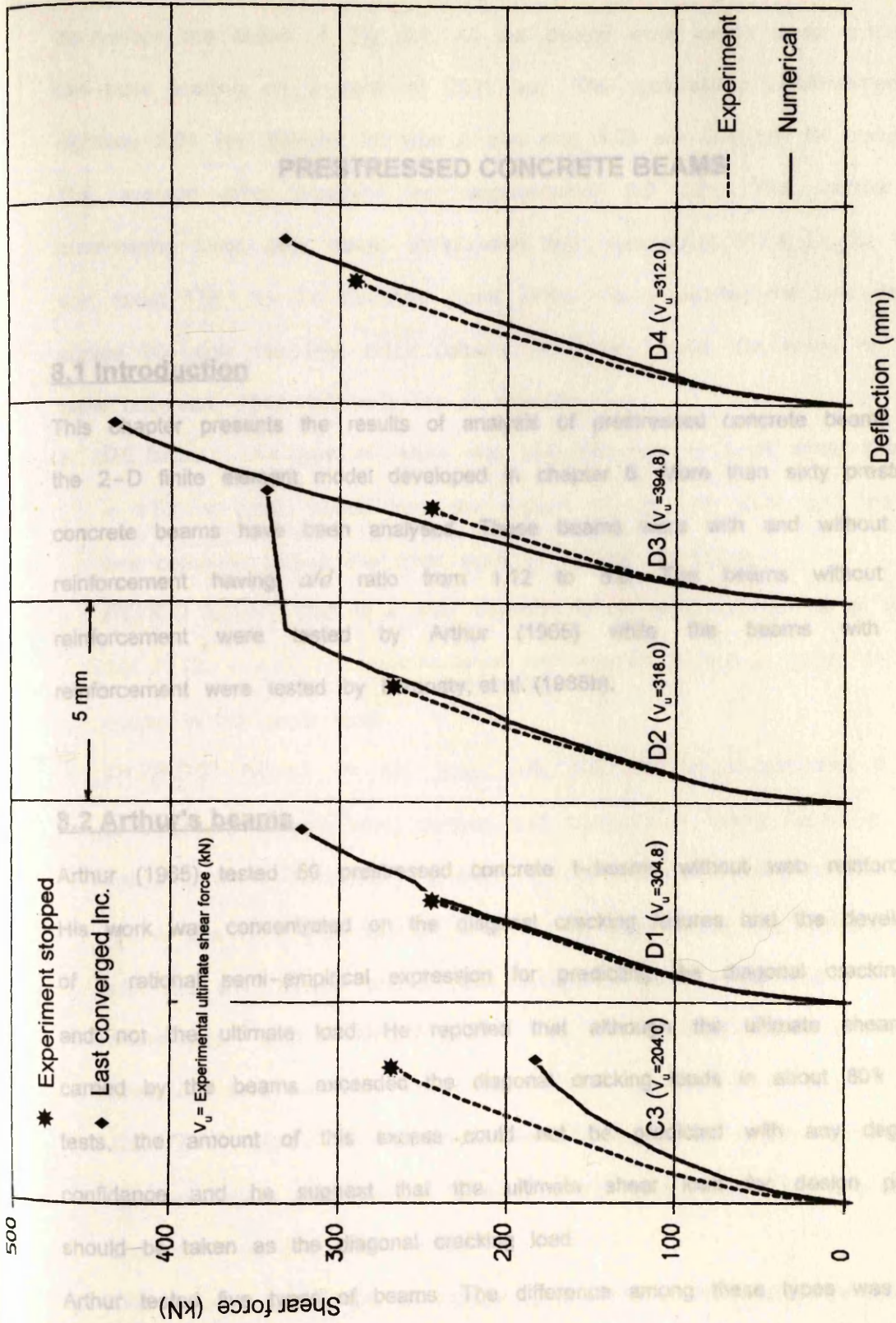


Fig. 7.39b Load-deflection curves of Clark's beams (C3, D1, D2, D3, and D4)

CHAPTER 8

PRESTRESSED CONCRETE BEAMS

8.1 Introduction

This chapter presents the results of analysis of prestressed concrete beams using the 2-D finite element model developed in chapter 6. More than sixty prestressed concrete beams have been analysed. These beams were with and without shear reinforcement having a/d ratio from 1.12 to 5.8. The beams without shear reinforcement were tested by Arthur (1965) while the beams with shear reinforcement were tested by Elzanaty, et al. (1986b).

8.2 Arthur's beams

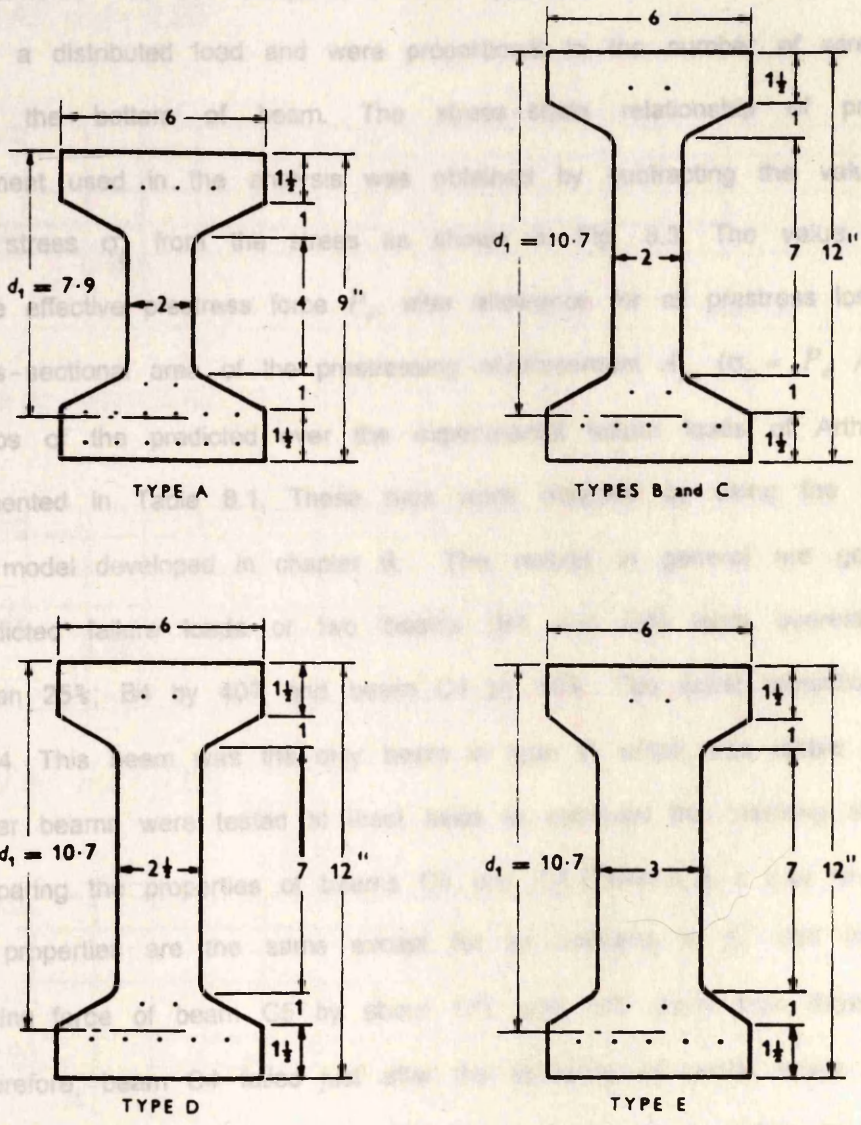
Arthur (1965) tested 50 prestressed concrete I-beams without web reinforcement. His work was concentrated on the diagonal cracking failures and the development of a rational semi-empirical expression for predicting the diagonal cracking load and not the ultimate load. He reported that although the ultimate shear loads carried by the beams exceeded the diagonal cracking loads in about 80% of the tests, the amount of this excess could not be predicted with any degree of confidence and he suggest that the ultimate shear load for design purposes should be taken as the diagonal cracking load.

Arthur tested five types of beams. The difference among these types was in the cross-section dimensions and the existence of a solid end-block. Two types (A and B) had solid end-blocks 304.8 mm long, while the other types (C, D, and E) had no end-blocks. All the beams were 2896 mm long. Due to the change of

the cross-section dimensions, a/d ratio varied from 1.12 to 4.57. The beams dimensions are shown in Fig. 8.1. All the beams were tested under symmetrical two-point loading on a span of 2591 mm. The prestressing reinforcement was eighteen 2.64 mm diameter for type A and nine 5.08 mm diameter for types B-E. The average initial prestress was approximately 6.9 MPa. The nominal initial prestressing force, after elastic compression loss, was about 117.4 kN for type A and about 176.1 kN for the other types. Arthur hasn't reported the load-deflection curves but only the final crack patterns of some beams. Six types of failures were observed. Their definitions are as follows:

- **DC** failure: This type of failure was observed only at short shear span, $a/d < 2.52$. A crack formed from the support to the load point, and the failure was complete without any other signs of distress developing.
- **DC/WD** failure: This is a web distortion failure which occurred at all ratios of a/d (1.12 - 4.57). It occurred when web tension formed a series of multiple cracks in the shear span.
- **DC/WD/F** failure: In this type, web distortion failures showed a further development, collapse being delayed until compression failure began in the top flange concrete under the load point. The range of a/d ratios for this type of failure was from 2.24 to 4.57. If a flexural shear crack was present together with the web tension cracks, (SC) designation was added and this type of failure was called **DC/WD/F (SC)**. The flexural shear cracks occurred only when a/d ratio was 4.57.
- **DC/WD/T** failure: This occurred when failure of the tension steel occurred near mid-span, after diagonal cracking in the shear span. This type of failure occurred when a/d ratio was 4.57.
- **WC** failure: This failure took place by crushing of the web in beams of a/d ratios of 1.12 and 3.36.
- **SC** failure: This type of failure initiated by a flexural crack in the shear span.

The data of the beams required for the analysis and the results of analysis are shown in Table 8.1. The finite element meshes used for the analysis are shown in Fig. 8.2. At the first increment, the total effective prestressing force was applied on the beam end as a horizontal compressive force. This force was divided into two components. The two components were applied at the top and the bottom of beam as a distributed load and were provided with the number of wires at the top and the bottom of beam. The stress-strain relations of concrete and prestressing reinforcement used in the analysis were obtained by adjusting the value of the effective stress of concrete as shown in Fig. 8.3. The value of σ_c is equal to the effective stress of concrete after allowance for prestress losses, over the cross-section, and the prestressing reinforcement stress is (σ_p / A_{ps}) . The ratios of the effective stress of concrete to the ultimate compressive strength are presented in Table 8.1. These data were used in the analysis of the 2-D finite element model developed in chapter 8. The model is generally good. Only the prediction of the load capacity of two beams is not very accurate. The load capacity was for more than 15% below the experimental value for beam C4. This was due to the fact that the beam was tested under shear force. The other beams were tested under flexure and the load capacity was very close to the experimental value. The properties of concrete and prestressing reinforcement used in the analysis are the same as that of the experimental beams. Therefore, the load capacity of beam C4. Therefore, the load capacity of beam C4 is 62.3 kN, while beam C3 failed at a load of 74.5 kN.



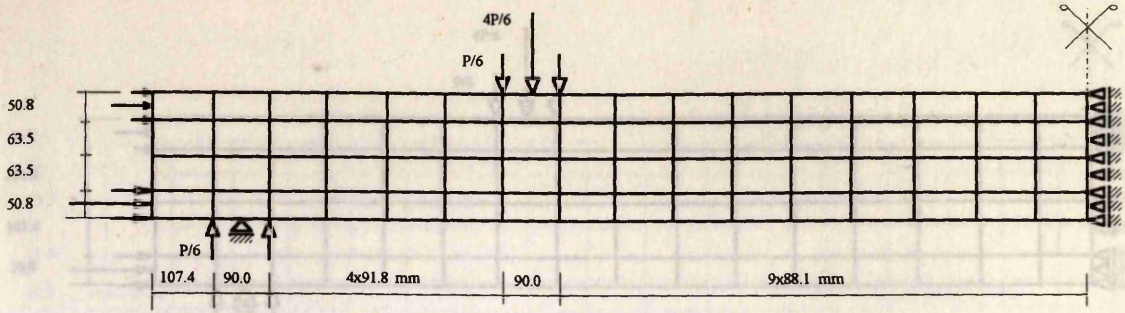
Prestressing wires are indented, Belgian pattern:
 type A, eighteen 0.104 in. diameter;
 types B-E, nine 0.2 in. diameter

Fig. 8.1 Cross-sections of Arthur's beams.
 (1 in. = 25.4 mm)

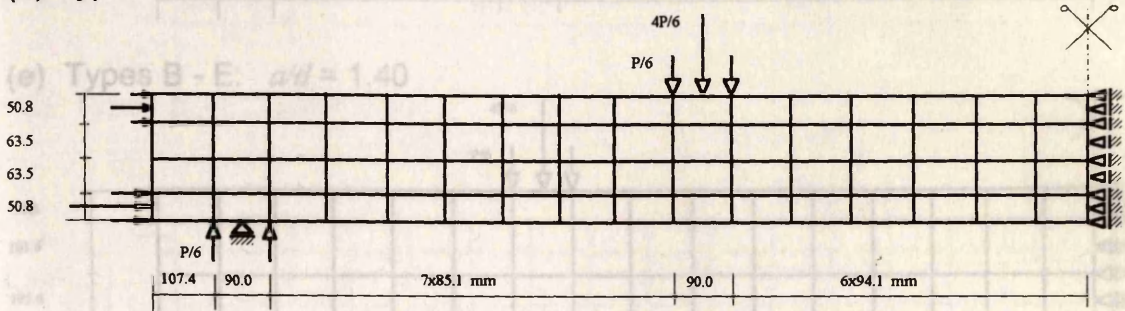
The data of the beams required for the analysis and the results of analysis are shown in Table 8.1. The finite element meshes used for the analysis are shown in Fig. 8.2. At the first increment, the total effective prestressing force was applied on the beam end as a horizontal compressive force. This force was divided into two components. The two components were applied at the top and the bottom of beam as a distributed load and were proportional to the number of wires at the top and the bottom of beam. The stress-strain relationship of prestressing reinforcement used in the analysis was obtained by subtracting the value of the effective stress σ_p from the stress as shown in Fig. 8.3. The value of σ_p is equal the effective prestress force P_e , after allowance for all prestress losses, over the cross-sectional area of the prestressing reinforcement A_{ps} ($\sigma_p = P_e / A_{ps}$).

The ratios of the predicted over the experimental failure loads of Arthur's beams are presented in Table 8.1. These runs were obtained by using the 2-D finite element model developed in chapter 6. The results in general are good. Only the predicted failure loads of two beams (B4 and C4) were overestimated by more than 25%; B4 by 40% and beam C4 by 90%. The worst prediction was for beam C4. This beam was the only beam in type C which was tested only once. The other beams were tested at least twice to measure the cracking shear force. By comparing the properties of beams C4 and C5 (Table 8.1), it can be seen that all the properties are the same except for an increase in f_c' and the effective prestressing force of beam C5 by about 17% and 10% more than those of beam C4. Therefore, beam C4 failed just after the formation of critical shear crack at a load of 62.3 kN, while beam C5 failed at a load which is higher by about 74% (108.5 kN).

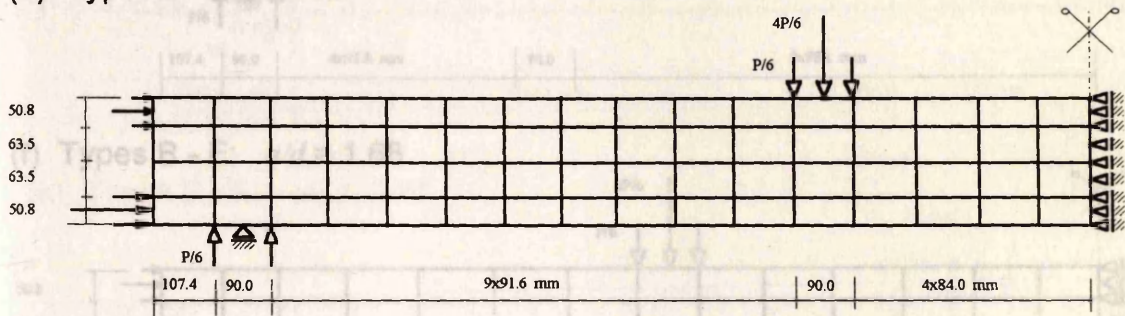
The mean value of the ratios of the predicted over the experimental failure loads of the all beams was 1.02 with standard deviation of 20.3%. By excluding beams B4 and C4 the mean value and the standard deviation became 0.99, 13.3%, respectively.



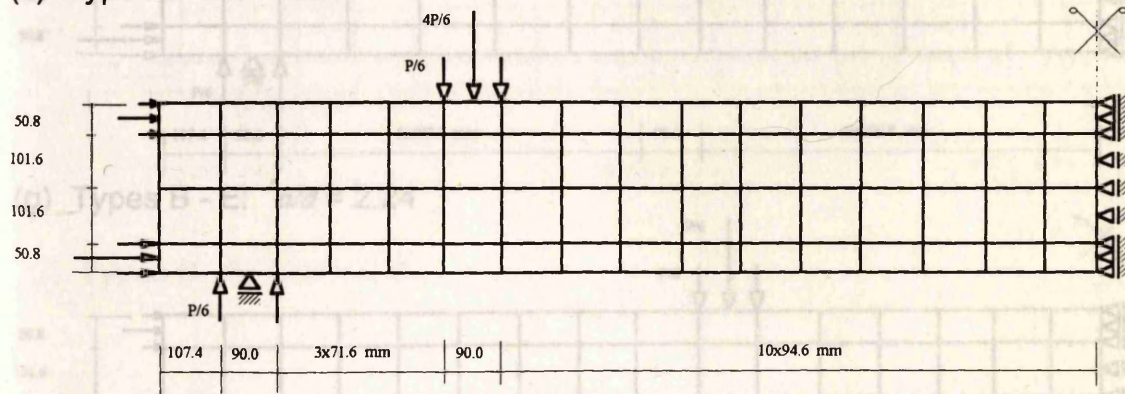
(a) Type A: $a/d = 2.28$



(b) Type A: $a/d = 3.42$



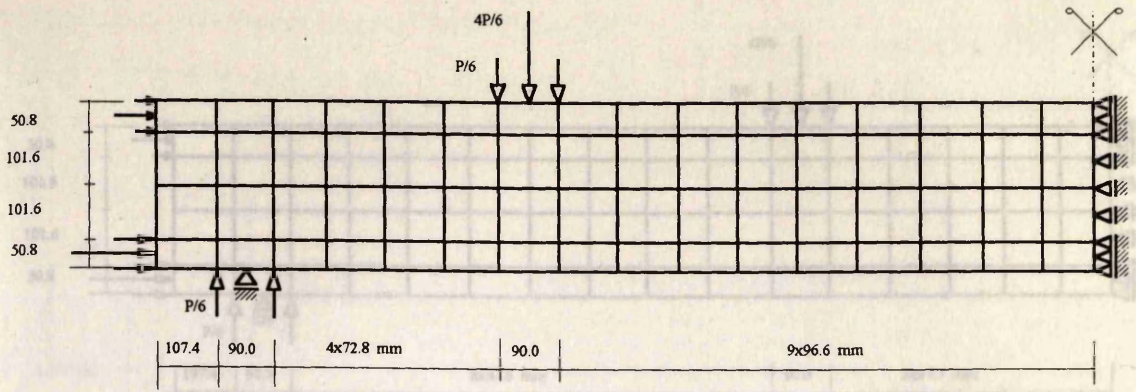
(c) Type A: $a/d = 4.56$



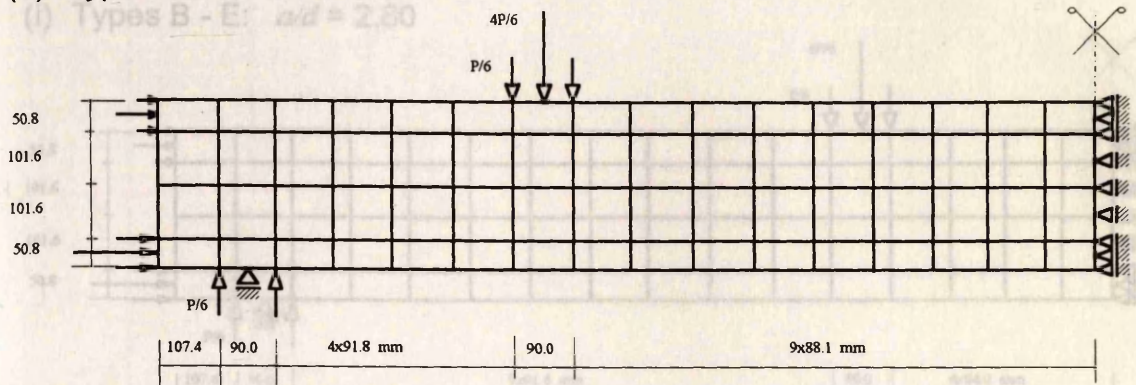
(d) Types B - E: $a/d = 1.12$

(h) Types B - E: Fig. 8.2 Finite element meshes for Arthur's beams

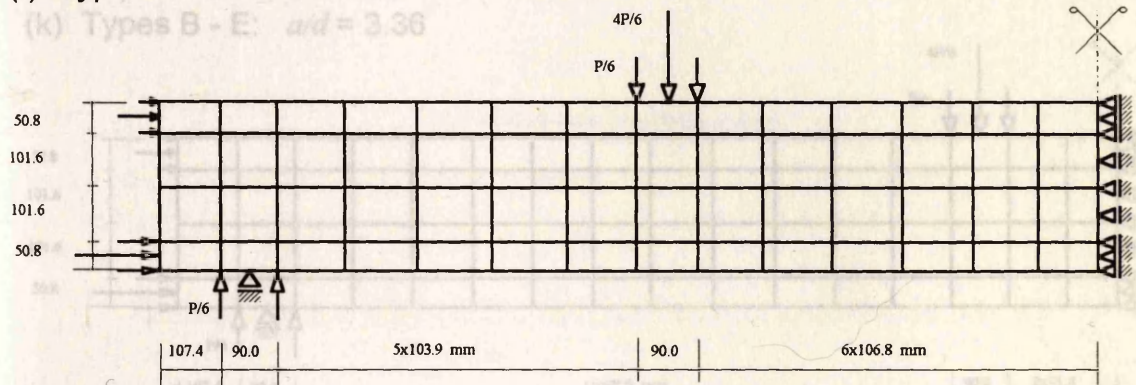
Fig. 8.2 Finite element meshes for Arthur's beams (continue)



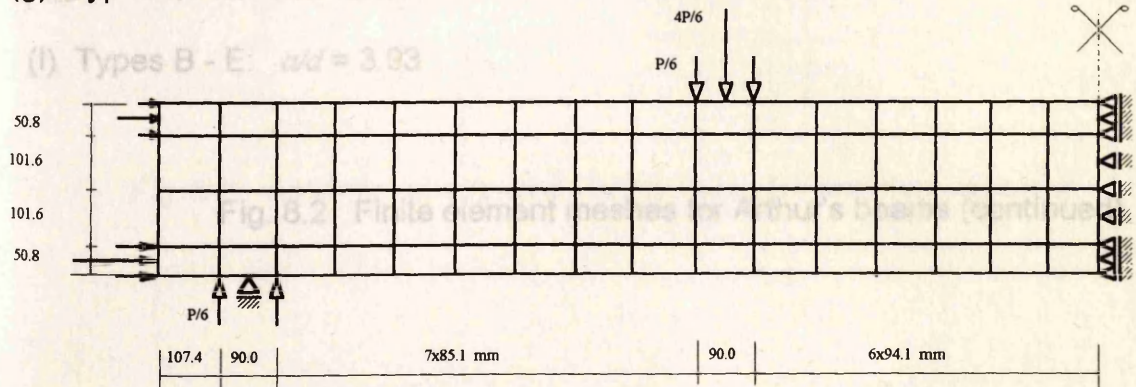
(e) Types B - E: $a/d = 1.40$



(f) Types B - E: $a/d = 1.68$

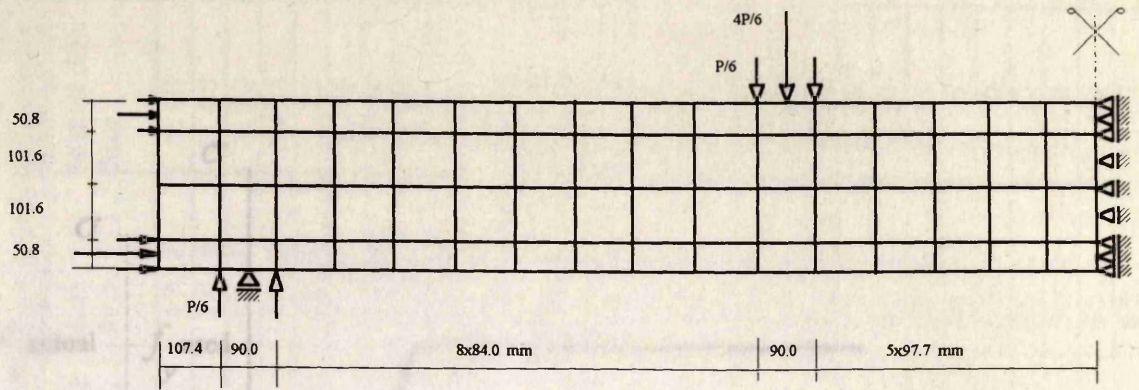


(g) Types B - E: $a/d = 2.24$

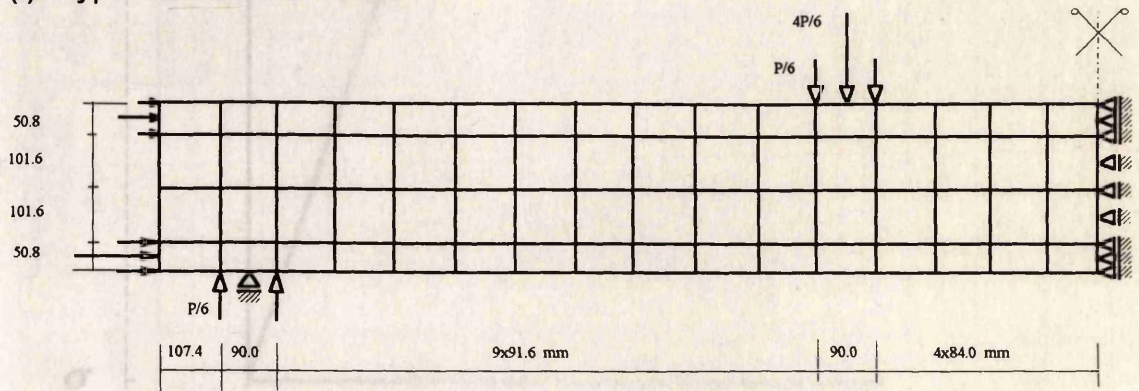


(h) Types B - E: $a/d = 2.52$

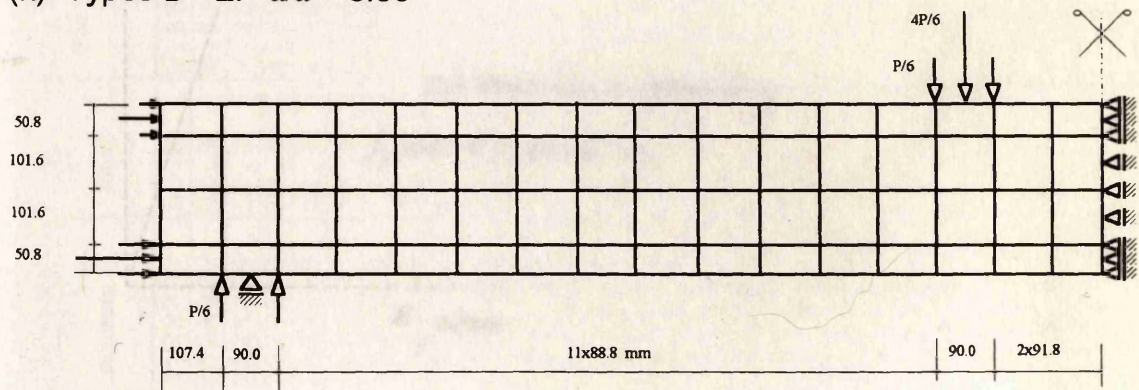
Fig. 8.2 Finite element meshes for Arthur's beams (continue).



(i) Types B - E: $a/d = 2.80$



(k) Types B - E: $a/d = 3.36$



(l) Types B - E: $a/d = 3.93$

Fig. 8.2 Finite element meshes for Arthur's beams (continued).

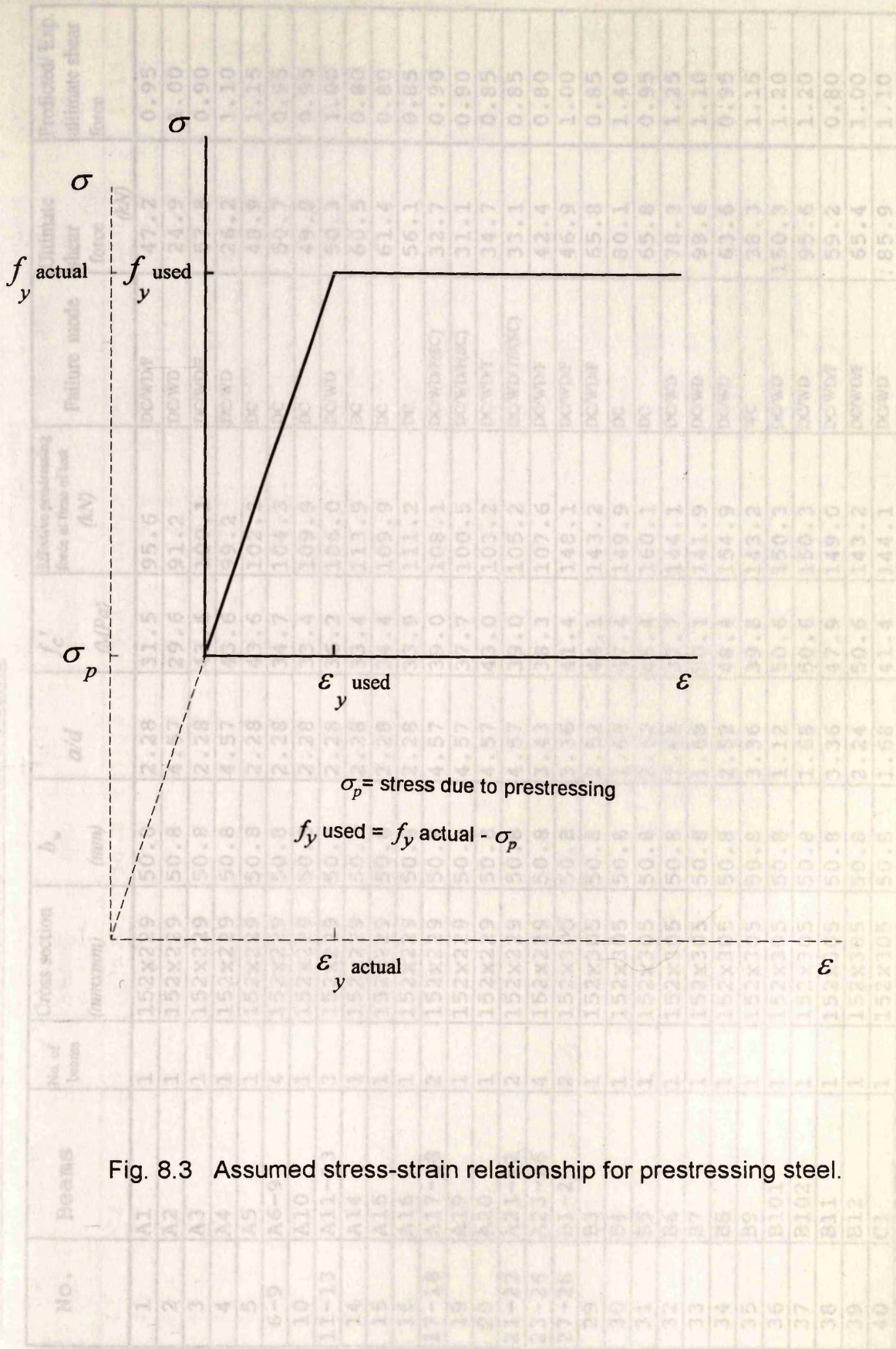


Fig. 8.3 Assumed stress-strain relationship for prestressing steel.

Table 8.1 Data and results of analysis of Arthur's beams

No.	Beams	No. of beams	Cross section (mmxmm)	b_w (mm)	a/d	f'_c (MPa)	Effective prestressing force at time of test (kN)	Failure mode	Ultimate shear force (kN)	Predicted/ Exp. ultimate shear force
1	A1	1	152x229	50.8	2.28	31.5	95.6	DC/WD/F	47.2	0.95
2	A2	1	152x229	50.8	4.57	29.6	91.2	DC/WD	24.9	1.00
3	A3	1	152x229	50.8	2.28	43.6	100.1	DC/WD/F	57.8	0.90
4	A4	1	152x229	50.8	4.57	43.6	99.2	DC/WD	26.2	1.10
5	A5	1	152x229	50.8	2.28	43.6	102.3	DC	48.9	1.15
6-9	A6-9	4	152x229	50.8	2.28	34.7	104.3	DC	50.7	0.95
10	A10	1	152x229	50.8	2.28	33.4	109.9	DC	49.8	0.95
11-13	A11-13	3	152x229	50.8	2.28	36.2	106.0	DC/WD	50.3	1.00
14	A14	1	152x229	50.8	2.28	33.4	113.9	DC	60.5	0.80
15	A15	1	152x229	50.8	2.28	34.4	109.9	DC	61.4	0.80
16	A16	1	152x229	50.8	2.28	33.9	111.2	DC	56.1	0.85
17-18	A17-18	2	152x229	50.8	4.57	39.0	108.1	DC/WD/F(SC)	32.7	0.90
19	A19	1	152x229	50.8	4.57	37.7	100.5	DC/WD/F(SC)	31.1	0.90
20	A20	1	152x229	50.8	4.57	43.0	103.2	DC/WD/T	34.7	0.85
21-22	A21-22	2	152x229	50.8	4.57	39.0	105.2	DC/WD/T(F(SC)	33.1	0.85
23-26	A23-26	4	152x229	50.8	3.43	38.3	107.6	DC/WD/F	42.4	0.80
27-28	B1-2	2	152x305	50.8	3.36	41.4	148.1	DC/WD/F	46.9	1.00
29	B3	1	152x305	50.8	2.52	44.1	143.2	DC/WD/F	65.8	0.85
30	B4	1	152x305	50.8	1.68	47.4	149.9	DC	80.1	1.40
31	B5	1	152x305	50.8	2.52	48.4	160.1	DC	65.8	0.95
32	B6	1	152x305	50.8	1.68	37.7	144.1	DC/WD	78.3	1.25
33	B7	1	152x305	50.8	1.68	50.1	141.9	DC/WD	99.6	1.10
34	B8	1	152x305	50.8	2.52	48.4	154.9	DC/WD	63.6	0.95
35	B9	1	152x305	50.8	3.36	39.8	143.2	WC	38.3	1.15
36	B101	1	152x305	50.8	1.12	50.6	150.3	DC/WD	150.3	1.20
37	B102	1	152x305	50.8	1.68	50.6	150.3	DC/WD	95.6	1.20
38	B11	1	152x305	50.8	3.36	47.9	149.0	DC/WD/F	59.2	0.80
39	B12	1	152x305	50.8	2.24	50.6	143.2	DC/WD/F	65.4	1.00
40	C1	1	152x305	50.8	1.68	41.4	144.1	DC/WD	85.9	1.10

Table 8.1 Data and results of analysis of Arthur's beams (continued)

No.	Beams	No. of beams	Cross section (mmxmm)	b_w (mm)	a/d	f'_c (MPa)	Effective prestressing force at time of test (kN)	Failure mode	Ultimate shear force (kN)	Predicted/ Exp. ultimate shear force
41	C2	1	152x305	50.8	1.12	45.2	147.2	WC	140.1	1.15
42	C3	1	152x305	50.8	2.24	41.4	149.9	DC/WD	66.7	0.95
43	C4	1	152x305	50.8	1.40	40.4	142.8	DC/WD	62.3	1.90
44	C5	1	152x305	50.8	1.40	47.4	156.6	DC	108.5	1.25
45	C6	1	152x305	50.8	1.12	48.4	156.6	DC	150.8	1.15
46	C7	1	152x305	50.8	2.24	48.4	149.9	DC/WD/F	67.4	0.95
47	C8	1	152x305	50.8	1.68	46.3	148.6	DC	87.5	1.05
48	D1	1	152x305	63.5	3.36	38.8	151.2	DC/WD	59.2	0.80
49	D2	1	152x305	63.5	3.92	44.1	146.8	SC	50.3	0.90
50	E1	1	152x305	76.2	2.80	42.5	142.3	DC/WD	57.4	1.05
51	E2	1	152x305	76.2	2.80	48.4	145.9	DC/WD	66.7	0.95
49 beams						Mean	value			0.99
51 beams						Standard	deviation			13.3%
						Mean	value			1.02
						Standard	deviation			20.3%

DC : Diagonal cracking

WD : Web distortion

F : Flexural compression

SC : Shear compression, initiated by a flexural crack

T : Fracture of tension steel

WC : Web crushing

This result is considered as a good result for beams without shear reinforcement. The predicted failure loads are plotted against the experimental failure loads in Fig. 8.4. If the predicted failure load is taken as 80% of the numerical failure load all the predicted failure loads except for two beams (B4 and C4) will be conservative.

To study the mode of failure of Arthur's beams, the predicted behaviours of some beams will be presented. The predicted failure mode will depend on four considerations;

- a) the deformed shape of the beam,
- b) the crack pattern,
- c) the stresses of concrete in the compression zone, and
- d) the stresses in the reinforcements.

Beam A1 (DC/WD/F failure)

The ratio of the predicted over the experimental failure load of beam A1 was 0.95. It failed in *DC/WD/F* failure type. The cracking shear force for this beam was about 80% of the ultimate shear force. The observed crack pattern is shown in Fig. 8.5a. Fig. 8.5b-e shows the predicted crack patterns and deformed shapes of the beam at some load factors. At load factor = 0.80 (Fig. 8.5b), no critical cracks has formed. The shear cracks started at a load level equal 0.85 of the experimental failure load (Fig. 8.5c). This load was higher than the observed critical cracking load by about 5% of the experimental failure load. At load factor = 0.90 (Fig. 8.5d), although the shear cracks became very large, the beam carried more load. Arthur reported that in this type of failure the collapse was delayed until compression failure began in the top flange concrete under the point load. The predicted crack pattern and deformed shape at the last converged increment (load factor = 0.95) are shown in Fig. 8.5e. Comparing Fig. 8.5a with

Fig. 8.5e it is seen clearly that the observed crack pattern was predicted to a good degree of accuracy. The stress-strain curves of concrete at a Gauss point near the mid-span and a Gauss point under the load point are shown in Fig. 8.6a. This figure shows that the stresses in the compression zone are less than f_c' up to the numerical failure. Fig. 8.6b shows the stresses in prestressing wire at some load factors. The steel was under nearly constant compressive stress at the beginning of vertical loading due to the existence of the axial force. By increasing the applied vertical load, most of the Gauss points on the steel started to carry tensile stresses. This behaviour of the prestressing steel was observed for the all beams. The tensile stresses were far from yielding up to the numerical failure load. From Fig. 8.6, it can be seen that the cause of failure was not the crushing of concrete in the compression zone or the yielding of tension steel. This leads to conclude that the beam failed in shear. To see how the beam failed, the distribution of the principal compressive stresses (stresses greater than 3 MPa) are plotted in Fig. 8.7. In Fig. 8.7a, the distribution of the principal compressive stresses are plotted at load factor = 0.1. At this level of load, nearly all the principal compressive stresses were horizontal. The maximum stress was 7.71 MPa and its location was near the end of the beam. At load factor = 0.50 (Fig. 8.7b), in the constant bending region, the principal compressive stresses (greater than 3 MPa) disappeared from the bottom of the beam and developed at the top of the beam. In the shear area, the stresses became inclined and arranged diagonally from the support toward the vertical load point. At load factor = 0.95 (last converged increment, Fig. 8.7c) the neutral axis moved up due to the flexural cracking and the compression zone depth became smaller. The maximum principal compressive stress, which reached the value of f_c' , was located in the shear area (in the compression thrust between the support and the vertical load point) and it was the cause of failure.

(a) Observed

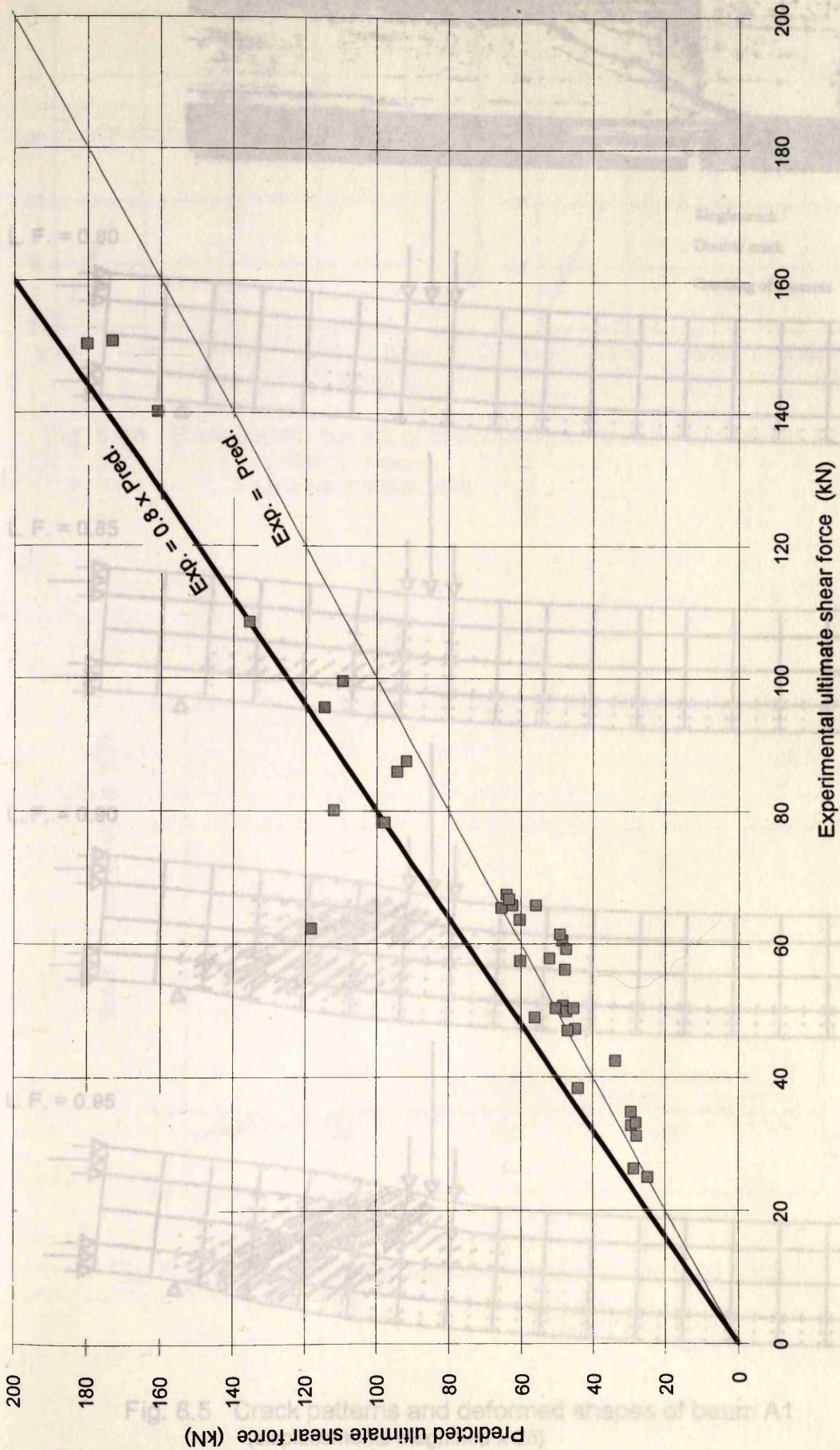
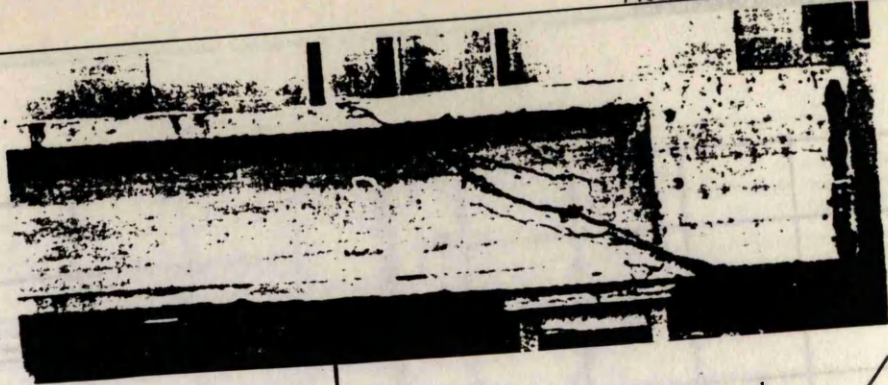


Fig. 8.4 Results of analysis of Arthur's beams

(a) Observed

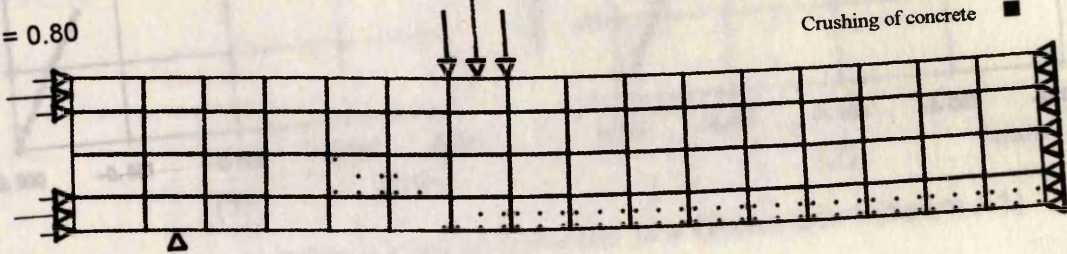


Single crack /

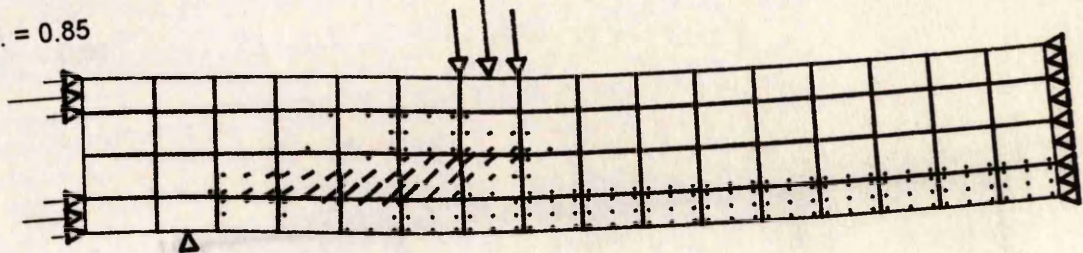
Double crack X

Crushing of concrete ■

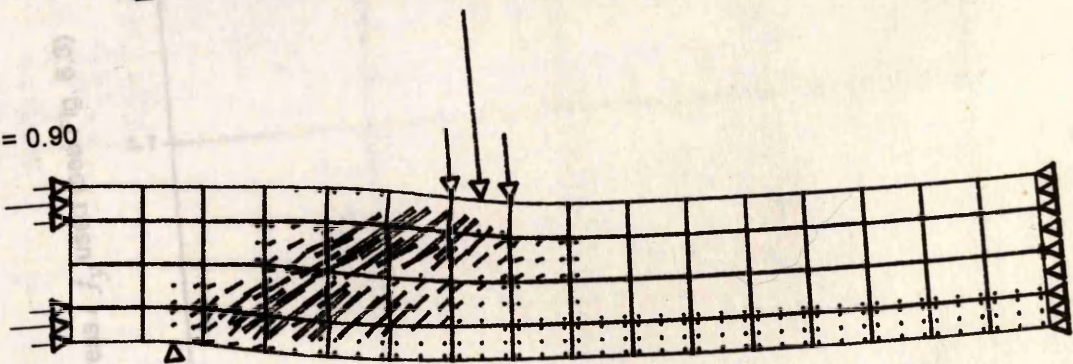
(b) L. F. = 0.80



(c) L. F. = 0.85



(d) L. F. = 0.90



(e) L. F. = 0.95

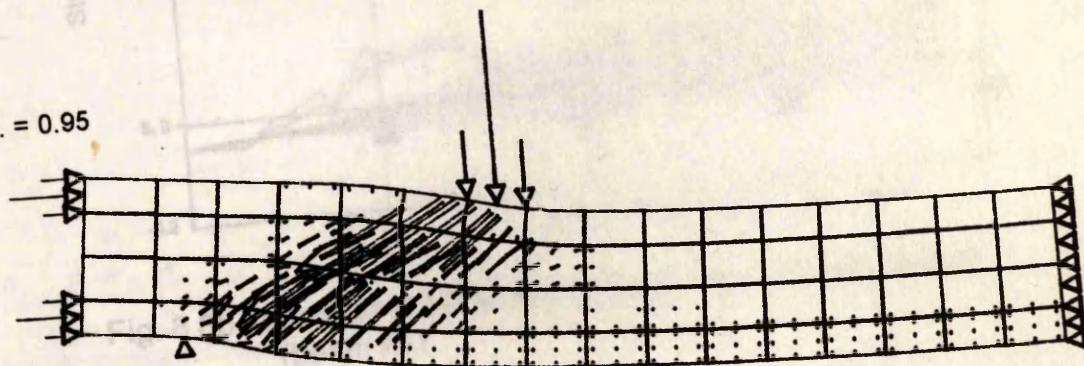


Fig. 8.5 Crack patterns and deformed shapes of beam A1
(displacements magnified x 20)

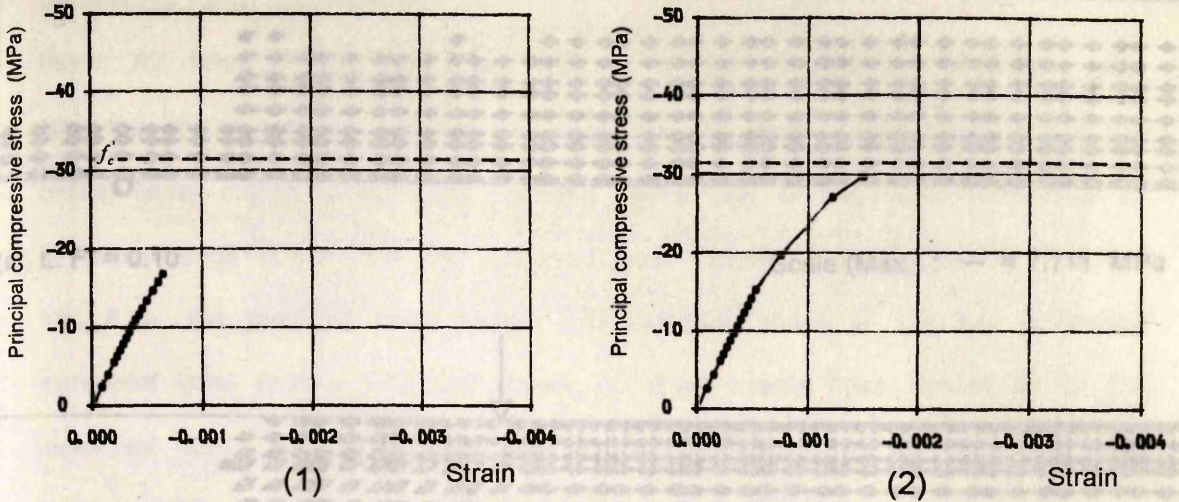


Fig. 8.6a Stress-strain curves of concrete at a Gauss point (beam A1)
 (1) near mid-span
 (2) under the load point

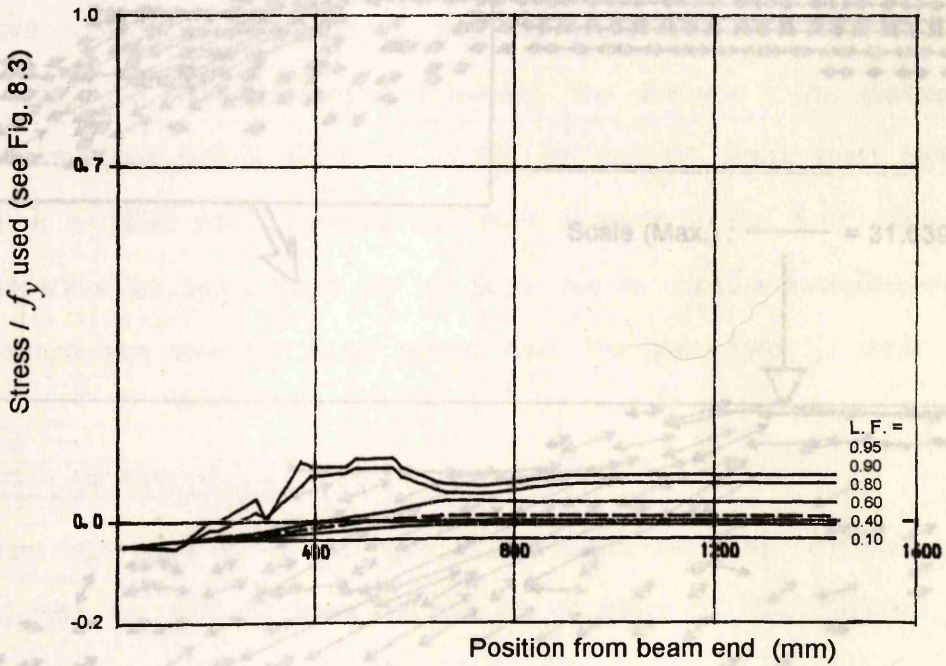
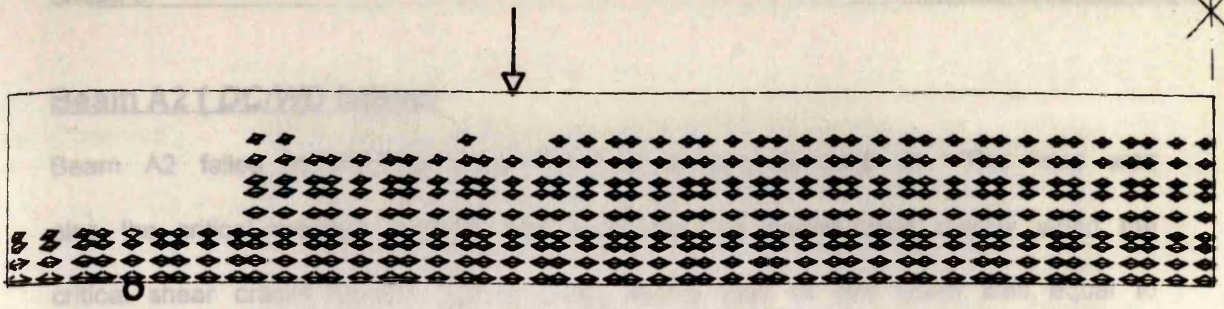
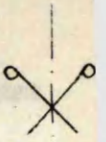
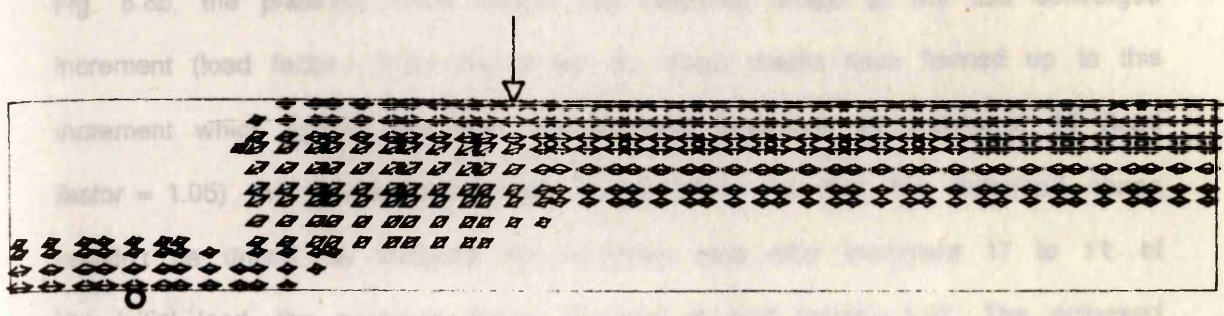


Fig. 8.6b Stresses in prestressing steel at some load factors (beam A1)



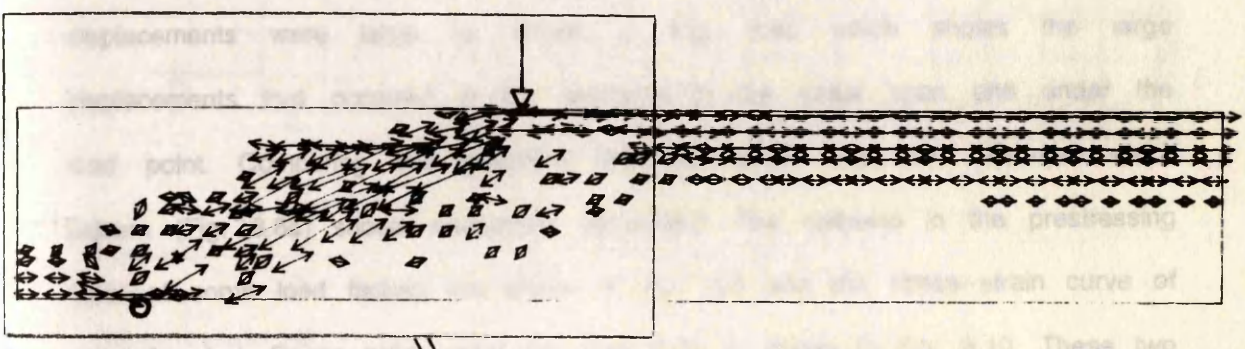
(a) L. F. = 0.10

Scale (Max.) : — = 7.711 MPa



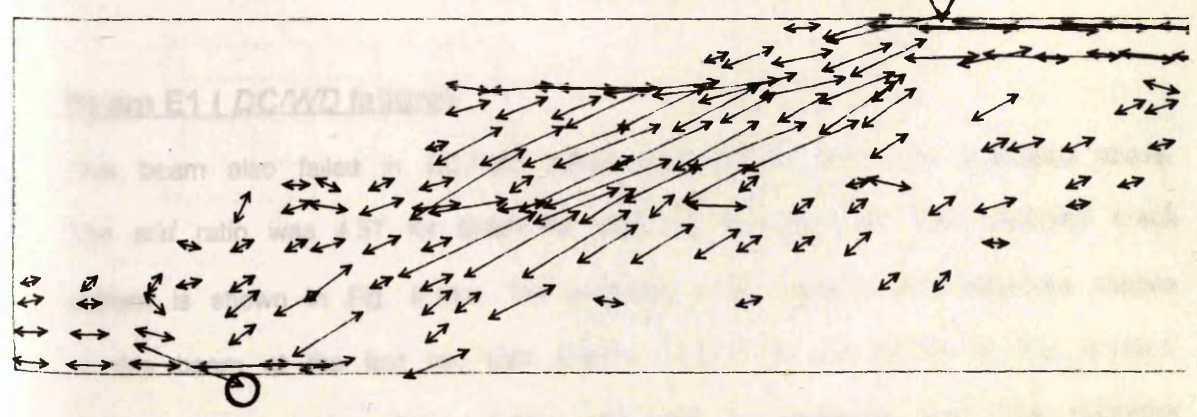
(b) L. F. = 0.50

Scale (Max.) : — = 9.996 MPa



(c) L. F. = 0.95

Scale (Max.) : — = 31.639 MPa



Scale (Max.) : — = 31.639 MPa

Fig. 8.7 Principal compressive stress distribution in beam A1 (stresses greater than 3 MPa)

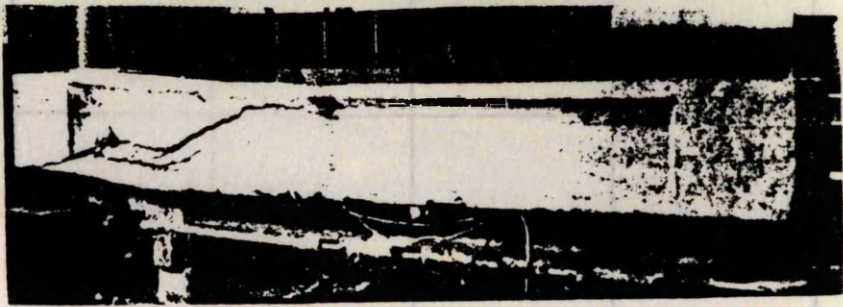
Beam A2 (DC/WD failure)

Beam A2 failed in DC/WD failure type at a load of 49.8 kN. This load was also the critical cracking load for this beam; i.e. the beam failed quickly when the critical shear cracks formed. The predicted failure load of this beam was equal to its experimental failure load. The observed crack pattern is shown in Fig. 8.8a. In Fig. 8.8b, the predicted crack pattern and deformed shape at the last converged increment (load factor = 1.00) are shown, no shear cracks have formed up to this increment which agreed well with the observed behaviour. At increment 18 (load factor = 1.05) the displacements were nearly infinity so that the deformed shape couldn't be drawn. By reducing the increment step after increment 17 to 1% of the initial load, the numerical failure occurred at load factor = 1.02. The deformed shape at load factor = 1.01, at which the convergence was not achieved and the displacements were large, is shown in Fig. 8.8c which shows the large displacements that occurred in the elements in the shear span and under the load point. Comparing this predicted deformed shape with the observed crack pattern (Fig. 8.8a) shows reasonable agreement. The stresses in the prestressing steel at some load factors are shown in Fig. 8.9 and the stress-strain curve of concrete at a Gauss point under the load point is shown in Fig. 8.10. These two figures show that the beam failure did not occur due to stresses exceeding neither in the compression zone nor in the tension steel. The beam failed in shear.

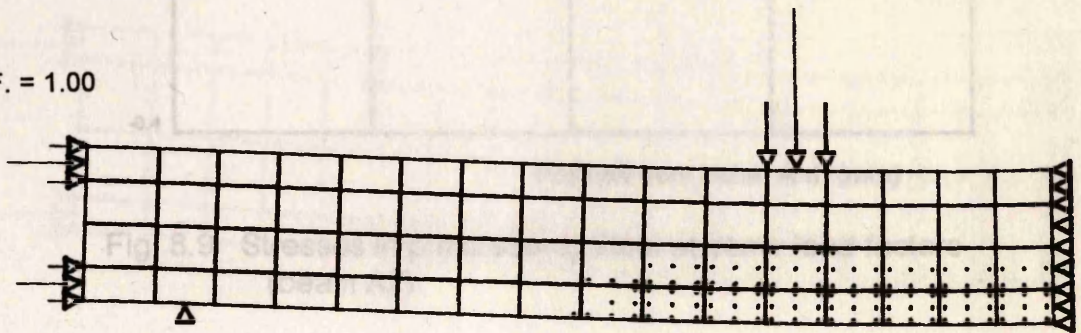
Beam E1 (DC/WD failure)

This beam also failed in DC/WD failure type as the beam A2 described above. The a/d ratio was 4.57 for beam A2 and 2.8 for beam E1. The observed crack pattern is shown in Fig. 8.11a. The predicted crack patterns and deformed shapes of this beam at the last two load factors (1.00, 1.05) are shown in Fig. 8.11b,c. The predicted crack pattern agreed well with the observed one. The predicted stress-strain curve of concrete at a Gauss point under the load point is shown in

(a) Observed



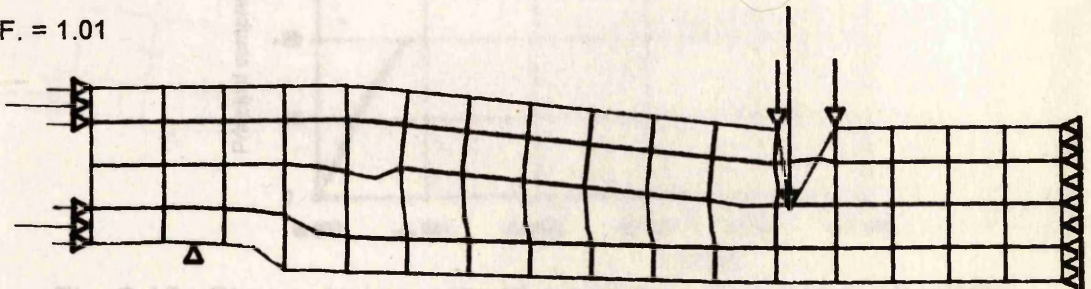
(b) L. F. = 1.00



- Single crack /
- Double crack X
- Crushing of concrete ■

Displacements magnified x 10

(c) L. F. = 1.01



Displacements reduced x 0.01

Fig. 8.10 Stress-strain curves at the load point of beam A2

Fig. 8.8 Crack patterns and deformed shapes of beam A2

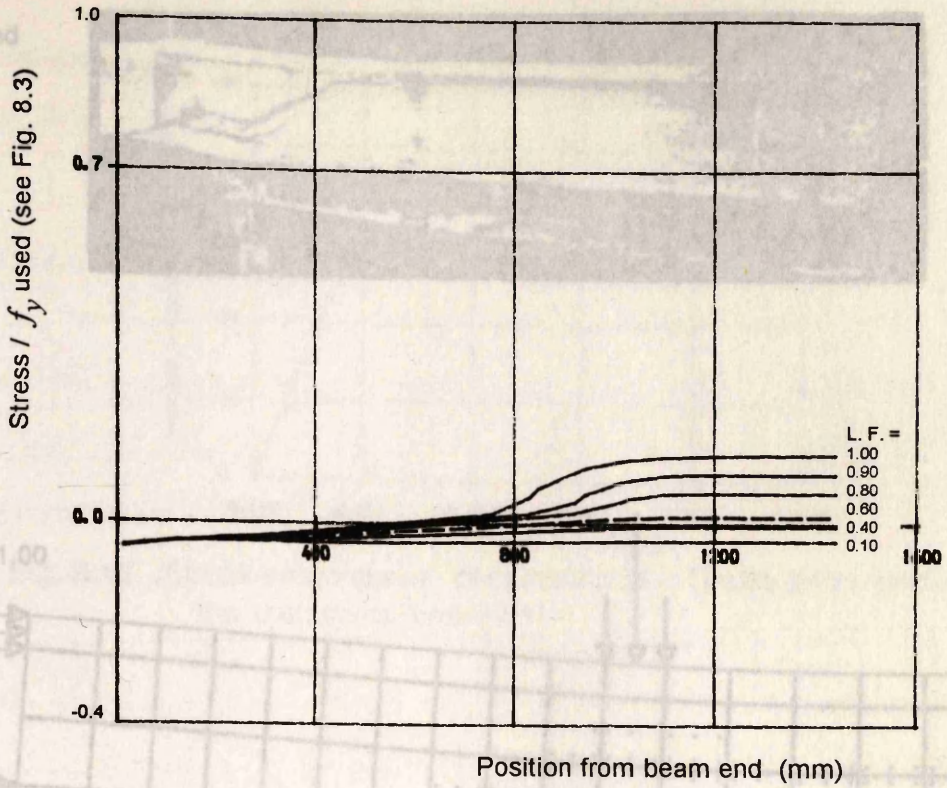


Fig. 8.9 Stresses in prestressing steel at some load factors (beam A2)

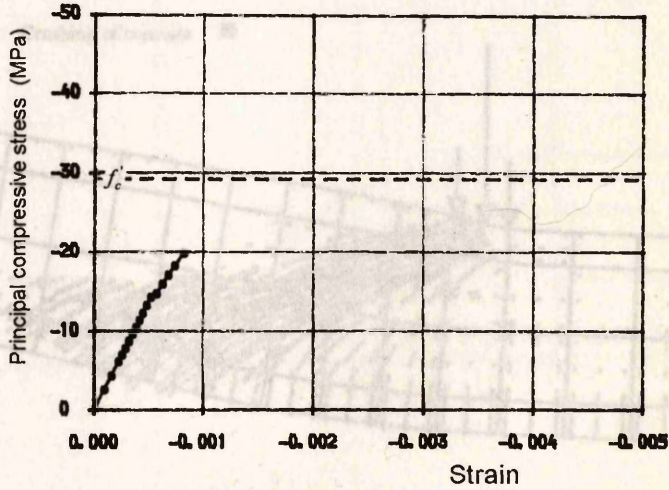
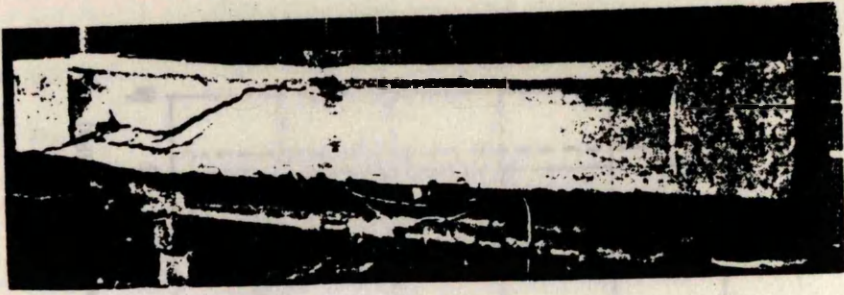
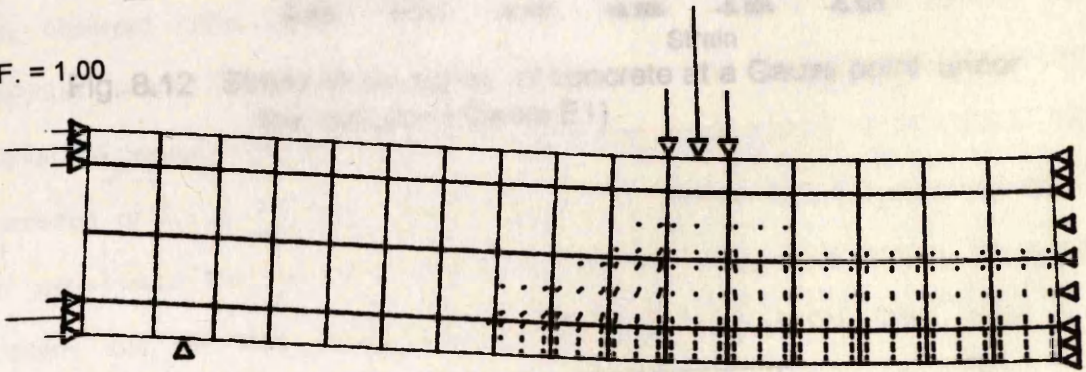


Fig. 8.10 Stress-strain curve of concrete at a Gauss point under the load point (beam A2)

(a) Observed



(b) L. F. = 1.00



(c) L. F. = 1.05

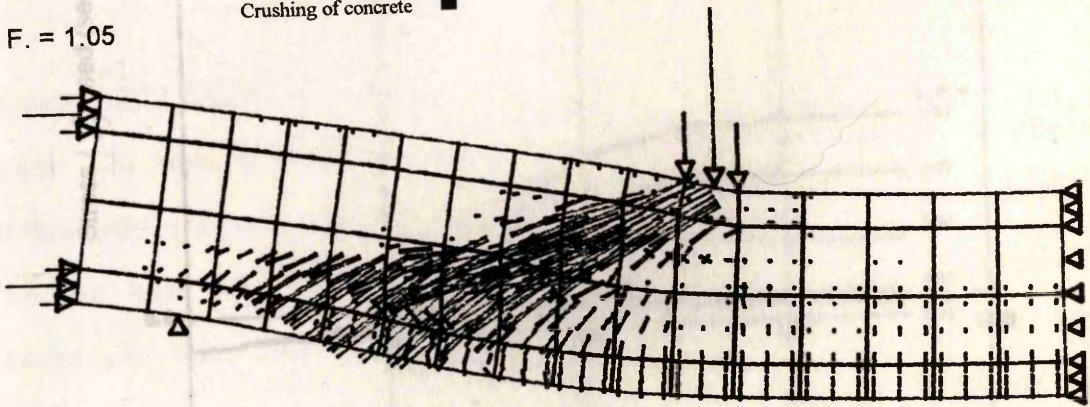


Fig. 8.11 Crack patterns and deformed shapes of beam E1 (displacements magnified x 10)

Fig. 8.13 Stresses in prestressing steel at some load factors (beam E1)

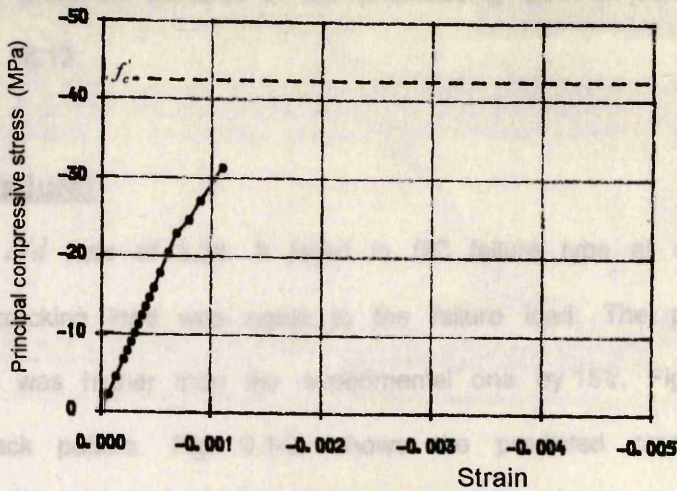


Fig. 8.12 Stress-strain curve of concrete at a Gauss point under the load point (beam E1)

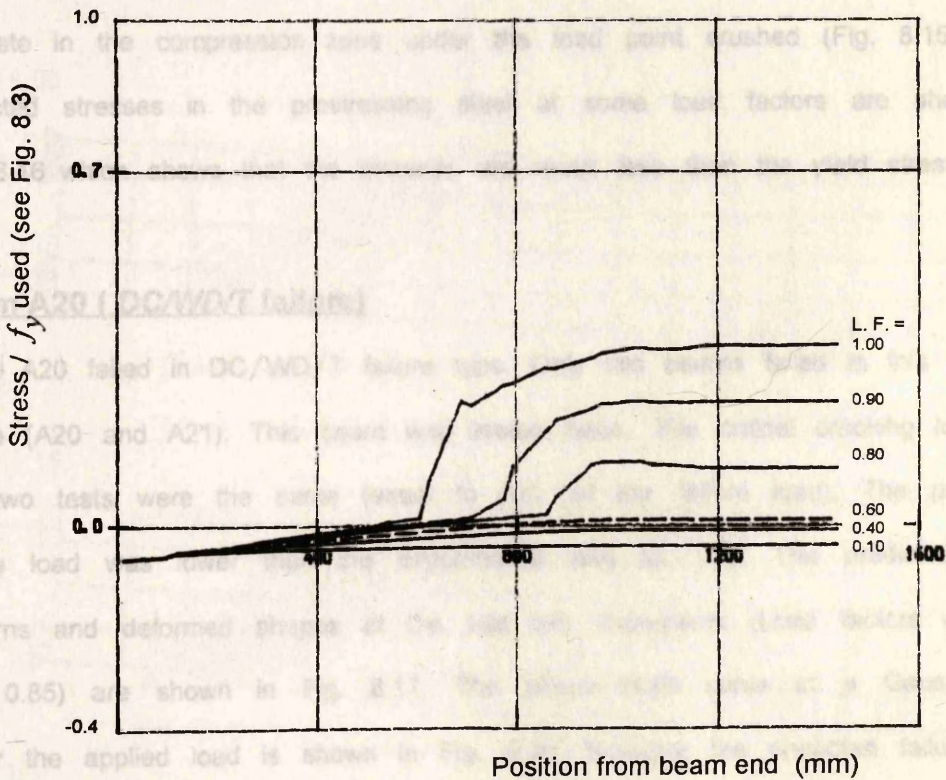


Fig. 8.13 Stresses in prestressing steel at some load factors (beam E1)

Fig. 8.12 and the predicted stresses in the prestressing steel at some load factors are shown in Fig. 8.13.

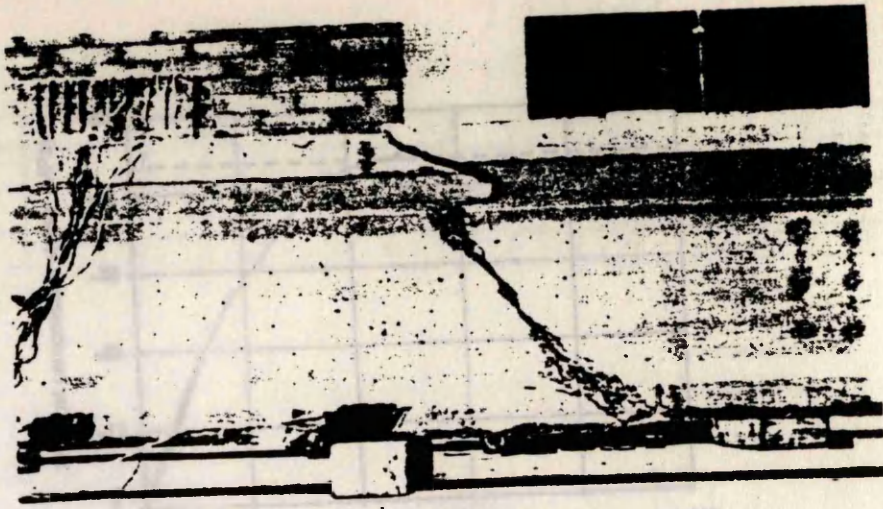
Beam A5 (DC failure)

Beam A5 had a a/d ratio of 2.28. It failed in DC failure type at a load of 97.9 kN. The critical cracking load was equal to the failure load. The predicted failure load of this beam was higher than the experimental one by 15%. Fig. 8.14a shows the observed crack pattern. Fig. 8.14b shows the predicted crack pattern and deformed shape at a load factor = 0.90, where no critical cracks formed. At a load equal the experimental failure load, the predicted crack pattern shows clearly the formation of the critical shear cracks (Fig. 8.14c). Despite this, the beam continued to carry more load up to a load factor of 1.15. Fig. 8.14d shows the crack pattern and deformed shape at this load level. The beam failed when the concrete in the compression zone under the load point crushed (Fig. 8.15). The predicted stresses in the prestressing steel at some load factors are shown in Fig. 8.16 which shows that the stresses are much less than the yield stress.

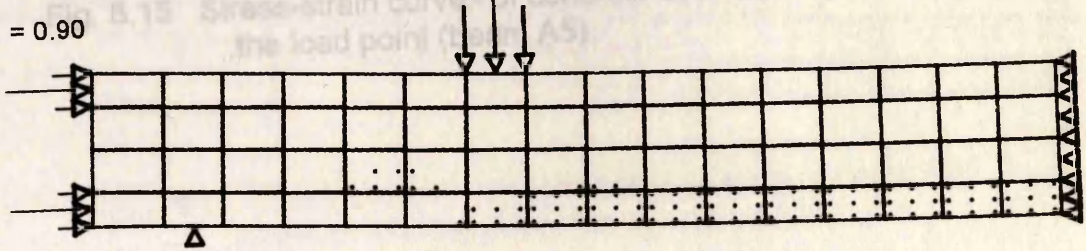
Beam A20 (DC/WD/T failure)

Beam A20 failed in DC/WD/T failure type. Only two beams failed in this type of failure (A20 and A21). This beam was tested twice. The critical cracking loads in the two tests were the same (equal to 82% of the failure load). The predicted failure load was lower than the experimental one by 15%. The predicted crack patterns and deformed shapes at the last two increments (Load factors of 0.80 and 0.85) are shown in Fig. 8.17. The stress-strain curve at a Gauss point under the applied load is shown in Fig. 8.18. Because the predicted failure load was less than the experimental one, no failure in the tension steel occurred as reported in this type of failure (Fig. 8.19), while the diagonal cracking in the shear span was very clear (Fig. 8.17b).

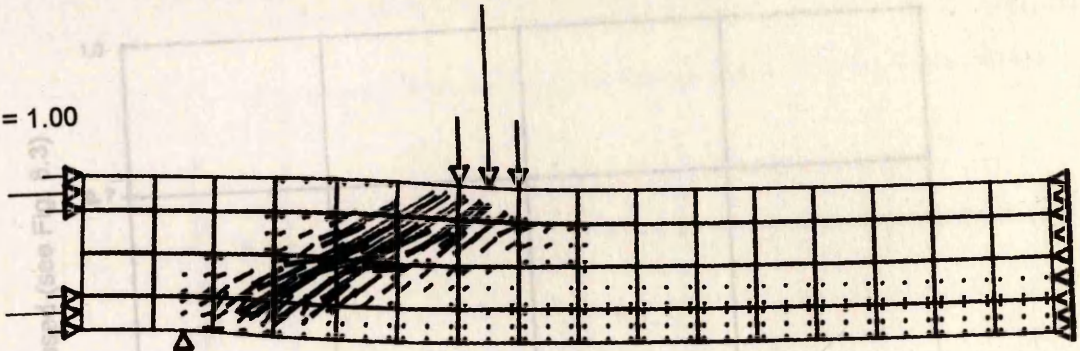
(a) Observed



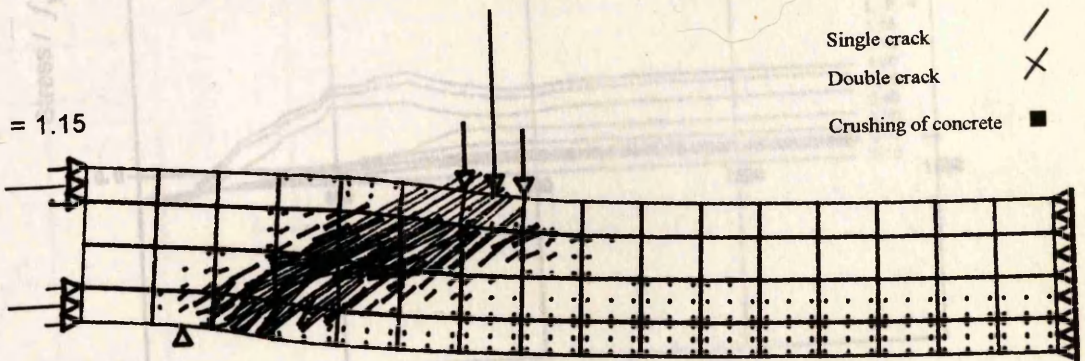
(b) L. F. = 0.90



(c) L. F. = 1.00



(d) L. F. = 1.15



Single crack /
 Double crack X
 Crushing of concrete ■

Fig. 8.14 Crack patterns and deformed shapes of beam A5 (displacements magnified x 10)

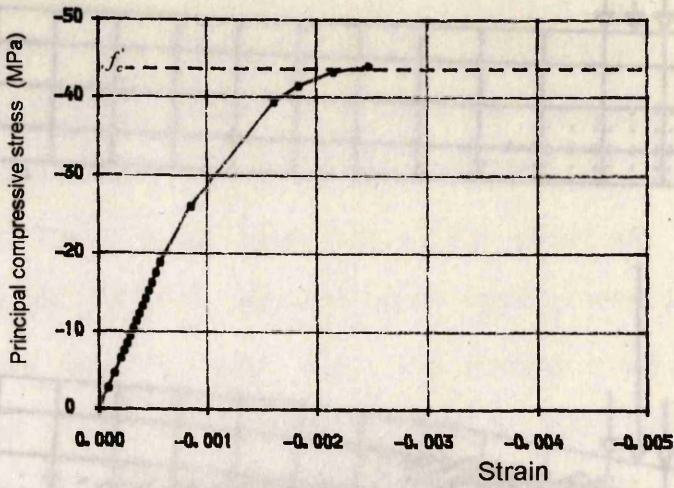


Fig. 8.15 Stress-strain curve of concrete at a Gauss point under the load point (beam A5)

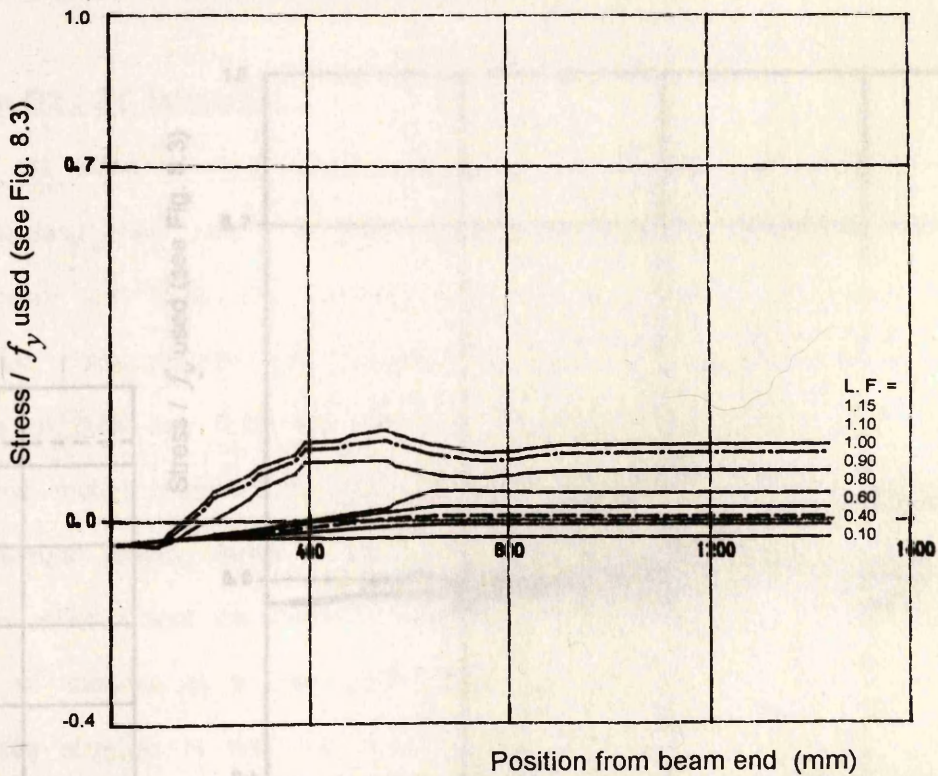


Fig. 8.16 Stresses in prestressing steel at some load factors (beam A5)

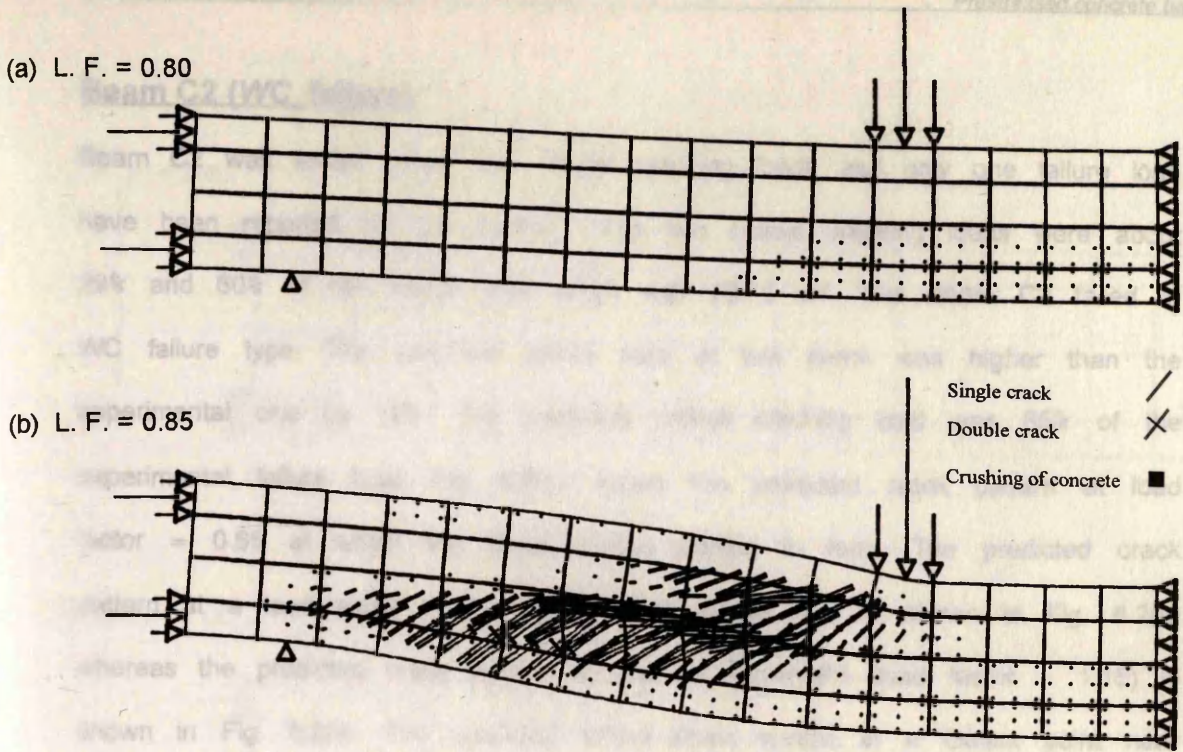


Fig. 8.17 Crack patterns and deformed shapes of beam A20 (displacements magnified x 10)

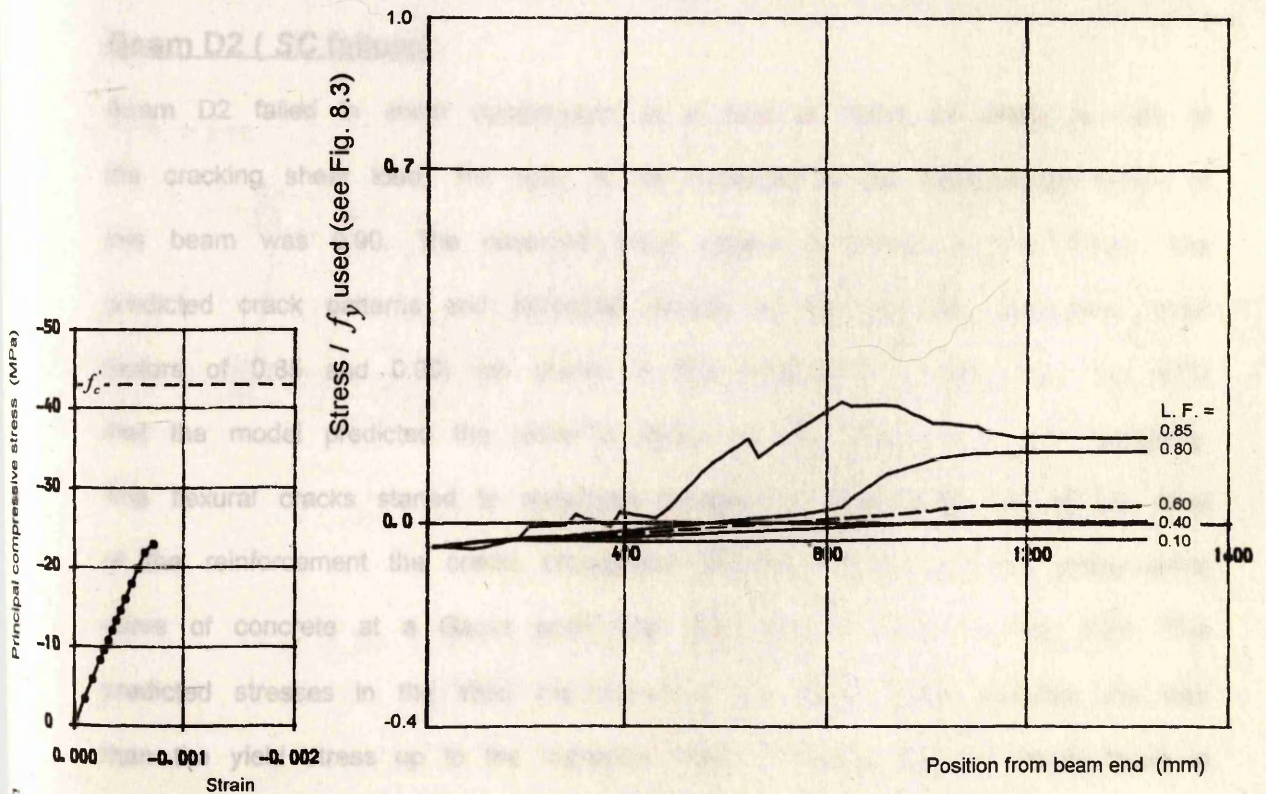


Fig. 8.18 Stress-strain curve of concrete at a Gauss point under the load point (beam A20)

Fig. 8.19 Stresses in prestressing steel at some load factors (beam A20)

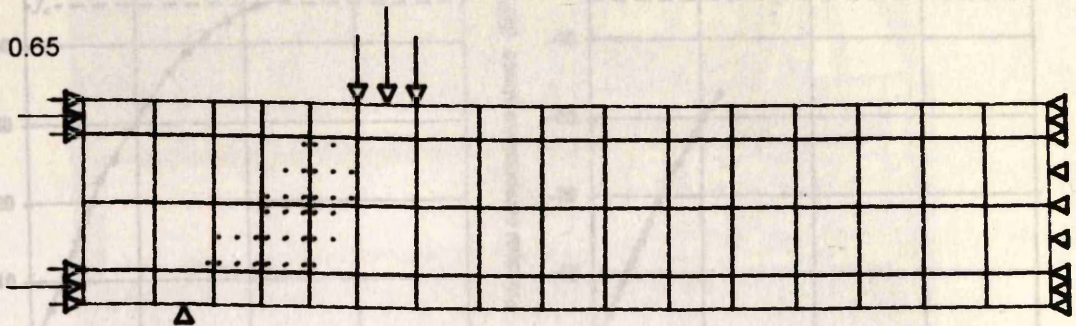
Beam C2 (WC failure)

Beam C2 was tested twice. Two critical cracking loads and only one failure load have been reported for this beam. The two critical cracking loads were about 29% and 60% of the failure load which was 280.2 kN. This beam C2 failed in WC failure type. The predicted failure load of this beam was higher than the experimental one by 15%. The predicted critical cracking load was 65% of the experimental failure load. Fig. 8.20a shows the predicted crack pattern at load factor = 0.65 at which the shear cracks started to form. The predicted crack pattern at a load equal to the experimental failure load is shown in Fig. 8.20b whereas the predicted crack pattern at the last increment (load factor = 1.15) is shown in Fig. 8.20c. The predicted stress-strain curves at a Gauss point near the mid-span and under the load point are shown in Figs. 8.21. The predicted stresses in the prestressing steel at some load factors are shown in Fig. 8.22.

Beam D2 (SC failure)

Beam D2 failed in shear compression at a load of 100.5 kN which is 1.33 of the cracking shear load. The ratio of the predicted to the experimental failure of this beam was 0.90. The observed crack pattern is shown in Fig. 8.23a. The predicted crack patterns and deformed shapes at the last two increments (load factors of 0.85 and 0.90) are shown in Fig. 8.23b,c. It is clear from Fig. 8.23 that the model predicted the mode of failure of this beam to a good accuracy. The flexural cracks started to propagate towards the load point and at the level of the reinforcement the cracks propagated towards the support. The stress-strain curve of concrete at a Gauss point near mid-span is shown in Fig. 8.24. The predicted stresses in the steel are shown in Fig. 8.25. These stresses are less than the yield stress up to the numerical failure indicating that the beam failed in shear and not in flexure.

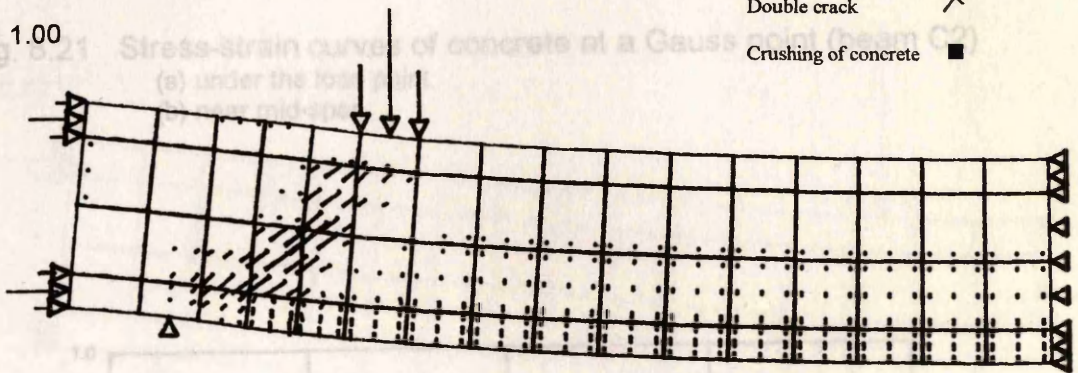
(a) L. F. = 0.65



(a)

- Single crack /
- Double crack X
- Crushing of concrete ■

(b) L. F. = 1.00



(b)

(c) L. F. = 1.15

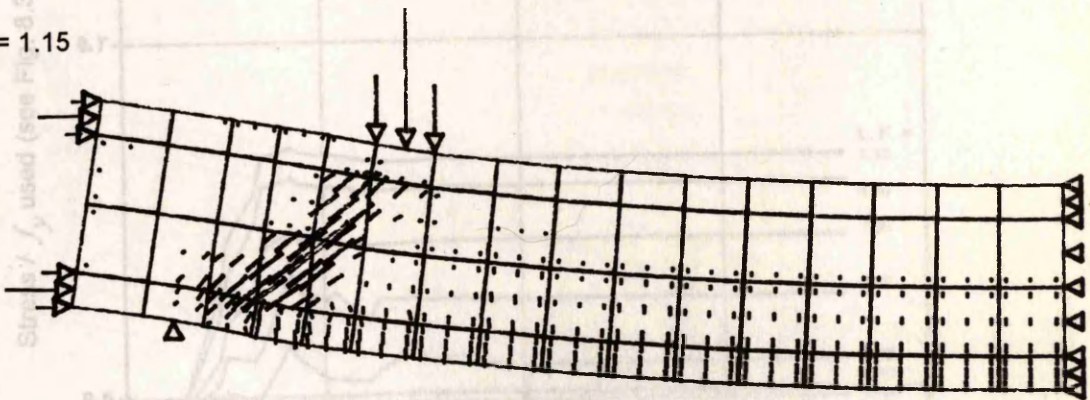


Fig. 8.20 Crack patterns and deformed shapes of beam C2 (displacements magnified x 10)

Fig. 8.22 Stresses in prestressing steel at some load factors (beam C2)

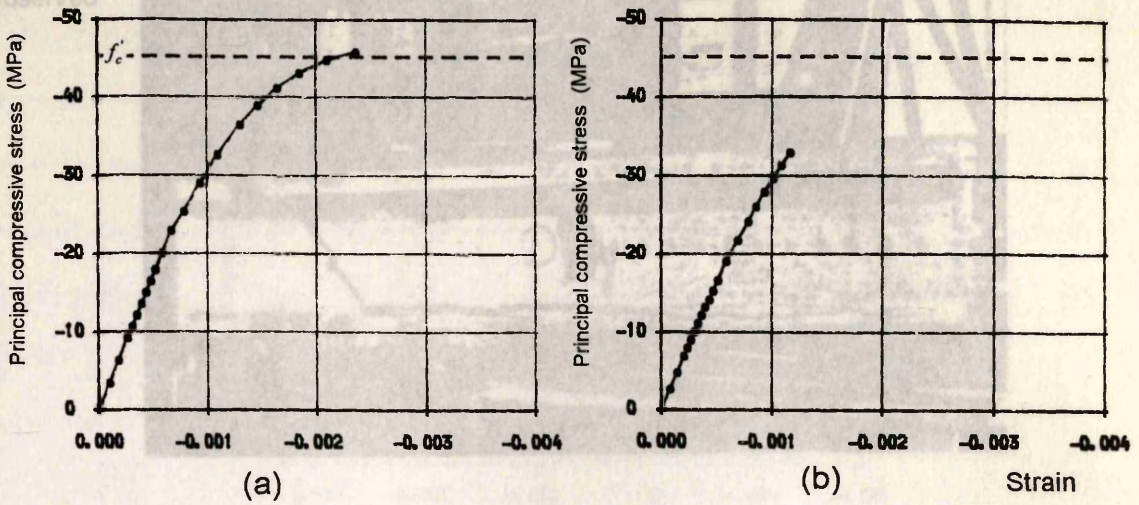


Fig. 8.21 Stress-strain curves of concrete at a Gauss point (beam C2)
 (a) under the load point
 (b) near mid-span

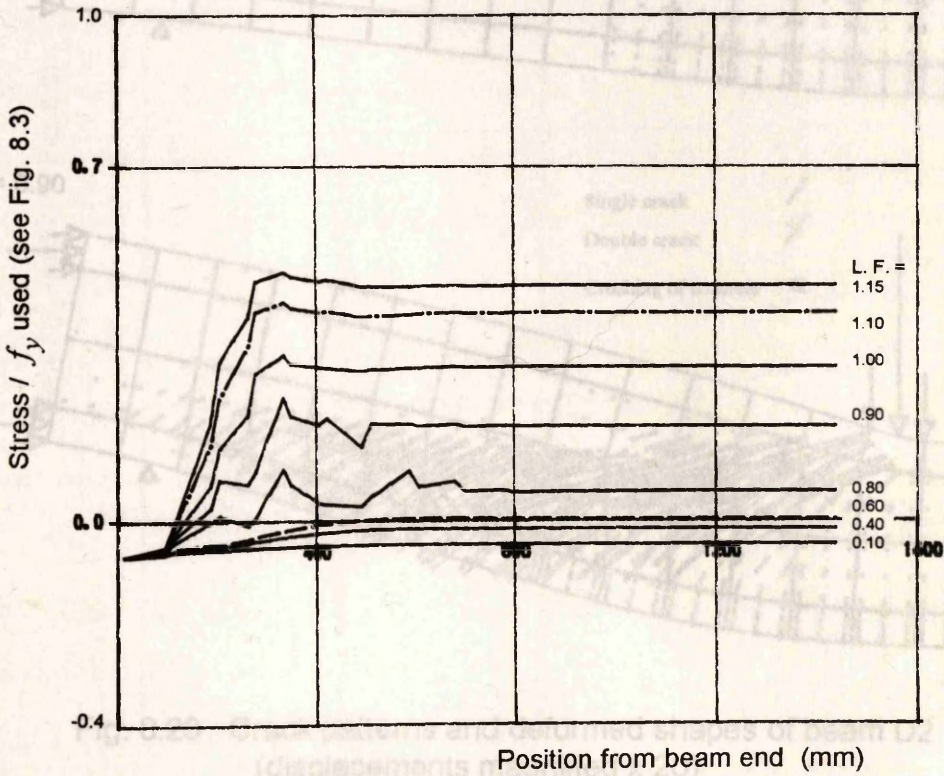
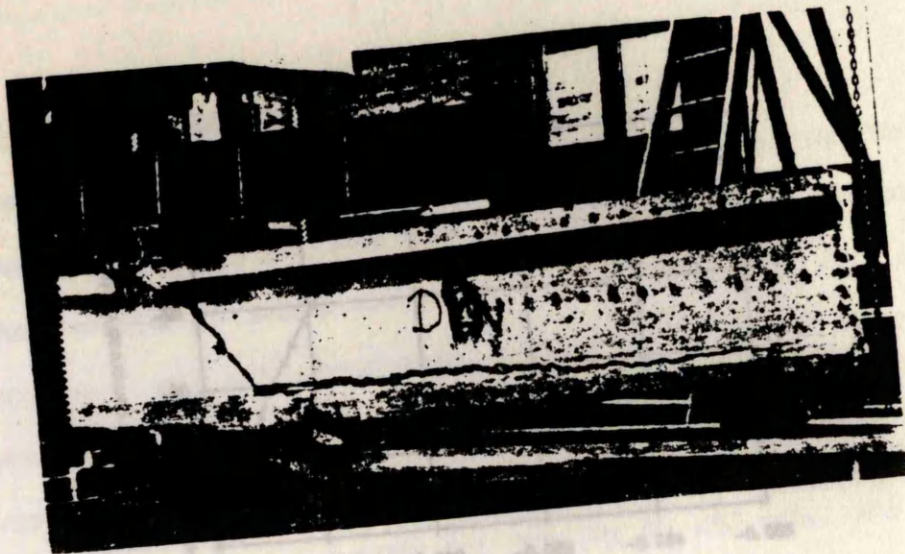
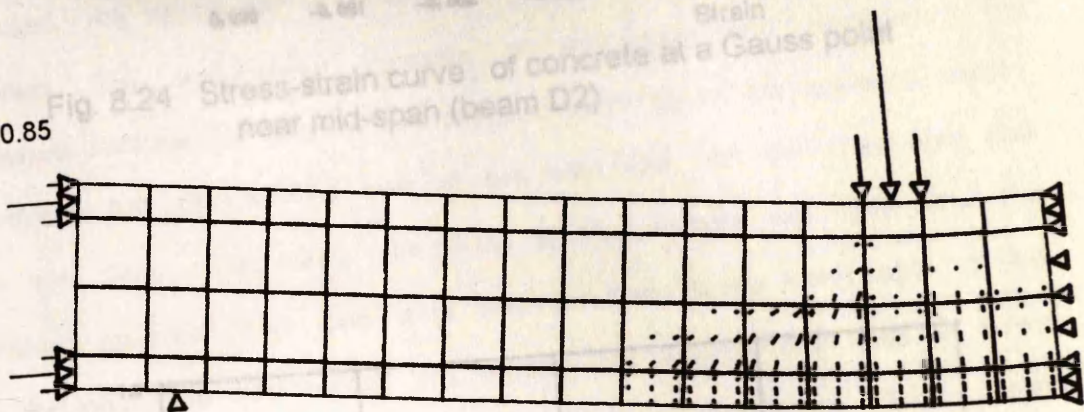


Fig. 8.22 Stresses in prestressing steel at some load factors (beam C2)

(a) Observed



(b) L. F. = 0.85



(c) L. F. = 0.90

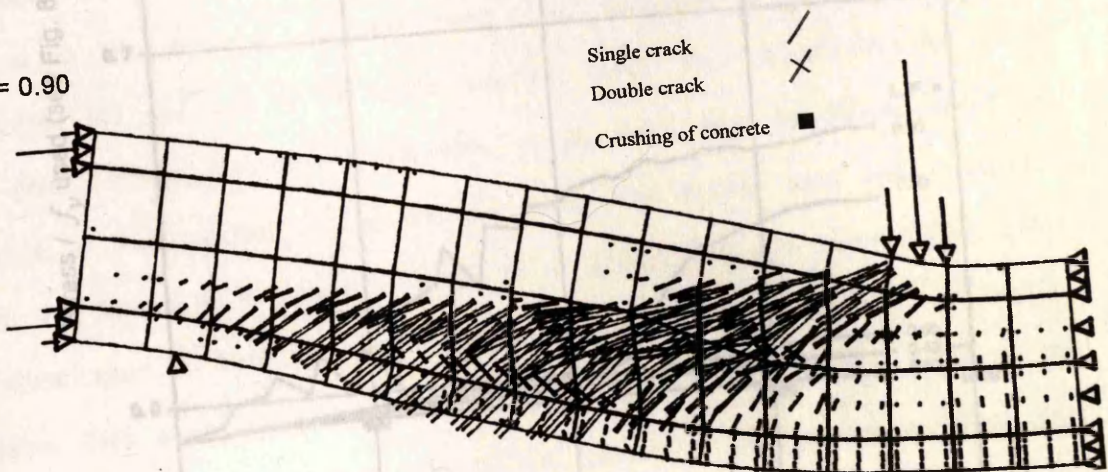


Fig. 8.23 Crack patterns and deformed shapes of beam D2 (displacements magnified x 20)

Fig. 8.25 Stresses in prestressing steel at some load factors (beam D2)

8.3 Elzanaty, et al's beams

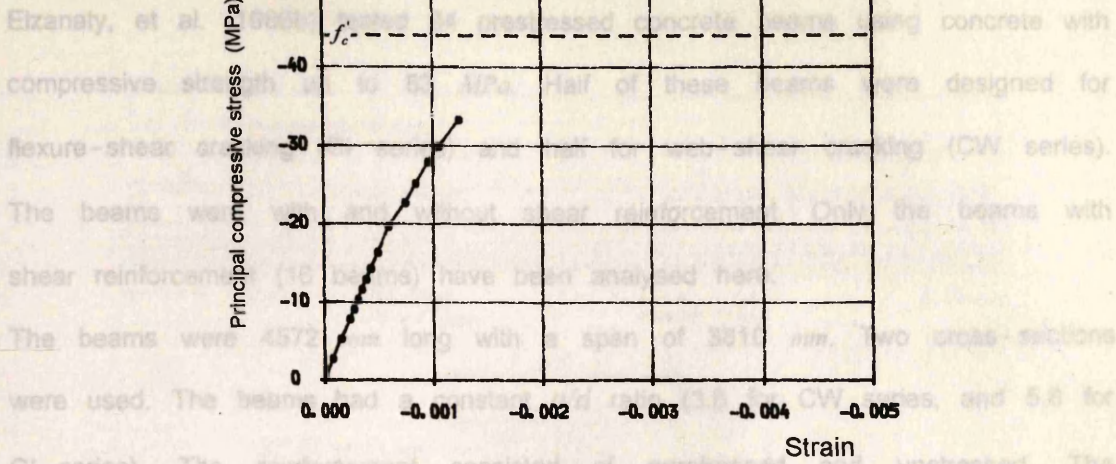


Fig. 8.24 Stress-strain curve of concrete at a Gauss point near mid-span (beam D2)

The beams were designed for flexure-shear and shear. The beams with shear reinforcement have been analysed here. The beams were 4570 mm long with a span of 3810 mm. Two cross-sections were used. The beam with a span of 3810 mm was analysed for two load factors, 0.8 and 0.9. The beam with a span of 4570 mm was analysed for two load factors, 0.8 and 0.9. The beams were analysed for flexure-shear and shear. The beams with shear reinforcement have been analysed here. The beams were 4570 mm long with a span of 3810 mm. Two cross-sections were used. The beam with a span of 3810 mm was analysed for two load factors, 0.8 and 0.9. The beam with a span of 4570 mm was analysed for two load factors, 0.8 and 0.9.

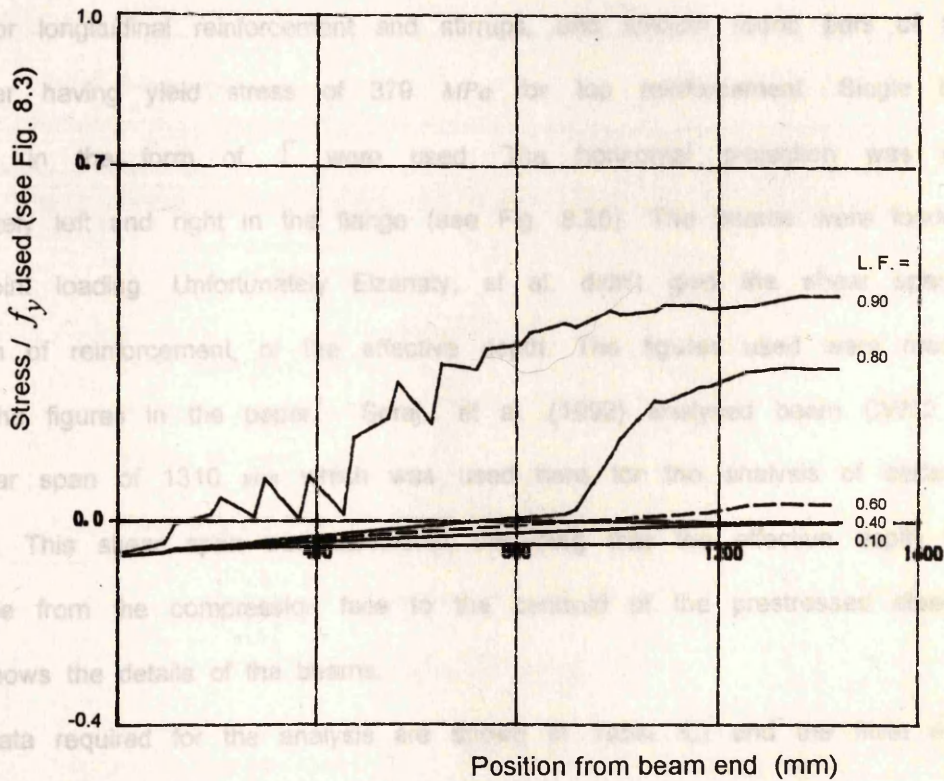


Fig. 8.25 Stresses in prestressing steel at some load factors (beam D2)

The data required for the analysis are shown in Fig. 8.27. The ratios of the prestressing steel stress to the yield stress are shown in Table 8.2. The mean value and standard deviation were 1.04 and 7.7%, respectively. All the predicted failure loads except two are within the range of 0.95 - 1.10 of

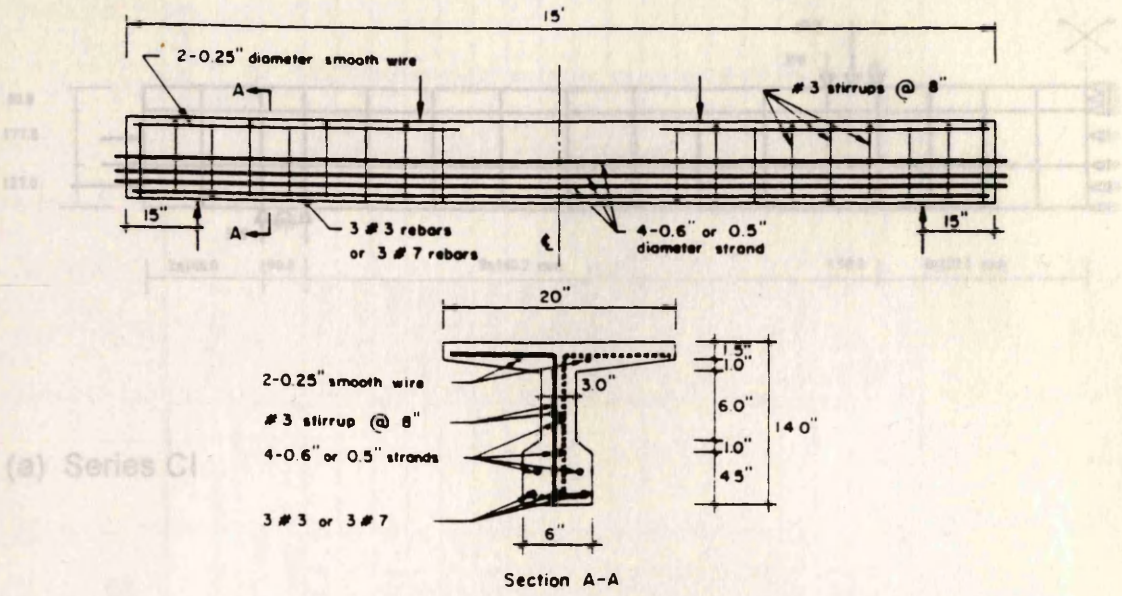
8.3 Elzanaty, et al's beams

Elzanaty, et al. (1986b) tested 34 prestressed concrete beams using concrete with compressive strength up to 83 MPa. Half of these beams were designed for flexure-shear cracking (CI series) and half for web-shear cracking (CW series). The beams were with and without shear reinforcement. Only the beams with shear reinforcement (16 beams) have been analysed here.

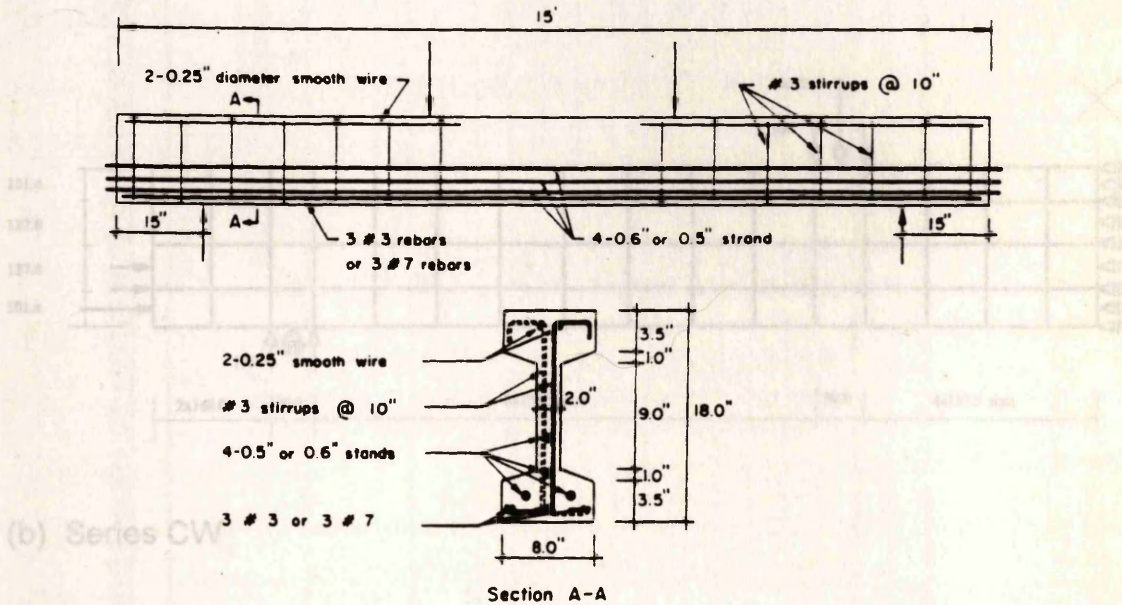
The beams were 4572 mm long with a span of 3810 mm. Two cross-sections were used. The beams had a constant a/d ratio (3.8 for CW series, and 5.8 for CI series). The reinforcement consisted of prestressed and unstressed. The prestressed reinforcement was 15 mm diameter made up of low-relaxation seven-wire Grade 270 strands. The area of this wire was 142 mm² (the area was taken from Seraj, et al. 1992). The stress at 1% extension was 1760 MPa. The unstressed reinforcing bars used were deformed bars having yield stress of 434 MPa for longitudinal reinforcement and stirrups, and smooth round bars of 6 mm diameter having yield stress of 379 MPa for top reinforcement. Single legged stirrups in the form of Γ were used. The horizontal projection was placed alternately left and right in the flange (see Fig. 8.26). The beams were loaded by two-point loading. Unfortunately Elzanaty, et al. didn't give the shear span, the position of reinforcement, or the effective depth. The figures used were measured from the figures in the paper. Seraj, et al. (1992) analysed beam CW12 using a shear span of 1310 mm which was used here for the analysis of series CW beams. This shear span was calculated assuming that the effective depth is the distance from the compression face to the centroid of the prestressed steel. Fig. 8.26 shows the details of the beams.

The data required for the analysis are shown in Table 8.2 and the finite element meshes used are shown in Fig. 8.27.

The ratios of the predicted over the experimental failure loads are presented in Table 8.2. The mean value and standard deviation were 1.04 and 7.7%, respectively. All the predicted failure loads except two are within the range of 0.95 – 1.10 of



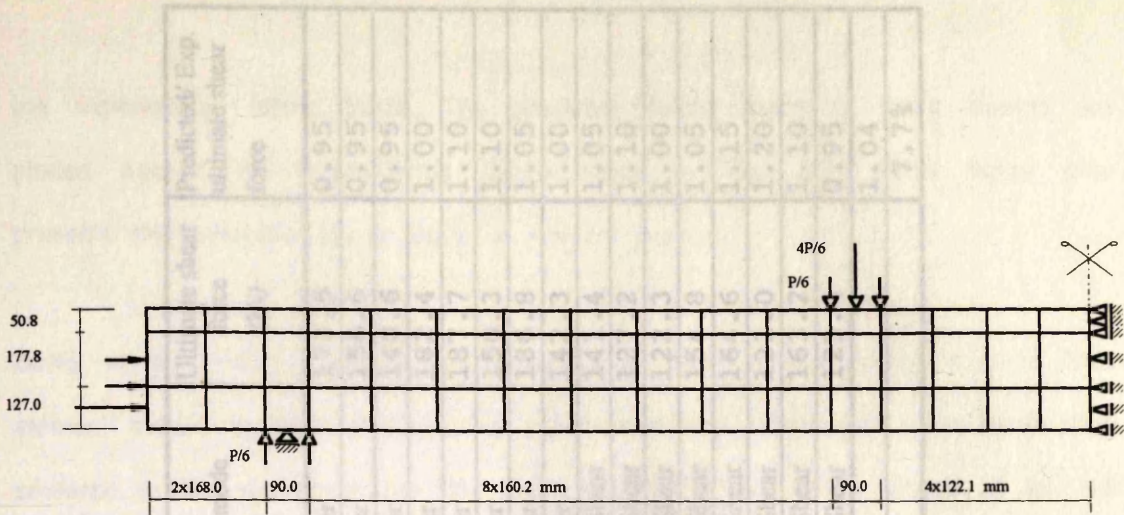
beams of CI series



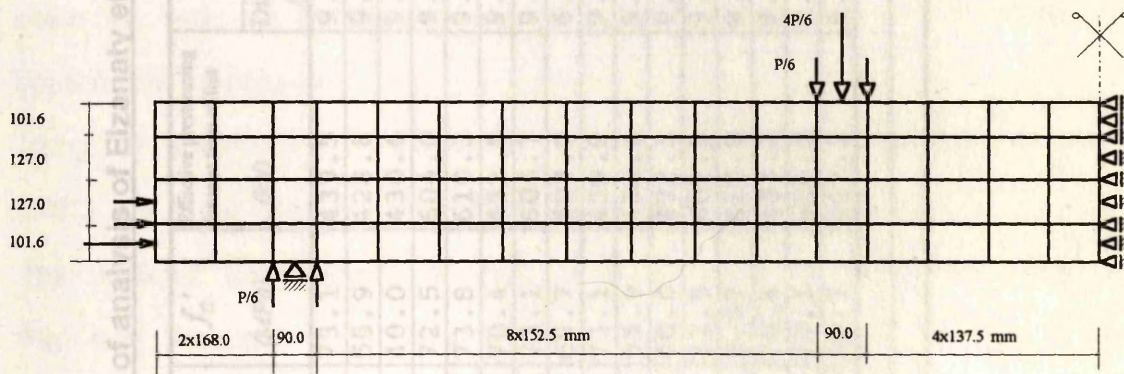
beams of CW series

Fig. 8.27 Finite element meshes for Elzanaty, et al's beams

Fig. 8.26 Dimensions of Elzanaty, et al' beams.



(a) Series CI



(b) Series CW

Table 8.2. Data and results of analysis of Elzanaty et al's beams

No. Beams	Shear reinforcement	Failure	Predicted/Exp. ultimate shear force
	Diameter (mm)		
1	254.0	Web-Shear	0.95
2	254.0	Web-Shear	0.95
3	254.0	Web-Shear	0.95
4	254.0	Web-Shear	1.00
5	177.8	Web-Shear	1.10
6	254.0	Web-Shear	1.10
7	254.0	Web-Shear	1.05
8	254.0	Web-Shear	1.00
9	281.2	Precracked	1.05
10	263.2	Precracked	1.15
11	263.2	Precracked	1.20
12	263.2	Precracked	1.10
13	263.2	Precracked	0.95
14	203.2	Precracked	1.04
15	203.2	Precracked	7.7%

Fig. 8.27 Finite element meshes for Elzanaty, et al's beams.

Table 8.2 Data and results of analysis of Elzanaty et al's beams

No.	Beams	a/d	f'_c (MPa)	Effective prestressing force at time of test (kN)	Shear reinforcement		Failure mode	Ultimate shear force (kN)	Predicted/ Exp. ultimate shear force
					Diameter (mm)	Spacing (mm)			
1	CW10	3.8	73.1	439.5	9.5	254.0	Web-Shear	173.5	0.95
2	CW11	3.8	55.9	428.8	9.5	254.0	Web-Shear	156.6	0.95
3	CW12	3.8	40.0	430.6	9.5	254.0	Web-Shear	140.6	0.95
4	CW13	3.8	72.5	604.0	9.5	254.0	Web-Shear	182.4	1.00
5	CW14	3.8	73.8	610.3	9.5	177.8	Web-Shear	187.7	1.10
6	CW15	3.8	70.4	432.8	9.5	254.0	Web-Shear	150.3	1.10
7	CW16	3.8	73.1	606.7	9.5	254.0	Web-Shear	186.8	1.05
8	CW17	3.8	69.7	608.0	6.4	254.0	Web-Shear	142.3	1.00
9	CI10	5.8	73.1	439.9	9.5	203.2	Flexural-Shear	141.4	1.05
10	CI11	5.8	55.9	430.6	9.5	203.2	Flexural-Shear	127.2	1.10
11	CI12	5.8	40.0	432.3	9.5	203.2	Flexural-Shear	122.3	1.00
12	CI13	5.8	72.5	602.3	9.5	203.2	Flexural-Shear	154.8	1.05
13	CI14	5.8	5.87	612.9	9.5	127.0	Flexural-Shear	164.6	1.15
14	CI15	5.8	70.4	433.2	9.5	203.2	Flexural-Shear	121.0	1.20
15	CI16	5.8	73.1	608.5	9.5	203.2	Flexural-Shear	163.2	1.10
16	CI17	5.8	69.7	607.2	6.4	203.2	Flexural-Shear	129.4	0.95
					Mean		value		
					Standard		deviation		
								1.04	7.7%

the experimental failure loads. The predicted failure loads of these beams are plotted against the experimental failure loads in Fig. 8.28. This figure also presents the predicted failure loads of Arthur's beams.

Seraj, et al. (1992) predicted the behaviour of beam CW12, using a 3-D finite element model. In their analysis, the prestressed and unstressed main steel were smeared to the element edges and the compression steel were placed at the top edge of the beam. They predicted a value of failure load equal 323.38 *kN* which is 15% higher than the experimental failure load (281.11 *kN*). Seraj, et al. referred the higher predicted failure load to the modelling of the stirrups. This was because they assumed symmetrical stirrups in order to keep, as they said, the computational efforts within the limit of available resources, while in the test the stirrups were arranged alternately in the flange. This modelling of stirrups, as they explained, introduced an additional confinement of the concrete. No attempt was made by Seraj, et al. to rerun the beam again without this part of stirrups to support their explanation.

Using the present 2-D finite element model the predicted failure load of beam CW12 was lower than the experimental failure load by about 5%.

The predicted crack patterns of Seraj, et al. at some increments are shown in Fig. 8.29. Elzanaty, et al. haven't reported the observed crack patterns of the beams but they mentioned that no cracks occurred up to the diagonal cracking load which for this beam was 170.8 *kN*. Seraj, et al. predicted a diagonal cracking load (182.8 *kN*) which is closer to the observed diagonal cracking load than the one predicted here (210 *kN*).

In Figs. 8.30 to 8.34, the predicted behaviours of beam CW12 are presented. Fig. 8.30 shows the predicted crack patterns and deformed shapes at some load factors. At the first increment (in which only the prestressed force was applied, Fig. 8.30a), the beam deflected upward. At load factor = 0.65 (Fig. 8.30b), the

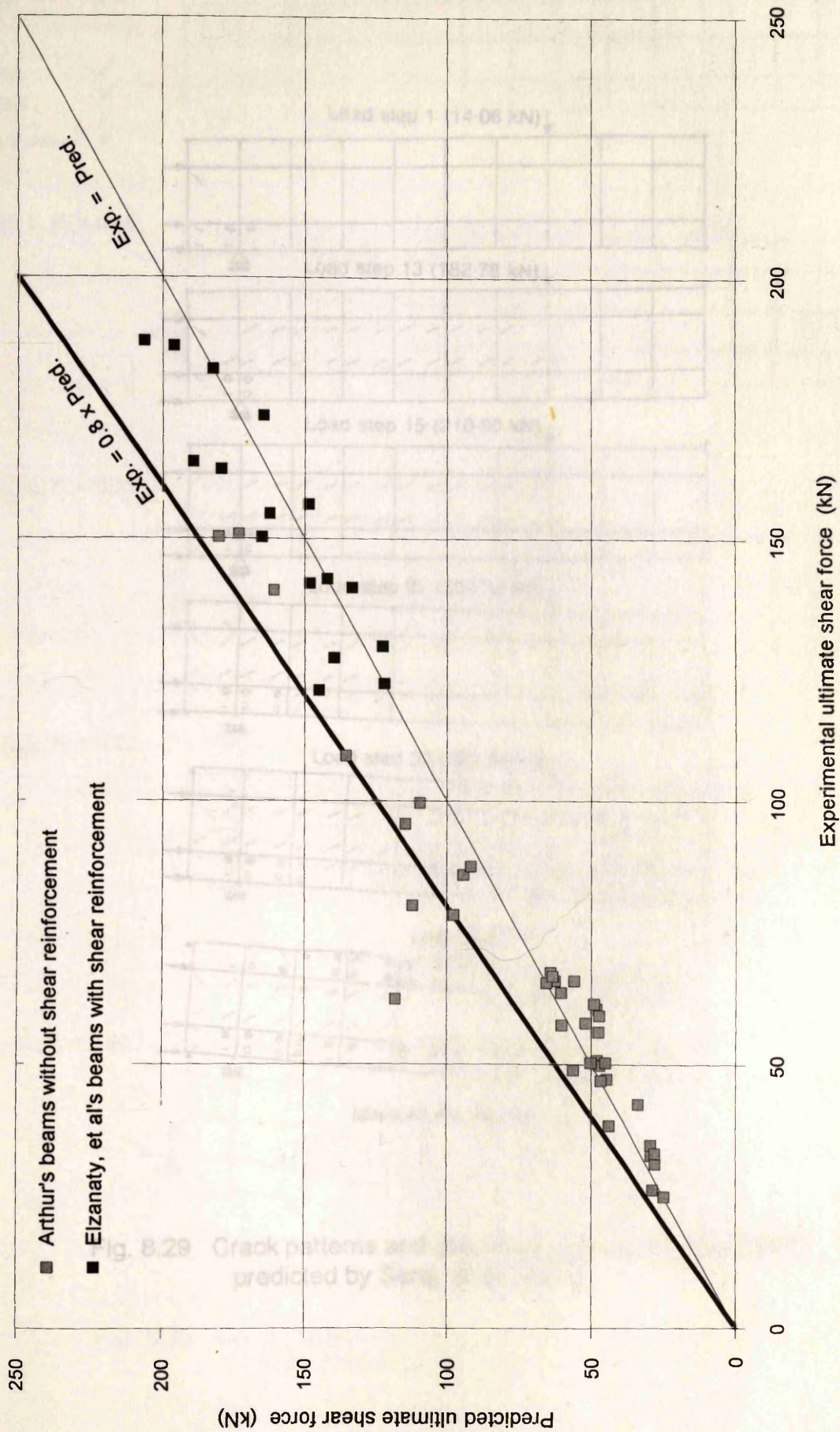


Fig. 8.28 Results of analysis of prestressed concrete beams

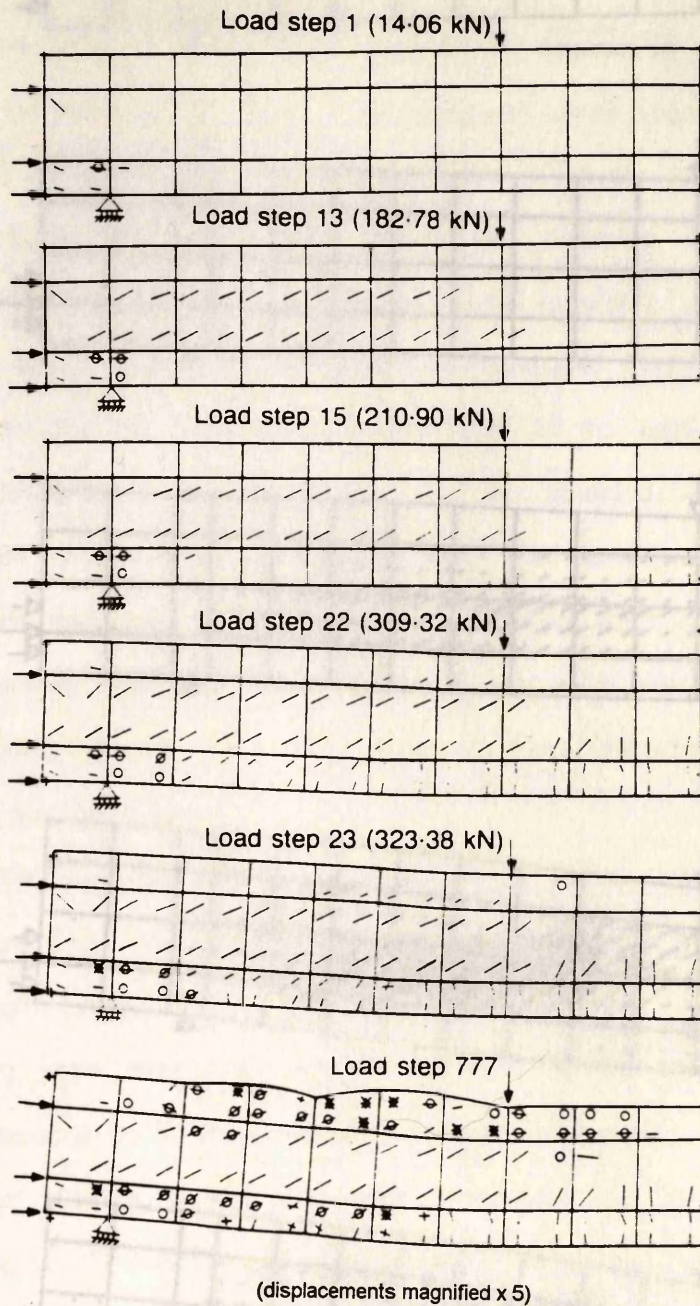


Fig. 8.29 Crack patterns and deformed shapes of beam CW12 predicted by Seraj, et al. (1992)

Fig. 8.30 Crack patterns and deformed shapes of beam CW12 (displacements magnified x 5)

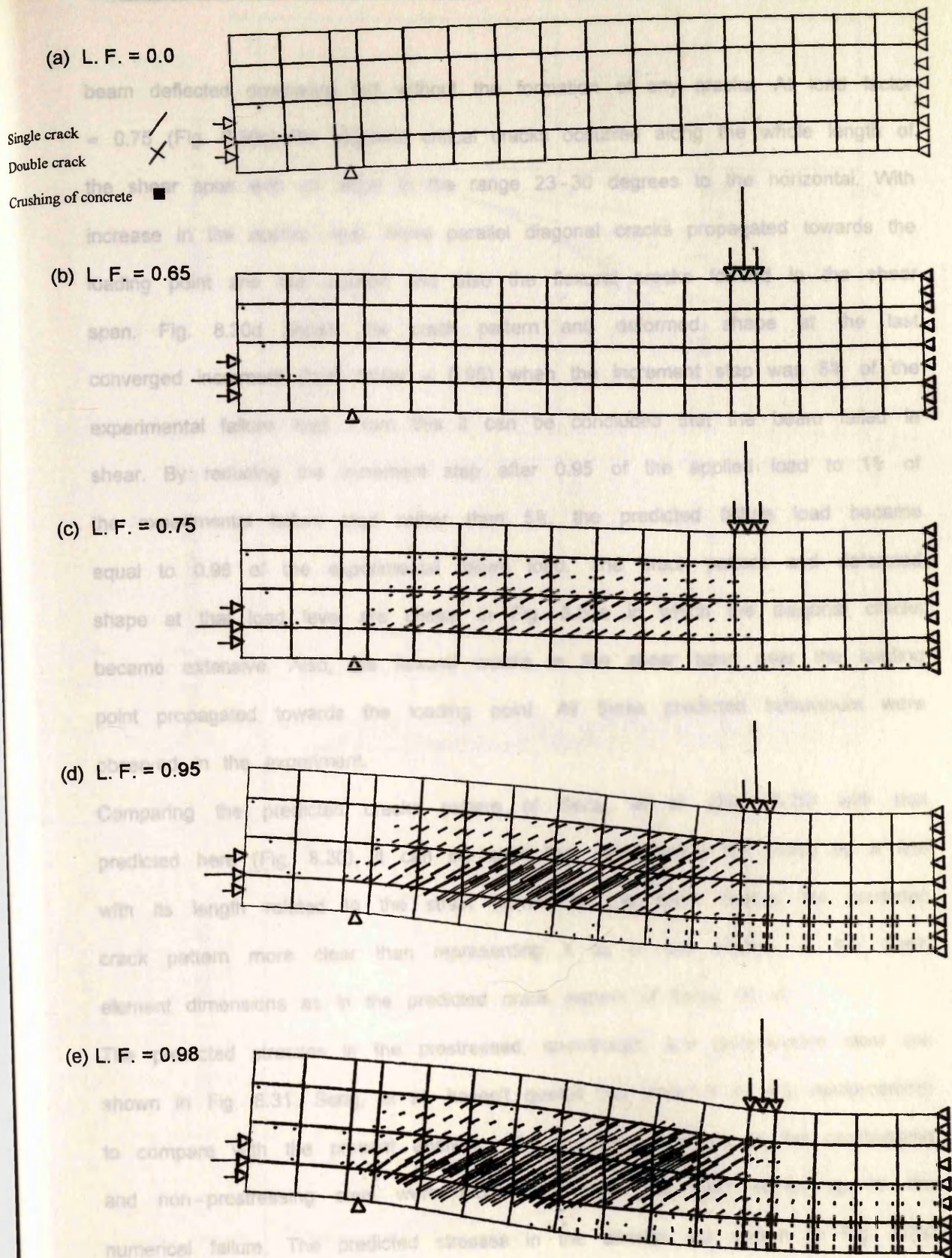


Fig. 8.30 Crack patterns and deformed shapes of beam CW12 (displacements magnified x 20)

beam deflected downward but without the formation of any cracks. At load factor = 0.75 (Fig. 8.30c) the diagonal critical cracks occurred along the whole length of the shear span with an angle in the range 23-30 degrees to the horizontal. With increase in the applied load, these parallel diagonal cracks propagated towards the loading point and the support and also the flexural cracks formed in the shear span. Fig. 8.30d shows the crack pattern and deformed shape at the last converged increment (load factor = 0.95) when the increment step was 5% of the experimental failure load. From this it can be concluded that the beam failed in shear. By reducing the increment step after 0.95 of the applied load to 1% of the experimental failure load rather than 5%, the predicted failure load became equal to 0.98 of the experimental failure load. The crack pattern and deformed shape at that load level are shown in Fig. 8.30e in which the diagonal cracks became extensive. Also, the flexural cracks in the shear span near the loading point propagated towards the loading point. All these predicted behaviours were observed in the experiment.

Comparing the predicted cracks pattern of Seraj, et al. (Fig. 8.29) with that predicted here (Fig. 8.30), it can be seen that representing the crack by a line with its length related to the strain normal to the crack makes the predicted crack pattern more clear than representing it by a line related to the mesh element dimensions as in the predicted crack pattern of Seraj, et al.

The predicted stresses in the prestressed, unstressed, and compression steel are shown in Fig. 8.31. Seraj, et al. haven't quoted the stresses in any reinforcement to compare with the present analysis. The predicted stresses in the prestressing and non-prestressing steel were much less than the yield stress up to the numerical failure. The predicted stresses in the stirrups are shown in Fig. 8.32. The stirrups started to sustain load after the formation of diagonal crack and started to yield before the numerical failure. The numerical failure occurred due to the compressive stress of concrete in the compression zone under the applied load equal to f_c' . This can be seen in Fig. 8.33 which shows the stress-strain

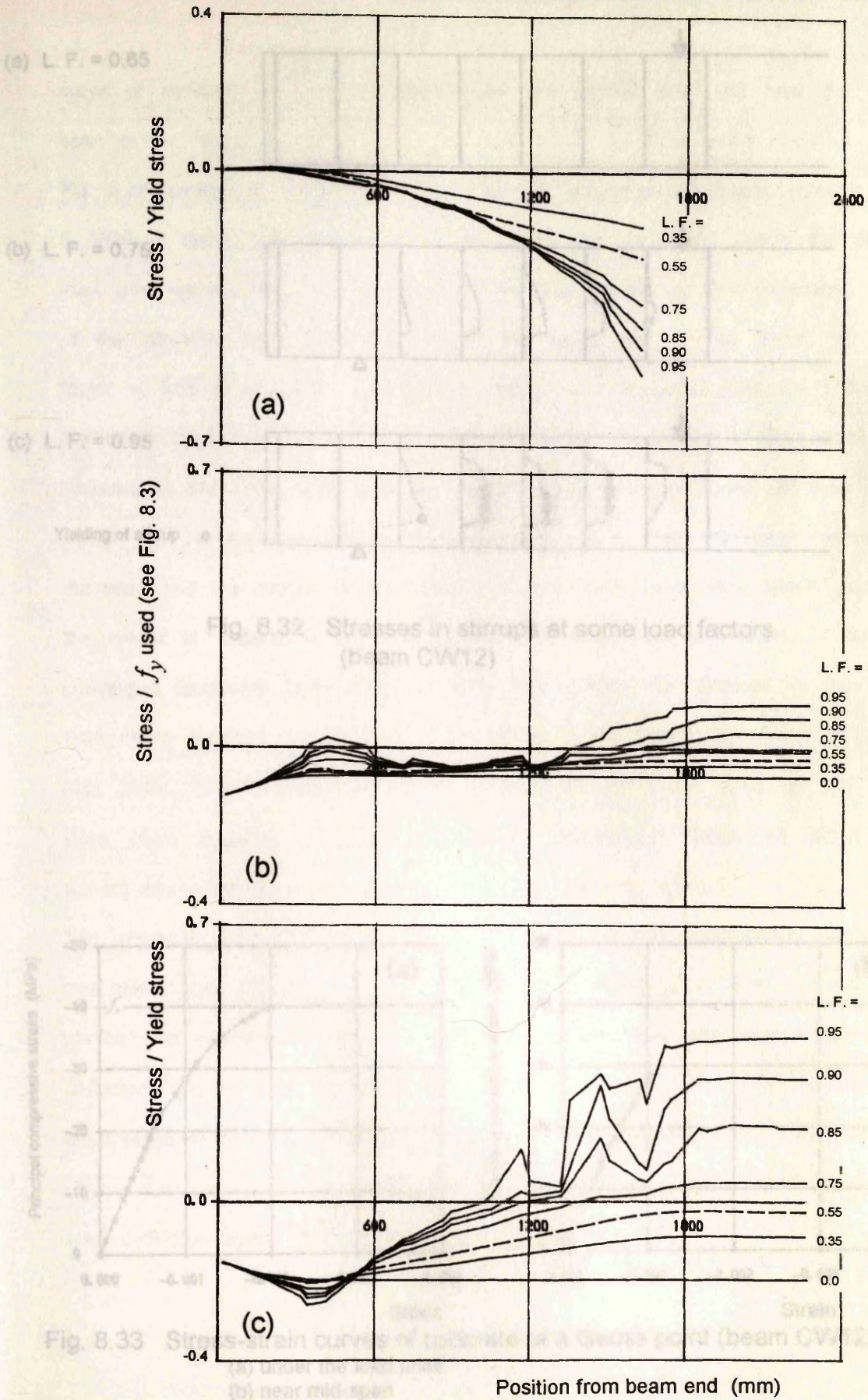


Fig. 8.31 Stresses in reinforcement at different load factors (beam CW12)
 (a) Compression steel (b) Prestressed steel (c) Unstressed steel

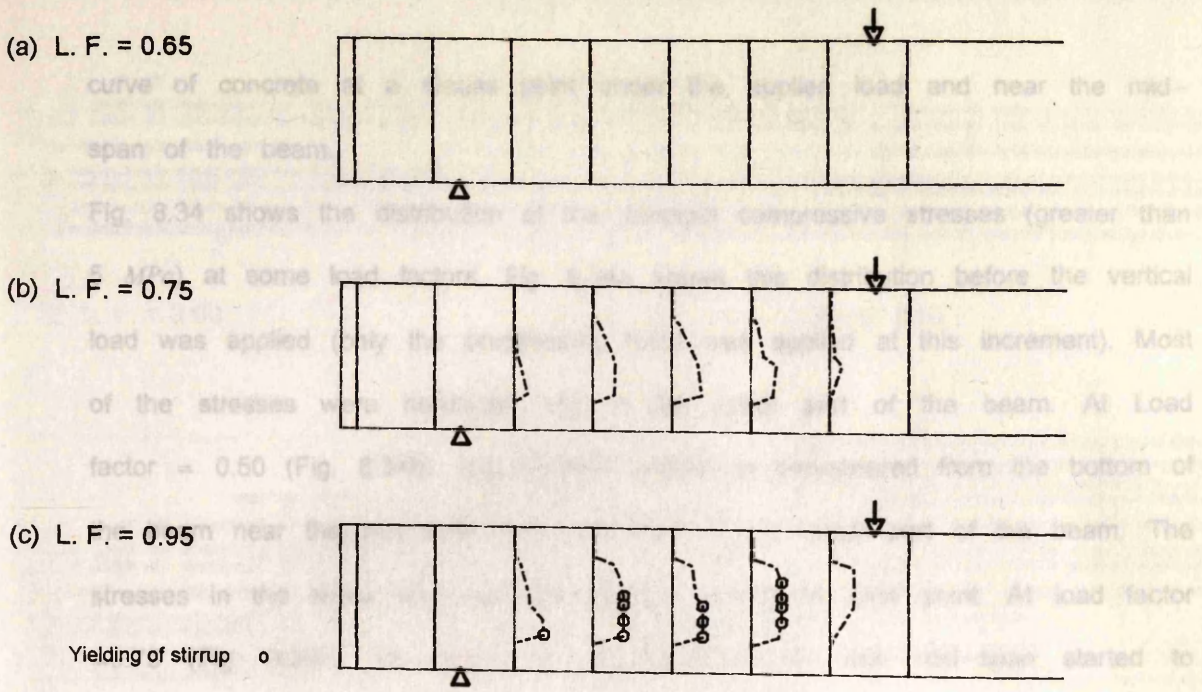


Fig. 8.32 Stresses in stirrups at some load factors (beam CW12)

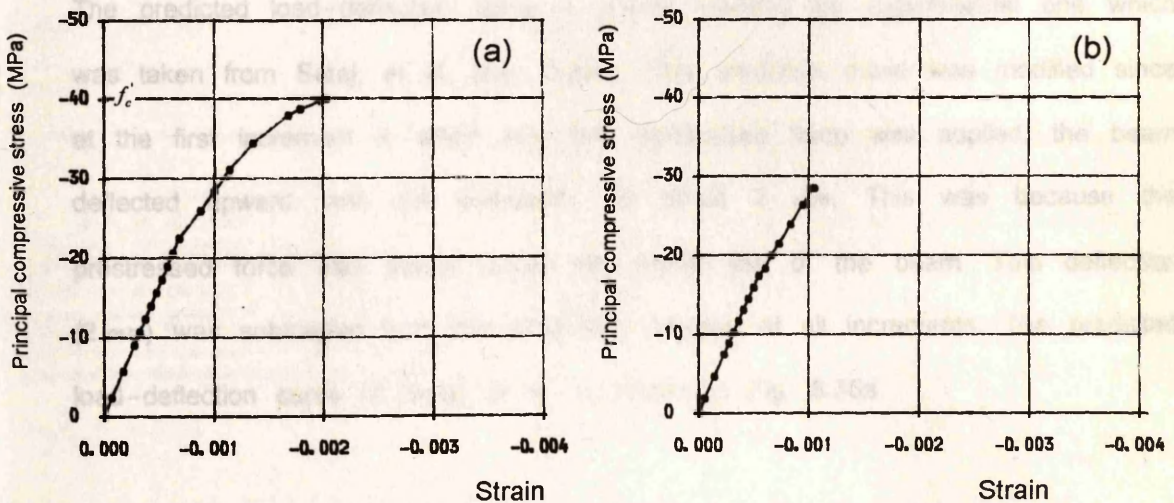


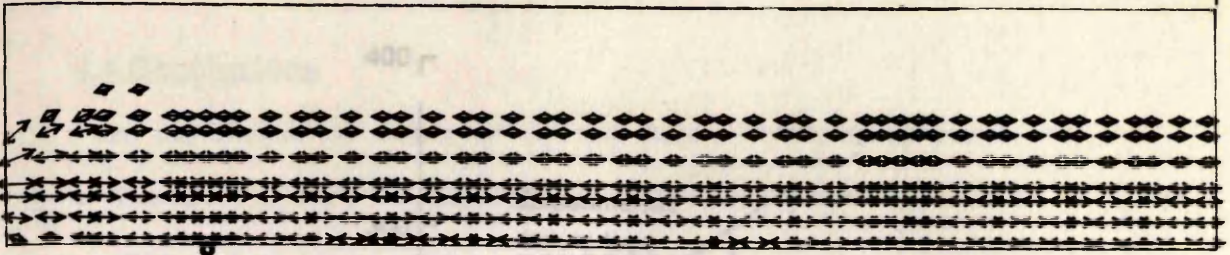
Fig. 8.33 Stress-strain curves of concrete at a Gauss point (beam CW12)
 (a) under the load point
 (b) near mid-span

curve of concrete at a Gauss point under the applied load and near the mid-span of the beam.

Fig. 8.34 shows the distribution of the principal compressive stresses (greater than 5 MPa) at some load factors. Fig. 8.34a shows this distribution before the vertical load was applied (only the prestressing force was applied at this increment). Most of the stresses were horizontal and in the lower part of the beam. At Load factor = 0.50 (Fig. 8.34b), the stresses started to disappear from the bottom of the beam near the mid-span and developed in the upper part of the beam. The stresses in the shear area became inclined toward the load point. At load factor = 0.75 (Fig. 8.34c), the depth of compression zone near mid-span started to decrease and the values of the stresses in the shear area were nearly equal to the values of stresses in the compression zone under the load point. At the last converged increment (load factor = 0.95, Fig. 8.34d), the stresses in the shear area nearly reached the value of f_c' as those in the compression zone under the load point. The principal compressive stresses in the shear area of this beam were more uniformly distributed than those stresses in beam A1 which was without shear reinforcement (compare Fig. 8.7 with Fig. 8.34).

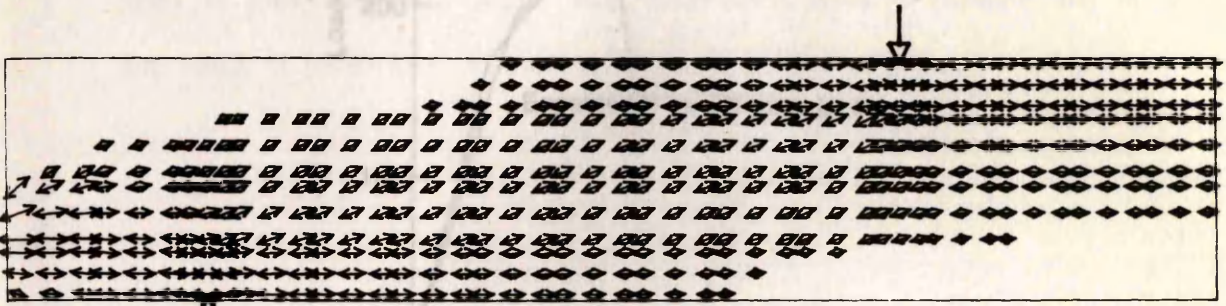
The predicted load-deflection curve is plotted against the experimental one which was taken from Seraj, et al. (Fig. 8.35b). This predicted curve was modified since at the first increment in which only the prestressed force was applied, the beam deflected upward, and not downward, by about 2 mm. This was because the prestressed force was placed under the centre line of the beam. This deflection (2 mm) was subtracted from the deflection obtained at all increments. The predicted load-deflection curve of Seraj, et al. is shown in Fig. 8.35a.

Fig. 8.34 Principal compressive stress distribution in beam CW12



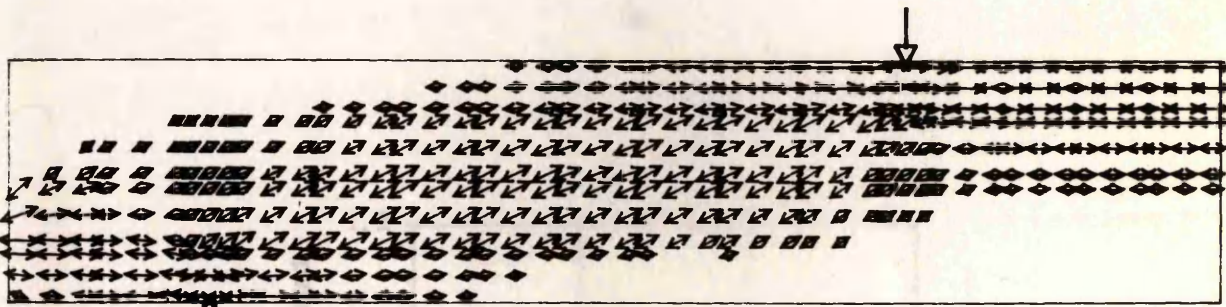
(a) L. F. = 0.00

Scale (Max.) : — = 20.826 MPa



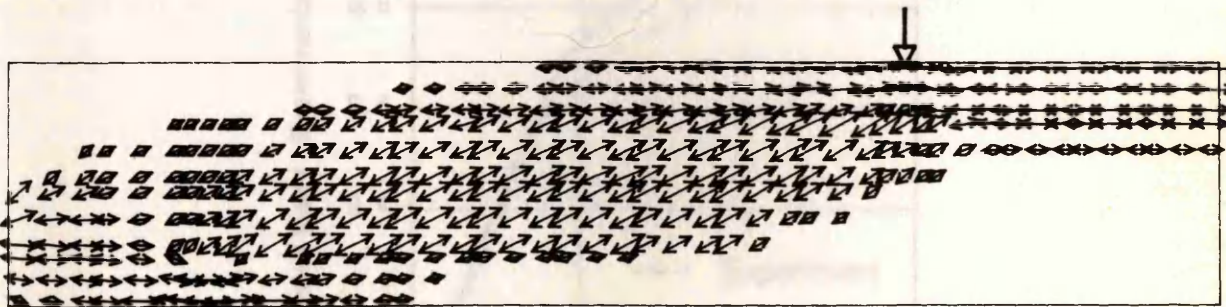
(b) L. F. = 0.50

Scale (Max.) : — = 21.074 MPa



(c) L. F. = 0.75

Scale (Max.) : — = 25.983 MPa



(d) L. F. = 0.95

Scale (Max.) : — = 37.179 MPa

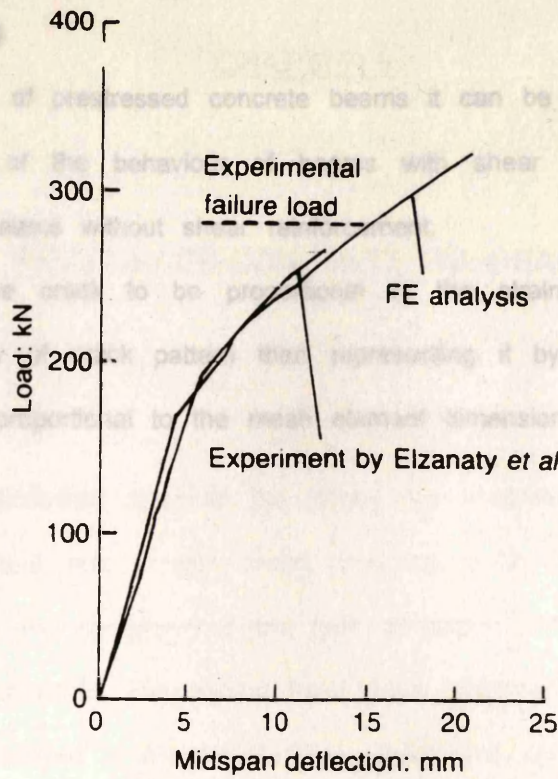
Fig. 8.34 Principal compressive stress distribution in beam CW12 (stresses greater than 5 MPa)

Fig. 8.35 Load-deflection curves for beam CW12

8.4 Conclusions

From the analysis of prestressed concrete beams it can be concluded that:

- The prediction of the behavior of beams with shear reinforcement is better than that of beams without shear reinforcement.
- Representing the crack pattern by a constant line or a line which is perpendicular to the mean diameter dimensions leads to clearly better results than representing it by a constant line or a line which is perpendicular to the mean diameter dimensions.



(a)

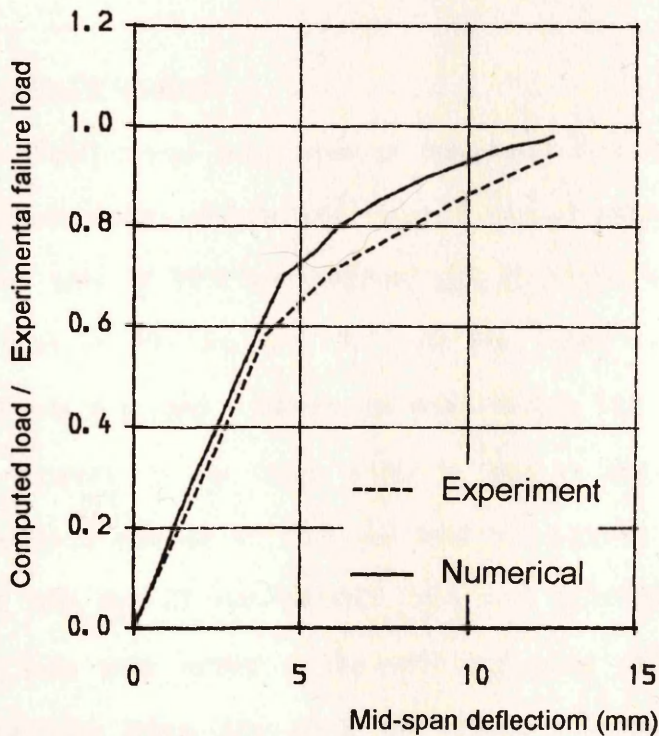


Fig. 8.35 Load-deflection curves for beam CW12
 (a) Model of Seraj, et al. (1992)
 (b) Present model

8.4 Conclusions

From the analysis of prestressed concrete beams it can be concluded that:

- The prediction of the behaviour of beams with shear reinforcement is better than that of beams without shear reinforcement.
- Representing the crack to be proportional to the strain normal to the crack leads to clarity of crack pattern than representing it by a constant line or a line which is proportional to the mesh element dimensions.

In Chapter 5, a reinforced concrete Tee-beam was analysed using 3-D and 2-D finite element models and it was found that the 2-D finite element model is sufficient to predict the behaviour of the type of beams. In this chapter, more than twenty reinforced concrete Tee-beams have been analysed using the 2-D finite element model developed in chapter 5. These reinforced concrete Tee beams were with and without shear reinforcement having λ ratio varying from 3.3 to 10.4. The beams without shear reinforcement were studied by Kotsyvos, et al. (1987), whereas the beams with shear reinforcement were studied by Tazari (1995).

9.2 Kotsyvos, et al's beams

Kotsyvos, et al. (1987) tested three types of reinforced concrete Tee beams. The beams were without shear reinforcement. Two of the beams were 6000 mm long with a shear span of 2500 mm and the other beam was 3000 mm long with a shear span of 800 mm. All the beams had the same Tee cross-section at mid span and a rectangular cross-section 400 mm wide and 350 mm high after the supports to the ends. The length of the rectangular section extended to a distance of 400 mm from the supports. The beams were under-reinforced with two 20 mm diameter high strength steel bars ($f_y = 540$ MPa). The bars were welded at the ends and the ends were used after the supports to prevent splitting along the longitudinal direction of the steel bars and concrete.

CHAPTER 9

REINFORCED CONCRETE TEE-BEAMS

9.1 Introduction

In Chapter 5, a reinforced concrete Tee-beam was analysed using 3-D and 2-D finite element models and it was found that the 2-D finite element model is sufficient to predict the behaviour of this type of beam. In this chapter, more than twenty reinforced concrete Tee-beams have been analysed using the 2-D finite element model developed in chapter 6. These reinforced concrete Tee beams were with and without shear reinforcement having a/d ratio varying from 3.3 to 10.4. The beams without shear reinforcement were tested by Kotsovos, et al. (1987), whereas the beams with shear reinforcement were tested by Taylor (1966).

9.2 Kotsovos. et al's beams

Kotsovos, et al. (1987) tested three types of reinforced concrete Tee beams. The beams were without shear reinforcement. Type I and II beams were 6600 mm long with a shear span of 2500 mm, whereas type III beams were 3200 mm long with a shear span of 800 mm (Fig. 9.1). All the beams had the same Tee cross-section at mid span and a rectangular cross-section 200 mm wide x 290 mm high after the supports to the beam ends. In type II beams the rectangular section extended to a distance of 1000 mm from the supports. The beams were under-reinforced with two 20 mm diameter high yield deformed steel bars ($f_y = 540$ MPa). The bars were welded at the ends onto steel plate to eliminate the possibility of anchorage failure. Also six 8 mm diameter mild steel links were used after the supports to prevent splitting along the interface between the steel bars and concrete.

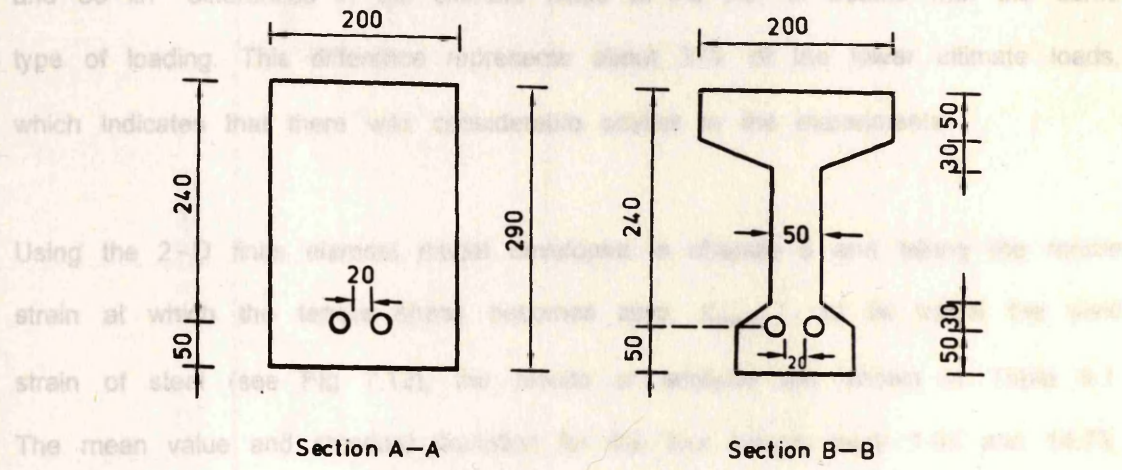
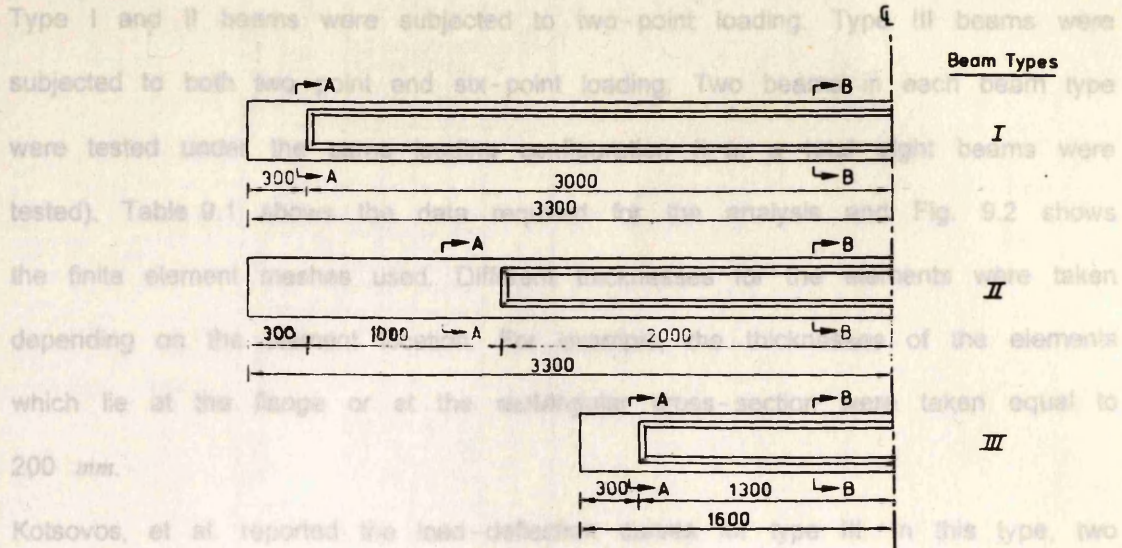


Fig. 9.1 Types of beams tested by Kotsovos, et al. (1987)
(all dimensions in mm)

Type I and II beams were subjected to two-point loading. Type III beams were subjected to both two-point and six-point loading. Two beams in each beam type were tested under the same loading configuration (i. e. a total eight beams were tested). Table 9.1 shows the data required for the analysis and Fig. 9.2 shows the finite element meshes used. Different thicknesses for the elements were taken depending on the element location. For example, the thicknesses of the elements which lie at the flange or at the rectangular cross-section were taken equal to 200 mm.

Kotsovos, et al. reported the load-deflection curves for type III. In this type, two beams were tested under two-point loading and two beams were tested under six-point loading. In this reported load-deflection curves, there was about 16 kN and 30 kN differences in the ultimate loads of the pair of beams with the same type of loading. This difference represents about 27% of the lower ultimate loads, which indicates that there was considerable scatter in the experiments.

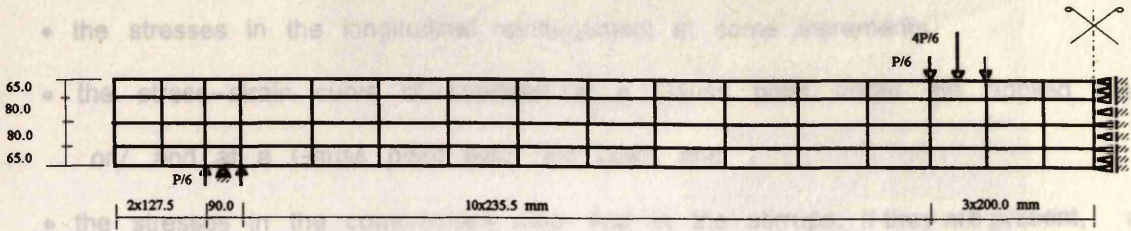
Using the 2-D finite element model developed in chapter 6 and taking the tensile strain at which the tensile stress becomes zero, ϵ_{tmax} , to be equal the yield strain of steel (see Fig. 7.12), the results of analysis are shown in Table 9.1. The mean value and standard deviation for the four beams were 1.05 and 14.7%, respectively. The worst prediction was for beam type II, the predicted to the experimental failure load was 1.25. Despite this it was noticed that at a load level a little greater than the ultimate load (load factor = 1.05), a large deflection was observed and also the number of iterations required for convergence in this increment was about 45 iterations (at other increments the number of iterations required was in the range of 1-8 iterations), which means that a large number of cracks occurred at that level.

To predict the mode of failure of beams, the following points will be looked at in greater detail:

Table 9.1 Data and results of Kotsovos, et al's beams

No.	Beam	a/d	Load type	f_{cu} MPa	f'_c MPa	Main steel	f_y MPa	Mode of failure	Ultimate Shear (kN)	Predicted/ Experimental ultimate shear
1	I	10.4	Two-point	44.1	40.4	2Y20	540	Shear	19.0	1.00
2	II	10.4	Two-point	44.1	40.4	2Y20	540	Shear	22.0	1.25
3	III2	3.3	Two-point	44.1	40.4	2Y20	540	Shear	37.0	1.05
4	III6	3.3	Six-point	44.1	40.4	2Y20	540	Shear	63.3	0.90
Mean value										
Standard deviation										
									1.05	14.7%

- the crack pattern and deformed shape of the beam,
- the stresses in the longitudinal reinforcement at some increments.

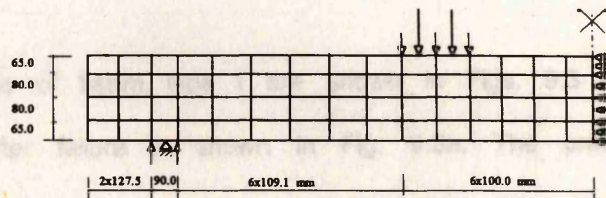


(a) Types I and II

are presented.

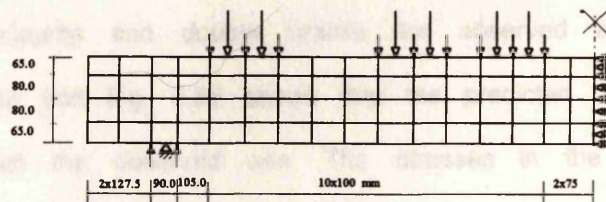
Beam KOD

The results of the analysis of beam KOD are shown in Fig. 9.2b. The observed crack pattern and deformed shape at the last converged increment (load factor = 1.00) are shown in Fig. 9.2b. Fig. 9.2c shows the deformed shape at increment 18 (load factor = 1.05) at which the convergence has not been achieved, both the crack pattern and deformed shape are drawn in Fig. 9.2d. It is clear from this figure that the beam failed in shear. Large vertical displacements are shown in the elements which lie in the shear span above the middle of the beam and a combination of nearly horizontal and vertical cracks are observed in this region. Comparing Fig. 9.2d with the crack pattern observed in the longitudinal reinforcement (Fig. 9.2e) suggests that the beam failed in shear, since the



(b) Type III2

here haven't yielded up to the maximum design load. The three curves shown in Fig. 9.4 are for the three test beams 0.9, 1.0, and 1.05. Fig. 9.5 shows the stress-strain curves of concrete at a Gauss point under the applied load (Fig. 9.5a) and at a Gauss point near the support (Fig. 9.5b). It is clear from these curves that the stress of concrete has not reached the value of f_{cu} at the time of failure. All these signs indicate that the beam failed in shear.



(c) Type III6

Fig. 9.2 Finite element meshes for Kotsovos, et al's beams.

(a) Observed

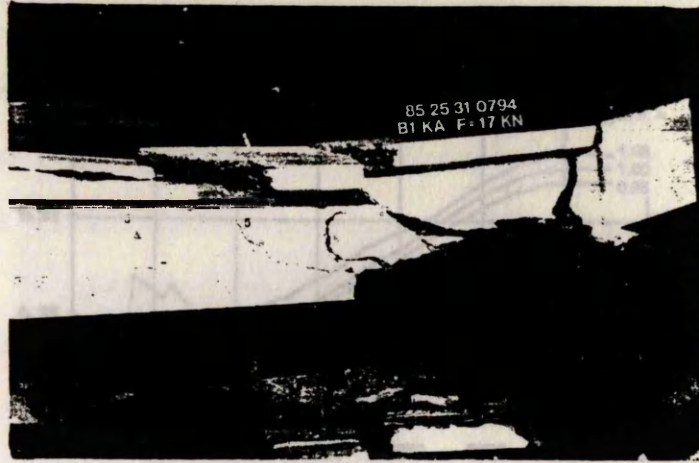
- the crack pattern and deflection shape of the beam,
- the stresses in the longitudinal reinforcement at some increments.
- the stress-strain curve of concrete at a Gauss point under the applied load or/ and at a Gauss point near mid span, and
- the stresses in the compression steel and in the stirrups, if they are present, at some increments.

In the following, a brief summary of the predicted behaviours of the four beams are presented.

Beam KOTI

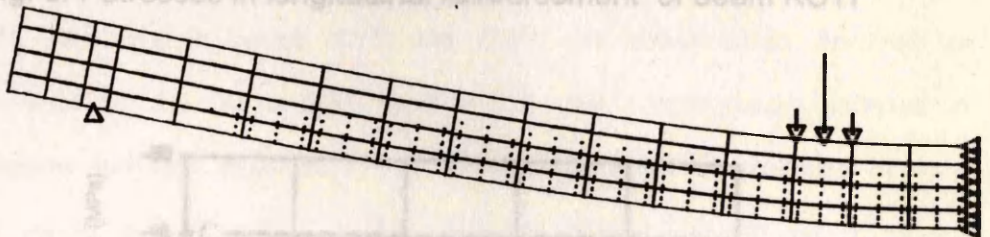
The results of the analysis of beam type I are shown in Figs. 9.3 to 9.6. The observed crack pattern after failure is shown in Fig. 9.3a. The predicted crack pattern and deformed shape at the last converged increment (load factor = 1.00) are shown in Fig. 9.3b. Fig. 9.3c shows the deformed shape at increment 18 (load factor = 1.05) at which the convergence has not been achieved, both the crack pattern and deformed shape are drawn in Fig. 9.3d. It is clear from this figure that the beam failed in shear. Large vertical displacements are shown in the elements which lie in the shear span above the middle of the beam and a combination of nearly horizontal and double cracks are observed also in this region. Comparing Fig. 9.3a and Fig. 9.3d shows that the predicted crack pattern is in good agreement with the observed one. The stresses in the longitudinal reinforcement (Fig. 9.4) supports the fact that the beam failed in shear, since the bars haven't yielded up to the numerical failure load. The three curves drawn in Fig. 9.4 are for the three load factors 0.95, 1.00, and 1.05. Fig. 9.5 shows the stress-strain curves of concrete at a Gauss point under the applied load (Fig. 9.5a) and at a Gauss point near the mid span (Fig. 9.5b). These curves show that The stress of concrete has not reached the value of f_c' up to the numerical failure. All these signs indicate that the beam failed in shear.

(a) Observed

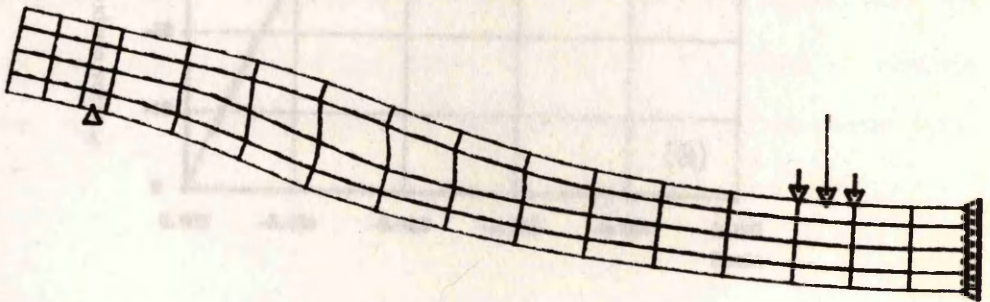


Position from beam end (mm)

(b) L. F. = 1.00



(c) L. F. = 1.05



(d) L. F. = 1.05

- Single crack /
- Double crack X
- Crushing of concrete ■

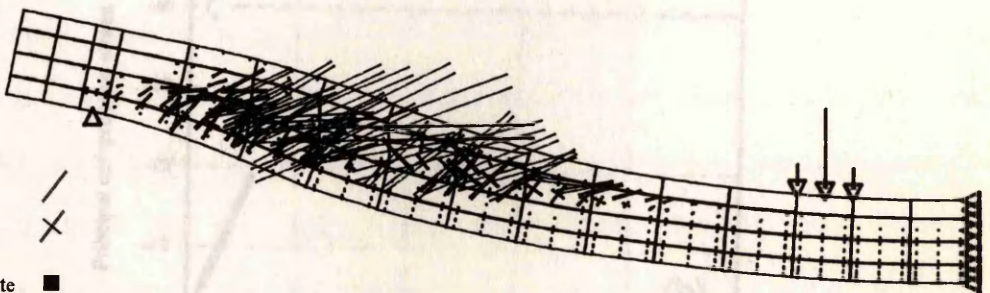


Fig. 9.3 Crack patterns and deformed shapes of beam KOTI (displacements magnified x 10)

Fig. 9.5 Stress-strain curves of concrete at a Gauss point (beam KOTI) (a) near mid-span (b) within the load points

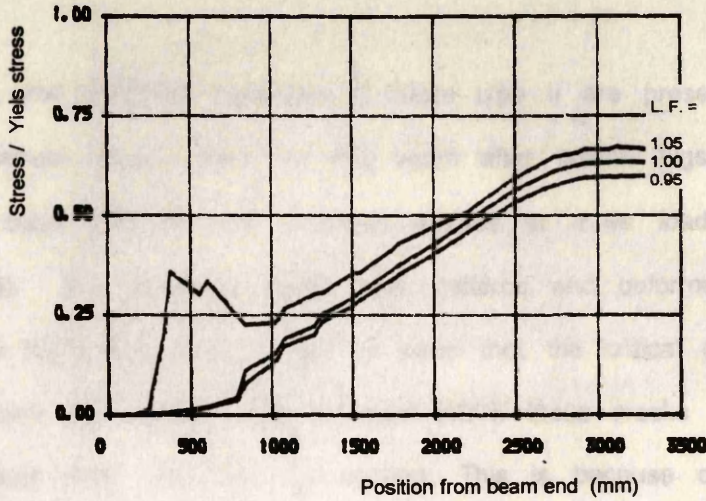


Fig. 9.4 Stresses in longitudinal reinforcement of beam KOTI

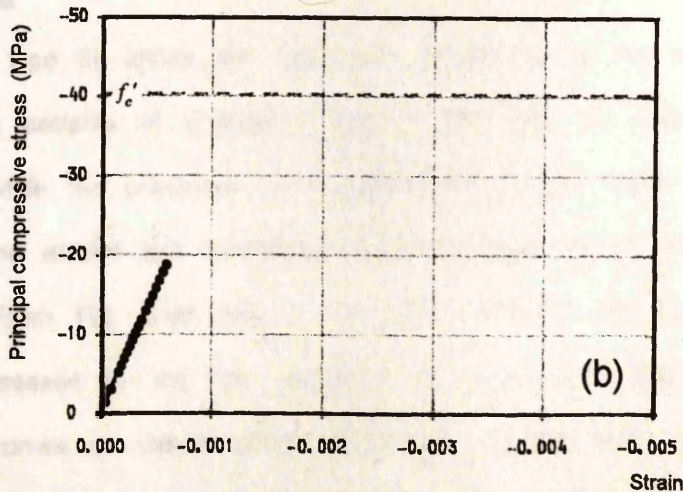
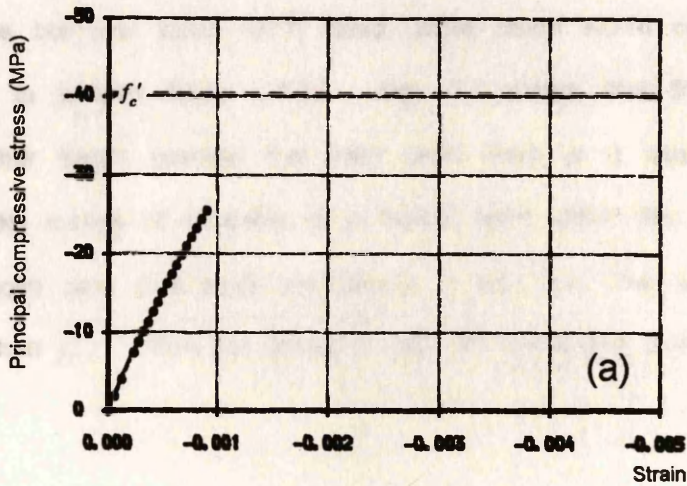


Fig. 9.5 Stress-strain curves of concrete at a Gauss point (beam KOTI)
 (a) near mid-span (b) under the load point

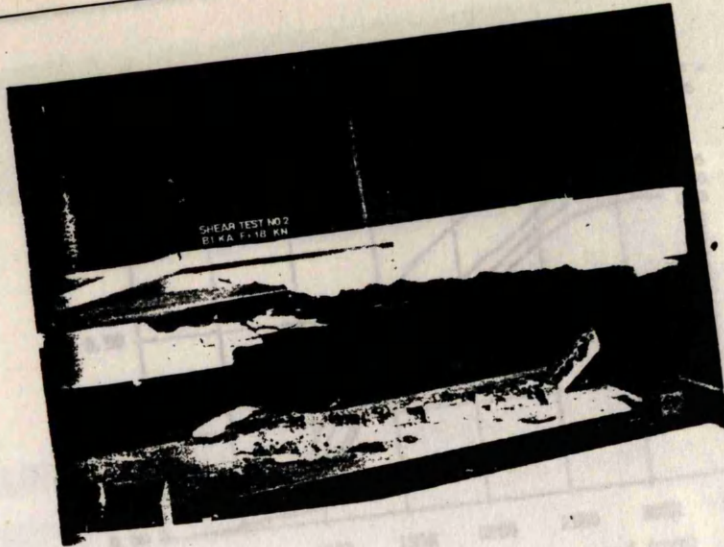
Beam KOTII

In Figs. 9.6-8, the predicted behaviours of beam type II are presented. Fig. 9.6a shows the observed crack pattern for this beam after failure. Figs. 9.6b-d show the predicted crack patterns and deformed shapes at three load factors (1.00, 1.05, and 1.25). By comparing these crack patterns and deformed shapes with those of beam KOTI (Fig. 9.3), it can be seen that the critical cracks in beam KOTI started from the support while in beam KOTII these cracks started from a distance of about 1000 mm from the support. This is because over this length the cross section of beam KOTII is rectangular (see Fig. 9.1) and not Tee as in beam KOTI. Also in both beams KOTI and KOTII, no critical cracks occurred up to a load factor = 1.0. At a load factor = 1.05, the critical cracks occurred in both the beams but only beam KOTI failed, while beam KOTII continued to carry more load up to a load factor = 1.25. Fig. 9.7 shows that the stress at any point on the bar hasn't reached the yield point even at a load factor of 1.25. The stress-strain curves of concrete at a Gauss point under the applied load and at a Gauss point near mid span are shown in Fig. 9.8. The stress in concrete is much less than f_c' . From the above it can be concluded that the beam failed in shear.

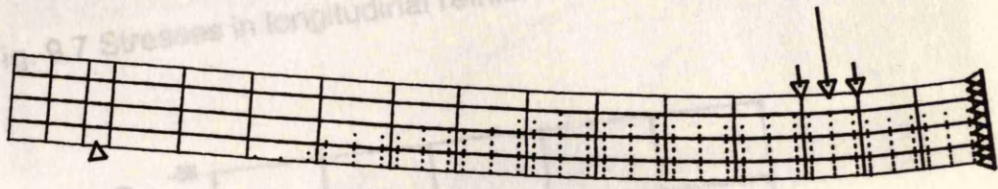
Beam KOTIII2

This beam is type III where the load was applied as a two-point loading. The observed crack patterns at a load of 24 kN and after the failure are shown in Fig. 9.9a-b, while the predicted crack patterns at a load factor = 0.65 (total load = 24.05 kN) and at the last converged increment (load factor = 1.05) are shown in Fig. 9.9c-d. From Fig. 9.9d only, it can be concluded that the beam failed in shear. The stresses in the bar support this conclusion (Fig. 9.10). Also the stress-strain curves at Gauss points under the applied load and near the mid span show that the stress in concrete is less than f_c' (Fig. 9.11).

(a) Observed



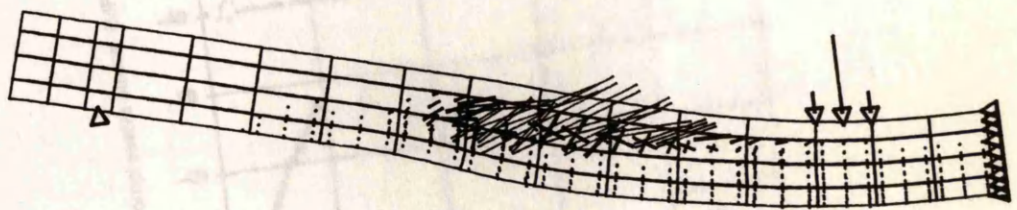
(b) L. F. = 1.00



(c) L. F. = 1.05



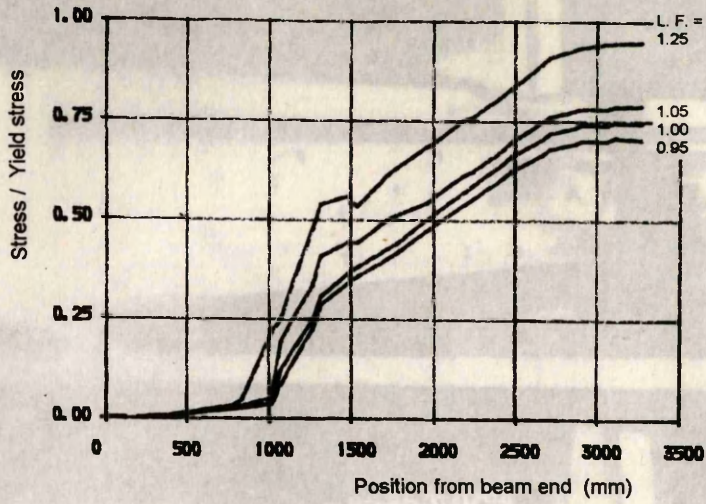
(d) L. F. = 1.25



Single crack /
Double crack X
Crushing of concrete ■

Fig. 9.6 Crack patterns and deformed shapes of beam KOTII (displacements magnified x 10)

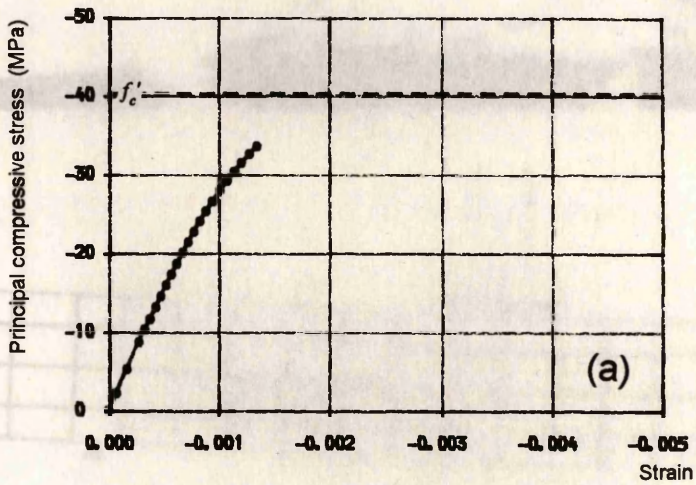
(a) Observed at 24 kN



(b) Observed at failure

Fig. 9.7 Stresses in longitudinal reinforcement of beam KOTII

(c) L.F. = 0.65



(d) L.F. = 1.05

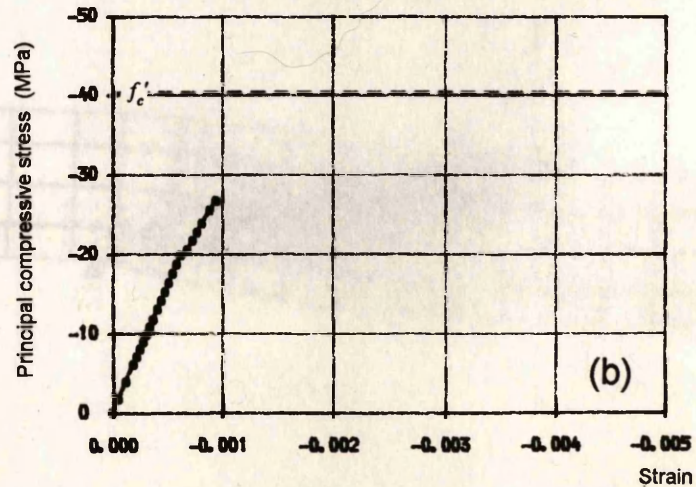


Fig. 9.8 Stress-strain curves of concrete at a Gauss point (beam KOTII)
 (a) near mid-span (b) under the load point

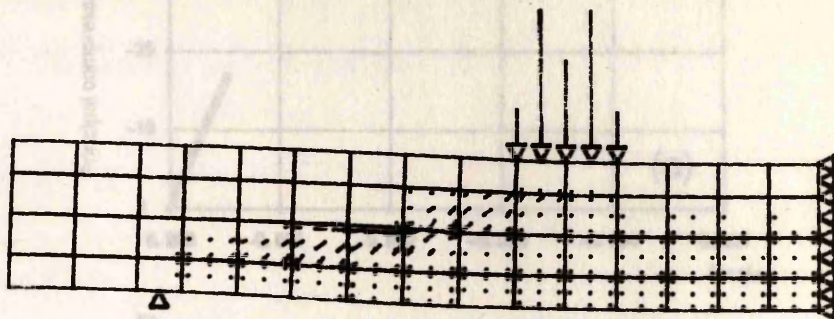
(a) Observed at 24 kN



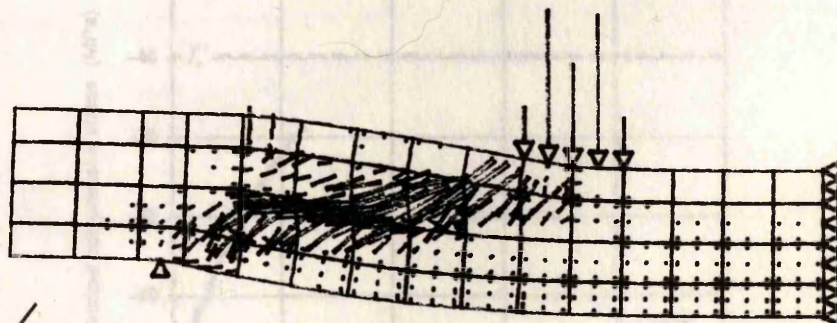
(b) Observed at failure



(c) L. F. = 0.65



(d) L. F. = 1.05



Single crack /

Double crack X

Crushing of concrete ■

Fig. 9.9 Crack patterns and deformed shapes of beam KOTIII2 (displacements magnified x 10)

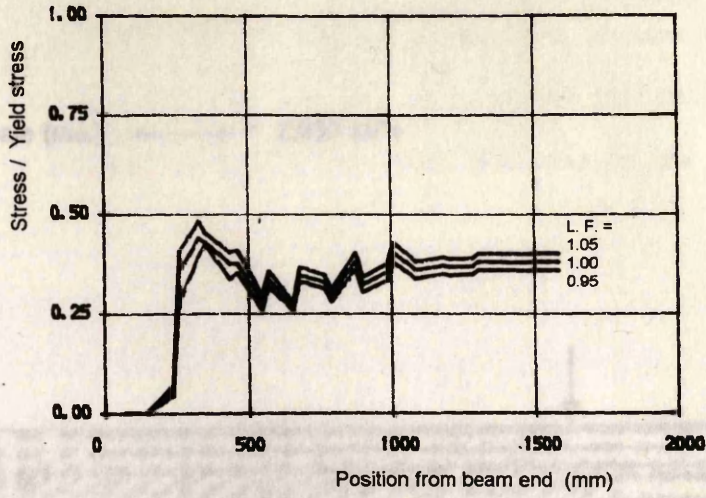


Fig. 9.10 Stresses in longitudinal reinforcement of beam KOTIII2

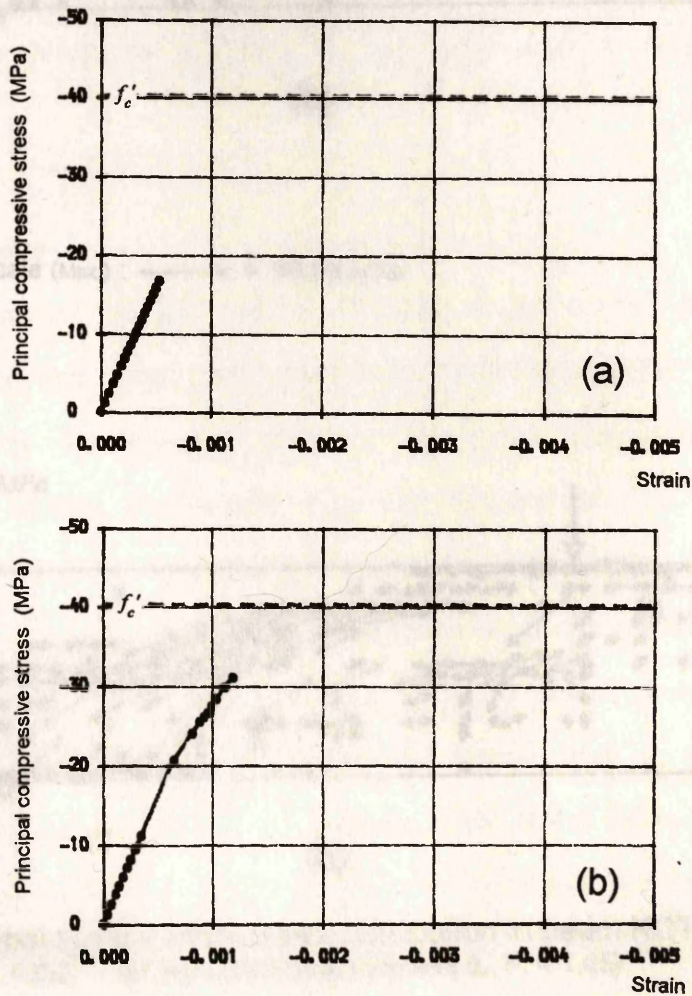
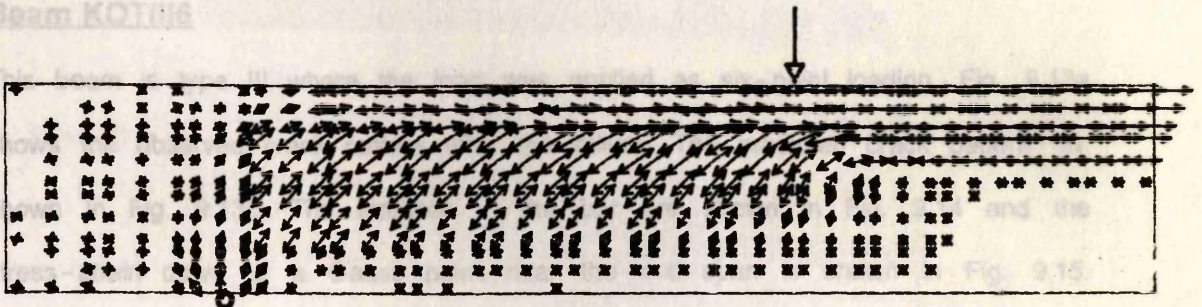


Fig. 9.11 Stress-strain curves of concrete at a Gauss point (beam KOTIII2) (a) near mid-span (b) under the load point

Fig. 9.12 shows the distribution of the principal compressive stresses at two load factors (0.2 and 1.05). From this figure it can be seen that the cause of failure was the crushing of concrete in web in the shear area due to the compressive stress exceeding f_c' .

Scale (Max.) : \longleftrightarrow = 2.553 MPa

Beam KOTIII2



(a)

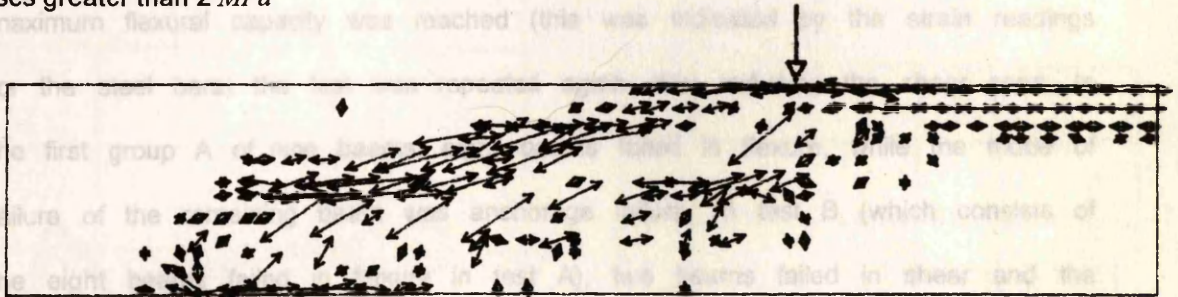
From these figures, it can be concluded that the beam failed in shear.

9.3 Taylor's beams

Scale (Max.) : \longleftrightarrow = 40.00 MPa

Taylor (1968) performed, on nine beams, 23 tests. All the beams were 3858 mm long. Some beams were tested only once, while some were tested two or three times depending on the mode of failure of the beam. Beams for which the maximum flexural capacity was reached (this was indicated by the strain readings

Stresses greater than 2 MPa



(b)

Fig. 9.12 Principal compressive stress distribution in beam KOTIII2 at (a) L. F. = 0.2 (b) last converged increment (L. F. = 1.05)

load was applied at mid-span in Tests B and C. Two point loads were applied. All the beams had the same cross-section. The difference was in the reinforcement ratio, type of steel and spacing of stirrups (Fig. 9.17).

(a) Observed

Fig. 9.12 shows the distribution of the principal compressive stresses at two load factors (0.2 and 1.05). From this figure it can be seen that the cause of failure was the crushing of concrete in web in the shear area due to the compressive stress exceeding f_c' .

Beam KOTIII6

This beam is type III where the load was applied as six-point loading. Fig. 9.13a shows the observed crack pattern after the failure. The predicted crack pattern is shown in Fig. 9.13b. The stresses in the bar are shown in Fig. 9.14 and the stress-strain curve at a Gauss point near the mid-span is shown in Fig. 9.15. From these figures, it can be concluded that the beam failed in shear.

Fig. 9.13 Crack patterns and deformed shapes of beam KOTIII6
displacements magnified $\times 10$

9.3 Taylor's beams

Taylor (1966) performed, on nine beams, 23 tests. All the beams were 3658 mm long. Some beams were tested only once, while some were tested two or three times depending on the mode of failure of the beam. Beams for which the maximum flexural capacity was reached (this was indicated by the strain readings for the steel bars) the test was repeated again after reducing the shear span. In the first group A of nine beams, eight beams failed in flexure, while the mode of failure of the remaining beam was anchorage failure. In test B (which consists of the eight beams failed in flexure in test A), two beams failed in shear and the others failed in flexure. In test C (six beams), three beams failed in shear and three failed in flexure. Thus a total 23 tests were performed. The shear spans of the three tests were 1600, 1143, 914 mm, respectively (Fig. 9.16). In Test A, the load was applied at mid-span. In Tests B and C, two point loads were applied. All the beams had the same cross-section. The difference was in the reinforcement ratio, type of steel, and spacing of stirrups (Fig. 9.17).

(a) Observed



(b) L. F. = 0.90

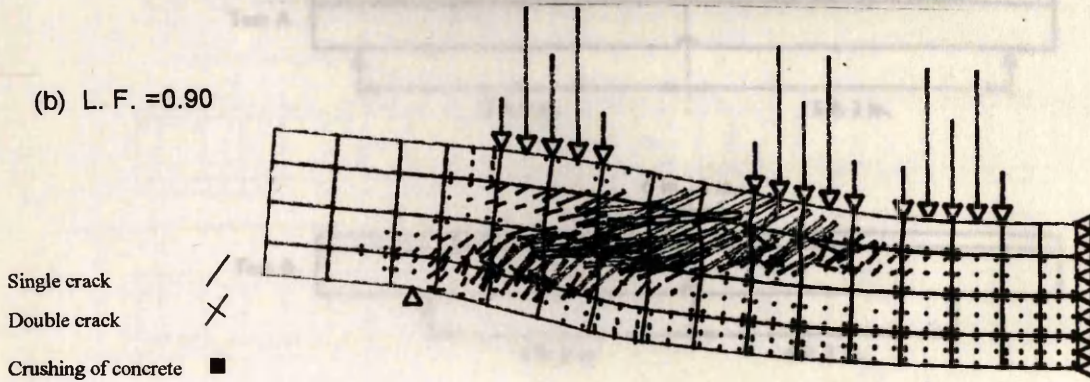


Fig. 9.13 Crack patterns and deformed shapes of beam KOTIII6 (displacements magnified x 10)

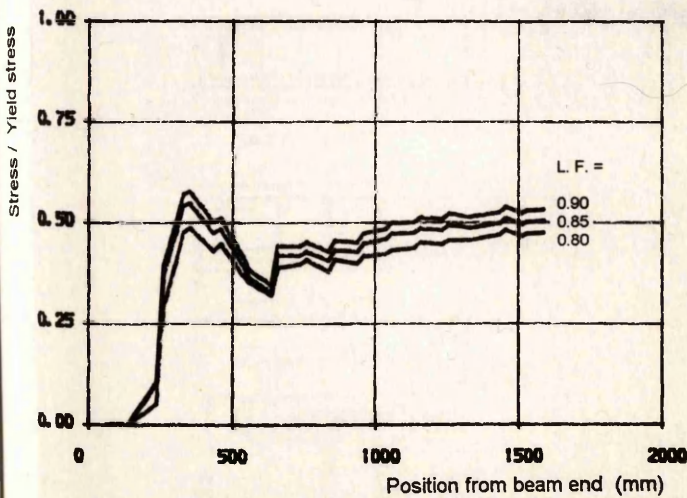


Fig. 9.14 Stresses in longitudinal reinforcement of beam KOTIII6

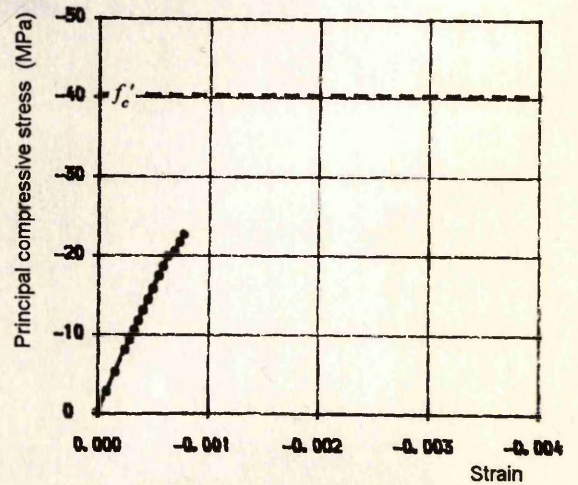


Fig. 9.15 Stress-strain curve of concrete at a Gauss point near mid-span (beam KOTIII6)

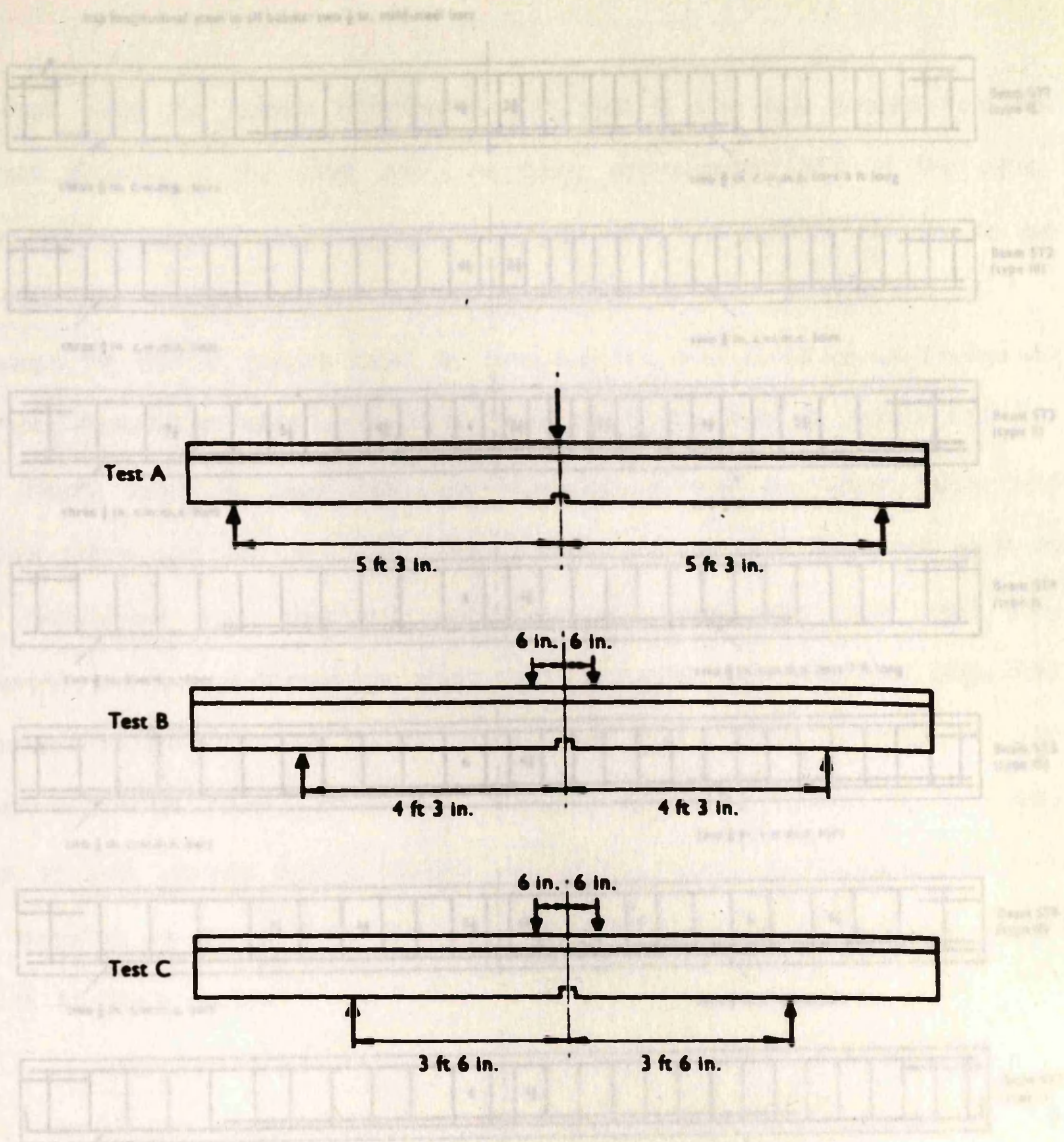


Fig. 9.16 Types of loading for Taylor's beams
(1 in. = 25.4 mm)

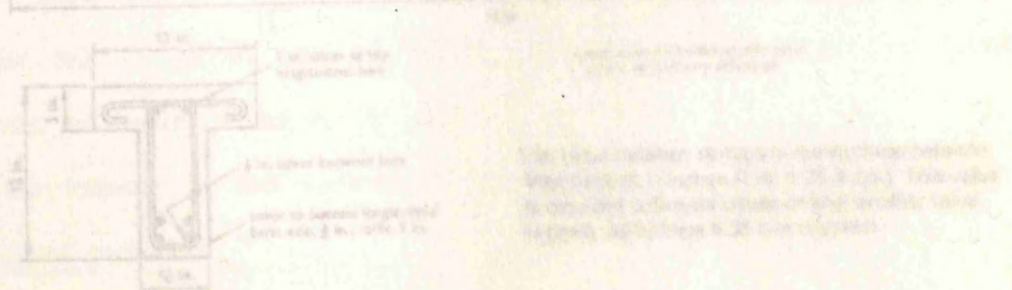


Fig. 9.17 Reinforcement details of Taylor's beams
(1 in. = 25.4 mm)

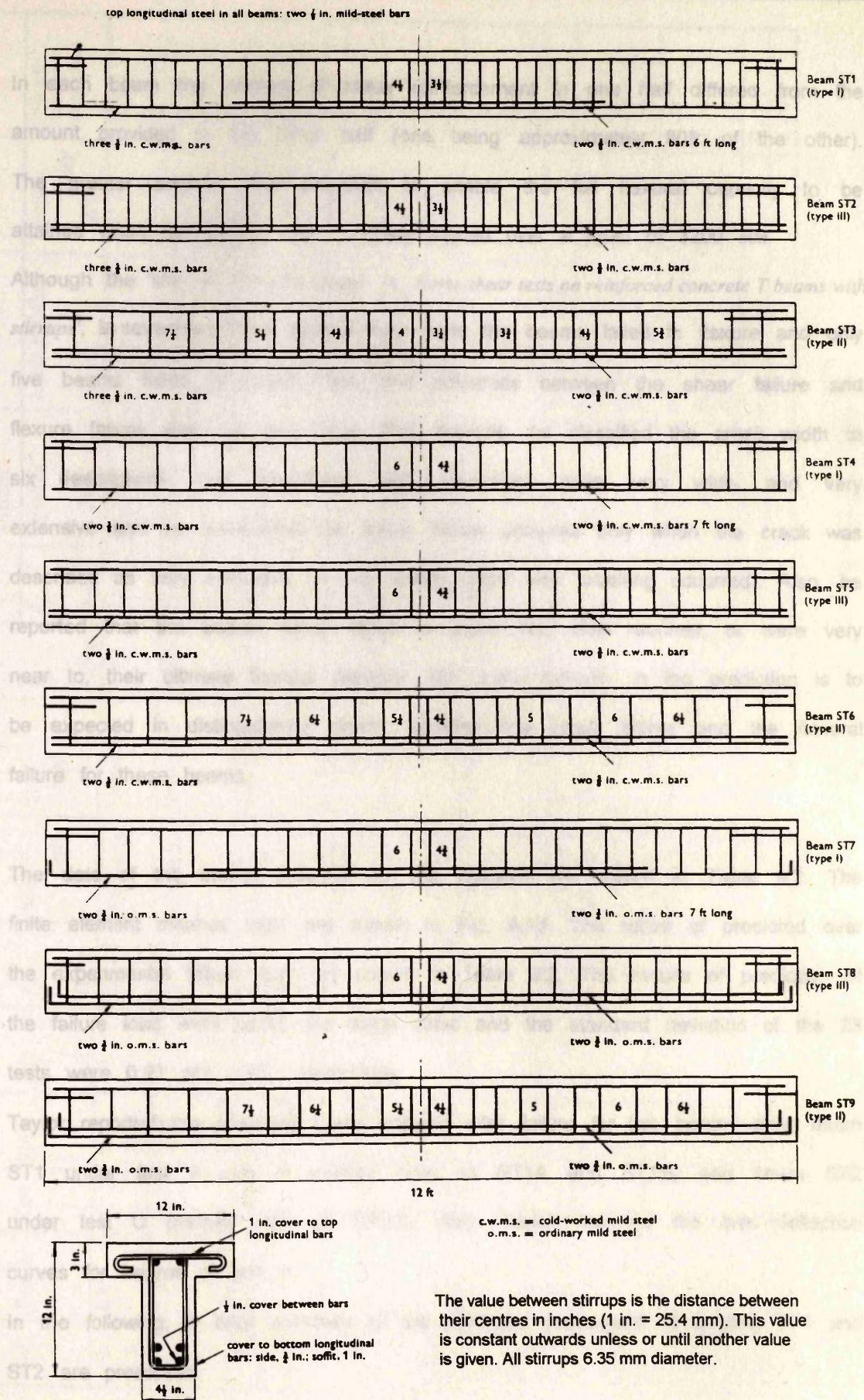


Fig. 9.17 Reinforcement details of Taylor's beams.
(1 in. = 25.4 mm)

In each beam the amount of shear reinforcement in one half differed from the amount provided in the other half (one being approximately 80% of the other). The greater amount was designed to enable the full flexural capacity to be attained when the beams were centrally loaded over a span of 3200 mm.

Although the title of Taylor's paper is '*Some shear tests on reinforced concrete T beams with stirrups*', in seventeen out of twenty-three tests the beams failed in flexure and only five beams failed in shear. Also, the difference between the shear failure and flexure failure was not very large. For example, he classified the crack width to six descriptions; fine, prominent, very prominent, wide, very wide, and very extensive and he considered the shear failure occurred only when the crack was described as very extensive (in one beam when web crushing occurred). Also, he reported that the beams which failed in shear had also reached, or were very near to, their ultimate flexural capacity. So, some difficulty in the prediction is to be expected in distinguishing clearly between the shear failure and the flexural failure for these beams.

The data of the beams required for the analysis are shown in Table 9.2. The finite element meshes used are shown in Fig. 9.18. The ratios of predicted over the experimental failure load are shown in Table 9.2. The results of prediction of the failure load were good, the mean value and the standard deviation of the 23 tests were 0.97 and 5.4%, respectively.

Taylor reported the observed crack patterns after failure for two beams only, beam ST1 under test A and B (named here as ST1A and ST1B) and beam ST2 under test C (named here as ST2C). Also, Taylor reported the load-deflection curves for beams of test A.

In the following, a brief summary of the predicted behaviours of beams ST1 and ST2 are presented.

Table 9.2 Data and results of Taylor's beams

No.	Beam	Test	a/d	f_{cu} (MPa)	f'_c (MPa)	Main steel	Steel type	f_y (MPa)	f_{yv} (MPa)	Stirrups		Mode of failure	Ultimate shear (kN)	Predicted/ Experimental ultimate shear
										Spacing (mm)				
1	ST1	A	6.2	25.9	20.2	5 ϕ 16mm	Deformed	442	290	114.3	FLEXURE	66.0	1.00	
2		B	4.4								SHEAR	89.2	0.90	
3	ST2	A	6.2	27.1	21.2	5 ϕ 16mm	Deformed	442	290	114.3	FLEXURE	68.5	0.95	
4		B	4.4								FLEXURE	93.9	0.90	
5		C	3.6								SHEAR	106.6	0.95	
6	ST3	A	6.2	27.1	21.2	5 ϕ 16mm	Deformed	442	290	101.6 - 190.5	FLEXURE	69.7	0.95	
7		B	4.4								FLEXURE	95.2	0.90	
8		C	3.6								SHEAR	105.6	0.90	
9	ST4	A	6.2	28.5	22.2	4 ϕ 16mm	Deformed	442	290	152.4	FLEXURE	53.3	1.00	
10		B	4.4								SHEAR	74.7	0.95	
11	ST5	A	6.2	28.5	22.2	4 ϕ 16mm	Deformed	442	290	152.4	FLEXURE	53.6	1.00	
12		B	4.4								FLEXURE	74.7	0.95	
13		C	3.6								FLEXURE	95.9	0.90	
14	ST6	A	6.2	23.3	18.2	4 ϕ 16mm	Deformed	442	290	139.7 - 190.5	FLEXURE	53.6	1.00	
15		B	4.4								FLEXURE	73.5	0.95	
16		C	3.6								SHEAR	86.7	0.95	
17	ST7	A	6.2	23.3	18.2	4 ϕ 19mm	Plain	278	290	152.4	ANCHORAGE	36.9	1.05	
18	ST8	A	6.2	25.9	20.2	4 ϕ 19mm	Plain	278	290	152.4	FLEXURE	47.6	1.05	
19		B	4.4								FLEXURE	66.0	1.00	
20		C	3.6								FLEXURE	81.5	1.00	
21	ST9	A	6.2	25.1	19.6	4 ϕ 19mm	Plain	278	290	139.7 - 190.5	FLEXURE	47.3	1.05	
22		B	4.4								FLEXURE	63.5	1.05	
23		C	3.6								FLEXURE	78.7	1.05	
Mean value													0.97	
Standard deviation													5.4%	

Fig. 9.18 Finite element meshes for Taylor's beams

Beams ST1A & ST1B

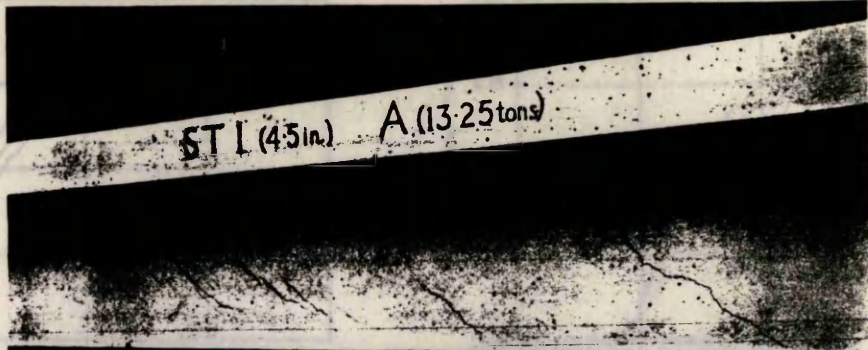
The observed crack patterns after failure for beam ST1 under test A and B are shown in Fig. 9.19a,b. Fig. 9.19a shows the crack pattern of test A where the beam failed in flexure, whereas Fig. 9.19b shows the crack pattern of test B where the beam failed in shear. The predicted crack patterns at the last convergent increment for the two tests A and B are shown in Fig. 9.19c,d. The difference between the two patterns is small, but the shear cracks in test B are slightly larger than that in test A. In Fig. 9.20, the stresses in the continuous longitudinal bars at the last three increments are shown for the two tests. Again, a small difference between the results of the two test are observed. But in test A, the stresses in the bar is higher than those in test B, also the bar has yielded at the last two increments in test A. Fig. 9.21 shows the stresses in the cut-off bar. The stress in the bar in test A is higher than in that in Test B. Fig. 9.22 shows the predicted stresses in the stirrups at the last converged increments. The circle at a Gauss point means that the stirrup yielded at this point. The stresses in the compression steel and the stress-strain curves at a Gauss point under the applied load are shown in Figs. 9.23 and 9.24.

Beams ST2A, ST2B, and ST2C

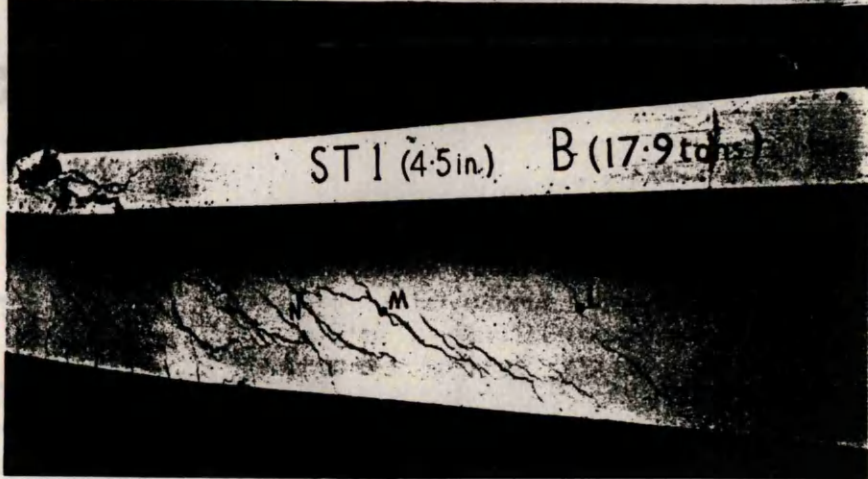
Taylor reported the observed crack pattern after failure for beam ST2 in Test C only (Fig. 9.25c). The predicted behaviours of the three tests (A, B, and C) of beam ST2 are shown in Figs. 9.25 to 9.29.

Fig. 9.25 shows the crack patterns. The shear crack in the crack pattern of test C is more critical than the shear crack in the crack patterns of tests A and B. The stresses in the tension steel at the last three increments are shown in Fig. 9.26. Again like beam ST1 in case of flexural failure (beams ST2A, ST2B), the tension steel has yielded at the last two increments while in shear failure (beam ST2C) the steel has yielded at the last increment only. The stresses in the compression steel at the last three increments are shown in Fig. 9.27. As the

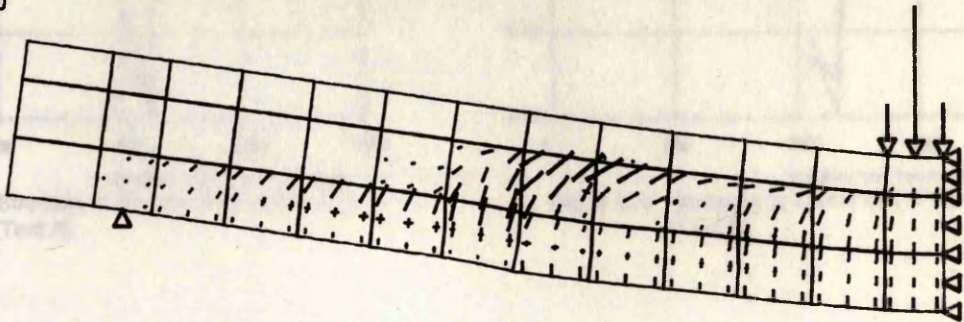
(a) Observed
(Test A)



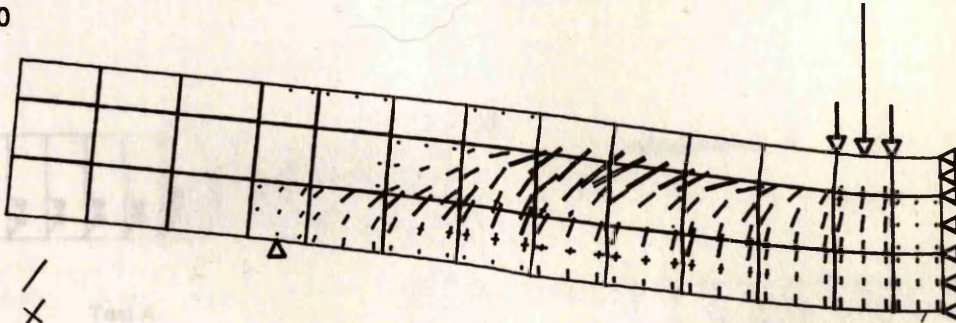
(b) Observed
(Test B)



(c) L. F. = 1.00
(Test A)



(d) L. F. = 0.90
(Test B)



- Single crack /
- Double crack X
- Crushing of concrete ■

Fig. 9.19 Crack patterns and deformed shapes of beam ST1 (displacements magnified x 10)

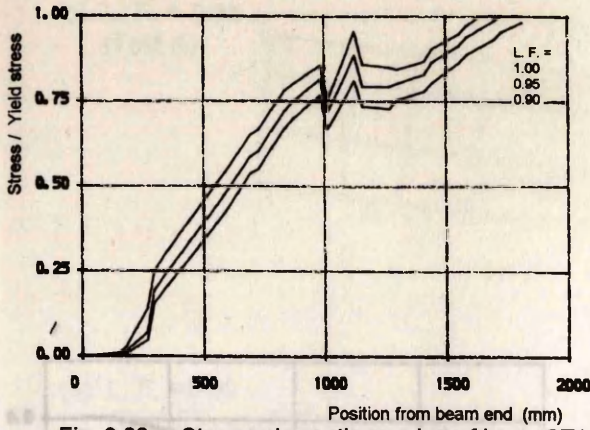


Fig. 9.20a Stresses in continuous bar of beam ST1 (Test A)

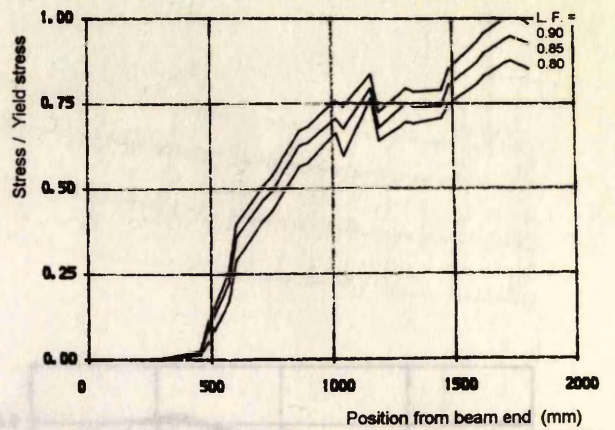


Fig. 9.20b Stresses in continuous bar of beam ST1 (Test B)

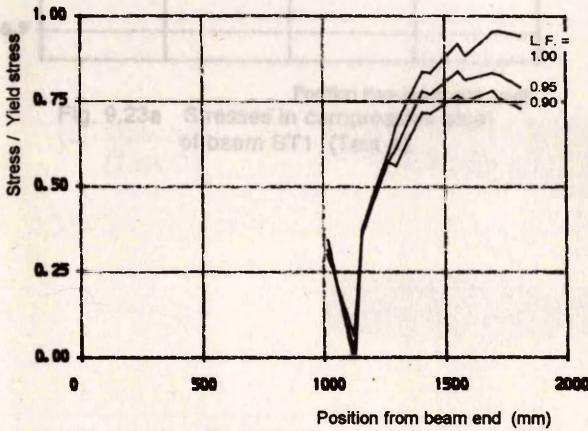


Fig. 9.21a Stresses in cut-off bar of beam ST1 (Test A)

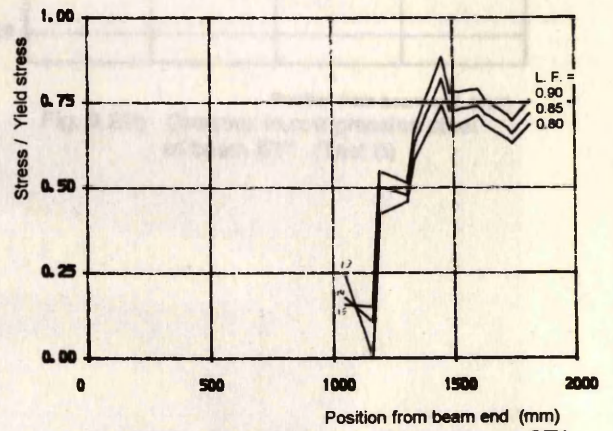


Fig. 9.21b Stresses in cut-off bar of beam ST1 (Test B)

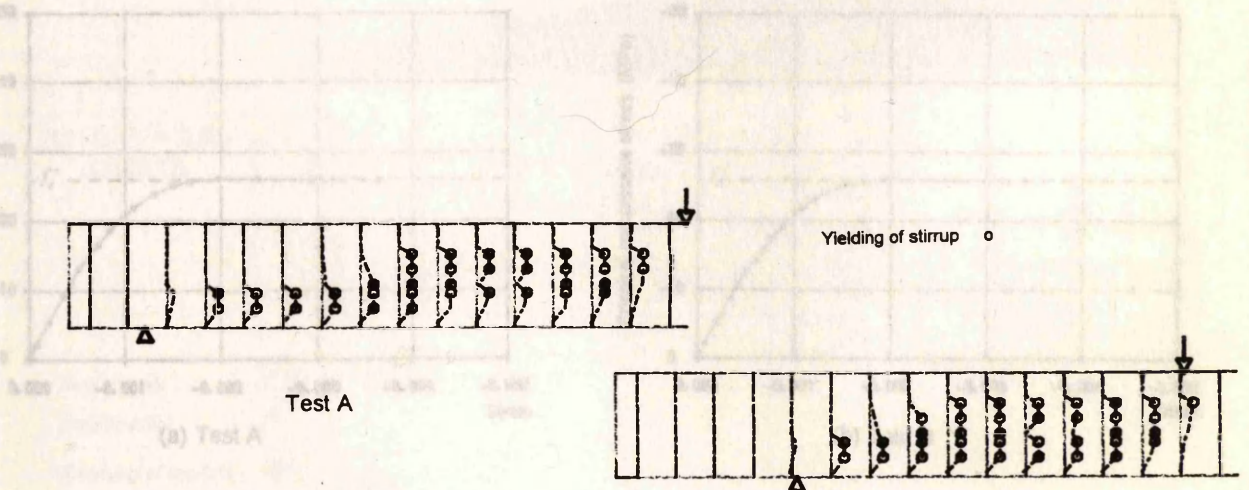


Fig. 9.22 Stresses in stirrups of beam ST1 at last converged increment

(a) L.F. = 0.95
(Test A)

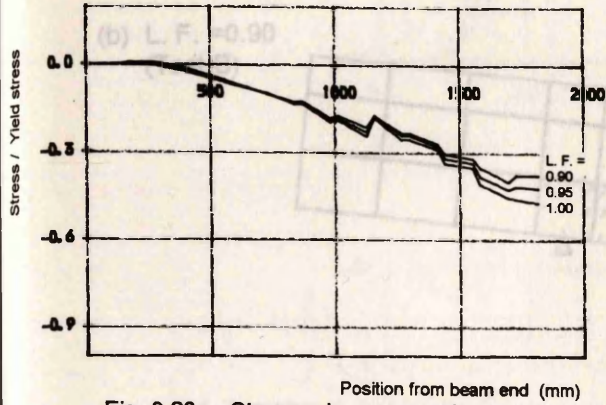
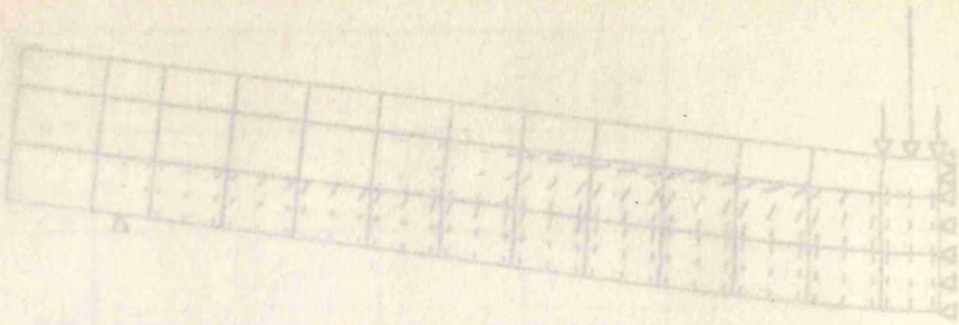


Fig. 9.23a Stresses in compression steel of beam ST1 (Test A)

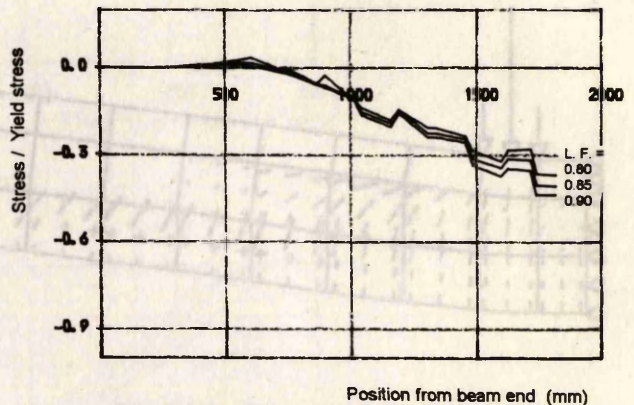
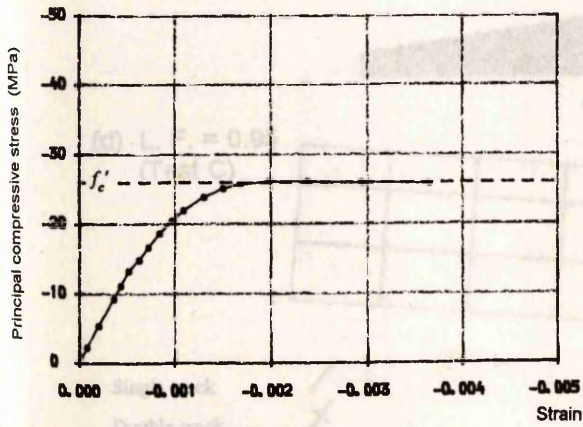
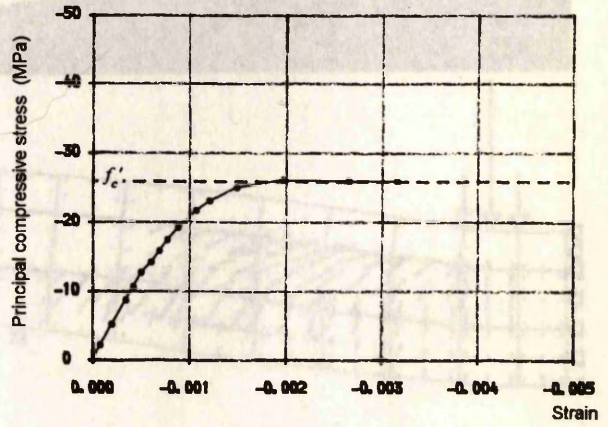


Fig. 9.23b Stresses in compression steel of beam ST1 (Test B)



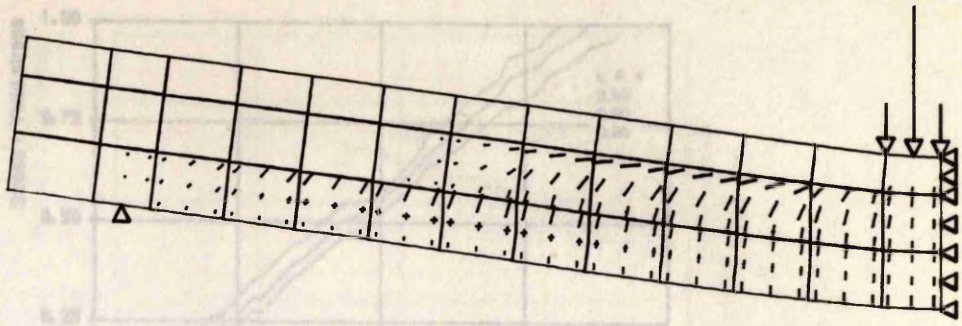
(a) Test A



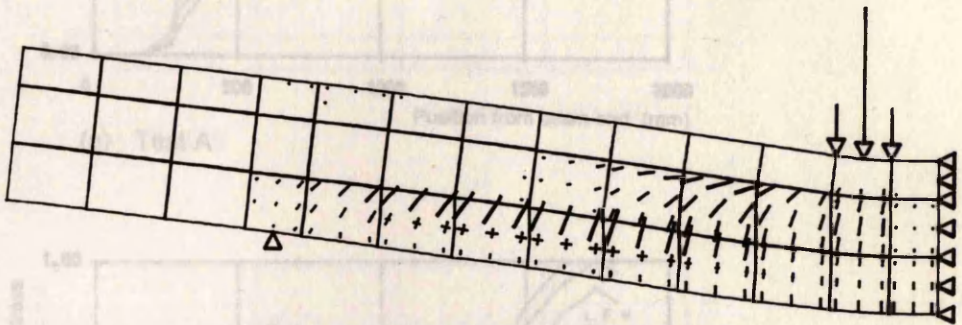
(b) Test B

Fig. 9.24 Stress-strain curves of concrete at a Gauss point under the load point (beam ST1)

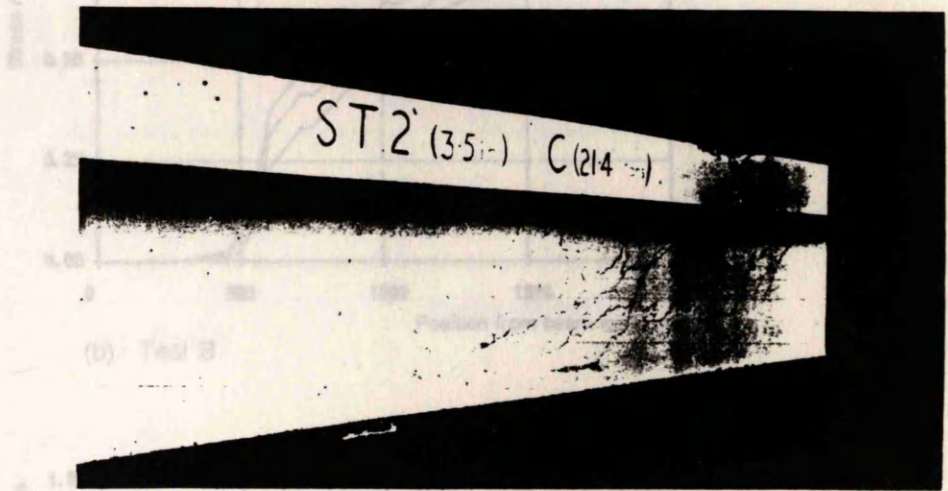
(a) L. F. = 0.95
(Test A)



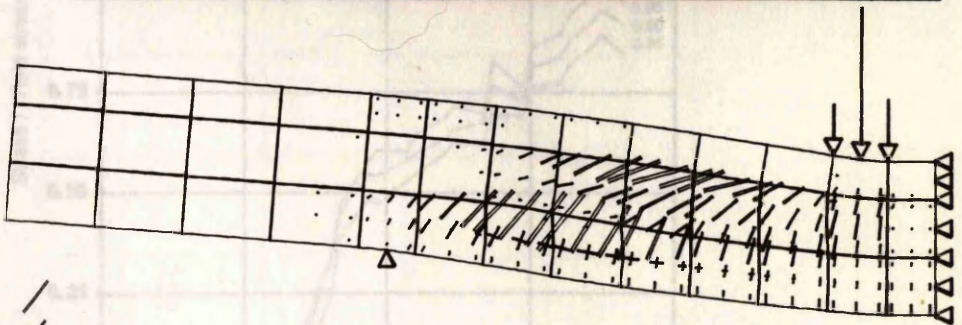
(b) L. F. = 0.90
(Test B)



(c) Observed
(Test C)



(d) L. F. = 0.95
(Test C)



- Single crack /
- Double crack X
- Crushing of concrete ■

Fig. 9.25 Crack patterns and deformed shapes of beam ST2 (displacements magnified x 10)

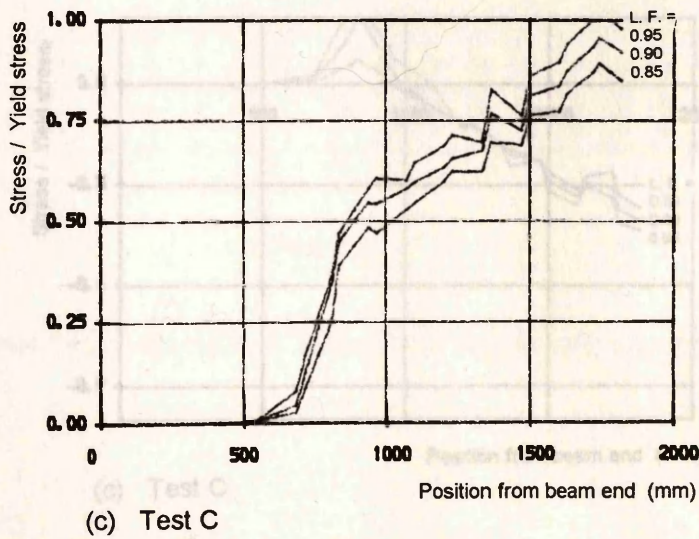
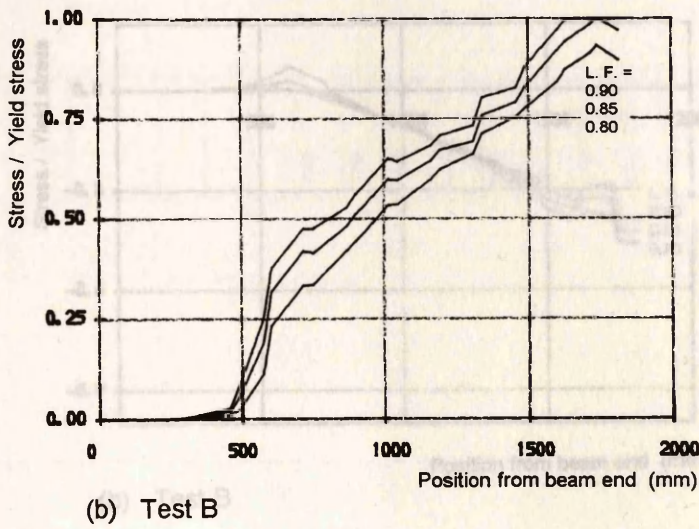
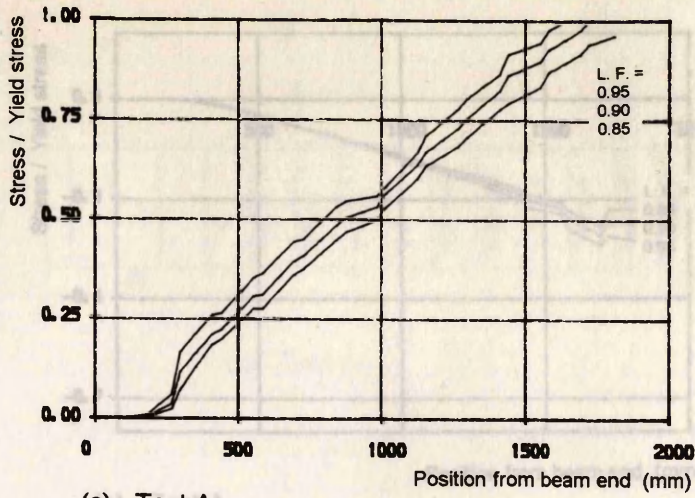
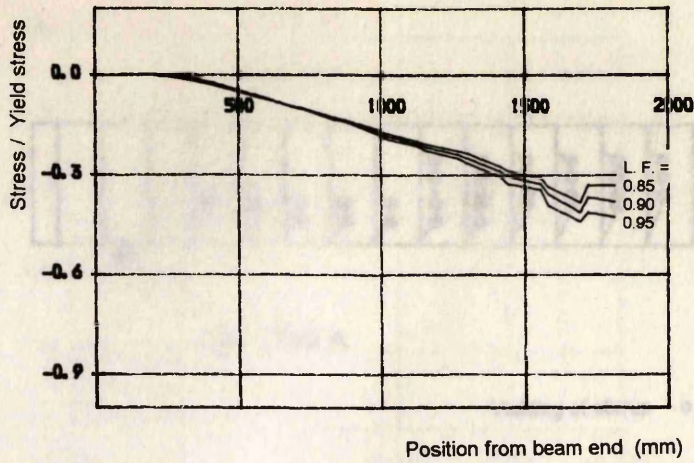
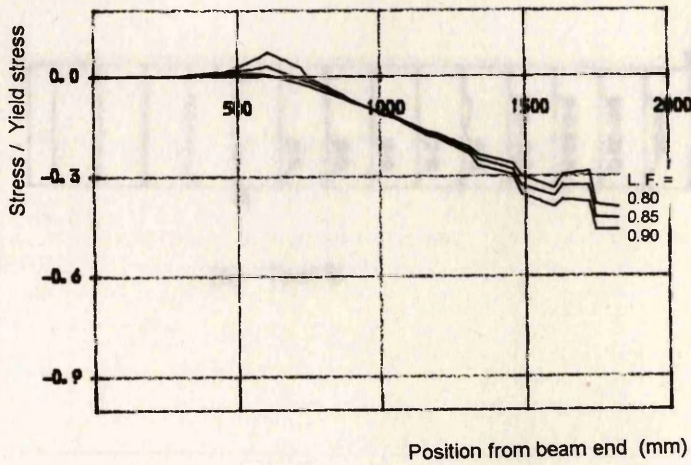


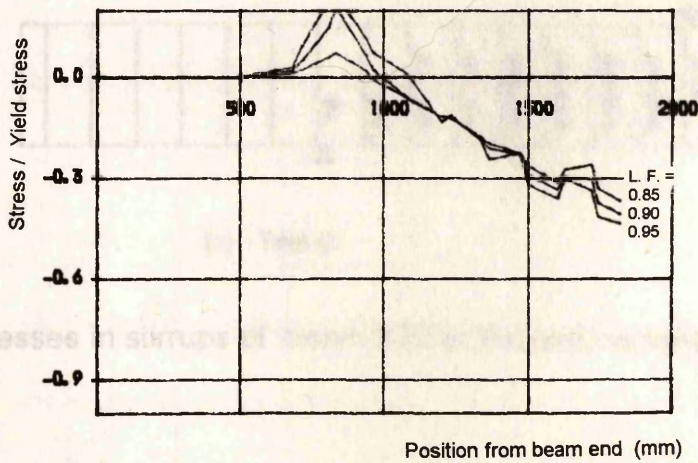
Fig. 9.26 Stresses in tension steel of beam ST2



(a) Test A



(b) Test B



(c) Test C

Fig. 9.27 Stresses in compression steel of beam ST2

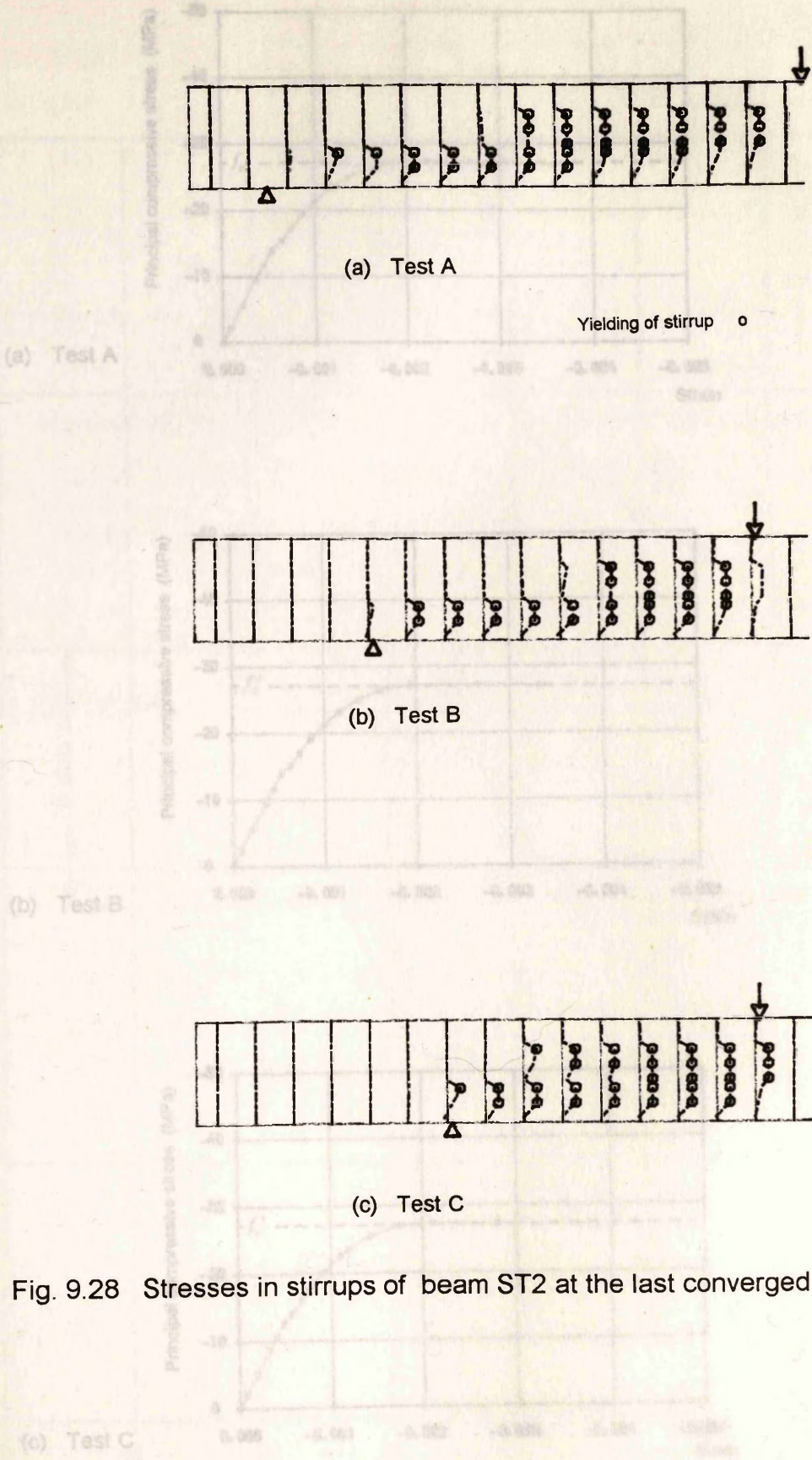


Fig. 9.28 Stresses in stirrups of beam ST2 at the last converged increments

Fig. 9.29 Stress-strain curves of concrete at a tension point under the load point (beam ST2)

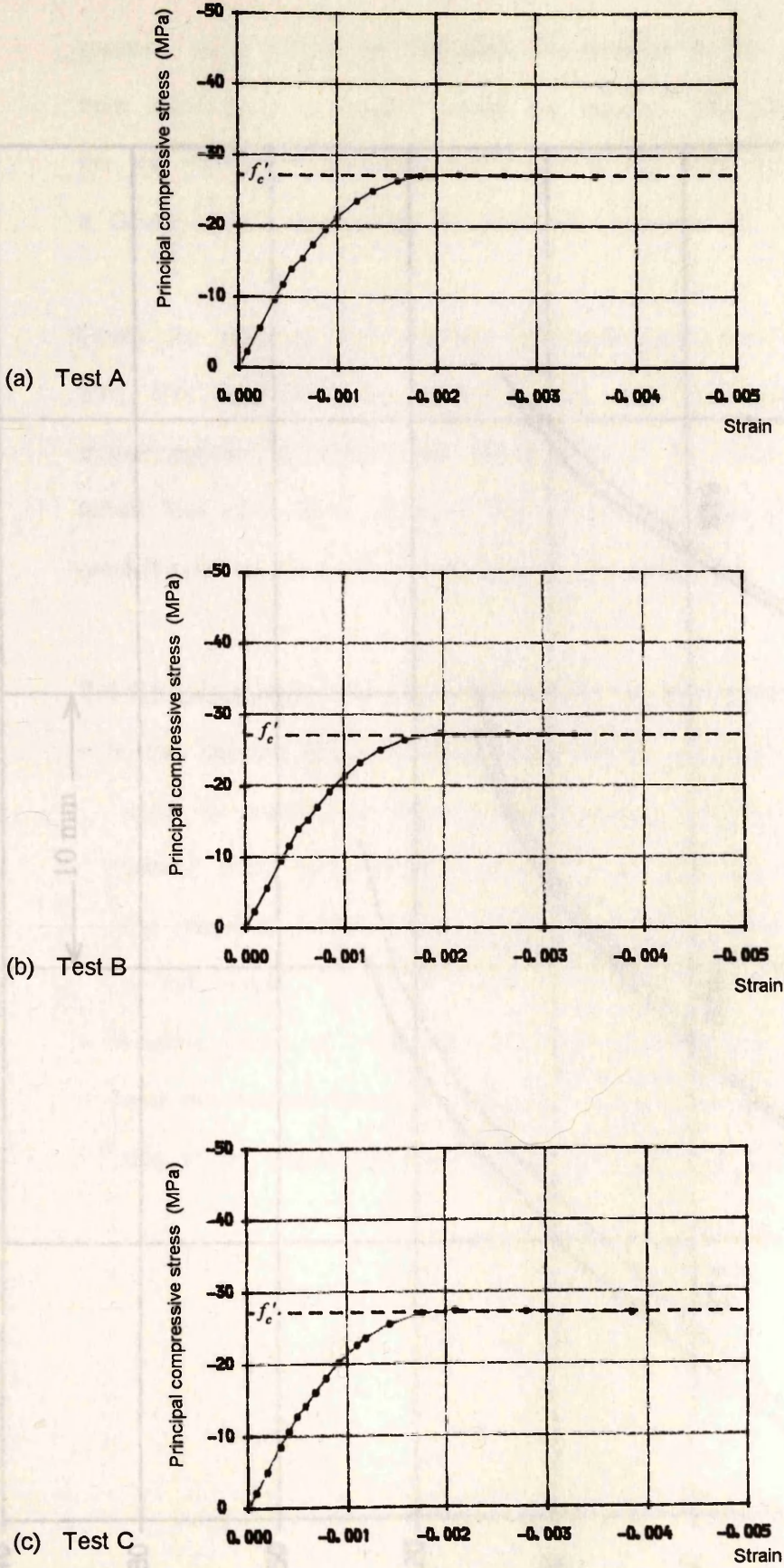


Fig. 9.29 Stress-strain curves of concrete at a Gauss point under the load point (beam ST2)

supports move toward the mid-span, the stresses in the compression steel change from compression to tension above the support. The stresses in the stirrups at

the east corner increase and are shown in Fig. 9.28. The stress-strain curves at a Gauss point near the corner are shown in Fig. 9.29.

Finally, the experimental and numerical load-deflection curves for five beams (beams ST1, ST6, and ST9) are shown in Fig. 9.30. The predicted failure loads are plotted against the experimental values in Fig. 9.31. Assuming the predicted failure load of a beam is 10% of the experimental failure load makes the predicted failure load of the beam conservative.

9.4 Conclusion

In this chapter, the 2-D finite element model developed in chapter 9 was used to predict the behavior of reinforced concrete Tee beams with and without shear reinforcement. The results of prediction of the ultimate load capacity of the beams are compared with the experimental results. In some cases, the model over-predicts the load capacity, but in most cases, the model under-predicts the load capacity. The reason for this is due to the linear description of the material behavior.

In some cases, the model over-predicts the load capacity, but in most cases, the model under-predicts the load capacity. The reason for this is due to the linear description of the material behavior.

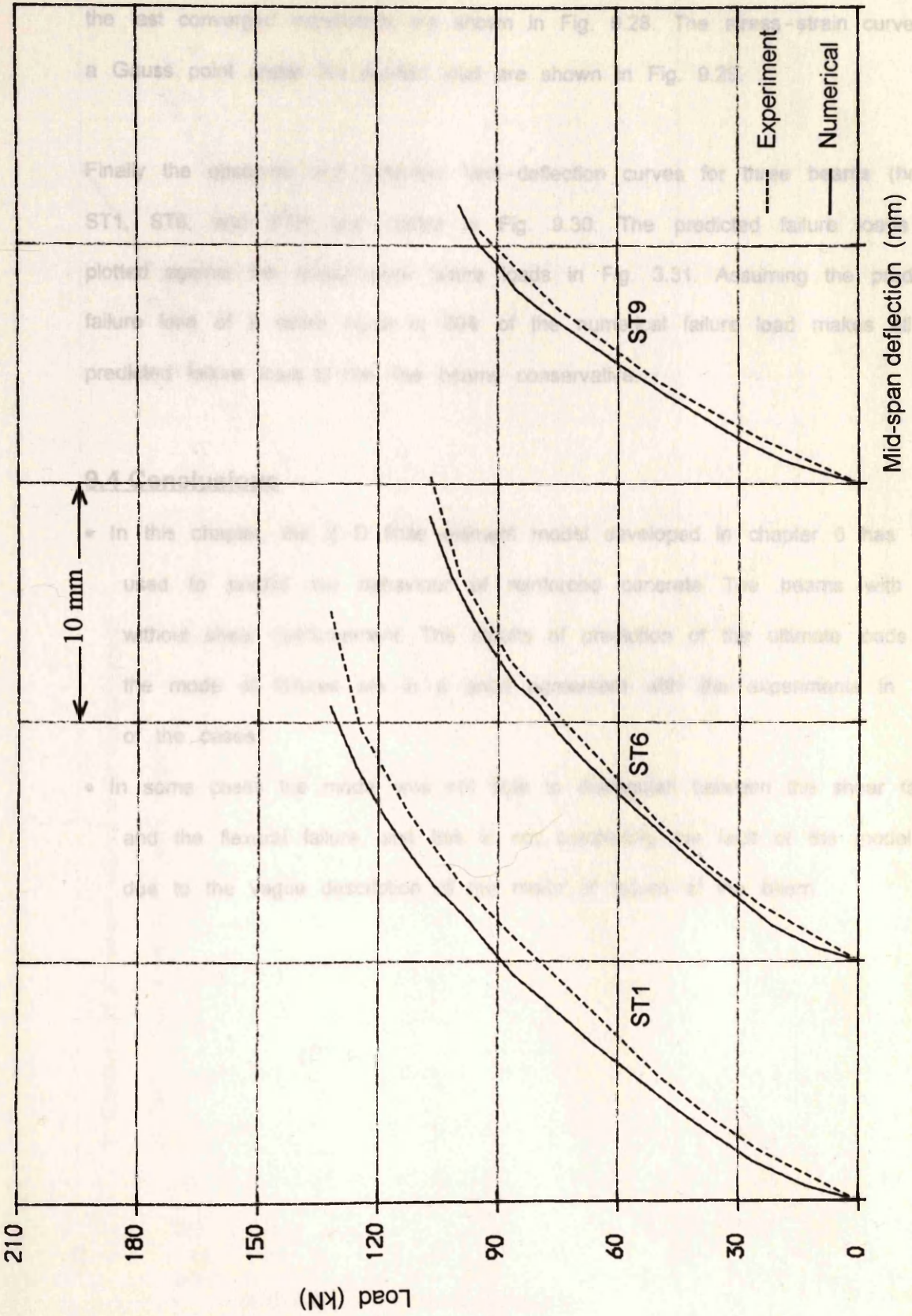


Fig. 9.30 Load-deflection curves of beams ST1, ST6, and ST9

supports move toward the mid-span, the stresses in the compression steel change from compression to tension above the support. The stresses in the stirrups at the last converged increments are shown in Fig. 9.28. The stress-strain curves at a Gauss point under the applied load are shown in Fig. 9.29.

Finally the observed and predicted load-deflection curves for three beams (beams ST1, ST6, and ST9) are plotted in Fig. 9.30. The predicted failure loads are plotted against the experimental failure loads in Fig. 3.31. Assuming the predicted failure load of a beam equal to 80% of the numerical failure load makes all the predicted failure loads of the Tee beams conservative.

9.4 Conclusions

- In this chapter, the 2-D finite element model developed in chapter 6 has been used to predict the behaviour of reinforced concrete Tee beams with and without shear reinforcement. The results of prediction of the ultimate loads and the mode of failures are in a good agreement with the experiments in most of the cases.
- In some cases the model was not able to distinguish between the shear failure and the flexural failure, and this is not completely the fault of the model but due to the vague description of the mode of failure of the beam.

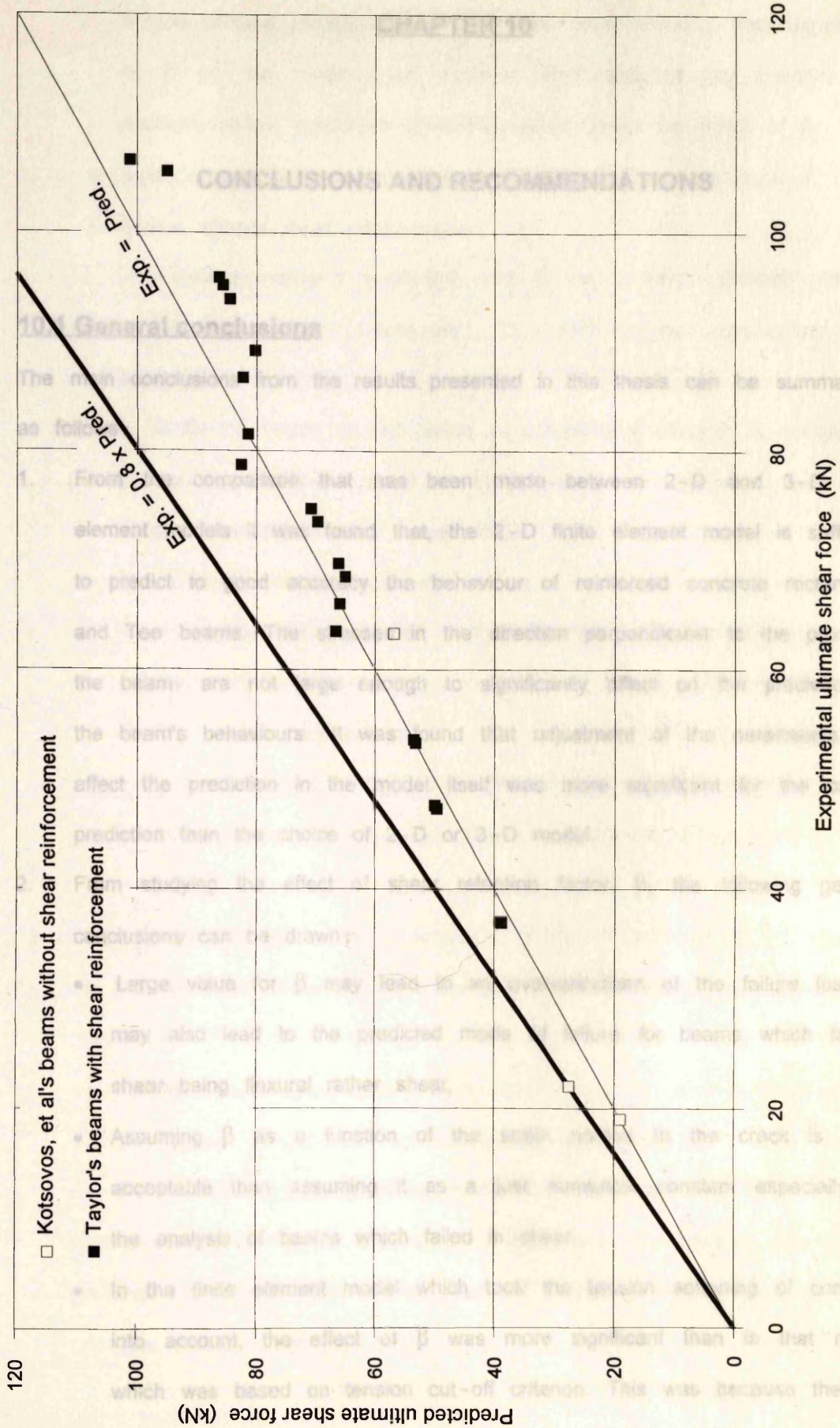


Fig. 9.31 Results of reinforced concrete Tee beams

CHAPTER 10

CONCLUSIONS AND RECOMMENDATIONS

10.1 General conclusions

The main conclusions from the results presented in this thesis can be summarised as follows:

1. From the comparison that has been made between 2-D and 3-D finite element models it was found that, the 2-D finite element model is sufficient to predict to good accuracy the behaviour of reinforced concrete rectangular and Tee beams. The stresses in the direction perpendicular to the plane of the beam are not large enough to significantly affect on the prediction of the beam's behaviours. It was found that adjustment of the parameters that affect the prediction in the model itself was more significant for the correct prediction than the choice of 2-D or 3-D model.
2. From studying the effect of shear retention factor, β , the following general conclusions can be drawn:
 - Large value for β may lead to an overestimation of the failure load. It may also lead to the predicted mode of failure for beams which fail in shear being flexural rather shear.
 - Assuming β as a function of the strain normal to the crack is more acceptable than assuming it as a just numerical constant especially for the analysis of beams which failed in shear.
 - In the finite element model which took the tension softening of concrete into account, the effect of β was more significant than in that model which was based on tension cut-off criterion. This was because the two

- models created different states of stresses after cracking. This dependency of β on the model itself explains why most of the previous finite element models concluded conflicting results about the effect of β .

In some classes of beams the following conclusions can be drawn:

- Beams without shear reinforcement:
 - In beams having a small a/d ratio, β had a very significant effect on the prediction of the failure load (25 - 125% of the experimental failure load).

4. From a study of the effect of tension softening of concrete on the prediction of the behaviour of reinforced concrete beams the following conclusions can be drawn:

- In beams having a high value of compressive strength of concrete, β had a very significant effect on the prediction of the failure load (up to 100% of the experimental failure load).

- Beams with shear reinforcement:
 - In beams having a high a/d ratio and high percentage of shear reinforcement (which was expected to fail in flexure), β had little or no effect on the predicted behaviours.
 - In beams having a small a/d ratio, β had a significant effect on the predicted failure load (10 - 25% of the experimental failure load).

3. From a study of the effect of tension softening of concrete on the prediction of the behaviour of reinforced concrete beams the following conclusions can be drawn:

- Taking tension softening into account was economical because it reduced the number of iterations required to achieve convergency.
- In beams with shear reinforcement having a high a/d ratio and high percentage of shear reinforcement, taking tension softening into account had very little effect on the predicted failure load, the mode of failure, and the load deflection curve.

- In beams without shear reinforcement having a high a/d ratio, taking tension softening into account had little effect on the predicted failure load although it improved the load deflection curve
 - In beams without shear reinforcement having low a/d ratio taking tension softening into account had a significant effect on the predicted failure load (20–35% of the experimental failure load). Also in these beams the strain at which the tension softening was terminated had a significant effect on the predicted failure load.
4. From a study of the effect of tensile strength of concrete on the prediction of reinforced concrete beams :
- In general, the less the assumed value of the tensile strength the less the predicted failure load. Also, the less the assumed value of tensile strength the less the scatter in the prediction.
 - The tensile strength of concrete had very little effect on the prediction of the behaviour of beams having a high a/d ratio and high percentage of shear reinforcement which failed in flexure.
 - It had a significant effect on the prediction of the behaviour of over reinforced beams without shear reinforcement which was expected to fail in shear
 - It had a very significant effect on beams without shear reinforcement having a/d ratio less than 4.
5. From a study of the effect of maximum compressive strain of concrete it was found that:
- In beams without shear reinforcement assuming the concrete to be crushed immediately after it reached the peak of stress with a maximum compressive strain ϵ_{max} of
- $$\epsilon_{max} = \frac{\sqrt{f'_c}}{2500}$$
- gave good results.

9. In beams with shear reinforcement assuming the concrete to be crushed when the maximum compressive strain ϵ_{max} reached to a value of 0.005 gave satisfactory results.
10. From a study of the effect of compression softening of concrete the following conclusions can be drawn:
- This effect was more important in beams having a high percentage of shear reinforcement, a high value of a/d ratio, and a low value of the compressive strength of concrete.
 - The shape of the curve in the descending portion of the stress-strain relationship had less effect on the prediction than the value of the compressive strain at which the concrete was assumed to be crushed (ϵ_{max}).
6. From the analysis of reinforced concrete T-beams it was found that:
- The essential features of the behaviour of Tee beams were predicted to a good accuracy using the 2-D finite element model. Neglecting the stresses variation in the flange had no significant effect on the prediction.
 - The prediction of the behaviour of Tee beams with shear reinforcement was more accurate than the prediction of the behaviour of beams without shear reinforcement.
7. From the analysis of prestressed concrete beams the following conclusions can be drawn:
- Like the reinforced concrete rectangular and Tee beams the prediction of the behaviours of beams with shear reinforcement was better than the prediction of the behaviours of beams without shear reinforcement.
 - Assuming the effective prestressing force as a constant horizontal load applied to the beam in the first load step seemed to be acceptable. Also modifying the stress strain curve of the prestressing reinforcement by subtracting the effective prestress and treating it as unstressed steel reasonably simulated the actual behaviour.
- 8.

9. From Fig. A1 (Appendix A) it is clear that the mesh used in the analysis is fine enough for the results to be only marginally affected by mesh dependency.
10. Finally, this thesis introduces a 2-D finite element model which can be used to predicted with satisfactory result the behaviour (e.g.; the ultimate load, the load-deflection curve, and the mode of failure) of reinforced and prestressed concrete beams. In this model the concrete and steel are modelled as follows :

- **Concrete:** is assumed to be elasto-plastic in compression and linear elastic in tension with a softening in both tension and compression as follows:

- (i) Compression: The stress-strain relationship of concrete in compression is assumed as shown in Fig. 10.1. In the analysis of beams without shear reinforcement, no compression softening is assumed (Fig. 10.1a). In the analysis of beams with shear reinforcement, a straight line with very small slope is assumed for the descending portion as follows (Fig. 10.1b).

$$\sigma = f_c' \frac{(0.1 - \varepsilon)}{(0.1 - \varepsilon_{cc})}; \quad \varepsilon < 0.005 \quad (10.1)$$

$$\varepsilon_{cc} = \sqrt{f_c' / 2500}$$

where f_c' in MPa

- (ii) Tension: The stress-strain relationship of concrete in tension is assumed as shown in Fig. 10.2. The tensile strength of concrete f_t' is estimated from the compressive strength f_c' as follows.

$$f_t' = 0.54 \sqrt{f_c'} \quad \text{MPa} \quad (10.2)$$

The equation which represents the descending portion of the stress-strain curve is.

$$\sigma = \frac{1}{2} \left(\frac{\varepsilon_{cr}}{\varepsilon_n} + \sqrt{\frac{\varepsilon_{cr}}{\varepsilon_n}} \right) f_t' ; \quad \varepsilon_n < \varepsilon_s \quad (10.3)$$

where ε_{cr} is the initial cracking strain of concrete and ε_s is the yield strain of steel used ($\varepsilon_s \approx 20 \varepsilon_{cr}$ for normal steel and $50 \varepsilon_{cr}$ for prestressing steel).

- (iii) Shear: After cracking, the shear retention factor β is assumed as a function of the strain normal to the crack ε_n as follows (Fig. 10.3).

$$\beta = 0.4 \frac{\varepsilon_{cr}}{\varepsilon_n} > 0.0 \quad (10.4)$$

- Young's modulus of concrete is taken as follows.

$$E = 5000 \sqrt{f_c'} \quad \text{MPa}$$

- **Steel:** is assumed to be elastic perfect plastic in tension and compression with the maximum stress equal to the yield stress. Fig. 10.4 shows the stress-strain curves of the normal and the prestressing steel.

The results of the model for more than two hundreds reinforced and prestressed concrete beams with and without shear reinforcement are shown in Fig. 10.5.

10.2 Recommendations for future work

This section recommends further work as follows :

- 1- Although the present equation (Eq. 10.4) used for shear retention factor gave acceptable results in most of the cases there is a need to study other equations obtained from the shear tests on concrete.
- 2- The compressive strain at which the concrete is assumed to be crushed needs more investigation. It is believed to be related to the percentage of reinforcement in reinforced concrete structure.
- 3- Further extensive analysis of the available test results, particularly for beams with shear reinforcement needs to be completed.

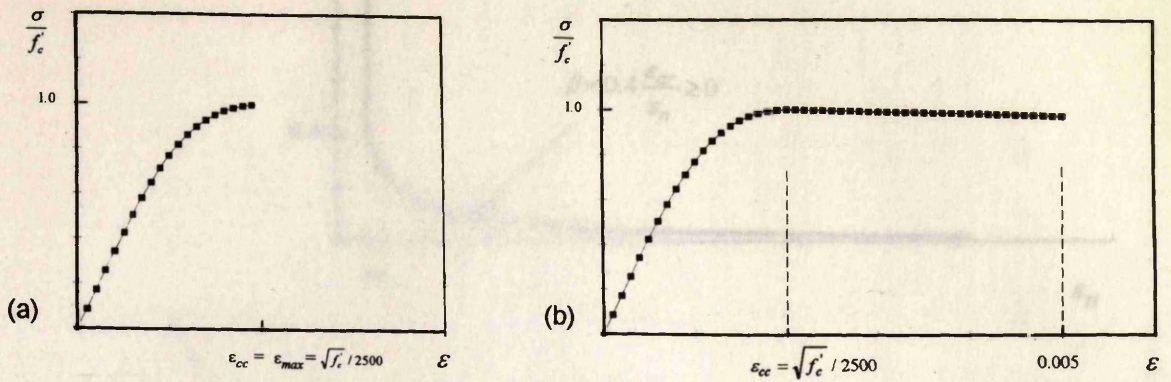


Fig. 10.1 Assumed stress-strain curve of concrete in compression
 (a) for beams without shear reinforcement
 (b) for beams with shear reinforcement

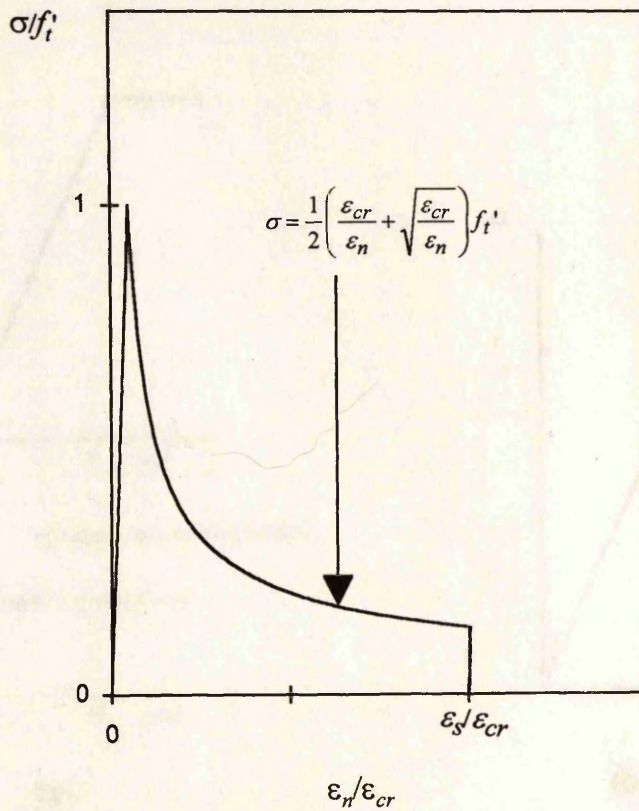


Fig. 10.2 Assumed stress-strain curve of concrete in Tension

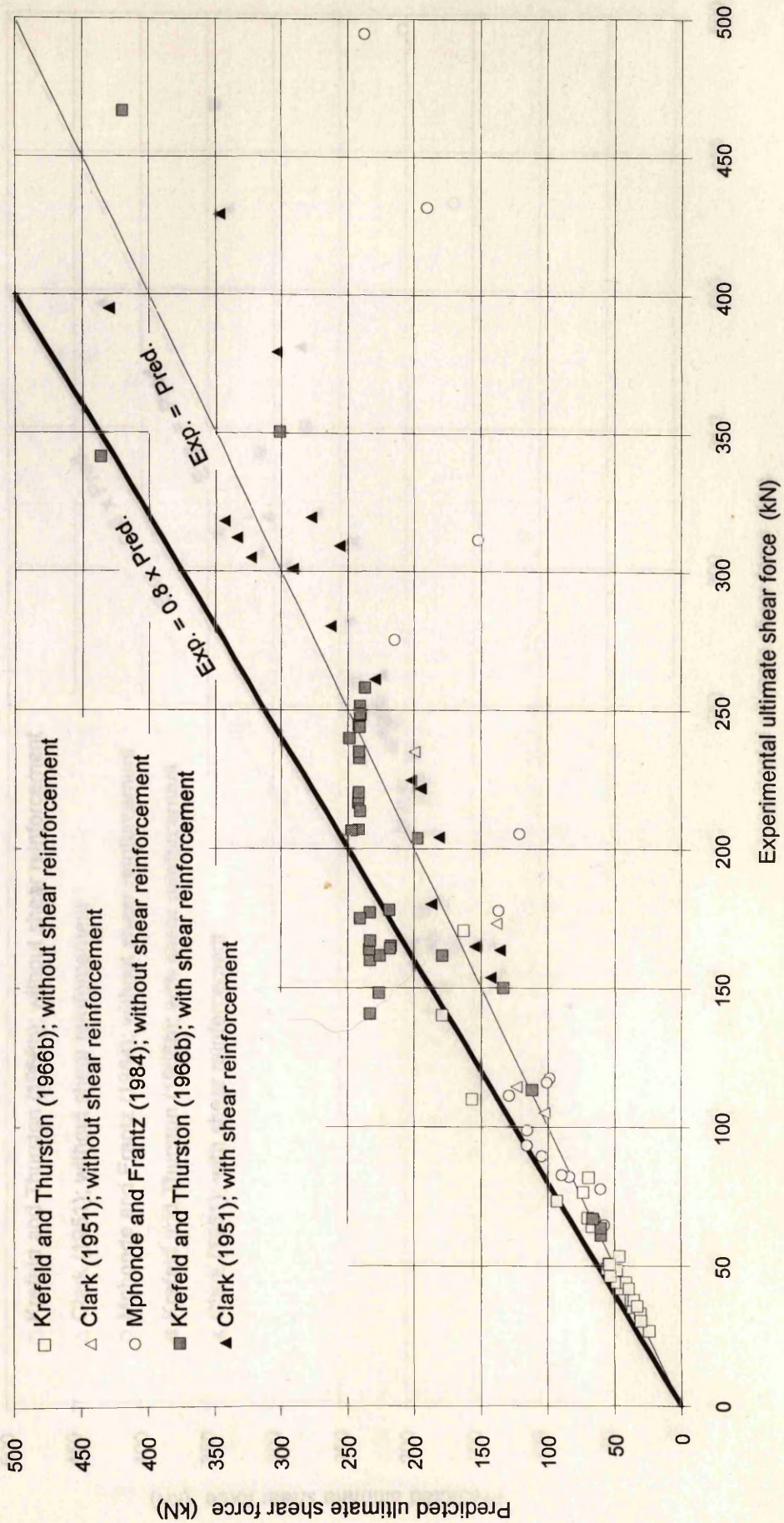


Fig. 10.5a Results of the model for reinforced concrete rectangular beams

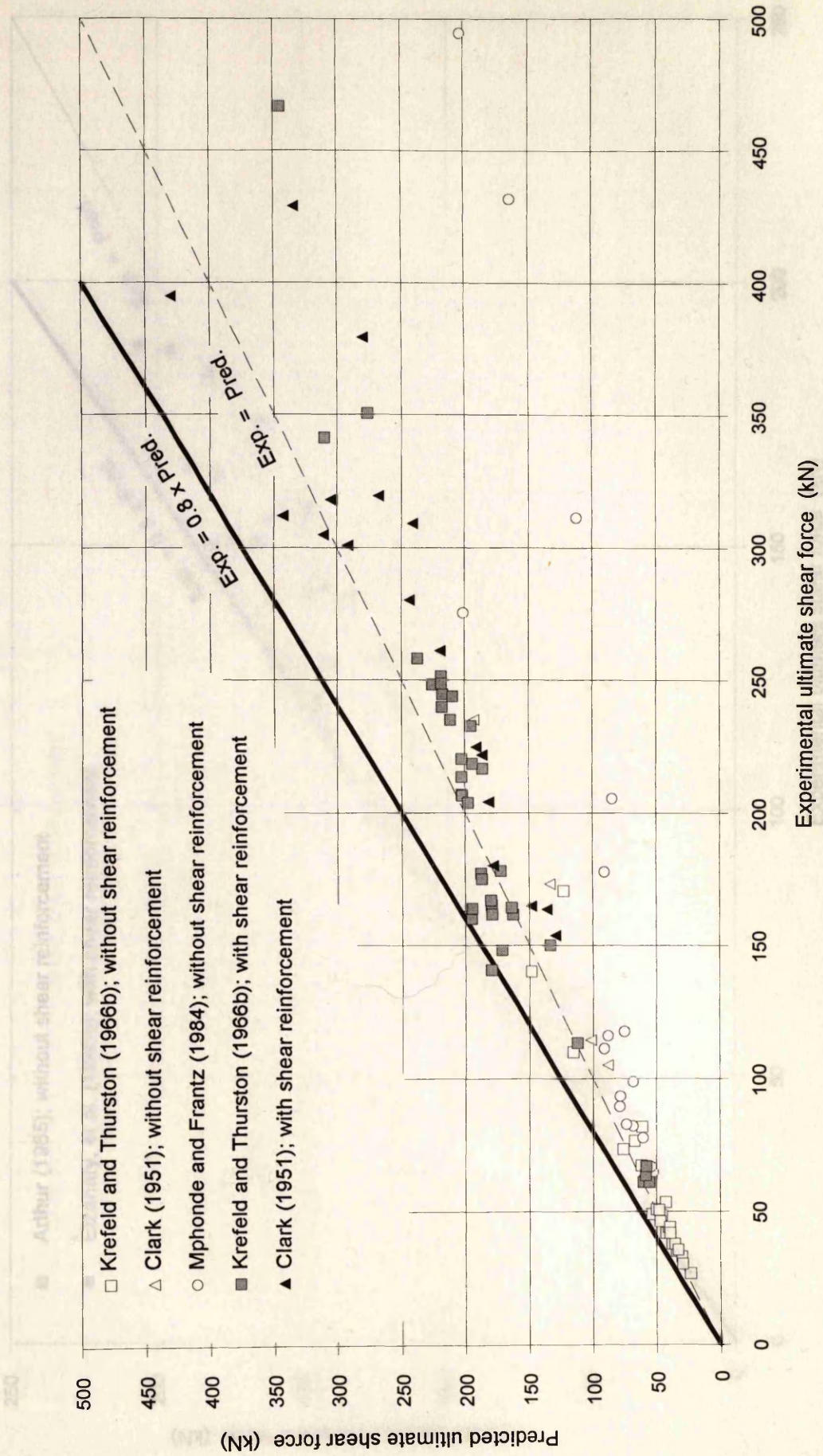


Fig. 10.5b Results of the model (except for using $f_t' = \sqrt[4]{f_c'}$) for reinforced concrete rectangular beams

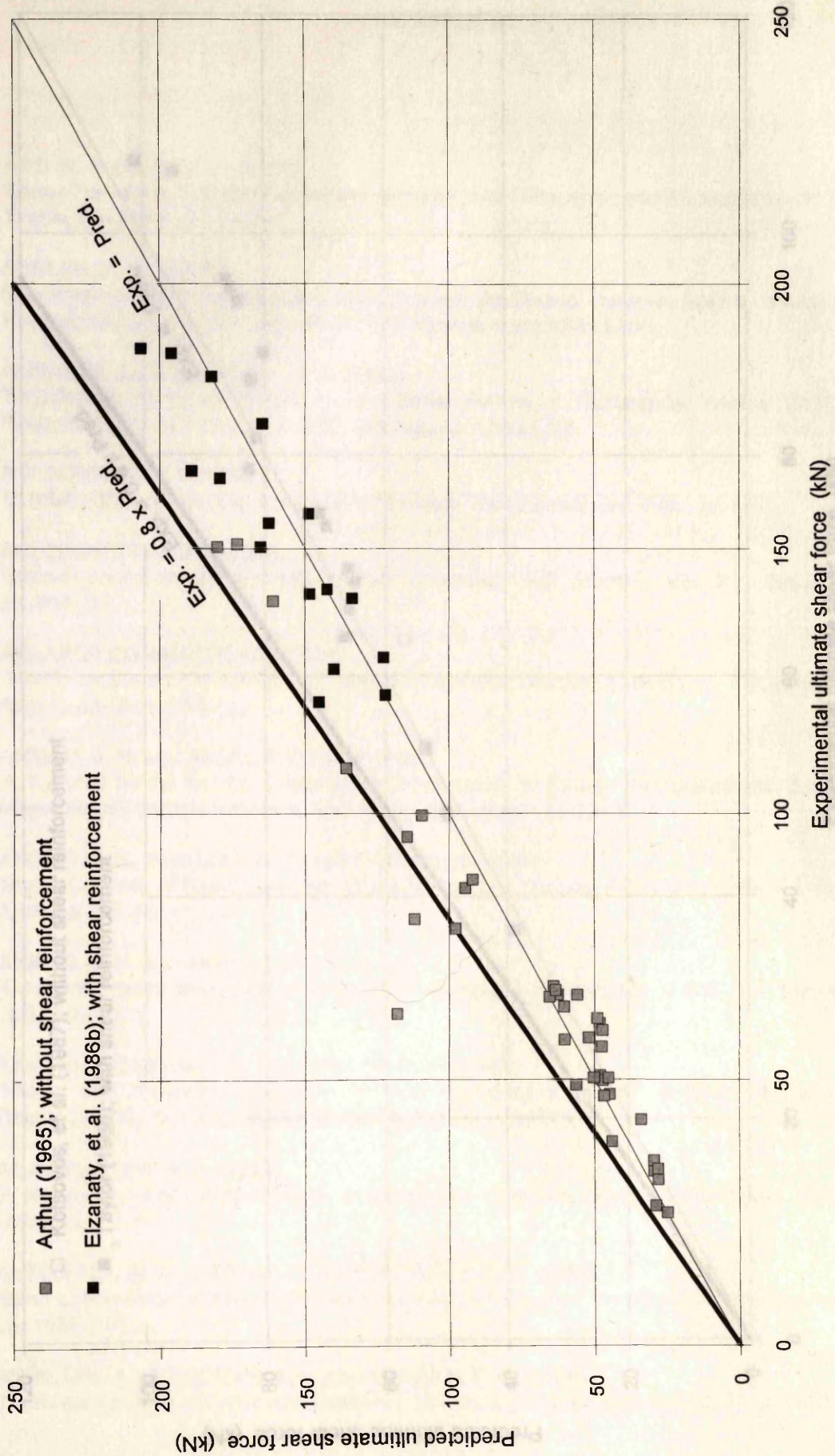


Fig. 10.5c Results of the model for prestressed concrete beams

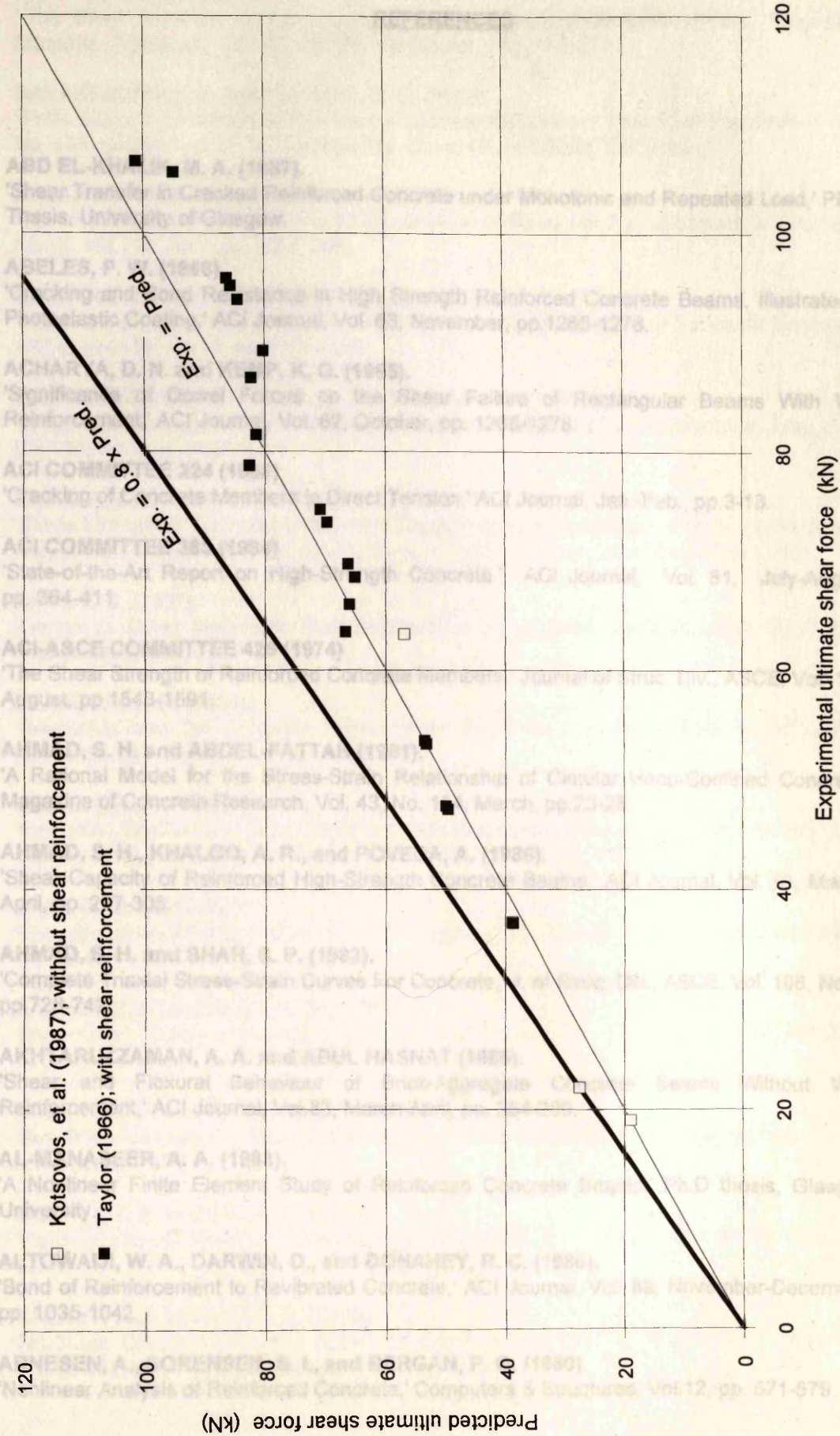


Fig. 10.5d Results of the model for reinforced concrete Tee-beams

REFERENCES

- ARTHUR, P. D. (1965).
'The Shear Strength of Reinforced Concrete Beams With Unreinforced Webs,' Magazine of Concrete Research, Vol. 17, No. 52, December, pp. 199-210.
- BALAKRISHNAN, S. and MURPHY, G. R. (1983).
'Finite Element Prediction of Reinforced Concrete Behaviour,' Structural Engineering Report No. 138, Department of Civil Engineering, University of Alberta, Edmonton.
- ABD EL-KHALIK, M. A. (1987).**
'Shear Transfer in Cracked Reinforced Concrete under Monotonic and Repeated Load,' Ph. D. Thesis, University of Glasgow.
- ABELES, P. W. (1966).**
'Cracking and Bond Resistance in High Strength Reinforced Concrete Beams, Illustrated by Photoelastic Coating,' ACI Journal, Vol. 63, November, pp.1265-1278.
- ACHARYA, D. N. and KEMP, K. O. (1965).**
'Significance of Dowel Forces on the Shear Failure of Rectangular Beams With Web Reinforcement,' ACI Journal, Vol. 62, October, pp. 1265-1278.
- ACI COMMITTEE 224 (1986)**
'Cracking of Concrete Members in Direct Tension,' ACI Journal, Jan.-Feb., pp.3-13.
- ACI COMMITTEE 363 (1984)**
'State-of-the-Art Report on High-Strength Concrete,' ACI Journal, Vol. 81, July-August, pp. 364-411.
- ACI-ASCE COMMITTEE 426 (1974)**
'The Shear Strength of Reinforced Concrete Members,' Journal of Struc. Div., ASCE, Vol. 100, August, pp 1543-1591.
- AHMAD, S. H. and ABDEL-FATTAH (1991).**
'A Rational Model for the Stress-Strain Relationship of Circular Hoop-Confined Concrete,' Magazine of Concrete Research, Vol. 43, No. 154, March, pp.23-28.
- AHMAD, S. H., KHALOO, A. R., and POVEDA, A. (1986).**
'Shear Capacity of Reinforced High-Strength Concrete Beams,' ACI Journal, Vol. 83, March-April, pp. 297-305.
- AHMAD, S. H. and SHAH, S. P. (1982).**
'Complete Triaxial Stress-Strain Curves For Concrete,' J. of Struc. Div., ASCE, Vol. 108, No. 4, pp.728-742.
- AKHTARUZZAMAN, A. A. and ABUL HASNAT (1986).**
'Shear and Flexural Behaviour of Brick-Aggregate Concrete Beams Without Web Reinforcement,' ACI Journal, Vol.83, March-April, pp. 284-289.
- AL-MANASEER, A. A. (1983).**
'A Nonlinear Finite Element Study of Reinforced Concrete Beams,' Ph.D thesis, Glasgow University.
- ALTOWAIJI, W. A., DARWIN, D., and DONAHEY, R. C. (1986).**
'Bond of Reinforcement to Revibrated Concrete,' ACI Journal, Vol. 83, November-December, pp. 1035-1042.
- ARNESEN, A., SORENSEN, S. I., and BERGAN, P. G. (1980).**
'Nonlinear Analysis of Reinforced Concrete,' Computers & Structures, Vol.12, pp. 571-579.

ARTHUR, P. D. (1965).

'The Shear Strength of Pre-Tensioned I Beams with Unreinforced Webs,' Magazine of Concrete Research, Vol. 17, No. 53, December., pp. 199-210.

BALAKRISHNAN, S. and MURRAY, D. W. (1986).

'Finite Element Prediction of Reinforced Concrete Behaviour,' Structural Engineering Report No. 138, Department of Civil Engineering, University of Alberta, Edmonton.

BALAKRISHNAN, S. and MURRAY, D. W. (1988a).

'Concrete Constitutive Model For NLFE Analysis of Structures,' J. of Structural Engineering, ASCE, Vol.114, No.7, pp.1449-1466.

BALAKRISHNAN, S. and MURRAY, D. W. (1988b).

'Prediction of R/C Panel and Deep Beam Behavior By NLFEA,' J. of Structural Engineering, ASCE, Vol.114, No.10, pp.2323-2342.

BALAKRISHNAN, S., ELWI, A. E., and MURRAY, D. W. (1988).

'Effect of Modeling on NLFE Analysis of Concrete Structures,' J. of Structural Eng., ASCE, Vol.114, No.7, pp.1467-1487.

BALMER, G. G. (1949).

'Shear Strength of Concrete under High Triaxial Stress-Computation of Mohr's Envelope as a Curve,' Struct. Res. Lab. Rep. SP-23, Denver, Colo., October. (quoted by Chen 1982).

BARI, M. S. (1987).

'Design of Shear Wall-Floor Slab Connections Using Shear Reinforcement,' Ph.D thesis, Glasgow University.

BARNARD, P. R. (1964).

'Researches into the Complete Stress-Strain Curve for Concrete,' Magazine of Concrete Research, Vol. 16, No. 49, Dec., pp. 203-210.

BAZANT, Z. P. (1976).

'Instability, Ductility and Size Effect in Strain-Softening Concret,' J. Engrg. Mech., ASCE, 102(2), 331-344, Discussions, 103, 357-358, 775-777;104, 501-502 .

BAZANT, Z. P. (1978).

'Endochronic Inelasticity and Incremental Plasticity,' Int. Journal. of Solids and Structures, Vol. 14, pp. 691-714.

BAZANT, Z. P. and BHAT, P. D. (1976).

'Endochronic Theory of Inelasticity and Failure of Concrete,' J. of Eng. Mech. Div., ASCE, Vol. 102, No. EM4, Aug., pp. 701-722.

BAZANT, Z. P. and KAZEMI, M. T. (1991).

'Size Effect on Diagonal Shear Failure of Beams Without Stirrups,' ACI Journal, Vol. 88, May-June, pp. 268-276.

BAZANT, Z. P. and KIM, S. S. (1979).

'Plastic-Fracturing Theory of Concrete,' J. of Eng. Mech. Div., ASCE, Vol. 105, No. EM3, June, 1979.

BAZANT, P. Z. and LIN, F. B. (1988).

'Nonlinear Smeared Cracking Model for Concrete Fracture,' J. of Structural Engineering, ASCE, Vol. 114, No. 11, November, pp. 2493-2510.

BAZANT, Z. P. and OH, B. H. (1983)

'Crack Band Theory for Fracture of Concrete,' Materials and Structures, RILEM, Paris, France, 16, 155-177.

BAZANT, Z. P. and OH, B. H. (1984)

'Rock Fracture Via Strain-Softening Finite Elements,' J. Eng. Mech., ASCE, 110(7), pp. 1015-1035.

BAZANT, Z. P., and PIJAUDIER-CABOT, G. (1988).

'Nonlocal Continuum damage, Localization Instability and Convergence,' J. Appl. Mech., ASME, 55(June), 287-293.

BAZANT, Z. P. and SHIEH, C. L. (1978).

'Endochronic Model for Nonlinear Triaxial Behaviour of Concrete,' Nuclear Eng. and Design, Vol. 47, pp.305-315.

BAZANT, Z. P. and SHIEH, C. L. (1980).

'Hysteretic Fracturing Endochronic Theory for Concrete,' J. of the Eng. Mech. Div., ASCE, Vol. 106, No. EM6, Dec., pp. 929-950.

BEDARD, C. and KOTSOVOS, M. D. (1985).

'Application of NLFEA to Concrete Structures,' J. of Structural Engineering, ASCE, Vol.111, No.12, pp.2691-2707.

BEDARD, C. and KOTSOVOS, M. D. (1986).

'Fracture Processes of Concrete for NLFEA Methods,' J. of Structural Engineering, ASCE, Vol.112, No.3, pp. 573-587.

BELARBI, A. and HSU, T. T. C. (1990).

'Stirrup Stresses in Reinforced Concrete Beams,' ACI Journal, Vol. 87, September-October, pp. 530-538.

BHATT, P. (1986).

'Programming the Matrix Analysis of Skeletal Structures,' John Willey & Sons, Chichester.

BRESLER, B. and MacGREGOR, J. G. (1967).

'Review of Concrete Beams Failing in Shear,' J. of Struc. Div., ASCE, Vol. 93, No. ST1, February, pp. 343-372.

BRESLER, B. and SCORDELIS, A. C. (1963).

'Shear Strength of Reinforced Concrete Beams,' Proc. ACI, Vol.60, No.1, pp.51-74.

BRESLER, B., and PISTER, K. S. (1958).

'Strength of Concrete under Combined Stresses,' ACI Journal, Vol.55, Sep., pp. 321-345.

BRETTMANN, B. B., DARWIN, D., and DONAHEY, R. C. (1986).

'Bond of Reinforcement to Superplasticized Concrete,' ACI Journal, Vol. 83, Jan.-Feb., pp. 98-107.

CEDERWALL, K., HEDMAN, O. and LOEBERG, A. (1974).

'Shear Strength of Partially Prestressed Beams With Pretension Reinforcement of High Grade Deformed Bars,' in SHEAR IN REINFORCED CONCRETE, Proceeding of the Shear Symposium, American Concrete Institute, ACI Special Publication SP-42, Vol.1, pp.215-230.

CEDOLIN, L., CRUTZEN, Y. R. J., and POLI, S. D. (1977).

'Triaxial Stress-Strain Relationship for Concrete,' J. of Eng. Mech. Div., ASCE, Vol. 103, No. EM3, June, pp. 423-439.

CEDOLIN, B. L. and Dei POLI, S. D. (1977).

'Finite Element Studies of Shear-Critical R/C Beams,' J. Eng. Mech. Div., Proc. of ASCE, Vol.103, No. EM3, pp.395-410.

CEDOLIN, B. L. and NILSON, A. H. (1978).

'A Convergence Study of Iterative Methods Applied to Finite Element Analysis of Reinforced Concrete,' Int. J. for Numerical Methods in Engineering, Vol.12, pp.437-451.

CERVENKA, V. (1970).

'Inelastic Finite Element Analysis of Reinforced Concrete Panels under In-Plane Loads,' Ph.D Thesis, University of Colorado.

CERVERA, M., HINTON, E. and HASSEN, O. (1987).

'Nonlinear Analysis of Reinforced Concrete Plate and Shell Structures Using 20-Noded Isoparametric Brick Elements,' Computer & Structures, Vol.25, No.6, pp.845-869.

CHANA, P. S. (1987).

'Investigation of the Mechanism of Shear Failure of Reinforced Concrete Beams,' Magazine of Concrete Research, Vol. 39, No. 141, December, pp. 196-204.

CHANA, P. S. (1988).

'Analytical and Experimental Studies of Shear Failures in Reinforced Concrete Beams,' Proc. Instn Civ. Engrs, Part 2, Vol. 85, December, pp. 609-628.

CHANG, T. Y., TANIGUCHI, H., and CHEN, W. F. (1987).

'Nonlinear Finite Element Analysis of Reinforced Concrete Panels,' J. of Structural Engineering, ASCE, Vol.113, No.1, pp.122-140.

CHEN, A. C. T. and CHEN, W. F. (1975a)

'Constitutive Relations for Concrete,' J. of Eng. Mech. Div., ASCE, Vol. 101, No. EM4, Aug., pp.465-481.

CHEN, A. C. T. and CHEN, W. F. (1975b)

'Constitutive Equations and Punch-Indentation of Concrete,' J. of Eng. Mech. Div., ASCE, Vol. 101, No. EM6, Dec., pp. 889-906.

CHEN, W. F. (1982).

'Plasticity in Reinforced Concrete,' McGraw Hill, New York.

CHEN, W. F. and TENG, E. C. (1980).

'Constitutive Models for Concrete,' J. of Mech. Div., Proc. of ASCE, Vol.106, No. EM1, February, pp. 1-19.

CHEN, W. F. and SALEEB, A. F. (1982).

'Constitutive equations for engineering materials,' Volume 1: Elasticity and Modelling. AWiley-Interscience Publication.

CLARK, A. P. (1951).

'Diagonal Tension in Reinforced Concrete Beams,' ACI Journal, Vol. 48, October, pp.145-156.

COLLINS, M. P. (1973).

'Torque-Twist Characteristics of Reinforced Concrete Beams, In Inelasticity and Non-Linearity in Structural Concrete. University of Waterloo Press, Waterloo Ontario. (quoted by Mau and Hsu 1990)

COLLINS, M. P. (1978).

'Towards a Rational Theory for RC Members in Shear,' J. of Struc. Div., ASCE, Vol. 104, April, pp. 649-666.

COLLINS, M. P. and MITCHELL, D. (1980).

'Shear and Torsion Design of Prestressed and Non-Prestressed Concrete Beams,' J. of the Prestressed Concrete Institute, Chicago, Vol.25, No.5, September-October, pp. 32-100.

COLLINS, M. P. and MITCHELL, D. (1986).

'A Rational Approach to Shear Design: The 1984 Canadian Code Provisions,' ACI Journal, Vol. 83, November-December, pp. 925-933.

CP-114 (1957).

British Standards Institution CP 114, 'The Structural Use of Reinforced Concrete in Buildings,' London.

DAHLBLOM, O. and OTTOSEN, N. S. (1990).

'Smearred Crack Analysis Using Generalized Fictitious Crack Model,' J. of Structural Engineering, ASCE, Vol. 116, No. 1, January, pp. 55-76.

DARWIN, D. and PECKNOLD, D. A. (1977).

'Nonlinear Biaxial Stress-Strain Law for Concrete,' J. of Eng. Mech. Div., ASCE, Vol. 103, April, pp. 229-241.

DIVAKAR, M. P., FAFITIS, A., and SHAH, S. P. (1987).

'Constitutive Model for Shear Transfer in Cracked Concrete,' J. of Struc. Eng., Vol. 113, No. 5, May, pp. 1046-1062.

DUNCAN, W. and JOHNARRY, T. (1979).

'Further studies on the Constant Stiffness method of Non-Linear Analysis of concrete structure,' Proc. Instn Civ. Engrs, Part 2, Vol. 67, Dec., pp. 951-969.

EIKLID G. E., GERSTLE, K. H. and TULIN, L. G. (1969).

'Strain-Hardening Effects in Reinforced Concrete,' Magazine of Concrete Research, Vol. 21, No. 69, December, pp.211-220.

EL-MEZAINI, N. and CITIPITIOGLU, E. (1991).

'Finite Element Analysis of Prestressed and Reinforced Concrete Structures,' J. of Struc. Eng., Vol. 117, No. 10, October, pp.-2851-2864.

ELNOUNU, G. F. (1985).

'Design of Shear Wall-Floor Slab Connections,' Ph.D thesis, Glasgow University.

ELWI, A. E. and HRUDEY, M. T. (1989).

'Finite Element Model for Curved Embedded Reinforcement,' J. of Engineering Mechanics, ASCE, Vol. 115, No. 4, April, pp.740-754.

ELWI, A. E. and MURRAY, D. W. (1979).

'A 3D Hypoelastic Concrete Constitutive Relationship,' J. of Eng. Mech. Div., ASCE, Vol. 105, No. EM4, Aug., 1979, pp. 623-641.

ELZANATY, A. H., NILSON, A. H., and SLATE, F. O. (1986a).

'Shear Capacity of Reinforced Concrete Beams Using High-Strength Concrete,' ACI Journal, Vol.83, March-April, pp.290-296.

ELZANATY, A. H., NILSON, A. H., and SLATE, F. O. (1986b).

'Shear Capacity of Prestressed Concrete Beams Using High-Strength Concrete,' ACI Journal, Vol. 83, May-June, pp. 359-368

EVANS, R. H. and SCHUMACHER (1963).

'Shear Strength of Prestressed Beams Without Web Reinforcement,' ACI Journal, Vol. 60, November, pp. 1621-1642.

FENWICK, R. C., and PAULAY, T. (1968).

'Mechanisms of Shear Resistance of Concrete Beams,' J. of Struc. Div., ASCE, Vol. 94, October, pp. 2325-2350.

FERGUSON, P. M. (1956).

'Some implications of recent diagonal tension tests,' ACI Journal, Vol. 53, August, pp. 157-172.

FLOEGL, H. and MANG, H. A. (1982).

'Tension Stiffening Concept Based on Bond Slip,' J. of Struc. Div., ASCE, Vol. 108, No. 12, December, pp. 2681-2701.

GAJER, G. and DUX, P. F. (1988).

'A Crack-Band Model for Finite Element Analysis of Concrete Structures,' Research Report No. CE89, University of Queensland.

GAJER, G. and DUX, P. F. (1990).

'Crack Band Based Model for FEM Analysis of Concrete Structure,' J. of Structural Engineering, ASCE, Vol. 116, No. 6, June, pp. 1696-1714.

GILBERT, R. I. and WARNER, R. F. (1978).

'Tension Stiffening Concept Based on Bond Slip,' J. of Struc. Div., ASCE, Vol. 104, No. 12, pp. 1885-1900.

GOPALARATNAM, V. S. and SHAH, S. P. (1985).

'Softening Response of Plain Concrete in Direct Tension,' ACI Journal, Vol. 82, pp. 310-323.

GUPTA, A. K. and MAESTRINI, S. R. (1989a).

'Post-Cracking Behaviour of Membrane Reinforced Concrete Elements Including Tension-Stiffening,' J. of Structural Engineering, ASCE, Vol. 115, No. 4, April, pp. 957-976.

GUPTA, A. K. and MAESTRINI, S. R. (1989b).

'Unified Approach to Modeling Post-cracking Membrane Behaviour of Reinforced Concrete,' J. of Structural Engineering, ASCE, Vol. 115, No. 4, April, pp. 977-993.

GUPTA, A. K. and MAESTRINI, S. R. (1990).

'Tension-Stiffness Model for Reinforced Concrete Bars,' J. of Structural Engineering, ASCE, Vol. 116, No. 3, March, pp. 769-790.

HARMON, T. G. and ZHARGYUAN, N. (1989).

'Shear Strength of Reinforced Concrete Plates and Shells Determined by Finite Element Analysis Using Layered Elements,' J. of Structural Engineering, ASCE, Vol. 115, No. 5, pp. 1141-1157.

HILLERBORG, A., MODEER, M. and PETERSSON, P. E. (1976).

'Analysis of Crack Formation and Crack Growth in Concrete By Means of Fracture Mechanics and Finite Element,' Cem. Concr. Res., 6(6), 773-782.

HINTON, E. and OWEN, D. R. G. (1977).

'Finite Element Programming,' Academic Press.

HOFBECK, J. A., IBRAHIM, I. O., and MATTOCK, A. H. (1969).

'Shear Transfer in Reinforced Concrete,' ACI Journal, Vol. 66, February, pp. 119-128.

HOUDE, J. and MIRZA, M. S. (1974)

'A Finite Element Analysis of Shear Strength of Reinforced Concrete Beams,' in SHEAR IN REINFORCED CONCRETE, Proceeding of the Shear Symposium, American Concrete Institute, ACI Special Publication SP-42, Vol. 1, pp. 103-128.

HSU, T. T. C. (1988).

'Softened Truss Model Theory for Shear and Torsion,' ACI Journal, Vol. 85, November-December, pp. 624-635.

HSU, T. T. C. (1991).

'Nonlinear Analysis of Concrete Membrane Elements,' ACI Journal, Vol. 88, September-October, pp. 552-561.

ISENBERG, J. and ADHAM, S. (1970).

'Analysis of Orthotropic Reinforced Concrete Structures,' J. of Struc. Div., ASCE, Vol. 96, ST 12, December, pp. 2607-2624.

IVEY, D. L. and BUTH, E. (1967).

'Shear Capacity of Lightweight Concrete Beams,' ACI Journal, Vol. 64, October, pp. 634-643.

IYENGAR, K. T. and RANGAN B. V. (1966).

Discussion of the paper by Kani (1966), ACI Journal, Vol. 63, December, pp. 1518-1522.

JIANG, D. H., SHAH, S. P., and ANDONIAN A. T. (1984).

'Study of the Transfer of Tensile Forces by Bond,' ACI Journal, Vol. 81, May-June, pp. 251-259.

JOHANRY, T. (1979).

'Elasto-Plastic Analysis of Concrete Structures Using Finite Elements,' Ph.D. Thesis, University of Strathclyde.

KENT, D. C., and PARK, R. (1971).

'Flexural Members With Confined Concrete,' J. of Struc. Div., ASCE, Vol. 97, No. ST7, Proc. Paper 8243, July, p. 1969. (quoted by Meyer and Bathe 1982)

KANI, G. N. J. (1964).

'The Riddle of Shear Failure and its Solution,' ACI Journal, Vol. 61, April, pp. 441-467.

KANI, G. N. J. (1966).

'Basic Facts Concerning Shear Failure,' ACI Journal, Vol. 63, June, pp. 675-691.

KANI, G. N. J. (1969).

'A Rational Theory for the Function of Web Reinforcement,' ACI Journal, Vol. 66, March, pp. 185-197.

KAR, J. N. (1969).

'Shear Strength of Prestressed Concrete Beams Without Web Reinforcement,' Magazine of Concrete Research, Vol. 21, No. 68, September, pp. 159-170.

KEMP, E. L. (1986).

'Bond in Reinforced Concrete: Behaviour and Design Criteria,' ACI Journal, Vol. 83, Jan-Feb, pp. 50-57.

KOTSOVOS, M. D. (1979).

'A Mathematical Description of the Strength Properties of Concrete under Generalised Stress,' Magazine of Concrete Research, Vol. 31, No. 108, Sept., pp. 151-158.

KOTSOVOS, M. D. (1983).

'Mechanisms of Shear Failure,' Magazine of Concrete Research, Vol. 35, No. 123, pp. 99-105.

KOTSOVOS, M. D. (1984).

'Behavior of Reinforced Concrete Beams With a Shear Span to Depth Ratio Between 1.0 and 2.5,' ACI Journal, Vol. 81, May-June, pp. 279-286.

- KOTSOVOS, M. D. (1986).**
'Behavior of Beams With Shear Span-to-Depth Ratios Greater Than 2.0,' ACI Journal, Vol. 83, November-December, pp. 1026-1034.
- KOTSOVOS, M. D., BOBROWSKI, J., and EIBL, J. (1987).**
'Behaviour of Reinforced Concrete T-Beams in Shear,' The Structural Engineer, Vol. 65B, No. 1, March, pp. 1-10.
- KOTSOVOS, M. D. and CHEONG, H. C. (1984).**
'Applicability of Test Specimen Results for the Description of the Behaviour of Concrete in a Structure,' ACI Journal, Vol. 81, July-August, pp. 358-363.
- KOTSOVOS, M. D. and LEFAS, I. D. (1990).**
'Behavior of Reinforced Concrete Beams Designed in Compliance with The Concept of Compressive-Force Path,' ACI Journal, Vol. 87, March-April, pp. 127-138.
- KOTSOVOS, M. D. and NEWMAN, J. B. (1977).**
'Behaviour of Concrete under Multiaxial Stress,' ACI Journal, Vol. 74, Sep., pp. 443-446.
- KOTSOVOS, M. D. and NEWMAN, J. B. (1978).**
'Generalised stress-strain relations for concrete,' J. of Eng. Mech. Div., ASCE, Vol. 104, No. EM4, August, pp. 845-856.
- KOTSOVOS, M. D. and NEWMAN, J. B. (1979).**
'A Mathematical Description of the Deformation Behaviour of Concrete under Complex Loading,' Mag. of Concrete Research, Vol 31, June, pp. 77-90.
- KOTSOVOS, M. D. and NEWMAN, J. B. (1980).**
'Mathematical Description of Deformation Behaviour of Concrete under Generalized Stress Beyond Ultimate Strength,' ACI Journal, Vol. 77, Sept.-Oct., pp. 340-346.
- KRUTHAMMER, T., FORCIER, G., PALMIERI, L., ROTH, J., and BERGSON, P. (1988).**
Discussion on 'Observed Stress-Strain Behaviour of Confined Concrete,' J. of Struc. Eng., ASCE, Vol. 114, No. 8, by Mander, et al., pp. 1469-1471.
- KREFELD, W. J. and THURSTON, C. W. (1966a).**
'Contribution of Longitudinal Steel to Shear Resistance of Reinforced Concrete Beams,' ACI Journal, March, pp. 325-343.
- KREFELD, W. J. and THURSTON, C. W. (1966b).**
'Studies of the Shear and Diagonal Tension Strength of Simply Supported Reinforced Concrete Beams,' ACI Journal, April, pp. 451-475.
- KUPFER, H., HILSDORF, H. K. and RUSCH, H. (1969).**
'Behavior of Concrete Under Biaxial Stresses,' ACI Journal, August, Vol. 66, pp. 656-666.
- LAHNERT, B. J., HOUDE, J., and GERSTLE, K. H. (1986).**
'Direct Measurement of Slip Between Steel and Concrete,' ACI Journal, Vol. 83, November-December, pp. 974-982.
- LIN, C. S. and SCORDELIS, A. C. (1975).**
'Nonlinear Analysis of RC shell of General Form,' J. of Struc. Div., ASCE, Vol. 111, No. 3, pp. 523-538.
- LIU, T. C. Y., NILSON, A. H. and SLATE, F. O. (1972).**
'Stress-Strain Response and Fracture of Concrete in Uniaxial and Biaxial Compression,' ACI Journal, Vol. 69, No. 5, May, pp. 291-295.

MacGREGOR, J. G. and WALTERS, J. R. V. (1967).

'Analysis of Inclined Cracking Shear in Slender Reinforced Concrete Beams,' ACI journal, Vol.64, October, pp. 644-653.

MANDER, J. B., PRIESTLEY, M. j., and PARK, R. (1988).

'Theoretical Stress-Strain Model for Confined Concrete,' J. of Struc. Eng., ASCE, Vol. 114, No. 8, August, pp. 1804-1826.

MASSICOTTE, B., ELWI, A. E., and MacGREGOR, J. G. (1990).

'Tension-Stiffening Model For Planar Reinforced Concrete Members,' J. of Structural Engineering, ASCE, Vol. 116, No.11, November, pp 3039-3058.

MATHEY, R. G. and WATSTEIN, D. (1963).

'Shear Strength of Beams Without Web Reinforcement Containing Deformed Bars of Different Yield Strength,' ACI Journal, February, pp.183-207.

MATTOCK, A. H. (1974).

'Shear Transfer in Concrete Having Reinforcement At An Angle to the Shear Plane,' in SHEAR IN REINFORCED CONCRETE, Proceeding of the Shear Symposium, American Concrete Institute, ACI Special Publication SP-42, Vol.1, pp.17-42.

MAU, S. T. and HSU, T. T. C. (1987).

'Shear Strength Prediction for Deep Beams with Web Reinforcement,' ACI Journal, Vol. 84, November-December, pp. 513-523.

MAU, S. T. and HSU, T. T. C. (1990).

'Shear Strength Prediction- Softened Truss Model,' in Reinforced Concrete Deep Beams, In Reinforced Concrete Deep Beams, Edited by F. K. Kong, Blackie.

MEYER, C. and BATHE, K. J. (1982.)

'Nonlinear Analysis of R/C Structures in Practice,' J. of Structural Engineering, ASCE, Vol. 108, No.7, July, pp 1605-1622.

MILLARD, S. G. and JOHNSON, R. P. (1984).

'Shear Transfer Across Cracks in Reinforced Concrete Due to Aggregate Interlock and to Dowel Action,' Magazine of Concrete Research, Vol. 36, No. 126, March, pp.9-21.

MITCHELL, D. and COLLINS, M. P. (1974).

'Diagonal Compression Field Theory A Rational Model for Structural Concrete in Pure Torsion,' ACI Journal, Vol. 71, No. 8, August, pp. 396-408.

MOODY, K. G., VIEST, M., ELSTNER, R. C., and HOGNESTAD, E. (1954).

'Shear Strength of Reinforced Concrete Beams Part 1-Tests of Simple Beams,' ACI Journal, November, pp. 317-332.

MOODY, K. G., VIEST, M., ELSTNER, R. C., and HOGNESTAD, E. (1955).

'Shear Strength of Reinforced Concrete Beams Part 2-Tests of Restrained Beams Without Web Reinforcement,' ACI Journal, January, pp. 417-434.

MOODY, K. G. and VIEST, M.(1955).

'Shear Strength of Reinforced Concrete Beams Part 4-Analytical Studies,' ACI Journal, March, pp. 697-729.

MPHONDE, A. G. and FRANTZ, G. C. (1984).

'Shear Tests of High-and Low-Strength Concrete Beams,' ACI Journal, July-August, Vol. 81, pp.350-357.

MPHONDE, A. G. (1988).

'Aggregate Interlock in High Strength Reinforced Concrete Beams,' Proc. Instn Civ. Engrs, Part 2, Vol. 85, Sept., pp.397-413.

MURRAY, D. W. (1979).

'Octahedral Based Incremental Stress Strain Matrices,' J. of Eng. Mech. Div., ASCE, Vol. 105, Aug., pp. 501-513.

MUSAVI, H. M. (1992).

'Punching Shear Strength of Unbonded Prestressed Flat Slabs at Edge Column Connections,' Ph.D thesis, Glasgow University.

NASSER, K. W. and KENYON, J. C. (1984).

'Why Not 3 x 6 Inch Cylinders for Testing Concrete Compressive Strength,' ACI Journal, Vol. 81, January-February, pp. 47-53.

NGO, D. and SCORDELIS, A. C. (1967).

'Finite Element Analysis of Reinforced Concrete Beams,' ACI Journal, Vol. 64, No. 3, pp. 152-163.

NILSON, A. H. (1971).

'Bond Stress-Slip Relations in Reinforced Concrete,' Report No.345, Dept. of Struct. Eng., Cornell Univ., Ithaca, N. Y. (quoted by Gupta and Maestrini 1990).

NIYOGI, L. L. (1974).

'Concrete Bearing Strength- Support, Mix, Size Effect,' J. of the Struc. Div., ASCE, Vol. 100, No. ST8, August, pp. 1685-1702.

OJHA, S. K. (1967).

'The Shear strength of Rectangular Reinforced and Prestressed Concrete Beams,' Magazine of Concrete Research, Vol. 19, September, pp. 173-184.

OTTOSEN, N. S. (1977).

'A Failure Criterion for Concrete,' J. of Eng. Mech. Div., ASCE, Vol.103, EM4, August, pp. 527-535.

OTTOSEN, N. S. (1982).

'2-D Finite Element Analysis of Massive RC Structure,' J. of Struc. Div., ASCE, Vol.108, No.ST8, August, pp. 1874-1893.

OWEN, D. R. J. and HINTON, E. (1980)

'Finite Element in Plasticity : Theory and Practice,' Pineridge Press Ltd, Swansea, U. K.

PALANISWAMY, R. and SHAH, S. P. (1974).

'Fracture and Stress-Strain Relationship of Concrete Under Triaxial Compression,' J. of the Struc. Div., ASCE, Vol. 100, No. St5, May, 1974, pp.901-916.

PAULAY, T. and LOEBER, P. J. (1974).

'Shear Transfer by Aggregate Interlock,' in SHEAR IN REINFORCED CONCRETE, Proceeding of the Shear Symposium, American Concrete Institute, ACI Special Publication SP-42, Vol.1, pp.1-15.

PERRY, E. S. and THOMPSON, J. N. (1966).

'Bond Stress Distribution on Reinforcing Steel in Beams and Pullout Specimens,' ACI Journal, Vol. 63, August, pp. 865-874.

PHILLIPS, D. V. (1992).

Discussion on 'Three-dimensional non-linear finite-element model for structural concrete: parts 1 and 2' by Vidosa, et al. (1991), Proc. Instn Civ. Engrs, Structs & Bldgs, Part 2, Vol. 94, August, pp. 365-374.

PHILLIPS, D. V. and WU, Z. P. (1990).

'An Oriented Embedded Bar Formulation with Bond-Slip,' Numerical Methods in Engineering: Theory and Application, Ed. Pande and Middleton, J., Vol. 1, pp. 320-328, Elsevier.

PHILLIPS, D. V. and ZIENKIEWICZ, O. C. (1976).

'Finite Element Non-Linear Analysis of Concrete Structures,' Proc. of Institution of Civil Engineers, Vol. 61, No. 2, pp. 59-88.

PIJAUDIER-CABOT, G. and BAZANT, Z. P. (1987).

'Nonlocal Damage Theory,' J. Engrg. Mech., ASCE, 113(10), 1512-1533.

RAMIREZ, J. A. and BREEN, J. E. (1983).

'Proposed Design Procedure for Shear and Torsion in Reinforced and Prestressed Concrete,' Research Report 248-4F, Center for Transportation Research, University of Texas at Austin, December, 254 pp (quoted by Ramirez and Breen 1991).

RAMIREZ, J. A. and BREEN, J. E. (1991).

'Evaluation of a Modified Truss-Model Approach for Beams in Shear,' ACI Journal, Vol. 88, September-October, pp. 562-571.

RANJBARAN, A. (1991).

'Embedding of Reinforcements in Reinforced Concrete Elements Implemented in DENA,' Computers & Structures, Vol. 40., No. 4, pp. 925-930.

RAPHAEL, J. M. (1984).

'Tensile Strength of Concrete,' ACI Journal, Vol. 81, March-April, pp. 158-165.

RASHID, Y. R. (1968).

'Ultimate Strength Analysis of Reinforced Concrete Pressure Vessels,' Nuclear Engineering and Design, Vol. 7, No. 4, April, pp. 334-344.

RAZAQPUR, A. G. and NOFAL, M. (1990).

'Analytical Modeling of Nonlinear Behavior of Composite Bridges,' J. of Struct. Eng., ASCE, Vol. 116, No. 6, June, pp. 1715-1733.

REGAN, P. E. (1969).

'Shear in Reinforced Concrete Beams,' Magazine of Concrete Research, Vol. 21, No. 66, March, pp. 31-42.

REINHARDT, H. W. (1985).

'Crack Softening Zone in Plain Concrete Under Static Loading,' Cement and Concrete Research, Vol. 15, pp. 42-52.

RILEM-DRAFT-RECOMMENDATION TC50-FMD (1985).

'Determination of the Fracture Energy of Mortar and Concrete by Means of Three-Point Bend Test on Notched Beams,' Materials and Structures, Vol. 18, No. 108.

RICHART, F. E., BRANDTZAEG, A. and BROWN, R. L. (1928).

'A Study of the Failure of Concrete Under Combined Compressive Stresses, Univ. Ill. Eng. Exp. St. Bull. 185. (quoted by Chen 1982).

'Nonlinear Finite Element Analysis of Reinforced Concrete Members,' ACI Journal, Vol. 86, January-February, pp. 22-32.

RUBLE, E. J. , TAUB, J., and AUTHORS (1955).

Discussion of series of papers by Moody, et al. (1954,1955) 'Shear Strength of Reinforced Concrete Beams,' ACI Journal, Vol. 51,Part 2 Dec., pp. 732-1 to 732-23.

SAENZ, I. P. (1964).

Discussion of 'Equation of the Stress-Strain Curve of Concrete' By Desayi P. and Krishnan S., ACI Journal, Vol. 61, No.9, September, pp. 1129-1235.

SCANLON, A. and MURRAY, D. W. (1974).

'Time Dependent Reinforced Concrete Slab Deflection,' J. of Struc. Div., ASCE, Vol. 100, No.9, pp.1911-1924.

SCORDELIS, A. C., NGO, O., and FRANKLIN, H. A. (1974).

'Finite Element Study of Reinforced Concrete Beams With Diagonal Tension Cracks,' Shear in Reinforced Concrete, Publication SP-42, American Concrete Institute, Detroit, pp.79-102.

SERAJ, S. M., KOTSOVOS, M. D., and PAVLOVIC, M. N. (1992).

'Non-Linear Finite-Element Analysis of Prestressed Concrete Members,' Proc. Instn Civ. Engrs Structs & Bldgs, Vol. 94, Nov., pp.403-418.

SHEIKH, S. A. and UZUMERI, S. M. (1982).

'Analytical Model for Concrete Confinement in Tied Columns,' J. of Struc. Div., ASCE, Vol. 108, No. ST12, December, pp. 2703-2722.

SOROUSHAN, P., OBASEKI, K., ROJAS, M. C., and SIM, J. (1986).

'Analysis of Dowel Bars Acting Against Concrete Core,' ACI Journal, Vol. 83, July-August, pp. 642-649.

STEVENS, N. J., UZUMERI, S. M., COLLINS, M. P., AND WILL, G. T. (1991).

'Constitutive Model for Reinforced Concrete Finite Element Analysis,' ACI Journal, Vol.88, No.1, January-February, pp.49-59.

SWAMY, R. N. AND ANDRIOPOULOS, A. D. (1974).

'Contribution of Aggregate Interlock and Dowel Action to the Shear Resistance of Reinforced Beams With Web Reinforcement,' in SHEAR IN REINFORCED CONCRETE, Proceeding of the Shear Symposium, American Concrete Institute, ACI Special Publication SP-42, Vol.1, pp. 129-165.

TAUB, J. and NEVILLE, A. M. (1970).

'Resistance to shear of reinforced concrete beams. Part 1 - Beams without web reinforcement,' ACI Journal, August, pp. 193-220.

TAYLOR, H. P. J. (1974).

'The Fundamental Behaviour of Reinforced Concrete Beams in Bending and Shear,' in SHEAR IN REINFORCED CONCRETE, Proceeding of the Shear Symposium, American Concrete Institute, ACI Special Publication SP-42, Vol.1, pp.43-77.

TAYLOR, R. (1966).

'Some Shear Tests on Reinforced Concrete T Beams With Stirrups,' Magazine of Concrete Research, Vol. 18, No. 57, December, pp. 221-230.

VAN MIER, J. G. M. (1986)

'Fracture of Concrete Under Complex Stress,' HERON, Vol. 31, No.3, Delft University of Technology, Delft, The Netherlands.

VECCHIO, F. J. (1989).

'Nonlinear Finite Element Analysis of Reinforced Concrete Membrances,' ACI Journal, Vol.86, January-February, pp.26-35.

VECCHIO, F. J. (1992).

'Finite Element Modeling of Concrete Expansion and Confinement,' J. of Struc. Eng., ASCE, Vol. 118, No. 9, September, pp. 2390-2406.

VECCHIO, F. and COLLINS, M. P. (1981).

'Stress-Strain Characteristics of Reinforced Concrete in Pure Shear,' Advanced Mechanics of Reinforced Concrete, IABSE Report, Vol.31 Delft, The Netherland, pp.35-42. (quoted by Mau and Hsu 1990).

VECCHIO, F. and COLLINS, M. P. (1986).

'Modified Compression-Field Theory for Reinforced Concrete Elements Subject to Shear,' ACI Journal, Proceedings Vol.83, No.2, March-April, pp.219-231.

VECCHIO, F. J. and NIETO, M. (1991).

'Shear-Friction Tests on Reinforced Concrete Panels,' ACI Journal, Vol. 88, May-June, pp. 371-379.

VIDOSA, F. G., KOTSOVOS, M. D., and PAVLOVIC, M. N. (1991a).

'Three-Dimensional Non-linear Finite Element Model for Structural Concrete. Part 1: main features and objectivity study,' Proc. Instn Civ. Engrs, Part 2, Vol. 91, pp.517-544.

VIDOSA, F. G., KOTSOVOS, M. D., and PAVLOVIC, M. N. (1991b).

'Three-Dimensional Non-linear Finite Element Model for Structural Concrete. Part 2: generality study,' Proc. Instn Civ. Engrs, Part 2, Vol. 91, pp.545-560.

VIDOSA, F. G., KOTSOVOS, M. D., and PAVLOVIC, M. N. (1991c).

'Non-linear Finite Element Analysis of Concrete Structures: performance of a fully three-dimensional brittle model,' Computer & Structures, Vol.40, No.5, pp.1287-1306.

VINTZELEOU, E. N. and TASSIOS, T. P. (1986).

'Mathematical models for dowel action under monotonic and cyclic conditions,' Magazine of Concrete Research, Vol 38, No. 134, March, pp. 13-22.

WANG, P., SHAH, S. P., and NAAMAN, A. E. (1978).

'High-Strength Concrete in Ultimate Strength Design,' J. of Struc. Div., ASCE, Vol. 104, No. ST11, November, pp.1761-1773.

WEGMULLER, A. W. (1974).

'Elast-plastic Finite Element Analysis of Plates,' Technical Notes TN99, Proc. of the Inst. of Civ. Engrs., Vol. 57(2), Sept., pp. 535-543.

WU, K. and ZHANG, B. (1988).

'Fracture Energy of Lightweight Concrete,' International Conference on Fracture Mechanics of Concrete, October, SENDAI, Japan.

YAMAGUCHI, E. and CHEN, W. F. (1990).

'Cracking Model for Finite Element Analysis of Concrete Materials,' J. of Structural Engineering, ASCE, Vol. 116, No. 6, June, pp.1242-1260.

YANKELEVSKY, D. Z. (1984).

'New Finite Element for Bond-Slip Analysis,' J. of Struc. Eng., Vol. 111, No. 7, July, pp. 1533-1542.

YANKELEVSKY, D. Z. and REINHARDT, H. W. (1987).

'Model for Cyclic Compressive Behavior of Concrete,' J. of Struc. Eng., ASCE, Vol. 113, No. 2, February, pp. 228-239.

YANNOPOULOS, P. J. and TASSIOS, T. P. (1991).

'Reinforced Concrete Axial Element Analyzed under Monotonic and Cyclic Actions,' ACI Journal, Vol. 88, Jan.-Feb., pp. 3-11.

YUZUGULLU, O. and SCHNOBRICH, W. C. (1973).

'A Numerical Procedure for the Determination of the Behaviour of a Shear Wall Frame System,' ACI Journal, Vol. 70, July, pp. 474-479.

ZIENKIEWICZ, O. C. (1977)

'The Finite Element Method,' McGraw Hill Book Company, 3rd. Edition.

ZWOYER, E. M. and SIESS, C. P. (1954).

'Ultimate Strength in Shear of Simply-Supported Prestressed Concrete Beams Without Web Reinforcement,' ACI Journal, Vol. 26, No. 2, October, pp. 181-200.

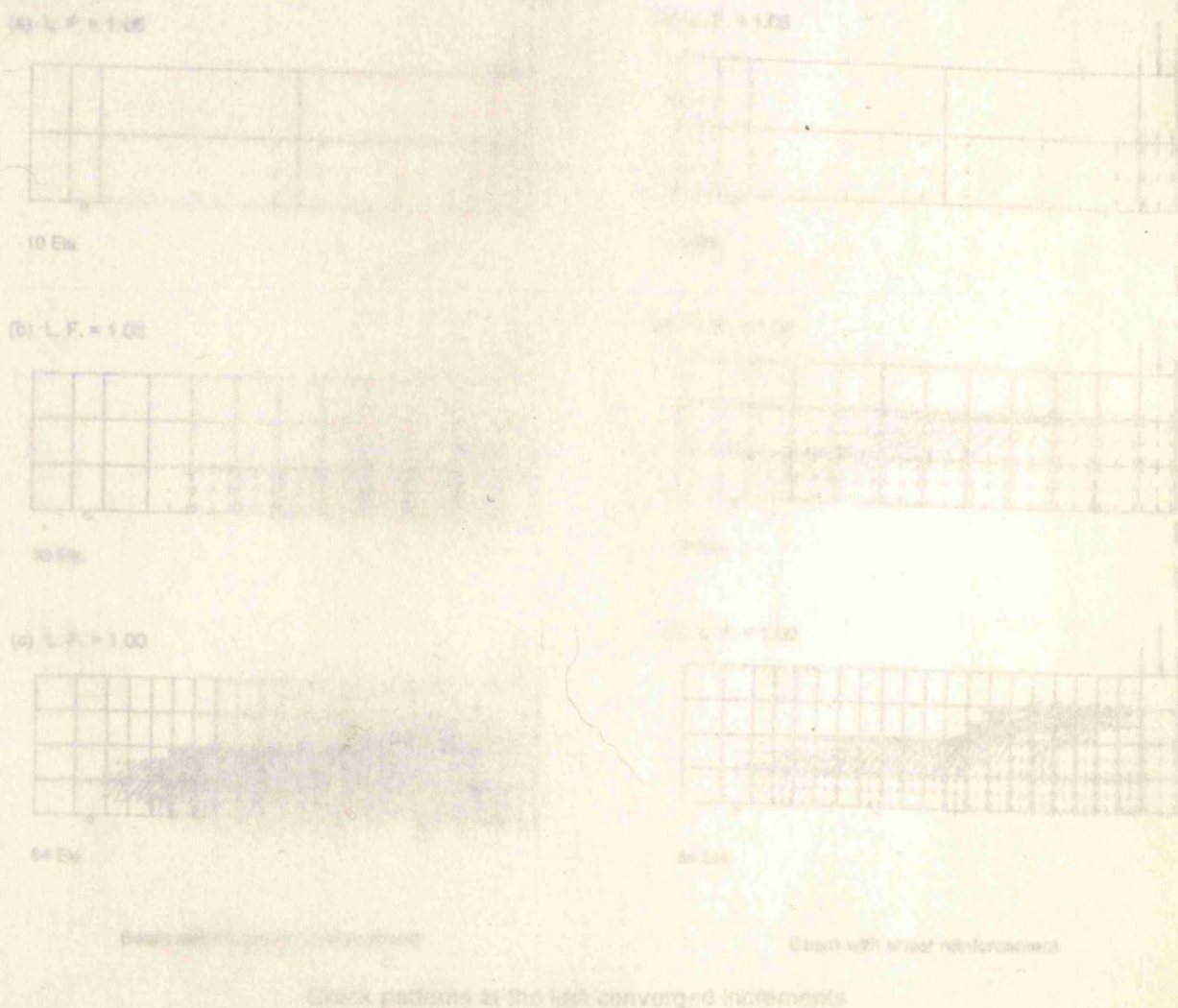
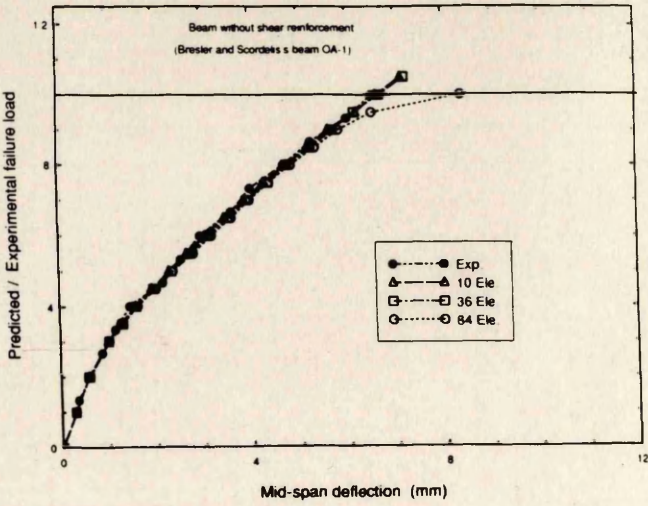


Fig. A1 Effect of number of elements on the prediction

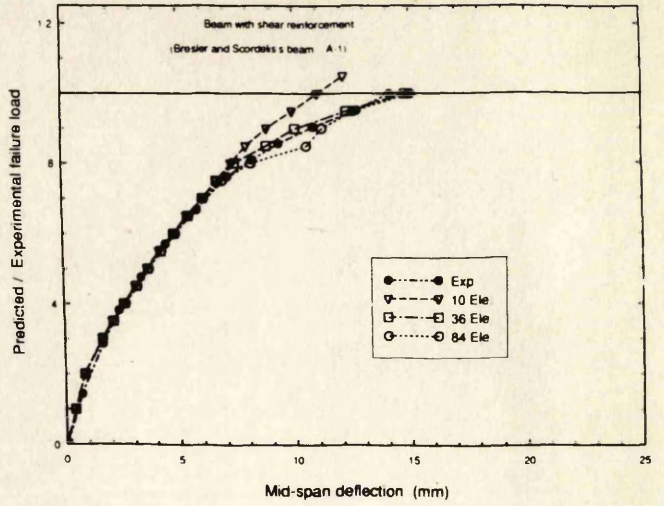
Appendix A

Effect of number of elements on the prediction

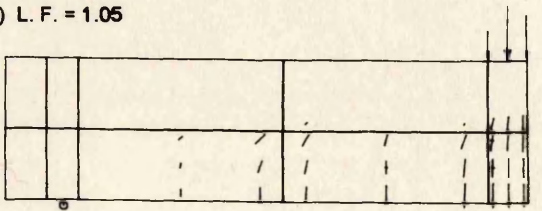
Effect of number of elements on the prediction



Effect of number of elements on the prediction

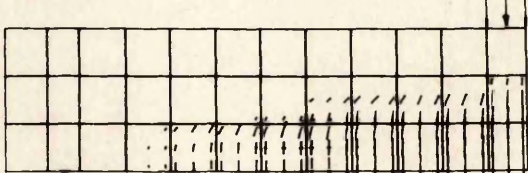


(a) L. F. = 1.05



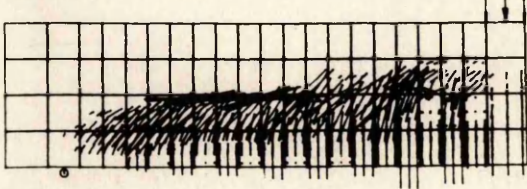
10 Ele.

(b) L. F. = 1.05



36 Ele.

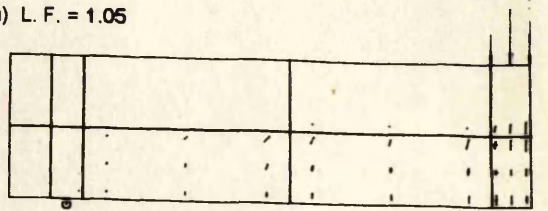
(c) L. F. = 1.00



84 Ele.

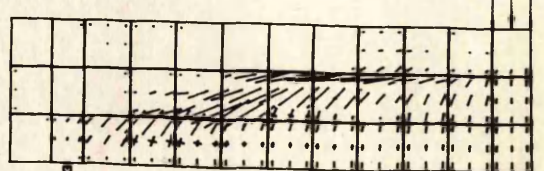
Beam without shear reinforcement

(a) L. F. = 1.05



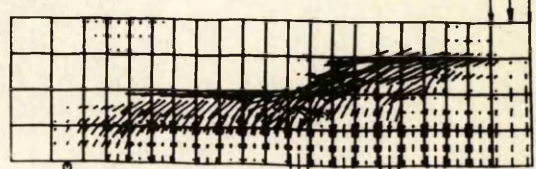
10 Ele.

(b) L. F. = 1.00



36 Ele.

(c) L. F. = 1.00



84 Ele.

Beam with shear reinforcement

Crack patterns at the last converged increments

Fig. A1 Effect of number of elements on the prediction.